NASA Technical Paper 3540

NASP TM–1186

1996

High-Temperature Strain Sensor and Mounting Development

W. Dan Williams
Lewis Research Center
Cleveland, Ohio

Jih-Fen Lei
U.S. Army Research Laboratory
Lewis Research Center
Cleveland, Ohio

Lawrence F. Reardon
Hugh L. Dryden Flight Research Center
Edwards, California

Keith Krake and M.M. Lemcoe
PRC, Inc.
Edwards, California

Harlan K. Holmes and Thomas C. Moore, Sr.
Langley Research Center
Hampton, Virginia

National Aeronautics and Space Administration

Office of Management

Scientific and Technical Information Program

1996

Preface

The purposes of Government Work Package Task 29 (GWP29) were to develop advanced resistance strain gage technology in support of the National Aerospace Plane (NASP) Program and to test these advanced sensors from room temperature to 2000 °F (1095 °C). The present phase of the development advances the technology to only 1500 °F (815 °C) primarily because of limitations in the materials selected for the program. GWP29 was a cooperative effort between NASA Lewis Research Center, NASA Langley Research Center, and NASA Dryden Flight Research Center to develop and test three strain gage types and to perfect gage attachment techniques. The end product of the effort was intended to characterize the behavior of the various gages over the temperature range on a selection of NASP materials and to arrive at recommendations regarding their use. Three test sites were selected for the development process because the NASP contractor team required independent verifications of the subject gages. Before testing could begin, significant delays were encountered, first in the selection of which NASP materials to use in the investigations and second in the delivery of adequate quantities of the selected materials for the many test specimens required. During the early phase an elaborate test procedure, complete with evaluation methodologies, was generated addressing the major gage properties of interest to an investigator: apparent strain, drift strain, and gage factor as a function of temperature. The three NASA centers conducted identical tests on three different high-temperature gages and on two NASP materials. Early during this phase significant advances in the gages being developed under this task led to a decision by the NASP Joint Program Office to apply them to several structural test articles being developed under other parts of the NASP program.

Langley Research Center developed an iron-chromium-aluminum (Kanthal A1) gage, consisting of two elements, one active and one inactive, connected in a half-bridge configuration. Lewis Research Center developed a dual-element, temperature-compensated gage of palladium-chromium (PdCr) with a platinum compensator. Dryden Flight Research Center developed a dual-element, iron-chromium-aluminum (BCL–3) compensated gage with a platinum compensator. The materials investigated were IN100 and β-21S titanium-matrix composite (TMC). Because of temperature limitations in the TMC material, tests were conducted principally to 1200 °F (650 °C) with additional excursions to 1350 °F (730 °C) and to 1500 °F (815 °C).

Extensive tests, as described in the test procedure (chapter 2), were performed on all three gage types for all gage parameters at each of the three centers. To gain statistical significance, data from all gage types were collected from all the centers and combined to give an average of the data for 12 gages of each type together with the upper and lower 95% confidence limits regarding those averages. Dryden collected and processed data from all three centers for apparent strain, Langley did the same for drift strain, and Lewis for gage factor. Close cooperation between the three centers was essential to ensure that data from gages tested at different laboratories by different personnel using different equipment could be combined to improve the statistics of the entire process. Although raw data were acquired on different systems, identical computational equipment and programs were used.

A tremendous amount of effort has been expended in the performance of this program: in developing the test procedure itself, in developing gage attachment techniques, in acquiring copious amounts of test data, and finally, in processing, displaying, and reporting the test results. New gages were developed, extensive apparent strain compensation techniques were explored, new gage application techniques were perfected, and new materials were examined. It was generally concluded that no one gage type is clearly better than the others although each has attributes that may be more applicable in certain test programs. It has been shown in this program that making valid strain measurements on new materials requires an investigation to ensure that the proper gage type is selected, that the necessary compensation for that material is determined, and that special gages are procured for the situation if needed.

The remainder of this report contains complete information on the test procedure, the evaluation methodologies, the test systems used at the various centers, and the gage attachment techniques used and provides curves of all data obtained in the course of testing.

Acknowledgments

The following contractor personnel contributed to this study:

1. At Lewis, Mike Tong (NYMA, Inc.) and Darwin Boyd (NRC fellow)
2. At Dryden, Anthony Piazza (PRC, Inc.)
3. At Langley, Fred Lamm and Robert Latinski (Modern Machine & Tool Co., Inc.)

And we are grateful for their help.

Contents

Chapter 1

Summary

1.1 Introduction

Before the formation of Government work packages, work within the NASP program on high-temperature, strain-sensing technology had proceeded under the Technology Maturation Program. In December 1990 the NASP contractor team reviewed the status of all instrumentation as it related to the NASP program and determined that strain-sensing technology was the major technical challenge needing to be addressed. The program to come out of that determination was Government Work Package Task 29 (GWP29). Its purpose was to develop advanced strain gage technology in support of the NASP program. The focus was to develop advanced resistance strain gages with a temperature range from room temperature to 2000 °F (1095 °C) and to develop methods for reliably attaching these gages to the various materials anticipated for use in the NASP program. An additional complication was the NASP program requirement for first-cycle data. Therefore, the installed gages were not prestabilized or heat treated before first-cycle data were recorded.

Most high-temperature gages on the market in the 1980's exhibited resistance changes with temperature that could be orders of magnitude greater than that due to the expected strain. These resistance changes were highly nonlinear, were not repeatable, and had significant zero shifts when the gages were returned to room temperature. Some of these traits could be corrected but that required extensive records on the temperature-time history for each gage. To minimize or eliminate these undesirable traits, NASA Lewis Research Center, together with United Technologies Research Center, embarked on a program a few years ago to find a new gage alloy and then develop methods for using this new gage. At the outset of GWP29 it was decided to continue development of the resulting Lewis palladium-chromium (PdCr) gage but also to revisit some more readily available iron-chromium-aluminum (FeCrAl) gages to develop techniques for minimizing the undesirable traits. Thus, the NASA Lewis Research Center, the lead center for GWP29, chose to continue development of the PdCr gage; NASA Langley Research Center chose to investigate a popular gage known as the NZ–2104 FeCrAl foil gage manufactured by JP Technologies, Inc.; and the NASA Dryden Flight Research Center, because of extensive experience with it, chose the well-known BCL–3 FeCrAl gage for their investigation. The work package was broken into four tasks. Task 1, conducted principally by Dryden and Langley, was to investigate prestabilization and compensation techniques for BCL–3 and NZ–2104, both FeCrAl gages. During this effort Langley replaced the NZ–2104 gage with a new concept gage using Kanthal A1 described in detail later in this report. Task 2, conducted principally by Lewis, was to continue the development of the PdCr gage and its compensation and attaching techniques. Task 3 was a combined effort, by all three centers, to follow a detailed test procedure primarily developed at Lewis and an evaluation methodology primarily developed at Dryden for the respective gages. Task 4 was the reporting of results, with this document being the final product.

The parameters investigated were those believed to be of greatest importance to the user: apparent strain, drift strain, and gage factor as a function of temperature, plus gage size and survival rate over the test period. Although a significant effort was made to minimize the differences in test equipment among the three test sites (e.g., the same hardware and software were used for final data processing), each center employed a different data acquisition system and furnace configuration; therefore, some inherent differences may be evident in the final results.

1.2 Program History

As stated previously, before the formation of Government Work Package Task 29, strain-sensing technology development, both optical and contact sensing techniques, had proceeded at several sites under the Technology Maturation Program. In December 1990 the NASP contractor team reviewed the status of all instrumentation relative to the NASP program; the following is a summary of their recommendations regarding strain sensing:

"Develop and test strain sensors applicable to high-temperature measurements on metals, metal-metrix composites (MMC), and carbon/carbon composites (C/C). Coordinate test plans with NASP contractors and current flight sensors contract effort. Specific tasks should include

1. Active coordination with NASP contractors.
2. Independent verification of reported successful results at high temperatures for FeCrAl and PdCr alloys. Issues include material source, coatings, and conflicting results between researchers.

3. Application of above alloys to NASP materials, e.g., molybdenum rhenium (MoRe) and titanium-matrix composites (TMC), and verification testing to establish operating limits for each of the sensor materials. Address foil or flattened configuration for PdCr to delete the "installed" high temperature stabilizing soak currently required.

4. Testing of alternative practical installation methods on NASP materials and evaluation of the effects of high acoustic levels (160–165 dB) on installed gauges.

5. Independent evaluation of the 1/4-in. HITEC capacitance gage for selected NASP required.

6. Proof of concept testing of new sensor candidates especially for the temperature range from 1500 to 2500 °F. For example, the DOE proposed thermographic phosphor method, an optical extensometer, fiber optics (if high temp fiber developed) or speckle techniques proposed."

These tasks were given a decreasing order of importance (as above) by the contractor teams and with these guidelines Lewis, as the lead center, with Langley and Dryden formulated a development and test program to further the development of high-temperature resistance strain gages. Emphasis was placed on the first three tasks and gage installation techniques. High acoustic levels, although of great concern, were not addressed because of insufficient funding levels, and evaluating the capacitance gage was not considered because of its sensitivity to the high vibration levels anticipated on the NASP vehicle. Optical techniques employing speckle imaging were being pursued under other auspices at both Lewis (ref. 1.1) and Langley and so were not considered further under this program. Over time several iterations were made concerning the materials to be used. Carbon/carbon was dropped as a material for the primary structure and MoRe was transferred to the contractor work package on strain. TMC and IN100 were selected for test with IN100 as the baseline material.

After many redirections the final program for GWP29 was formulated as follows:

1. Task objective: Develop and test contact strain sensors capable of providing valid first-cycle data for use in the NASP program from room temperature to 2000 °F (1095 °C).

2. Approach: Use the latest gage attachment techniques to perform a laboratory evaluation of the latest versions of the BCL–3, NZ–2104, and PdCr gages installed on test bars and coupons of IN100, MoRe, and TMC materials. (MoRe was subsequently transferred to the contractor work package.)

3. Relationship to other Government and contractor work packages: This is a companion effort to the contractor's High-Temperature Strain Sensor Work Package and will provide the test techniques for the contractor's phase IID test article instrumentation efforts in support of the phase II exit criteria.

4. Schedule and milestones:

Original date	Revised date	Task element or milestone
1/92	6/92	a. Develop compensation techniques for FeCrAl gage types.
6/92	3/93	b. Develop PdCr gages.
12/92	1/95	c. Independently test and evaluate the BCL–3, NZ–2104, and PdCr gages on IN100, TMC, and MoRe materials.
3/93	5/95	d. Produce final report on gage evaluation and on gage attachment techniques.

The first two tasks were essentially completed according to this schedule, allowing time to improve the gages before testing. Task 3 was delayed considerably due to delays in delivery of material. The first IN100 deliveries were made in August 1992, but the material was found to be unusable. Salvage attempts proved unsuccessful and more material was procured with delivery in April 1994. Initial deliveries of the TMC material were made in January 1993, but the initial plates were warped significantly. A series of tests were conducted to determine the material's usefulness for this program (see appendix). Significant x-ray and ultrasonic studies done under NASP WBS 5.6.7 led to the conclusion that the material was acceptable. These evaluations delayed the testing phase.

1.3 Technical Background

Measuring mechanical strain is a difficult task at elevated temperatures, particularly where first-cycle data are required. Temperatures as high as 1500 °F (815 °C) and above are encountered in engine testing and were anticipated in structural testing in the NASP program. Not only are gages difficult to work with at these temperatures, but new materials have idiosyncrasies of their own that complicate the task. At the beginning of the NASP program numerous gages were available commercially, most of which were either platinum-tungsten, nickel-chromium, or FeCrAl alloys. The FeCrAl strain gage formulations were studied extensively in the late 1960's and early 1970's, and a great deal of effort was directed to finding formulations that would minimize the apparent strain of those materials, particularly at 700 to 900 °F (370 to 480 °C), where a metallurgical phase change occurs. Two formulations of the FeCrAl alloys have been extensively studied. One formulation, developed under Langley contracts (refs. 1.2 to 1.4) with Battelle Columbus Laboratories is designated the BCL–3 alloy. A second formulation was developed in China, hence the name "Chinese Alloy," in both 1300 and 1475 °F (700 and 800 °C) versions. The large magnitude, nonlinearity, and cooling rate sensitivity of the apparent strain for the non-temperature-compensated FeCrAl gages motivated the NASA Lewis Research Center and the United Technologies Research Center to develop the PdCr gage. Figure 1.1 illustrates the apparent strain as a function of temperature for four high-temperature

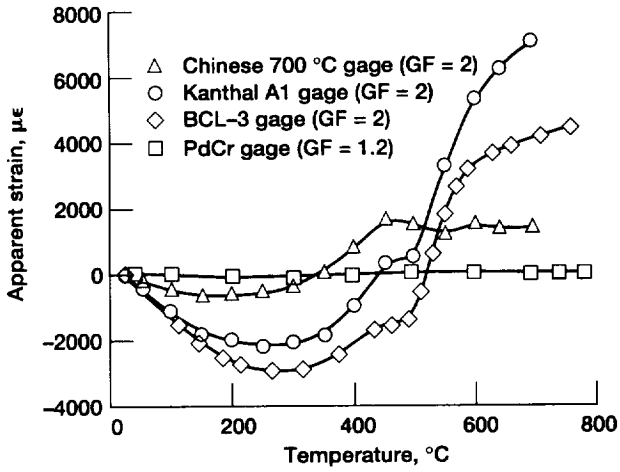

Figure 1.1.—Comparison of apparent strain versus temperature among four high-temperature strain gages.

resistance strain gages that were available when the GWP29 program started. It is apparent from figure 1.1 that the FeCrAl gages had large apparent strain variations as a function of temperature, perhaps an order of magnitude greater than the strains of interest (ref. 1.1). (Note that the result for the PdCr gage was from a gage that was prestabilized on the test article before testing.) Meaningful apparent strain correction, unless further compensation is accomplished, demands a rather precise knowledge of the temperature. In addition to the apparent strain variation with temperature, apparent strain variations over time at temperature must also be accounted for. Indeed, heating and cooling rates can affect the apparent strain magnitude and cause a non-return-to-zero condition that must also be dealt with. This test program sought to address all these concerns by a test sequence that attempted to determine the magnitude of the various effects (refs. 1.5 and 1.6).

Resistance strain gages measure strain by measuring the fractional change in resistance of a gage material, usually a fine wire, thin foil, or thin film. This change is expressed as

$$\Delta R / R = \Delta\varepsilon \times \mathrm{GF} \tag{1.1}$$

where

ΔR fractional change in gage resistance

R unstrained resistance of strain-sensing element

$\Delta\varepsilon$ applied mechanical strain

GF gage factor

For elevated temperatures the gage changes resistance with temperature T and with time τ at temperature, and the measured strain ε results from both true strain, apparent strain, and drift strain expressed as

$$\Delta\varepsilon_{\text{measured strain}} = \Delta\varepsilon_{\text{true strain}} + \Delta\varepsilon_{\text{apparent strain}} + \Delta\varepsilon_{\text{drift strain}} \tag{1.2}$$

where

$$\Delta\varepsilon_{\text{measured strain}} = \frac{\Delta R_{\varepsilon,T,\tau}/R_T}{\mathrm{GF}_T}$$

$$\Delta\varepsilon_{\text{apparent strain}} = \frac{\Delta R_T/R_0}{\mathrm{GF}_T}$$

$$\Delta\varepsilon_{\text{drift strain}} = \frac{\Delta R_{T,\tau}/R_T}{\mathrm{GF}_T}$$

R_0 unrestrained resistance at room temperature of strain-sensing element

R_T unrestrained resistance at temperature T of strain-sensing element

GF_T gage factor at temperature T

Various approaches have been taken to minimize the magnitude of the last two terms in equation (1.2). All techniques must resort to some method, either resistance or voltage offset compensation, to minimize the apparent strain (ref. 1.7). Different temperature-compensating alloy compositions are used to control or linearize the apparent strain versus temperature as well as to minimize the drift strain terms. Greatly reducing the effect of apparent strain by matched gage elements connected electrically in adjacent arms of a Wheatstone bridge circuit is another means to the same end. These approaches have been employed in this work package and make certain compromises that the user must evaluate to determine which method is best for a specific application. It must be emphasized that before applying any of these gages to new materials, particularly composite materials, one must test samples of the new material to determine compensator resistance magnitude. These specialized gages can then be obtained with a compensator so that they will be optimized for that new material.

1.4 Strain Gage Selection

As is evident from the preceding section, continued development and characterization of high-temperature strain gages presented a formidable challenge at the outset of the test program. Several approaches to selecting gages to evaluate and their compensation techniques were addressed. Factors leading to these selection and compensation techniques are now described.

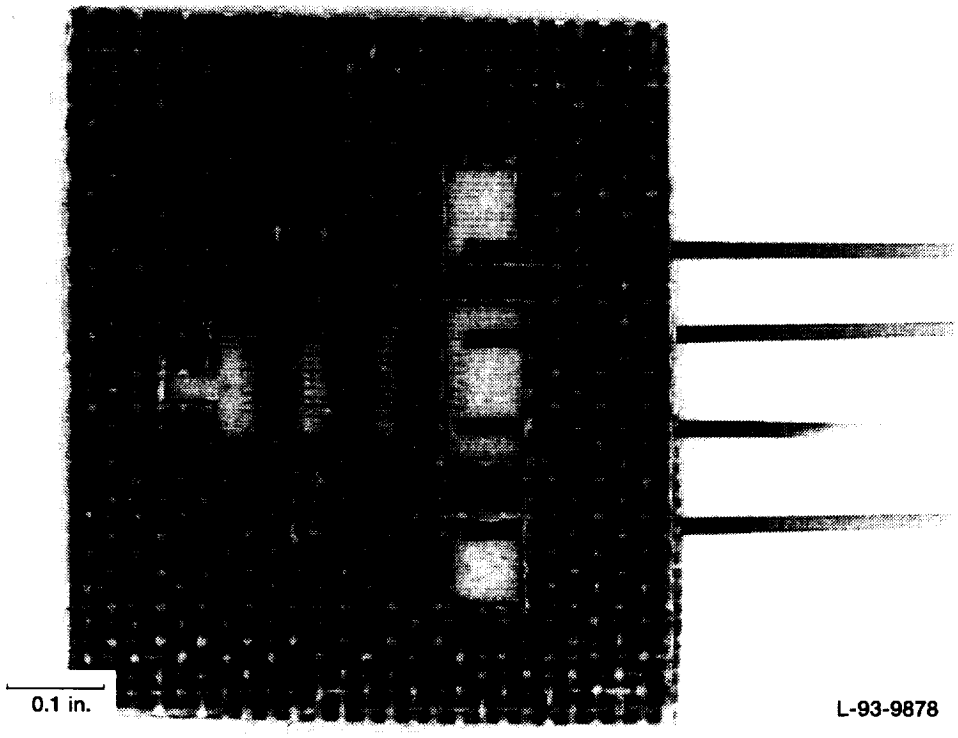

Figure 1.2.—Langley compensated Kanthal gage (CKA1).

1.4.1 Langley Research Center's Compensated Kanthal A1 Gage (CKA1)

To minimize the effects of apparent strain due to temperature and drift strain over time, a multielement gage was designed using a closely matched pair of gages. The gages were matched in both material and resistance. One gage element was firmly bonded to the structure; a second gage element, surrounding the first, was not bonded and was therefore isolated from the mechanical strain (ref. 1.8). Thus, both gage elements were exposed to a similar thermal environment. The gage is shown in figure 1.2. Connecting these two gage elements in adjacent arms of a Wheatstone bridge ideally balanced the thermal inputs and yet retained sensitivity to the mechanical strain. To correct for differences in thermal expansion between the gage and the structure materials, such as TMC's, an additional 0.001-in.-diameter platinum element was added in the arm that would generate the proper sign of the apparent strain. Originally, an NZ–2104–120L, free-filament, foil gage with a dual element for compensation had been considered; however, it was felt that structural damage caused by plasma spray attachment techniques and oxidation of the thin foil, above approximately 1200 °F (650 °C), would result in both yield and reliability problems. In changing to a wire construction the 1300 °F (700 °C) Chinese Alloy was considered, but its availability was always in question. The BCL–3 wire was also considered, but its cost and the fact that Dryden was advancing the development of that gage made selection of an inexpensive, readily available wire an alternative to expand the knowledge base. As a result, Langley selected 0.001-in.-diameter Kanthal A1 wire for the construction of their gages.

1.4.2 Lewis Research Center's Palladium-Chromium Gage (PdCr)

The PdCr gage was developed by the United Technologies Research Center with further refinements at Lewis. It was selected by Lewis for continued development under the NASP program. The gage material, palladium plus 13 wt% chromium, was selected after an extensive study (ref. 1.9) as having the most stable electrical properties among a number of alloys studied. The gage (ref. 1.10), consisting of a 0.001-in.-diameter PdCr wire, a 0.001-in.-diameter platinum compensator, and 0.03-in.-diameter PdCr lead-wire attachments, is shown in figure 1.3. The gage was connected in a half-bridge configuration, with the compensator and a ballast resistor in an adjacent arm completing the bridge. The resistance of the ballast resistor was selected to balance the bridge. The apparent strain of the PdCr element was essentially linear and the compensator was strain sensitive. This approach compensated for both apparent strain and mismatch in thermal coefficient of expansion between the gage and the substrate.

1.4.3 Dryden Flight Research Center's Dual-Element, Temperature-Compensated BCL Gage (DETCBCL)

Dryden selected this dual-element, temperature-compensated gage because of their extensive experience with the standard

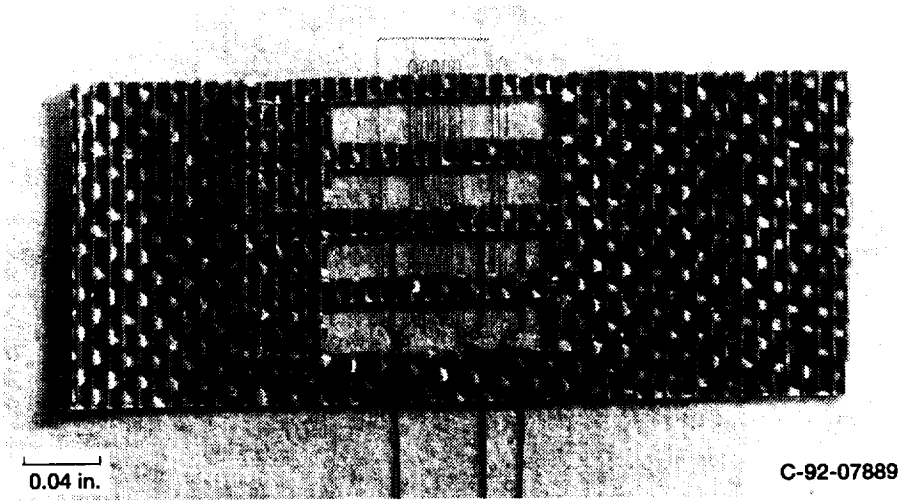

Figure 1.3.—Lewis PdCr high-temperature static strain gage with platinum compensating element.

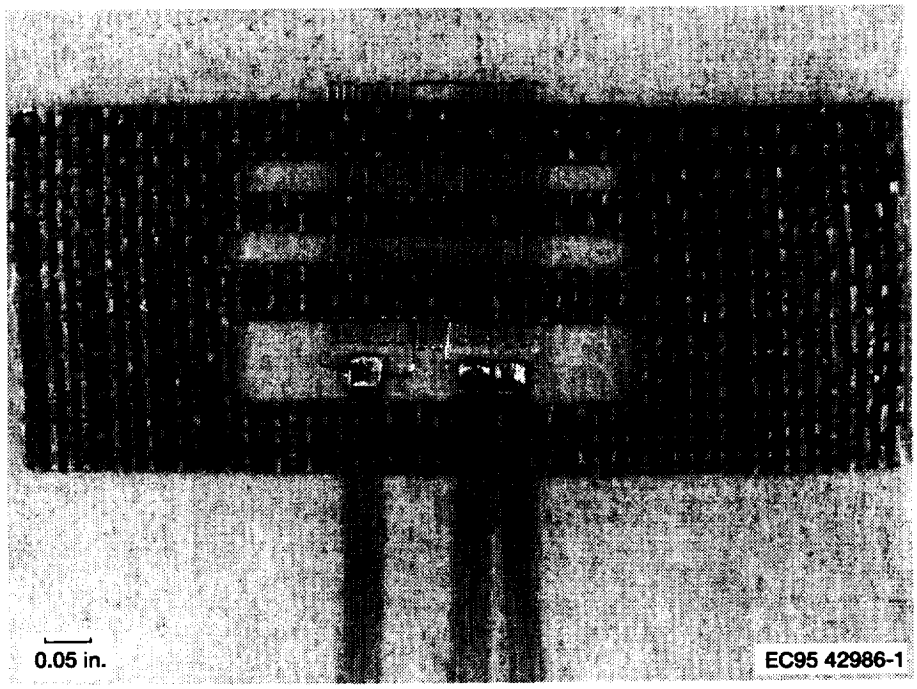

Figure 1.4.—Dryden DETCBCL gage with platinum compensating element.

BCL–3 gage, an FeCrAl gage. The DETCBCL comprised two wire grids connected in series. The primary grid was fabricated from 0.002-in.-diameter BCL–3 alloy wire, a special high-purity FeCrAl strain gage alloy wire originally developed a number of years ago by Battelle Columbus Laboratories (ref. 1.2) under contract to Langley. The compensating grid was also 0.002-in.-diameter wire and was fabricated from a high-grade platinum metal. Temperature compensation was achieved during gage manufacture by selecting the resistance of the compensating grid to adjust the apparent strain of the compensated gage to zero at the test temperature, in this case 1500 °F (815 °C). This procedure reduced the requirement for precise knowledge of the temperature for which compensation has been determined, but at intermediate temperatures this requirement still existed. The lead-wire attachment tabs were 0.031-in. by 0.02-in. Hoskins 875 ribbon. The nominal resistance of the gage was 120 Ω. Figure 1.4 shows the gage. The gage required no external temperature compensation and was connected to the data acquisition equipment in a standard three-wire, quarter-bridge configuration.

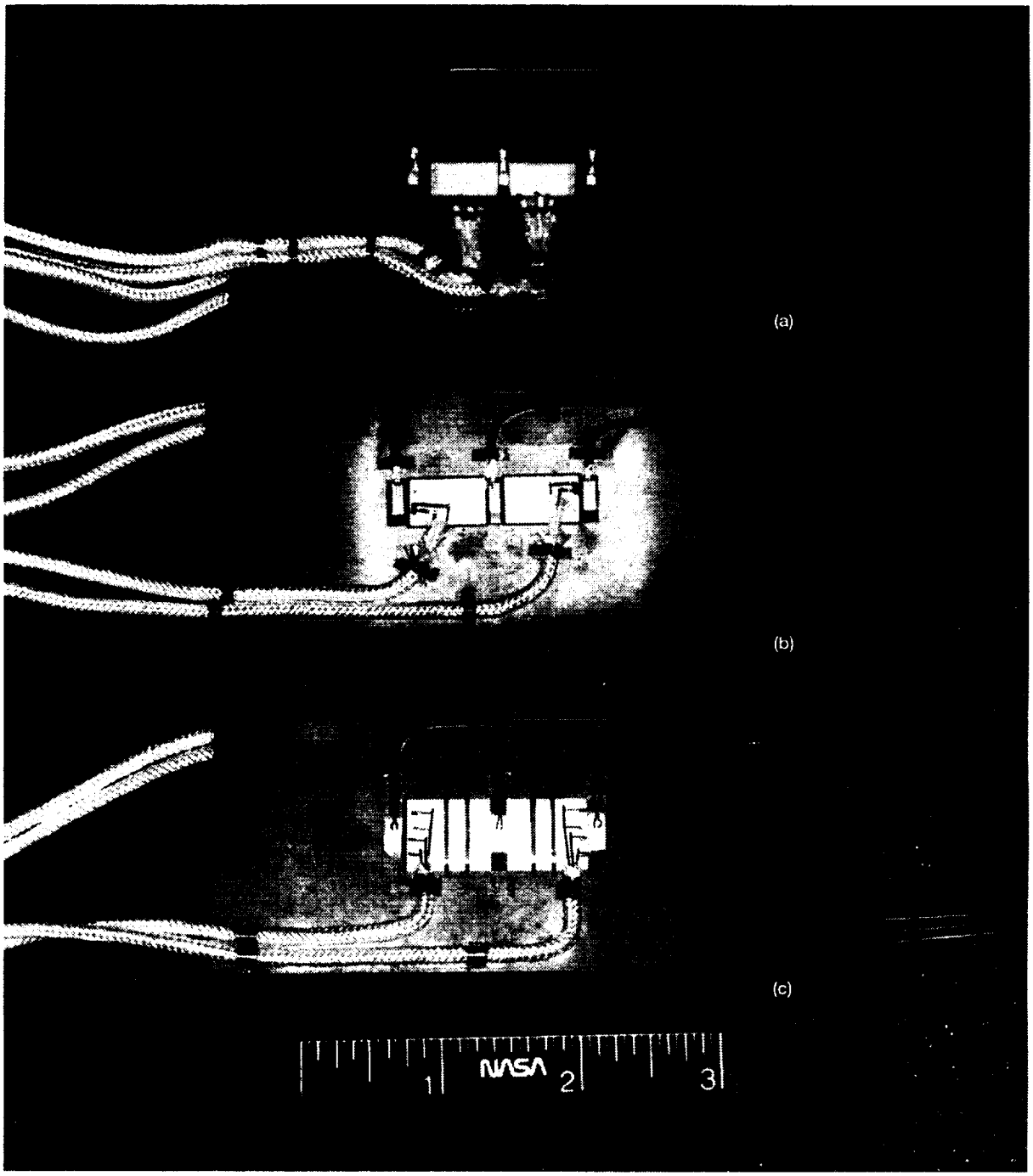

Figure 1.5.—Gages installed on IN100 coupon and tested under NASP GWP29 program. (a) PdCr. (b) DETCBCL. (c) CKA1.

The three candidate gages finally selected are shown in figure 1.5. Here the gages are installed on an IN100 coupon.

1.5 Summary of Test Results

A total of 216 gages, 72 of each gage kind, were tested on two types of specimen, IN100 and SCS–6/β-21S TMC. All the CKA1 gages tested were procured and installed at Langley, and all the DETCBCL gages tested were procured and installed at Dryden. There were, however, some variations for the PdCr gages. During the testing of the PdCr gages on IN100, it was determined that the welds between the gage lead wire, 0.003-in. PdCr, and the trunk lead, American wire gage (AWG) #25 Hoskins 875, were not durable enough for shipping. All the PdCr gages on TMC that later were tested at Langley and

Dryden were therefore reworked along the welds at Langley. These gages, however, showed a much larger apparent strain and higher drift rate than those gages without reworking that were tested at Lewis. This discrepancy may result from possible contamination introduced during the reworking. The average results from the PdCr gages on TMC are therefore not as representative as those from the gages on IN100.

1.5.1 Apparent Strain

This section discusses the apparent strain characteristics, scatter, magnitude, slope, and repeatability, for each type of gage. The actual gage application will determine which characteristic is the most important. Center-to-center differences in heating and cooling rates have not been accounted for in the data reduction; therefore, the characteristics for apparent strain are affected by these heating and cooling differences. Apparent strain tests were performed on two materials, IN100 and TMC, and their results for each are discussed here. This discussion is based on figures 5.1 to 5.72 and the results of chapter 5.

1.5.1.1 Scatter.—When tested on IN100 the CKA1 gage canceled the metallurgical instabilities in the Kanthal A1 alloy very well. Second cycles to a given temperature tended to stabilize this gage. The figures of merit from section 5.4 indicate that this gage was superior to the others in this characteristic, with the exception of the cooldown on cycle 1, C1CD. The PdCr gage had little sensitivity to heating rate changes but was sensitive to cooling rate changes because Hoskins 875 (FeCrAl) lead wires were used in a non-one-to-one bridge circuit. Scatterbands increased significantly on cycles to 1500 °F (815 °C), indicating a phase change transformation of the PdCr wire at approximately that temperature. The figures of merit for this characteristic of the DETCBCL gage show that it did not perform as well as the other two for all first-cycle tests, which is believed to be a result of the center-to-center heating and cooling rate differences.

The tests on TMC indicated the same results, except at the 1500 °F (815 °C) test points, where the DETCBCL gage had the least scatter.

1.5.1.2 Magnitude.—The CKA1 gage had a smaller magnitude of apparent strain throughout the temperature range tested than the other high-temperature strain gages tested on IN100. As shown by the figures of merit in section 5.4 this gage was superior in apparent strain magnitude through all cycles tested. The PdCr gage showed a greater magnitude than the CKA1 gage, but it was generally less than 1000 με and was relatively constant over the 12 cycles. The figures of merit show the PdCr gage to be second in this characteristic. The magnitude of the DETCBCL gage was consistent throughout all cycles but was higher than the magnitudes of the other two gages.

The tests on TMC showed that the CKA1 gage again had a small magnitude of apparent strain. The magnitude was even smaller than that measured during IN100 tests. This gage was superior on all cycles except cycle 1 heating, where the PdCr gage was superior; for all other cycles the DETCBCL gage was second to the CKA1.

1.5.1.3 Slope.—The CKA1 gage showed very little slope in the apparent strain plots when tested on IN100. The figures of merit indicate that the CKA1 gage was superior for all cycles. The PdCr gage had a relatively flat slope for all cycles except at 1500 °F (815 °C). The figures of merit show the PdCr gage to be second to the CKA1 gage for all cycles tested. The slope of the apparent strain curves for the DETCBCL gage was negative to approximately 600 °F (315 °C) and then became positive to the end test temperature. The figures of merit indicate that this type of gage did not perform as well as the other two.

Tests on TMC once again showed that the CKA1 gage had very little slope in the apparent strain plots. As in the IN100 tests, the CKA1 gage changed slope between 300 and 750 °F (150 and 400 °C) because the installation stress had been relieved. The CKA1 gage was superior for all half-cycles except cycle 1 heating, where the PdCr gage was superior. After the first half-cycle the PdCr and DETCBCL gages were close in performance throughout the test range.

1.5.1.4 Repeatability.—In tests on IN100 the figures of merit show that the PdCr gage was superior in four of the seven selected cycles and the CKA1 gage was superior in the other three cycles. The figures of merit also show the DETCBCL gage to be second in two of the designated cycles and third in the others. A factor in this poor showing of the DETCBCL gage is the time-at-temperature difference from center to center caused by the difference in the furnaces used for heating.

The tests on TMC indicated that the CKA1 gage had good repeatability for the selected cycles but was superior in only three of the seven cycles. The PdCr gage did not appear to be as rate sensitive as it was in the IN100 tests but did show some large zero shifts. Again, this may have resulted from the reworking done at Langley. Although the DETCBCL gage showed some first-cycle zero shift, it was significantly less than on IN100 and less than that shown by the other gages. The figures of merit show the DETCBCL gage to be superior in four of the seven selected cycles and second in the other three cycles.

1.5.2 Drift Strain

This discussion is based on figures 5.73 to 5.114 and the results of chapter 5.

In performing drift strain testing the test procedure called for heating the specimen to the test temperature, allowing the temperature along the coupon to stabilize, and then beginning the 4-hr soak. Given that Langley and Lewis used environmentally controlled chambers (ovens) and Dryden used a faster radiant heat facility, some bias resulting from disparate heating rates might be expected. Historically, it has been observed that the major portion of the drift strain occurs in the first hour at temperature. Indeed, the Dryden data have

somewhat higher drift values, particularly for the CKA1 and DETCBCL gages around 900 °F (480 °C), where known phase changes occur in the gage alloy. Similar comments apply to tests of the CKA1 gage and to a lesser extent for the DETCBCL gage on TMC material. It is noteworthy that, in nearly all cases, data from four gages on TMC, as tested at each center, seem to cluster together rather than be randomly distributed, confirming some degree of bias.

Drift magnitude and scatter were lowest for the PdCr gage on IN100. At 1500 °F (815 °C) the PdCr gage was very marginal and several installations did fail. The CKA1 gage exhibited a larger scatter among the 12 gages, which increased as the temperature increased and appeared consistent on both materials. This scatter may be attributable to the CKA1 gage being only 0.001 in. in diameter and possibly experiencing a higher oxidation of the unbonded compensating element. This gage had the lowest drift rate on TMC except in the phase transformation temperature range and was reasonably good in terms of scatter. Clearly, the DETCBCL gage revealed a tighter pattern among the 12 gages than the CKA1 gage, even as the scatter increased with temperature. The drift magnitude was highest for the DETCBCL particularly at the lower temperatures, but this steadied out at higher temperatures, an attribute observed in the past.

1.5.3 Gage Factor

This discussion is based on figures 5.115 to 5.186 and the results of chapter 5.

Gage factor tests were performed on both IN100 and TMC. Langley performed tensile tests and therefore had their load bars placed under only tension. Dryden and Lewis, on the other hand, performed bending tests and therefore had their load bars placed under both tension and compression. The test results indicated that the gage factor of all three gage types decreased as the temperature increased from room temperature to 1200 °F (650 °C) and then slightly increased as temperature increased up to 1500 °F (815 °C). The measured gage factor of all three gage types decreased after the first thermal cycle to 1200 °F (650 °C), suggesting increase in strain transfer after the first thermal and mechanical loading. The gage factor characteristics of CKA1 and DETCBCL gages under tension or compression were slightly different in the temperature range 750 to 1050 °F (400 to 565 °C), the gage factor measured under compression being generally smaller than that measured under tension. The measured gage factors of all three gage types on TMC were generally larger than those of the gages tested on IN100, and the differences increased with thermal cycling.

The CKA1 gage had the largest gage factor magnitude among the three gage types tested on both IN100 and TMC. The CKA1 gage, however, also had the largest gage factor–temperature sensitivity (highest slope) among the three gage types. The PdCr gage, on the other hand, had the smallest gage factor magnitude and the lowest temperature sensitivity among the three gage types. The larger the slope, the greater the possible uncertainty in the gage factor correction. The gage factors of the CKA1, DETCBCL, and PdCr gages decreased approximately 25 to 30%, 20 to 25%, and 15 to 20%, respectively, as the temperature increased from room temperature to 1200 °F (650 °C) and then slightly increased as temperature increased up to 1500 °C (815 °C). On IN100 the CKA1 gage had the best repeatability for the first thermal cycle to 1200 and 1350 °F (650 and 730 °C) under tension and was second to the PdCr gage for all other cycles. On TMC, the PdCr gage had the best repeatability for all thermal cycles except for the first thermal cycle to 1500 °F (815 °C); CKA1 was the best for this cycle. As for the gage-to-gage scatter the DETCBCL gage had the least scatter for all thermal cycles under tension on IN100 and was second to the PdCr gage for all thermal cycles under compression. The PdCr gage also had the least gage-to-gage scatter for all thermal cycles under tension on TMC and was second to the CKA1 gage for all the cycles under compression.

1.5.4 Gage Size and Survivability

The PdCr required the smallest installation area of the three gages tested, the DETCBCL required a somewhat larger area, and the CKA1 required the largest area.

The IN100 testing showed the CKA1 to have the superior figure of merit for survival rate, followed closely by the DETCBCL. The TMC testing showed the PdCr to have the superior figure of merit for overall failure, followed closely by the CKA1 and the DETCBCL.

1.6 Conclusions

Personnel from all three NASA centers, combining decades of experience in high-temperature strain measurements, developed a comprehensive test procedure and an evaluation methodology for testing and characterizing the performance of high-temperature strain gages. Three types of wire strain gage, each with a radically different approach to compensating for thermally induced apparent strain, were subjected to extensive testing at three disparate test sites on two candidate NASP materials. The gages' apparent strain versus temperature, drift strain at temperature, gage factor as a function of temperature, gage size, and survivability were characterized. Data from 12 gages of each gage type (three groups of four gages with one group tested at Langley, one at Lewis, and one at Dryden) were collected, providing statistical significance in the average performance and 95% confidence interval for each parameter. Thus, the data presented suggest where the average of another group of gages might be expected to fall and give confidence that the mean of the population would fall within the confidence interval obtained from the samples tested.

A major contribution to strain gage technology is the comprehensive test procedures and evaluation methodology for testing

and characterizing gages developed in this study. This document will, no doubt, serve as a handbook for strain gage evaluation.

It is surprising that after such a detailed study it is not possible to be absolutely definitive regarding a single best gage. But it is not. All three gages exhibited some positives and some negatives. All three showed some effect of the metallurgical phase transition, which affected the CKA1 and DETCBCL gages at about 700 to 900 °F (370 to 480 °C) and the PdCr gage at 1500 °F (815 °C). All three gages used some form of temperature compensation. The gages were tested on coupons over the test temperature range so that the results could be used for apparent strain compensation through either selection of the external ballast resistor for each PdCr gage (ref. 1.11), modification of the internal gage compensation element for the DETCBCL gage, or addition of an internal gage compensation element for the CKA1 gage. For the CKA1, which is a half-bridge configuration, an internal gage compensation element was needed only for the gages tested on TMC coupons.

In very general terms, and with some reservations, it may be claimed that the CKAl gage is superior for apparent strain measurements and that the PdCr gage is superior for drift strain measurements. The CKAl gage has a larger gage factor magnitude. The PdCr gage is superior in gage factor temperature insensitivity and also in gage size and calculated transverse sensitivity. The CKA1 gage has superior survival on IN100; the PdCr gage has superior survival on TMC. However, selection of a gage depends on a particular application. If long-duration measurements are required, drift will be more important than if the measurement is performed during rapid heating and cooling, where smaller apparent strain is important. Large apparent strain may not be a factor where change in strain is required only at a constant temperature. Furthermore, if durability is an issue, survivability must be considered. The user must also consider if the gage will fit into the area allowed and how large a gage length will be acceptable for the measurement. Finally, the requirement for first-cycle data meant that the gages could not be heat treated (or prestabilized) on the part. If that could be done, all of these results would be vastly different.

A general conclusion from this test program is that no single gage developed in this program is clearly superior to the others but that each gage type has attributes that may make it the gage of choice for a specific application. The advantage is that three high-temperature gages have been extensively tested and their attributes, including statistical information from which to make a choice, are described in this report. It must also be emphasized that apparent strain tests must be conducted prior to any major test program, particularly if new materials are involved. The optimum gage compensation can then be determined, when necessary, so that accurate corrections can be made to the measured data.

Early in the program the NASP Joint Program Office recognized significant progress in the development of new gages and requested that they be used on a number of test panels and engine structures actively being developed in other task areas. Principal among these were the McDonnell Douglas lightly loaded splice subelement; the McDonnell Douglas beta beaded buckling panel; two Rockwell International highly loaded joint panels, where some of the first data at design loads and temperature were obtained; the McDonnell Douglas sigma buckling panel; the Rockwell International side shear panel; the Rockwell International actively cooled Haynes 188 panel (1 in. × 4 in.); and the Pratt & Whitney actively cooled panel (1 in. × 4 in.) (refs. 1.12 to 1.17). Non-NASP applications include the Pratt & Whitney Integrated High Performance Turbine Engine Technology (IHPTET) test and tests at the NASA Lewis Structures Division (refs. 1.18 and 1.19).

Major spinoffs of the technology developed under this program have occurred. All of these gages are now available on the market. Several applications are being planned with the electric power and automotive industries.

1.7 Recommendations

Should funding for additional work be obtained, a number of topics beyond the scope of the present work need to be addressed:

1. Major efforts need to be expended on new materials and on new methods, such as optical or x-ray-based concepts, for measuring strain above 2000 °F (1095 °C).
2. The gages and attachment techniques should be evaluated for use at cryogenic temperatures.
3. Studies should be continued to improve attachment to new difficult-to-bond materials.
4. Gages should be evaluated for durability and sensitivity to hydrogen environments.
5. Gage performance should be evaluated in high acoustic, vibration, and shock environments.
6. Studies should also be continued on enhancing the present gage material by heat treating the wire before the gage is installed.
7. Further characterization of the mechanical and physical properties of complex candidate materials will be necessary to permit proper interpretation of strain measurements made on these materials.

References

1.1 Williams, W. Dan: Strain Sensing Technology for High Temperature Applications. NASA TM–4498, 1993.

1.2 Lemcoe, M.M.: Development of High Temperature Strain Gages. NASA CR–112241, 1973.

1.3 Lemcoe, M.M.: Development of Strain Gages for Use to 1311 K (1900 °F). NASA CR–132485, 1974.

1.4 Lemcoe, M.M.: Characterization of BCL Strain Gages for Use to 1366 K (2000 °F). NASA CR–132739, 1975.

1.5 Englund, D.R.; and Lei, J.-F.: The Apparent Strain of FeCrAl Alloys: A Model for Improved Repeatability? NASP Workshop Publication 1010, 1991.

1.6 Lei, J.-F.: The Apparent Strain Stability and Repeatability of a BCL–3 Resistance Strain Gage. NASP CR–1114, 1991.

1.7 Strain Gage Users Handbook. R.L. Hannah and S.E. Reed, eds., Elsevier Science Publishers, Ltd., 1992.

1.8 Holmes, H.K.; and Moore, Sr., T.C.: High Temperature Strain Gage Apparent Strain Compensation. NASA CP-3161, 1992, pp. 211-222.

1.9 Hulse, C.O., et al.: High Temperature Static Strain Gage Development. NASA CR-189044, 1991.

1.10 Lei, J.-F.: Palladium-Chromium Static Strain Gages for High Temperatures. NASA CP-3161, 1992, pp. 189-209.

1.11 Lei, J.-F.; Englund, D.R.; and Croom, C.: The Temperature Compensation Technique for a PdCr Resistance Strain Gage. Structural Testing Technology at High Temperature, Society for Experimental Mechanics Fall Meeting, 1991, pp. 190-196.

1.12 Hussong, F.; and Pappas, J.: Instrumentation of the Lightly Loaded Splice Subcomponent. Society for Experimental Mechanics Fall Meeting, 1993.

1.13 Seidensticker, D.; and Hellwing, T.: Structural Analysis and High-Temperature Testing of a Titanium Matrix Composite NASP Fuselage Joint. Society for Experimental Mechanics Fall Meeting, 1993.

1.14 Final Test Report for McDonnell Douglas Aerospace Beaded Beta Buckling Panel. (Contract F33657-91-C-2012.) NASP Contract Report X30MD94001, Feb. 1994.

1.15 Sawyer, J.W.; Rothgeb, T.M.; and Austel, L.G.: Mechanical Test of TMC Highly Loaded Joint. Society for Experimental Mechanics Fall Meeting, 1993.

1.16 Sawyer, J.W.; Austel, L.G.; and Rothgeb, T.M.: Thermal Mechanical Test of TMC Highly Loaded Joint, Test Article #1. NASP Technology Review, 1993.

1.17 Final Test Report for McDonnell Douglas Aerospace Sigma Buckling Panel. (Contract F33657-91-C-2012.) NASP Contract Report X30MD94003, Sept. 1994.

1.18 Fichetl, E.J.; and McDaniel, A.D.: High Temperature Strain Gage Technology for Gas Turbine Engines. NASA CR-191177, 1994.

1.19 Castelli, M.G.; and Lei, J.-F.: A Comparison Between High Temperature Extensometry and PdCr Based Resistance Strain Gages With Multiple Application Techniques. NASA CP-10146, 1994.

Chapter 2

Test Procedure

2.1 Description

Government Work Package Task 29 was a development and testing activity for high-temperature static strain gages in support of structure and flight testing in the NASP program. A test procedure was devised to verify the independent test results on various gages developed by groups as part of GWP29 and to establish methodologies and data sets for proper utilization of these gages.

After several months of intense development by NASA Dryden Flight Research Center, NASA Langley Research Center, and NASA Lewis Research Center, three gages were selected for evaluation. These were the dual-element, temperature-compensated BCL–3 gage (DETCBCL) developed by Dryden, the compensated gage based on Kanthal A1 (CKA1) developed by Langley, and a temperature-compensated, palladium-chromium gage (PdCr) developed by Lewis. Details of these gages can be found in references 1.6 and 1.8. All three gages were tested in the strain gage development laboratories at all three NASA centers.

The tests selected were those required to determine calibration curves for using the gages on test structures and for comparing gage performance. These tests were apparent strain, drift strain, and gage factor determination. Each test center tested four gages of each type on specimens of IN100 and SCS–6/β-21S titanium-matrix composite (TMC) for each of the three test types listed above. A total of 216 gages were tested.

The gages were tested under conditions in keeping with program concerns, including the requirement of recording first-cycle data. Therefore, the gages were not heat treated or preconditioned after installation. The heating rates and cooling rates selected were typical of structural tests and yet within the constraints of the available facilities. All tests were conducted in air.

2.1.1 Objectives

The major objectives included the following:

1. Determine apparent strain, drift strain, and gage factors versus temperature for using the gages on test structures and for comparing gage performance.
2. Estimate the relative reliability for the limited number of gages tested.
3. Determine the relative suitability of each gage type for various tests applications.

2.1.2 Success Criteria

Test success was determined by meeting the three objectives. The first two objectives are self-evident, but the last requires elaboration. Because at this point there did not appear to be a "standout" superior gage that was the best gage for all applications, we decided not to try to recommend one gage over another. Instead, we chose to evaluate the gages against a set of parameters by which a user can select a gage for a specific application. A test application may require extremely low apparent strain magnitude and may take so short a time as to allow a large drift rate. In this application low apparent strain magnitude is much more important than drift rate. Another test application may require longer duration measurements where low drift magnitude is necessary but apparent strain magnitude correction is somewhat less important. Therefore, the particular application for which strain measurements are needed will determine gage selection. Since the gage must survive to produce valid data, gage survivability is an important parameter. The size of the gage installation may be important in some applications and is therefore included as an evaluation parameter. Five evaluation parameters were established to indicate to the user which gage has the most favorable parameter. Each evaluation parameter consists of one or more characteristics that have equal value in determining the relative quality or usefulness of the gages in each area (e.g., gage factor or apparent strain). The evaluation parameters and characteristics are listed in table 2.1. Figures-of-merit evaluation methods for these parameters are described in section 2.3.

TABLE 2.1.—EVALUATION PARAMETERS FOR GAGE SELECTION

Evaluation parameter	Characteristics
Apparent strain	Magnitude Cycle-to-cycle repeatability Gage-to-gage scatter Slope of apparent strain versus temperature
Drift rate	Magnitude Gage-to-gage scatter
Gage factor	Magnitude Cycle-to-cycle repeatability Gage-to-gage scatter Slope of gage factor versus temperature
Gage size	Installed area Transverse sensitivity
Survival rate	Number of gages surviving test

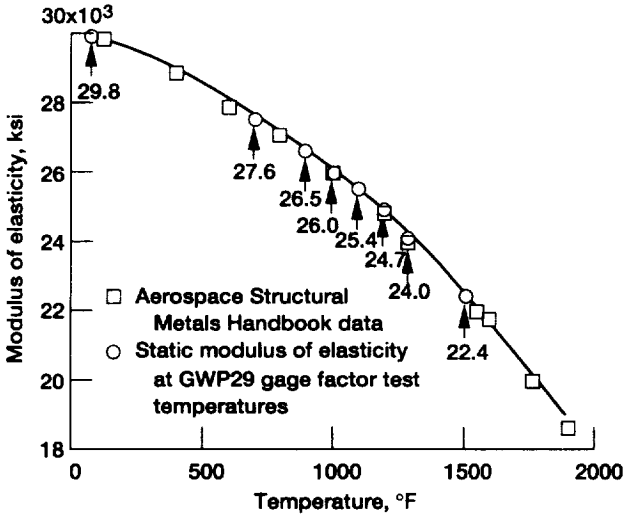

Figure 2.1.—IN100 modulus of elasticity.

TABLE 2.2.—TENSILE PROPERTIES OF SCS–6/β-21S TMC

Temperature		Modulus of elasticity		Ultimate tensile strength		Failure strain, percent	First elastic strain limit, με
°F	°C	Msi	GPa	ksi	MPa		
77	25	17.6	121	131	903	1.3	1000
1200	650	13.2	91	62	429	.9	1000
1350	732	13.0	90	59	407	.9	800
1500	816	12.2	84	49	335	.7	600

TABLE 2.3.—BENDING PROPERTIES OF SCS–6/β-21S TMC

Temperature		Modulus of elasticity		Ultimate tensile strength		First elastic strain limit, με
°F	°C	Msi	GPa	ksi	MPa	
77	25	18.3	126	209.4	1444	1700
900	482	17.6	121	164.3	1133	1380
1200	649	15.2	105	120.8	833	2100
1300	704	12.3	85	106.6	735	2200
1500	816	13.9	96	70.8	488	1100

2.1.3 Test Materials

The IN100 specimen tested in this program was manufactured by Howmet Co. and machined by Port City Machine & Tool Co. The materials were cast and heat treated for 8 hr at 1975 °F (1080 °C) and then for 12 hr at 1600 °F (870 °C) in vacuum. A tensile test was then performed by Howmet to determine the Young's modulus, 0.02% offset and 0.2% offset yield strengths, and ultimate tensile strength of this batch of IN100 material. The average results obtained from 16 test coupons were very close to the Aerospace Structural Metals Handbook values. The Young's-modulus-versus-temperature curve for IN100 is shown in figure 2.1. Material properties data for the IN100 material were taken from references 2.1 and 2.2.

The SCS–6/β-21S TMC coupons and load bars were fabricated by Rockwell International and were cut from three 1/8-in.-thick, 16-ply panels with layup of $[0, \pm 45, 90]_{2S}$. The fiber diameter was 5.4 mils and the fiber volume was 39%. Two panels were evaluated at Langley by three nondestructive evaluation technologies: magnetic-optical imaging, thermography, and ultrasonics (see appendix). Except for warping panels and surface blemishes called bird's-eyes, the two panels tested had no defects. The bird's-eyes were not expected to affect measurements. Dimensional measurements showed that the warpage was typically 0.15 in. over the 4-in. length of the coupons.

Material properties data for the TMC's were to be supplied by the contractors but were not received. Therefore, Lewis performed tensile and four-point bending tests and used the results to select the loads for the gage factor tests. Reference 2.3 describes the tests performed. The properties are given in tables 2.2 and 2.3. The fit to the coefficient of thermal expansion (CTE) curves is given by

$$\text{CTE(/F deg)} = 2.1913\times10^{-6} + 1.9613\times10^{-9}T - 2.5143\times10^{-13}T^2 \quad (2.1)$$

$$\text{CTE(/C deg)} = 4.6153\times10^{-6} + 9.9883\times10^{-9}T - 1.4373\times10^{-12}T^2 \quad (2.2)$$

2.1.4 Gages

The DETCBCL, CKA1, and PdCr gages were tested. Each center procured its gages and installed them with leads and thermocouples for testing in all three facilities. Extra gages were procured to replace gages lost during installation, shipping, or handling. Each center received the following instrumented load bars and coupons of each material:

1. One load bar with four DETCBCL gages from Dryden
2. One load bar with four CKA1 gages from Langley
3. One load bar with four PdCr gages from Lewis
4. Two coupons each with four DETCBCL gages from Dryden
5. Two coupons each with four CKA1 gages from Langley
6. Two coupons each with four PdCr gages from Lewis

Each center tested four gages per specimen times two material types times three gage types times three tests for a total of 72 gages. See table 2.4. Each center received a total of 6 load bars for gage factor tests (3 of each substrate material) and 12 coupons for apparent strain and drift tests (6 of each material). The total for each center was 18 specimens each with 4 gages for a total of 72 gages. The total number of gages tested was 216: 72 gages of DETCBCL, 72 gages of CKA1, and 72 gages of PdCr.

TABLE 2.4.—NUMBER OF GAGES TESTED AT EACH CENTER

Gage	Test						Total
	A (apparent strain)		B (drift strain)		C & D (gage factor) total		
	IN100 coupon	TMC coupon	IN100 coupon	TMC coupon	IN100 bar	TMC bar	
DETCBCL	4	4	4	4	4	4	24
CKAl	4	4	4	4	4	4	24
PdCr	4	4	4	4	4	4	24

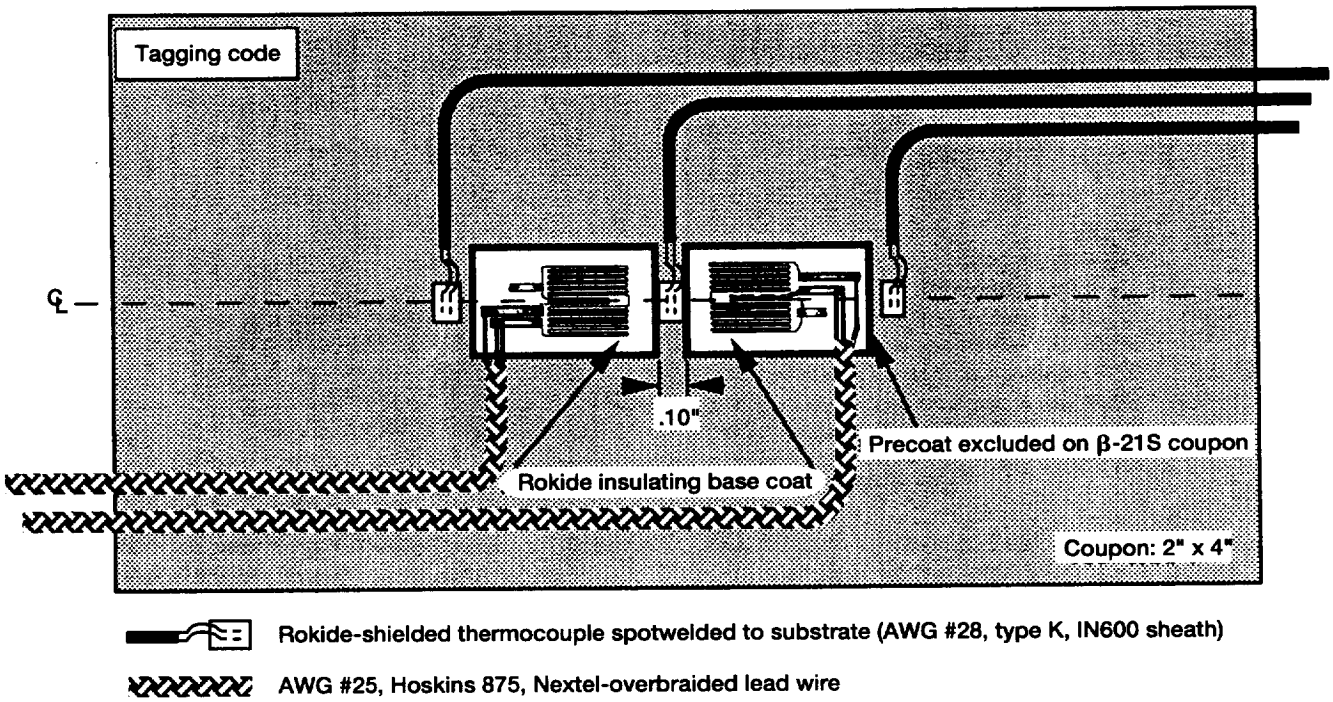

Figure 2.2—Tag location for apparent strain and drift coupon instrumentation and wiring layout.

TABLE 2.5.—SPECIMEN CODING SYSTEM

Item	Description	Symbol
Location of test	Dryden Flight Research Center	D
	Langley Research Center	A
	Lewis Research Center	E
Strain gage type	Dual-element, temperature-compensated DETCBCL	B
	Compensated Kanthal A1	K
	PdCr	P
Test type	Apparent strain	A
	Drift	D
	Gage factor	F
Coupon serial number	Serial number supplied with specimen	e.g., 1023, 3013, or 1A–4

The specimens were identified by two different methods. The IN100 specimens were marked with vibrator pencil, and the β-21S TMC specimens were tagged with a spotweld coded shim. See figure 2.2. The coding system is given in table 2.5. For example, a specimen coded as DPD3–23 is a drift test of PdCr gages at Dryden Flight Research Center. The designator 3–23 is the coupon number for a TMC coupon supplied.

2.1.5 Specimen Preparation and Arrangement

First-cycle data to 1200 °F (650 °C) were collected and analyzed. Gages requiring heat treatment were heat treated before being attached to the test bars or coupons. Non-heat-treated gages were attached and tested with no further heat treatment on the specimen.

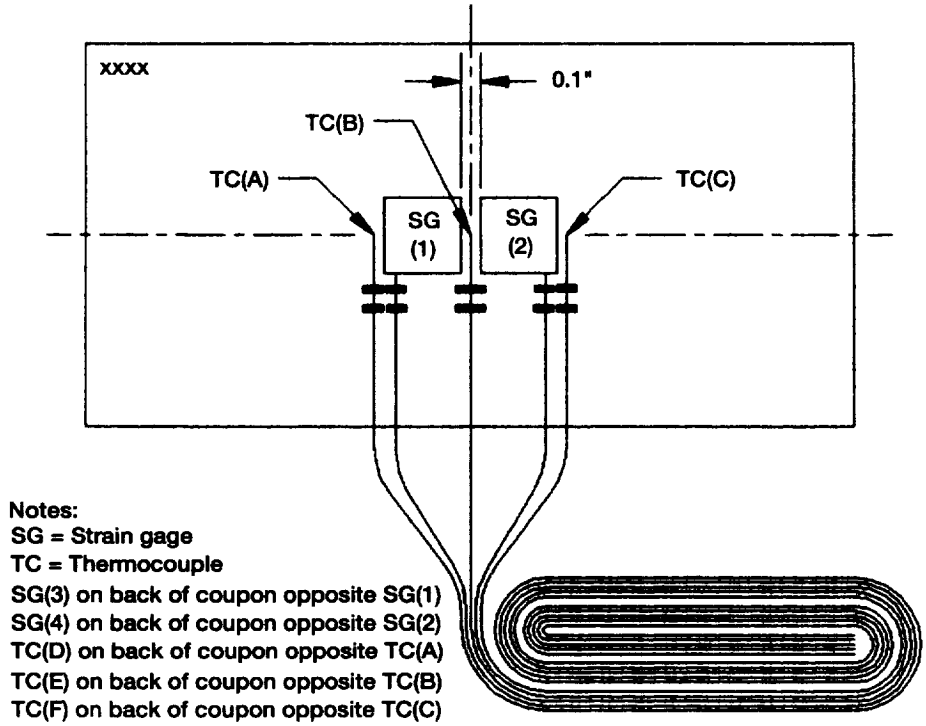

Figure 2.3.—Instrumentation layout for GWP29 coupon.

Four gages were used on each test specimen, two on each side. On each side of the test specimen there were also three type K thermocouples to determine temperature and temperature gradient along the specimen centerline. A total of six thermocouples were used. (See figs. 2.2 and 2.3.) The thermocouples were spotwelded to the substrate and then covered with Rokide. All thermocouples were identical and installed as described in chapter 3.

Nextel braided, three-conductor, AWG #25 Hoskins 875 wire was used for the lead wires (trunk leads). IN600 sheathed, AWG #28 type K thermocouples were used. The thermocouples and leads were 24 in. long. The length in the hot zone was 13 in. for apparent strain and drift strain tests. Each center stated the length in the hot zone for gage factor testing.

2.1.6 Test Procedures

The tests performed were apparent strain (test A), drift strain (test B), and gage factor (tests C and D). Each center used the strain gage measurement equipment modified as required for the different types of gage tested. All modifications and uses are documented in this report. Each center supplied a schematic representation of their measurement system with instrument type and model number. Each center calibrated their instruments before testing began. In all tests temperature versus time was recorded every minute to provide a time-versus-temperature history. A gage factor setting of 2.0 was used in tests A and B. After the gages had been installed and before shipment, each center measured the gage resistance including lead-wire resistance, the compensator resistance including lead-wire resistance, the resistance to ground, and the ballast resistance at room temperature as shown in figure 2.4. This information was recorded in record 1 as shown in section 2.2. The receiving center then recorded in record 1 the gage plus lead-wire resistance and the compensator plus lead-wire resistance. If the before-shipment and after-shipment values did not agree, each center was consulted as to the appropriate steps to take.

Also the gage resistance plus lead-wire resistance, the compensator plus lead-wire resistance, the resistance to ground, and the ballast resistance at room temperature were measured and recorded in record 2 (section 2.2) before and after each temperature excursion. Record 2 was used for each temperature excursion and had another record (i.e., record 3, record 4, or record 5 in section 2.2) attached to it for a data record.

2.1.6.1 Test A (apparent strain).—This test measured apparent strain versus temperature from room temperature to maximum test temperature for 12 thermal cycles with two heating and cooling rates as listed in table 2.6. Data were taken every 150 F deg (84 C deg) during heatup and cooldown. Test temperature was taken as the temperature of thermocouple B on side one with thermocouple E on the other side as backup. (See fig. 2.3.) A pause was held at each test temperature to ensure that the temperature had stabilized within ±5 F deg (±3 C deg) during data taking. If needed, a maximum of 10 min was allowed to stabilize the temperature. To ensure that the coupon was isothermal, all thermocouples had to agree to within ±5 F deg (±3 C deg). The test temperatures were room temperature and 150, 300, 450, 600, 750, 900, 1050, 1200, 1350,

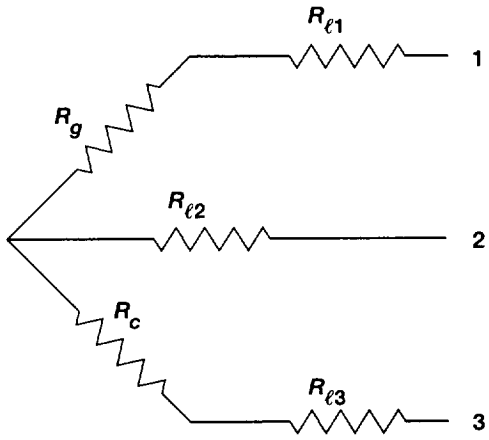

$R_{12} = R_{\ell 1} + R_g + R_{\ell 2}$
$R_{13} = R_{\ell 1} + R_g + R_c + R_{\ell 3}$
$R_{23} = R_{\ell 2} + R_c + R_{\ell 3}$
$R_{1g} = R_{\ell 1}$ + Resistance to ground

Figure 2.4.—Schematic representation of gage R_g, compensating element R_c, and lead wires $R_{\ell 1}$, $R_{\ell 2}$, and $R_{\ell 3}$. R_{12}, R_{13}, R_{23} and R_{1g} are measured before and after shipping and recorded in record 1.

TABLE 2.6.—THERMAL CYCLES FOR TEST A

Cycle	Maximum test temperature		Heating rate		Cooling rate	
	°F	°C	F deg/min	C deg/min	F deg/min	C deg/min
1	1200	650	10±5	5.6±3	10±5	5.6±3
2	1200	650	10±5	5.6±3	10±5	5.6±3
3	1200	650	60±5	33±3	10±5	5.6±3
4	1200	650	60±5	33±3	10±5	5.6±3
5	1200	650	60±5	33±3	[a] 60±5	33±3
6	1200	650	60±5	33±3	60±5	33±3
7	1200	650	10±5	5.6±3	10±5	5.6±3
8	1200	650	10±5	5.6±3	10±5	5.6±3
9	1350	730	10±5	5.6±3	10±5	5.6±3
10	1350	730	10±5	5.6±3	10±5	5.6±3
11	1500	815	10±5	5.6±3	10±5	5.6±3
12	1500	815	10±5	5.6±3	10±5	5.6±3

[a]60±5 F deg/min (33±3 C deg/min) cooling was maintained until 750 °F (400 °C). Below 750 °F (400 °C), 60±5 F deg/min (33±3 C deg/min) was maintained as closely as possible by using natural convection cooling.

and 1500 °F (65, 150, 230, 315, 400, 480, 565, 650, 730, and 815 °C).

The data are presented as plots of apparent strain (με) versus temperature (degrees Fahrenheit and Celsius) and as plots of time versus temperature for each test run. Data were also recorded in tabular form in records 2 and 3 for review.

2.1.6.2 Test B (drift strain).—The drift strain was measured by the following technique: heating the test coupon from room temperature to the first test temperature at 60±5 F deg/min (33±3 C deg/min); stabilizing at the test temperature and holding for 4 hr and then cooling to room temperature at 60±5 F deg/min (33±3 C deg/min) (see footnote to table 2.6); repeating for the second test temperature and so on for each test temperature; stabilizing the test temperature to within ±5 F deg (±3 C deg) before taking data; and recording data every 15 min while holding at the test temperature. Convective cooling could be used below 550 °F (285 °C). The test temperatures were 600, 750, 900, 1050, 1200, 1350, and 1500 °F (315, 400, 480, 565, 650, 730, and 815 °C).

The data are presented as plots of drift strain (με) versus time (hours) for each test run. Data were also recorded in tabular form in records 2 and 4 for review.

2.1.6.3 Test C (gage factor for IN100 bars).—Before starting gage factor testing the testing equipment was calibrated with a calibration bar of the same geometry as that used for the gage factor testing. The calibration bar was instrumented with Micro-Measurements room-temperature or WK foil strain gages. The equipment was calibrated at room temperature at loads, or deflections, that produce the strains shown in table 2.7. A minimum of two room-temperature cycles to ±2000 με was required. The data, including zero shifts and permanent set in the calibration bar, were recorded. Sufficient room-temperature gages were installed on the bending calibration bars to permit variations across the width and faces to be assessed at the corresponding gage locations on the GWP29 specimens. A sufficient number of gages were installed on the tensile calibration load bars to determine variations across and longitudinally along the test section.

Before testing, each instrumented GWP29 gage factor load bar was mechanically precycled three times at room temperature to ±2000 με. The gage factor was determined at selected strain levels at the indicated temperatures. The process was as follows: stabilizing the load bar at the test temperature to within ±5 F deg (3 C deg); recording data at the first temperature for the five selected strain levels; recording data for all positive deflections and then all negative deflections; and then increasing the temperature to the next temperature and taking data for the five strain levels. This process was repeated to the first-cycle maximum temperature of 1200 °F (650 °C). After the maximum temperature had been reached, data were recorded again at each test temperature as the bars were cooled back to

TABLE 2.7.—TEST TEMPERATURES AND STRAIN LEVELS FOR TEST C (IN100 LOAD BARS)

Temperature, °F (°C)							
77 (21)	700 (370)	900 (480)	1000 (540)	1100 (590)	1200 (650)	1350 (730)	1500 (815)
Strain level, με							
0	0	0	0	0	0	0	0
±400	±400	± 400	±400	±400	±400	± 400	±400
±800	±800	±800	±800	±800	±800	±800	± 800
±1200	±1200	±1200	±1200	±1200	±1200	±1200	±1200
±1600	±1600	±1600	±1600	±1600	±1600	±1600	±1600
±2000	±2000	±2000	±2000	±2000	±2000	±2000	±2000

TABLE 2.8.—TEST TEMPERATURES AND STRAIN LEVELS FOR TEST D (TMC LOAD BARS)

Temperature, °F (°C)							
77 (21)	700 (370)	900 (480)	1000 (540)	1100 (590)	1200 (650)	1350 (730)	1500 (815)
Strain level in tension, με							
0	0	0	0	0	0	0	0
+300	+300	+300	+300	+300	+300	+300	+200
+600	+600	+600	+600	+600	+600	+600	+400
+900	+900	+900	+900	+900	+900	+700	+500
Strain level in bending, με							
0	0	0	0	0	0	0	0
−400	−400	−400	−400	−400	−400	−400	−400
−800	−800	−800	−800	−800	−800	−800	−800
−1200	−1200	−200	−1200	−1200	−1200	−1200	−1000

room temperature. Heating and cooling rates were 15±5 F deg/min (8±3 C deg/min). See table 2.7 for strain levels. Langley performed tensile tests and therefore their load bars were not placed under compression.

The test sequence was as follows:

1. Cycle 1—To 1200 °F (650 °C) and return to room temperature
2. Cycle 2—To 1200 °F (650 °C) again and return to room temperature without load
3. Cycle 3—To 1200 °F (650 °C) again and return to room temperature without load
4. Cycle 4—To 1200 °F (650 °C) again and return to room temperature
5. Cycle 5—To 1350 °F (730 °C) and return to room temperature
6. Cycle 6—To 1350 °F (730 °C) again and return to room temperature
7. Cycle 7—To 1500 °F (815 °C) and return to room temperature
8. Cycle 8—To 1500 °F (815 °C) again and return to room temperature

The data are presented as plots of gage output versus true strain (με) at each temperature and gage factor versus temperature for each test run. Each center recorded its data in tabular form in records 2 and 5 for review, including the zero shift for the two runs. The equation for deriving gage factor from strain data was included. The determined gage factor and other corrections were used to correct measured apparent strain data to true data in test A (με versus temperature) and test B (με versus time). Corrections for permanent set in the load bar were also made.

2.1.6.4 Test D (gage factor for TMC bars).—The gage factor was determined from the TMC gage factor calibration bar surface strains, which were determined from Micro-Measurements room-temperature or WK gages. Test conditions were the same as specified for test C except for the reduced strain levels given in table 2.8.

Prior to gage factor testing each instrumented GWP29 gage factor load bar was mechanically precycled three times at room temperature to 900 με in tension and to 1200 με in bending.

The test sequence was as follows:

1. Cycle 1—To 1200 °F (650 °C) and return to room temperature
2. Cycle 2—To 1200 °F (650 °C) again and return to room temperature without load
3. Cycle 3—To 1200 °F (650 °C) again and return to room temperature without load
4. Cycle 4—To 1200 °F (650 °C) again and return to room temperature
5. Cycle 5—To 1350 °F (730 °C) and return to room temperature
6. Cycle 6—To 1350 °F (730 °C) again and return to room temperature
7. Cycle 7—To 1500 °F (815 °C) and return to room temperature
8. Cycle 8—To 1500 °F (815 °C) again and return to room temperature

The data are presented as for test C plus a plot of GF_C/GF_D versus temperature where GF_C is the gage factor determined in test C and GF_D is the gage factor determined in test D. Data were also recorded in tabular form in record 5 for review.

Each center used strain gage measurement equipment modified as required for different gage needs. All modifications and uses are documented in this report.

2.2 Example Records

RECORD 1.—NASP GWP29 SHIPPING RECORD

Specimen code: _____
Test center: ☐ NASA Dryden ☐ NASA Langley ☐ NASA Lewis
Gage type: ☐ DETCBCL ☐ CKA1 ☐ PdCr
Substrate: ☐ IN100 ☐ TMC
Shipment date: _____
Electrical resistance of gages before shipment, Ω:

Resistance	Gage 1	Gage 2	Gage 3	Gage 4
R_{12}				
R_{13}				
$R23$				
R_{1g}				

Date of receipt: _____
Electrical resistance of gages after shipment, Ω:

Resistance	Gage 1	Gage 2	Gage 3	Gage 4
R_{12}				
R_{13}				
R_{23}				
R_{1g}				

RECORD 2.—NASP GWP29 TEST RECORD

Specimen code: _____
Test center: ☐ NASA Dryden ☐ NASA Langley ☐ NASA Lewis
Gage type: ☐ DETCBCL ☐ CKA1 ☐ PdCr
Substrate: ☐ IN100 ☐ TMC
Test type: ☐ Apparent strain ☐ Drift ☐ Gage factor
Date: _____

Cycle	Resistance, Ω			$\Delta R_{12}/R_{12}$, percent	$\Delta R_{13}/R_{13}$, percent	$\Delta R_{23}/R_{23}$, percent	Resistance, Ω	
	R_{12}	R_{13}	R_{23}				R_B	R_G
As received				0.0	0.0	0.0		
1								
2								
3								
4								
5								
6								
7								
8								
9								
10								
11								
12								

RECORD 3.—APPARENT STRAIN TEST A DATA

Specimen code: _____ Thermal cycle: _____ Gage factor setting: _____
Heating rate: _____ Cooling rate: _____

Thermocouple output, °F						Strain gage ouput, με				Time, min
TC_1	TC_2	TC_3	TC_4	TC_5	TC_6	SG_1	SG_2	SG_3	SG_4	

RECORD 4.—DRIFT TEST B DATA

Specimen code: _____ Gage factor setting: _____

Time, min	Temperature, °F		Drift strain, με			
	TC_B	TC_E	SG_1	SG_2	SG_3	SG_4

RECORD 5.—GAGE FACTOR TEST C AND D DATA

Specimen code: _____ Cycle: _____

Temperature, °F (°C)	Recorded gage factor				Maximum strain	Zero shift	Permanent set	Tare load	Strain (tare)	Gage factor variation, percent			
	SG_1	SG_2	SG_3	SG_4						SG_1	SG_2	SG_3	SG_4
77 (21)													
700 (370)													
900 (480)													
1000 (540)													
1100 (590)													
1200 (650)													
1350 (730)													
1500 (815)													

2.3 Strain Gage Figure-of-Merit Evaluation Methodology

2.3.1 Introduction

Government Work Package Task 29 required a methodology that would permit an objective quantitative assessment of several types of high-temperature strain gage. Therefore, figure-of-merit evaluation methodology was used to determine the relative performance of three GWP29 candidate strain gages in terms of their basic performance characteristics.

The parameters chosen for evaluation were apparent strain, strain due to drift, gage factor, gage size, and survival rate. The parameters were divided into characteristics to permit a more comprehensive assessment of gage performance on the basis of the figures of merit calculated for each characteristic. Higher scores indicate superior performance. All figures of merit defined herein were scaled between 0 and 1, with 1 being the best score for a particular characteristic. This scaling enabled the figures of merit for individual characteristics to be summed to determine an overall figure of merit for a given parameter. It must be remembered, however, that one of these characteristics may be more important to an individual user than another characteristic. Thus, any sums should be used with considerable caution in selecting a "best gage" for a particular test.

The methodology as a whole was intended to account for multiple gages by calculating figures of merit from the average strain data for a sample of n gages of some gage type i, unless otherwise noted. Therefore, the user, such as a structural test engineer, can know statistically what performance to expect for the strain gage type. The intent was to avoid making figure-of-merit calculations based on data from individual gages, which may or may not be statistically indicative of the gage type.

Strain gage behavior generally depends on the time-temperature history that the gage has experienced, even within a single cycle. Unless the gages are preconditioned or effectively temperature compensated, first-cycle data tend to differ from data in successive cycles, and within the first cycle there tend to be differences between heatup and cooldown. Also, strain gage installation onto a substrate and the substrate itself can have profound effects on the strain data. Bearing these phenomena in mind we defined the figures of merit so as to separate out, as well as possible, the various effects. Thus, all figures of merit were based on half-cycle data so that heatup and cooldown could be treated separately for all cycles.

The individual characteristics related to each parameter evaluated in this methodology are analogous in some respects to the characteristics evaluated in instruments. The concepts of full scale, linearity, repeatability, etc., that are common in evaluating instruments can be found throughout this methodology, although the specific definitions as they relate to high-temperature strain gages are quite different in many cases from those associated with instruments.

Several requirements were established for a software package that could effect the necessary data reduction to do the figure-of-merit analysis. Automated operation was necessary to enable the same analysis to be applied to different sets of similar data. As several types of data needed to be reduced, power and flexibility in data analysis capabilities were also required, such as numerical integration and curve fitting for figure-of-merit calculation. Further, integrated data analysis and presentation-quality graphics were necessary to minimize the time required to reduce data for reporting. An Apple Macintosh-based program, IGOR, from WaveMetrics was selected. The internal programming language, extensive data analysis operations, and graphics capabilities in IGOR met all established requirements.

The data used for the examples in the methodology do not necessarily reflect data generated from GWP29. In fact, the apparent strain data shown in the examples are transient apparent strain for several small samples of experimental derivatives of the BCL gage. Although different data reduction methods were used to obtain the data for the examples and the GWP29 static apparent strain data, the figure-of-merit equations themselves were exactly the same.

No attempt was made to determine an overall best gage. Instead, we tried to determine five figures of merit, one for each evaluation parameter. However, it was not possible to reconcile the need to report first-cycle data with the relatively large numbers of cycles being conducted and the three first cycles in the apparent strain test in a single figure of merit for each parameter. Table 2.9 shows the reported figures of merit. Table 2.10, a much expanded version of table 2.9, shows all individual calculated figures of merit.

2.3.2 Methodology for Calculating Apparent Strain Figures of Merit

Figures of merit were used to quantitatively evaluate gage performance in terms of four apparent strain characteristics over a specified temperature range. The first figure of merit varies with gage type according to the scatter in apparent strain data from gage to gage. The second varies with gage type according to the relative magnitude of apparent strains for two or more evaluated gage types. The third varies with gage type according to the magnitude of the slopes of the apparent strain curves. The fourth varies with gage type according to the relative repeatability of the evaluated gages.

2.3.2.1 Apparent strain scatter figure of merit.—A fundamental user requirement for a strain gage, beyond the desire for small magnitudes, small slopes, and excellent repeatability, is that gages of a certain type and of a particular lot exhibit essentially identical performance. Regardless of the magnitude, slope, or repeatability of apparent strain of a single gage, if the gage-to-gage scatter in the data is large, the gage type cannot be considered dependable. The area between the 95% confidence limits is an excellent measure of the scatter. Because

TABLE 2.9.—GWP29 FIGURE-OF-MERIT SUMMARY

Parameter	Characteristic	Cycle or temperature	IN100			β-21S TMC		
			CKA1	PdCr	DETCBCL	CKA1	PdCr	DETCBCL
Apparent strain	Scatter	Cycle 1						
		Cycle 9						
		Cycle 11						
		Other cycles						
	Magnitude	Cycle 1						
		Cycle 9						
		Cycle 11						
		Other cycles						
	Slope	Cycle 1						
		Cycle 9						
		Cycle 11						
		Other cycles						
	Repeatability	C1HU,C1CD						
		C9HU,C9CD						
		C11HU,C11CD						
		C2CD,C3HU						
		C1HU,C8CD						
		C2CD,C4CD						
		C4HU,C6HU						
Gage factor (tension)	Scatter	Cycle 1						
		Cycle 5						
		Cycle 7						
		Other cycles						
	Magnitude	Cycle 1						
		Cycle 5						
		Cycle 7						
		Other cycles						
	Slope	Cycle 1						
		Cycle 5						
		Cycle 7						
		Other cycles						
	Repeatability	C1HU,C1CD						
		C5HU,C5CD						
		C7HU,C7CD						
Gage factor (compression)	Scatter	Cycle 1						
		Cycle 5						
		Cycle 7						
		Other cycles						
	Magnitude	Cycle 1						
		Cycle 5						
		Cycle 7						
		Other cycles						
	Slope	Cycle 1						
		Cycle 5						
		Cycle 7						
		Other cycles						
	Repeatability	C1HU,C1CD						
		C5HU,C5CD						
		C7HU,C7CD						

half-cycle-to-half-cycle apparent strain characteristics are not necessarily repeatable, gage-to-gage scatter figures of merit must be evaluated for individual half-cycles.

The following equation was used to determine the figure of merit (FoM) for a given strain gage type on the basis of its gage-to-gage scatter in apparent strain:

$$\mathrm{FoM}\left[\mathbf{SC}(\varepsilon_{\mathrm{app}})_{i,j}\right]_m = \frac{\left\{\int_{T_{\mathrm{lower}}}^{T_{\mathrm{upper}}} [\mathrm{U95CL}(T) - \mathrm{L95CL}(T)]_j \, dT\right\}_m}{\left\{\int_{T_{\mathrm{lower}}}^{T_{\mathrm{upper}}} [\mathrm{U95CL}(T) - \mathrm{L95CL}(T)]_i \, dT\right\}_m} \tag{2.3}$$

TABLE 2.9.—Concluded.

Parameter	Characteristic	Cycle or temperature	IN100			β-21S TMC		
			CKA1	PdCr	DETCBCL	CKA1	PdCr	DETCBCL
Drift strain	Rate	600 °F (315 °C)						
		750 °F (400 °C)						
		900 °F (480 °C)						
		1050 °F (565 °C)						
		1200 °F (650 °C)						
		1350 °F (730 °C)						
		1500 °F (815 °C)						
	Scatter	600 °F (315 °C)						
		750 °F (400 °C)						
		900 °F (480 °C)						
		1050 °F (565 °C)						
		1200 °F (650 °C)						
		1350 °F (730 °C)						
		1500 °F (815 °C)						
Gage size	Installed area		0.42	1.00	0.60	0.42	1.00	0.60
	Calculated transverse sensitivity		0.88	1.00	0.89	0.88	1.00	0.89
	Sum		1.30	2.00	1.49	1.30	2.00	1.49
Survival rate	Apparent strain	1200 °F (650 °C)						
		1350 °F (730 °C)						
		1500 °F (815 °C)						
	Drift	1200 °F (650 °C)						
		1350 °F (730 °C)						
		1500 °F (815 °C)						
	Gage factor	1200 °F (650 °C)						
		1350 °F (730 °C)						
		1500 °F (815 °C)						
	Overall	1200 °F (650 °C)						
		1350 °F (730 °C)						
		1500 °F (815 °C)						

where

FoM figure of merit

SC (ε_{app}) scatter in apparent strain, gage to gage

i designator for gage type

j designator for gage type for which difference between upper and lower 95% confidence limits is minimum

m designator for half-cycle number

T_{upper} upper temperature limit

T_{lower} lower temperature limit

U95CL(T) upper 95% confidence limit

L95CL(T) lower 95% confidence limit

The general confidence limit (ref. 2.4) for small samples ($n < 30$) is

$$CL = \bar{X} \pm t\frac{s}{\sqrt{n}} \tag{2.4}$$

where

CL confidence limit

$\bar{X}$ sample mean

t Student's t distribution value

s standard deviation for small samples, $s = \sqrt{\frac{\sum(X - \bar{X})}{n-1}}$

n number of samples

TABLE 2.10.—GWP29 FIGURES OF MERIT

Parameter	Characteristic	Cycle or temperature	IN100			β-21S TMC		
			CKA1	PdCr	DETCBCL	CKA1	PdCr	DETCBCL
Apparent strain	Scatter	C1HU						
		C1CD						
		C2HU						
		C2CD						
		C3HU						
		C3CD						
		C4HU						
		C4CD						
		C5HU						
		C5CD						
		C6HU						
		C6CD						
		C7HU						
		C7CD						
		C8HU						
		C8CD						
		C9HU						
		C9CD						
		C10HU						
		C10CD						
		C11HU						
		C11CD						
		C12HU						
		C12CD						
	Magnitude	C1HU						
		C1CD						
		C2HU						
		C2CD						
		C3HU						
		C3CD						
		C4HU						
		C4CD						
		C5HU						
		C5CD						
		C6HU						
		C6CD						
		C7HU						
		C7CD						
		C8HU						
		C8CD						
		C9HU						
		C9CD						
		C10HU						
		C10CD						
		C11HU						
		C11CD						
		C12HU						
		C12CD						
	Slope	C1HU						
		C1CD						
		C2HU						
		C2CD						

TABLE 2.10.—Continued.

Parameter	Characteristic	Cycle or temperature	IN100			β-21S TMC		
			CKA1	PdCr	DETCBCL	CKA1	PdCr	DETCBCL
Apparent strain	Slope	C3HU						
		C3CD						
		C4HU						
		C4CD						
		C5HU						
		C5CD						
		C6HU						
		C6CD						
		C7HU						
		C7CD						
		C8HU						
		C8CD						
		C9HU						
		C9CD						
		C10HU						
		C10CD						
		C11HU						
		C11CD						
		C12HU						
		C12CD						
	Repeatability	C1HU,C1CD						
		C1HU,C2HU						
		C1CD,C2HU						
		C1CD,C2CD						
		C2HU,C2CD						
		C2HU,C3HU						
		C2CD,C3HU						
		C2CD,C3CD						
		C2CD, C4CD						
		C3HU,C3CD						
		C4CD,C6CD						
		C5HU,C5CD						
		C6HU,C7HU						
		C6CD,C7CD						
		C7HU,C7CD						
		C1HU,C8CD						
		C9HU,C9CD						
		C9CD,C10HU						
		C10HU,C10CD						
		C11HU,C11CD						
		C11CD,C12HU						
		C12HU,C12CD						
Gage factor (tension)	Scatter	C1HU						
		C1CD						
		C4HU						
		C4CD						
		C5HU						
		C5CD						
		C6HU						
		C6CD						
		C7HU						
		C7CD						

TABLE 2.10.—Continued.

Parameter	Characteristic	Cycle or temperature	IN100			β-21S TMC		
			CKA1	PdCr	DETCBCL	CKA1	PdCr	DETCBCL
Gage factor (tension)	Scatter	C8HU						
		C8CD						
	Magnitude	C1HU						
		C1CD						
		C4HU						
		C4CD						
		C5HU						
		C5CD						
		C6HU						
		C6CD						
		C7HU						
		C7CD						
		C8HU						
		C8CD						
	Slope	C1HU						
		C1CD						
		C4HU						
		C4CD						
		C5HU						
		C5CD						
		C6HU						
		C6CD						
		C7HU						
		C7CD						
		C8HU						
		C8CD						
	Repeatability	C1HU,C1CD						
		C1HU,C4HU						
		C1CD,C4CD						
		C4HU,C4CD						
		C5HU,C5CD						
		C5HU,C6HU						
		C5CD,C6CD						
		C6HU,C6CD						
		C7HU,C7CD						
		C7HU,C8HU						
		C7CD,C8CD						
		C8HU,C8CD						
Gage factor (compression)	Scatter	C1HU						
		C1CD						
		C4HU						
		C4CD						
		C5HU						
		C5CD						
		C6HU						
		C6CD						
		C7HU						
		C7CD						
		C8HU						
		C8CD						
	Magnitude	C1HU						
		C1CD						
		C4HU						
		C4CD						
		C5HU						

TABLE 2.10.—Continued.

Parameter	Characteristic	Cycle or temperature	IN100			β-21S TMC		
			CKA1	PdCr	DETCBCL	CKA1	PdCr	DETCBCL
Gage factor (compression)	Magnitude	C5CD						
		C6HU						
		C6CD						
		C7HU						
		C7CD						
		C8HU						
		C8CD						
	Slope	C1HU						
		C1CD						
		C4HU						
		C4CD						
		C5HU						
		C5CD						
		C6HU						
		C6CD						
		C7HU						
		C7CD						
		C8HU						
		C8CD						
	Repeatability	C1HU,C1CD						
		C1HU,C4HU						
		C1CD,C4CD						
		C4HU,C4CD						
		C5HU,C5CD						
		C5HU,C6HU						
		C5CD,C6CD						
		C6HU,C6CD						
		C7HU,C7CD						
		C7HU,C8HU						
		C7CD,C8CD						
		C8HU,C8CD						
Drift strain	Rate	600 °F (315 °C)						
		750 °F (400 °C)						
		900 °F (480 °C)						
		1050 °F (565 °C)						
		1200 ° F (650 °C)						
		1350 °F (730 °C)						
		1500 °F (815 °C)						
	Scatter	600 °F (315 °C)						
		750 °F (400 °C)						
		900 °F (480 °C)						
		1050 °F (565 °C)						
		1200 °F (650 °C)						
		1350 °F (730 °C)						
		1500 °F (815 °C)						
Gage size	Installed area		0.42	1.00	0.60	0.42	1.00	0.60
	Transverse sensitivity		0.88	1.00	0.89	0.88	1.00	0.89
Survival rate	Apparent strain	1200 °F (650 °C)						
		1350 °F (730 °C)						
		1500 °F (815 °C)						
	Drift	1200 °F (650 °C)						

TABLE 2.10.—Concluded.

Parameter	Characteristic	Cycle or temperature	IN100			β-21S TMC		
			CKA1	PdCr	DETCBCL	CKA1	PdCr	DETCBCL
Survival rate	Drift	1350 °F (730 °C)						
	Gage factor	1200 °F (650 °C)						
		1350 °F (730 °C)						
		1500 °F (815 °C)						
	Overall	1200 °F (650 °C)						
		1350 °F (730 °C)						
		1500 °F (815 °C)						

TABLE 2.11.—PERCENTILE VALUES (t_p) OF STUDENT'S t DISTRIBUTION WITH n–1 DEGREES OF FREEDOM (TWO TAILED)

$n-1$	$t_{0.99}$	$t_{0.98}$	$t_{0.95}$	$t_{0.90}$	$t_{0.80}$	$t_{0.60}$	$t_{0.50}$	$t_{0.40}$	$t_{0.20}$	$t_{0.10}$
1	63.66	31.82	12.71	6.31	3.08	1.376	1.000	.727	.325	.158
2	9.92	6.96	4.30	2.92	1.89	1.061	.816	.617	.289	.142
3	5.84	4.54	3.18	2.35	1.64	.978	.765	.584	.277	.137
4	4.60	3.75	2.78	2.13	1.53	.941	.741	.569	.271	.134
5	4.03	3.36	2.57	2.02	1.48	.920	.727	.559	.267	.132
6	3.71	3.14	2.45	1.94	1.44	.906	.718	.553	.265	.131
7	3.50	3.00	2.36	1.90	1.42	.896	.711	.549	.263	.130
8	3.36	2.90	2.31	1.86	1.40	.889	.706	.546	.262	.130
9	3.25	2.82	2.26	1.83	1.38	.883	.703	.543	.261	.129
10	3.17	2.76	2.23	1.81	1.37	.879	.700	.542	.260	.129
11	3.11	2.72	2.20	1.80	1.36	.876	.697	.540	.260	.129
12	3.06	2.68	2.18	1.78	1.36	.873	.695	.539	.259	.128
13	3.01	2.65	2.16	1.77	1.35	.870	.694	.538	.259	.128
14	2.98	2.62	2.14	1.76	1.34	.868	.692	.537	.258	.128
15	2.95	2.60	2.13	1.75	1.34	.866	.691	.536	.258	.128

Values of t are given in table 2.11 for various sample sizes and percent confidence limits. As we are subtracting the lower 95% confidence limit from the upper 95% confidence limit, the figure-of-merit equation can be expressed another way by using the general expression

$$\mathrm{U95CL}(T) - \mathrm{L95CL}(T) = \left[\overline{\varepsilon_{\mathrm{app},n}}(T) + t_{0.95}(n)\frac{s_{\mathrm{app},n}(T)}{\sqrt{n}}\right] - \left[\overline{\varepsilon_{\mathrm{app},n}}(T) - t_{0.95}(n)\frac{s_{\mathrm{app},n}(T)}{\sqrt{n}}\right] = 2t_{0.95}(n)\frac{s_{\mathrm{app},n}(T)}{\sqrt{n}} \tag{2.5}$$

Thus,

$$\mathrm{FoM}\left[\mathrm{SC}(\varepsilon_{\mathrm{app}})_{i,j}\right]_m = \frac{\left[\int_{T_{\mathrm{lower}}}^{T_{\mathrm{upper}}} t_{0.95}(n_j)\frac{s_{\mathrm{app},n_j}(\mathrm{T})}{\sqrt{n_j}}\,dT\right]_m}{\left[\int_{T_{\mathrm{lower}}}^{T_{\mathrm{upper}}} t_{0.95}(n_j)\frac{s_{\mathrm{app},n_j}(\mathrm{T})}{\sqrt{n_j}}\,dT\right]_m} \tag{2.6}$$

where

$t_{0.95}$ Student's t for 95% confidence (Note that the quantity $n - 1$ is used for computing or locating tabular values of Student's t for a sample size n.)

n number of gages (samples) of given type

$s_{\mathrm{app},n}(T)$ standard deviation of apparent strain for sample of n gages as function of temperature

Although ideally the statistical sample size should be the same for all gage types, this was not always feasible in the event of gage failures. One such failure-related problem was a gage failure in midcycle (i.e., during heatup or cooldown at some fraction of the maximum temperature). In this event the failed gage (or gages) were eliminated from consideration for the entire half-cycle. The gage sample size for this half-cycle and all subsequent half-cycles was decreased by the number of failed gages. The 95% confidence limit curves were affected, but the figure-of-merit calculation method was the same. In the event that gage failures reached the point that the gage sample size n was only 1 (or 0), this gage type i was assigned a figure of merit of 0. The reduction in knowledge of and confidence in gage behavior with increasing failures intuitively implies that the upper and lower confidence limits tend toward infinity. The

difference between these curves also tends toward infinity, and the figure of merit decreases to zero.

EXAMPLE 1: Figure 2.5 illustrates the areas between the upper and lower 95% confidence limits of the cycle 1 heatup apparent strain scatter curves for gage types A and B. It is clear from the figure that gage type B had much less scatter from gage to gage than did gage type A. By using the definition for figure of merit, we determined the relative merits of these gage types.

Upper and lower 95% confidence limits were obtained from the raw data for the set of each gage type at each temperature interval. An average apparent strain curve was determined as well as the standard deviation of the average at the specified temperature level. Because there can be variation in the temperature data as well, an average temperature was determined at each specified nominal temperature. Table 2.12 is a slice of data for gage type B near the nominal temperature of 1200 °F (650 °C); it shows the averages and standard deviation obtained. Student's t was found from statistical tables for 95% confidence by using the appropriate number of gages (table 2.11).

The area between the confidence limits for gage type A was 2 030 380 με·F deg from 75 to 1500 °F (20 to 815 °C), and the area between the confidence limits for gage type B was 172 907 με·F deg in the same temperature range. Thus, the figures of merit for these gages are

Gage type A:

$$\mathrm{FoM}\left[\mathrm{SC}(\varepsilon_{app})_{A,B}\right]_{CIHU} = \frac{172\ 907}{2\ 030\ 380} = 0.09$$

Gage type B:

$$\mathrm{FoM}\left[\mathrm{SC}(\varepsilon_{app})_{B,B}\right]_{CIHU} = \frac{172\ 907}{172\ 907} = 1.00$$

in the temperature range 75 to 1500 °F (20 to 815 °C).

Because collecting valid first-cycle data was an important goal for GWP29, we calculated figures of merit for both first-cycle heatup and first-cycle cooldown, as well as for cycles 9 and 11 (both heatup and cooldown) because these are the first cycles to 1350 and 1500 °F (730 and 815 °C), respectively.

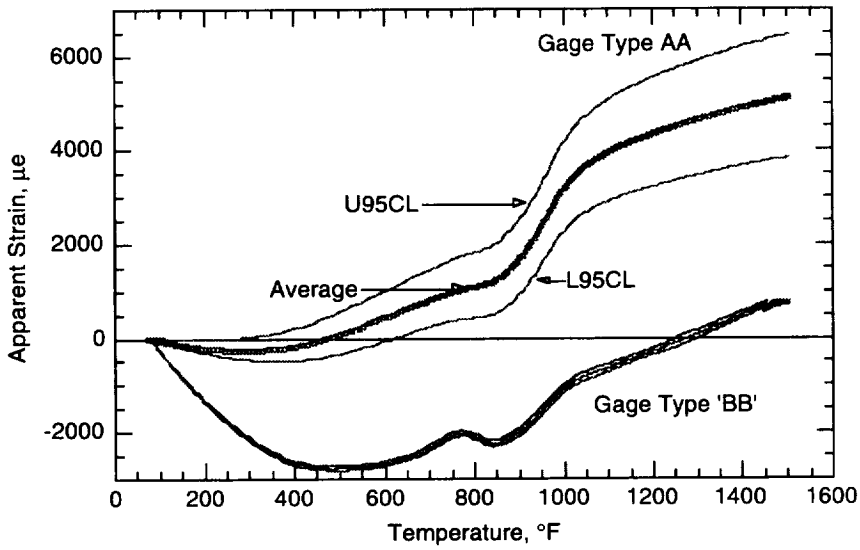

Figure 2.5.—Apparent strain scatter figure-of-merit example.

TABLE 2.12.—DETERMINATION OF CONFIDENCE LIMITS AT GIVEN TEMPERATURE
[Gage type B; n = 4; nominal temperature, 1200 °F (650 °C).]

Gage	Apparent strain, με
1	-381
2	-296
3	-351
4	-356

Average strain, με	-346
Standard deviation, με	±35.8
Student's t	3.18
U95CL, με	-289
L95CL, με	-403

In the general version of the methodology this figure of merit was defined so that it could be used to look in detail at gage-to-gage scatter in various temperature subranges, for instance, the phase transformation temperature range of the BCL gage. In this example it is clear from the figure that the division of the scatter data into temperature ranges was not necessary, as the scatter trend was similar throughout the entire range from room temperature to 1500 °F (815 °C). For GWP29 the temperature ranges were from room temperature to the respective maximum temperatures of the cycles defined above.

2.3.2.2 Apparent strain magnitude figure of merit.—Large apparent strain magnitudes can magnify measurement errors, making accurate measurement more difficult when small mechanical strain levels are to be measured. We awarded a higher figure of merit to a gage type with smaller apparent strains.

The following equation for figure of merit was used to quantitatively evaluate relative gage performance on the basis of the magnitude of apparent strain:

$$\mathrm{FoM}\left[\mathrm{M}\left(\overline{\varepsilon_{app}}\right)_{i,j}\right]_m = \frac{\left(\overline{\varepsilon_{app,n,max}} - \overline{\varepsilon_{app,n,min}}\right)_{j,m}}{\left(\overline{\varepsilon_{app,n,max}} - \overline{\varepsilon_{app,n,min}}\right)_{i,m}} \qquad (2.7)$$

where

$\mathrm{M}\left(\overline{\varepsilon_{app}}\right)$ magnitude of average apparent strain

$\overline{\varepsilon_{app,n,max}}$ maximum apparent strain of average of n gages over entire temperature range

$\overline{\varepsilon_{app,n,min}}$ minimum apparent strain of average of an gages over entire temperature range

EXAMPLE 2: Figure 2.6 shows curves of average first-cycle heatup apparent strain for four gages each of gage types A and B. Gage type A had significantly higher peak apparent strain magnitude than did gage type B (and higher average magnitude, for that matter), and this fact is reflected in the figures of merit for the two gage types:

$$\mathrm{FoM}\left[\mathrm{M}\left(\overline{\varepsilon_{app}}\right)_{A,B}\right]_{CIHU} = \frac{0-(-3980)}{17\,416-0} = \frac{3980}{17\,416} = 0.23$$

$$\mathrm{FoM}\left[\mathrm{M}\left(\overline{\varepsilon_{app}}\right)_{B,B}\right]_{CIHU} = \frac{0-(-3980)}{0-(-3980)} = \frac{3980}{3980} = 1.00$$

Note that the maximum magnitude of apparent strain occurred at 1500 °F (815 °C) for gage type A but at 588 °F (305 °C) for gage type B. Maximum magnitude of apparent strain may occur at different temperatures for different gage types. In this case the maximum magnitude for gage type B occurred at a temperature that may not be in the most useful temperature range for the gage nor in the most critical temperature range of interest. We therefore caution against evaluating a gage on the basis of a single criterion.

Note that the apparent strain data were not averaged over the entire temperature range, as was done for several other figures of merit in this methodology. Averaging the apparent strain magnitude over the whole temperature range would tend to hide the information about the peak (or full scale) values of apparent strain.

2.3.2.3 Apparent strain slope figure of merit.—Sensitivity to temperature (slope) is another characteristic of high-temperature strain gages that can contribute to uncertainty in strain measurement. Gage types that are less sensitive to temperature, and thus have smaller apparent strain slopes, were awarded higher figures of merit than gages with large apparent strain slopes.

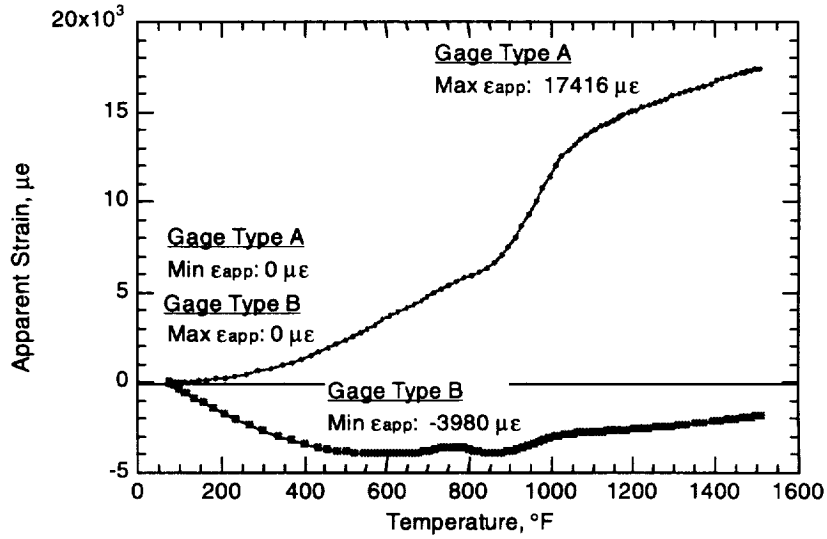

Figure 2.6.—Apparent strain magnitude figure-of-merit example.

The following equation was used to quantitatively evaluate relative gage performance from the slope of average apparent strain:

$$\mathrm{FoM}\left[\mathrm{SL}\left(\overline{\varepsilon_{\mathrm{app}}}\right)_{i,j}\right]_m = \frac{\int_{T_{\mathrm{lower}}}^{T_{\mathrm{upper}}} \left| \left(\frac{d\overline{\varepsilon_{\mathrm{app},n}(T)}}{dT} \right)_{j,m} \right| dT}{\int_{T_{\mathrm{lower}}}^{T_{\mathrm{upper}}} \left| \left(\frac{d\overline{\varepsilon_{\mathrm{app},n}(T)}}{dT} \right)_{i,m} \right| dT} \qquad (2.8)$$

where

$\mathrm{SL}\left(\overline{\varepsilon_{\mathrm{app}}}\right)$ slope of average apparent strain

j designator for gage type for which average slope is smallest over temperature range

$\frac{d\overline{\varepsilon_{\mathrm{app},n}(T)}}{dT}$ derivative of average apparent strain curve of n gages with respect to temperature

The equation was defined in a manner to account for an apparent strain curve which had its slope evenly distributed with both positive and negative values across the temperature range of interest. By integrating the absolute value of the derivative rather than the derivative itself, positive and negative slopes were accumulated, making the figure of merit an accurate measure of slope.

EXAMPLE 3: Figures 2.7 and 2.8 show, respectively, the apparent strain versus temperature and the derivative of the apparent strain versus temperature for gage types A and B. Average slopes were obtained from the instantaneous derivatives by averaging across the temperature range from 75 °F (25 °C) to the maximum temperature, 1500 °F (815 °C) in this example. The average slopes were included in figure 2.7.

The figures of merit for gage types A and B are

$$\mathrm{FoM}\left[\mathrm{SL}\left(\overline{\varepsilon_{\mathrm{app}}}\right)_{\mathrm{A,B}}\right]_{\mathrm{CIHU}} = \frac{|7011.7|}{|11\,095.8|} = 0.63$$

$$\mathrm{FoM}\left[\mathrm{SL}\left(\overline{\varepsilon_{\mathrm{app}}}\right)_{\mathrm{B,B}}\right]_{\mathrm{CIHU}} = \frac{|7011.7|}{|7011.7|} = 1.00$$

The importance of the slope of apparent strain as a performance parameter is evident in these data. If there were a 5 F deg (3 C deg) error in the temperature measurement, gage type A would have an average error in measured strain of 38 με and gage type B, 25 με.

2.3.2.4 Apparent strain repeatability figure of merit.— Repeatability of apparent strain is an important requirement in any application where temperature excursions will be made, even for a single cycle. Many phenomena affect the repeatability of the apparent strain of the high-temperature strain gage itself: oxidation, heating and cooling rates, metallurgical phase transformations, and residual stresses in the gage installation, among others. In addition, substrate phenomena, such as warping, creep, viscoplasticity, and relaxation of residual stresses, can significantly affect the gage's measured apparent strain. All of the various effects combine to make high-temperature strain gages very dependent on the thermal history of the gage and substrate.

The thermal history must be considered to make meaningful figure-of-merit comparisons among the different gage types. Apparent strain repeatability typically improves considerably after the first thermal cycle. The goal of obtaining valid first-cycle data required that this method be able to account separately for the first cycle and for subsequent cycles.

The following equation was used to determine the figure of merit for a given gage type on the basis of apparent strain repeatability:

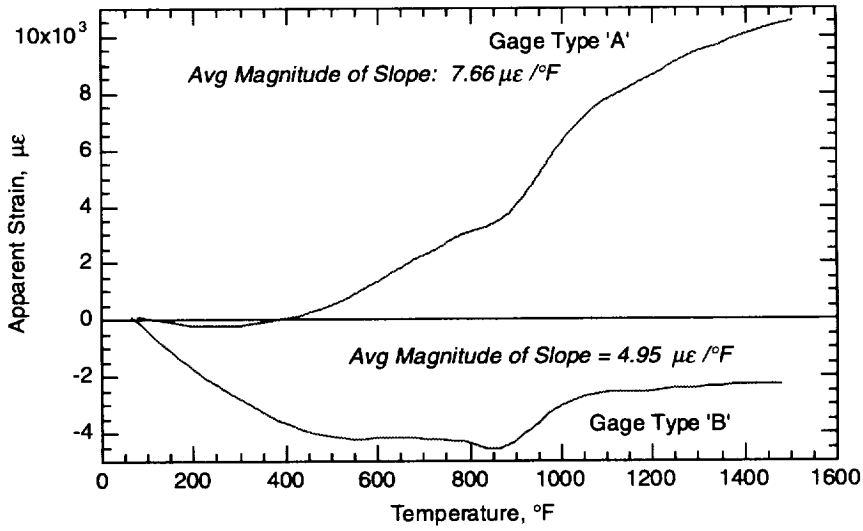

Figure 2.7.—Apparent strain slope figure-of-merit example.

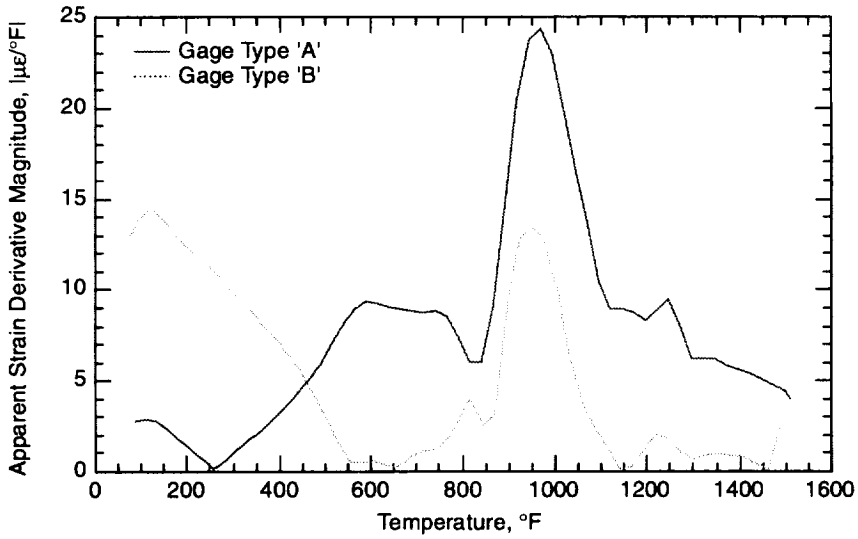

Figure 2.8.—Apparent strain derivatives for slope figure-of-merit example.

$$\mathrm{FoM}\left[\mathbf{R}\left(\overline{\varepsilon_{\mathrm{app}}}\right)_{i,j}\right]_{m_1,m_2} = \frac{\int_{T_{\mathrm{lower}}}^{T_{\mathrm{upper}}} \left|\overline{\varepsilon_{\mathrm{app},n,m_1}}(T) - \overline{\varepsilon_{\mathrm{app},n,m_2}}(T)\right|_j dT}{\int_{T_{\mathrm{lower}}}^{T_{\mathrm{upper}}} \left|\overline{\varepsilon_{\mathrm{app},n,m_1}}(T) - \overline{\varepsilon_{\mathrm{app},n,m_2}}(T)\right|_i dT} \qquad (2.9)$$

where

$\mathbf{R}\left(\overline{\varepsilon_{\mathrm{app}}}\right)$ repeatability of average apparent strain

j designator for gage type for which apparent strain deviation is minimum for all gage types

m_1 designator for first half-cycle number

m_2 designator for second half-cycle number

$\overline{\varepsilon_{\mathrm{app},n,m}}(T)$ average apparent strain of n gages for given half-cycle as function of temperature

The GWP29 test plan called for 12 apparent strain cycles on each coupon. It is easy to see that with 12 cycles (24 half-cycles) this method could become cumbersome. However, not all of the possible comparisons that could be made are important. Table 2.13 indicates the cycles for which figures of merit were calculated and describes the designated half-cycles.

EXAMPLE 4: Figure 2.9 shows the areas between the first-cycle heatup and first-cycle cooldown of gage types A and B. The areas between these curves for the two gage types, as calculated by equation (2.9), were 897 925 με·F deg for gage type A and 1 744 220 με·F deg for gage type B, over the temperature range 75 to 1500 °F (20 to 815 °C).

These areas yielded the following figures of merit:

$$\mathrm{FoM}\left[\mathbf{R}\left(\overline{\varepsilon_{\mathrm{app}}}\right)_{\mathrm{A,B}}\right]_{\mathrm{CIHU,CICD}} = \frac{897\,925}{897\,925} = 1.00$$

$$\mathrm{FoM}\left[\mathbf{R}\left(\overline{\varepsilon_{\mathrm{app}}}\right)_{\mathrm{B,B}}\right]_{\mathrm{CIHU,CICD}} = \frac{897\,925}{1\,744\,220} = 0.51$$

2.3.3 Methodology for Calculating Drift Strain Figures of Merit

Figures of merit were used to quantitatively evaluate gage performance in terms of two drift strain characteristics over a specified time period. The first varies according to the drift rate of the evaluated gages. The second varies according to the scatter in drift strain data from gage to gage.

2.3.3.1 Drift rate figure of merit.—Because drift is a time-dependent property by definition, the drift rate, rather than the absolute drift itself, is more important as a performance characteristic when evaluating gage types. Complicating the evaluation of drift characteristics is the fact that drift rates themselves are a function of both time and temperature. Figures 2.10 and 2.11 graphically illustrate these points. Figure 2.10 demonstrates that the drift rate can vary significantly with temperature, meaning that a separate figure of merit had to be evaluated for all gages in the test matrix at *each* test temperature. The time period over which the figure of merit was calculated had to be carefully selected because, as is shown in figure 2.11, the drift rate also depends on the elapsed time during the test. The early part of the test, up to 4 hr, was characterized by high drift rates. After 4 hr the drift rate became much more moderate, and after 12 hr the drift rate was essentially constant. Although time periods of this length were not used in GWP29 tests, the reasoning remains the same: drift properties must be evaluated

TABLE 2.13.—APPARENT STRAIN REPEATABILITY COMPARISONS

Cycle designations	Description of cycles
C1HU, C1CD	First cycle
C1HU, C2HU	First two heatups
C1CD, C2HU	First retraceability
C1CD, C2CD	First two cooldowns
C2HU, C2CD	Second cycle (effect of thermal cycling)
C2HU, C3HU	First faster heatup change of rate
C2CD, C3HU	First retraceability comparison involving rate change
C2CD, C3CD	Effect of intermediate heatup at higher rate
C2CD, C4CD	Effect on cooldown of intermediate cycle with fast heatup
C3HU, C3CD	First cycle at fast heatup rate
C4HU, C6HU	Effect on heatup of faster intermediate cycle
C4CD, C5CD	First faster cooldown change of rate
C5HU, C5CD	First cycle at fast cooldown rate
C6HU, C7HU	First slower heatup change of rate
C6CD, C7CD	First slower cooldown change of rate
C7HU, C7CD	Return to slow heating and cooling rates
C1HU, C8CD	First and last 1200 °F (650 °C) half-cycles
C9HU, C9CD	First cycle to 1350 °F (730 °C)
C9CD, C10HU	First retraceability comparison to 1350 °F (730 °C)
C10HU, C10CD	Second cycle to 1350 °F (730 °C)
C11HU, C11CD	First cycle to 1500 °F (815 °C)
C11CD, C12HU	First retraceability comparison to 1500 °F (815 °C)
C12HU, C12CD	Second cycle to 1500 °F (815 °C)

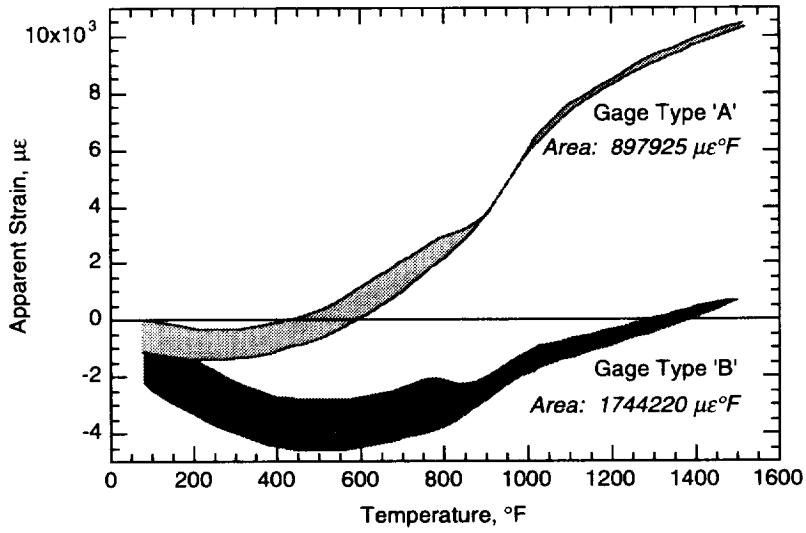

Figure 2.9.—Apparent strain repeatability example.

at discrete temperatures rather than across temperature ranges, and the time interval over which drift is considered is important.

The following equation was used to determine the figure of merit for a given strain gage type on the basis of drift rate:

$$\mathrm{FoM}\left[\mathbf{M}\left(\overline{\dot{\varepsilon}_{\mathrm{drift}}}\right)_{i,j}\right]_T = \frac{\int_{\tau_1}^{\tau_2}\left|\left(\frac{d\overline{\varepsilon_{\mathrm{drift}}}(\tau)}{d\tau}\right)_{j,T}\right|d\tau}{\int_{\tau_1}^{\tau_2}\left|\left(\frac{d\overline{\varepsilon_{\mathrm{drift}}}(\tau)}{d\tau}\right)_{i,T}\right|d\tau} \qquad (2.10)$$

where

$\mathbf{M}\left(\overline{\dot{\varepsilon}_{\mathrm{app}}}\right)$ magnitude of average drift rate as a function of time at constant temperature

T designator for temperature level

τ_1 time 1, start of time interval

τ_2 time 2, end of time interval

$\frac{d\overline{\varepsilon_{\mathrm{drift}}}(\tau)}{d\tau}$ derivative of average drift strain with respect to time at constant temperature

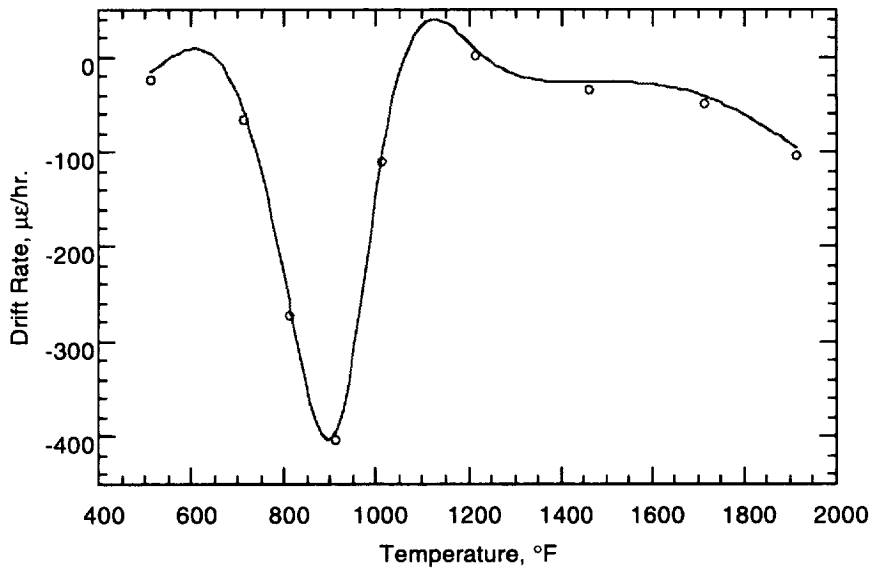

Figure 2.10.—Average 4-hr drift rate versus temperature.

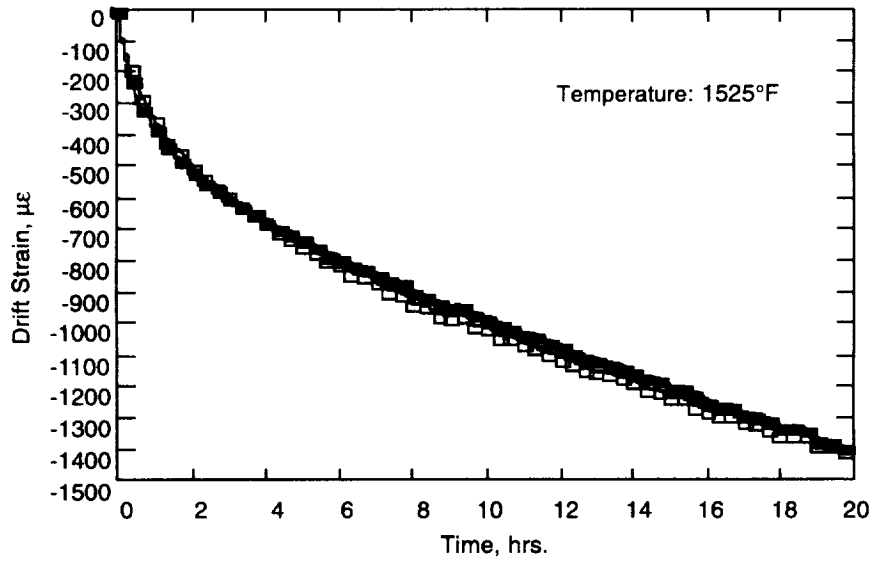

Figure 2.11.—First-cycle, untreated-BCL gage prestabilization drift.

EXAMPLE 5: As noted above, it was necessary to select the temperature and the time interval or intervals over which figures of merit would be calculated. Because the example data shown for gage types A and B in figure 2.12 are for 1500 °F (815 °C), the selection of temperature for the example was easy. Three time intervals (1, 2, and 4 hr) were selected for the example to illustrate the time dependency of the drift rate and that it may be best to evaluate drift properties over several time intervals when selecting a gage if the test duration is such that there is a large change in drift rate. For GWP29 the time period was 4 hr.

The drift rates for the first hour of the test shown in figure 2.12 were −151 με/hr for gage type A and −174 με/hr for gage type B. The figures of merit for these two gages

Gage type A:

$$\mathrm{FoM}\left[\mathbf{M}\left(\dot{\varepsilon}_{\mathrm{drift}}\right)_{\mathrm{A,A}}\right]_{1500} = \frac{|-151|}{|-151|} = 1.00$$

Gage type B:

$$\mathrm{FoM}\left[\mathbf{M}\left(\dot{\varepsilon}_{\mathrm{drift}}\right)_{\mathrm{B,A}}\right]_{1500} = \frac{|-151|}{|-174|} = 0.87$$

indicate that gage type A was somewhat better than gage type B in terms of drift rate for the first hour of a soak at 1500 °F (815 °C). For the first 2 hr of the test the average drift rates for the two gages were −129 με/hr for gage type A and −136 με/hr for gage type B. The figures of merit for the two gage types

Gage type A:

$$\mathrm{FoM}\left[\mathbf{M}\left(\dot{\varepsilon}_{\mathrm{drift}}\right)_{\mathrm{A,A}}\right]_{1500} = \frac{|-129|}{|-129|} = 1.00$$

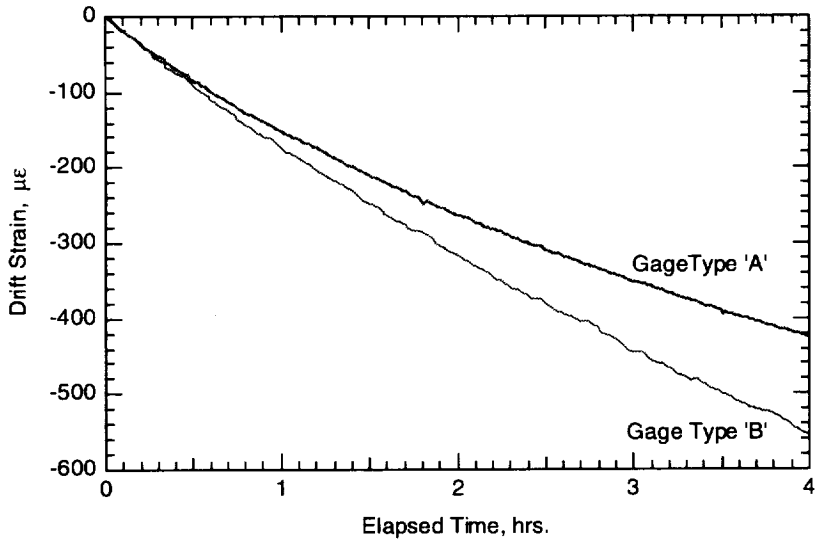

Figure 2.12.—Drift strain comparison for gage types A and B.

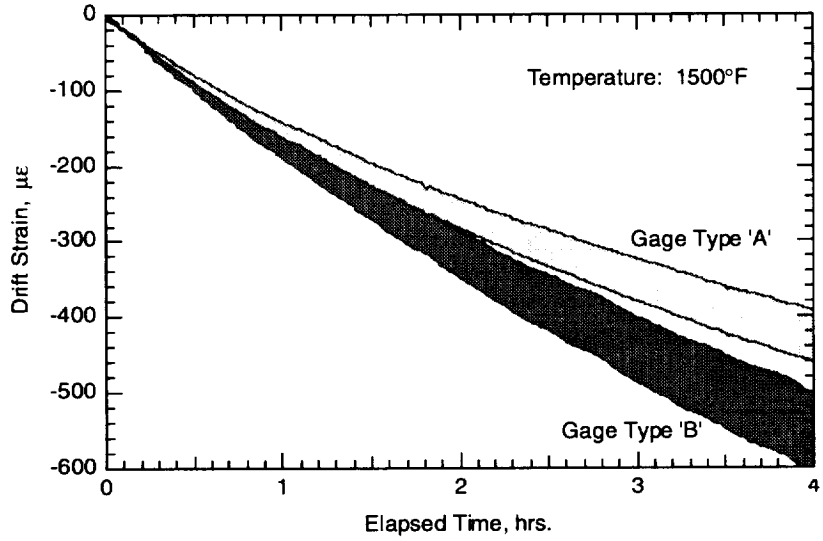

Figure 2.13.—Drift scatter comparison for gage types A and B.

Gage type B:

$$\mathrm{FoM}\left[\mathrm{M}\left(\dot{\varepsilon}_{\mathrm{drift}}\right)_{\mathrm{B,A}}\right]_{1500} = \frac{|-129|}{|-136|} = 0.95$$

indicate that gage type A was still better than gage type B over this time interval and that the margin of superiority was less than over the first hour. For the full 4 hr of the test the average drift rates of the two gages were −103 με/hr for gage type A and −136 με/hr for gage type B. The figures of merit obtained for these two gages

Gage type A:

$$\mathrm{FoM}\left[\mathrm{M}\left(\dot{\varepsilon}_{\mathrm{drift}}\right)_{\mathrm{A,A}}\right]_{1500} = \frac{|-103|}{|-103|} = 1.00$$

Gage type B:

$$\mathrm{FoM}\left[\mathrm{M}\left(\dot{\varepsilon}_{\mathrm{drift}}\right)_{\mathrm{B,A}}\right]_{1500} = \frac{|-103|}{|-136|} = 0.76$$

indicate that gage type A was even better over the 4-hr period than over the 1-hr and 2-hr periods, in comparison with gage type B. The significance of this superiority depends on the application.

2.3.3.2 Drift strain gage-to-gage scatter figure of merit.— It is important that the gage-to-gage scatter be small in order to give confidence in the corrections for drift applied to test data. The area between statistical limits, such as 95% confidence limits, provides an excellent measure of the scatter in data over a wide range. Figure 2.13 shows the area between the 95% confidence limits for gage types A and B.

The following figure of merit was used for evaluating strain gages on the basis of gage-to-gage scatter in the drift data:

$$\mathrm{FoM}\left[\mathbf{SC}\left(\varepsilon_{\mathrm{drift}}\right)_{i,j}\right]_T = \frac{\left[\int_{\tau_1}^{\tau_2}\left[\mathrm{U95CL}(\tau)-\mathrm{L95CL}(\tau)\right]_j d\tau\right]_T}{\left[\int_{\tau_1}^{\tau_2}\left[\mathrm{U95CL}(\tau)-\mathrm{L95CL}(\tau)\right]_i d\tau\right]_T} \tag{2.11}$$

where

$\mathbf{SC}(\varepsilon_{\mathrm{drift}})$ scatter in drift strain data

j designator for gage type for which difference between upper and lower 95% confidence limits is minimum

U95CL(τ) upper statistical limit as function of time at constant temperature

L95CL(τ) lower statistical limit as function of time at constant temperature

This equation can be simplified in the same manner as equation (2.1) such that

$$\mathrm{FoM}\left[\mathbf{SC}\left(\varepsilon_{\mathrm{drift}}\right)_{i,j}\right]_T = \frac{\left[\int_{\tau_1}^{\tau_2} t_{0.95}(n_j)\frac{s_{\mathrm{drift},n_j}(\tau)}{\sqrt{n_j}}d\tau\right]_T}{\left[\int_{\tau_1}^{\tau_2} t_{0.95}(n_i)\frac{s_{\mathrm{drift},n_i}(\tau)}{\sqrt{n_i}}d\tau\right]_T} \tag{2.12}$$

where

$s_{\mathrm{drift},n}(\tau)$ drift strain standard deviation for sample of n gages as function of time at constant temperature

EXAMPLE 6: Although it is evident from figure 2.13 that gage type A had lower drift rates than gage type B, it is not as evident that the area defining the amount of scatter in the gage was smaller in all time periods of interest. Over the first hour of the test gage the scatter was 21 με·hr for gage type A and 32 με·hr for gage type B. Thus, the figures of merit for the two gage types were
Gage type A:

$$\mathrm{FoM}\left[\mathbf{SC}\left(\varepsilon_{\mathrm{drift}}\right)_{A,A}\right]_{1500} = \frac{21}{21} = 1.00$$

Gage type B:

$$\mathrm{FoM}\left[\mathbf{SC}\left(\varepsilon_{\mathrm{drift}}\right)_{B,A}\right]_{1500} = \frac{21}{32} = 0.66$$

For the first 2 hr of the test the gage scatter was 81 με·hr for gage type A and 125 με·hr for gage type B. Thus, the figures of merit for the two gage types were
Gage type A:

$$\mathrm{FoM}\left[\mathbf{SC}\left(\varepsilon_{\mathrm{drift}}\right)_{A,A}\right]_{1500} = \frac{81}{81} = 1.00$$

Gage type B:

$$\mathrm{FoM}\left[\mathbf{SC}\left(\varepsilon_{\mathrm{drift}}\right)_{B,A}\right]_{1500} = \frac{81}{125} = 0.65$$

Finally, for the whole 4 hr of the test the gage scatter between the statistical limits was 300 με·hr for gage type A and 461 με·hr for gage type B. Thus, the figures of merit for the two gage types were
Gage type A:

$$\mathrm{FoM}\left[\mathbf{SC}\left(\varepsilon_{\mathrm{drift}}\right)_{A,A}\right]_{1500} = \frac{300}{300} = 1.00$$

Gage type B:

$$\mathrm{FoM}\left[\mathbf{SC}\left(\varepsilon_{\mathrm{drift}}\right)_{B,A}\right]_{1500} = \frac{300}{461} = 0.65$$

It is coincidental that the figures of merit were so close for gage type B for all three calculations. Clearly, gage type A had less scatter in the drift data from gage to gage and thus is a better gage from that standpoint.

Table 2.14 summarizes the drift characteristic figures of merit for gage types A and B. Only the figures of merit calculated for the period 0 to 4 hr were used for GWP29. Those for the other time periods show that figures of merit can change, depending on the time period over which they are calculated.

For each time period table 2.14 sums the individual figures of merit for each performance parameter for each gage type to obtain a composite score. Summing characteristics in this way enables the user to determine from one set of numbers how the gages compare with one another for a given parameter. This table shows that gage type A was superior to gage type B, in

TABLE 2.14.—FIGURES OF MERIT FOR DRIFT CHARACTERISTICS

Gage type	$\mathrm{FoM}\left[\mathrm{M}\left(\overline{\varepsilon_{\mathrm{drift}}}\right)\right]$	$\mathrm{FoM}\left[\mathrm{SC}\left(\varepsilon_{\mathrm{drift}}\right)\right]$	$\sum$ FoM
0 to 1 hr			
A	1.00	1.00	2.00
B	.87	.66	1.53
0 to 2 hr			
A	1.00	1.00	2.00
B	.95	.65	1.60
0 to 4 hr			
A	1.00	1.00	2.00
B	.76	.65	1.41

TABLE 2.15.—SUMMARY OF DRIFT RATES AND DEVIATIONS

Gage type	Mean drift rate, με/hr	Average deviation from mean, με/hr	Percent deviation from mean
1050 °F (565 °C)			
C	−50	1.8	3.60
D	−26	2.0	7.69
E	−88	6.9	7.84
1200 °F (650 °C)			
C	7	0.8	11.43
D	12	1.3	10.83
E	−81	7.2	8.89
1350 °F (730 °C)			
C	−19	1.6	8.42
D	−58	2.5	4.31
E	−118	10.0	8.47
1500 °F (815 °C)			
C	−37	2.2	5.95
D	−149	10.3	6.91
E	−181	16.6	9.17

both drift rate and gage-to-gage scatter aspects of drift performance, over all time periods of interest up to 4-hr duration.

Table 2.15 is another way of presenting similar information. It shows the mean values for drift rate at each temperature in the test matrix, as well as the average deviations from the mean for each gage type. In this table all time intervals for comparison are the same, 1 hr. Three new gage types are introduced here as data for them were readily available from past work. The gage types are gage type C—prestabilized, preconditioned BCL; gage type D—untreated BCL; and gage type E—NZ–2104–120L.

2.3.4 Methodology for Calculating Gage Factor Figures of Merit

Figures of merit were used to quantitatively evaluate strain gage performance in terms of four gage factor characteristics over a specified temperature range. The first varies with gage type according to the scatter of the gage factor from gage to gage. The second varies with gage type according to the magnitude of the gage factor over a specified temperature range. The third varies with gage type according to the sensitivity of gage factor to temperature. The fourth varies with gage type according to the repeatability of gage factor with cycling.

The figures of merit that are defined here are all referenced by cycle. Caution must be observed in interpreting these definitions with regard to the implied dependency of gage factor on cyclic effects. Gage factor is an intrinsic property of a strain gage alloy; thus, the true gage factor should not change with thermal or mechanical cycling. However, because the strain gage is attached to a substrate by various means, there can be the appearance of gage factor changes due to cycling. These apparent changes in gage factor are the result of changes due to cycling within the gage attachment, within the interface between the gage attachment and substrate, and/or within the substrate itself. Because the performance of the strain gage system depends on its attachment, it is appropriate that the effects of cycling on the attachment are reflected in the figures of merit.

Gage factor can vary depending on whether the gage was loaded in tension or in compression, and this behavior may differ from gage type to gage type. Accordingly, separate figures of merit were calculated for tension and compression.

In all of the analyses that follow, all corrections for factors such as lead-wire resistance, gage standoff, and gage factor setting were assumed to have already been made to the data. This approach was required for analyzing actual GWP29 test data.

2.3.4.1 Gage factor scatter figure of merit.—A fundamental user requirement for a strain gage, beyond the desire for large gage factors or low temperature sensitivity, is that gages of a certain type and of a particular lot exhibit essentially identical performance. Regardless of the magnitude, temperature sensitivity, or repeatability of gage factor for a single gage, if the gage-to-gage scatter in the data is large, the gage type cannot be considered dependable. The area between the 95% confidence limits is an excellent measure of the scatter.

The following equation was used to determine the figure of merit for a given strain gage type on the basis of its gage-to-gage scatter in gage factor:

$$\mathrm{FoM}\left[\mathbf{SC}(\mathrm{GF})_{i,j,l}\right]_m = \frac{\left[\int_{T_{\mathrm{lower}}}^{T_{\mathrm{upper}}} \left[\mathrm{U95CL}(T) - \mathrm{L95CL}(T)\right]_{j,l} dT\right]_m}{\left[\int_{T_{\mathrm{lower}}}^{T_{\mathrm{upper}}} \left[\mathrm{U95CL}(T) - \mathrm{L95CL}(T)\right]_{i,l} dT\right]_m} \tag{2.13}$$

where

SC scatter in gage factor, gage to gage

j designator for gage type for which difference between upper and lower 95% confidence limits is minimum

l designator for tension or compression

This equation can be simplified in the same manner as equation (2.1), such that

$$\mathrm{FoM}\left[\mathbf{SC}(\mathrm{GF})_{i,j,l}\right]_m = \frac{\left[\int_{T_{\mathrm{lower}}}^{T_{\mathrm{upper}}} t_{0.95(n_j)} \frac{\left(s_{\mathrm{GF},n_j}(T)\right)_l}{\sqrt{n_j}} dT\right]_m}{\left[\int_{T_{\mathrm{lower}}}^{T_{\mathrm{upper}}} t_{0.95(n_i)} \frac{\left(s_{\mathrm{GF},n_i}(T)\right)_l}{\sqrt{n_i}} dT\right]_m} \tag{2.14}$$

where

$s_{GF,n}(T)$ gage factor standard deviation for sample of n gages as function of temperature

The requirement for valid first-cycle data necessitated that a figure of merit be calculated for the first cycle. For a prospective user, data were obtained in which the effects from the strain gage installer and the attachment technique and/or the substrate were minimized. These data were the average of second-cycle heatup and cooldown to each maximum temperature and can be used as additional figures of merit for gage factor.

EXAMPLE 7: Figure 2.14 illustrates the areas between the upper and lower statistical limits of the gage factor scatter curves for gage types A and B. By using the preceding definition for the figure of merit, we determined the relative merits of these gage types.

The areas between upper and lower 95% confidence limits are 136.50 GF·F deg for gage type A and 133.25 GF·F deg for gage type B over the temperature range 75 to 1500 °F (20 to 815 °C), yielding the following figures of merit:

Gage type A:

$$\mathrm{FoM}\left[\mathrm{SC(GF)}_{A,B,\sigma_t}\right]_{C2HU} = \frac{133.25}{136.50} = 0.98$$

Gage type B:

$$\mathrm{FoM}\left[\mathrm{SC(GF)}_{B,B,\sigma_t}\right]_{C2HU} = \frac{133.25}{133.25} = 1.00$$

Although the figures of merit permit an accurate quantitative comparison of multiple gage types, they tend to mask certain important facets of the data. Gage type B had a slightly superior figure of merit over the whole temperature range from 75 to 1500 °F (20 to 815 °C) than did gage type A, but above 900 °F (480 °C) gage type A clearly exhibited less scatter than gage type B. If we assume, for example, that some low-temperature strain gage with excellent scatter properties was used in parallel with the high-temperature gage to 900 °F (480 °C), overall measurement accuracy would actually be worse if gage type B were selected for the high-temperature part of a test solely on the figure of merit. This is all the more reason for the user to be careful when interpreting figures of merit calculated over broad temperature ranges without regard for the regions in which data overlap—important aspects of gage behavior may disappear in the calculations.

2.3.4.2 Gage factor magnitude figure of merit.—In general, it is beneficial to use a gage with a high gage factor, with added benefits from smaller changes in temperature sensitivity and linearity of gage factor versus temperature. This benefit is illustrated graphically in figure 2.15, where gage type A has the higher average gage factor throughout the temperature range from 75 to 1500 °F (20 to 815 °C) and gage type B has less change in sensitivity and less nonlinearity.

The following equation for figure of merit was used to quantitatively evaluate relative gage performance on the basis of the magnitude of average gage factor:

$$\mathrm{FoM}\left[\mathrm{M}\left(\overline{\mathrm{GF}}\right)_{i,j,l}\right]_m = \frac{\left[\int_{T_{\mathrm{lower}}}^{T_{\mathrm{upper}}} \overline{\mathrm{GF}}_{i,l}(T)\,dT\right]_m}{\left[\int_{T_{\mathrm{lower}}}^{T_{\mathrm{upper}}} \overline{\mathrm{GF}}_{j,l}(T)\,dT\right]_m} \qquad (2.15)$$

where

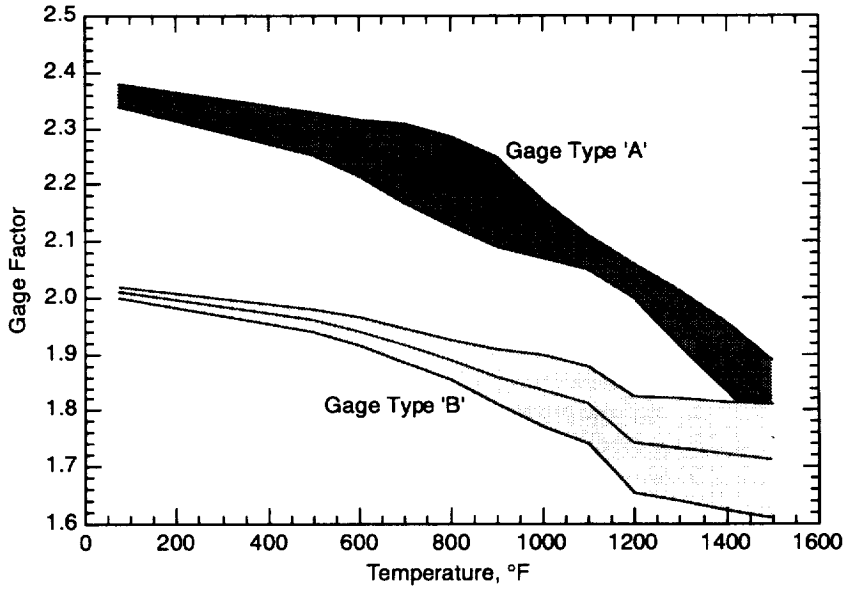

Figure 2.14.—Gage factor gage-to-gage scatter.

$\mathbf{M}(\overline{\mathrm{GF}})$ magnitude of average gage factor

j designator for gage type with largest gage-factor-versus-temperature area

Using the quotient of the areas under the gage-factor-versus-temperature curves for each gage type accounts for the variation in gage factor magnitude over the temperature range of interest. The gage-factor-versus-temperature curve for each gage type i is the average curve for a sample of n gages of that type. In this way the figure-of-merit calculation is statistically more meaningful than a calculation based on gage factor for a single gage.

EXAMPLE 8: The areas under the gage-factor-versus-temperature curves for gage types A and B in figure 2.15 are 3090.48 GF·F deg for gage type A and 2671.12 GF·F deg for gage type B. The figures of merit for these gages are Gage type A:

$$\mathrm{FoM}\left[\mathbf{M}(\mathrm{GF})_{\mathrm{A,A},\sigma_t}\right]_{\mathrm{C2HU}} = \frac{3090.48}{3090.48} = 1.00$$

Gage type B:

$$\mathrm{FoM}\left[\mathbf{M}(\mathrm{GF})_{\mathrm{B,A},\sigma_t}\right]_{\mathrm{C2HU}} = \frac{2671.12}{3090.48} = 0.86$$

2.3.4.3 Gage factor temperature sensitivity figure of merit.—Gage factor changes with temperature can contribute to uncertainty in strain-gage-based measurements. Desensitization of the strain gage alloy as the temperature increases reduces the gage output, making the strain-measuring system more susceptible to errors. Further, gage factor changes tend to be nonlinear for high-temperature strain gages, making calibration of a strain gage type with respect to gage factor that much more difficult. A figure of merit ranging from 0 to 1 will be calculated for each gage type, where a higher number indicates less gage factor change with temperature.

The following equation was used to quantitatively evaluate relative gage performance on the basis of the gage factor temperature sensitivity, or slope:

$$\mathrm{FoM}\left[\mathbf{SL}\left(\overline{\mathrm{GF}}\right)_{i,j,l}\right]_m = \frac{\int_{T_{\mathrm{lower}}}^{T_{\mathrm{upper}}} \left| \left(\frac{d\overline{\mathrm{GF}}(T)}{dT} \right)_{j,l,m} \right| dT}{\int_{T_{\mathrm{lower}}}^{T_{\mathrm{upper}}} \left| \left(\frac{d\overline{\mathrm{GF}}(T)}{dT} \right)_{i,l,m} \right| dT} \qquad (2.16)$$

where

$\mathbf{SL}\left(\overline{\mathrm{GF}}\right)$ average slope of gage factor

j designator for gage type which has least gage factor sensitivity to temperature

$\frac{d\overline{\mathrm{GF}}(T)}{dT}$ derivative of average gage factor curve with respect to temperature

EXAMPLE 9: Figure 2.16 shows the average gage factor slope for samples of two strain gage types, A and B. Gage type A has an average slope over the temperature range from 75 to 1500 °F (20 to 815 °C) of -4.42×10^{-3} GF·F deg, and gage type B has an average slope of -2.25×10^{-3} GF·F deg over the same range. Thus, the figures of merit for these gage types are

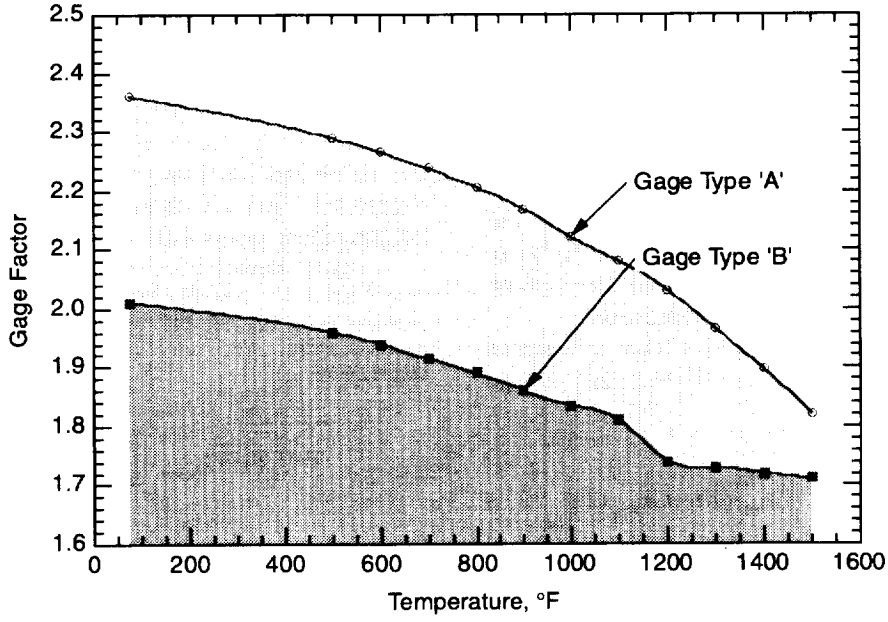

Figure 2.15.—Areas beneath gage-factor-versus-temperature curves.

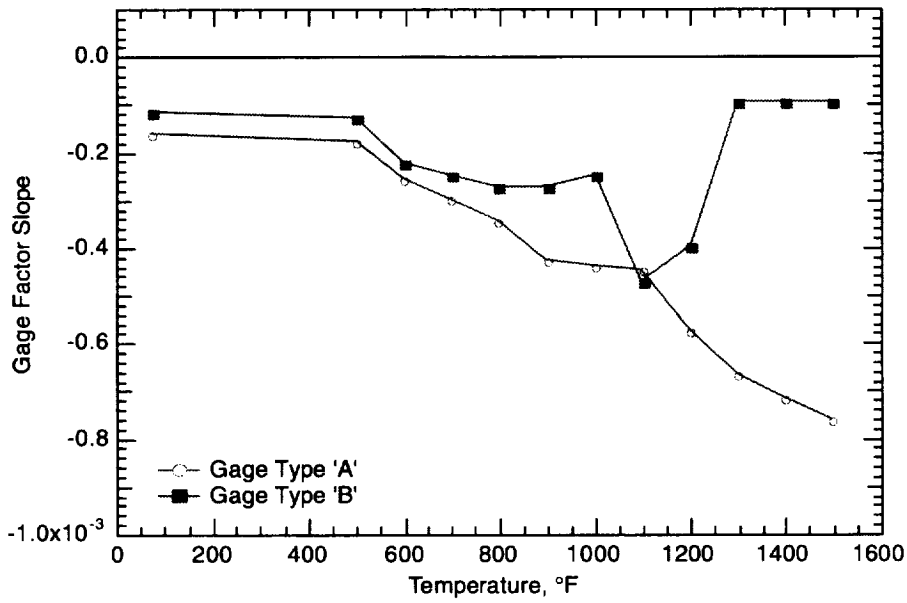

Figure 2.16.—Gage factor sensitivity to temperature.

Gage type A:

$$\mathrm{FoM}\left[\mathrm{SL}\left(\overline{\mathrm{GF}}\right)_{\mathrm{A,B},\sigma_t}\right]_{\mathrm{C2HU}} = \frac{\left|-2.25\times10^{-3}\right|}{\left|-4.42\times10^{-3}\right|} = 0.51$$

Gage type B:

$$\mathrm{FoM}\left[\mathrm{SL}\left(\overline{\mathrm{GF}}\right)_{\mathrm{B,B},\sigma_t}\right]_{\mathrm{C2HU}} = \frac{\left|-2.25\times10^{-3}\right|}{\left|-2.25\times10^{-3}\right|} = 1.00$$

2.3.4.4 Gage factor repeatability figure of merit.—Repeatability of the gage factor of the strain gage alloy itself was not an issue because it is an intrinsic property of the alloy. The effective gage factor was determined by the amount of strain transfer from the substrate to the strain gage. This effective gage factor was subject to the attachment technique and the skill of the technician. Repeatability of this effective gage factor because the strain gage was attached to a substrate was the reason for defining a repeatability figure of merit for gage factor. Repeatability had to be considered between like loading cycles (i.e., either both tension or both compression).

The following equation was used to determine the figure of merit for a given gage type on the basis of repeatability of gage factor:

$$\mathrm{FoM}\left[\mathbf{R}\left(\overline{\mathrm{GF}}\right)_{i,j,l}\right]_{m_1,m_2} = \frac{\int_{T_{\mathrm{lower}}}^{T_{\mathrm{upper}}}\left|\overline{\mathrm{GF}_{m_1}}(T)-\overline{\mathrm{GF}_{m_2}}(T)\right|_{j,l}dT}{\int_{T_{\mathrm{lower}}}^{T_{\mathrm{upper}}}\left|\overline{\mathrm{GF}_{m_1}}(T)-\overline{\mathrm{GF}_{m_2}}(T)\right|_{i,l}dT} \qquad (2.17)$$

where

$\mathbf{R}\left(\overline{\mathrm{GF}}\right)$ repeatability of gage factor

j designator for gage type for which gage factor deviation is minimum for all gage types

$\overline{\mathrm{GF}_m}(T)$ average gage factor of n gages for given half-cycle as function of temperature

The GWP29 test procedure included four thermal cycles to a maximum temperature of 1200 °F (650 °C), with mechanical loading cycles conducted at several intermediate temperatures during the first and fourth cycles. Also included were two thermal cycles to each of the maximum temperatures, 1350 and 1500 °F (730 and 815 °C), with mechanical loading cycles conducted at several intermediate temperatures during each thermal cycle. As was the case with apparent strain repeatability, not all combinations of half-cycles that can be made are significant. Table 2.16 indicates the combinations considered important and describes the designated half-cycles.

EXAMPLE 10: Figure 2.17 shows data for two heatup half-cycles for gage types A and B. The areas between the two heatups are 43.8036 GF-F deg for gage type A and 27.2744 GF-F deg for gage type B, yielding the following figures of merit:

Gage type A:

$$\mathrm{FoM}\left[\mathbf{R}\left(\overline{\mathrm{GF}}\right)_{\mathrm{A,B},\sigma_t}\right]_{\mathrm{C1HU,C2HU}} = \frac{27.2744}{43.8046} = 0.62$$

Gage type B:

$$\mathrm{FoM}\left[\mathbf{R}\left(\overline{\mathrm{GF}}\right)_{\mathrm{B,B},\sigma_t}\right]_{\mathrm{C1HU,C2HU}} = \frac{27.2744}{27.2744} = 1.00$$

TABLE 2.16.—GAGE FACTOR REPEATABILITY COMPARISONS

Cycles	Description
C1HU, C1CD	First cycle to 1200 °F (650 °C) (likelihood of deviations is greatest)
C1HU, C4HU	First two heatups to 1200 °F (650 °C) with mechanical loading
C1CD, C4CD	First two cooldowns from 1200 °F (650 °C) with mechanical loading
C4HU, C4CD	Second cycle to 1200 °F (650 °C) with mechanical loading (compare with C1HU, C1CD)
C5HU, C5CD	First cycle to 1350 °F (730 °C) (likelihood of deviations is greatest)
C5HU, C6HU	First two heatups to 1350 °F (730 °C) (check on heatup effects)
C5CD, C6CD	First two cooldowns from 1350 °F (730 °C) (check on cooldown effects)
C6HU, C6CD	Second cycle to 1350 °F (730 °C) (compare with C5HU, C5CD)
C7HU, C7CD	First cycle to 1500 °F (815 °C) (likelihood of deviations is greatest)
C7HU, C8HU	First two heatups to 1500 °F (815 °C) (check on heatup effects)
C7CD, C8CD	First two cooldowns from 1500 °F (815 °C) (check on cooldown effects)
C8HU, C8CD	Second cycle to 1500 °F (815 °C) (compare with C7HU, C7CD)

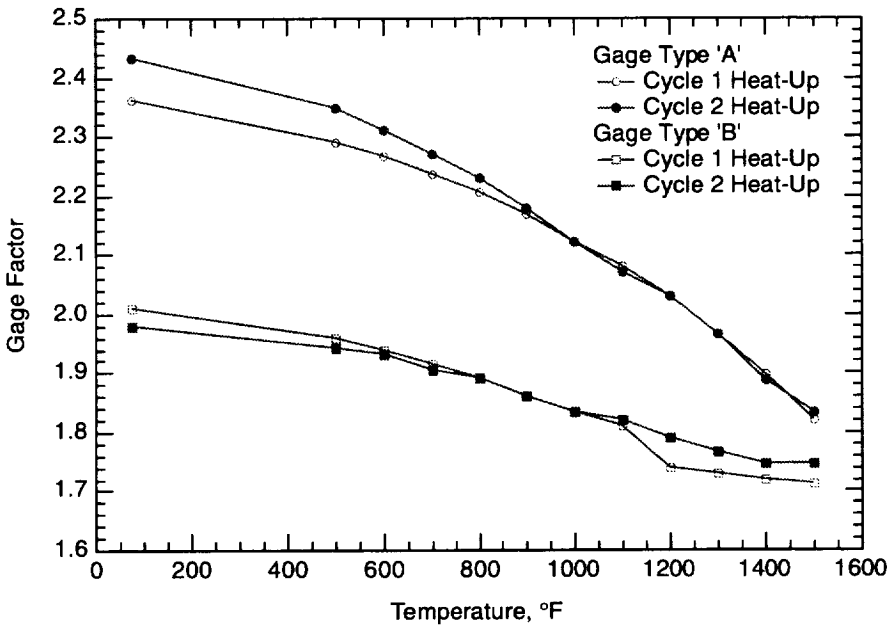

Figure 2.17.—Repeatability of gage factor.

2.3.5 Methodology for Calculating Gage Size Figures of Merit

Figures of merit were used to quantitatively evaluate strain gages in terms of two gage size characteristics. The first varies with gage type according to the respective areas required for the gage installations. The second varies with gage type according to the estimated transverse sensitivity of the respective gages.

2.3.5.1 Gage installation area figure of merit.—The area required for a strain gage installation can determine whether the gage can be used for a particular application, depending on the envelope into which the gage must fit and the space surrounding the gage in which to work. A large strain gage may not fit into the available area, so regardless of its performance, it may not be the gage of choice for an application where the available area is small.

The area required for a gage installation is defined as the product of the minimum length times the minimum width required for the strain gage, including the minimum area required for any and all precoats, overcoats, straps, etc., used to attach the gage to the substrate. The following equation was used to determine the figure of merit for a given strain gage type on the basis of the area required for the gage installation:

$$\mathrm{FoM}\left(\mathbf{A}_{i,j}\right) = \frac{\left(\text{Overall length} \times \text{Overall width}\right)_j}{\left(\text{Overall length} \times \text{Overall width}\right)_i} \qquad (2.18)$$

where

A	area required for installed gage
j	designator for gage type for which area required for gage installation is minimum
Overall length	grid length plus added length for installation
Overall width	grid width plus added width for installation

EXAMPLE 11: The relative sizes of the three GWP29 gages when installed are shown in figure 2.18. Their dimensions are shown in figures 2.19 to 2.21. The overall areas of the DETCBCL, PdCr, and CKAl gages were 0.24, 0.15, and 0.36 in.^{2}, respectively.

DETCBCL :

$$\mathrm{FoM}\left(A_{\mathrm{DETCBCL,\ PdCr}}\right) = \frac{0.5 \times 0.3}{0.6 \times 0.4} = 0.62$$

CKAl :

$$\mathrm{FoM}\left(A_{\mathrm{CKA1,\ PdCr}}\right) = \frac{0.5 \times 0.3}{0.6 \times 0.6} = 0.42$$

PdCr :

$$\mathrm{FoM}\left(A_{\mathrm{PdCr,\ PdCr}}\right) = \frac{0.5 \times 0.3}{0.5 \times 0.3} = 1.00$$

2.3.5.2 Transverse sensitivity figure of merit.—Testing the transverse sensitivity of the gages was beyond the scope of GWP29, but the relative transverse sensitivity of each gage type was estimated from the respective gage geometries. The transverse sensitivity of a gage was estimated from the resistance changes of the individual elements. The equation (ref. 2.5, p. 60) for the transverse sensitivity of a single element is

$$K_t = \frac{\left(\frac{\Delta R/R}{\varepsilon_t}\right)_{\varepsilon_a = 0}}{\left(\frac{\Delta R/R}{\varepsilon_a}\right)_{\varepsilon_t = 0}} \qquad (2.19)$$

where

K_t transverse sensitivity of gage

ΔR change in resistance of gage

R initial (unstrained) resistance of gage

ε_a strain axial direction

ε_t strain in transverse direction ($= -\nu\varepsilon_a$ in uniaxial strain field, where ν is Poisson's ratio of substrate)

$\varepsilon_t = 0$ corresponds to calibration under conditions such that there is strain at right angles to direction of gage axis but none parallel to gage axis

$\varepsilon_a = 0$ corresponds to calibration under conditions such that there is strain in direction of gage axis but none at right angles

The equation (ref. 2.5, p. 62) for change in resistance was estimated in terms of a resistance per unit length and the length affected by strains in a given direction:

$$\Delta R_\chi = \mathcal{R} L_\chi \mathrm{GF} \varepsilon_\chi \qquad (2.20)$$

where

ΔR_χ change in resistance due to strain in given direction χ

$\mathcal{R}$ resistance per unit length of gage wire

L_χ length of gage wire affected by strains in χ direction

GF gage factor of element

ε_χ strain in χ direction

For a strain gage bonded to a substrate subjected to a uniaxial strain field, applying equation (2.20) resulted in the following:

$$\Delta R_{\mathrm{element}} = \frac{R_{\mathrm{element}}}{L_{\mathrm{element}}} \mathrm{GF}\left[\left(\sum \text{length affected by axial strain}\right)\varepsilon_a + \left(\sum \text{length affected by transverse strain}\right)\varepsilon_t\right] \qquad (2.21)$$

where

$\Delta R_{\mathrm{element}}$ change in resistance of individual gage element, active or compensating

R_{element} initial (unstrained) resistance of element

L_{element} initial (unstrained) length of element

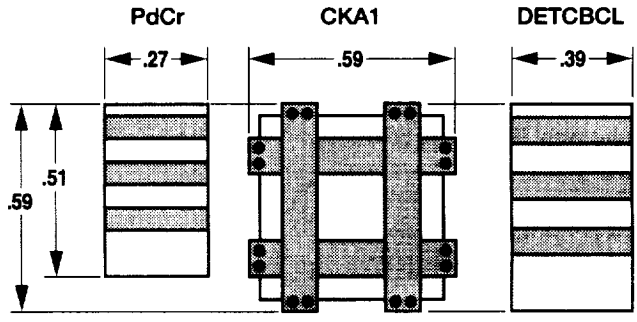

Figure 2.18.—Relative sizes (in inches) of GWP29 strain gages when installed.

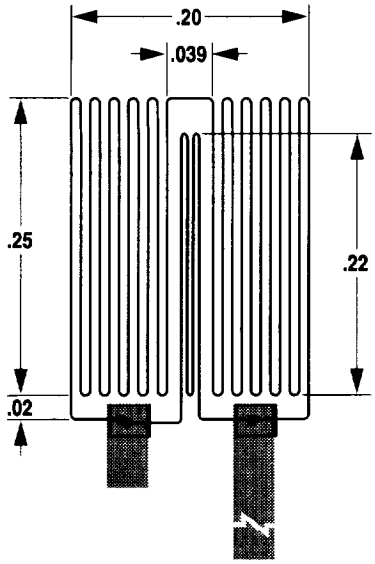

Figure 2.19.—Dimensions of the dual element, temperature-compensated BLC gage (in inches).

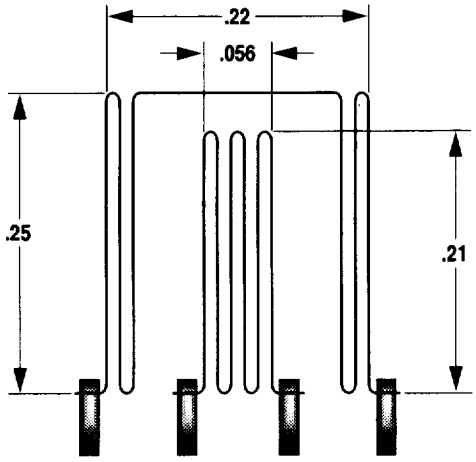

Figure 2.20.—Dimensions of compesated Kanthal A1 gage (in inches).

The resistance changes in the individual elements were then combined to give the resistance change for the gage,

$$\Delta R/R_{\text{gage}} = \frac{\Delta R_{\text{active}} + \Delta R_{\text{compensating}}}{R_{\text{active}} + R_{\text{compensating}}} \qquad (2.22)$$

As the following example shows, the transverse and axial strains, ε_t and ε_a, in equation (2.22) mathematically cancel out of the numerator and denominator, respectively.

EXAMPLE 12: Figures of merit for the relative transverse sensitivities of the three GWP29 gages were calculated. It is important to note that these are only relative numbers. The only precise method for determining transverse sensitivity

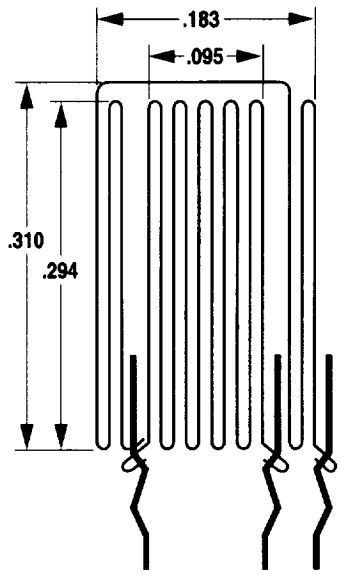

Figure 2.21.—Dimensions of palladium-chromium gage (in inches).

is testing. However, for the purposes of computing figures of merit, which are themselves relative relationships between the gages, the approach outlined here provided a meaningful way to assess gage performance with respect to transverse sensitivity.

In applying equations (2.19) to (2.22) to the CKA1 gage, note that because there was negligible strain in the compensating element, the resistance terms for the compensating element in equation (2.21) were assumed to be 0. From equation (2.21)

$$\Delta R_{\text{CKA1}} = \frac{120}{L_{\text{CKA1}}} 2.67\left[6\left(0.210 - 2\frac{0.0112}{2} + \pi\frac{0.0112}{4}\right)\varepsilon_a + 6\pi\frac{0.0112}{4}\varepsilon_t\right]\Omega$$

where

$$L_{\text{CKA1}} = 6\left(0.210 - 2\frac{0.0112}{2} + \pi\frac{0.0112}{2}\right) = 1.298 \text{ in}$$

so that

$$\Delta R_{\text{CKA1}} = 246.841\left(1.2456\varepsilon_a + 0.0528\varepsilon_t\right)$$

Inserting these values into equation (2.19) gave the transverse sensitivity of the CKA1:

$$K_{t,\text{CKA1}} = \frac{\dfrac{246.841\left[1.2456(0) + 0.0528\varepsilon_t\right]/120}{\varepsilon_t}}{\dfrac{246.841\left[1.2456\varepsilon_a + 0.0528(0)\right]/120}{\varepsilon_a}} = \frac{0.0528}{1.2456} = 0.0424 = 4.24\%$$

The pertinent gage factor and resistance quantities of the DETCBCL gage were

$$GF_{active} = 2.36 \qquad GF_{compensating} \sim 4$$

$$R_{active} = 120.00 \qquad R_{compensating} = 1.57$$

From equation (2.21) the resistance change term for the active element was

$$\Delta R_{BCL} = \frac{120}{L_{BCL}} 2.36\left\{\left[21\left(0.25 - 2\frac{0.007}{2}\right) + 2\left(0.02\frac{0.007}{2}\right) + 22\pi\frac{0.007}{4}\right]\varepsilon_a + \left(22\pi\frac{0.007}{4} + 0.039 + 0.045 + 0.020 - 4\frac{0.007}{2}\right)\varepsilon_t\right\}$$

where

$$L_{BCL} = 21\left(0.25 - 2\frac{0.007}{2} + \pi\frac{0.007}{2}\right) + 2\left(0.02 - \frac{0.007}{2}\right) + \left(0.039 - 2\frac{0.007}{2}\right) + \left(0.045 - \frac{0.007}{2}\right) + \left(0.020 - \frac{0.007}{2}\right) + \pi\frac{0.007}{2} = 5.468$$

so that

$$\Delta R_{BCL} = 51.7932\left(5.257\varepsilon_a + 0.211\varepsilon_t\right)$$

Similarly,

$$\Delta R_{Pt} = \frac{1.57}{L_{Pt}} 4\left\{\left[4\left(0.22 - 2\frac{0.007}{2} + \pi\frac{0.007}{4}\right) + 2\left(0.02 - \frac{0.007}{2}\right)\right]\varepsilon_a + \left(4\pi\frac{0.007}{4} + 0.85\right)\varepsilon_t\right\}$$

with

$$L_{Pt} = 4\left(0.22 - 2\frac{0.007}{2} + \pi\frac{0.007}{2}\right) + 2\left(0.02 - \frac{0.007}{2}\right) + 0.85 + 2\pi\frac{0.007}{2} = 1.035 \text{ in.}$$

so that

$$\Delta R_{Pt,(series)} = 6.0619\left(0.907\varepsilon_a + 0.107\varepsilon_t\right)$$

where the subscript Pt denotes platinum.

For the two-element gage

$$\Delta R / R_{DETCBCL} = \frac{51.7932(5.257\varepsilon_a + 0.211\varepsilon_t) + 6.0619(0.907\varepsilon_a + 0.107\varepsilon_t)}{120 + 1.57}$$

$$= 2.2849\varepsilon_a + 0.0952\varepsilon_t$$

Thus, the transverse sensitivity of the gage was

$$K_{t,DETCBCL} = \frac{\dfrac{2.2849(0) + 0.0952\varepsilon_t}{\varepsilon_t}}{\dfrac{2.2849\varepsilon_a + 0.0952(0)}{\varepsilon_a}}$$

$$= 0.0416 = 4.16\%$$

The transverse sensitivity of the palladium-chromium gage was found in a similar manner to that of the DETCBCL. The gage factors and resistances of the PdCr gage elements were

$$GF_{active} = 1.8 \qquad GF_{compensating} \sim 4$$

$$R_{active} = 120 \qquad R_{compensating} = 8$$

The active element had a resistance change of

$$\Delta R_{PdCr} = \frac{120}{L_{PdCr}} 1.8\left\{\left[10\left(0.294 - 2\frac{0.0106}{2}\right) + 9\pi\frac{0.0106}{4}\right]\varepsilon_a + \left(9\pi\frac{0.0106}{4}\right)\varepsilon_t\right\}$$

with

$$L_{PdCr} = 10\left(0.294 - 2\frac{0.0106}{2} + 9\pi\frac{0.0106}{4}\right) = 2.984 \text{ in.}$$

so that

$$\Delta R_{PdCr} = 72.3896(2.909\varepsilon_a + 0.075\varepsilon_t)$$

The compensating element had

$$\Delta R_{Pt} = \frac{8}{L_{Pt}} 4\left\{\left[2\left(0.310 - 2\frac{0.0106}{2}\right) + 4\left(0.294 - 2\frac{0.0106}{2}\right) + 5\pi\frac{0.0106}{4}\right]\varepsilon_a + \left[\left(0.183 - 2\frac{0.0106}{2}\right) + 5\pi\frac{0.0106}{4}\right]\varepsilon_t\right\}$$

where

$$L_{Pt} = 2\left(0.310 - 2\frac{0.0106}{2}\right) + 4\left(0.294 - 2\frac{0.0106}{2}\right)$$

$$+5\pi\frac{0.0106}{2} + \left(0.183 - 2\frac{0.0106}{2}\right) = 1.988 \text{ in.}$$

Thus,

$$\Delta R_{Pt} = 16.0966(1.774\varepsilon_a + 0.214\varepsilon_t)$$

Inserting these values into equation (2.22) yielded

$$\Delta R / R_{PdCr/Pt} = \frac{172.3896(2.909\varepsilon_a + 0.075\varepsilon_t) + 16.0966(1.77\varepsilon_a + 0.21\varepsilon_t)}{120 + 8 + 109}$$

$$= 1.009\varepsilon_a + 0.037\varepsilon_t$$

The transverse sensitivity of the gage was

$$K_{t,PdCr/Pt} = \frac{\dfrac{1.009(0) + 0.037\varepsilon_t}{\varepsilon_t}}{\dfrac{1.009\varepsilon_a + 0.037(0)}{\varepsilon_a}} = 0.0371 = 3.71\%$$

The figure-of-merit equation for transverse sensitivity was simply the ratio of the transverse sensitivities of the gage types as follows:

$$\text{FoM}\left(K_{t,i,j}\right) = \frac{\left(K_t\right)_j}{\left(K_t\right)_i} \tag{2.23}$$

where

j designator for gage type which has minimum transverse sensitivity

The figures of merit for the three gage types were DETCBCL:

$$\text{FoM}\left(K_{t,\text{DETCBCL,PdCr}}\right) = \frac{3.71}{4.16} = 0.89 \tag{2.24}$$

CKA1:

$$\text{FoM}\left(K_{t,\text{CKA1,PdCr}}\right) = \frac{3.71}{4.24} = 0.88 \tag{2.25}$$

PdCr:

$$\text{FoM}\left(K_{t,\text{PdCr, PdCr}}\right) = \frac{3.71}{3.71} = 1.00 \tag{2.26}$$

2.3.6 Methodology for Calculating Survival Rate Figures of Merit

Figures of merit were used to quantitatively evaluate strain gage performance in terms of the overall survival rate for the sum of all apparent strain, strain due to drift, and gage factor tests conducted for GWP29. Although other parameters, such as strain limit to failure, the number of failures during a low-cycle fatigue strength test, or the number of thermal and mechanical cycles to failure, may provide more detailed information on how strain gages fail, measurements of this nature were outside the scope of GWP29 and were not considered for the figure-of-merit evaluation methodology.

Several conditions can be considered a failure of a strain gage:

1. Open gage
2. Partial or complete debonding of the gage
3. Unstable or excessive drift at room temperature
4. Spikes in data that cannot be explained by data-acquisition-related causes or power supply problems
5. Gage shorted to ground
6. Partial or complete loss of temperature compensation
7. Erratic behavior at certain strain levels

For the purposes of GWP29 one type of failure was as significant as any other. No attempt was made in this methodology to distinguish between types of failure. The failures were grouped by the test in which they occurred in order that some insight might be gained into the relative strengths and weaknesses of the gage types for a particular appplication.

Mathematically, it was preferable to consider the number of gages that survived a test rather than the number that failed. The probability of a zero in the denominator was reduced because it was unlikely that all gages for all three gage types would fail during testing. Thus, the figures of merit was based on survival rate rather than on failure rate.

A general form of the equation for these figures of merit is

$$\text{FoM}\left(\mathbf{SR}_{i,j}\right) = \frac{\left(\dfrac{\text{No. of surviving gages}}{\text{No. of gages tested}}\right)_i}{\left(\dfrac{\text{No. of surviving gages}}{\text{No. of gages tested}}\right)_j} \tag{2.27}$$

where

SR survival rate

j designator for gage type for which number of surviving gages is maximum

For all GWP29 tests the same number of gages were tested for all gage types, allowing the general equation to be simplified to

$$\mathrm{FoM}\left(\mathbf{SR}_{i,j}\right) = \frac{(\text{No. of surviving gages})_i}{(\text{No. of surviving gages})_j} \qquad (2.28)$$

For each test-related parameter (i.e., apparent strain, drift, and gage factor), this equation was applied to get the following specific figure-of-merit equations:

$$\mathrm{FoM}\left[\mathbf{SR}\left(\varepsilon_{\mathrm{app}}\right)_{i,j}\right] = \frac{(\text{No. of surviving gages})_i}{(\text{No. of surviving gages})_j} \qquad (2.29)$$

$$\mathrm{FoM}\left[\mathbf{SR}\left(\varepsilon_{\mathrm{drift}}\right)_{i,j}\right] = \frac{(\text{No. of surviving gages})_i}{(\text{No. of surviving gages})_j} \qquad (2.30)$$

$$\mathrm{FoM}\left[\mathbf{SR}(\mathrm{GF})_{i,j}\right] = \frac{(\text{No. of surviving gages})_i}{(\text{No. of surviving gages})_j} \qquad (2.31)$$

where

$\varepsilon_{\mathrm{app}}$ apparent strain
$\varepsilon_{\mathrm{drift}}$ strain due to drift
GF gage factor

Also, it may be useful for the user to know an overall survival rate for each gage type. The following equation combines equations (2.29) to (2.31) to get an overall figure of merit for survival rate:

$$\mathrm{FoM}\left(\mathbf{SR}_{i,j}\right) = \frac{\left[(\text{No. of surviving gages})_{\varepsilon_{\mathrm{app}}} + (\text{No. of surviving gages})_{\varepsilon_{\mathrm{drift}}} + (\text{No. of surviving gages})_{\mathrm{GF}}\right]_i}{\left[(\text{No. of surviving gages})_{\varepsilon_{\mathrm{app}}} + (\text{No. of surviving gages})_{\varepsilon_{\mathrm{drift}}} + (\text{No. of surviving gages})_{\mathrm{GF}}\right]_j} \qquad (2.32)$$

Example 13: Four each of gage types A and B were tested for apparent strain, drift, and gage factor. Table 2.17 illustrates the survival results for the gages in each test.

TABLE 2.17.—EXAMPLE SURVIVAL DATA FOR STRAIN GAGES

Gage type	$\varepsilon_{\mathrm{app}}$	$\varepsilon_{\mathrm{drift}}$	GF	Summary
A	4/4	4/4	2/4	10/12
B	3/4	4/4	2/4	9/12

The apparent strain figures of merit were
Gage type A:

$$\mathrm{FoM}\left[\mathbf{SR}\left(\varepsilon_{\mathrm{app}}\right)_{\mathrm{A,A}}\right] = \frac{4}{4} = 1.00$$

Gage type B:

$$\mathrm{FoM}\left[\mathbf{SR}\left(\varepsilon_{\mathrm{app}}\right)_{\mathrm{B,A}}\right] = \frac{3}{4} = 0.75$$

The drift and gage factor figures of merit were all 1.00 because the same number of gages of both types survived both tests. The overall figures of merit were
Gage type A:

$$\mathrm{FoM}\left(\mathbf{SR}_{\mathrm{A,A}}\right) = \frac{(4)\varepsilon_{\mathrm{app}} + (4)\varepsilon_{\mathrm{drift}} + (2)\mathrm{GF}}{(4)\varepsilon_{\mathrm{app}} + (4)\varepsilon_{\mathrm{drift}} + (2)\mathrm{GF}} = \frac{10}{10} = 1.00$$

Gage type B:

$$\mathrm{FoM}\left(\mathbf{SR}_{\mathrm{B,A}}\right) = \frac{(3)\varepsilon_{\mathrm{app}} + (4)\varepsilon_{\mathrm{drift}} + (2)\mathrm{GF}}{(4)\varepsilon_{\mathrm{app}} + (4)\varepsilon_{\mathrm{drift}} + (2)\mathrm{GF}} = \frac{9}{10} = 0.90$$

2.3.7 Methodology for Calculating Figures of Merit for Special Case of Zero in Denominator

In the unlikely event that one gage type were to exhibit perfect behavior for a given characteristic, the mathematical problem of a 0 in the denominator could occur. Therefore, when a gage exhibited perfect behavior, it was automatically assigned a figure of merit of 1. However, all other gage types that did not exhibit perfect behavior were then forced to have figures of merit of 0, implying that their relative behaviors were the same, which may not be true. To avoid this inaccurate ranking of the other gage types, we used an additional figure-of-merit definition in this special case. The figures of merit subject to this special case included all apparent strain figures of merit (scatter, magnitude, slope, and repeatability), both drift figures of merit (rate and scatter), and gage factor scatter, slope, and repeatability figures of merit.

The general formula for determining the figure of merit for the case of a 0 in the denominator is

$$\mathrm{FoM}\left[\left\{(\varepsilon)_{i,\, j \equiv 1,k}\right\}_m\right] = 1 - \frac{\left\{g_i[\varepsilon(T,\tau,\ldots)]\right\}_m}{\left\{g_k[\varepsilon(T,\tau,\ldots)]\right\}_m} \qquad (2.33)$$

where

$\mathfrak{f}(\varepsilon)$	function derived from strain behavior, such as scatter or magnitude
$\mathfrak{g}[\varepsilon(T,\tau,\ldots)]$	function of strain behavior (e.g., difference between maximum and minimum strain magnitudes)
$j \equiv 1$	designator for gage type for which FoM is assigned value of 1
k	designator for gage type for which function $\mathfrak{g}[\varepsilon(T,\tau,\ldots)]$ indicates poorest performance of all gage types

The form of equation (2.33) suggests that this equation would yield figures of merit for all gage types, regardless of the existence of a special case. Although this is true, the figures of merit would then be scaled such that a value of 0 would indicate superior performance and a value of 1, poorest performance. As pointed out in section 2.3.1, the methodology was designed to permit summation of the figures of merit for individual characteristics into a single figure of merit for a given parameter. The easy summation of figures of merit was deemed to be more important than the use of a single figure-of-merit definition.

For each of the three gage-to-gage scatter figures of merit, apparent strain, drift, and gage factor, the use of equation (2.33) is very similar. In the special case of a gage type that does not exhibit any gage-to-gage scatter, the sample standard deviation is 0, and the difference between upper and lower 95% confidence limits is also 0. This 0 value would then appear in the denominator of the figure-of-merit equation. In this case this gage type also has to be the gage type with the minimum scatter because it is not possible to have less scatter than 0. The gage type would then be assigned a figure of merit of 1. It is evident that, as defined above, the figures of merit for any and all other gage types would be 0, even in cases of significant difference between these gages. For this special case the application of equation (2.33) is very similar for each of the three gage-to-gage scatter figures of merit (i.e., apparent strain, drift, and gage factor). Table 2.18 shows the appropriate functions inserted into equation (2.33).

In the special case of a gage type that has a perfectly flat apparent strain curve, the maximum and minimum apparent strains are both 0, and the difference between the maximum and minimum values is 0. This 0 value would then appear in the

TABLE 2.18.—SPECIAL CASE VARIABLES FOR SCATTER FIGURES OF MERIT

$$\mathfrak{f}(\varepsilon) = \begin{cases} \mathrm{SC}\left(\varepsilon_{\mathrm{app}}\right) & \text{for apparent strain} \\ \mathrm{SC}\left(\varepsilon_{\mathrm{drift}}\right) & \text{for drift strain} \\ \mathrm{SC}(\mathrm{GF}) & \text{for gage factor} \end{cases}$$

$$\mathfrak{g}[\varepsilon(T,\tau,\ldots)] = \int_{\text{lower limit}}^{\text{upper limit}} t_{0.95}\left(n_{\text{gage type}}\right) \frac{s_{\text{characteristic},n_{\text{gage type}}}(\text{unit})}{\sqrt{n_{\text{gage type}}}}$$

where

$$\text{upper limit} = \begin{cases} T_{\text{upper}} & \text{for apparent strain and gage factor} \\ \tau_2 & \text{for drift strain} \end{cases}$$

$$\text{lower limit} = \begin{cases} T_{\text{lower}} & \text{for apparent strain and gage factor} \\ \tau_1 & \text{for drift strain} \end{cases}$$

$$\text{characteristic} = \begin{cases} \varepsilon_{\text{app}} & \text{for apparent strain} \\ \varepsilon_{\text{app}} & \text{for drift strain} \\ \mathrm{GF} & \text{for gage factor} \end{cases}$$

$$\text{gage type} = \begin{cases} i & \text{for gage type } i \\ k & \text{for poorest performing gage type} \\ \mathrm{GF} & \text{for gage factor} \end{cases}$$

$$\text{unit} = \begin{cases} T & \text{for temperature} \\ \tau & \text{for time} \end{cases}$$

denominator of the figure-of-merit equation. In this case this gage type also has to be the gage type with the minimum magnitude because it is not possible to have a difference in magnitudes of less than 0. The gage type would then be assigned a figure of merit of 1. The variables to be inserted into equation (2.33) to calculate the figures of merit for the other gages for this special case are shown in table 2.19.

The use of equation (2.33) is similar for both apparent strain, gage factor slope, and drift rate figures of merit, as they are all based on generically similar derivative equations. In the special case of a gage type that has no sensitivity to temperature or time change, the average slope, or rate, would be 0. This 0 value would then appear in the denominator of the figure-of-merit equation. In this case this gage type also has to be the gage type with the minimum slope (rate) because it is not possible to have a slope (rate) with an absolute value of less than 0. The gage type would then be assigned a figure of merit of 1. The variables to be inserted into equation (2.33) to calculate the figures of merit for the other gages for these special cases are expressed in table 2.20.

The use of equation (2.33) is very similar for both apparent strain and gage factor repeatability figures of merit. In the special case of a gage type that has perfect repeatability, the deviation between half-cycles would be 0. This 0 value would then appear in the denominator of the figure-of-merit equation. In this case this gage type also has to be the gage type with the minimum deviation because it is not possible to have deviation magnitudes of less than 0. The gage type would then be

TABLE 2.19.—SPECIAL-CASE VARIABLES FOR APPARENT STRAIN MAGNITUDE FIGURE OF MERIT

$$\phi(\varepsilon) = M\left(\varepsilon_{app}\right)$$

$$g\left[\varepsilon\left(T, \tau, \ldots\right)\right] = \overline{\varepsilon}_{app,\, n,\, max} - \overline{\varepsilon}_{app,\, n,\, min}$$

TABLE 2.20. —SPECIAL-CASE VARIABLES FOR SLOPE AND RATE FIGURES OF MERIT

$$\phi(e) = \begin{cases} SL\left(\overline{\varepsilon_{app}}\right) & \text{for apparent strain} \\ M\left(\overline{\varepsilon_{drift}}\right) & \text{for drift strain} \\ SL\left(\overline{GF_{\ell}}\right) & \text{for gage factor} \end{cases}$$

$$g[\varepsilon(T, \tau, \ldots)] = \int_{\text{lower limit}}^{\text{upper limit}} \left| \left(\frac{d \text{ characteristic (unit)}}{d \text{ unit}} \right)_{\text{gage type, designator}} \right| d \text{ unit}$$

where

$$\text{upper limit} = \begin{cases} T_{upper} & \text{for apparent strain and gage factor} \\ \tau_2 & \text{for drift strain} \end{cases}$$

$$\text{lower limit} = \begin{cases} T_{lower} & \text{for apparent strain and gage factor} \\ \tau_1 & \text{for drift strain} \end{cases}$$

$$\text{characteristic} = \begin{cases} \overline{\varepsilon_{app}} & \text{for apparent strain} \\ \overline{\varepsilon_{app}} & \text{for drift strain} \\ \overline{GF_{\ell}} & \text{for gage factor} \end{cases}$$

$$\text{gage type} = \begin{cases} i & \text{for gage type } i \\ k & \text{for poorest performing gage type} \end{cases}$$

$$\text{unit} = \begin{cases} T & \text{for temperature} \\ \tau & \text{for time} \end{cases}$$

TABLE 2.21.—SPECIAL-CASE VARIABLES FOR REPEATABILITY FIGURES OF MERIT

$$\natural(e) = \begin{cases} \mathbf{R}\left(\overline{\varepsilon_{app}}\right) & \text{for apparent strain} \\ \mathbf{R}\left(\overline{GF_\ell}\right) & \text{for gage factor} \end{cases}$$

$$g[\varepsilon(T, \tau, \ldots)] = \int_{T_{\text{lower limit}}}^{T_{\text{upper limit}}} \left| \overline{\text{characteristic}_{n,m_1}}(T) - \overline{\text{characteristic}_{n,m_2}}(T) \right|_{\text{gage type}} dT$$

where

$$\text{characteristic} = \begin{cases} \overline{\varepsilon_{app}} & \text{for apparent strain} \\ \overline{GF_\ell} & \text{for gage factor} \end{cases}$$

$$\text{gage type} = \begin{cases} i & \text{for gage type} \\ k & \text{for poorest performing gage type} \end{cases}$$

assigned a figure of merit of 1. The variables to be inserted into equation (2.33) to calculate the figures of merit for the other gages for these special cases are expressed in table 2.21.

References

2.1 INCO: High Temperature High Strength Nickel Base Alloys. International Nickel Company, Inc., New York, 1977.

2.2 Belfour Stulen, Inc.: Aerospace Structure Metals Handbook. Mechanical Properties Data Center, Traverse City, Michigan, 1978.

2.3 Salem, J.A.; Lerch, B.A.; and Lei, J.-F.: Mechanical Behaviors of a 16-Ply Quasi-Isotropic SCS–6/β-21S TMC. NASP TM–1174, 1994.

2.4 Spiegel, M.R.: Schaum's Outline of Theory and Problems of Statistics. McGraw-Hill, New York, 1961.

2.5 Murray, W.M.; and Stein, P.K.: Strain Gage Techniques: Fundamentals (July 9–13, 1962), Applications (July 16–20, 1962). Massachusetts Institute of Technology, 1962.

Chapter 3

Test Equipment and Operational Procedures

3.1 Specimen Preparation

3.1.1 Strain Gages and Attachments

3.1.1.1 Langley.—Detailed here are the procedures for installing the Langley high-temperature gage, including the attachment of the lead wires to the gage.

Design and specifications: A serious concern for the user of high-temperature strain gages is the large magnitude of the apparent strains typically associated with the commercially available gages. This concern was the primary driver in the design of the Langley gage. The large apparent strains in single-element gages can be reduced by using a two-element, half-bridge configuration for making strain measurements. The Langley design employs an active element bonded to the surface to be measured and an inactive or "compensating" element that is not bonded to the surface. This element, therefore, will be insensitive to strain. The Langley two-element gage is designed with the compensating element surrounding the active element on three sides. Both elements are installed on an aluminum oxide base coat at the same time. The active element is flame sprayed in place whereas the compensating element is only tack bonded in such a manner that it cannot respond to actual surface strains. The dimensions and basic configuration of both elements of the gage are shown in section 2.3.5.2 (fig. 2.20). As shown, the elements are not yet wired together to form the half-bridge, allowing for ease in making electrical checks of each individual element. Following these checks the gage is wired to a three-lead-wire system to form the half-bridge. The Wheatstone bridge wiring configuration is illustrated in section 3.2.3 (fig. 3.12). Figure 3.12(b) shows how the gage was modified to include a length of platinum wire. The wire was used only with the gages on the TMC test coupons to correct for the mismatch in expansion coefficients of the gage alloy and the TMC. This piece of wire was not bonded to the substrate; therefore, it was not subjected to mechanical strains. Early prototypes of the Langley gage included two-element gages made with the Chinese Alloy, the BCL–3 alloy, and a foil version of the Langley-designed half-bridge furnished by Micro-Engineering, Inc. Insufficient funding prevented BCL–3 from being the alloy of choice. Early testing of the foil version of the compensated half-bridge generated excellent data, but repeated excursions to 1500 °F (815 °C) appeared to degrade the gage more rapidly than the wire versions. Kanthal A1 was selected for the gage elements for three reasons: (1) It has an operating range up to 1500 °F (815 °C); (2) gages manufactured from this alloy are relatively inexpensive; and (3) the wire necessary to make the gages was readily available as well as affordable.

Installation procedures: The following basic steps were developed and used at Langley for installing compensated strain gages on IN100 and β-21S TMC surfaces. No effort was made here to describe the details for using the spray gun. Working distances between the spray gun and the surface to be gaged, the number of passes over the area being sprayed, settings for the spray equipment, and other gaging installation steps using thermal spray equipment are all experience driven. A more detailed description of the installation procedures is obtainable from JP Technologies, Inc., and Advanced Hi-Temp Strain Sensors, Inc., manufacturers of the gage.

1. Locate the area where the strain gages are to be installed and clean with an appropriate degreaser.
2. Mask around the area to be gaged; then microgrit blast the open area within the masking with 50-μm aluminum oxide (Al_2O_3) abrasive powder. This step removes any surface coatings or surface oxidation while providing a uniformly textured surface, which is beneficial (visually) during the coarse-grit blasting step.
3. Coarse-grit blast the microgrit-blasted area with a #30-grit silicon carbide abrasive powder to generate a coarse texture for the later thermal spraying operations.
4. Remove the masking tape and clean the area with an appropriate surface degreaser.
5. Remask around the grit-blasted area.
6. Plasma spray a base coat of Al_2O_3 onto the grit-blasted surface within the masked area. This first layer of gaging base coat should be approximately 0.001 in. thick.

Note: The initial base-coating step (step 6) with plasma-sprayed Al_2O_3 is optional, but fewer gage failures on TMC have been observed at 1500 °F (815 °C) when this technique has been employed.

7. To complete the base coat, apply a second coat of Al_2O_3 to the initial base coat (step 6) using a Rokide flame spray gun. This layer of Al_2O_3 plus the original layer should total approximately 0.003 in. thick.
8. Position and secure the pair of gages (active and compensating) with their top carrier and subcarrier to the Al_2O_3 base coat.

9. Initial bond the partially exposed active gage convolutes, the exposed gage ribbons, and the exposed tack-bonded areas of the compensating gage (fig. 3.1) with a Rokide gun. Keep the amount of Al_2O_3 to a minimum.

10. Carefully remove the top carrier and subcarrier tape segments from the active gage. With this done, inspect and remove any ridges of Al_2O_3 that may have formed adjacent to the carrier tape strips. An Al_2O_3 abrasive stone or a pointed diamond file can be employed for this task. Figure 3.2 is a closeup of the gage ready for final flame spraying.

11. Final bond the active gage using the Rokide gun. Using Al_2O_3 rods of the same type used for the initial bonding of the gage convolutes, flame spray all exposed areas, making certain to cover the entire gage. Keep the total Al_2O_3 thickness to a minimum. A typical completed installation should be approximately 0.015 in. thick.

12. Remove the remaining top carrier, being careful to ensure that the subcarrier remains in place.

Note: Steps 13 to 16 are optional. These steps detail the procedure for adding a "window-frame border" of Al_2O_3 around the entire installation to minimize the temperature difference between the active gage and the compensating gage when fast heatup rates or airflows are expected. This window-frame border is actually a ridge of Al_2O_3 that forms a boundary for the thermal blanket.

13. Remove 0.100 in. of the subcarrier tape from the lead-wire end of the gages. Also, remove 0.030 in. (this dimension may be revised depending on the overall width of the carrier tape furnished with the gages) from the remaining three sides (outside perimeter) of the subcarrier tape to expose the base coat of Al_2O_3 and allow for the forming of the window-frame border.

14. Add two layers of high-temperature tape around the perimeter of the subcarrier tape, leaving a 0.030-in. gap on all four sides. Also, add two layers of high-temperature tape over the subcarrier tape, cut to the same size as the subcarrier tape (fig. 3.3).

15. Using Rokide, flame spray the 0.030-in. perimeter gap until the Al_2O_3 fills the gap to the top of the tape, completing the formation of the window-frame border (ridge of Al_2O_3).

16. Remove all added tape, being careful not to disturb the subcarrier tape.

17. *Carefully* remove the individual segments of the subcarrier tape. Compensating gage convolutes must be kept flat against the base coat. Figure 3.4 shows the installed gage after all tape has been removed. This gage is now ready for the thermal blanket, which is also shown in the photograph.

18. Install the thermal blanket. The thermal blanket consists of a sheet of Nextel 312 cloth, 0.010 in. thick, which has had its

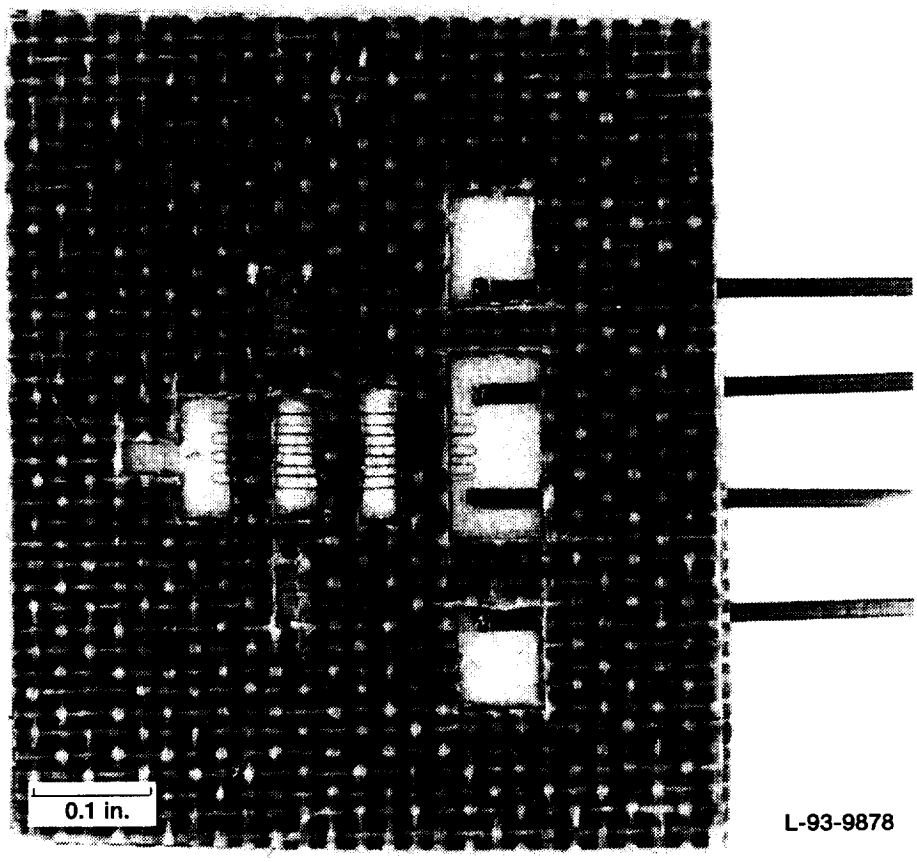

Figure 3.1.—Closeup of CKA1 gage ready for installation.

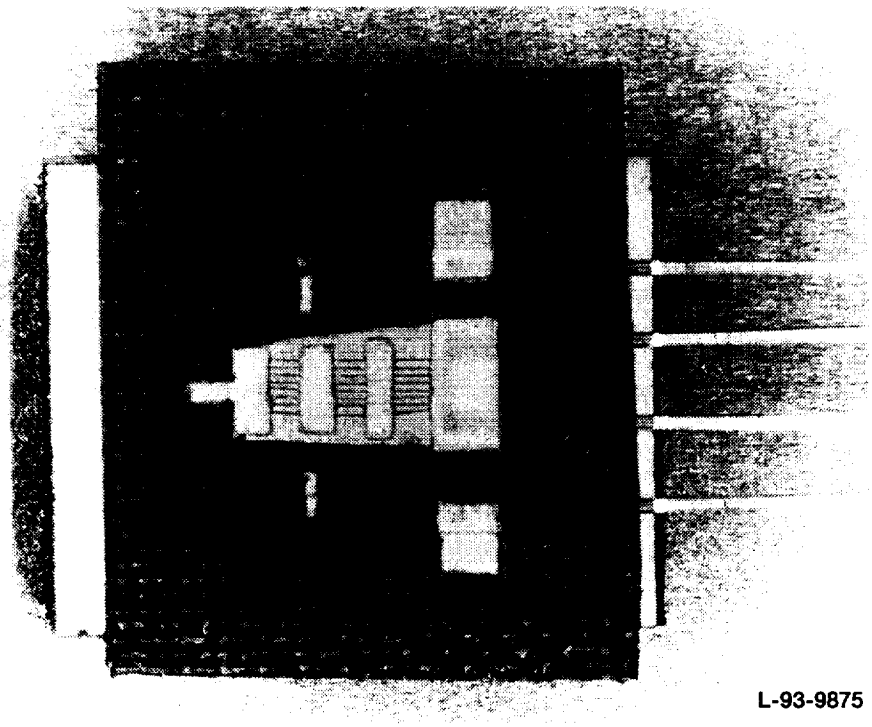

Figure 3.2.—Closeup of CKA1 gage following initial flame spray operation.

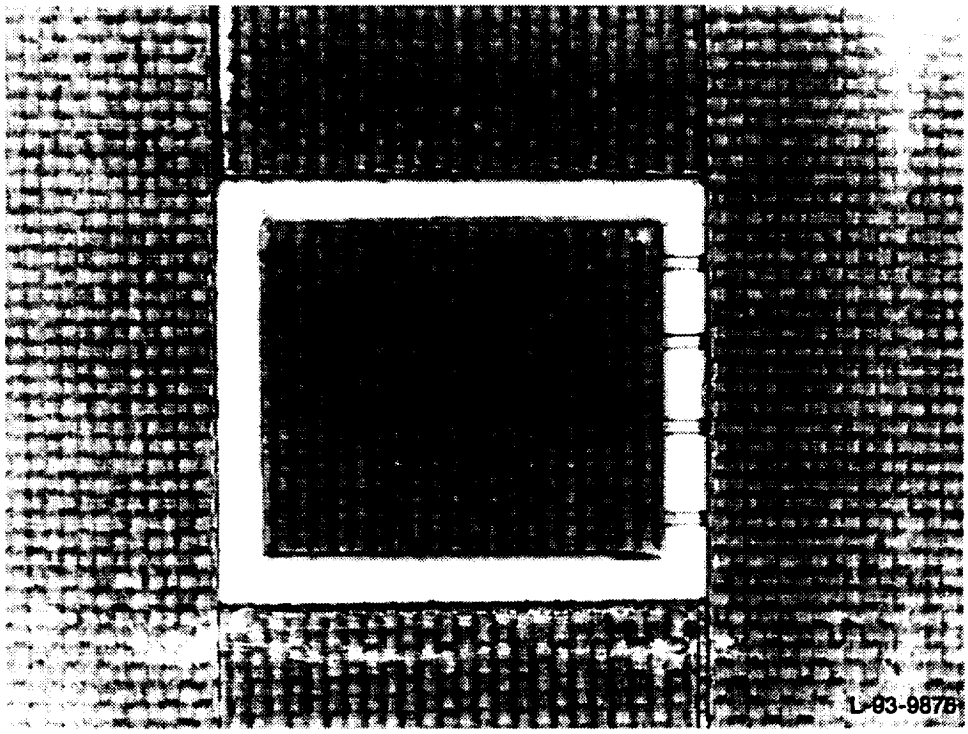

Figure 3.3.—Gage masking for Al_2O_3 around perimeter of installed CKA1 gage.

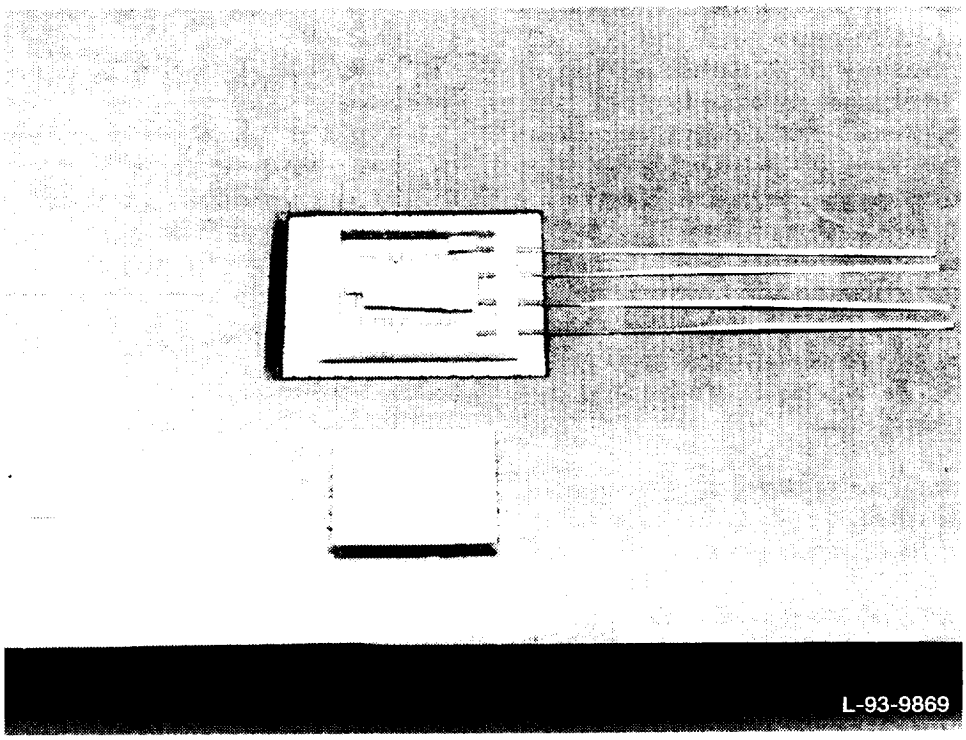

Figure 3.4.—Installed CKA1 gage showing exposed compensating element and thermal blanket.

top surface flame sprayed with a 0.005-in.-thick layer of Al_2O_3. The blanket should be cut to fit within the confines of the window-frame border (when a border is used).

19. Secure the thermal blanket with spotwelded straps or ceramic cement.

20. The installation is now ready for its final electrical checks and lead-wire hookup.

Lead wires: The Langley gage is a two-element gage designed such that one element is in each adjacent arm of a Wheatstone bridge circuit. A typical three-lead-wire system works well for the hookup of the two gage elements. Following electrical checks of each individual gage element, the gage elements are wired in adjacent arms of a Wheatstone bridge circuit configuration to form a half-bridge. This hookup is shown in section 3.2.3 (fig. 3.12). As shown, one ribbon from each gage is spotwelded to one of the three lead wires. The other ribbon from each of the gages is spotwelded (one each) to the remaining two lead wires to form a two-arm half-bridge with one active gage and one compensating gage. The actual spotwelding of the gage ribbons to the lead wires uses a technique developed by Dryden in which the ribbon wraps around the lead wire so that one spotwelder probe contacts the ribbon while the other spotwelder probe contacts the lead wire. The probes are maintained in intimate contact with the ribbon and lead wire as the junction is being spotwelded. Identical three-lead-wire systems used by all three centers for this program consist of a braided three-conductor cable. Each conductor is a Hoskins 875 (FeCrAl) wire, AWG #25, insulated with Rayon-served Nextel 312 braiding. An additional braiding over the three braided conductors is also Rayon-served Nextel 312. All strain gage cables are "heat cleaned" for 1 hr at 1000 °F (540 °C) before installation on the test coupons and test beams.

3.1.1.2 Lewis.—The free-filament PdCr wire gage was mounted on the test article by using a flame spray technique described here. The installation technique for this gage is described in detail in reference 3.1.

1. Lightly grit blast the gage bonding area to remove the existing surface oxide and then clean with solvent.

2. Mask the gage bonding area perimeter with flame spray masking tape. Tape must be well bonded to the surface to prevent tape lifting by heat from the flame spray process. Apply a 50- to 76-μm (2- to 3-mil) thick nickel aluminide coating to the substrate as the bond coat. If the substrate is less than 3.2 mm (1/8 in.) thick, use cooling air during the coating process to prevent heat from distorting the parts. The cooling air must be desiccant filtered to remove all oil; otherwise, an oil-less air compressor should be used. Remove masking tape and gently run an industrial razor over the coating to remove any loose particles. A clean wire brush may also be used to gently remove any loose particles.

3. Remask using flame spray masking tape. Place the tape exactly at the edge of the nickel aluminide bond coat. Apply a 50- to 76-μm (2- to 3-mil) Al_2O_3 precoat over the bond coat. Examine the coating under a microscope to be sure that it is continuous.

4. Hold the gage in position with tweezers and press the gage down onto the precoat with the tape carrier.

5. Apply a coating mixture of Al_2O_3 and zirconium oxide (Zr_2O_3), which provides oxidation protection for the gage, to the open areas between the strips. Hold the spray gun perpendicular to the gage surface at about 25-cm (10-in.) distance, and apply a tack coat with rapid passes. The gage grid temperature should not exceed 390 °F (200 °C), and the gage grid should return to room temperature before the next pass.

6. Remove all perimeter tape with sharp tweezers. Examine the gage carefully and remove any debris with an artist's brush.

7. Remask with a single layer of the tape and apply a final Al_2O_3 mixture overcoat. Remove all the tape and dress any sharp corners with an Al_2O_3 stone.

Because both PdCr and platinum are very sensitive to impurities such as aluminum and silicon, care must be taken during handling and each installation step to protect the gage from contamination.

3.1.1.3 Dryden.—Dryden tested three candidate strain gages, all based on the BCL–3 alloy. The first gage was the standard BCL gage, the second was a heat-treated version of the standard BCL gage, and the third was the dual-element, temperature-compensated BCL gage (DETCBCL). Using an early version of the figure-of-merit methodology described in section 2.3, the DETCBCL was selected for this study. See section 1.4.3 for a description of the DETCBCL.

Dryden developed the following general step-by-step procedure for installing the DETCBCL gage. The installations on β-21S TMC did not use either a bond coat or a graded layer; therefore, steps 11 to 14 were performed only on gages installed on IN100 specimens.

1. Degrease the entire specimen with Micro-Measurements CSM–1 or equivalent.

2. Mask an area of the specimen to be instrumented, using CHR Industries A2008 Teflon-impregnated tape or equivalent.

3. Degrease the specimen area to be instrumented with methyl ethyl ketone (MEK).

4. For specimens thinner than approximately 1/16 in., microgrit blast the specimen surface to remove any oxidation or contaminants in order to minimize the time spent coarse-grit blasting the specimen surface.

5. Coarse-grit blast the area to be gaged with –30, +200 mesh (54 grit), brown, fused Al_2O_3 at a pressure sufficient to clean and abrade the surface but not so high as to embed abrasive particles in the material. For metals this generally would be 40 to 70 psi (55 psi was used).

6. Remove the Teflon tape.

7. Blast with filtered air at 60 psi or higher (90 psi was used).

8. Degrease the specimen area to be instrumented with MEK.

9. Remask the grit-blasted area with Teflon tape.

10. Measure the specimen thickness in the grit-blasted area with a micrometer.

11. Plasma-arc spray a 4-mil-thick coating of 80/20 Nichrome (e.g., Metco 461).

12. Measure the specimen thickness after spraying to verify actual coating thickness.

13. Plasma-arc spray a 4-mil-thick coating of a 50/50 (by volume) homogeneous mixture of 80/20 Nichrome (Metco 461) and Al_2O_3 (e.g., Metco 105NS) on top of the Nichrome coating.

Note: Steps 11 and 13 are required when using gages on nickel- or cobalt-based substrates at temperatures above 1400 °F (760 °C). Different bond coat materials and graded layer materials are required for different substrate materials. The selection of these materials depends on the match of coefficient of thermal expansion to the substrate material.

14. Measure the specimen thickness again to verify the thickness of the Nichrome/Al_2O_3 coating.

15. Remove the Teflon tape.

16. Mask off an area not less than 5/8 in. × 1/2 in. (actual dimensions depend on the gage configuration) with Teflon tape at the specified locations.

17. Apply a 4-mil-thick coating of Al_2O_3, using the Rokide flame spray process.

18. Measure the specimen thickness again to verify the thickness of the Al_2O_3 coating.

19. Establish the precise location and alignment of the gage with a non-graphite-based colored lead pencil by putting alignment marks outside the Rokide-coated area and never in the area occupied by the gage filament.

20. Carefully remove the gage from the glass slide.

21. Carefully position the gage on the specimen with respect to the location markings.

22. Mask off the remaining areas of the substrate not covered by the carrier tape.

23. Smooth down the tape by pressing firmly, making certain that the tape edges are "down."

24. Apply the tack coat by flame spraying through the windows left by the strips of tape, using the Rokide process. The tack coat is of proper thickness when gage filaments are slightly visible through the coating.

25. Mask the upper portion of the gage with Teflon tape, leaving the ribbon area exposed.

26. Rokide a thicker tack coat onto the ribbons until the "button" is flush with the tape surface.

27. Carefully chip away any alumina that has bridged from the button to the tape and round all sharp corners of the Al_2O_3 to avoid strain concentrations.

28. Carefully remove the strips of tape by folding one end of the strip back over the gage at a low angle, pulling the tape across the gage while keeping it as close to the specimen as possible.

29. Verify, if applicable, that the ends of the compensating element end loops are flush to the Rokide surface.

30. Remask the gage area, leaving the entire gage exposed.

31. Rokide the final coat. The coat should be sufficient to just encapsulate the gage wires but not thicker.

32. If needed, mask off the upper portion of the gage with Teflon tape. Rokide the heavier final coat to the ribbons to securely anchor them. This will require a heavier coat than used to just encapsulate the gage filaments.

33. Remove all masking tape.

34. Knock down all sharp edges and corners of the Al_2O_3 with an Al_2O_3 stone.

3.1.2 Thermocouples and Attachments

All thermocouples were made of AWG #28, type K, magnesium-oxide-insulated, Inconel 600, sheathed, 0.63-in.-outside-diameter cable. The procedure for attaching thermocouples was as follows:

1. Strip sheath and insulation back 0.50 in. (plus 0.03 in., minus 0) from each end of the cut thermocouple cable. Seal the exposed ends of the cable with a moisture-proof coating, such as Micro-Engineering, Inc., Gagekote 1 or alternative.

2. Install miniature type K thermocouple connectors on one end of the cut thermocouple cable before shipping completed coupons and load bars to the other centers. Excess conductor material may be cut off the end of the stripped wire so that it will fit in the connector properly. It is suggested that the connectors be installed before attaching the thermocouple to the coupon or load bar in order to minimize handling of coupons and load bars once the gages are installed.

3. Use intrinsic thermocouple junctions for all thermocouples on all coupons and load bars. (An intrinsic junction is formed by separately attaching the two thermocouple wires to the substrate: they do not contact one another except through the substrate.)

4. Separate the centerlines of the two thermocouple wires by 0.025 in. at the thermocouple junction.

5. Make strain relief loops when installing thermocouple junctions. Thermocouple wires should exit straight from the cable for approximately 0.10 in. Make a loop in each thermocouple wire starting at 0.10 in. This loop should reach no more than 0.10 in. above the coupon surface at a distance of 0.15 in. from the cable end and finish 0.20 in. from the cable end. At this distance the thermocouple junction is formed (fig. 3.5).

6. Attach thermocouple wires to the substrate by spotwelding. A combination of 10 W-sec at 10-lb electrode force on a Measurements Group, Model 700 portable strain gage welding/soldering unit is recommended for welding both Chromel and Alumel leads to β-21S TMC. These weld schedules may vary depending on the welding equipment.

7. Use two welds on each thermocouple wire. The first weld is 0.20 in. from the end of the cable. Cut excess material off so that the second weld is 0.05 in. from the first weld. Make this second weld with enough force on the electrode to flatten the end of the wire (fig. 3.6).

8. Use Inconel 600 straps for staking thermocouple cable to the surface of the IN100 and β-21S TMC load bars and coupons. The weld schedules for joining these materials are 12 W-sec/10 lb for Inconel 600/IN100 and 20 W-sec/10 lb for Inconel 600/β-21S TMC. These weld schedules may vary depending on the welding equipment.

9. Completely cover spotwelded thermocouple junctions with Rokide. The edge of the Rokide coating should be 0.25 in. from the lines formed by the welds (fig. 3.7).

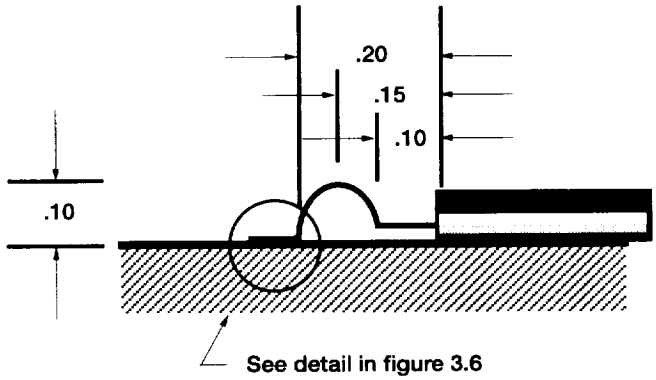

Figure 3.5.—Thermocouple installation with strain relief loop. (Dimensions are in inches.)

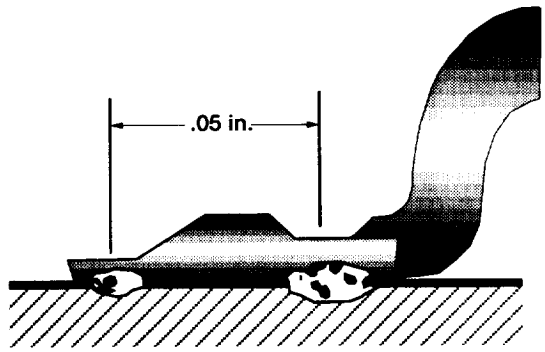

Figure 3.6.—Relative locations of thermocouple spot welds.

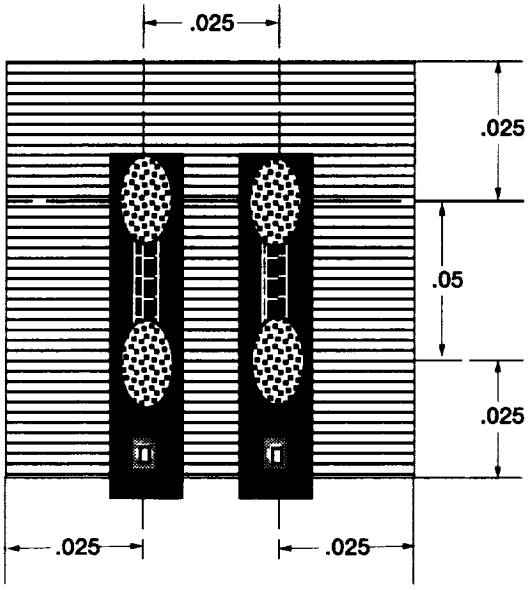

Figure 3.7.—Top view of thermocouple installation showing relation to Rokide coating. (Dimensions are in inches.)

3.2 Langley Test Equipment and Operational Procedures

The test equipment, procedures, and data acquisition system described here were used at the Langley Research Center in gage performance characterization testing for this work package and in testing the three GWP29 gages.

3.2.1 Test Equipment

Specifically designed equipment was used for each of the three types of test that Langley performed on the three GWP29 gages (i.e., apparent strain, drift strain, and gage factor). This equipment is listed below. The data acquisition system shown in the equipment photographs is described in section 3.2.3.

3.2.1.1 Apparent strain test apparatus.—The following apparatus (figs. 3.8 and 3.9) was used for conducting the apparent strain runs:

1. IN100 test coupons, three each
2. β-21S TMC test coupons, three each
3. Applied Test Systems (ATS) Series 3350 furnace

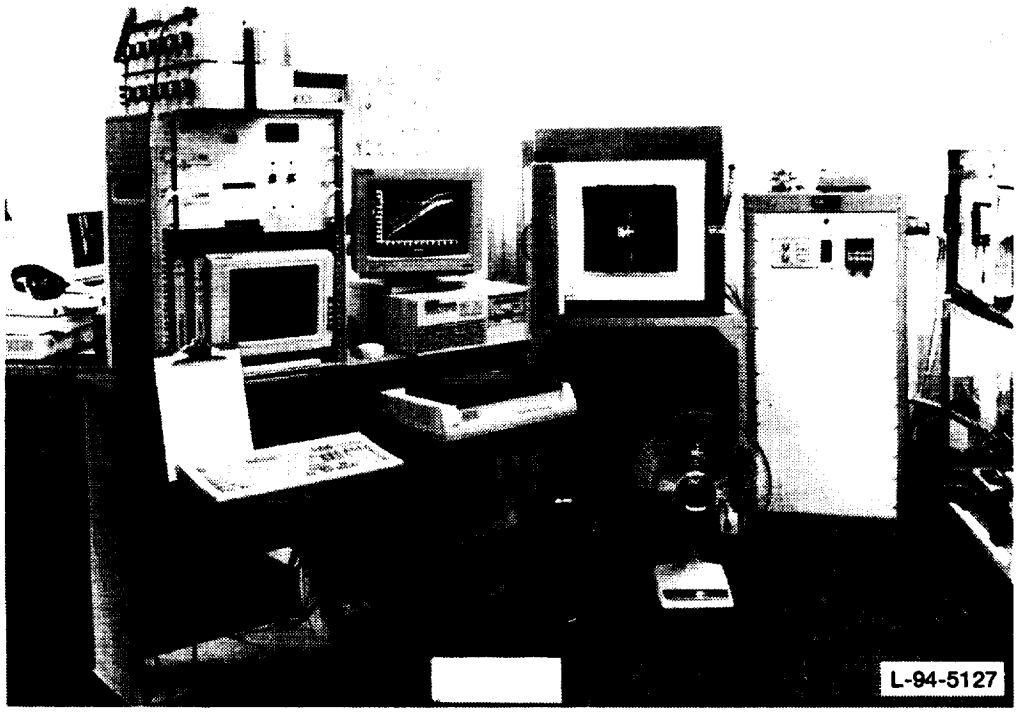

Figure 3.8.—Langley apparent strain test chamber and data acquisition system.

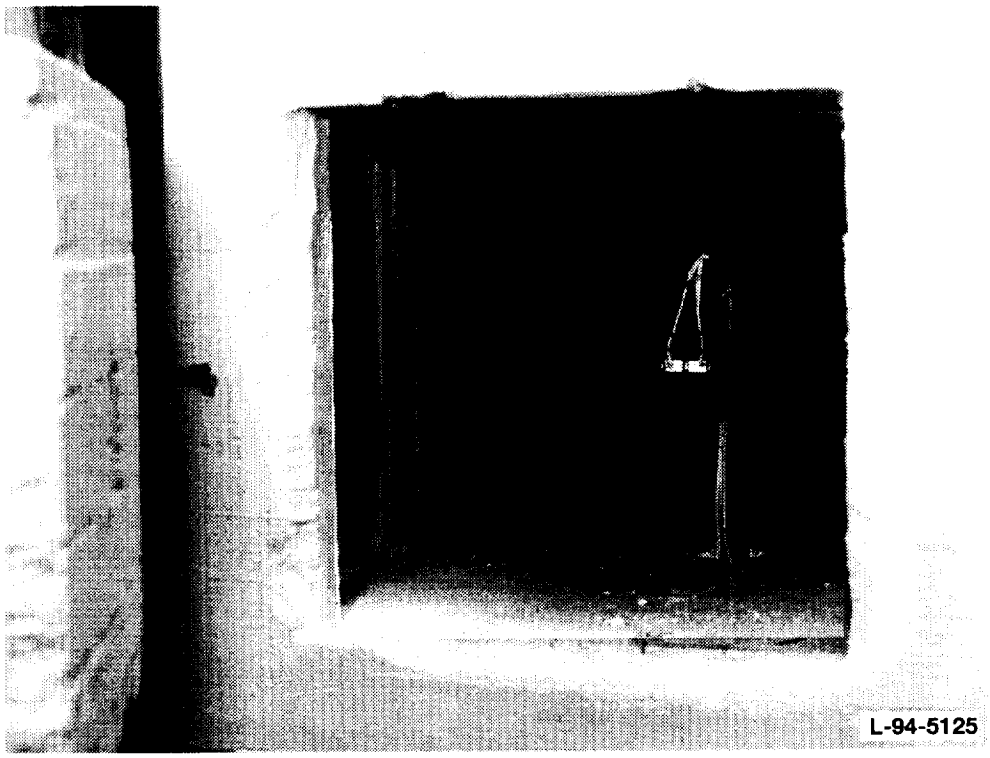

Figure 3.9.—Closeup of Langley apparent strain test chamber with radiant heat cover around test coupon.

4. ATS two-zone furnace controller with RS/232 compatibility
5. IBM PC/AT for temperature control programming
6. Two-piece radiant heat cover (figs. 3.8 and 3.9).

3.2.1.2 Drift strain test apparatus.—The following apparatus (fig. 3.10) was used for conducting the drift strain runs:

1. IN100 test coupons, three each
2. β-21S TMC test coupons, three each
3. ATS Series 3150 furnace
4. ATS furnace temperature control system

3.2.1.3 Gage factor test apparatus.—The following apparatus (fig. 3.11) was used for conducting the gage factor tests:

1. IN100 tensile load bars, three each
2. β-21S TMC tensile load bars, three each
3. ATS Series 3210 split-tube furnace
4. ATS three-zone furnace controller
5. Materials Test Systems (MTS) Model 810 tensile load machine
6. MTS Model 458.20 microconsole
7. MTS Model 647 hydraulic wedge grips
8. MTS Model 609.10A–01 alignment fixture
9. Steel calibration load bar

3.2.2 Operational Test Procedures

The test procedures described here were incorporated into apparent strain, drift strain, and gage factor testing at Langley. Operational procedures for the three types of test are described individually.

3.2.2.1 Apparent strain test procedures.—At Langley each apparent strain coupon was placed in the ATS furnace (Series 3350) and suspended by the strain gage and thermocouple cables so that the coupon was in a strain-free position. A two-piece metal shield was then placed around the coupon to assist in providing a uniform heating and cooling environment for the coupon during the test. Twelve apparent strain runs were conducted for each coupon. The heatup rates, cooldown rates, and maximum temperature for each of the 12 cycles are listed in chapter 2. Using the IBM PC/AT, a program was written to accommodate the various heatup and cooldown rates required for the apparent strain runs. The capability of the program to provide the rates required was tested on spare coupons before commencing the actual runs. Because of the mass of the furnace used for these apparent strain tests, forced-air cooling was incorporated for certain rapid cooldown portions of some runs. The electrical hookup for the gages and the thermocouples is described in section 3.2.3.

3.2.2.2 Drift strain test procedures.— At Langley each drift strain coupon was placed in the ATS furnace (Series 3150) and

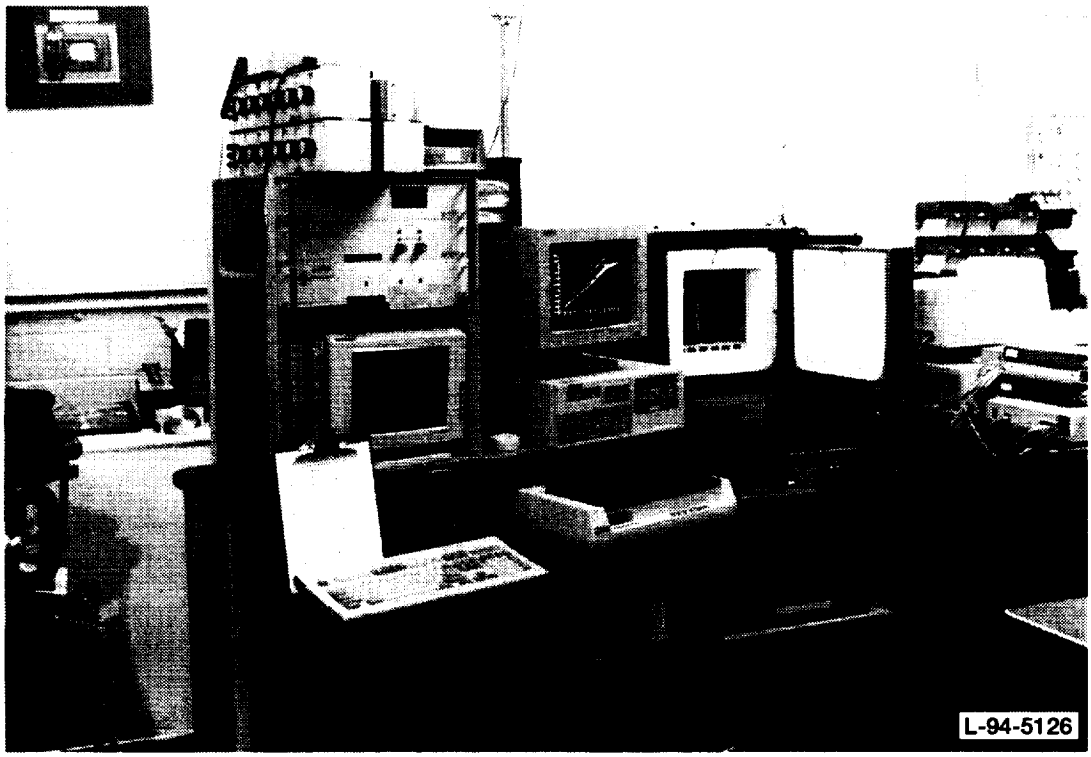

Figure 3.10.—Langley drift strain test chamber and data acquisition system.

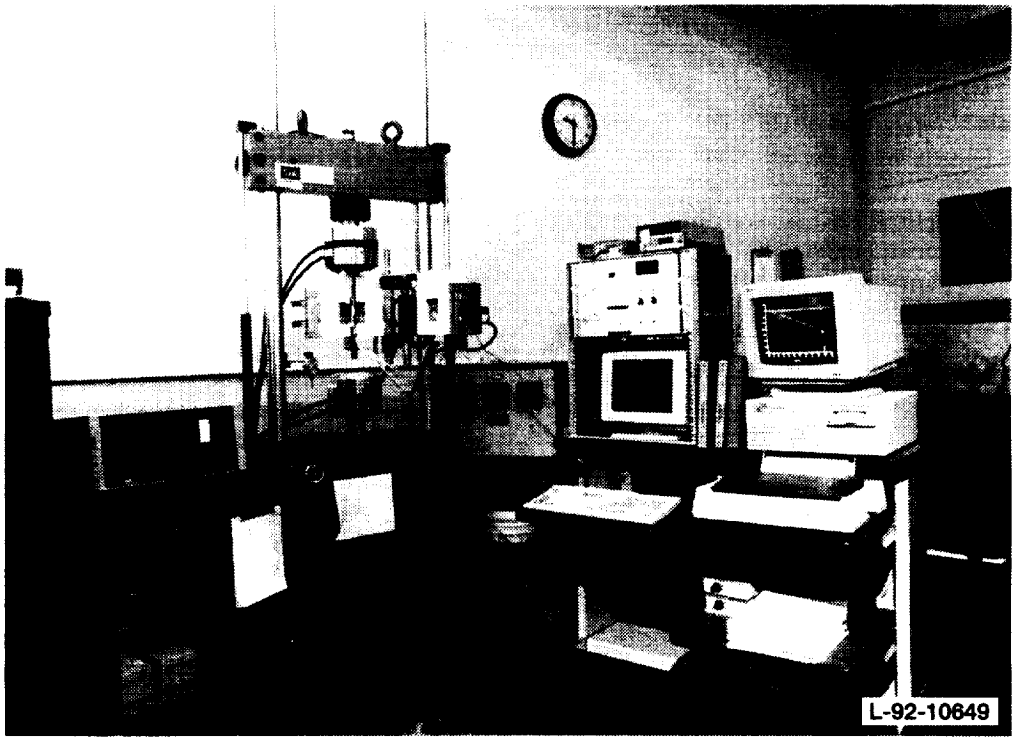

Figure 3.11.—Langley high-temperature tensile load machine and data acquisition system.

suspended by the strain gage and thermocouple cables so that the coupon was in a strain-free position. For each drift strain test the coupon was heated to the desired test temperature, stabilized with respect to uniform temperature, soaked for 4 hr at that temperature, and then cooled to room temperature. This procedure was repeated at seven different temperatures ranging from 600 to 1500 °F (315 to 815 °C). Because of the mass of the furnaces used at Langley and Lewis, a considerable amount of time was required to stabilize the coupon temperature at each of the designated test temperatures. The type of furnace used by Dryden could stabilize the coupon temperature in a much shorter time. Therefore, the gages tested at Langley and Lewis were subjected to a longer soak time *at almost* the designated test temperature before testing. Because of the difference in time required to heat the coupons, the shape and slope of the drift strains for a given gage type may have differed when comparing drift strain data from Langley and Lewis with those from Dryden for a given test. The electrical hookup for the gages and the thermocouples is described in section 3.2.3.

3.2.2.3 Gage factor test procedures.—Each of the three centers participated in the gage factor testing. Langley tested the same gage types and materials as Lewis and Dryden. However, because of equipment constraints the gage factor testing at Langley was conducted on IN100 and β-21S TMC tensile load beams, whereas Lewis and Dryden generated gage factor characterization on beams in a bending configuration. Therefore, the Langley gage factor data were obtained on gages in a tension direction only. Before testing, a steel calibration load bar was strain gaged with 12 conventional gages configured to provide a means of verifying the test beam alignment in a bend-free tensile mode. This calibration bar was fabricated with the same geometry as that of the beams to be tested. A MTS Model 609 alignment fixture was used to accurately align the clamping grips for the tension tests. Once accurate alignment had been assured, the calibration load bar was loaded to the strain levels specified. The deflection was recorded for these levels and then used for applying the required strains at the various test temperatures. Once the setup was completed, the load beams were tested with the three gage types from the three centers. Each beam was placed in the grips, with the upper end of the beam clamped in the top grip. Zeros and gage resistances were then recorded. Next, the bottom end of the beam was clamped in its grip and electrical gage checks were again conducted. The test was then begun. A predetermined tare was applied and the specified strains were then generated. This procedure was repeated at each test temperature for each material.

3.2.3 Data Acquisition System

A single stand-alone, preprogrammed data acquisition system was used for the three types of test conducted on the three types of GWP29 gage. It contains a personal computer, a controller (interface between the computer and the scanners), a strain gage scanner, a thermocouple scanner, and a universal scanner. This Measurements Group, Inc., System 4000 was used by Dryden and Langley for these tests. This unit and its accompanying data analysis electronics are described here after the Wheatstone bridge circuit configuration used for each of the three gage types is reviewed.

3.2.3.1 Wheatstone bridge circuit configurations.—The Langley CKA1 gage was a two-element gage configuration with one active gage element (strain sensitive) and one compensating gage element (unbonded and insensitive to strain). These two elements were wired in adjacent arms of a four-arm Wheatstone bridge circuit forming a half-bridge (fig. 3.12(a)). One ribbon from each of the gage elements was spotwelded to the three-external-lead-wire attachment point near the gages. This lead-wire system was then connected to a half-bridge completion network in the System 4000 data acquisition system, forming the classic Wheatstone bridge circuit. A length of platinum wire was added to the group of Langley gages installed on the β-21S TMC coupons to minimize the total apparent strain generated with these gages on that particular material. This wire was added to the active gage element in such a way that it was not bonded to the surface and was insensitive to strain. Its wiring configuration is illustrated in figure 3.12(b).

The Lewis PdCr gage (fig. 3.13) was a single-element active gage with a compensating resistor in an adjacent arm of the bridge circuit. Because the compensating resistance was nominally 15 Ω, an additional ballast resistance was added externally to balance this half of the Wheatstone bridge circuit. The compensating resistor was fabricated as part of the gage and was bonded to the surface along with the active single element. The three wires exiting the gage were configured such that one provided a hookup to one of the bridge completion resistors, one provided a hookup to the ballast resistor, and the third was routed to the signal readout. The ballast resistance value for each gage tested was provided by Lewis. After hookup (fig. 3.13) this Wheatstone bridge circuit was connected to the System 4000 data acquisition system.

The Dryden DETCBCL gage (fig. 3.14) was a dual-element gage. The primary active element was of BCL–3 alloy. In series with this element a platinum element served as an apparent strain compensator. The compensating element was positioned in the gage center among the BCL–3 convolutes. It was fabricated as part of the gage and subsequently bonded to the test coupon along with the active gage element. The strain gage ribbon shown on the left-hand side of the figure was not hooked up electrically to any external lead wires. Thus, the platinum element was in series with the gage. This dual-element gage formed one arm of a Wheatstone bridge circuit. A standard three-lead-wire attachment to the two gage ribbons provided the quarter-bridge hookup to the System 4000 data acquisition system.

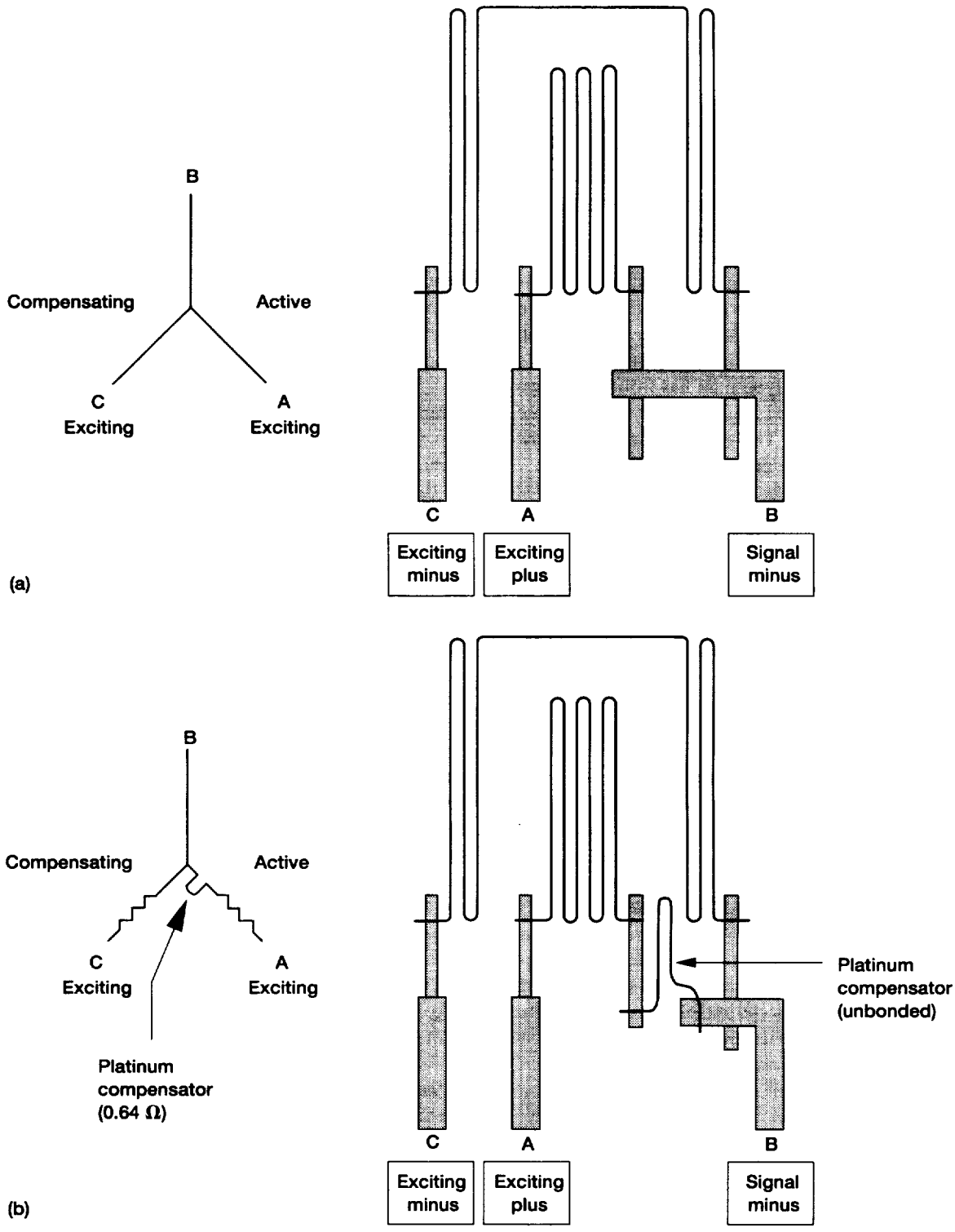

Figure 3.12.—Wiring configuration for Langley CKA1 gage (half-bridge). (Note: When polarities are utilized as shown, an up-scale reading will result with a tension load applied to the active gage.) (a) On IN100. (b) On β-21S TMC.

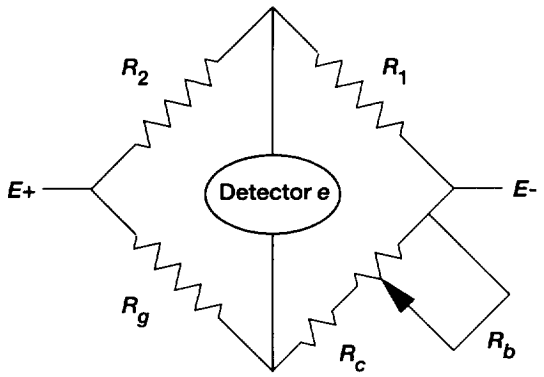

Figure 3.13.—Wiring configuration for Lewis PdCr gage. (Strain gage resistance R_g; compensating gage resistance, R_c; ballast resistance, R_b; bridge completion resistors, R_1 and R_2.)

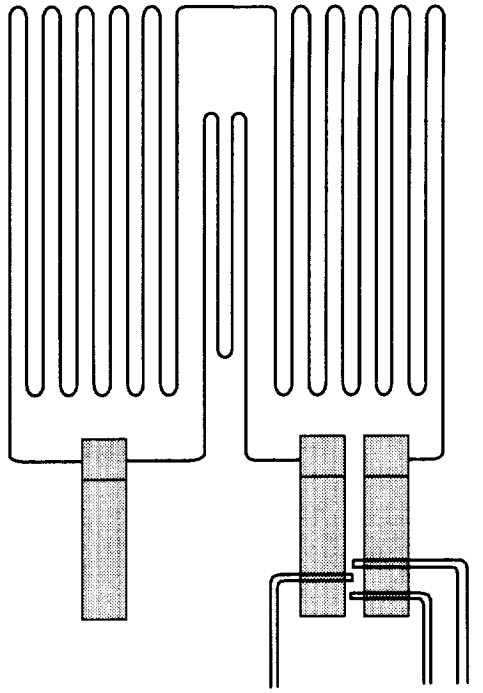

Figure 3.14—Wiring configuration for Dryden DETCBCL gage (dual element, temperature compensated).

3.2.3.2 Strain and thermocouple data measurement system.—All strain and temperature data were recorded with the System 4000. Strain gage connections to the system were made in accordance with the respective Wheatstone bridge configurations described previously. For the Lewis gages precision trim pots and resistance boxes were also used. The resistance values used with these gages were designated by Lewis. All thermocouples used in the gage testing were type K. The electrical hookup was directly to the System 4000 thermocouple scanner.

3.2.3.3 Data analysis system.—In conjunction with the System 4000, additional electronics were used in processing and analyzing data, generating plots and tables, and providing documentation for this program. Included were a Hewlett-Packard Laserjet IIIP printer for the data records from System 4000, an IGOR program for data analysis, a Macintosh Centris 650 personal computer for data entry to IGOR, a Macintosh Laserwriter Pro for providing plots, tables, etc., 0.01-Ω resistance boxes, and 2K-at-0.01-Ω trim pots for hookup with the Lewis gages. The raw data from the System 4000 were reduced to a file in which the data had been corrected by using specified parameters and engineering units. This reduced file was then translated to a Lotus 123-compatible text file and transported to the Macintosh Centris 650. There, the final analysis and plotting were accomplished by using the IGOR program provided by WaveMetrics. Data reduction and analysis methods are described in chapter 4.

3.3 Lewis Test Equipment and Operational Procedures

All test data were taken after the furnace temperature stabilized. The testing system consisted of a 10-channel scanning thermometer for measuring six thermocouple outputs, a digital-to-analog converter for programming the furnace temperatures, and four digital multimeters for measuring the four gages' output. A Zenith 286PC was used for computer control of furnace temperature, actuator displacement, and data sampling. The computer communicated with the instrumentation by means of an IEEE–488 bus. An in-house-developed software system (ref. 3.2) was used to provide flexible, natural language process control capability. Figure 3.15 shows a block diagram of the measurement system, and figure 3.16 presents the strain gage testing laboratory at NASA Lewis.

3.3.1 Apparent Strain and Drift Apparatus

A self-programmable furnace (Omegalux LMF–6525) was used for apparent strain and drift strain testing because of its high heating/cooling rate capability. The 60 F deg/min (33 C deg/min) heating/cooling rate required for some apparent strain cycles was beyond the limit of the Fisher muffle

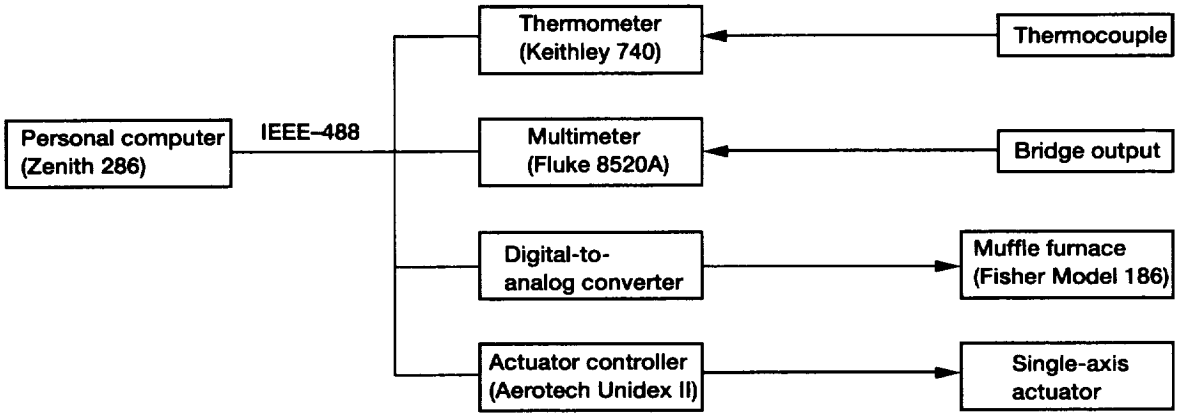

Figure 3.15.—Schematic of Lewis testing system.

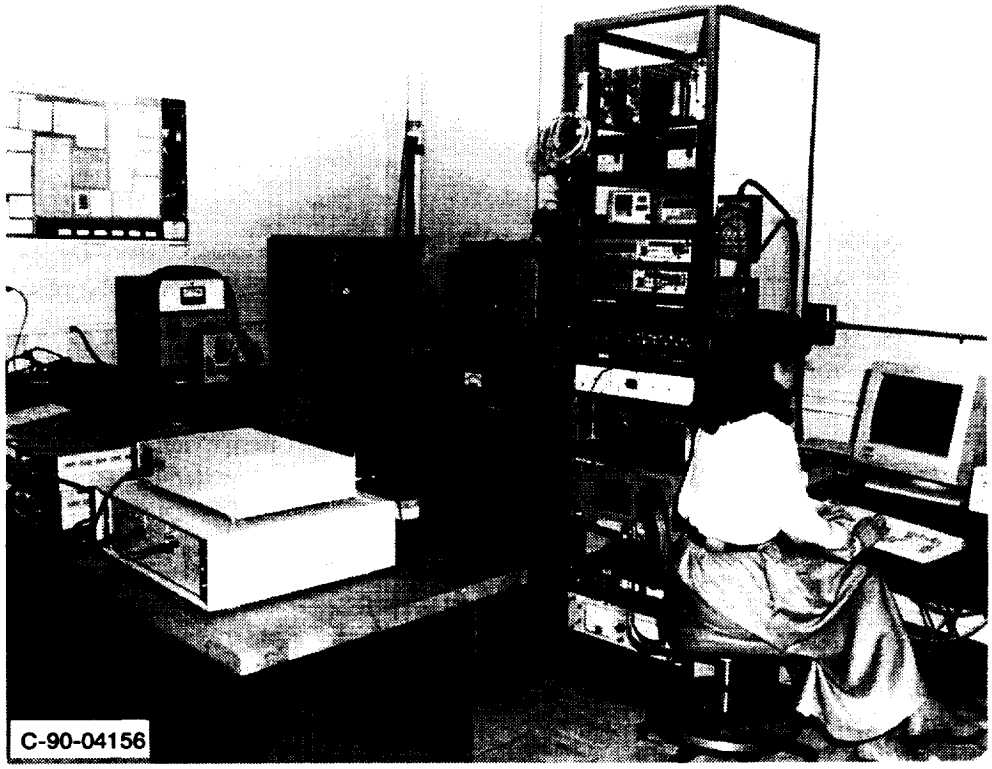

Figure 3.16.—Lewis high-temperature strain gage laboratory.

furnace used for gage factor testing. The three GWP29 test gages were connected to a Wheatstone bridge circuit with different configurations (fig. 3.17). As shown, the bridges were balanced at room temperature before testing. Shunt calibration was taken by shunting the active gage. The equipment used in the bridge completion network is listed in table 3.1 and shown in figure 3.18.

3.3.2 Gage Factor Apparatus

Gage factor determination tests at Lewis used constant-moment beams (fig. 3.19). An IN100 beam with six reference gages was mounted in the bending fixture made of SAE 1010–1030 steel and stressed to about 2000 με (fig. 3.20). A relation between the deflection of the beam d and the strain ε experienced

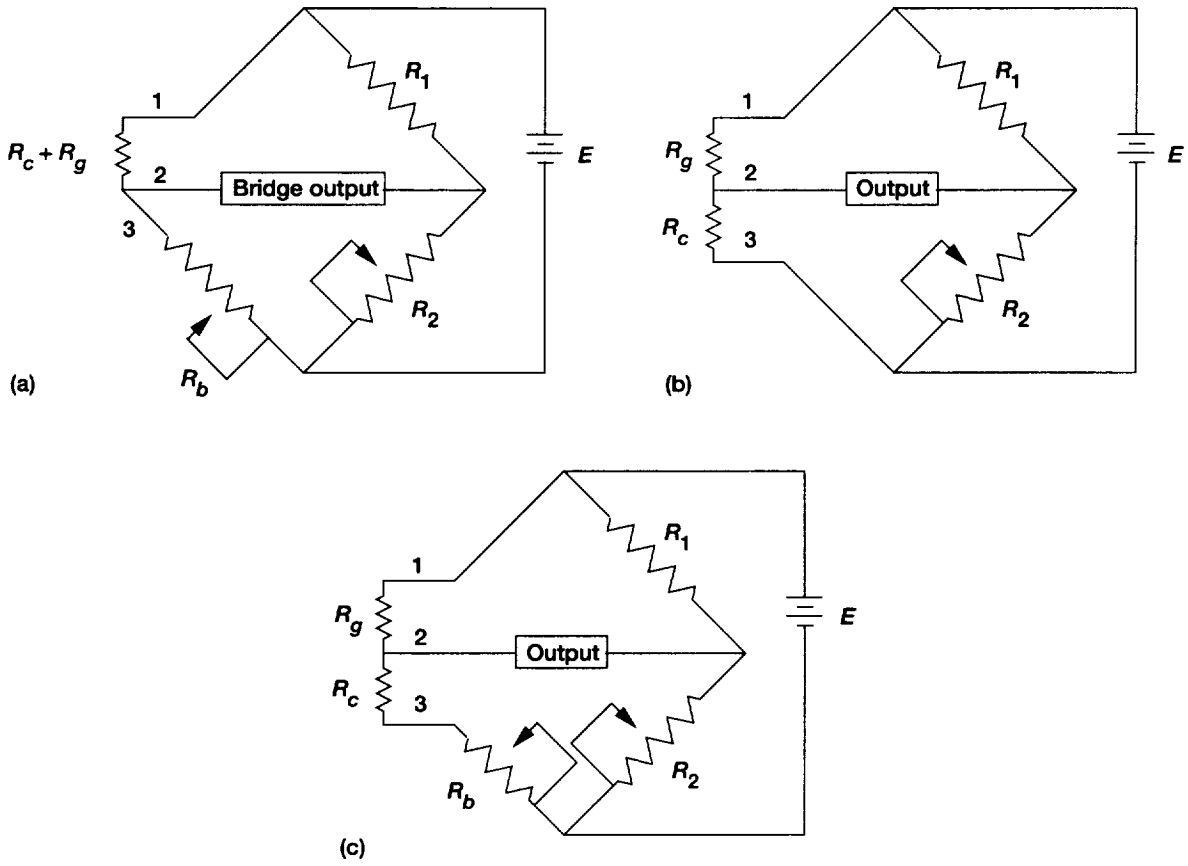

Figure 3.17.—Schematic of Wheatstone bridge completion network for DETCBCL gage, CKA1 gage, and PdCr gage. (a) Bridge with DETCBCL gage balanced at room temperature so that $R_g + R_c/(R_g + R_c + R_b) = R_1/(R_1 + R_2)$. (b) Bridge with CKA1 gage balanced at room temperature so that $R_g + R_c/(R_g + R_c) = R_1/(R_1 + R_2)$. (c) Bridge with PdCr gage balanced at room temperature so that $R_g + R_c/(R_g + R_c + R_b) = R_1/(R_1 + R_2)$.

TABLE 3.1.—EQUIPMENT USED IN BRIDGE COMPLETION NETWORK

Gage	Excitation voltage source, E	Ballast resistor, R_B	Bridge completion resistor, $R_1 + R_2$
1 & 2	Tri-Com SN321 signal conditioner	Measurements Group v/E–40 decade resistor	Hallcross 837 decade voltage divider
3 & 4	Raytheon Co. power source	Measurements Group v/E–40 decade resistor	Measurements Group v/E–40 decade resistors

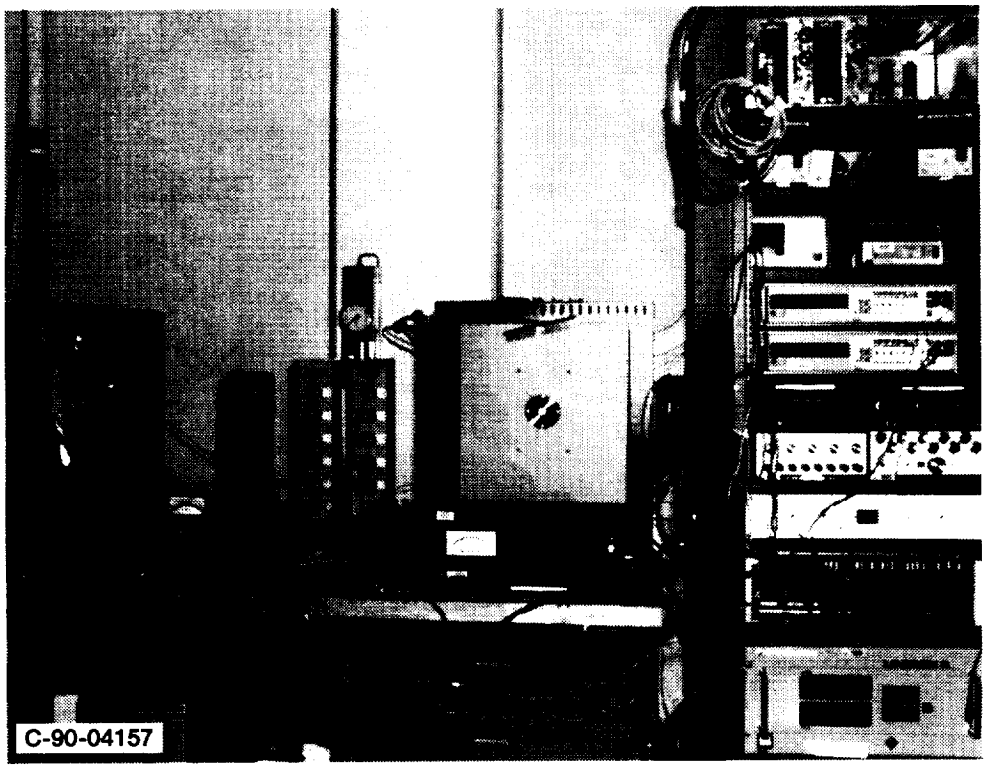

Figure 3.18—Lewis equipment used in bridge completion network.

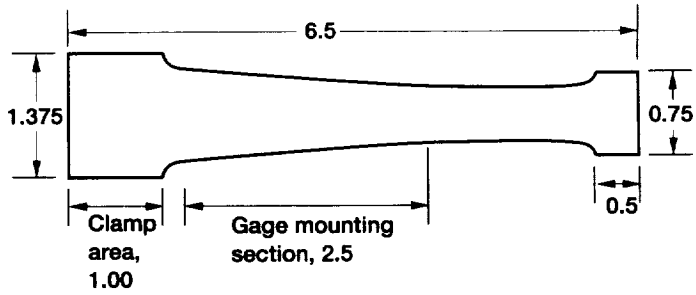

Figure 3.19.—Geometry of constant-moment beam used at Lewis for gage factor determination test. (Dimensions are in inches.)

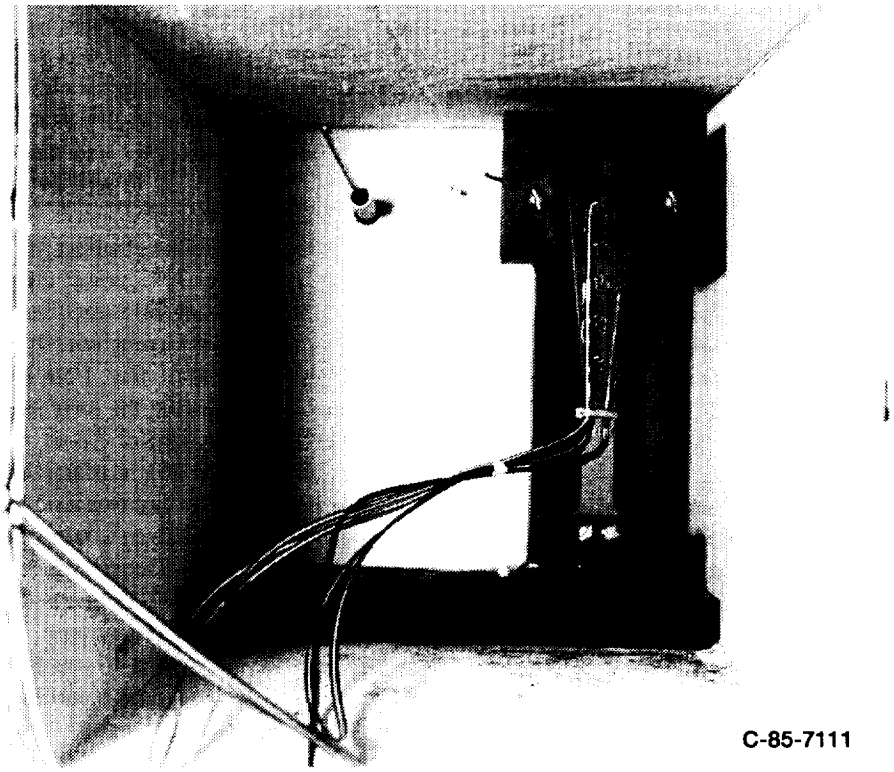

Figure 3.20.—Lewis bending fixture.

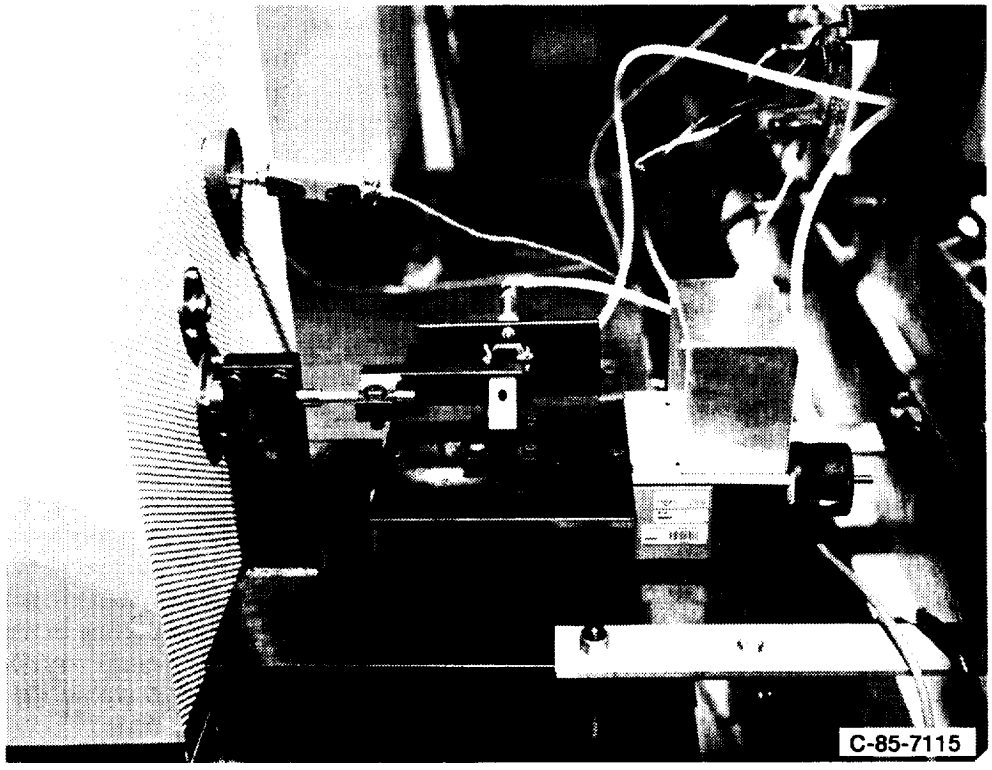

Figure 3.21.—Fisher muffle furnace.

by the gages was thus determined for calibration. The strain in the test beam was calculated from

$$\varepsilon = t \times d/l^2$$

where t is thickness and l is length of the beam. A deflection of about 1.2 cm of an IN100 beam is equivalent to approximately 2000 με on the beam. The strain calculations based on beam deflection have an uncertainty of approximately 1%.

A Fisher Model 186 isotemperature muffle furnace equipped with bending fixture and deflection actuator (fig. 3.21) was used for gage factor testing. Beam deflection was automatically controlled with an Aerotech Unidex II controller.

3.3.3 Data Acquisition System

A Zenith 286PC was used to collect test data, as mentioned earlier. The test data, which included time, temperature, and gage output, were printed and also saved on a diskette as ASCII files. The data files were then transported to a Macintosh II computer for IGOR data analysis.

3.4 Dryden Test Equipment and Operational Procedures

3.4.1 Apparent Strain and Drift Test Equipment

The system used at Dryden Flight Research Center to conduct the apparent strain and drift tests consisted of a high-temperature, infrared, radiant heating furnace; a susceptor to shield the test coupons from direct radiation; a power controller; and a temperature programmer/controller.

Dryden used a Research Inc. Model 4068 parabolic clamshell, infrared, radiant heating chamber as the furnace for all apparent strain and drift tests. The infrared heating chamber consisted of a circular array of quartz lamps installed in water-cooled, polished-aluminum parabolic reflectors. Each reflector provided a highly directional heating pattern, directing the radiant energy from a tungsten filament, tubular, quartz lamp to the center of the chamber. The chamber itself was capable of rapid heatup rates, depending on the voltage applied to the lamps and the thermal characteristics of the specimen. Maximum specimen temperatures of 2000 °F (1095 °C) were possible. Rapid, controlled cooldown was possible because radiant energy dissipated rapidly after power was cut owing to the low thermal mass of the emitter system. Using this furnace permitted accurate temperature control and excellent time-temperature response. It also introduced the potential for radiation errors in the temperature measurement. This problem was avoided by using a susceptor to block the direct radiant heat of the quartz lamps in the furnace. After several iterations an acceptable susceptor geometry and coupon support system were determined. A 0.005-in.-thick sheet of Inconel 600 foil was rolled into a 12-in.-long tube with a 2.35-in. inner diameter. The seam was spotwelded at several locations along the tube. Oversized holes were punched into the sheet before it was rolled into the tube to allow ceramic tubes to be used to support both the susceptor and the test coupons inside the susceptor. Figure 3.22 shows the furnace and susceptor arrangement.

Power to the parabolic chamber initially was furnished by a Research Inc. Model 7447 power controller. The Model 7447 used a system of a magnetic amplifier, two thyratrons, and two water-cooled ignitrons for proportioning single-phase, alternating-current voltage to the furnace, from zero to the maximum line voltage of 480 V. During the early stages of testing the power controller failed. A state-of-the-art Control Concepts Model 1037–A silicon-controlled-rectifier power controller replaced the failed power controller and was used for all subsequent tests. A checkout test conducted on a temperature calibration coupon showed that the time-temperature behavior and temperature distributions on the GWP29 coupons were unaffected by the change in the power control system.

Temperature profile control was provided by a Research Inc. Micristar dual-loop process controller and setpoint programmer. The programmer provided 50 profile segments for ramping and soaking. A wide range of adjustment was available for proportional, integral, and derivative (PID) control constants, as well as for selectable levels of digital filtering of the control thermocouple signal. Initial temperature controller PID tuning efforts revealed that direct control of the coupon temperatures was not feasible with the susceptor in place. Cascade control, in which the output of the primary controller becomes the setpoint of the secondary controller, was used so that feedback from both the susceptor and the coupon was factored into the control circuit. The dual loops of the controller allowed it to be used as a cascade controller. To accomplish this, an AWG #24, type S thermocouple spotwelded to the susceptor was used as the control thermocouple for the primary loop, and one of the type K thermocouples on the test coupon was branched to the temperature controller for secondary loop control as well as for data acquisition. Figure 3.23 is a schematic of the cascade control configuration used for testing.

System calibrations were conducted for both transient response and steady-state temperature distributions. The most difficult GWP29 transient requirement was the 60 F deg/min (33 C deg/min) heating and cooling rate on the IN100 coupon. One coupon instrumented with thermocouples was used to calibrate the PID parameters to best match the coupon time-temperature history to the required test procedures. The calibration was checked by conducting an apparent strain cycle using a data sampling rate of once every 30 sec. Analyzing the data showed that the GWP29 profile was met acceptably in all heatup segments, except from 75 to 150 °F (25 to 65 °C), where there was some lag in heating rate and overshoot of the setpoint temperature. The lag and overshoot in this segment

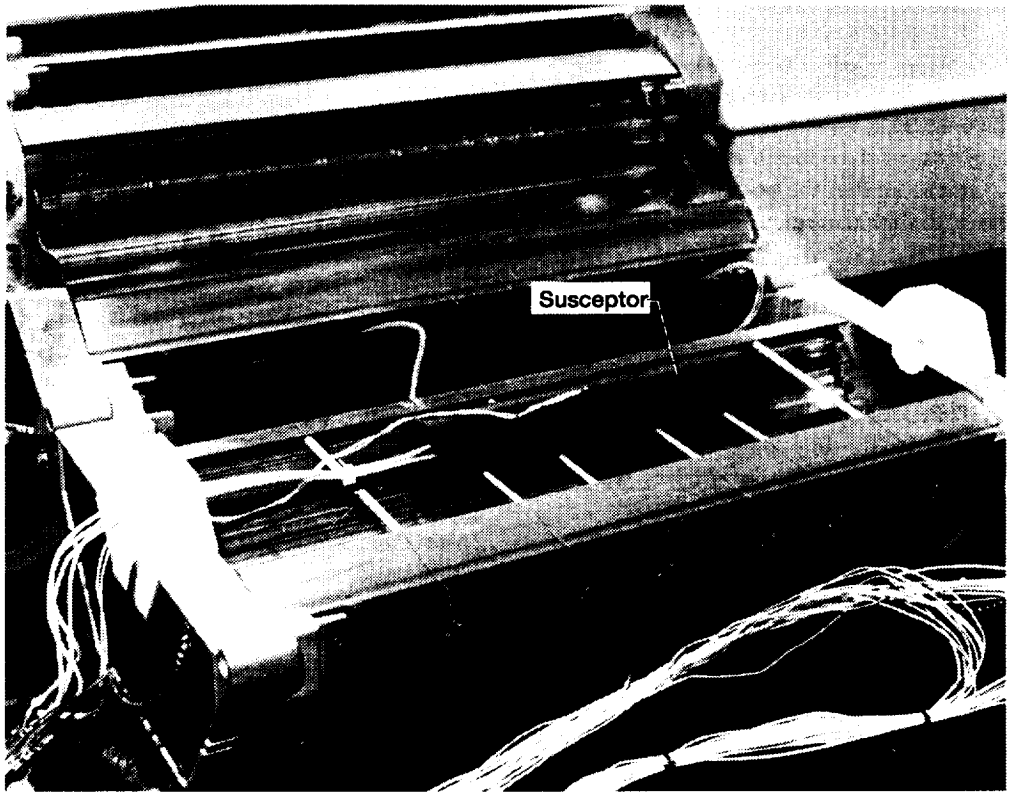

Figure 3.22.—Dryden parabolic clamshell, infrared, radiant heating chamber and susceptor.

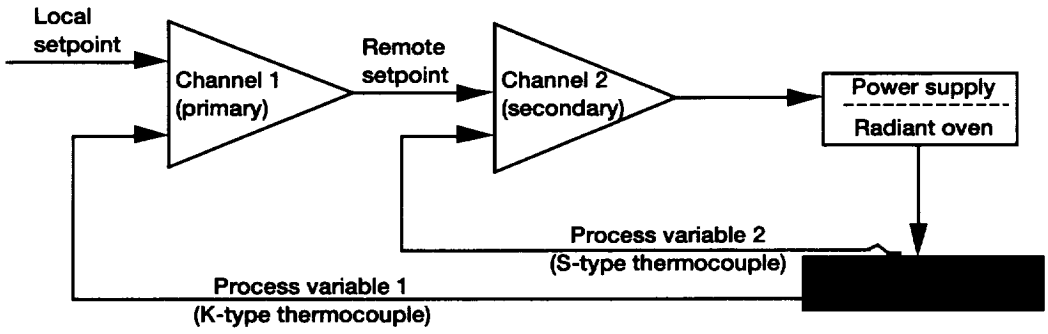

Figure 3.23.—Block diagram of Dryden apparent strain and drift coupon cascade temperature control.

existed in all of the Dryden apparent strain time-temperature data, although it is not believed to have significantly affected the actual apparent strain data. The cooling rate requirement was attained in all segments from 1500 °F (815 °C) down to 750 °F (400 °C), below which temperature natural cooling dominated.

The performance improved at the 10 F deg/min (5.6 C deg/min) heating/cooling rate. Also, heating and cooling performance on a β-21S TMC coupon was observed to be improved over that on an IN100 coupon because the β-21S has lower thermal mass.

The general test procedure (chapter 2) required that the temperature be stabilized to within ±5 F deg (± 3 C deg) of the required temperature during the process of taking the data at each test temperature. Also, to ensure that the coupon was isothermal, all thermocouples on a test specimen had to agree to within ±5 F deg (± 3 C deg) at steady-state conditions. To determine the ability of the radiant furnace to meet these criteria, Dryden conducted a test to determine the temperature distribution on the calibration coupon. The coupon was instrumented with thermocouples at several locations around its face and through its thickness

at one location. Using the time-temperature profile from chapter 2, coupon temperature distributions were determined after hold periods of 5 min at each test temperature. The conditions described in chapter 2 were met across the gaged section of the coupon at all test temperatures. Gradients through the thickness of the coupon were less than 6 F deg (± 3.3 C deg), indicating that the potential for thermal strain effects on the strain measurement was small.

3.4.2 Operational Procedures for Apparent Strain and Drift Tests

The procedures used to conduct each test were nearly identical, with the only differences being in the setup of the data acquisition system display and the time-temperature profile set into the temperature programmer. The procedures were as follows:

1. The position of the coupon was checked to ensure that it was level and centered inside the susceptor.
2. Resistance measurements were made by using the four-wire method (chapter 2).
3. Data acquisition system recording and real-time graphics were set up.
4. The time-temperature profiles for the test and cycle were entered into the temperature programmer.
5. The temperature programmer was then enabled and automatically ran the test.
6. The furnace was opened at the appropriate cooldown temperature for the test (chapter 2).
7. Resistance measurements were made by using the four-wire method (chapter 2).

3.4.3 Gage Factor Test Equipment

To conduct the gage factor tests, Dryden used a high-temperature furnace, a power and temperature control system, and a special fixture for deflecting a cantilevered-beam load bar to specified surface strains. The Dryden load bars were designed to fit precisely in the fixture. Figure 3.24 shows the equipment.

The furnace, a Marshall Furnace Co. Model 2250, was of conventional split-tube design with resistance heating elements embedded in ceramic insulation and was 24 in. long with a 5-in. bore. It was capable of continuous operation to at least 2200 °F (1205 °C). In use the furnace surrounded the load bar, the truss structure, and the clamping beam. The furnace had a total of four zones, one each surrounding the load bar and the clamping beam plus two end zones.

Power control was furnished by a single, 45-A maximum load, alternating-current-operating, solid-state relay for each zone. Temperature control of the individual zones was provided by Eurotherm Model 847 PID setpoint controllers. In the zone

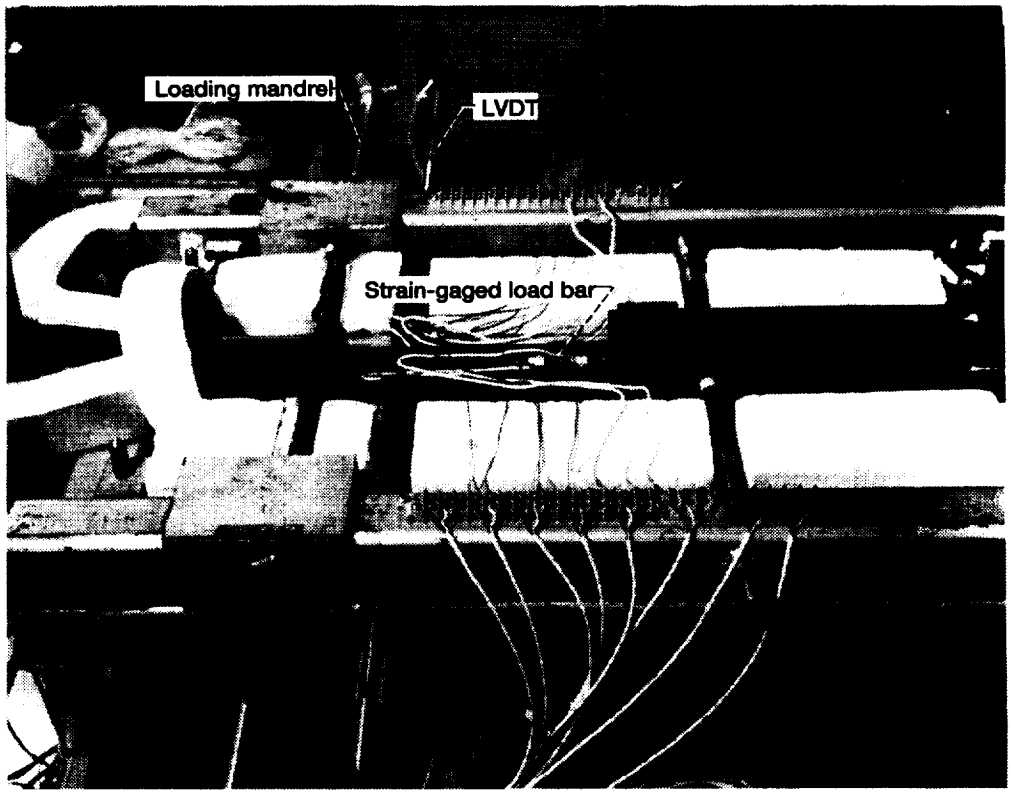

Figure 3.24.—Dryden high-temperature furnace and fixture for deflection of load bar.

surrounding the load bar, temperature control for large setpoint changes was provided by a thermocouple located at the heating element surface. Control for fine setpoint adjustment was switched to a thermocouple attached to the load bar. Feedback control in each of the other zones was provided by AWG #8, type K thermocouples located at the element surface.

The fixture consisted of an exterior carbon steel support frame mounted on legs with leveling screws, the cantilevered clamping beam assembly, a deflection gage support structure, deflection measurement instruments, and loading mandrels. The exterior box frame was designed to resist the mandrel loads and moment induced at the root end of the cantilevered clamping beam, with a minimum amount of deflection in the frame.

The cantilevered clamping beam was fabricated from 2.25-in.-square Inconel X750 bar stock. It was clamped to the support structure by means of six Inconel bolts. To minimize heat flow from the clamping beam into the cooler support structure, high-compressive-strength, low-thermal-conductivity Al_2O_3 thermal insulation spacer blocks were used between the support structure and the side faces of the clamping beam. The clamping beam rigidly clamped the end of the load bar but resulted in temperature gradients along the length of the load bar. These gradients, although small, can cause errors in the strain measurement due to small variations in Young's modulus caused by these gradients. Experiments to characterize these gradients were conducted on a load bar specially instrumented along its length with thermocouples. The temperature gradient was essentially the same at each GWP29 gage factor test temperature, varying from –5 to 8 F deg (–3 to 5 C deg). A least-squares, curve-fitted equation supplied the basis for corrections made to the test data.

The deflection gage truss, fabricated from Inconel X750, was welded to the end of the clamping beam. Consequently, the measured deflections represent the relative deflection of the load bar between the plane of fixity and the point of deflection measurement as shown in figure 3.25. The deflection measurement was therefore essentially independent of the deflection of the clamping beam itself, which was relatively small.

Schaevitz Model GCA–121 linear variable displacement transducers (LVDT's) were used to measure the actual deflections of the load bar. Before use, the LVDT's were calibrated by measuring their output versus the deflection of a precision micrometer mounted in a dedicated LVDT calibration stand. Corrections for small amounts of instrument nonlinearity and hysteresis were applied to the measured deflection data before calculating load bar strains. The LVDT's were protected from heat by thermally isolating the LVDT yoke from the deflection gage support truss.

With loading mandrels on each side of the load bar, it is possible to subject a gage to reverse strain cycles (i.e., 0 to $+\varepsilon$ to 0 to $-\varepsilon$ to 0) or to the opposite sequence without removing and repositioning the load bar.

The true-strain-versus-deflection calibration curve for each GWP29 gage location was obtained from a least-squares curve fit of the average strain of two commercial foil gages installed on either side of the load bar centerline at these locations. A schematic diagram of the fixture is shown in figure 3.25. The

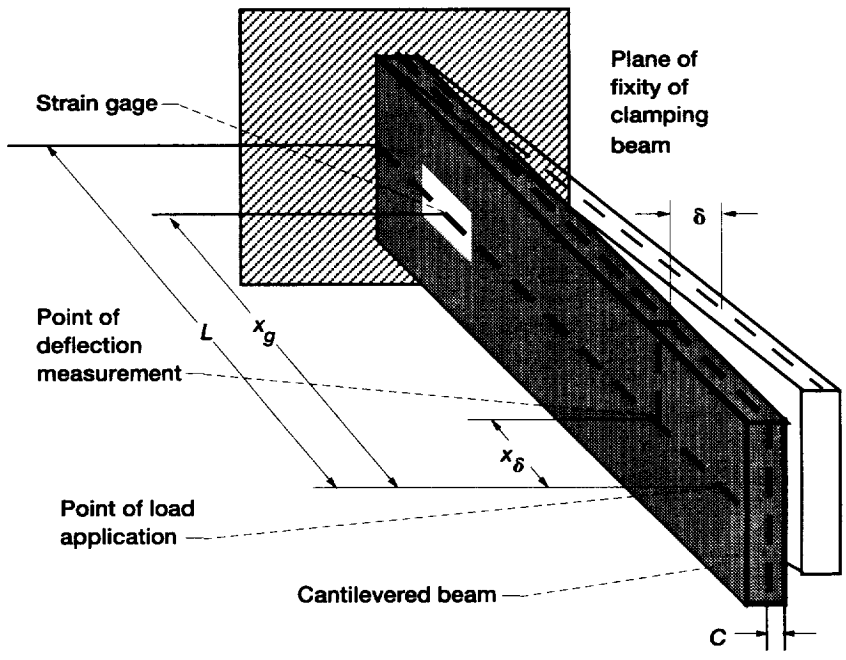

Figure 3.25.—Schematic of Dryden gage factor equipment.

theoretical strain versus deflection at a point where a gage was located is given by the equation

$$\varepsilon = \frac{6\delta x_g c}{\left(L - x_\delta\right)^2 \left(2L + x_\delta\right)} \tag{3.1}$$

where

ε strain on surface of load bar, με

δ deflection of load bar, in.

x_g gage location (distance from point of application of load to gage center), in.

c distance from neutral axis to surface of load bar, in.

L length of load bar (distance from point of application of load to plane of fixity of cantilevered beam), in.

x_δ deflection measurement location (distance from point of application of load to location at which deflections are measured), in.

The equation for calculating the estimated uncertainty in the strain measurements was found by differentiating the absolute value of the logarithm of the theoretical strain equation and collecting terms. The strain uncertainty, or error, was then given by

$$d\varepsilon = \varepsilon\left[\frac{d\delta}{\delta} + \frac{dx_g}{x_g} + \frac{dc}{c} + 2dL\left(\frac{1}{L - x_\delta} + \frac{1}{2L + x_\delta}\right) + dx_\delta\left(\frac{2}{L - x_\delta} - \frac{1}{2L - x_\delta}\right)\right] \tag{3.2}$$

The uncertainty in the deflection measurement $d\delta$ from manufacturers' literature was 0.0001 in. The constituent uncertainties of the various distance terms come from the standard deviation of a survey of historical measured data for these quantities in the fixture. The uncertainty in gage location dx_g was 0.01 in. The uncertainty in the neutral axis distance dc was 0.0005 in. The uncertainty in the length of the cantilevered beam dL was 0.056 in., and the uncertainty in location of the deflection measurement dx_δ was 0.01 in. For IN100 load bars the uncertainty varied from 1.93% of the measured strain at ±400 με down to 1.80% of the measured strain at ±2000 με. For TMC load bars the uncertainties varied from 1.88% down to 1.84% from ±400 με to ±1200 με.

The Dryden load bar was a cantilevered beam with a constant cross section and dogbone-style ends. See figure 3.26. It was designed to be heated either by driving direct current through the bar by means of electrodes connected to the dogbone ends of the bar or by conventional furnace heating. The latter mode was ultimately selected for GWP29 tests because lower thermal gradients resulted along the length of the load bar with furnace heating.

3.4.4 Operational Procedures for Gage Factor Tests

The following procedures were used for all gage factor tests:

1. Load bar alignment and clamping bolts were checked.
2. Resistance measurements were made using the four-wire method (chapter 2).
3. Data acquisition system recording and real-time graphics were set up. For open-loop control during heating, displays showed the thermocouples along the length of the load bar.
4. The furnace was heated and cooled to the test temperature by using the procedure established during the temperature calibration test, until a steady-state condition was reached and thermal gradients along the length of the load bar were minimized.
5. The strain gages were recalibrated and rezeroed in order to reference the gage factor measurement to the test temperature. LVDT's were also rezeroed to correct for the effects of thermal expansion in the load bar.

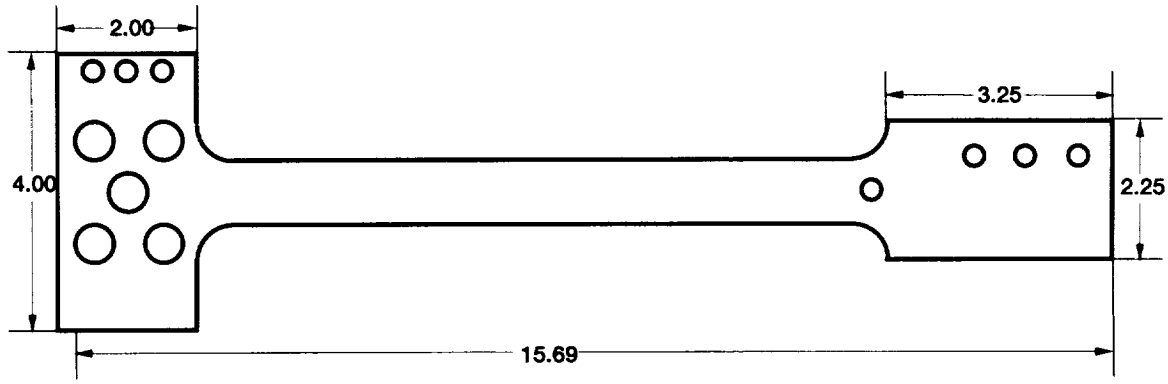

Figure 3.26.—Dryden constant-cross-section, cantilevered-beam load bar used for GWP29 gage factor tests. (Dimensions are in inches.)

6. Deflection was applied to the load bar by the increments listed in chapter 2 up to the maximum deflection to apply 2000 με to the load bar surface, recording gage output at each increment. Deflection was removed from the load bar in the same increments, again recording gage output at each increment.

7. LVDT's were rezeroed. Strain gages were not rezeroed between opposed-direction deflections of the load bar but were rezeroed during data reduction.

8. Steps 6 to 9 were repeated for each of the other test temperatures.

9. Resistance measurements were made per chapter 2 by using the four-wire method after the final step of the cycle had been completed.

3.4.5 Data Acquisition System

All GWP29 testing at Dryden used a Measurements Group, Inc., System 4000 fifty-channel data acquisition system, complete with signal conditioning and direct-current power supply. Being a turnkey package the System 4000 had simplified setup, operation, maintenance, and calibration, such that all test-related activities were accomplished by one test engineer and one test technician. Before entering the GWP29 test phase all strain gage and thermocouple signal-conditioning channels were calibrated to ensure maximum measurement accuracy. Gage factor setting was 2.0 for all tests, although the true gage factor obtained from these tests was used to correct the apparent strain and drift data. Shunt calibration was selected to simulate 2000 με for all gages, although the actual value used for System 4000 varied slightly after being corrected for lead-wire desensitization on each gage.

The dual-element, temperature-compensated BCL (DETCBCL) gage was set up as a quarter-bridge. The internal 350-Ω completion resistors and the 120-Ω dummy of the signal-conditioning system were used in the bridge. The System 4000 option for correcting measurements for quarter-bridge nonlinearity was used. Excitation voltage was 5 V. The schematic of this bridge circuit is shown in figure 3.27.

The Langley compensated Kanthal A1 (CKA1) signal-conditioning configuration was set up as a half-bridge, using the gage and compensating element on one side of the bridge and data acquisition system internal 350-Ω resistors for bridge completion. The System 4000 parameters were entered as for a quarter-bridge, except that the option for correcting measurements for quarter-bridge nonlinearity was not used. Excitation voltage was 5 V. The schematic of this bridge circuit is shown in figure 3.28.

The signal-conditioning configuration for the Lewis palladium-chromium (PdCr) gage depended on the type of data collected (apparent strain, drift, or gage factor). The apparent strain setup used a full-bridge configuration so that external completion resistors could be used to satisfy the need for unequal completion resistor values. See bridge schematic in figure 3.29. One precision resistor and one potentiometer per channel were used for the completion resistors, and precision decade boxes were used for the ballast resistance. The System 4000 configuration was also used for a full bridge. Excitation voltage was 2 V for all PdCr gages.

Preliminary work was conducted to determine the interface for the PdCr gage to the data acquisition system used at Dryden for apparent strain testing. The standard full-bridge equation used by the System 4000 software assumes that initial resistances in each arm of the bridge are equal and thus reduces to

$$\varepsilon = \frac{\frac{e_o}{E}}{GF} \tag{3.3}$$

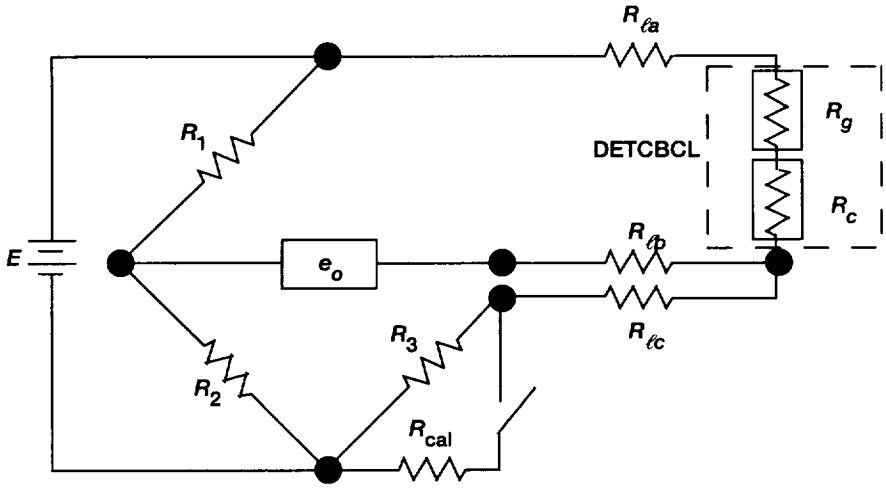

Figure 3.27—Schematic of Wheatstone bridge for Dryden DETCBCL gage.

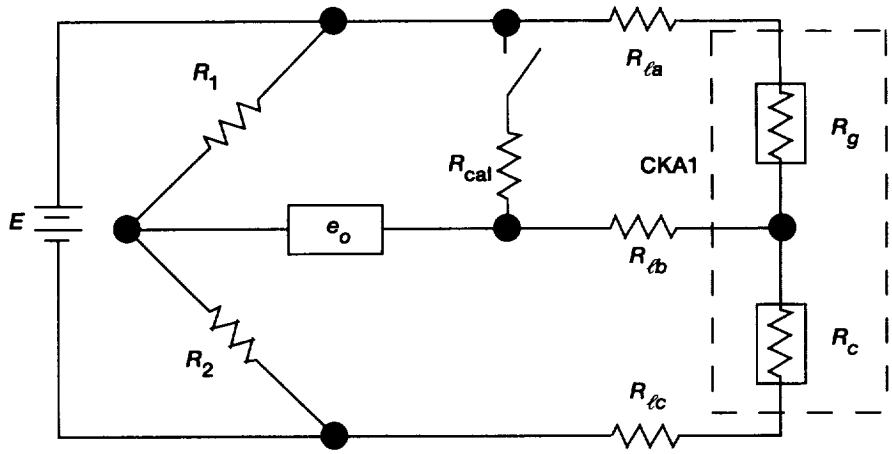

Figure 3.28.—Schematic of Dryden Wheatstone bridge for Langley CKA1 gage.

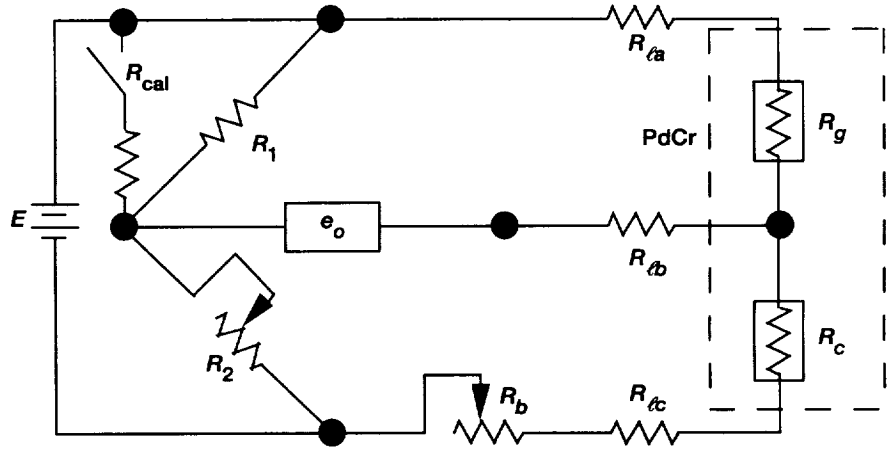

Figure 3.29.—Schematic of Dryden Wheatstone bridge for Lewis PdCr apparent strain tests.

where

ε	strain
e_o	output voltage
E	excitation voltage
GF	gage factor

The initial resistances in the arms of the PdCr apparent strain bridge were not all equal. The completion resistors were not necessarily equal, and the total resistance in the compensating arm (compensating element resistance plus ballast resistance) was not necessarily equal to the resistance in the gage arm. The schematic for this bridge circuit is shown in figure 3.30. The bridge equation (ref. 3.3) for the PdCr gage is thus

$$(\Delta\varepsilon)_T = \frac{\left(\frac{e_o}{E}\right)_T \left(R_b + R_c' + R_g'\right)\left(\frac{1}{R_b + R_c'}\right) + \left(\frac{1}{R_g'}\right)}{\mathrm{GF}} \qquad (3.4)$$

where

$(\Delta\varepsilon)_T$	apparent strain
T	temperature
R_b	ballast resistance
R_c'	$R_c + r_c$, where R_c is original room-temperature resistance of compensating element and r_c is original room-temperature resistance of compensating element lead wire

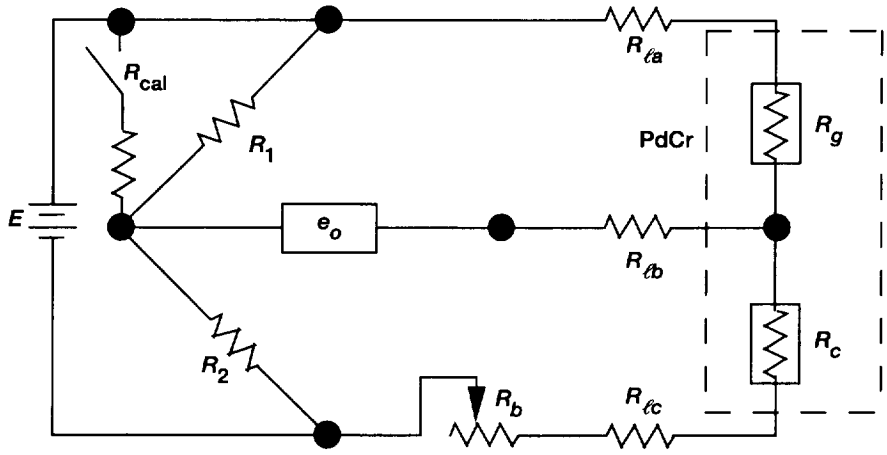

Figure 3.30.—Schematic of Dryden Wheatstone bridge for Lewis PdCr drift strain and gage factor tests.

R_g' $R_g + r_g$, where R_g is original room temperature resistance of gage element and r_g is original room-temperature resistance of gage element lead wire

GF′ gage factor of compensated gage

Correction factors equal to the ratio of equation (3.3) to equation (3.4) were applied to the entries into the data acquisition system in order to acquire the proper engineering units for the PdCr gage by using the built-in equation of the data acquisition system. Similar corrections were made for drift and gage factor tests, although the correction factor was always 4 because a one-to-one bridge was used, in which the total resistance in the compensating arm is equal to the resistance in the gage arm.

References

3.1 Wnuk, S.P., Jr.: Final Report on Procedure for Installation of PdCr Gages by Flame Spraying. NASA CR–195389, 1994.

3.2 Will, H.A.; and Mackin, M.A.: Laboratory Process Control Using Natural Language Commands From a Personal Computer. NASA TM–101988, 1989.

3.3 Lei, J.-F.; Euglund, D.R.; and Croom, C.: The Temperature Compensation Technique for a PdCr Resistance Strain Gage. Society for Experimental Mechanics Fall Meeting, 1991.

Chapter 4

Data Reduction and Analysis Methods

4.1 Introduction

The large volume of data and the diversity of data parameters posed unique challenges to the data reduction process. Contrasting requirements regarding the complexity and volume of data to be analyzed were balanced against the available resources and the need for identical treatment of data at distant locations by close cooperation between the three centers and prudent judgment.

Two steps were involved in converting the test data into the results presented herein. The raw test data, which were collected as described in chapter 2, were reduced into static apparent strain, drift strain, and gage factor from the indicated strains, temperatures, times, and true strains recorded in the respective tests. Although specific data reduction methods were determined by consensus between the three test centers, the actual computational routines used to reduce the original raw data varied slightly because different test equipment and operational procedures were used.

After reduced data were obtained by each test center, the data for each parameter for each gage type were combined to improve statistical significance. Each center led the development of data-processing procedures and display of results for one of the parameters, using feedback from each of the other centers to ensure the suitability of the computational routines. An Apple Macintosh program, IGOR, from WaveMetrics was used for all routines. The internal programming language, extensive data analysis operations, and graphics capabilities in IGOR met all the established requirements. Conformity in the display of results for each parameter was achieved by having the center that led in developing the procedures also perform the processing. Dryden processed the apparent strain data, Langley processed the drift strain data, and Lewis processed the gage factor data.

Each center also conducted the figure-of-merit analysis for the respective parameter for which data were processed. Much of the input to the figure-of-merit analysis was included in the routines that combined the data from the three centers, with the exception of the analyses of gage repeatability with respect to a certain parameter. These inputs were quantities derived from gage performance data and are described in section 2.3.

4.2 Apparent Strain

4.2.1 Data Reduction Procedures

The key elements in reducing apparent strain data were the selection of static apparent strain points from raw test data, the combination of static data from the three test centers into a statistical analysis of each gage type and the presentation of the average apparent strain curve. Figure 4.1 is a flowchart of the entire process.

An automated routine was written that selected static apparent strain points from the entire set of apparent strain raw test data on the basis of the temperature stability criteria specified in chapter 2. The one point that best matched the set of criteria was selected. The correction for lead-wire desensitization was applied by each test center to the raw test data.

An automated routine was used to combine the individual static apparent strains from each test center into one data set and then to determine the statistical average and the upper and lower 95% confidence limits for the set of 12 gages tested at the three test centers. Although failed gages were excluded from the calculation of the average apparent strain curve, the upper and lower 95% confidence limits were affected by failed gages because Student's t distribution changed for each failed gage.

This same routine also applied a correction for the true gage factor at the appropriate test temperature to the data for each of the 12 gages before making the statistical calculations. Table 4.1 indicates which cycle of gage factor data was used to correct which cycles of apparent strain data. For the purposes of data correction, only the heatup half of the tension portion of the respective cycle was used.

TABLE 4.1.—CORRELATION OF APPARENT STRAIN AND GAGE FACTOR CYCLES FOR CORRECTION OF GAGE -FACTOR -VERSUS-TEMPERATURE VARIATION

Apparent strain cycle	Gage factor cycle
1, 2, 3	1
4, 5, 6, 7, 8	4
9	5
10	6
11	7
12	8

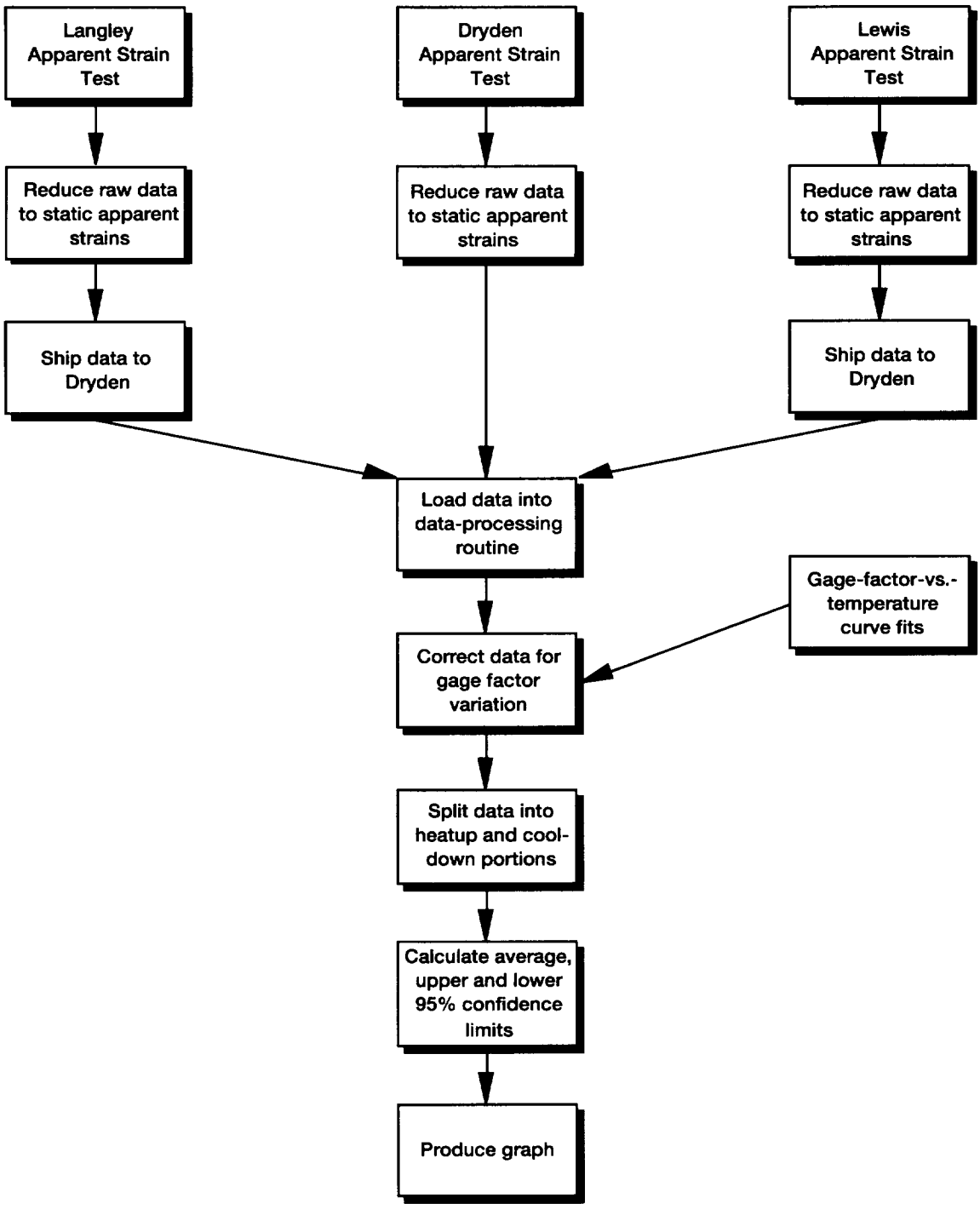

Figure 4.1.—Flowchart for apparent strain data processing.

4.2.2 Data Reduction Routines

The following set of IGOR macros were used to process GWP29 static apparent strain data into the graphs included in the report. Although certain specific elements are somewhat generic IGOR code, as a whole they were written specifically for that purpose and would require considerable modification to be used for data generated according to a different test plan.

PageMaker is a utility macro that executed the data-processing macros to automatically create a page for the report containing graphs for two apparent strain cycles. Inputs include the gage type, the substrate material, and the cycle numbers for the two graphs to be created.

```
Macro PageMaker (GageType,Substrate,CycleX,CycleY)
    Variable GageType,Substrate,CycleX,CycleY
    Prompt GageType,"1) DETCBCL, 2) CKA1, 3) PdCr"
    Prompt Substrate,"1) IN100, 2) ß21S TMC"
    Prompt CycleX,"Initial cycle no: 1 - 12"
    Prompt CycleY,"Next cycle no: 1 - 12"

    if (CycleY<=CycleX)
        Abort "Next cycle no. must be after the Initial cycle no."
    else
        AppStrain (GageType,Substrate,CycleX,0,1)
        AppStrain (GageType,Substrate,CycleY,1,1)
        Layout0()
    endif
End
```

AppStrain is a utility macro that integrated the individual data-processing macros into one routine. For a single cycle of data AppStrain executed the individual data-processing macros that loaded the data, corrected them for gage-factor-versus-temperature variation, split the data into heatup and cooldown portions, and performed the statistical calculations to determine the average and 95% confidence limits and to graph the information.

```
Macro AppStrain (GageType,Substrate,CycleNo,PNswitch,LAxisSwitch)
    Variable GageType,Substrate,CycleNo,PNswitch=0,LAxisSwitch=1
    Prompt GageType,"1) DETCBCL, 2) CKA1, 3) PdCr"
    Prompt Substrate,"1) IN100, 2) ß21S TMC"
    Prompt CycleNo,"1 - 12"
    Prompt PNswitch,"Select page numbering type: 0) None, 1) from file, 2) user input"
    Prompt LAxisSwitch,"Select left axis scaling type: 0) Auto, 1) CL+10%, 2) user input"

    PauseUpdate;Silent 1
    DataLoader(GageType, Substrate, CycleNo)
    GFTcorrector(GageType, Substrate, CycleNo)
    SplitCycle()
    StatCalc(GageType, Substrate, CycleNo)
    EappGraph(GageType, Substrate, CycleNo, PNswitch,LAxisSwitch)
    Beep
End
```

DataLoader built the names of files containing static apparent strain data and associated temperature data from input codes for the gage type, substrate material, and cycle number. It also determined the path on the hard disk to follow to find these files and then loaded these files into IGOR for processing.

```
Macro DataLoader(GageType, Substrate, CycleNo)
    Variable GageType, Substrate, CycleNo
    Prompt GageType, "1) DETCBCL, 2) CKA1, 3) PdCr"
    Prompt Substrate, "1) IN100, 2) ß21S TMC"
    Prompt CycleNo,"1 - 12"

    PauseUpdate;Silent 1;Slow 0
    String load1="A", load2="D", load3="E", loadi, DataPathString, DataFileString, OWaveString, RWaveString
    String lpath1, lpath2, lpath3, lpath="Keith-80HD:Files:GWP29:GWP-29 Test Data:", CycleString
    if (GageType==1)
        load1+="B";load2+="B";load3+="B"
    endif
    if (GageType==2)
        load1+="K";load2+="K";load3+="K"
    endif
    if (GageType==3)
        load1+="P";load2+="P";load3+="P"
    endif
    load1+="A";load2+="A";load3+="A"
    if (Substrate==1)
        NewPath/O CoupNums "Keith-80HD:Files:GWP29:GWP-29 Test Data:DR&A Routines:Apparent Strain:IN100 Folder:"
        LoadWave/O/T/Q/P=CoupNums "IN100.awav"
        RemovePath CoupNums
    endif
    if (Substrate==2)
        NewPath/O CoupNums "Keith-80HD:Files:GWP29:GWP-29 Test Data:DR&A Routines:Apparent Strain:TMC Folder:"
        LoadWave/O/T/Q/P=CoupNums "TMC.awav"
        RemovePath CoupNums
    endif
    if (GageType==1)
        load1+=num2istr(BSN[0]);load2+=num2istr(BSN[1]);load3+=num2istr(BSN[2])
    endif
    if (GageType==2)
        load1+=num2istr(KSN[0]);load2+=num2istr(KSN[1]);load3+=num2istr(KSN[2])
    endif
    if (GageType==3)
        load1+=num2istr(PSN[0]);load2+=num2istr(PSN[1]);load3+=num2istr(PSN[2])
    endif
    print "Data will be analyzed for coupons "+LOAD1+", "+LOAD2+", and "+LOAD3
    iterate (3)
        if (i==0)
            loadi=load1
        else
            if (i==1)
                loadi=load2
            else
                loadi=load3
            endif
        endif
        DataPathString=lpath+loadi+":Cycle "
        if (CycleNo<10)
            CycleString=num2istr(0)+num2istr(CycleNo)
        else
            CycleString=num2istr(CycleNo)
        endif
        DataPathString+=CycleString+" DR&A Folder:"
        NewPath/O DataPath DataPathString
        iterate (11)
```

```
            if ((i>0)*(i<5))
                DataFileString="TblSG"+num2istr(i)
                if (j<2)
                    DataFileString+=".bwav"
                else
                    DataFileString+=".awav"
                endif
            else
                DataFileString="TblTC"+num2char(i+60)
                if (j<2)
                    DataFileString+=".bwav"
                else
                    DataFileString+=".awav"
                endif
            endif
            if (i==0)
                DataFileString="TblTET"
                if (j<2)
                    DataFileString+=".bwav"
                else
                    DataFileString+=".awav"
                endif
            endif
            if (j<2)
                LoadWave/O/Q/P=DataPath DataFileString
            else
                LoadWave/T/O/Q/P=DataPath DataFileString
            endif
            RWaveString=loadi+"C"+CycleString+DataFileString[3, strlen(DataFileString)-6]
            OWaveString=DataFileString[0, strlen(DataFileString)-6]
            Rename $OWaveString $RWaveString
        loop
        RemovePath DataPath
        Variable str_end
        if (Substrate==1)
            str_end=9
        else
            str_end=8
        endif
        String/G Abase,Dbase,Ebase
        if (i==0)
            Abase=RWaveString[0,str_end]
        else
            if (i==1)
                Dbase=RWaveString[0,str_end]
            else
                Ebase=RWaveString[0,str_end]
            endif
        endif
    loop
    KillWaves BSN,KSN,PSN
End
```

GFTcorrector determined the appropriate file of gage-factor-versus-temperature, curve-fit coefficients for making corrections (see tables 5.16 to 5.27) based on the input codes for gage type, substrate material, and cycle number. It then loaded the file and applied the correction to all 12 sets of apparent strain data.

```
Macro GFTcorrector (GageType, Substrate, CycleNo)
	Variable GageType, Substrate, CycleNo
	Prompt GageType, "1) DETCBCL, 2) CKA1, 3) PdCr"
	Prompt Substrate, "1) IN100, 2) ß21S TMC"
	Prompt CycleNo, "1 - 12"

	PauseUpdate;Silent 1
	String pathstring="Keith-80HD:Files:GWP29:True GFvTs:", coeffile, Base, ModSG, ModTC
	Variable RGCN, ngages=12, GN, Ccnt, GFT, a0, a1, a2, a3
	if (Substrate==1)
		coeffile="I"
	endif
	if (Substrate==2)
		coeffile="T"
	endif
	if (GageType==1)
		coeffile+="B"
	endif
	if (GageType==2)
		coeffile+="K"
	endif
	if (GageType==3)
		coeffile+="P"
	endif
	coeffile+="GFta.awav"
	NewPath/O GFvTpath pathstring
	LoadWave/O/T/Q/P=GFvTpath coeffile
	RemovePath GFvTpath
	if (CycleNo<4)
		RGCN=1
	endif
	if ((CycleNo>3)*(CycleNo<9))
		RGCN=4
	endif
	if (CycleNo>8)
		RGCN=CycleNo-4
	endif
	if (RGCN==1)
		Ccnt=RGCN-1
	else
		Ccnt=RGCN-3
	endif
	iterate (ngages)
		if (i<4)
			Base=Abase
			GN=i+1
		endif
		if ((i>3)*(i<8))
			Base=Dbase
			GN=i-3
		endif
		if (i>7)
			Base=Ebase
			GN=i-7
		endif
		ModSG=Base+"SG"+num2istr(GN)
		ModTC=Base+"TCB"
		a0=GFta0[Ccnt];a1=GFta1[Ccnt];a2=GFta2[Ccnt];a3=GFta3[Ccnt]
```

```
        iterate (numpnts($ModSG))
            $ModSG[i]=$ModSG[i]*2.0/(a0+a1*$ModTC[i]+a2*$ModTC[i]^2+a3*$ModTC[i]^3)
        loop
    loop
    KillWaves GFta0,GFta1,GFta2,GFta3
End
```

SplitCycle is another macro that expedited the data processing, but in and of itself did not process data. Instead, SplitCycle set the inputs for and executed two other macros, ZeroShift and SplitData.

```
Macro SplitCycle()
    PauseUpdate;Silent 1
    String Base, DegF, Strain1, Strain2, Strain3, Strain4
    iterate (3)
        if (i==0)
            Base=Abase
        else
            if (i==1)
                Base=Dbase
            else
                Base=Ebase
            endif
        endif
        DegF=Base+"TCB"; Strain1=Base+"SG1"; Strain2=Base+"SG2"
        Strain3=Base+"SG3"; Strain4=Base+"SG4"
        ZeroShift(Base)
        SplitData(DegF, Strain1, Strain2, Strain3, Strain4)
                KillWaves $DegF, $Strain1, $Strain2, $Strain3, $Strain4    |comment this line out to keep input waves

    loop
End
```

ZeroShift was called from the macro SplitData. It used as the only input a base string from which names of several associated data waves were built. It also created a new wave, also built on the base string, into which the zero shift values were placed for the particular set of apparent strain data waves referenced by the base string. Finally, the zero shifts were subtracted from each of the points in the apparent strain waves. Thus, the data displayed in the report were corrected for zero shifts. The wave containing the zero shift values was saved as a separate file in order to expedite production of tables 5.2 to 5.13 in chapter 5.

```
Proc ZeroShift(Base)                |Corrects for Zero Shift
    String Base
    PauseUpdate;Silent 1
    String ZSV=Base+"ZSV",Strain,destpath="Keith-80HD:Files:GWP29:Eapp ZS:",destfile
    Make/N=4/O $ZSV,rezero
    iterate (4)
        Strain=Base+"SG"+num2istr(i+1)
        $ZSV[i]=$Strain[numpnts($Strain)-1]-$Strain[0]
        rezero[i]=$Strain[0]
        $Strain=$Strain-rezero[i]
    loop
    destfile=ZSV+".awav"
    NewPath/O savepath, destpath
```

```
    Save/T/O/P=savepath $ZSV as destfile
    RemovePath Savepath
    KillWaves rezero
EndMacro
```

SplitData did the actual dividing up of data into heatup and cooldown portions. The four apparent strain data waves and their associated wave of temperature data were input to the macro from SplitCycle. The IGOR WaveStats operation was used to determine the relative location in the temperature wave of the maximum temperature and the number of points in the wave. Using this information about the wave of temperature data, it created new waves for the heatup and cooldown data.

```
Proc SplitData (ReferenceWave, DataWave1, DataWave2, DataWave3, DataWave4)
    String ReferenceWave, DataWave1, DataWave2, DataWave3, DataWave4

    PauseUpdate;Silent 1
    String SplitRefI=ReferenceWave+"_H", SplitRefD=ReferenceWave+"_C", SplitDat1I=DataWave1+"_H", SplitDat1D=DataWave1+"_C"
    String SplitDat2I=DataWave2+"_H", SplitDat2D=DataWave2+"_C", SplitDat3I=DataWave3+"_H",SplitDat3D=DataWave3+"_C"
    String SplitDat4I=DataWave4+"_H",SplitDat4D=DataWave4+"_C"
    WaveStats/Q $ReferenceWave
    Make/N=(V_maxloc+1)/O $SplitRefI, $SplitDat1I, $SplitDat2I, $SplitDat3I, $SplitDat4I
    Make/N=(V_npnts-V_maxloc)/O $SplitRefD, $SplitDat1D, $SplitDat2D, $SplitDat3D, $SplitDat4D
    iterate (V_maxloc+1)
        $SplitRefI[i]=$ReferenceWave[i]; $SplitDat1I[i]=$DataWave1[i]
        $SplitDat2I[i]=$DataWave2[i]; $SplitDat3I[i]=$DataWave3[i];$SplitDat4I[i]=$DataWave4[i]
        $SplitRefD[i]=$ReferenceWave[V_npnts-1-i]; $SplitDat1D[i]=$DataWave1[V_npnts-1-i]
        $SplitDat2D[i]=$DataWave2[V_npnts-1-i]; $SplitDat3D[i]=$DataWave3[V_npnts-1-i]
        $SplitDat4D[i]=$DataWave4[V_npnts-1-i]
        loop
End
```

StatCalc was used to determine the average of the 12 gages and the upper and lower 95% confidence limits, as well as for making the calculations for the inputs to the scatter, magnitude, and slope figures of merit. Using the input gage type, the substrate material, and the cycle number, it built names for each of the 12 static apparent strain waves Waves were created for the statistical parameters, as well as for an average of the three reference temperature waves. As the routine scrolled down each heatup and cooldown wave for each of the 12 gages, the points for equivalent temperatures were picked off and placed into an intermediate wave. By using the IGOR WaveStats operation, the average of the 12 gages was determined, as well as the standard deviation, which was used for the confidence limit calculation. Failed gages, which were assigned nonnumeric values, were automatically accounted for by the WaveStats operation. WaveStats decremented an internal counter of the valid data points by the number of nonnumeric values found in the data. Once the average strain and temperature waves had been obtained, the figure-of-merit inputs were calculated.

```
Macro StatCalc(GageType, Substrate, CycleNo)
    Variable GageType, Substrate, CycleNo
    Prompt GageType, "1) DETCBCL, 2) CKA1, 3) PdCr"
    Prompt Substrate, "1) IN100, 2) B21S TMC"
    Prompt CycleNo, "1 - 12"

    PauseUpdate;Silent 1
    String name0, name1, name2
        String gage="SG", TC="TCB", hh="_H", ch="_C", Base, ModSGh, ModSGc, ModTCh, ModTCc, GT, SM, CN
    Variable npnts, ngages=12, GN
    Make/N=(ngages)/O transferSGh, transferTCh, transferSGc, transferTCc
    if (GageType==1)
        GT="B"
```

```
else
    if (GageType==2)
        GT="K"
    else
        GT="P"
    endif
endif
if (Substrate==1)
    SM="I"
else
    SM="T"
endif
if (CycleNo<10)
    CN=num2istr(0)+num2istr(CycleNo)
else
    CN=num2istr(CycleNo)
endif
if (CycleNo<9)
    npnts=9
else
    if (CycleNo<11)
        npnts=10
    else
        npnts=11
    endif
endif
    String ASGh=GT+SM+CN+"_AH", ATCh=GT+SM+CN+"_TH", ASGc=GT+SM+CN+"_AC", ATCc=GT+SM+CN+"_TC"
    String USGh=GT+SM+CN+"_UH", LSGh=GT+SM+CN+"_LH", USGc=GT+SM+CN+"_UC", LSGc=GT+SM+CN+"_LC"
Make/N=(npnts)/O $ASGh, $ATCh, $ASGc, $ATCc, $USGh, $LSGh, $USGc, $LSGc
iterate (npnts)
    iterate (ngages)
        if (i<4)
            Base=Abase
            GN=i+1
        endif
        if ((i>3)*(i<8))
            Base=Dbase
            GN=i-3
        endif
        if (i>7)
            Base=Ebase
            GN=i-7
        endif
        ModSGh=Base+"SG"+num2istr(GN)+hh
        ModSGc=Base+"SG"+num2istr(GN)+ch
        ModTCh=Base+"TCB"+hh
        ModTCc=Base+"TCB"+ch
        transferSGh[i]=$ModSGh[j]
        transferTCh[i]=$ModTCh[j]
        transferSGc[i]=$ModSGc[j]
        transferTCc[i]=$ModTCc[j]

        loop
        WaveStats/Q transferSGh
        $ASGh[i]=V_avg
        $USGh[i]=V_avg+t95CL(V_npnts)*V_sdev
        $LSGh[i]=V_avg-t95CL(V_npnts)*V_sdev
        WaveStats/Q transferTCh
        $ATCh[i]=V_avg
```

```
        WaveStats/Q transferSGc
        $ASGc[i]=V_avg
        $USGc[i]=V_avg+t95CL(V_npnts)*V_sdev
        $LSGc[i]=V_avg-t95CL(V_npnts)*V_sdev
        WaveStats/Q transferTCc
        $ATCc[i]=V_avg
    loop
    String FMinH=GT+SM+CN+"_FMinH", FMinC=GT+SM+CN+"_FMinC"
    Make/N=3/O $FMinH, $FMinC
    String ASGhI=GT+SM+CN+"_AHi", ATChI=GT+SM+CN+"_THi", ASGcI=GT+SM+CN+"_ACi", ATCcI=GT+SM+CN+"_TCi"
    String USGhI=GT+SM+CN+"_UHi", LSGhI=GT+SM+CN+"_LHi", USGcI=GT+SM+CN+"_UCi", LSGcI=GT+SM+CN+"_LCi"
    Make/N=256/O $ASGhI,$USGhI,$LSGhI,$ASGcI,$USGcI,$LSGcI
    Interpolate/N=256/E=1/I/Y=$USGhI/X=$ATChI $USGh /X=$ATCh
    Interpolate/N=256/E=1/I/Y=$LSGhI/X=$ATChI $LSGh /X=$ATCh
    Interpolate/N=256/E=1/I/Y=$ASGhI/X=$ATChI $ASGh /X=$ATCh
    Interpolate/N=256/E=1/I/Y=$USGcI/X=$ATCcI $USGc /X=$ATCc
    Interpolate/N=256/E=1/I/Y=$LSGcI/X=$ATCcI $LSGc /X=$ATCc
    Interpolate/N=256/E=1/I/Y=$ASGcI/X=$ATCcI $ASGc /X=$ATCc
    WaveStats/Q $ATChI
    Make/N=256 UCL_LCL;UCL_LCL=$USGhI-$LSGhI
    UCL_LCL=abs(UCL_LCL)
    $FMinH[0]=AreaXY($ATChI,UCL_LCL,V_min+1,V_max-1)          |Scatter
    Duplicate/O $ASGhI dedT
    Duplicate/O $ATChI dTdp
    Differentiate dedT,dTdp
    dedT/=dTdp
    dedT=abs(dedT)
    $FMinH[2]=AreaXY($ATChI,dedT,V_min+1,V_max-1)             |Slope
    WaveStats/Q $ASGhI
    $FMinH[1]=V_max-V_min                                     |Magnitude
    WaveStats/Q $ATCcI
    UCL_LCL=$USGcI-$LSGcI
    UCL_LCL=abs(UCL_LCL)
    $FMinC[0]=AreaXY($ATCcI,UCL_LCL,V_min+1,V_max-1)          |Scatter
    Duplicate/O $ASGcI dedT
    Duplicate/O $ATCcI dTdp
    Differentiate dedT,dTdp
    dedT/=dTdp
    dedT=abs(dedT)
    $FMinC[2]=AreaXY($ATCcI,dedT,V_min+1,V_max-1)             |Slope
    WaveStats/Q $ASGcI
    $FMinC[1]=V_max-V_min                                     |Magnitude
    destfile=GT+SM+CN+".awav"
    NewPath/O savepath, destpath
    Save/T/O/P=savepath $FMinH,$FMinC, as destfile
    RemovePath savepath
    KillWaves dedT,dTdp, transferSGh, transferTCh, transferSGc, transferTCc
        KillWaves $ASGhI, $USGhI, $LSGhI, $ASGcI, $USGcI, $LSGcI, UCL_LCL
End
```

The function t95CL used a curve fit to the table of 95% confidence values versus the degrees of freedom to determine a Student's *t* value.

```
Function t95CL(nsamples)
    Variable nsamples
        Variable a=1.655565351, b=12.4319945888558, c=-6.8427630580109, d=-7.7736507612652, studt, x=nsamples-1
```

```
    |fit good for x≤120
    studt=a+b/(x*sqrt(x))+c*ln(x)/x^2+d/x^2
    Return studt
End
```

AreaXY and BinarySearch are functions provided by WaveMetrics as extras to IGOR that enable area calculations to arbitrarily spaced *x–y* data. (Note that IGOR's internal area function requires data to be evenly spaced.)

```
| return p such that x is straddled by  xwave[p] and xwave[p+1]
| return -1 if offscale at zero end or -2 if offscale at other end


|
Function BinarySearch(xwave, x)
    Wave xwave
    Variable x
;
    variable n= numpnts(xwave), tmp
    variable increasing= xwave[n-1] > xwave[0]

    variable jl= -1, ju= n          | lower and upper bounds
    variable jm                     | midpoint

    if( x == xwave[0] )
        return 0                    | special case for endpoints
    endif
    if( x == xwave[n-1] )
        return n-1
    endif

    if( increasing )
        if( x > xwave[n-1] )
            return -2
        endif
    else
        if( x < xwave[n-1] )
            return -2
        endif
    endif
    do
        if( ju-jl <= 1 )
            break;
        endif
        jm= floor((ju+jl)/2)
        if( (x >= xwave[jm]) == increasing )
            jl= jm
        else
            ju= jm
        endif
    while(1)
    return jl
end

| given a tabulated function with monotonically increasing or decreasing
| x values, return the trapezoidal area over an interval.  NaN is
```

```
| returned if the interval is out of range.
|
| REQUIRES: BinarySearch()
|
Function AreaXY(xwave, ywave, a, b)
    Wave xwave, ywave                    | xwave must be monotonic!
    Variable a, b                        | limits of integration
;
    variable n= numpnts(xwave), tmp
    variable increasing= xwave[n-1] > xwave[0], reversed=0
        if( increasing )
        if( a > b )
            tmp= a
            a= b
            b= tmp
            reversed= 1
        endif
    else
        if( a < b )
            tmp= a
            a= b
            b= tmp
            reversed= 1
        endif
    endif

    variable pa=BinarySearch(xwave,a),pb=BinarySearch(xwave,b)
    if( (pa<0) %^ (pb<0) )
        return NaN              | a or b is out of range
    endif
    pb += 1
    | now we know that a and b are somewhere between xwave[pa} and xwave[pb] inclusive
    variable f= (xwave[pa+1]-a)/(xwave[pa+1]-xwave[pa])
    variable y= f*ywave[pa]+(1-f)*ywave[pa+1]          | interpolated y at a
    variable area= (y+ywave[pa+1])*(xwave[pa+1]-a)/2   | area from a to next point
    do
        pa += 1
        if( pa >= pb )
            break;
        endif
        area += (ywave[pa]+ywave[pa+1])*(xwave[pa+1]-xwave[pa])/2
    while(1)
    if( pb != n )
        f= (xwave[pb]-b)/(xwave[pb]-xwave[pb-1])
        y= f*ywave[pb-1]+(1-f)*ywave[pb]                | interpolated y at b
        area -= (y+ywave[pb])*(xwave[pb]-b)/2           | correct for area from b to last point
    endif
    if(reversed)
        return -area
    endif
    return area
End
```

EappGraph plotted each heatup and cooldown wave for all 12 gages, used cubic-spline interpolation to graph smooth curves for the average and the confidence limits, and added the necessary annotation and legend to the graph for a single cycle of apparent strain data.

```
Macro EappGraph(GageType,Substrate,CycleNo,PNswitch,LAxisSwitch)
	Variable GageType,Substrate,CycleNo,PNswitch=0,LAxisSwitch=1
	Prompt GageType,"1) DETCBCL, 2) CKA1, 3) PdCr"
	Prompt Substrate,"1) IN100, 2) ß21S TMC"
	Prompt CycleNo,"1 - 12"
	Prompt PNswitch,"Select page numbering type: 0) None, 1) from file, 2) user input"
	Prompt LAxisSwitch,"Select left axis scaling type: 0) Auto, 1) CL+10%, 2) user input"

	PauseUpdate; Silent 1		| building window...
	String gage="SG", TC="TCB", hh="_H", ch="_C", Base, ModSGh, ModSGc, ModTCh, ModTCc, GT, SM, CN, GageT, SubMat
	Variable npnts, ngages=12, GN, LARct=7, FN0
	if (GageType==1)
		GT="B";GageT="DETCBCL"
	else
		if (GageType==2)
			GT="K";GageT="CKA1"
		else
			GT="P";GageT="PdCr"
		endif
	endif
	if (Substrate==1)
		SM="I";SubMat="IN100"
	else
		SM="T";SubMat="ß21S TMC"
	endif
	if (CycleNo<10)
		CN=num2istr(0)+num2istr(CycleNo)
	else
		CN=num2istr(CycleNo)
	endif
	String ASGh=GT+SM+CN+"_AH", ATCh=GT+SM+CN+"_TH", ASGc=GT+SM+CN+"_AC", ATCc=GT+SM+CN+"_TC"
	String USGh=GT+SM+CN+"_UH", LSGh=GT+SM+CN+"_LH", USGc=GT+SM+CN+"_UC", LSGc=GT+SM+CN+"_LC"
	String ASGhI=GT+SM+CN+"_AHi", ATChI=GT+SM+CN+"_THi", ASGcI=GT+SM+CN+"_ACi", ATCcI=GT+SM+CN+"_TCi"
	String USGhI=GT+SM+CN+"_UHi", LSGhI=GT+SM+CN+"_LHi", USGcI=GT+SM+CN+"_UCi", LSGcI=GT+SM+CN+"_LCi"
	Make/N=256/O $ASGhI, $USGhI, $LSGhI, $ASGcI, $USGcI, $LSGcI
	Interpolate/N=256/E=1/I/Y=$USGhI/X=$ATChI $USGh /X=$ATCh
	Interpolate/N=256/E=1/I/Y=$LSGhI/X=$ATChI $LSGh /X=$ATCh
	Interpolate/N=256/E=1/I/Y=$ASGhI/X=$ATChI $ASGh /X=$ATCh
	Interpolate/N=256/E=1/I/Y=$USGcI/X=$ATCcI $USGc /X=$ATCc
	Interpolate/N=256/E=1/I/Y=$LSGcI/X=$ATCcI $LSGc /X=$ATCc
	Interpolate/N=256/E=1/I/Y=$ASGcI/X=$ATCcI $ASGc /X=$ATCc
	Display $ASGhI, $USGhI, $LSGhI vs $ATChI	/W=(3, 42,637,477)
	Append $ASGcI, $USGcI, $LSGcI vs $ATCcI
	Make/O/N=8 LAxisRange
	WaveStats/Q $USGhI
	LAxisRange[0]=V_max
	LAxisRange[1]=V_min
	WaveStats/Q $LSGhI
	LAxisRange[2]=V_max
	LAxisRange[3]=V_min
	WaveStats/Q $USGcI
	LAxisRange[4]=V_max
	LAxisRange[5]=V_min
	WaveStats/Q $LSGcI
	LAxisRange[6]=V_max
	LAxisRange[7]=V_min
	iterate (ngages)
		if (i<4)
			Base=Abase
```

```
        GN=i+1
    endif
    if ((i>3)*(i<8))
        Base=Dbase
        GN=i-3
    endif
    if (i>7)
        Base=Ebase
        GN=i-7
    endif
    ModSGh=Base+"SG"+num2istr(GN)+hh
    ModSGc=Base+"SG"+num2istr(GN)+ch
    ModTCh=Base+"TCB"+hh
    ModTCc=Base+"TCB"+ch
    Append $ModSGh vs $ModTCh
    Append $ModSGc vs $ModTCc
    Redimension/N=(numpnts(LAxisRange)+4) LAxisRange
    WaveStats/Q $ModSGh
    LAxisRange[LARct+i+1]=V_max
    LAxisRange[LARct+i+2]=V_min
    WaveStats/Q $ModSGc
    LAxisRange[LARct+i+3]=V_max
    LAxisRange[LARct+i+4]=V_min
    if (i<4)
        Modify marker($ModSGh)=8, marker($ModSGc)=19
    endif
    if ((i>3)*(i<8))
        Modify marker($ModSGh)=5, marker($ModSGc)=16
    endif
    if (i>7)
        Modify marker($ModSGh)=6, marker($ModSGc)=17
    endif
    Modify mode($ModSGh)=3, mode($ModSGc)=3
loop
String CelSGdat=ModSGc+"_C", CelTCdat=ModTCc+"_C", heatrate, coolrate
Duplicate/O $ModSGc $CelSGdat
Duplicate/O $ModTCc $CelTCdat
$CelTCdat=($ModTCc-32)/1.8
Append/T $CelSGdat vs $CelTCdat
Modify gFont="Helvetica", gfSize=12, gmSize=3, mode($ASGhI)=0, lSize($ASGhI)=1.5, lStyle($ASGhI)=0, mode($ASGcI)=0,
lSize($ASGcI)=1.5, lStyle($ASGcI)=1
Modify mode($USGhI)=0, lStyle($USGhI)=2, mode($LSGhI)=0, lStyle($LSGhI)=2
Modify mode($USGcI)=0, lStyle($USGcI)=3, mode($LSGcI)=0, lStyle($LSGcI)=3
Modify grid(left)=2, grid(bottom)=2, tick=2, zero(left)=1, mirror(left)=1, minor=1, lblMargin(left)=10, lblMargin(bottom)=6, standoff=0
Label left "Apparent Strain, \F'Symbol'me"
Label bottom "Temperature, °F"
Label top "Temperature, °C"
if (LAxisSwitch==0)
    SetAxis/A left
endif
if (LAxisSwitch==1)
    WaveStats/Q LAxisRange
    print "Left Axis Range Max:",V_max,"Left Axis Range Min:",V_min
    SetAxis left V_min-.1*abs(V_min),V_max+.1*abs(V_max)
endif
if (LAxisSwitch==2)
    NewPath/O LAR "Keith-80HD:Files:GWP29:Final Report:Apparent Strain Grapher Folder:"
    LoadWave/O/T/Q/P=LAR "LftAxRng.awav"
    RemovePath LAR
```

```
    SetAxis left LftAxRng[0],LftAxRng[1]
    KillWaves LftAxRng
endif
WaveStats/Q $ATChI
SetAxis bottom 0, V_max+10
SetAxis top -17.7778, ((V_max+10)-32)/1.8
Modify mode($CelSGdat)=2, mSize=0
if ((CycleNo<3)+(CycleNo>6))
    heatrate="10"
else
    heatrate="60"
endif
if ((CycleNo==5)+(CycleNo==6))
    coolrate="60"
else
    coolrate="10"
endif
Variable/G FN
if (GageType==1)
    if (Substrate==1)
        FN0=25
    else
        FN0=61
    endif
else
    if (GageType==2)
        if (Substrate==1)
            FN0=1
        else
            FN0=37
        endif
    else
        if (GageType==3)
            if (Substrate==1)
                FN0=13
            else
                FN0=49
            endif
        else
            Abort
        endif
    endif
endif
FN=FN0+CycleNo-1
Textbox /F=0/A=MB/E "Figure 5.1."+num2istr(FN)+".  "+GageT+" Gage Cycle " +num2istr(CycleNo)+" Apparent Strain on "+SubMat
Legend/J /A=LB/T={100} "\Z10Heat-up:\t Cool-down:"
AppendText "\s("+Abase+"SG1"+hh+") LaRC data    \s("+Abase+"SG1"+ch+") LaRC data"
AppendText "\s("+Dbase+"SG1"+hh+") DFRC data   \s("+Dbase+"SG1"+ch+") DFRC data"
AppendText "\s("+Ebase+"SG1"+hh+") LeRC data    \s("+Ebase+"SG1"+ch+") LeRC data"
AppendText  "\s("+GT+SM+CN+"_AHi) Average      \s("+GT+SM+CN+"_ACi)  Average"
AppendText "\s("+GT+SM+CN+"_UHi) 95% CL      \s("+GT+SM+CN+"_UCi) 95% CL"
AppendText "Heating/Cooling Rate (°F/min):  "+heatrate+"/"+coolrate
if (PNswitch==0)
    TextBox /F=0/Y=-10/A=MB/E " "
endif
if (PNswitch==1)
        NewPath/O Numbers "Keith-80HD:Files:GWP29:Final Report:Apparent Strain Grapher Folder:"
    LoadWave/O/T/Q/P=Numbers "PNo_FNo.awav"
    RemovePath Numbers
```

```
        FindLevel/Q FigNo, FN
        Variable PN
        PN=PageNo[V_LevelX]
        TextBox /F=0/Y=-10/A=MB/E "5."+num2istr(PN)
        KillWaves PageNo,FigNo
    endif
    if (PNswitch==2)
        String/G UPN=""
        UserPN()
        TextBox /F=0/Y=-10/A=MB/E UPN
    endif
EndMacro
Proc UserPN(UserPageNo)
    String UserPageNo
    Prompt UserPageNo, "Enter custom page number for graph:"
    UPN=UserPageNo
End
```

This IGOR layout scales and places graphs for two apparent strain cycles onto one page.

```
Window Layout0() : Layout
    PauseUpdate; Silent 1          | building window...
    Layout /I/W=(.25,.25,6,6.5) Graph0(1,1,7.5,5.63)/O=1/F=0,Graph1(1,5.56,7.5,10.25)/O=1/F=0
EndMacro
```

The apparent strain repeatability figures of merit were calculated by using the routines ReportCompares and EappRepeat. ReportCompares is a utility macro that executed EappRepeat for each of the repeatability comparisons to be made and saved the resultant inputs to the figure-of-merit comparison in a separate file for each gage type/substrate combination. The cycle designations for the repeatability comparisons were stored in waves "First" and "Second," and loaded into the routine for execution. Other repeatability comparisons could be made quickly and easily simply by entering different cycle numbers into these waves.

```
Macro ReportCompares(GageType,Substrate)
    Variable GageType,Substrate
    Prompt GageType,"Enter gage type:  1) DETCBCL, 2) CKA1, 3) PdCr"
    Prompt Substrate,"Enter material type:  1) IN100, 2) ß21S TMC"

    PauseUpdate;Silent 1
    String SeqPath="Keith-80HD:Files:GWP29:Final Report:Apparent Strain Repeat Folder:",GT,SM
    NewPath/O GWP29Seq SeqPath
    LoadWave/O/T/Q/P=GWP29Seq "RepeatComp.awav"
    RemovePath GWP29Seq
    Make/N=(numpnts(Second))/O FM_AS_Rw
    iterate (numpnts(First))
        EappRepeat(GageType,Substrate,First[i],Second[i],0)
        FM_AS_Rw[i]=FM_AS_R
    loop
    KillWaves First,Second
    if (GageType==1)
        GT="B"
    else
        if (GageType==2)
            GT="K"
        else
```

```
            GT="P"
        endif
    endif
    if (Substrate==1)
        SM="I"
    else
        SM="T"
    endif
    String repeat=GT+SM+"r"
    NewPath/O savepath, "Keith-80HD:Files:GWP29:Eapp FoM:"
    Save/T/O/P=savepath FM_AS_Rw as repeat
    RemovePath savepath
    Beep;Beep
End
```

EappRepeat determined the appropriate file names and paths for loading the apparent strain and temperature data for making the repeatability comparisons and then performed the calculations and stored them in a special variable. EappRepeat can be run independently of ReportCompares and optionally can report certain statistics regarding the equality of the temperature data for the two input apparent strain waves to determine the quality of the comparison.

```
Macro EappRepeat(GageType,Substrate,Half1,Half2,Messages)
    Variable GageType,Substrate,Half1=1.0,Half2=1.1,Messages=1
    Prompt GageType,"Enter gage type:  1) DETCBCL, 2) CKA1, 3) PdCr"
    Prompt Substrate,"Enter material type:  1) IN100, 2) ß21S TMC"
    Prompt Half1,"Enter first half-cycle designation"      |should be entered in format "x.y" where x is
    Prompt Half2,"Enter second half-cycle designation"     |cycle number and y is 0 for HU and 1 for CD
    Prompt Messages,"Print Messages? 0-N,1-Y"

    PauseUpdate;Silent 1
    String hh="HU",ch="CD",HCcode1,HCcode2,GT,SM,HCN1,HCN2
    Variable npnts,ngages=12,GN
    if (GageType==1)
        GT="B"
    else
        if (GageType==2)
            GT="K"
        else
            GT="P"
        endif
    endif
    if (Substrate==1)
        SM="I"
    else
        SM="T"
    endif
    if (Half1<10)
        HCN1=num2istr(0)+num2istr(trunc(Half1))+"_A"
    else
        HCN1=num2istr(trunc(Half1))+"_A"
    endif
    if (round((Half1-trunc(Half1))*10)==0)
        HCN1+="H";HCcode1=hh
    else
        HCN1+="C";HCcode1=ch
    endif
```

```
if (Half2<10)
    HCN2=num2istr(0)+num2istr(trunc(Half2))+"_A"
else
    HCN2=num2istr(trunc(Half2))+"_A"
endif
if (round((Half2-trunc(Half2))*10)==0)
    HCN2+="H";HCcode2=hh
else
    HCN2+="C";HCcode2=ch
endif
String gage1=GT+SM+HCN1+"i", gage2=GT+SM+HCN2+"i", FolderName1=GT+SM, FolderName2=GT+SM
String temp1=gage1[0,4]+"T"+gage1[6,7],temp2=gage2[0,4]+"T"+gage2[6,7]
if (mod(trunc(Half1),2)==1)
    if (Half1<10)
        FolderName1+=num2istr(0)+num2istr(trunc(Half1))
    else
        FolderName1+=num2istr(trunc(Half1))
    endif
    if (Half1+1<10)
        FolderName1+=num2istr(0)+num2istr(trunc(Half1)+1)
    else
        FolderName1+=num2istr(trunc(Half1)+1)
    endif
else
    if (Half1-1<10)
        FolderName1+=num2istr(0)+num2istr(trunc(Half1)-1)
    else
        FolderName1+=num2istr(trunc(Half1)-1)
    endif
    if (Half1<10)
        FolderName1+=num2istr(0)+num2istr(trunc(Half1))
    else
        FolderName1+=num2istr(trunc(Half1))
    endif
endif
if (mod(trunc(Half2),2)==1)
    if (Half2<10)
        FolderName2+=num2istr(0)+num2istr(trunc(Half2))
    else
        FolderName2+=num2istr(trunc(Half2))
    endif
    if (Half2+1<10)
        FolderName2+=num2istr(0)+num2istr(trunc(Half2)+1)
    else
        FolderName2+=num2istr(trunc(Half2)+1)
    endif
else
    if (Half2-1<10)
        FolderName2+=num2istr(0)+num2istr(trunc(Half2)-1)
    else
        FolderName2+=num2istr(trunc(Half2)-1)
    endif
    if (Half2<10)
        FolderName2+=num2istr(0)+num2istr(trunc(Half2))
    else
        FolderName2+=num2istr(trunc(Half2))
    endif
endif
FolderName1+=" Folder";FolderName2+=" Folder"
```

```
    String lpath="Keith-80HD:Files:GWP29:Final Report:Apparent Strain graphs:"
    NewPath/O load1 lpath+FolderName1
    LoadWave/O/Q/P=load1 gage1+".bwav"
    LoadWave/O/Q/P=load1 temp1+".bwav"
    RemovePath load1
    NewPath/O load2 lpath+FolderName2
    LoadWave/O/Q/P=load2 gage2+".bwav"
    LoadWave/O/Q/P=load2 temp2+".bwav"
    RemovePath load2
    String repeat=GT+SM+"_C"+HCN1[0,1]+HCcode1+"C"+HCN2[0,1]+HCcode2
    Make/N=256/O $repeat,tempstats,tempavg
    $repeat=abs($gage1-$gage2)
    tempstats=$temp1-$temp2
    if (Messages==1)
        print ""
        print "Repeatability Comparison Temperature Statistics for"+repeat+" :"
        WaveStats tempstats
    endif
    iterate (256)
        tempavg[i]=($temp1[i]+$temp2[i])/2
    loop
    WaveStats/Q tempavg
    Variable/G FM_AS_R=AreaXY(tempavg,$repeat,V_min+1,V_max-1)
    if (Messages==1)
        print "Area between "+gage1+" and "+gage2+" = "+num2str(FM_AS_R)
    endif
    KillWaves tempstats,$gage1,$gage2,$temp1,$temp2
End
```

4.3 Drift Strain

4.3.1 Data Reduction Procedures

Data taken at all three centers were reduced and formalized before being sent to the designated reporting center. The reduced data were loaded into the analysis software package IGOR and then represented as "waves," or columns of data, and arranged for processing. Data processing included selecting the group of consecutive points within the test parameters, extracting specific test points, performing calculations, curve fitting, and presenting. The original data were taken every minute for the entire test from the beginning of heatup to the cooldown to room temperature.

The first routines, InCN, Gage Type, and Specimen Code, set up the preliminary information of cycle number, type of gage tested, and specimen identification code, respectively.

The data were restructured using StrainvsTemp, which extracted the specific data points record at 15-min intervals at the required test temperature for the minimum of 4 hr at temperature.

The routine Split selected the points where all six thermocouples were within ±5 F deg (±3 C deg) of the test temperature and created the final data waves for the 4-hr drift test.

The routine ComAvgCl called the routine AVGALL, which calculated the average of the 12 gages and then calculated the upper and lower confidence limits at each point for the 12 gages. The average, upper-confidence-limit, and lower-confidence-limit waves were then fitted by using the spline curve-fit functions. The spline curve-fit functions were written in the IGOR procedure file as "functions" and were labeled Spline and Splint. The fitted waves were then plotted with the individual data points versus the test time, beginning with time 0 and ending with time 240 (240 min).

The routine MeansConf calculated the average and the upper and lower confidence limits for the four gages tested at Langley. The routine Fit produced the spline curve-fit waves for the waves created by the routine MeansConf.

The routine Calculations calculated the values used to determine figures of merit and could be used for either 4 or 12 gages because the routine used the fitted waves for the average and the upper and lower confidence limits in calculating scatter, slope, repeatability, and magnitude. The routine called IntegrateAbs returned the area of the absolute value of a function with respect to the Y axis by using trapezoidal integration and also called AreaXY , which is an internal IGOR routine.

The routine DriftwCorrectGF called another routine, GFCorrection, which adjusted the strain by converting the measured strain of gage factor 2.0 to the correct strain for the gage factor for the respective temperature. The routine then calculated the average and the upper and lower confidence limits and repeated the process for a second cycle, if applicable. The plots for final printing were called and placed onto a page

layout. Accessory routines used in data analysis were Zeroshift, Unzero, and CalcFinal, which zeroed the data, restored original values to data, and called the necessary routines to process data for 12 gages, respectively. Other routines were set up for graphs, tables, and layouts for final plots and presentation.

4.3.2 Data Reduction Routines

```
Macro InCN(CN)              |Input cycle number
Variable CN
string/G Cn,Tp
Prompt CN,"Enter cycle number: "
Silent 1
if ((CN>7) + (CN<1))
Abort "Invalid cycle number — Test Plan 9/17/93 has 7 cycles for Drift strain"
endif
CycleNumber=CN;Cn=num2str(CycleNumber);Tp=num2str((CycleNumber*150)+450)
EndMacro

Macro GageType(GTyp)            |Input type of gages
string/G Gages
variable  GTyp
Prompt GTyp, "Enter Gage Type: 1=DETC BCL-3; 2=LaRC-CKA1B; 3=PdCr",popup,"1;2;3"
If (GTyp==1)
Gages="DETC BCL-3"
endif
If (GTyp==2)
Gages="LaRC-CKA1B"
endif
If (GTyp==3)
Gages="PdCr"
endif
EndMacro

Macro SpecimenCode(SpNm)      |Input ID code of specimen or type of material
string SpNm
Prompt SpNm, "Enter Specimen Code:"
SpecNum=SpNm
EndMacro

Proc StrainvsTemp()           |Select data for final points
Silent 1                  | Don't display macro commands
Variable Last             | Last is the last point in the full data set
Variable L, i,Tlast,Lgh
WaveStats/Q ATCB;Make/n=8/O TTemp;Tlast=(numpnts(ATCB)/15)+1;Last=numpnts(ATCB)
Make/O Time2, TA, TB, TC, TD, TE, TF, Strain1, Strain2, Strain3, Strain4
MAKE/O DTIME2,DTA,DTB,DTC,DTD,DTE,DTF,Strain5, Strain6, Strain7, Strain8
TTemp(1)=600;TTemp(2)=750;TTemp(3)=900;TTemp(4)=1050
(StrainvsTemp continued)
TTemp(5)=1200;TTemp(6)=1350;TTemp(7)=1500
L=0;i=0
Do
Time2[L]=ATime1[i]
TA[L]=ATCA[i]
TB[L]=ATCB[i]
TC[L]=ATCC[i]
TD[L]=ATCD[i]
TE[L]=ATCE[i]
TF[L]=ATCF[i]
Strain1[L]=ASG1[i]
```

```
Strain2[L]=ASG2[i]
Strain3[L]=ASG3[i]
Strain4[L]=ASG4[i]
L=L+1;i=i+15
While(i<=Last)
Redimension/N=(Tlast) Time2 TA TB TC TD TE TF Strain1 Strain2 Strain3 Strain4
nar=numpnts(TB)
L=0;i=0
Do
DTime2[L]=DTime1[i]
DTA[L]=DTCA[i]
DTB[L]=DTCB[i]
DTC[L]=DTCC[i]
DTD[L]=DTCD[i]
DTE[L]=DTCE[i]
DTF[L]=DTCF[i]
Strain5[L]=DSG1[i]
Strain6[L]=DSG2[i]
Strain7[L]=DSG3[i]
Strain8[L]=DSG4[i]
L=L+1;i=i+15
While(i<=Last)
Redimension/N=(Tlast) DTime2 DTA DTB DTC DTD DTE DTF
Redimension/N=(Tlast) Strain5 Strain6 Strain7 Strain8
EndMacro

Proc Split()                    |Create final data waves (** 4 Gages **)
Silent 1
Variable J,K,Tmp
Make/N=(nar)/O TempD,TDE,TTimD,Strain1D,Strain2D,Strain3D,Strain4D,AvgStrainD
Make/N=(nar)/O DTempD,DTDE,DTTimD,Strain5D,Strain6D,Strain7D,Strain8D
J=0;K=0;NumPts=0;Tmp=TTemp(CycleNumber)
Do
K=K+1
While(TB(K)<(Tmp-5))
Do
(Split continued)
TempD(J)=TB(K);TDE(J)=TE(K);TTimD(J)=Time2(K);Strain2D(J)=Strain2(K)
Strain3D(J)=Strain3(K);Strain4D(J)=Strain4(K)
AvgStrainD(J)=(Strain1(K)+Strain2(K)+Strain3(K)+Strain4(K))/4
J=J+1;K=K+1;NumPts=NumPts+1
While(TB(K)>=(Tmp-5))
Redimension/N=(NumPts) TempD,TDE,TTimD,Strain1D,Strain2D,Strain3D,Strain4D,AvgStrainD
J=0;K=0;NumPts=0;Tmp=TTemp(CycleNumber)
Do
K=K+1
While(DTB(K)<(Tmp-5))
Do
DTempD(J)=DTB(K);DTDE(J)=DTE(K);DTTimD(J)=DTime2(K)Strain5D(J)=Strain5(K)
Strain6D(J)=Strain6(K);Strain7D(J)=Strain7(K);Strain8D(J)=Strain8(K)
AvgStrainD(J)=(AvgStrainD(J)+(Strain5(K)+Strain6(K)+Strain7(K)+Strain8(K))/4)/2
J=J+1;K=K+1;NumPts=NumPts+1
While(DTB(K)>=(Tmp-5))
Redimension/N=(NumPts) DTempD,DTDE,DTTimD,
Strain5D,Strain6D,Strain7D,Strain8D
KillWaves/F Time2, TA, TB, TC, TD, TE, TF, Strain1
KillWaves/F Strain2, Strain3, Strain4, Strain6, Strain7, Strain8
KillWaves/F DTIME2,DTA,DTB,DTC,DTD,DTE,DTF,Strain5
EndMacro
```

```
Macro AVGALL()              |Average data from 12 gages
Silent 1
Variable J
J=0;AvgStrainD[0,16]=0
iterate(17)
AvgStrainD(J)=Strain1D(J)+Strain2D(J)+Strain3D(J)+Strain4D(J)
AvgStrainD(J)=AvgStrainD(J)+Strain5D(J)+Strain6D(J)+Strain7D(J)+Strain8D(J)
AvgStrainD(J)=(AvgStrainD(J)+ESG1(J)+ESG2(J)+ESG3(J)+ESG4(J))/12;J=J+1
loop
EndMacro

Proc MeansConf()            |Create Confidence limits
Silent 1
Variable C1
print "GAGES TESTED AT LaRC ONLY!! (** 4 GAGES **)'
Make/N=(NumPts)/O ConfidenceD, UConfidenceD, LConfidenceD
C1=2.353/2/sqrt(3)          | C1=t/sqr(n)/sqrt(n-1)
iterate (NumPts)
AvgStrainD(i)=(Strain1D(i)+Strain2D(i)+Strain3D(i)+Strain4D(i))/4
ConfidenceD(i)=(Strain1D(i)-AvgStrainD(i))*(Strain1D(i)-AvgStrainD(i))
ConfidenceD(i)=ConfidenceD(i)+(Strain2D(i)-AvgStrainD(i))*(Strain2D(i)-AvgStrainD(i))
ConfidenceD(i)=ConfidenceD(i)+(Strain3D(i)-AvgStrainD(i))*(Strain3D(i)-AvgStrainD(i))
 (MeansConf continued)
ConfidenceD(i)=ConfidenceD(i)+(Strain4D(i)-AvgStrainD(i))*(Strain4D(i)-AvgStrainD(i))
ConfidenceD(i)=sqrt(ConfidenceD(i))*C1
UConfidenceD(i)=AvgStrainD(i)+ConfidenceD(i)
LConfidenceD(i)=AvgStrainD(i)-ConfidenceD(i)
loop
EndMacro

Proc Fit()                  |Create curve fits for average and C.limits
Variable Dummy
Silent 1
Make/N=(NumPts)/O U, AvgStrainDY2,UConfidenceDY2, LConfidenceDY2
Make/N=256/O AvgStrainDFit, UConfidenceDFit, LConfidenceDFit
SetScale/I x (TTimD(0)), (TTimD(NumPts)), "" AvgStrainDFit, UConfidenceDFit, LConfidenceDFit
Dummy=Spline(TTimD, AvgStrainD, AvgStrainDY2, NumPts)
Dummy=Spline(TTimD, UConfidenceD, UConfidenceDY2, NumPts)
Dummy=Spline(TTimD, LConfidenceD, LConfidenceDY2, NumPts)
AvgStrainDFit=SplInt(TTimD, AvgStrainD, AvgStrainDY2, NumPts, x)
UConfidenceDFit=SplInt(TTimD, UConfidenceD, UConfidenceDY2, NumPts, x)
LConfidenceDFit=SplInt(TTimD, LConfidenceD, LConfidenceDY2, NumPts, x)
KillWaves/F AvgStrainDY2,UConfidenceDY2, LConfidenceDY2
EndMacro

Macro CalcFinal()
DoAlert 1,"Calculates Final Data for all 12 Gages. Continue?"
StrainvsTemp();Split();ComAvgCl();Fit()
EndMacro()

Macro PlotFinal()
Silent 1
CloseWindows();GraphD();Graph2D();LayoutP()
EndMacro

Macro Calculations()        |Calculates Figure of Merit Numbers
Variable  RepeatX
Variable i, lim,j
```

```
Silent 1
Variable Magnitude, Scatter, Slope,Repeatability
String Mag,Sca,Slo,Rep
Make/N=17/O DerD
Make/N=256/O DerivativeD, Repeatability1
Make/N=256/O AvgStrainDFitX
WaveStats/Q AvgStrainDFit
j=1
do
AvgStrainD[j-1]=AvgStrainD[NumPts-(18-j)]
j=j+1
(Calculations continued)
while(j<18)
DerD=AvgStrainD;Differentiate DerD;Magnitude=IntegrateAbs(DerD)
Scatter=AreaXY(ETIME1,UConfidenceD,0,240)
Scatter=Scatter-AreaXY(ETIME1,LConfidenceD,0,240)
DerivativeD=AvgStrainDFit
Differentiate DerivativeD
Slope=IntegrateAbs(DerivativeD)/240
i=0
lim=255
do
if (i>lim)
break
endif
AvgStrainDFitX[i]=pnt2x(AvgStrainDFit,i)
i=i+1
while (1)
i=0
lim=255
do
if (i>lim)
break
endif
RepeatX=pnt2x(Repeatability1,i)
Repeatability1[i]=interp(RepeatX,AvgStrainDFitX,AvgStrainDFit)
i=i+1
while (1)
Repeatability=IntegrateAbs(Repeatability1)
Mag=num2istr(Magnitude);Sca=num2istr(Scatter);Slo=num2istr(Slope)
Rep=num2istr(Repeatability)
DoWindow/F Layout02
Modify height(Graph02)=366;Print Mag,Sca,Slo,Rep
TextBox/N=Calc/T={12,24,36,48}/F=2/S=1/a=MC/x=1/y=-42
AppendText "Magnitude\t"+"Scatter\t"+"Slope\t"+"Repeatability"
AppendText Mag+"\t\t\t"+Sca+"\t\t\t"+Slo+"\t\t\t"+Rep
AppendText "Drift Rate (Avg)="+num2istr(Magnitude/4)+"µ\F'Symbol'e\F]0/hr"
Save/T TDA,TempD,TDC,TDD,TDE,TDF,Strain1D,Strain2D,Strain3D,Strain4D,TTimD KillWaves/F
DerD,DerivativeD,AvgStrainDFitX,Repeatability1
EndMacro

Macro CloseWindows()
DoWindow/K Table0;DoWindow/K TableA;DoWindow/K TableD
DoWindow/K Tables;DoWindow/K TableE;DoWindow/K Tableall
DoWindow/K TableC2DoWindow/K GraphD;DoWindow/K Graph2D
DoWindow/K LayoutP;DoWindow/K LayoutL
EndMacro
```

```
Macro Zeroshift()              |Corrects for Zero Shift
VARIABLE/G ZDSV1,ZDSV2,ZDSV3,ZDSV4,ZESV1,ZESV2,ZESV3,ZESV4
VARIABLE/G ZSFLAG,ZSV1,ZSV2,ZSV3,ZSV4
Silent 1
IF (ZSFLAG==1)
Beep
Print ZDSV1,ZDSV2,ZDSV3,ZDSV4,ZESV1,ZESV2,ZESV3,ZESV4, ZSV1,ZSV2,ZSV3,ZSV4
Abort " Data already zeroed!! "
endif
ZSV1=Strain1D[0];ZSV2=Strain2D[0];ZSV3=Strain3D[0];ZSV4=Strain4D[0]
Strain1D=Strain1D-ZSV1;Strain2D=Strain2D-ZSV2;Strain3D=Strain3D-ZSV3
Strain4D=Strain4D-ZSV4
ZDSV1=Strain5D[0];ZDSV2=Strain6D[0];ZDSV3=Strain7D[0];ZDSV4=Strain8D[0]
Strain5D=Strain5D-ZDSV1;Strain6D=Strain6D-ZDSV2;Strain7D=Strain7D-ZDSV3
Strain8D=Strain8D-ZDSV4
ZESV1=ESG1[0];ZESV2=ESG2[0];ZESV3=ESG3[0];ZESV4=ESG4[0]
ESG1=ESG1-ZESV1;ESG2=ESG2-ZESV2
ESG3=ESG3-ZESV3;ESG4=ESG4-ZESV4
ZSFLAG=1
EndMacro

Macro Unzero()
Strain1D=Strain1D+ZSV1;Strain2D=Strain2D+ZSV2
Strain3D=Strain3D+ZSV3;Strain4D=Strain4D+ZSV4
Strain5D=Strain5D+ZDSV1;Strain6D=Strain6D+ZDSV2
Strain7D=Strain7D+ZDSV3;Strain8D=Strain8D+ZDSV4
ESG1D=ESG1D+ZESV1;ESG2D=ESG2D+ZESV2
ESG3D=ESG3D+ZESV3;ESG4D=ESG4D+ZESV4
ZSFLAG=0
Print "Waves zeroshift replaced."
EndMacro

Macro ComAvgCl()               |
Silent 1
Variable C1
Make/N=(17)/O CConfidenceD, CUConfidenceD, CLConfidenceD
Make/N=(17)/O U,AvgStrainDY2,CUConfidenceDY2,  CLConfidenceDY2
Make/N=(17)/O AvgStrainDFit,CUConfidenceDFit,  CLConfidenceDFit
Print "<< Average and Confidence Limits for 12 Gages >>"
AvgStrainD[0,16]=0
C1=1.80/sqrt(12)/sqrt(11)          | C1=t/sqr(n)/sqrt(n-1)
AVGALL()
iterate (17)
CConfidenceD(i)=(Strain1D(i)-AvgStrainD(i))*(Strain1D(i)-AvgStrainD(i))
CConfidenceD(i)=CConfidenceD(i)+(Strain2D(i)-AvgStrainD(i))*(Strain2D(i)-AvgStrainD(i))
CConfidenceD(i)=CConfidenceD(i)+(Strain3D(i)-AvgStrainD(i))*(Strain3D(i)-AvgStrainD(i))
(ComAvgCl continued)
CConfidenceD(i)=CConfidenceD(i)+(Strain4D(i)-AvgStrainD(i))*(Strain4D(i)-AvgStrainD(i))
CConfidenceD(i)=CConfidenceD(i)+(Strain5D(i)-AvgStrainD(i))*(Strain5D(i)-AvgStrainD(i))
CConfidenceD(i)=CConfidenceD(i)+(Strain6D(i)-AvgStrainD(i))*(Strain6D(i)-AvgStrainD(i))
CConfidenceD(i)=CConfidenceD(i)+(Strain7D(i)-AvgStrainD(i))*(Strain7D(i)-AvgStrainD(i))
CConfidenceD(i)=CConfidenceD(i)+(Strain8D(i)-AvgStrainD(i))*(Strain8D(i)-AvgStrainD(i))
CConfidenceD(i)=CConfidenceD(i)+(ESG1(i)-AvgStrainD(i))*(ESG1(i)-AvgStrainD(i))
CConfidenceD(i)=CConfidenceD(i)+(ESG2(i)-AvgStrainD(i))*(ESG2(i)-AvgStrainD(i))
CConfidenceD(i)=CConfidenceD(i)+(ESG3(i)-AvgStrainD(i))*(ESG3(i)-AvgStrainD(i))
CConfidenceD(i)=CConfidenceD(i)+(ESG4(i)-AvgStrainD(i))*(ESG4(i)-AvgStrainD(i))
CConfidenceD(i)=sqrt(CConfidenceD(i))*C1
CUConfidenceD(i)=AvgStrainD(i)+CConfidenceD(i)
```

```
CLConfidenceD(i)=AvgStrainD(i)-CConfidenceD(i)
loop
VARIABLE DUMMY;Dummy=Spline(TTimD, AvgStrainD, AvgStrainDY2, NumPts)
Dummy=Spline(TTimD, CUConfidenceD, CUConfidenceDY2, NumPts)
Dummy=Spline(TTimD, CLConfidenceD, CLConfidenceDY2, NumPts)
AvgStrainDFit=SplInt(TTimD, AvgStrainD, AvgStrainDY2, NumPts, x)
CUConfidenceDFit=SplInt(TTimD, CUConfidenceD, CUConfidenceDY2, NumPts, x)
CLConfidenceDFit=SplInt(TTimD, CLConfidenceD, CLConfidenceDY2, NumPts, x)
KillWaves/F AvgStrainDY2,CUConfidenceDY2, CLConfidenceDY2
EndMacro

Function Spline(X,Y,Y2,N)  |Spline curve fit
Wave X, Y, Y2
Variable N, i, lim, SIG, P
Y2[0]=0
U[0]=0; Y2[N-1]=0; i=1; lim=N-2 |Lower & Upper b.c. set to natural
do
if (i>lim)
    break
endif
SIG=(X[i]-X[i-1])/(X[i+1]-X[i-1]); P=SIG*Y2[i-1]+2; Y2[i]=(SIG-1)/P
U[i]=(6*((Y[i+1]-Y[i])/(X[i+1]-X[i])-(Y[i]-Y[i-1])/(X[i]-X[i-1]))/(X[i+1]-X[i-1])-SIG*U[i-1])/P
i+=1
while (1)
i=N-2; lim=1
do
if (i<lim)
    break
endif
Y2[i]=Y2[i]*Y2[i+1]+U[i]; i-=1
while (1)
End

Function SplInt(XA,YA,Y2A,N,X)
Wave XA, YA, Y2A
Variable N, X
Variable KLO, KHI, K, H, A, B,Y
KLO=1
KHI=N
do
if ((KHI-KLO-0.5)>1)
K=((KHI+KLO)/2)-0.5
if (XA[round(K-1)]>X)
KHI=round(K)
else
KLO=round(K)
endif
else
break
endif
while (1)
H=XA[round(KHI-1)]-XA[round(KLO-1)]
A=(XA[round(KHI-1)]-X)/H
B=(X-XA[round(KLO-1)])/H
Y=A*YA[round(KLO-1)]+B*YA[round(KHI-1)]
Y=Y+((A^3-A)*Y2A[round(KLO-1)]+(B^3-B)*Y2A[round(KHI-1)])*(H^2)/6
return (Y)
End
```

```
Function IntegrateAbs(Y)
Wave Y
Variable i, lim
i=0
lim=numpnts(Y)-1
do
if (i>lim)
    break
endif
Y[i]=abs(Y[i])
i+=1
while (1)
return (area(Y,leftx(Y),pnt2x(Y,numpnts(Y)-1)))
End

Window TITLE():Graph
Textbox /N=TextBox_0/F=0/A=MC/X=-1.78571/Y=41.4545
AppendText "\f01\F'Helvetica'\Z18        LaRC GWP#29 TEST"
AppendText "GWP 29 COUPON #"+SpecNum+" CYCLE "+Cn
EndMacro
Window GraphD() : Graph
PauseUpdate; Silent 1          | building window...
Display /W=(17,41,421,298) AG1C1,AG2C1,AG3C1,AG4C1 vs ETIME1
Append DG1C1,DG2C1,DG3C1,DG4C1 vs ETIME1
Append EG1C1,EG2C1,EG3C1,EG4C1 vs ETIME1
Append UCLGFCD,LCLGFCD,AVSCGFD vs ETIME1
Modify mode(AG1C1)=3,mode(AG2C1)=3,mode(AG3C1)=3,mode(AG4C1)=3
Modify mode(DG1C1)=3,mode(DG2C1)=3,mode(DG3C1)=3,mode(DG4C1)=3
Modify mode(EG1C1)=3,mode(EG2C1)=3,mode(EG3C1)=3,mode(EG4C1)=3
Modify marker(AG1C1)=8,marker(AG2C1)=8,marker(AG3C1)=8
Modify marker(AG4C1)=8,marker(DG1C1)=5,marker(DG2C1)=5
Modify marker(DG3C1)=5,marker(DG4C1)=5,marker(EG1C1)=6
Modify marker(EG2C1)=6,marker(EG3C1)=6,marker(EG4C1)=6
Modify lStyle(AG3C1)=2,lStyle(AG4C1)=3
Modify lStyle(UCLGFCD)=3,lStyle(LCLGFCD)=2
Modify rgb(UCLGFCD)=(26300,0,0),rgb(LCLGFCD)=(2608,8563,65535)
Modify grid=1; Modify mirror=1; Modify nticks(left)=7; Modify fSize=10
Modify lblMargin(bottom)=50
Modify axOffset(left)=1.875,axOffset(bottom)=4
Modify manTick(bottom)={0,30,0,0},manMinor(bottom)={0,0}
Label bottom "\Z10Time (min)"
SetAxis left -2000,2000; SetAxis bottom 0,245
Legend/J /A=MB/X=-29.9652/Y=60 "\Z08\s(AG1C1) Tested@LaRC\r\s(EG1C1) Tested@LeRC"
AppendText "\s(DG1C1) Tested@DFRC\r\s(AVSCGFD) AverageStrain"
AppendText "\s(UCLGFCD) UpperConfidenceLimit\r\s(LCLGFCD) LowerConfidenceLimit"
EndMacro

Window Graph2D() : Graph
PauseUpdate; Silent 1          | building window...
Display /W=(134,96,538,353) C2AG1C1,C2AG2C1,C2AG3C1 vs C2ETIME1
Append C2AG4C1 vs C2ETIME1
Append C2DG1C1,C2DG2C1,C2DG3C1,C2DG4C1 vs C2ETIME1
Append C2EG1C1,C2EG2C1,C2EG3C1,C2EG4C1 vs C2ETIME1
Append C2AVSCGFD,C2UCLGFCD,C2LCLGFCD vs C2ETIME1
Modify mode(C2AG1C1)=3,mode(C2AG2C1)=3
Modify mode(C2AG3C1)=3,mode(C2AG4C1)=3
Modify mode(C2DG1C1)=3,mode(C2DG2C1)=3
Modify mode(C2DG3C1)=3,mode(C2DG4C1)=3
Modify mode(C2EG1C1)=3,mode(C2EG2C1)=3
```

```
Modify mode(C2EG3C1)=3,mode(C2EG4C1)=3
Modify marker(C2AG1C1)=8,marker(C2AG2C1)=8,marker(C2AG3C1)=8
Modify marker(C2AG4C1)=8,marker(C2DG1C1)=5,marker(C2DG2C1)=5
Modify marker(C2DG3C1)=5,marker(C2DG4C1)=5,marker(C2EG1C1)=6
Modify marker(C2EG2C1)=6,marker(C2EG3C1)=6,marker(C2EG4C1)=6
Modify lStyle(C2UCLGFCD)=3,lStyle(C2LCLGFCD)=2
Modify rgb(C2UCLGFCD)=(26300,0,0),rgb(C2LCLGFCD)=(2608,8563,65535)
Modify grid=1;Modify mirror=1;Modify nticks(left)=7;Modify fSize=10
(Graph2D continued)
Modify lblMargin(bottom)=48
Modify axOffset(left)=1.875,axOffset(bottom)=4
Modify manTick(bottom)={0,30,0,0},manMinor(bottom)={0,0}
Label bottom "\Z10Time (min)"
SetAxis left -2000,2000;SetAxis bottom 0,245
Legend/J /A=MB/X=-29.6167/Y=60.6452 "\Z08\s(C2AG1C1) Tested@LaRC\r\s(C2EG1C1) Tested@LeRC"
AppendText "\s(C2DG1C1) Tested@DFRC\r\s(C2UCLGFCD) UpperConfidenceLimit"
AppendText "\s(C2LCLGFCD) LowerConfidenceLimit\r\s(C2AVSCGFD) AverageStrain"
EndMacro

Window LayoutP() : Layout
PauseUpdate; Silent 1          | building window...
Layout /W=(59,40,474,422) GraphD(73,56,515,376)/O=1/F=0,Graph2D(73,396,517,704)/O=1/F=0
Textbox /N=YTitle/F=0/A=MC/X=-40.3636/Y=29.9451 "\Z08   Strain\rDue to Drift\r  (μin/in)"
Textbox /N=TextBox_3/A=MC/X=2.18182/Y=6.86813
AppendText "Figure 5.2."+Cn+"  12 "+Gages+" Gages on IN100 - Cycle"+Cn
AppendText "("+Tp+"\F'Symbol'∞\F]0F)"
Textbox /N=YTitle_1/F=0/A=MC/X=-40.3636/Y=-15.6593 "\Z08   Strain\rDue to Drift\r  (μin/in)"
Textbox /N=TextBox_1/A=MC/X=1.81818/Y=-39.2857
AppendText "Figure 5.2."+(Cn+1)+"  12 " +Gages+" Gages on IN100 - Cycle "+Cn
AppendText "("+Tp+"\F'Symbol'∞\F]0F)"
EndMacro

Window Table0() : Table
PauseUpdate; Silent 1          | building window...
Edit /W=(5,42,197,167) IKDC1FoM.y  |Material,Gagetype,D,& Cycle # FoM
Modify width(Point)=64
EndMacro

Window TableA() : Table
PauseUpdate; Silent 1          | building window...
Edit /W=(5,42,515,251) ATime1.y,Strain1D.y,Strain2D.y,Strain3D.y,Strain4D.y,ATCB.y
Modify width=50;Modify format=1
EndMacro

Window TableD() : Table
PauseUpdate; Silent 1          | building window...
Edit /W=(13,114,597,281) DTimD.y,DSG1.y,DSG2.y,DSG3.y,DSG4.y
Append DTCB.y;Modify width=48;Modify format=1
EndMacro

Window TableE() : Table
PauseUpdate; Silent 1          | building window...
Edit /W=(5,42,515,251) ETime1.y,ESG1.y,ESG2.y,ESG3.y,ESG4.y,ETCB.y
Modify width(Point)=50;Modify format=1
EndMacro

Window Tableall() : Table
PauseUpdate; Silent 1          | building window...
Edit /W=(5,44,642,351) ESG1.y,ESG2.y,ESG3.y,ESG4.y,ETime1.y,Strain1D.y
```

```
Append Strain2D.y,Strain3D.y,Strain4D.y,AvgStrainD.y,Strain5D.y
Append Strain6D.y,Strain7D.y,Strain8D.y
Modify width=41;Modify format=1
EndMacro

Proc GFCorrection()          |Procedure for correcting Gage Factor
variable /G GFC,A0,A1,A2,A3,CF
make /O/N=17 AG1C1,AG2C1,AG3C1,AG4C1,DG1C1,DG2C1,DG3C1,DG4C1
make /O/N=17 EG1C1,EG2C1,EG3C1,EG4C1,C2AG1C1,C2AG2C1
make /O/N=17 C2AG3C1,C2AG4C1,C2DG1C1,C2DG2C1,C2DG3C1
make /O/N=17 C2DG4C1,C2EG1C1,C2EG2C1,C2EG3C1,C2EG4C1
PRINT "GAGE FACTOR CORRECTION MADE."
A0=2.0001;A1=.0003666;A2=-1.8390e-07;A3=-3.329e-10 |Cycle X GF Correction
GFC=A0+(A1*600)+(A2*(600^2))+(A3*(600^3));print GFC;CF=2.0/GFC
AG1C1=STRAIN1D*CF;AG2C1=STRAIN2D*CF;AG3C1=STRAIN3D*CF
AG4C1=STRAIN4D*CF;DG1C1=STRAIN5D*CF;DG2C1=STRAIN6D*CF
DG3C1=STRAIN7D*CF;DG4C1=STRAIN8D*CF;EG1C1=ESG1*CF
EG2C1=ESG2*CF;EG3C1=ESG3*CF;EG4C1=ESG4*CF
A0=2.0001;A1=.0003666;A2=-1.8390e-07;A3=-3.329e-10 |Cycle X GF Correction
GFC=A0+(A1*750)+(A2*(750^2))+(A3*(750^3));print GFC
CF=2.00/GFC
C2ESG1=C2ESG1*CF;C2ESG2=C2ESG2*CF;C2ESG3=C2ESG3*CF
C2ESG4=C2ESG4*CF;C2AG1C1=C2STRAIN1D*CF
C2AG2C1=C2STRAIN2D*CF;C2AG3C1=C2STRAIN3D*CF
C2AG4C1=C2STRAIN4D*CF;C2DG1C1=C2STRAIN5D*CF
C2DG2C1=C2STRAIN6D*CF;C2DG3C1=C2STRAIN7D*CF
C2DG4C1=C2STRAIN8D*CF
EndMacro

Macro DriftwCorrectGF()          |Corrects drift data with proper gage factor
GFCorrection()
Variable C1
Silent 1
Make/N=(17)/O CLGFCD, UCLGFCD, LCLGFCD,AVSCGFD
Make/N=(17)/O U,AVSCGFDY2,UCLGFCDY2,  LCLGFCDY2
Make/N=(256)/O AVSCGFDFit,UCLGFCDFit,  LCLGFCDFit
Print "<< Average and Confidence Limits for 12 Gages >>"
AVSCGFD[0,16]=0
C1=1.80/sqrt(12)/sqrt(11)          | C1=t/sqr(n)/sqrt(n-1)
iterate (17)
( DriftwCorrectGF continued)
AVSCGFD(i)=DG1C1(i)+DG2C1(i)+DG3C1(i)+DG4C1(i)
AVSCGFD(i)=AVSCGFD(i)+AG1C1(i)+AG2C1(i)+AG3C1(i)+AG4C1(i)
AVSCGFD(i)=(AVSCGFD(i)+EG1C1(i)+EG2C1(i)+EG3C1(i)+EG4C1(i))/12
CLGFCD(i)=(AG1C1(i)-AVSCGFD(i))*(AG1C1(i)-AVSCGFD(i))
CLGFCD(i)=CLGFCD(i)+(AG2C1(i)-AVSCGFD(i))*(AG2C1(i)-AVSCGFD(i))
CLGFCD(i)=CLGFCD(i)+(AG3C1(i)-AVSCGFD(i))*(AG3C1(i)-AVSCGFD(i))
CLGFCD(i)=CLGFCD(i)+(AG4C1(i)-AVSCGFD(i))*(AG4C1(i)-AVSCGFD(i))
CLGFCD(i)=CLGFCD(i)+(DG1C1(i)-AVSCGFD(i))*(DG1C1(i)-AVSCGFD(i))
CLGFCD(i)=CLGFCD(i)+(DG2C1(i)-AVSCGFD(i))*(DG2C1(i)-AVSCGFD(i))
CLGFCD(i)=CLGFCD(i)+(DG3C1(i)-AVSCGFD(i))*(DG3C1(i)-AVSCGFD(i))
CLGFCD(i)=CLGFCD(i)+(DG4C1(i)-AVSCGFD(i))*(DG4C1(i)-AVSCGFD(i))
CLGFCD(i)=CLGFCD(i)+(EG1C1(i)-AVSCGFD(i))*(EG1C1(i)-AVSCGFD(i))
CLGFCD(i)=CLGFCD(i)+(EG2C1(i)-AVSCGFD(i))*(EG2C1(i)-AVSCGFD(i))
CLGFCD(i)=CLGFCD(i)+(EG3C1(i)-AVSCGFD(i))*(EG3C1(i)-AVSCGFD(i))
```

```
CLGFCD(i)=CLGFCD(i)+(EG4C1(i)-AVSCGFD(i))*(EG4C1(i)-AVSCGFD(i))
CLGFCD(i)=sqrt(CLGFCD(i))*C1
UCLGFCD(i)=AVSCGFD(i)+CLGFCD(i)
LCLGFCD(i)=AVSCGFD(i)-CLGFCD(i)
loop
VARIABLE DUMMY
Dummy=Spline(ETIME1, AVSCGFD, AVSCGFDY2, 17)
Dummy=Spline(ETIME1, UCLGFCD, UCLGFCDY2, 17)
Dummy=Spline(ETIME1, LCLGFCD, LCLGFCDY2, 17)
AVSCGFDFit=SplInt(ETIME1, AVSCGFD, AVSCGFDY2, 17, x)
UCLGFCDFit=SplInt(ETIME1, UCLGFCD, UCLGFCDY2, 17, x)
LCLGFCDFit=SplInt(ETIME1, LCLGFCD, LCLGFCDY2, 17, x)
KillWaves/F AVSCGFDY2,UCLGFCDY2, LCLGFCDY2
C2DriftwCorrectGF();GraphD();Graph2D();LayoutP()
EndMacro

Proc C2DriftwCorrectGF()          |Next cycle correction (2 cycles/page)
VARIABLE C1
Silent 1                          | Don't display macro commands
Make/N=(17)/O C2CLGFCD, C2UCLGFCD, C2LCLGFCD,C2AVSCGFD
Make/N=(17)/O U,C2AVSCGFDY2,C2UCLGFCDY2, C2LCLGFCDY2
Make/N=(256)/O C2AVSCGFDFit,C2UCLGFCDFit  C2LCLGFCDFit
Print "<< Average and Confidence Limits for 12 Gages >>"
C2AVSCGFD[0,16]=0
C1=1.80/sqrt(12)/sqrt(11)         | C1=t/sqr(n)/sqrt(n-1)
iterate (17)
C2AVSCGFD(i)=C2DG1C1(i)+C2DG2C1(i)+C2DG3C1(i)+C2DG4C1(i)
C2AVSCGFD(i)=C2AVSCGFD(i)+C2AG1C1(i)+C2AG2C1(i)+C2AG3C1(i)+ C2AG4C1(i)
C2AVSCGFD(i)=(C2AVSCGFD(i)+C2EG1C1(i)+C2EG2C1(i)+C2EG3C1(i)+ C2EG4C1(i))/12
C2CLGFCD(i)=(C2AG1C1(i)-C2AVSCGFD(i))*(C2AG1C1(i)-C2AVSCGFD(i))
C2CLGFCD(i)=C2CLGFCD(i)+(C2AG2C1(i)-C2AVSCGFD(i))*(C2AG2C1(i)-C2AVSCGFD(i))
(C2DriftwCorrectGF continued)
C2CLGFCD(i)=C2CLGFCD(i)+(C2AG3C1(i)-C2AVSCGFD(i))*(C2AG3C1(i)-C2AVSCGFD(i))
C2CLGFCD(i)=C2CLGFCD(i)+(C2AG4C1(i)-C2AVSCGFD(i))*(C2AG4C1(i)-C2AVSCGFD(i))
C2CLGFCD(i)=C2CLGFCD(i)+(C2DG1C1(i)-C2AVSCGFD(i))*(C2DG1C1(i)-C2AVSCGFD(i))
C2CLGFCD(i)=C2CLGFCD(i)+(C2DG2C1(i)-C2AVSCGFD(i))*(C2DG2C1(i)-C2AVSCGFD(i))
C2CLGFCD(i)=C2CLGFCD(i)+(C2DG3C1(i)-C2AVSCGFD(i))*(C2DG3C1(i)-C2AVSCGFD(i))
C2CLGFCD(i)=C2CLGFCD(i)+(C2DG4C1(i)-C2AVSCGFD(i))*(C2DG4C1(i)-C2AVSCGFD(i))
C2CLGFCD(i)=C2CLGFCD(i)+(C2EG1C1(i)-C2AVSCGFD(i))*(C2EG1C1(i)-C2AVSCGFD(i))
C2CLGFCD(i)=C2CLGFCD(i)+(C2EG2C1(i)-C2AVSCGFD(i))*(C2EG2C1(i)-C2AVSCGFD(i))
C2CLGFCD(i)=C2CLGFCD(i)+(C2EG3C1(i)-C2AVSCGFD(i))*(C2EG3C1(i)-C2AVSCGFD(i))
C2CLGFCD(i)=C2CLGFCD(i)+(C2EG4C1(i)-C2AVSCGFD(i))*(C2EG4C1(i)-C2AVSCGFD(i))
C2CLGFCD(i)=sqrt(C2CLGFCD(i))*C1
C2UCLGFCD(i)=C2AVSCGFD(i)+C2CLGFCD(i)
C2LCLGFCD(i)=C2AVSCGFD(i)-C2CLGFCD(i)
loop
VARIABLE DUMMY
Dummy=Spline(ETIME1, C2AVSCGFD, C2AVSCGFDY2, 17)
Dummy=Spline(ETIME1, C2UCLGFCD, C2UCLGFCDY2, 17)
Dummy=Spline(ETIME1, C2LCLGFCD, C2LCLGFCDY2, 17)
C2AVSCGFDFit=SplInt(ETIME1, C2AVSCGFD, C2AVSCGFDY2, 17, x)
C2UCLGFCDFit=SplInt(ETIME1, C2UCLGFCD, C2UCLGFCDY2, 17, x)
C2LCLGFCDFit=SplInt(ETIME1, C2LCLGFCD, C2LCLGFCDY2, 17, x)
KillWaves/F C2AVSCGFDY2,C2UCLGFCDY2, C2LCLGFCDY2
EndMacro
```

4.4 Gage Factor

4.4.1 Data Reduction Procedures

Gage factor data taken at all three centers were collected and formalized before being loaded into IGOR for processing. Data from all three centers were combined to obtain the average gage factor data under tension, but only Dryden and Lewis data were combined to obtain the average gage factor data under compression. A second-degree polynomial was used for curve fitting. Failed gages were not included in the calculation of the average data, but the upper and lower 95% confidence limits were affected by the number of the failed gages.

The IGOR routines used in the process and their functions are listed as follows:

1. Load: Load the data file from hard drive.
2. InCN, Gage Type, Specimen Code: Specify cycle number, gage type, and specimen material.
3. Arrange: Assign waves to each column of the data file.
4. Split: Split data for heatup and cooldown cycles.
5. MeansConf: Calculate average data and upper and lower 95% confidence limits.
6. Fit: Perform curve fitting using second-degree polynomial.
7. HeatUpGFvsTemp: Present gage-factor-versus-temperature curves for heatup cycle.
8. CoolDownGFvsTemp: Present gage-factor-versus-temperature curves for cooldown cycle.
9. Calculations: Calculate the magnitude, slope, scatter, and repeatability of the data later used to calculate the figure of merit for gage performance.

4.4.2 Data Reduction Routines

```
Macro Load()
variable/G CycleNumber,NumPts,GTyp,FitTyp
String/G Gages,SpecNum
String base="wave"      Silent 1
NewPath/O Pathname, "Macintosh HD:IGOR Folder:GWP Folder:"
LoadWave/G/N/P=Pathname
    ZSV1=0;ZSV2=0;ZSV3=0;ZSV4=0
EndMacro
Macro Arrange()
String matchStr     String exceptStr     Silent 1
        matchStr="Time*";exceptStr="";KillMatchWaves(matchStr,exceptStr)
        matchStr="TC*";exceptStr="";KillMatchWaves(matchStr,exceptStr)
                matchStr="GF*";exceptStr="";KillMatchWaves(matchStr,exceptStr)
        Rename wave0, TCB; Rename wave1, GF1; Rename wave2, GF2;  Rename wave3,GF3; Rename wave4, GF4
        Rename wave5, TCB1; Rename wave6,GF5; Rename wave7, GF6;  Rename wave8,GF7; Rename wave9, GF8
End Macro
Macro InCN(CN)
Variable CN
        Prompt CN,"Enter cycle number: "    Silent 1
if ((CN>12) + (CN<1))  Abort "Invalid cycle number  --  Test Plan 9/17/93 has 12 cycles for apparent strain"
        endif
CycleNumber=CN
EndMacro
Macro GageType(GTyp)
string/G Gages      variable  GTyp
Prompt GTyp, "Enter Gage Type: 1=BCL; 2=CKA1; 3=PdCr",popup,"1;2;3"
If (GTyp==1) Gages="BCL"  endif
If (GTyp==2) Gages="CKA1"  endif
If (GTyp==3) Gages="PdCr"  endif
EndMacro
Macro SpecimenCode(SpNm)
string SpNm
Prompt SpNm, "Enter Specimen Code: (input IN100 or TMC)"
        SpecNum=SpNm
EndMacro
Macro Split()
```

```
        Silent 1
        NumPts=6
        Make/N=(NumPts)/O Temp1H,Temp2H,Temp3H,TempH,Temp1C,Temp2C,Temp3C,TempC,
        Make/N=(NumPts)/O GF1H, GF1C, GF2H, GF2C, GF3H, GF3C, GF4H, GF4C,GF5H, GF5C,GF6H,GF6C
        Make/N=(NumPts)/O GF7H, GF7C, GF8H, GF8C, GF9H, GF9C, GF10H, GF10C,GF11H, GF11C,GF12H,GF12C"
        Make/N=(NumPts)/O AvgGFH, AvgGFC, AvgLaRCH, AvgDryH, AvgLeRCH, AvgLaRC, AvgDryC, AvgLeRC
        Make/N=(NumPts)/O ConfidenceH, ConfidenceC, UConfidenceH, LConfidenceH, UConfidenceC, LConfidenceC
        iterate (NumPts)
        Temp1H(i)=TCB(i) Temp2H(i)=TCB1(i)  Temp3H(i)=TCB2(i)  TempH(i)=(TCB(i)+TCB1(i)+TCB2(i))/3
        GF1H(i)=GF1(i);GF2H(i)=GF2(i);GF3H(i)=GF3(i);GF4H(i)=GF4(i)
        GF5H(i)=GF5(i);GF6H(i)=GF6(i);GF7H(i)=GF7(i);GF8H(i)=GF8(i)
        GF9H(i)=GF9(i);GF10H(i)=GF10(i);GF11H(i)=GF11(i);GF12H(i)=GF12(i)
        Temp1C(i)=TCB(2*NumPts-2-i) Temp2C(i)=TCB1(2*NumPts-2-i) Temp3C(i)=TCB2(2*NumPts-2-i)
        TempC(i)=(TCB(2*NumPts-2-i)+TCB1(2*NumPts-2-i)+TCB2(2*NumPts-2-i))/3
        GF1C(i)=GF1(2*NumPts-2-i);GF2C(i)=GF2(2*NumPts-2-i);GF3C(i)=GF3(2*NumPts-2-i)
        GF4C(i)=GF4(2*NumPts-2-i);GF5C(i)=GF5(2*NumPts-2-i);GF6C(i)=GF6(2*NumPts-2-i)
        GF7C(i)=GF7(2*NumPts-2-i);GF8C(i)=GF8(2*NumPts-2-i);GF9C(i)=GF9(2*NumPts-2-i)
        GF10C(i)=GF10(2*NumPts-2-i);GF11C(i)=GF11(2*NumPts-2-i);GF12C(i)=GF12(2*NumPts-2-i)
        loop
EndMacro
Macro MeansConf()
        Variable C1  Silent 1
        /calculate means and 95% confidence levels for each half cycle C1=2.20/sqrt(12)/sqrt(11)!C1=t/sqrt(n)/sqrt(n-1)
        iterate (NumPts)
        AvgDryH(i)=(GF1H(i)+GF2H(i)+GF3H(i)+GF4H(i))/4
        AvgLeRCH(i)=(GF5H(i)+GF6H(i)+GF7H(i)+GF8H(i))/4
        AvgLaRCH(i)=(GF9H(i)+GF10H(i)+GF11H(i)+GF12H(i))/4
        AvgGFH(i)=(AvgDryH(i)*4+AvgLeRCH(i)*4+AvgLaRCH(i)*4)/12
        AvgDryC(i)=(GF1C(i)+GF2C(i)+GF3C(i)+GF4C(i))/4
        AvgLeRC(i)=(GF5C(i)+GF6C(i)+GF7C(i)+GF8C(i))/4
        AvgLaRC(i)=(GF9C(i)+GF10C(i)+GF11C(i)+GF12C(i))/4
        AvgGFC(i)=(AvgDryC(i)*4+AvgLeRC(i)*4+AvgLaRC(i)*4)/12 ConfidenceH(i)=(GF1H(i)-AvgGFH(i))*(GF1H(i)-AvgGFH(i))
                        ConfidenceH(i)=ConfidenceH(i)+(GF2H(i)-AvgGFH(i))*(GF2H(i)-AvgGFH(i))
                        ConfidenceH(i)=ConfidenceH(i)+(GF3H(i)-AvgGFH(i))*(GF3H(i)-AvgGFH(i))
                        ConfidenceH(i)=ConfidenceH(i)+(GF4H(i)-AvgGFH(i))*(GF4H(i)-AvgGFH(i))
                        ConfidenceH(i)=ConfidenceH(i)+(GF5H(i)-AvgGFH(i))*(GF5H(i)-AvgGFH(i))
                        ConfidenceH(i)=ConfidenceH(i)+(GF6H(i)-AvgGFH(i))*(GF6H(i)-AvgGFH(i))
                        ConfidenceH(i)=ConfidenceH(i)+(GF7H(i)-AvgGFH(i))*(GF7H(i)-AvgGFH(i))
                        ConfidenceH(i)=ConfidenceH(i)+(GF8H(i)-AvgGFH(i))*(GF8H(i)-AvgGFH(i))
                        ConfidenceH(i)=ConfidenceH(i)+(GF9H(i)-AvgGFH(i))*(GF9H(i)-AvgGFH(i))
                        ConfidenceH(i)=ConfidenceH(i)+(GF10H(i)-AvgGFH(i))*(GF10H(i)-AvgGFH(i))
                        ConfidenceH(i)=ConfidenceH(i)+(GF11H(i)-AvgGFH(i))*(GF11H(i)-AvgGFH(i))
                        ConfidenceH(i)=ConfidenceH(i)+(GF12H(i)-AvgGFH(i))*(GF12H(i)-AvgGFH(i))
        ConfidenceH(i)=sqrt(ConfidenceH(i))*C1
        ConfidenceC(i)=(GF1C(i)-AvgGFC(i))*(GF1C(i)-AvgGFC(i))
                ConfidenceC(i)=ConfidenceC(i)+(GF2C(i)-AvgGFC(i))*(GF2C(i)-AvgGFC(i))
                        ConfidenceC(i)=ConfidenceC(i)+(GF3C(i)-AvgGFC(i))*(GF3C(i)-AvgGFC(i))
                        ConfidenceC(i)=ConfidenceC(i)+(GF4C(i)-AvgGFC(i))*(GF4C(i)-AvgGFC(i))
                        ConfidenceC(i)=ConfidenceC(i)+(GF5C(i)-AvgGFC(i))*(GF5C(i)-AvgGFC(i))
                        ConfidenceC(i)=ConfidenceC(i)+(GF6C(i)-AvgGFC(i))*(GF6C(i)-AvgGFC(i))
                        ConfidenceC(i)=ConfidenceC(i)+(GF7C(i)-AvgGFC(i))*(GF7C(i)-AvgGFC(i))
                        ConfidenceC(i)=ConfidenceC(i)+(GF8C(i)-AvgGFC(i))*(GF8C(i)-AvgGFC(i))
                        ConfidenceC(i)=ConfidenceC(i)+(GF9C(i)-AvgGFC(i))*(GF9C(i)-AvgGFC(i))
                        ConfidenceC(i)=ConfidenceC(i)+(GF10C(i)-AvgGFC(i))*(GF10C(i)-AvgGFC(i))
                        ConfidenceC(i)=ConfidenceC(i)+(GF11C(i)-AvgGFC(i))*(GF11C(i)-AvgGFC(i))
                        ConfidenceC(i)=ConfidenceC(i)+(GF12C(i)-AvgGFC(i))*(GF12C(i)-AvgGFC(i))
        ConfidenceC(i)=sqrt(ConfidenceC(i))*C1
        UConfidenceH(i)=AvgGFH(i)+ConfidenceH(i)
```

```
        LConfidenceH(i)=AvgGFH(i)-ConfidenceH(i) UConfidenceC(i)=AvgGFC(i)+ConfidenceC(i)
        LConfidenceC(i)=AvgGFC(i)-ConfidenceC(i)
 loop
EndMacro
Macro Fit()
Variable Dummy   Silent 1
Make/N=2/O A0, A1, A2
        Make/N=(NumPts)/O
        AvgGFHY2,AvgGFCY2,AvgLaRCHY2,AvgDryHY2,AvgLeRCHY2,AvgLaRCY2,AvgDryCY2,AvgLeRCY2
        Make/N=(NumPts)/O UConfidenceHY2, LConfidenceHY2, UConfidenceCY2,LConfidenceCY2
        Make/N=(NumPts)/O AvgGFHFit,AvgGFCFit,UConfidenceHFit,LConfidenceHFit,UConfidenceCFit,LConfidenceCFit
        Make/N=(NumPts)/O AvgLaRCHFit, AvgDryHFit, AvgLeRCHFit, AvgLaRCFit, AvgDryCFit,AvgLeRCFit
        WaveStats/Q AvgGFH
CurveFit poly 3, AvgGFH(V_minloc,V_maxloc)/D=AvgGFHFit/X=TempH
    A0[0]=K0; A1[0]=K1; A2[0]=K2
WaveStats/Q UConfidenceH
CurveFit poly 3, UConfidenceH(V_minloc,V_maxloc)/D=UConfidenceHFit/X=TempH
        WaveStats/Q LConfidenceH
CurveFit poly 3, LConfidenceH(V_minloc,V_maxloc)/D=LConfidenceHFit/X=TempH
WaveStats/Q AvgGFC
        CurveFit poly 3, AvgGFC(V_minloc,V_maxloc)/D=AvgGFCFit/X=TempC
        A0[1]=K0; A1[1]=K1; A2[1]=K2
WaveStats/Q UConfidenceC
CurveFit poly 3, UConfidenceC(V_minloc,V_maxloc)/D=UConfidenceCFit/X=TempC
WaveStats/Q LConfidenceC
CurveFit poly 3, LConfidenceC(V_minloc,V_maxloc)/D=LConfidenceCFit/X=TempC
  Edit A0, A1, A2
EndMacro
Macro HeatUpGFvsTemp()
        Silent 1
        Variable p1, p2, p3
        Display  GF1H vs Temp1H as "Gage 1 G.F. vs.Temperature"
        DoWindow/K Graph01 DoWindow/CGraph01
        Make/N=(NumPts)/O TCBC
        Make/N=(NumPts)/O GF1H2;GF1H2=GF1H
        TCBC=(Temp1H-32)*5/9
        Append/T GF1H2 vs TCBC
        Append AvgGFHFit vs TempH
        Append UConfidenceHFit vs TempH
        Append LConfidenceHFit vs TempH
        Append GF2H vs Temp1H
        Append GF3H vs Temp1H
        Append GF4H vs Temp1H
        Append GF5H vs Temp2H
        Append GF6H vs Temp2H
        Append GF7H vs Temp2H
        Append GF8H vs Temp2H
        Append GF9H vs Temp3H
        Append GF10H  vs Temp3H
        Append GF11H   vs Temp3H
        Append GF12H   vs Temp3H
        Label bottom, "Temperature (°F)"      p1=1200      p2=(0-32)*5/9      p3=(p1-32)*5/9
Modify mirror(left)=1;Modify tick(left)=2;SetAxis bottom 0,p1;Modify grid(left)=1;SetAxis left 1.5,3.0
Modify width=340, height=190
Modify manTick(bottom)={0,200,0,0},manMinor(bottom)={0,0}; Modify grid(bottom)=1
SetAxis top p2,p3; Label top, "Temperature (°C)"
Modify manTick(top)={0,100,0,0},manMinor(top)={0,0}
Modify mode(GF1H2)=3,marker(GF1H2)=8, mrkThick(GF1H2)=0
Modify mode(GF1H)=3,marker(GF1H)=8;Modify mode(GF2H)=3,marker(GF2H)=8;
```

```
            Modify mode(GF3H)=3,marker(GF3H)=8;Modify mode(GF4H)=3,marker(GF4H)=8
Modify mode(GF5H)=3,marker(GF5H)=5;Modify mode(GF6H)=3,marker(GF6H)=5;
Modify mode(GF7H)=3,marker(GF7H)=5;Modify mode(GF8H)=3,marker(GF8H)=5
Modify mode(GF9H)=3,marker(GF9H)=6;Modify mode( GF10H)=3,marker( GF10H)=6;
            Modify mode(GF11H)=3,marker(GF11H)=6;Modify mode(GF12H)=3,marker(GF12H)=6
            Modify lstyle(UConfidenceHFit)=2;Modify lstyle(LConfidenceHFit)= 2
            Legend/X=-12/Y=-28/J /A=MC
            AppendText "\Z08\s(GF1H)       DFRC testdata"
            AppendText "\Z08\s(GF5H)       LeRC testdata"
            AppendText "\Z08\s(GF9H)       LaRC test data"
            AppendText "\Z08\s(AvgGFHFit)      Average"
            AppendText "\Z08\s(UConfidenceHFit)     95% CL"
            Textbox/N=TextBox_1/F=0/A=MC/X=-5/Y=-50
            AppendText "\Z10  "+Gages+" on "+SpecNum+" for cycle "+num2str(CycleNumber)+ "Heating, Tension"  LayoutP()
EndMacro
Macro CoolDownGFvsTemp()
            Silent 1
Variable p1, p2, p3"
Display  GF1C vs Temp1C as "Gage 1 G.F. vs. Temperature"
            DoWindow/K Graph02   DoWindow/C Graph02
Make/N=(NumPts)/O TCBC Make/N=(NumPts)/O GF1C2; GF1C2=GF1C
TCBC=(Temp1C-32)*5/9
Append/T GF1C2 vs TCBC
Append AvgGFCFit vs TempC
Append UConfidenceCFit vs TempC
Append LConfidenceCFit vs TempC
Append GF2C vs Temp1C
Append GF3C vs Temp1C
Append GF4C vs Temp1C
Append GF5C vs Temp2C
Append GF6C vs Temp2C
Append GF7C vs Temp2C
Append GF8C vs Temp2C
Append GF9C vs Temp3C
Append GF10C vs Temp3C
Append GF11C vs Temp3C
Append GF12C vs Temp3C
    Label bottom, "Temperature (°F)"
    p1=1200       p2=(0-32)*5/9            p3=(p1-32)*5/9
Modify mirror(left)=1;Modify tick(left)=2;SetAxis bottom 0,p1;Modify grid(left)=1;SetAxis left 1.5,3.0
Modify width=340, height=190
Modify manTick(bottom)={0,200,0,0},manMinor(bottom)={0,0}; Modify grid(bottom)=1
SetAxis top p2,p3; Label top, ""Temperature (°C)"
Modify manTick(top)={0,100,0,0},manMinor(top)={0,0}
Modify mode(GF1C2)=3,marker(GF1C2)=19, mrkThick(GF1C2)=0
Modify mode(GF1C)=3,marker(GF1C)=19;Modify mode(GF2C)=3,marker(GF2C)=19;
    Modify mode(GF3C)=3,marker(GF3C)=19;Modify mode(GF4C)=3,marker(GF4C)=19
Modify mode(GF5C)=3,marker(GF5C)=16;Modify mode(GF6C)=3,marker(GF6C)=16;
    Modify mode(GF7C)=3,marker(GF7C)=16;Modify mode(GF8C)=3,marker(GF8C)=16
Modify mode(GF9C)=3,marker(GF9C)=17;Modify mode( GF10C)=3,marker(GF10C)=17;
    Modify mode(GF11C)=3,marker(GF11C)=17;Modify mode(GF12C)=3,marker(GF12C)=17
Modify lstyle(UConfidenceCFit)=2;Modify lstyle(LConfidenceCFit)=2
        Legend/X=-12/Y=-28/J /A=MC
        AppendText "\Z08\s(GF1C)     DFRC test data"
        AppendText "\Z08\s(GF5C)     LeRC test data"
        AppendText "\Z08\s(GF9C)     LaRC test data"
        AppendText "\Z08\s(AvgGFCFit)      Average"
        AppendText ""\Z08\s(UConfidenceCFit)  95% CL"
        Textbox /N=TextBox_2/F=0/A=MC/X=-5/Y=-50
AppendText "\Z10  "+Gages+" on "+SpecNum+" for cycle "+num2str(CycleNumber)+ " Cooling,Tension"
```

```
LayoutP()
EndMacro
Macro Calculations()
        Variable  RepeatX
Variable i, lim, MaxSlopeH,MaxSlopeC,MaxLoc0,MaxLoc1
        Silent 1
        Make/N=2/O Magnitude, Scatter,Slope
        Make/N=2/O Repeatability
        Make/N=256/O DerivativeH, DerivativeC, Repeatability1,DerivativeTH,DerivativeTC
        SetScale/I x (TempH(0)), (TempH(NumPts-1)),"" DerivativeH;
SetScale/I x (TempC(0)), (TempC(NumPts-1)),"" DerivativeC;
    if (TempH(0)>=TempC(0))
        SetScale/I x (TempH(0)), (TempH(NumPts-1)), ""Repeatability1;
    else
        SetScale/I x (TempC(0)), (TempC(NumPts-1)), ""Repeatability1;
        endif
        Make/N=256/O AvgGFHFitX,AvgGFCFitX,AvgGFHFit1,AvgGFCFit1,UConfidenceHFit1,LConfidenceHFit1,UConfidenceCFit1,
        LConfidenceCFit1
        SetScale/I x (TempH(0)), (TempH(NumPts-1)), FitX,AvgGFHFit1,UConfidenceHFit1,LConfidenceHFit1
SetScale/I x (TempC(0)), (TempC(NumPts-1)), AvgGFCFitX,AvgGFCFit1,UConfidenceCFit1,LConfidenceCFit1
WaveStats/Q AvgGFHFit
Magnitude[0]=Area(AvgGFHFit,TempH(0),TempH(NumPts-1))
WaveStats/Q AvgGFCFit
Magnitude[1]=Area(AvgGFCFit,TempC(0),TempC(NumPts-1))
AvgGFHFit1=AvgGFHFit    AvgGFCFit1=AvgGFCFit
UConfidenceHFit1=UConfidenceHFit  LConfidenceHFit1=LConfidenceHFit
        UConfidenceCFit1=UConfidenceCFit  LConfidenceCFit1=LConfidenceCFit
        Scatter[0]=Area(UConfidenceHFit1,TempH(0),TempH(NumPts-1))-Area(LConfidenceHFit1,TempH(0),TempH(Nu mPts-1))
        Scatter[1]=Area(UConfidenceCFit1,TempC(0),TempC(NumPts-1))-Area(LConfidenceCFit1,TempC(0),TempC(Nu mPts-1))
        DerivativeH=AvgGFHFit  Differentiate DerivativeH      DerivativeH=abs(DerivativeH)
        DerivativeC=AvgGFCFit  Differentiate DerivativeC      DerivativeC=abs(DerivativeC)
        Slope[0]=IntegrateAbs(DerivativeH)/(TempH(NumPts-1)-TempH(0))
            Slope[1]=IntegrateAbs(DerivativeC)/(TempC(NumPts-1)-TempC(0))
        i=0  lim=255        do
if (i>lim)      break           endif
        AvgGFHFitX[i]=pnt2x(AvgGFHFit1,i)
        AvgGFCFitX[i]=pnt2x(AvgGFCFit1,i)
    i=i+1           while (1)
        i=0  lim=255  do
if (i>lim)      break     endif
RepeatX=pnt2x(Repeatability1,i)
        Repeatability1[i]=interp(RepeatX,AvgGFHFitX,AvgGFHFit1)-interp(RepeatX,AvgGFCFitX,AvgGFCFit1)"
        i+=1 while (1)
        Repeatability[0]=IntegrateAbs(Repeatability1)
        Repeatability[1]=IntegrateAbs(Repeatability1)
        Edit  Scatter, Magnitude,Slope, Repeatability, A0,A1,A2
        DoWindow/K Table00
        DoWindow/C Table00   | Subsequent macros expect this name
Modify format(Magnitude.y)=3
        Modify format(Scatter.y)=3
Modify format(Slope.y)=0
Modify format(Repeatability.y)=3
Modify width(Point)=50
Modify width(Repeatability)=100
        DoWindow/F Layout0
KillWaves/F   Repeatability1 |
        Edit/W=(0,270,635,478)
        Scatter[0],Scatter[1],Magnitude[0],Magnitude[1],Slope[0],Slope[1],Repeatability[0],Repeatability[1]
EndMacro
```

Chapter 5

Test Data

5.1 Apparent Strain Data

Figures 5.1 to 5.72 show plots of microstrain versus temperature for each of the three selected gages attached to two different materials, IN100 and β-21S TMC. There are 12 figures for each type of gage and each figure represents a temperature cycle as defined in chapter 2. Data from all 12 gages of a particular type are shown on each plot unless a failure occurred; then only data from surviving gages are shown. Also shown on each figure are the average values for the 12 gages and the upper and lower 95% confidence limits. Except where noted, scales for the IN100 figures are identical, as are those for the β-21S figures. Also shown in this section in tabular form are the incremental zero shifts for each cycle and the accumulated zero shifts through each temperature cycle. A list of the apparent strain figures is given in table 5.1.

For each of the three gage types installed on IN100, figures 5.1 to 5.36 plot apparent strain and tables 5.2 to 5.7 tabulate zero shifts resulting from each complete cycle and the sums of these shifts as they accumulated through each of the 12 cycles. Figures 5.37 to 5.72 and tables 5.8 to 5.13 do the same for the gages installed on β-21S TMC.

Two PdCr gages failed on the first cycle of IN100 coupon testing; therefore, all data for PdCr gages on IN100 are based on 10 gages. Two PdCr gages failed on the cooldown of cycle 12 on β-21S; therefore, those data are based on 10 gages.

All plots for apparent strain on IN100 material are to the same scale except figures 5.23(b) and 5.24(b), which have expanded scales to allow inclusion of all data points. Plots of β-21S data use the same scale except for figures 5.57(b), 5.58(b), 5.59(b), and 5.60(b), which are also expanded to include all data points.

TABLE 5.1—FIGURES FOR APPARENT STRAIN

Figure	Gage type	Substrate material	Maximum temperature		Heat/cool rates		Cycle
			°F	°C	F deg/min	C deg/min	
5.1	CKA1	IN100	1200	650	10/10	5.6/10	1
5.2	CKA1	IN100	1200	650	10/10	5.6/10	2
5.3	CKA1	IN100	1200	650	60/10	33/10	3
5.4	CKA1	IN100	1200	650	60/10	33/10	4
5.5	CKA1	IN100	1200	650	60/60	33/10	5
5.6	CKA1	IN100	1200	650	60/60	33/10	6
5.7	CKA1	IN100	1200	650	10/10	5.6/10	7
5.8	CKA1	IN100	1200	650	10/10	5.6/10	8
5.9	CKA1	IN100	1350	730	10/10	5.6/10	9
5.10	CKA1	IN100	1350	730	10/10	5.6/10	10
5.11	CKA1	IN100	1500	815	10/10	5.6/10	11
5.12	CKA1	IN100	1500	815	10/10	5.6/10	12
5.13	PdCr	IN100	1200	650	10/10	5.6/10	1
5.14	PdCr	IN100	1200	650	10/10	5.6/10	2
5.15	PdCr	IN100	1200	650	60/10	33/10	3
5.16	PdCr	IN100	1200	650	60/10	33/10	4
5.17	PdCr	IN100	1200	650	60/60	33/10	5
5.18	PdCr	IN100	1200	650	60/60	33/10	6
5.19	PdCr	IN100	1200	650	10/10	5.6/10	7
5.20	PdCr	IN100	1200	650	10/10	5.6/10	8
5.21	PdCr	IN100	1350	730	10/10	5.6/10	9
5.22	PdCr	IN100	1350	730	10/10	5.6/10	10
5.23	PdCr	IN100	1500	815	10/10	5.6/10	11
5.24	PdCr	IN100	1500	815	10/10	5.6/10	12
5.25	DETCBCL	IN100	1200	650	10/10	5.6/10	1
5.26	DETCBCL	IN100	1200	650	10/10	5.6/10	2
5.27	DETCBCL	IN100	1200	650	60/10	33/10	3
5.28	DETCBCL	IN100	1200	650	60/10	33/10	4
5.29	DETCBCL	IN100	1200	650	60/60	33/10	5
5.30	DETCBCL	IN100	1200	650	60/60	33/10	6
5.31	DETCBCL	IN100	1200	650	10/10	5.6/10	7
5.32	DETCBCL	IN100	1200	650	10/10	5.6/10	8
5.33	DETCBCL	IN100	1350	730	10/10	5.6/10	9
5.34	DETCBCL	IN100	1350	730	10/10	5.6/10	10
5.35	DETCBCL	IN100	1500	815	10/10	5.6/10	11
5.36	DETCBCL	IN100	1500	815	10/10	5.6/10	12
5.37	CKA1	TMC	1200	650	10/10	5.6/10	1
5.38	CKA1	TMC	1200	650	10/10	5.6/10	2
5.39	CKA1	TMC	1200	650	60/10	33/10	3
5.40	CKA1	TMC	1200	650	60/10	33/10	4
5.41	CKA1	TMC	1200	650	60/60	33/10	5
5.42	CKA1	TMC	1200	650	60/60	33/10	6
5.43	CKA1	TMC	1200	650	10/10	5.6/10	7
5.44	CKA1	TMC	1200	650	10/10	5.6/10	8
5.45	CKA1	TMC	1350	730	10/10	5.6/10	9
5.46	CKA1	TMC	1350	730	10/10	5.6/10	10
5.47	CKA1	TMC	1500	815	10/10	5.6/10	11
5.48	CKA1	TMC	1500	815	10/10	5.6/10	12

TABLE 5.1—Concluded.

Figure	Gage type	Substrate material	Maximum temperature		Heat/cool rates		Cycle
			°F	°C	F deg/min	C deg/min	
5.49	PdCr	TMC	1200	650	10/10	5.6/10	1
5.50	PdCr	TMC	1200	650	10/10	5.6/10	2
5.51	PdCr	TMC	1200	650	60/10	33/10	3
5.52	PdCr	TMC	1200	650	60/10	33/10	4
5.53	PdCr	TMC	1200	650	60/60	33/10	5
5.54	PdCr	TMC	1200	650	60/60	33/10	6
5.55	PdCr	TMC	1200	650	10/10	5.6/10	7
5.56	PdCr	TMC	1200	650	10/10	5.6/10	8
5.57	PdCr	TMC	1350	730	10/10	5.6/10	9
5.58	PdCr	TMC	1350	730	10/10	5.6/10	10
5.59	PdCr	TMC	1500	815	10/10	5.6/10	11
5.60	PdCr	TMC	1500	815	10/10	5.6/10	12
5.61	DETCBCL	TMC	1200	650	10/10	5.6/10	1
5.62	DETCBCL	TMC	1200	650	10/10	5.6/10	2
5.63	DETCBCL	TMC	1200	650	60/10	33/10	3
5.64	DETCBCL	TMC	1200	650	60/10	33/10	4
5.65	DETCBCL	TMC	1200	650	60/60	33/10	5
5.66	DETCBCL	TMC	1200	650	60/60	33/10	6
5.67	DETCBCL	TMC	1200	650	10/10	5.6/10	7
5.68	DETCBCL	TMC	1200	650	10/10	5.6/10	8
5.69	DETCBCL	TMC	1350	730	10/10	5.6/10	9
5.70	DETCBCL	TMC	1350	730	10/10	5.6/10	10
5.71	DETCBCL	TMC	1500	815	10/10	5.6/10	11
5.72	DETCBCL	TMC	1500	815	10/10	5.6/10	12

TABLE 5.2.—CKA1 INCREMENTAL ZERO SHIFTS ON IN100

Gage	Cycle											
	1	2	3	4	5	6	7	8	9	10	11	12
Tested at Langley												
1	246	135	26	33	-17	72	-71	121	529	113	-312	-482
2	9	139	64	18	2	79	-83	42	261	97	139	-359
3	-61	83	73	26	6	3	-171	51	192	-152	-175	-148
4	1322	219	134	60	50	70	-29	112	345	110	-199	-306
Tested at Lewis												
5	-273	9	-74	-78	-41	-40	-30	0	-252	-73	-775	-423
6	-710	12	7	-8	-14	-37	-1	2	-94	20	-72	-59
7	0	207	39	-2	17	1	-24	3	-30	-81	-179	-131
8	-80	139	39	11	75	119	-14	-18	-146	-40	-491	-123
Tested at Dryden												
9	-34	206	143	131	23	-29	-34	-25	95	1	-36	-115
10	961	-736	212	194	70	11	32	-8	270	50	60	9
11	-145	204	74	57	14	-28	-14	17	61	-50	-554	-205
12	-532	541	116	132	0	1	-36	-37	-18	-15	-209	-124

TABLE 5.3—CKA1 ACCUMULATED ZERO SHIFTS ON IN100

Gage	Cycle											
	1	2	3	4	5	6	7	8	9	10	11	12
Tested at Langley												
1	246	381	408	440	424	496	425	545	1074	1188	876	394
2	9	148	211	229	231	310	226	268	530	626	765	407
3	–61	22	95	121	116	119	–52	–1	191	39	–136	–283
4	1322	1541	1676	1736	1785	1855	1826	1938	2284	2393	2194	1888
Tested at Lewis												
5	–273	–263	–338	–416	–458	–498	–528	–528	–780	–853	–1628	–2051
6	–710	–697	–690	–699	–713	–750	–751	–749	–842	–823	–895	–954
7	0	207	246	244	261	262	238	241	211	129	–49	–181
8	–80	60	99	110	184	303	289	271	126	85	–405	–528
Tested at Dryden												
9	–34	172	315	445	468	439	405	380	475	476	439	325
10	961	225	437	631	701	712	744	736	1006	1056	1116	1125
11	–145	95	169	227	241	213	199	215	276	226	–329	–534
12	–532	9	125	257	257	258	222	185	167	152	–57	–181

TABLE 5.4.—PdCr INCREMENTAL ZERO SHIFTS ON IN100

Gage	Cycle											
	1	2	3	4	5	6	7	8	9	10	11	12
Tested at Langley												
1	–1001	–443	–181	865	–1742	–56	467	–390	197	1022	6582	–986
2	failed											
3	117	120	106	273	–370	–9	420	167	–650	515	–1394	–328
4	331	–72	354	378	–298	102	581	331	334	620	3	–333
Tested at Lewis												
5	234	45	45	103	171	74	19	109	13	451	5001	–25
6	88	79	79	45	44	88	–20	37	56	327	7626	114
7	243	102	102	68	28	116	4	55	106	606	7479	996
8	179	73	73	42	39	126	–24	32	9	352	8269	1295
Tested at Dryden												
9	227	35	72	–129	–213	65	–32	16	–304	–255	–2120	–984
10	432	–207	32	–47	–603	–69	248	–209	–1398	–79	–2523	–870
11	failed											
12	–976	–122	50	–134	–474	74	124	2	–666	247	–138	–3035

TABLE 5.5.—PdCr ACCUMULATED ZERO SHIFTS ON IN100

Gage	Cycle											
	1	2	3	4	5	6	7	8	9	10	11	12
Tested at Langley												
1	−1001	−1444	−1625	−760	−2502	−2557	−2090	−2480	−2283	−1261	5321	4335
2	failed											
3	117	237	343	616	246	236	656	823	173	687	−707	−1035
4	331	258	612	991	693	795	1376	1707	2040	2660	2663	2330
Tested at Lewis												
5	234	279	324	427	599	672	691	801	813	1264	6265	6241
6	88	167	245	290	334	422	401	438	493	820	8447	8561
7	243	345	447	515	543	659	663	718	824	1430	8908	9905
8	179	252	325	367	406	531	508	540	549	901	9170	10465
Tested at Dryden												
9	227	262	333	205	−9	56	24	40	−265	−520	−2640	−3624
10	432	225	256	209	−394	−462	−214	−424	−1821	−1900	−4423	−5293
11	failed											
12	−976	−1098	−1048	−1182	−1656	−1582	−1458	−1456	−2122	−1876	−2014	−5049

TABLE 5.6.—DETCBCL INCREMENTAL ZERO SHIFTS ON IN100

Gage	Cycle											
	1	2	3	4	5	6	7	8	9	10	11	12
Tested at Langley												
1	−1733	284	−149	213	957	147	−1903	886	−346	−1717	541	−890
2	−1664	269	−136	210	958	156	−1900	893	−344	−1711	567	−868
3	−1762	276	−137	213	957	153	−1901	893	−343	−1711	587	−848
4	−1748	264	−119	210	957	153	−1902	903	−370	−1708	589	−853
Tested at Lewis												
5	−1424	−196	−60	−215	−180	157	97	−239	−372	−414	−1635	−712
6	−1385	−207	−57	−194	−212	182	89	−242	−350	−394	−1501	−644
7	−1369	−204	−61	−212	−183	152	109	−240	−371	−405	−1617	−695
8	−1476	−205	−63	−217	−204	161	98	−241	−371	−414	−1662	−724
Tested at Dryden												
9	−1090	−87	57	91	1091	−58	−1389	−79	−259	−207	−1116	−640
10	−1220	−126	94	63	1008	92	−1396	−23	−232	−265	−1130	−609
11	−1092	−218	−8	44	1304	−87	−1301	−36	−258	−205	−1079	−593
12	−1066	−200	6	45	1067	−60	−1297	−16	−308	−180	−1073	−592

TABLE 5.7.—DETCBCL ACCUMULATED ZERO SHIFTS ON IN100

Gage	Cycle											
	1	2	3	4	5	6	7	8	9	10	11	12
Tested at Langley												
1	−1733	−1448	−1598	−1385	−427	−280	−2183	−1297	−1644	−3361	−2820	−3710
2	−1664	−1394	−1530	−1320	−361	−206	−2106	−1213	−1557	−3267	−2700	−3568
3	−1762	−1486	−1622	−1409	−452	−299	−2200	−1307	−1650	−3361	−2774	−3623
4	−1748	−1485	−1604	−1394	−436	−284	−2186	−1283	−1653	−3361	−2771	−3625
Tested at Lewis												
5	−1424	−1620	−1679	−1894	−2074	−1917	−1820	−2058	−2431	−2845	−4480	−5192
6	−1385	−1592	−1649	−1843	−2055	−1873	−1784	−2026	−2376	−2769	−4270	−4914
7	−1369	−1572	−1633	−1845	−2028	−1875	−1766	−2006	−2377	−2781	−4398	−5093
8	−1476	−1681	−1743	−1960	−2164	−2004	−1906	−2147	−2518	−2932	−4594	−5318
Tested at Dryden												
9	−1090	−1177	−1120	−1030	62	4	−1386	−1465	−1724	−1931	−3047	−3687
10	−1220	−1347	−1252	−1189	−182	−89	−1485	−1508	−1740	−2005	−3135	−3744
11	−1092	−1310	−1318	−1274	29	−58	−1359	−1395	−1653	−1858	−2936	−3529
12	−1066	−1266	−1260	−1215	−148	−208	−1506	−1521	−1829	−2010	−3083	−3674

TABLE 5.8.—CKA1 INCREMENTAL ZERO SHIFTS ON β-21S TMC

Gage	Cycle											
	1	2	3	4	5	6	7	8	9	10	11	12
Tested at Langley												
1	855	102	77	132	60	98	2	155	7	37	−182	5753
2	960	105	63	49	83	106	8	179	383	72	369	5074
3	1379	71	26	−46	−127	20	−11	119	88	−86	172	5268
4	827	56	6	56	2	5	−71	182	259	64	198	2960
Tested at Lewis												
5	829	106	54	41	34	84	20	18	−138	−62	−852	−96
6	707	95	53	50	−40	53	34	35	−173	−44	−896	−246
7	976	112	42	40	−8	36	35	35	−134	−38	−404	221
8	1205	91	39	43	−49	25	27	25	−176	−59	−824	−303
Tested at Dryden												
9	550	131	61	29	73	88	58	41	−29	25	−361	43
10	440	124	56	−1	47	76	90	72	−12	22	−588	−132
11	736	118	83	57	65	72	70	55	−18	5	−564	−44
12	801	99	40	−4	62	19	62	38	−7	14	−478	−116

TABLE 5.9—CKA1 ACCUMULATED ZERO SHIFTS ON β-21S TMC

Gage	Cycle											
	1	2	3	4	5	6	7	8	9	10	11	12
Tested at Langley												
1	855	957	1034	1166	1226	1324	1326	1481	1487	1525	1342	7095
2	960	1065	1129	1178	1261	1366	1375	1553	1936	2009	2377	7451
3	1379	1451	1477	1430	1303	1323	1312	1431	1519	1434	1606	6874
4	827	883	890	945	948	953	882	1064	1324	1387	1585	4545
Tested at Lewis												
5	829	935	989	1030	1064	1148	1168	1186	1048	986	134	38
6	707	803	855	905	865	918	952	986	814	770	−126	−372
7	976	1087	1129	1169	1160	1196	1231	1266	1132	1094	690	911
8	1205	1296	1335	1378	1329	1354	1381	1406	1231	1171	347	44
Tested at Dryden												
9	550	681	742	771	845	933	991	1032	1004	1029	668	711
10	440	564	620	619	666	742	832	904	892	914	326	193
11	736	854	937	994	1059	1132	1202	1256	1238	1243	679	635
12	801	899	940	936	998	1016	1078	1116	1109	1124	646	529

TABLE 5.10.—PdCr INCREMENTAL ZERO SHIFTS ON β-21S TMC

Gage	Cycle											
	1	2	3	4	5	6	7	8	9	10	11	12
Tested at Langley												
1	−3342	−1002	−430	−195	−330	−80	66	96	4337	2476	11366	4194
2	−4685	−1191	−544	−286	−361	−144	71	83	4008	2327	10289	3994
3	−5048	−1356	−584	−360	−428	−238	−1	19	4051	2640	12153	6934
4	−2689	−939	−433	−250	−344	−134	60	91	3420	2351	9848	4243
Tested at Lewis												
5	−123	−156	−146	−116	−115	−107	76	63	7592	4000	20626	11258
6	−228	−190	−176	−133	−141	−88	78	81	8035	4191	21751	11240
7	−247	−226	−208	−160	−188	−135	78	61	9346	4724	25002	3866
8	−338	−272	−248	−118	−173	−114	72	177	7731	4110	28608	12239
Tested at Dryden												
9	−4961	−2123	−1169	−638	−802	−469	−921	−751	3101	2760	13244	failed
10	−5923	−2138	−873	−17	−625	−402	−546	−706	4765	3008	8761	failed
11	−4180	−2132	−1142	−788	−801	−479	−754	−761	2788	2231	18469	−14200
12	−4714	−2056	−1174	−642	−708	−281	−709	−716	1857	2717	17705	−23121

TABLE 5.11.—PdCr ACCUMULATED ZERO SHIFTS ON β-21S TMC

Gage	Cycle											
	1	2	3	4	5	6	7	8	9	10	11	12
Tested at Langley												
1	−3342	−4344	−4774	−4969	−5298	−5379	−5313	−5217	−880	1597	12963	17157
2	−4685	−5876	−6420	−6706	−7067	−7211	−7140	−7057	−3049	722	9567	13561
3	−5048	−6404	−6989	−7349	−7777	−8015	−8016	−7997	−3945	−1305	10848	17782
4	−2689	−3627	−4060	−4310	−4654	−4788	−4728	−4637	−1217	1134	10981	15225
Tested at Lewis												
5	−123	−279	−425	−541	−656	−763	−687	−624	6968	10968	31594	42853
6	−228	−418	−594	−726	−868	−956	−877	−797	7239	1430	33181	44421
7	−247	−473	−681	−840	−1028	−1163	−1085	−1024	8322	13045	38047	41913
8	−338	−610	−859	−977	−1150	−1264	−1192	−1016	6716	10826	39434	51673
Tested at Dryden												
9	−4961	−7084	−8253	−8891	−9693	−10162	−10863	−11834	−8733	−5973	7272	failed
10	−5923	−8061	−8934	−8951	−9577	−9979	−10524	−11230	−6465	−3457	5304	failed
11	−4180	−6312	−7454	−8242	−9042	−9521	−10275	−11036	−8248	−6017	12452	−1748
12	−4714	−6770	−7944	−8585	−9293	−9575	−10284	−11000	−9143	−6426	11279	−11842

TABLE 5.12.—DETCBCL INCREMENTAL ZERO SHIFTS ON β-21S TMC

Gage	Cycle											
	1	2	3	4	5	6	7	8	9	10	11	12
Tested at Langley												
1	−678	−570	694	−95	879	−20	−779	−239	−389	85	−1177	−706
2	−706	−571	659	−71	874	79	−757	−208	53	139	−1094	−711
3	60	−527	662	−96	861	−34	−739	−239	−427	77	−1149	−637
4	101	−523	668	−86	869	−29	−740	−249	−409	88	−1042	−597
Tested at Lewis												
5	−962	−54	−155	−31	−265	42	292	−63	139	−786	−1036	−1225
6	−1032	−53	−154	−26	−278	48	310	−64	169	−784	−1050	−969
7	−136	−27	−149	−32	−288	20	308	−62	99	−816	−1090	−658
8	−123	−23	−147	−36	−292	53	323	−52	118	−806	−1060	−618
Tested at Dryden												
9	−464	−6	−127	54	1017	66	−1180	147	−167	14	−617	−441
10	−365	26	−113	39	1128	−69	−1199	160	−204	7	−589	−420
11	130	−9	−153	24	1171	−65	−1194	155	−160	19	−587	−435
12	62	12	−125	18	1090	−80	−1196	108	−133	23	−577	−449

TABLE 5.13.—DETCBCL ACCUMULATED ZERO SHIFTS ON β-21S TMC

Gage	Cycle											
	1	2	3	4	5	6	7	8	9	10	11	12
Tested at Langley												
1	−678	−1248	−554	−650	229	209	−570	−809	−1197	−1112	−2289	−2995
2	−706	−1276	−618	−689	186	265	−492	−700	−647	−508	−1602	−2314
3	60	−467	195	99	960	926	186	−53	−481	−404	−15553	−2190
4	101	−422	246	160	1029	1000	260	11	−398	−310	−1352	−1949
Tested at Lewis												
5	−962	−1016	−1172	−1203	−1469	−1426	−1135	−1198	−1059	−1845	−2880	−4105
6	−1032	−1085	−1239	−1265	−1543	−1495	−1185	−1249	−1080	−1864	−2914	−3882
7	−136	−163	−311	−343	−631	−610	−302	−364	−265	−1081	−2175	−2832
8	−123	−146	−293	−329	−621	−568	−245	−297	−179	−985	−2045	−2663
Tested at Dryden												
9	−464	−471	−597	−544	473	539	−641	−493	−661	−647	−1263	−1705
10	−365	−338	−452	−412	716	647	−552	−392	−596	−589	−1178	−1599
11	130	121	−33	−8	1163	1098	−97	58	−101	−82	−669	−1104
12	62	73	−52	−34	1056	976	−220	−112	−245	−222	−799	−1248

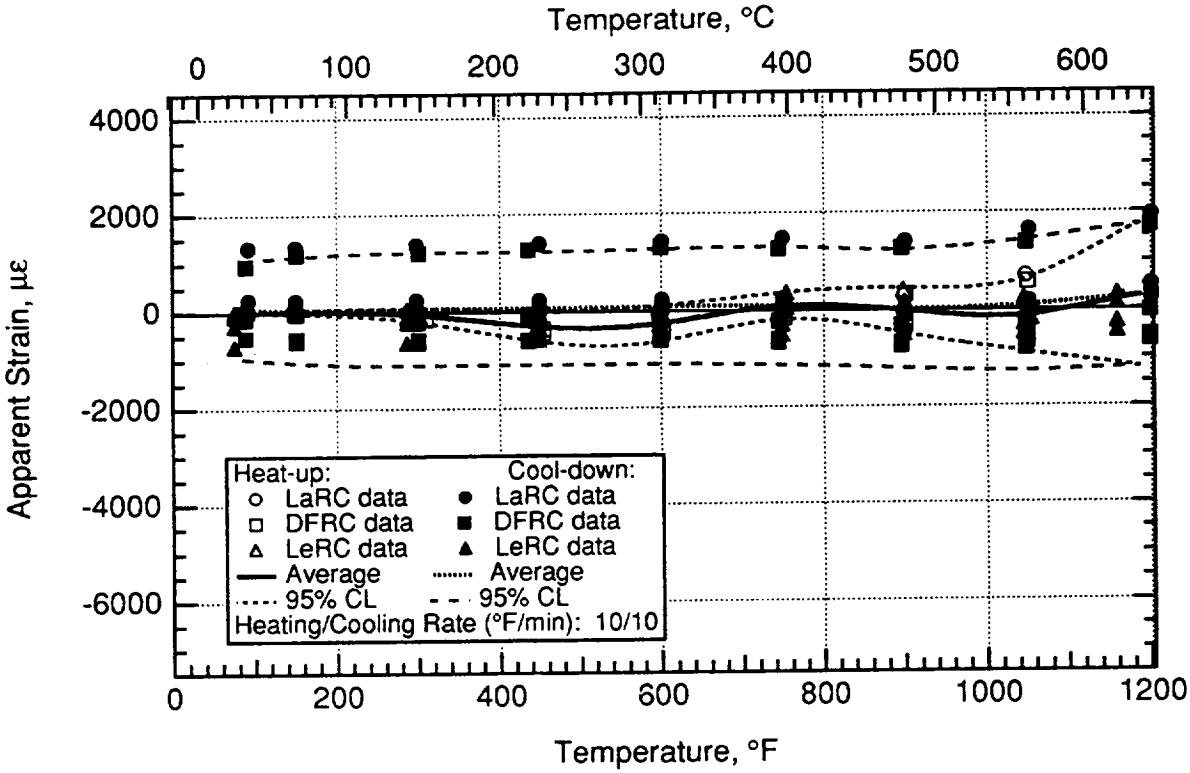

Figure 5.1.—CKA1 gage cycle 1 apparent strain on IN100.

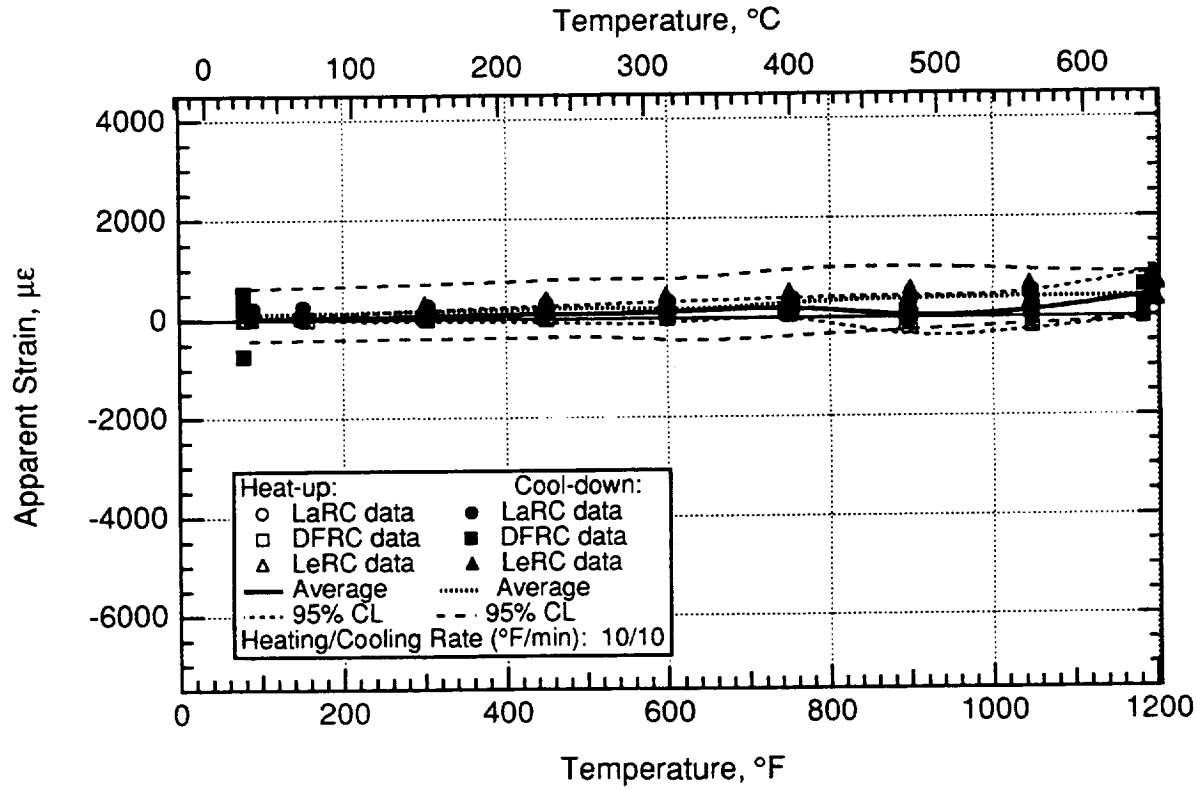

Figure 5.2.—CKA1 gage cycle 2 apparent strain on IN100.

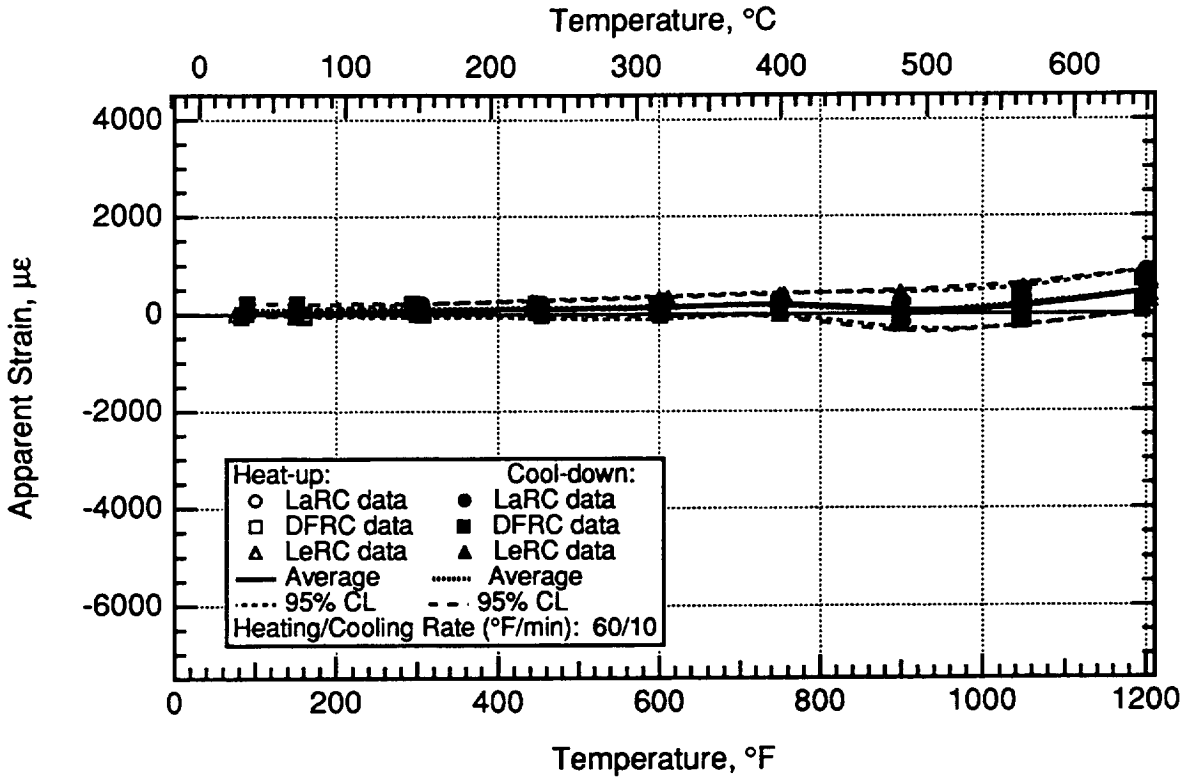

Figure 5.3.—CKA1 gage cycle 3 apparent strain on IN100.

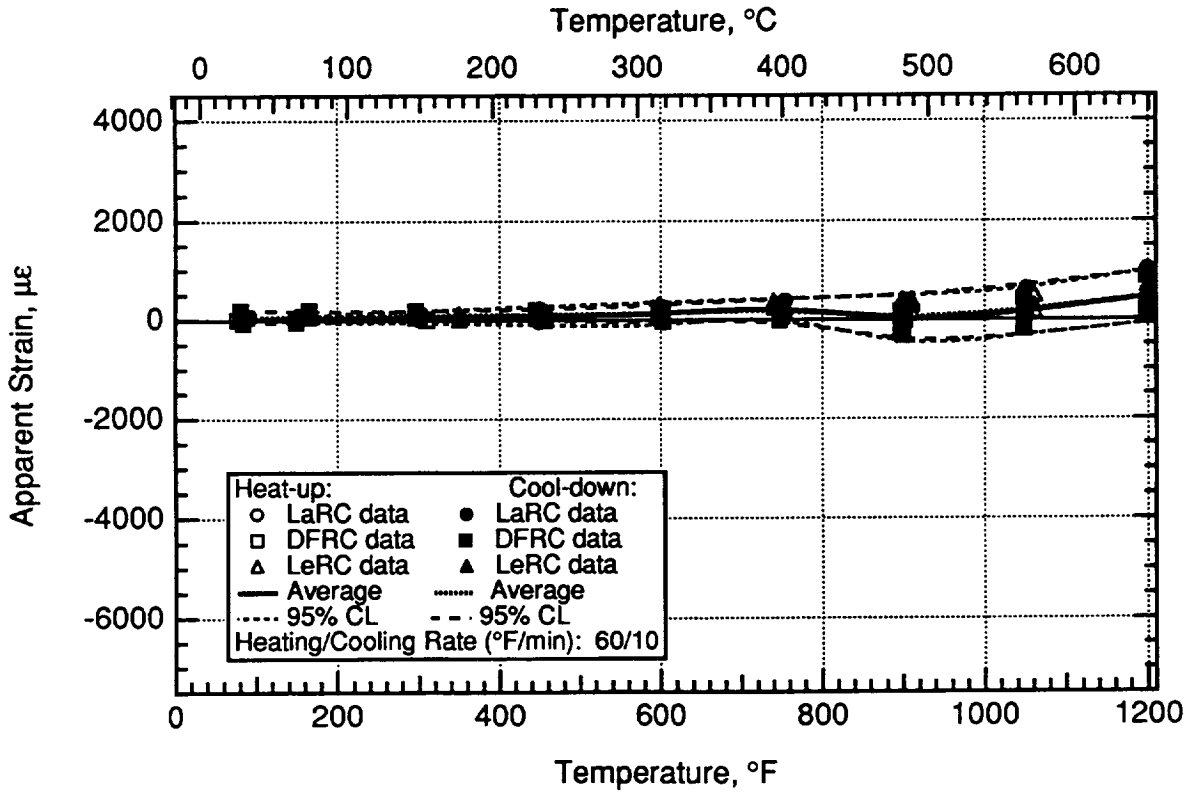

Figure 5.4.—CKA1 gage cycle 4 apparent strain on IN100.

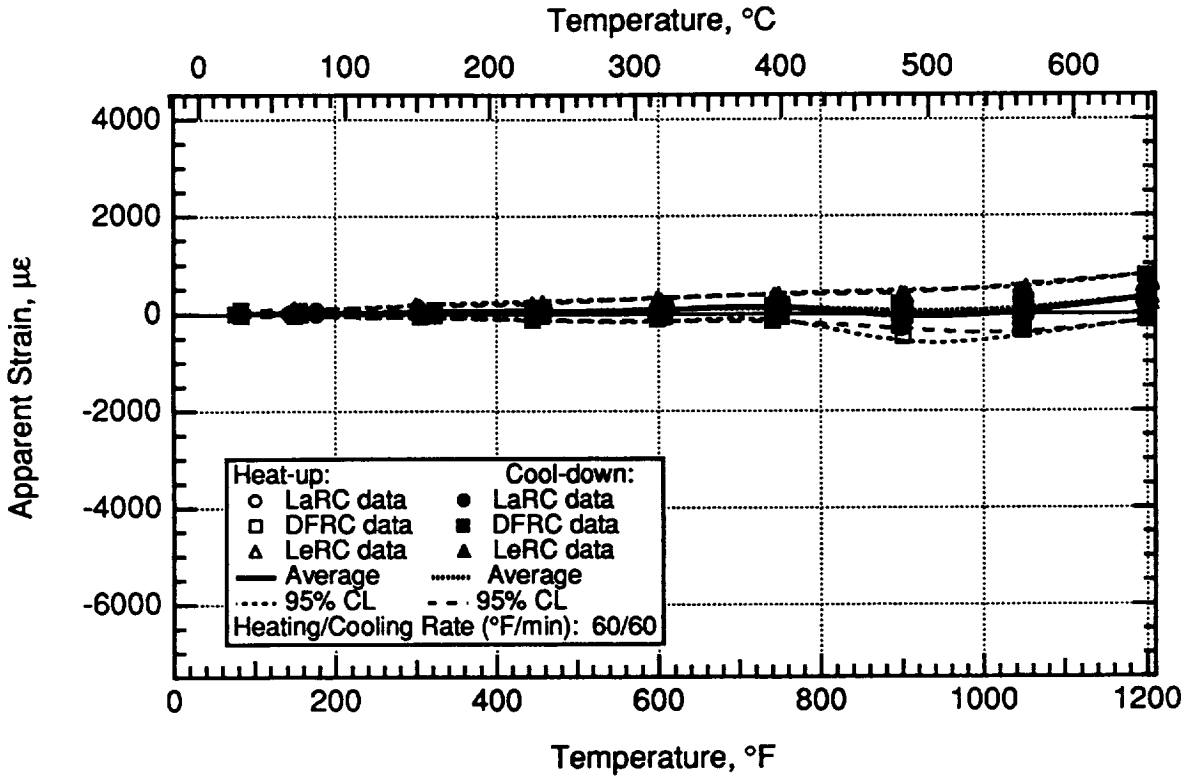

Figure 5.5.—CKA1 gage cycle 5 apparent strain on IN100.

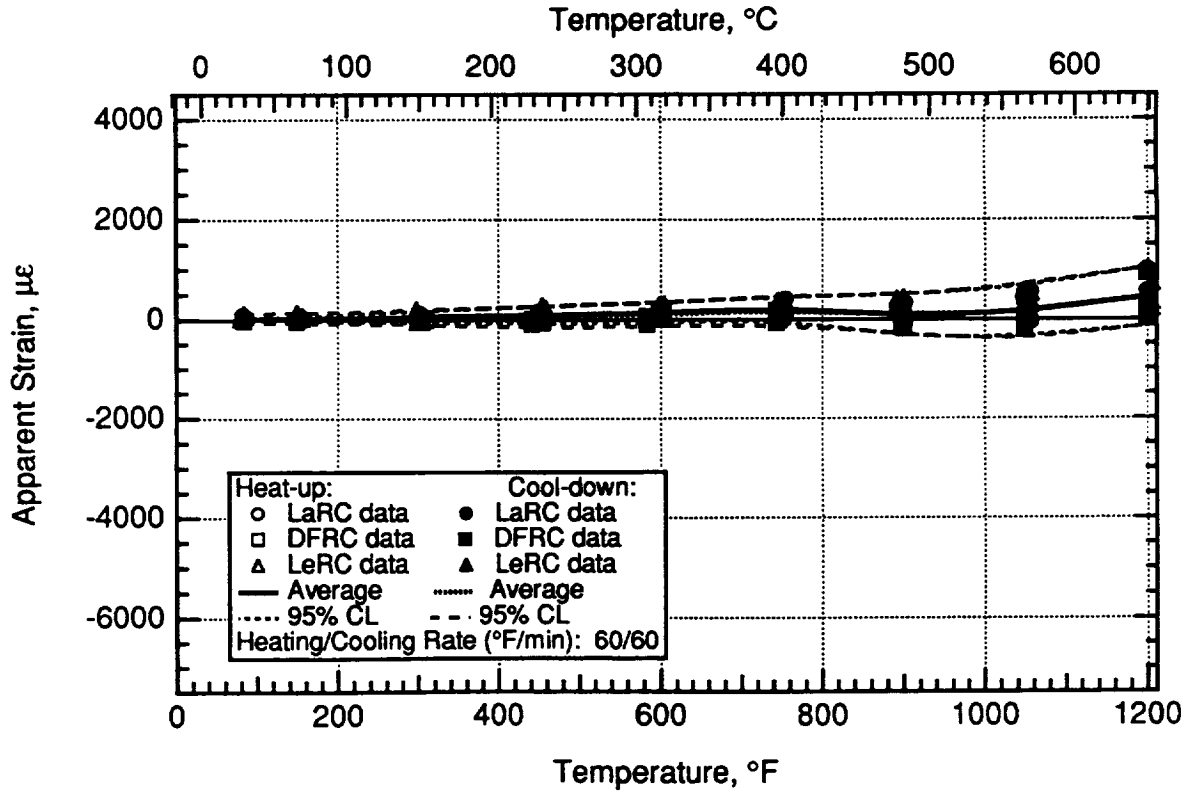

Figure 5.6.—CKA1 gage cycle 6 apparent strain on IN100.

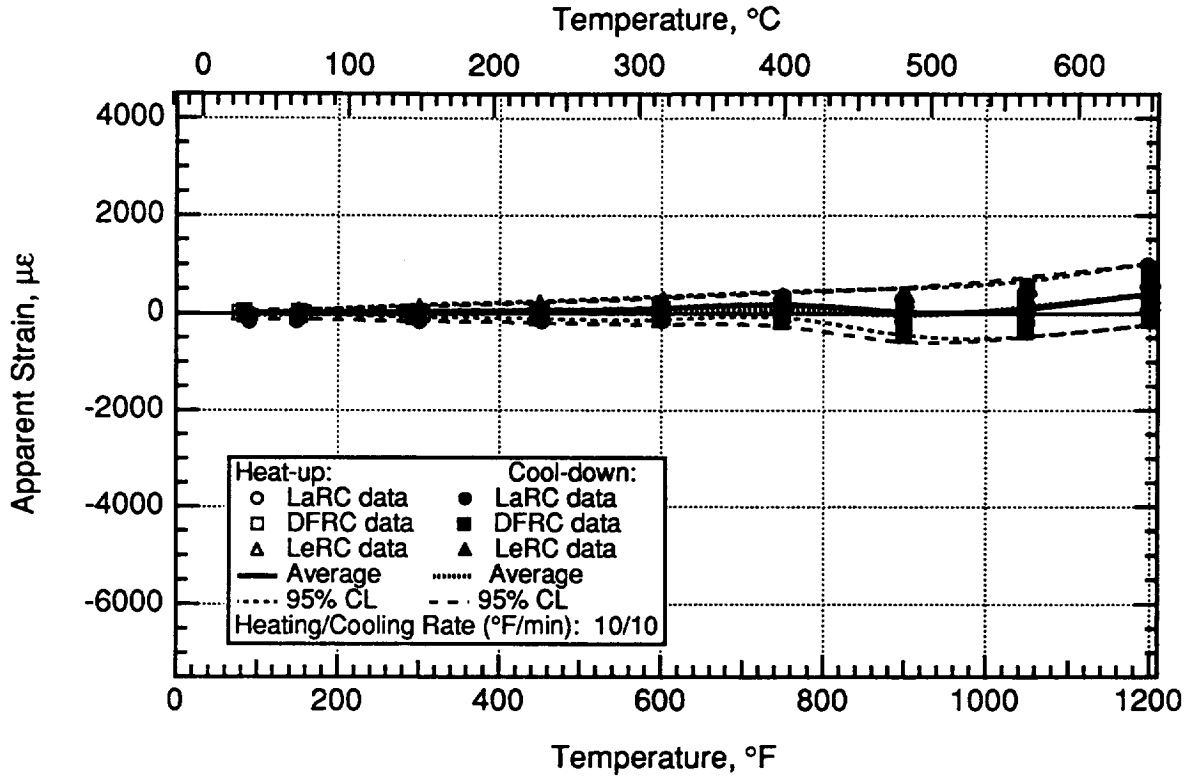

Figure 5.7.—CKA1 gage cycle 7 apparent strain on IN100.

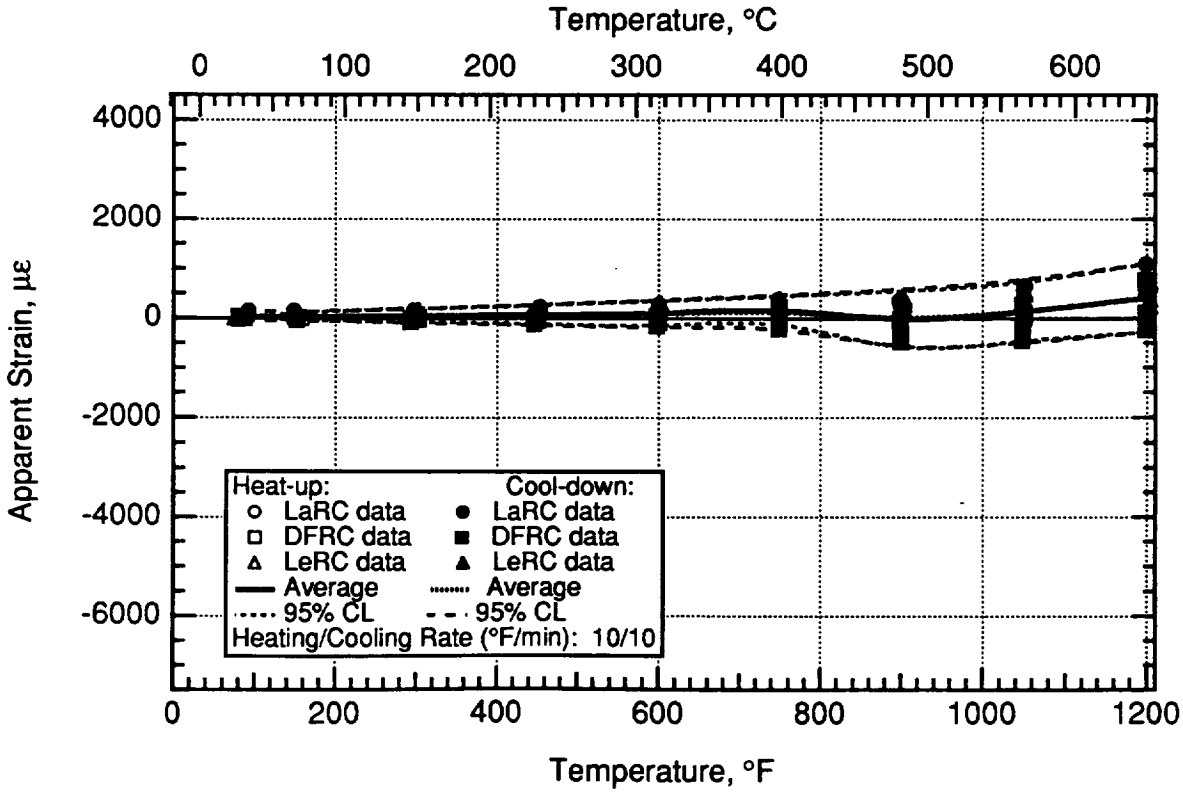

Figure 5.8.—CKA1 gage cycle 8 apparent strain on IN100.

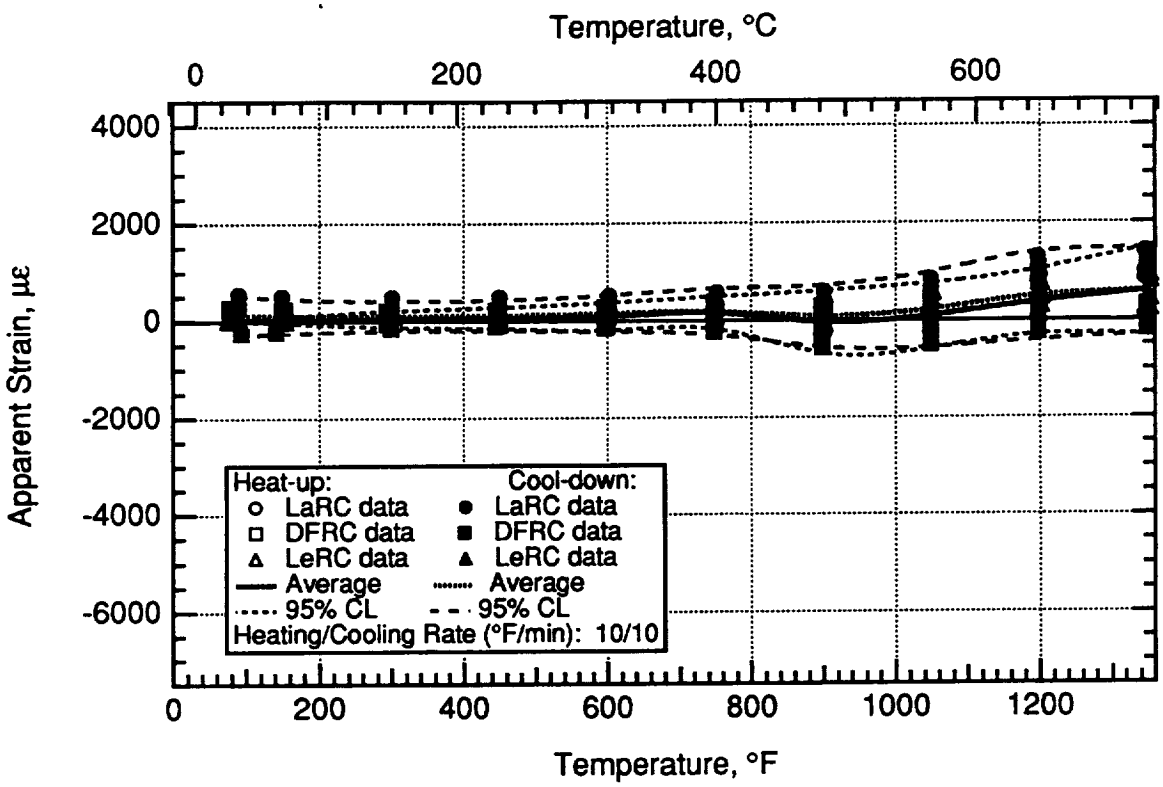

Figure 5.9.—CKA1 gage cycle 9 apparent strain on IN100.

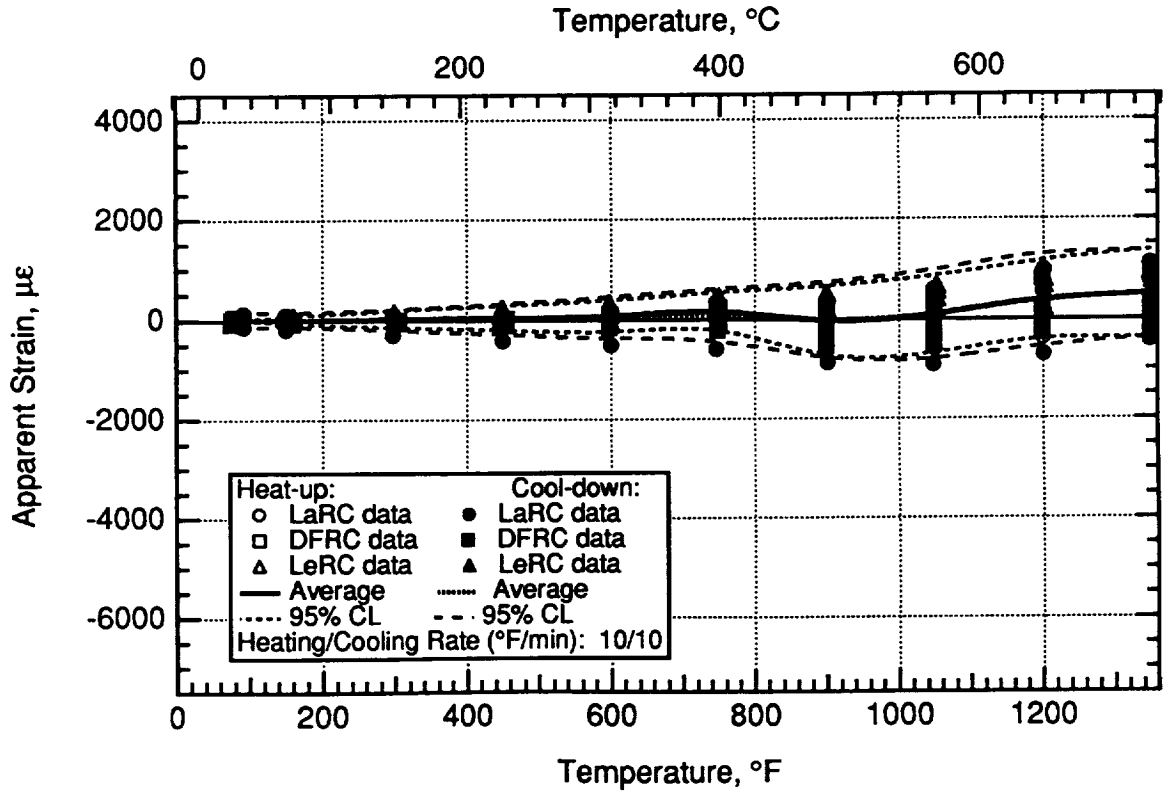

Figure 5.10.—CKA1 gage cycle 10 apparent strain on IN100.

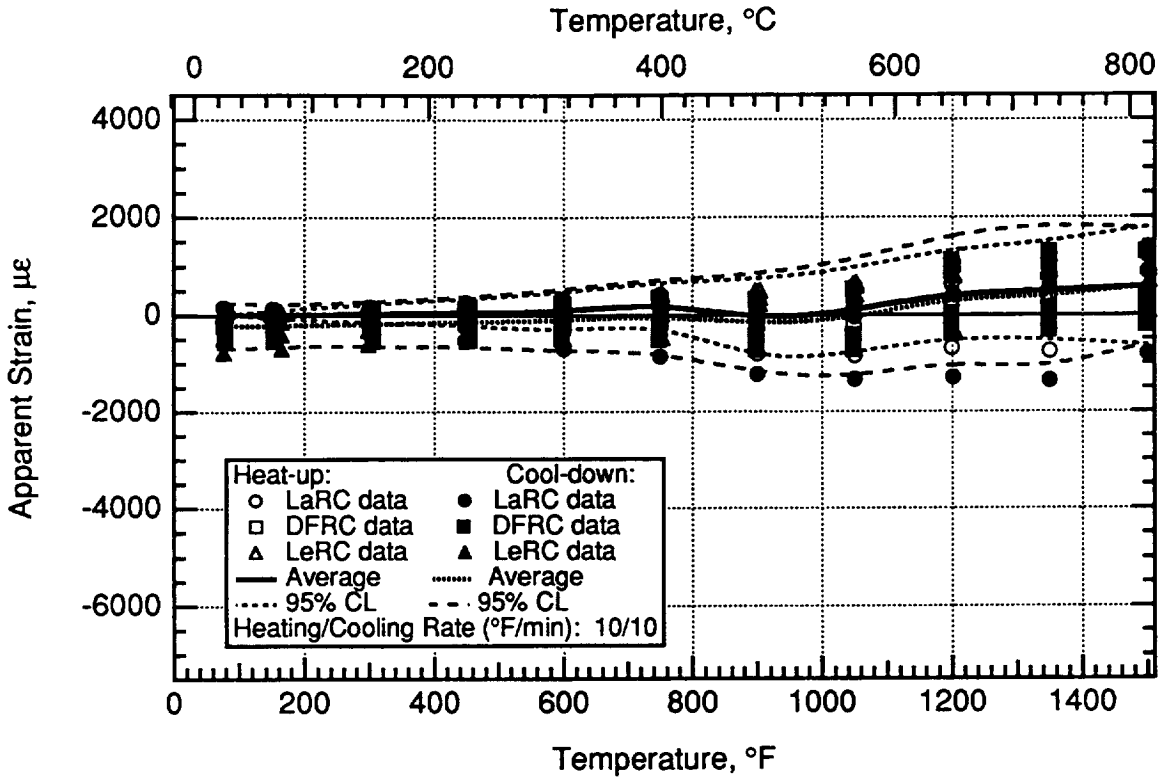

Figure 5.11.—CKA1 gage cycle 11 apparent strain on IN100.

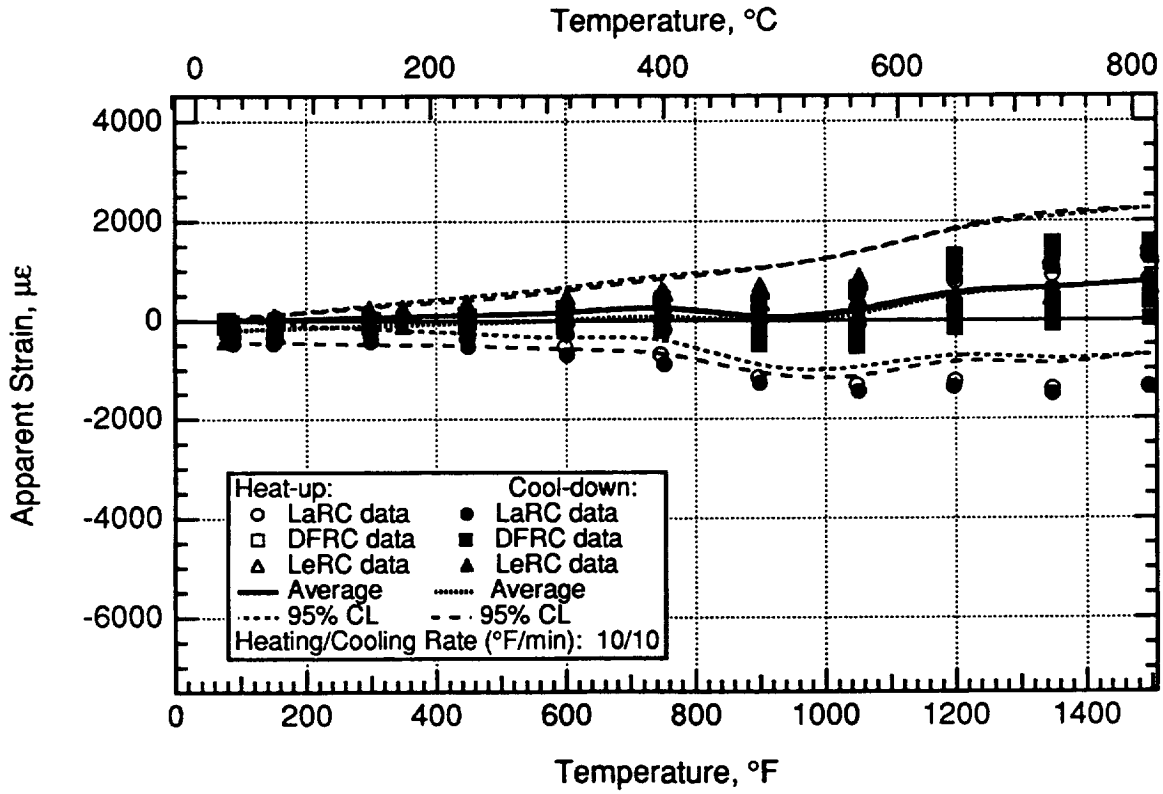

Figure 5.12.—CKA1 gage cycle 12 apparent strain on IN100.

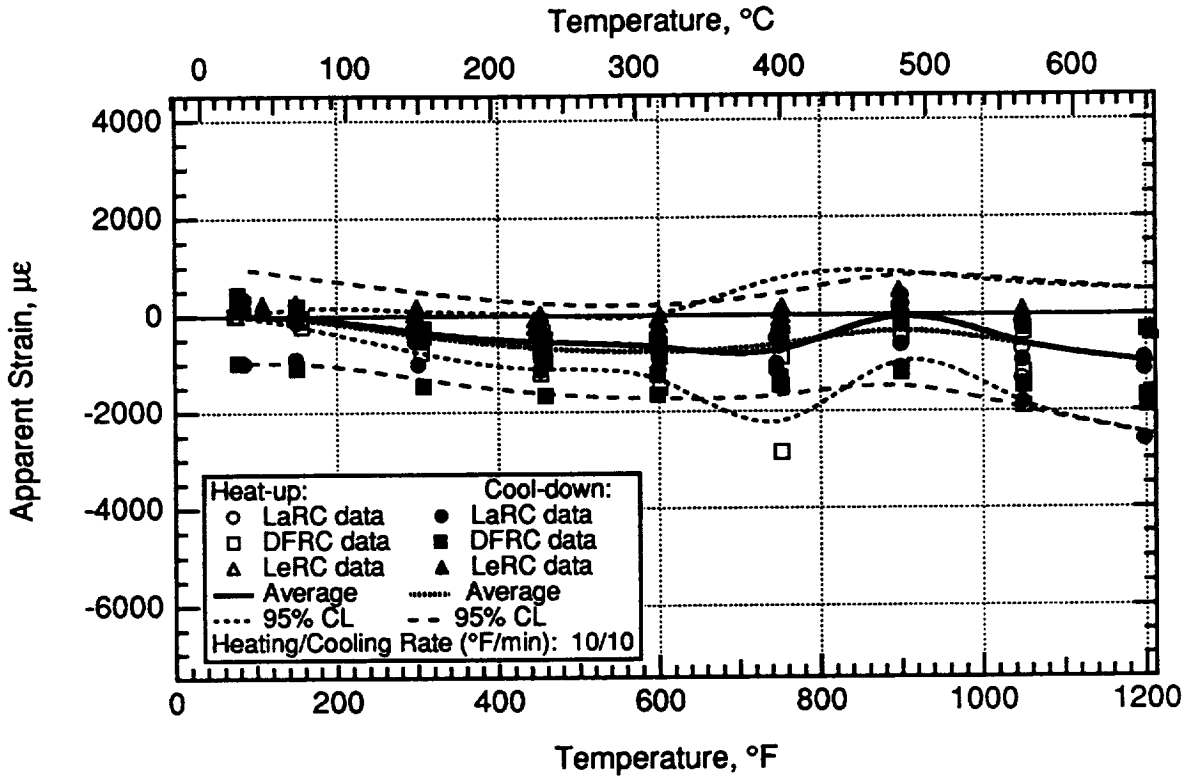

Figure 5.13.—PdCr gage cycle 1 apparent strain on IN100.

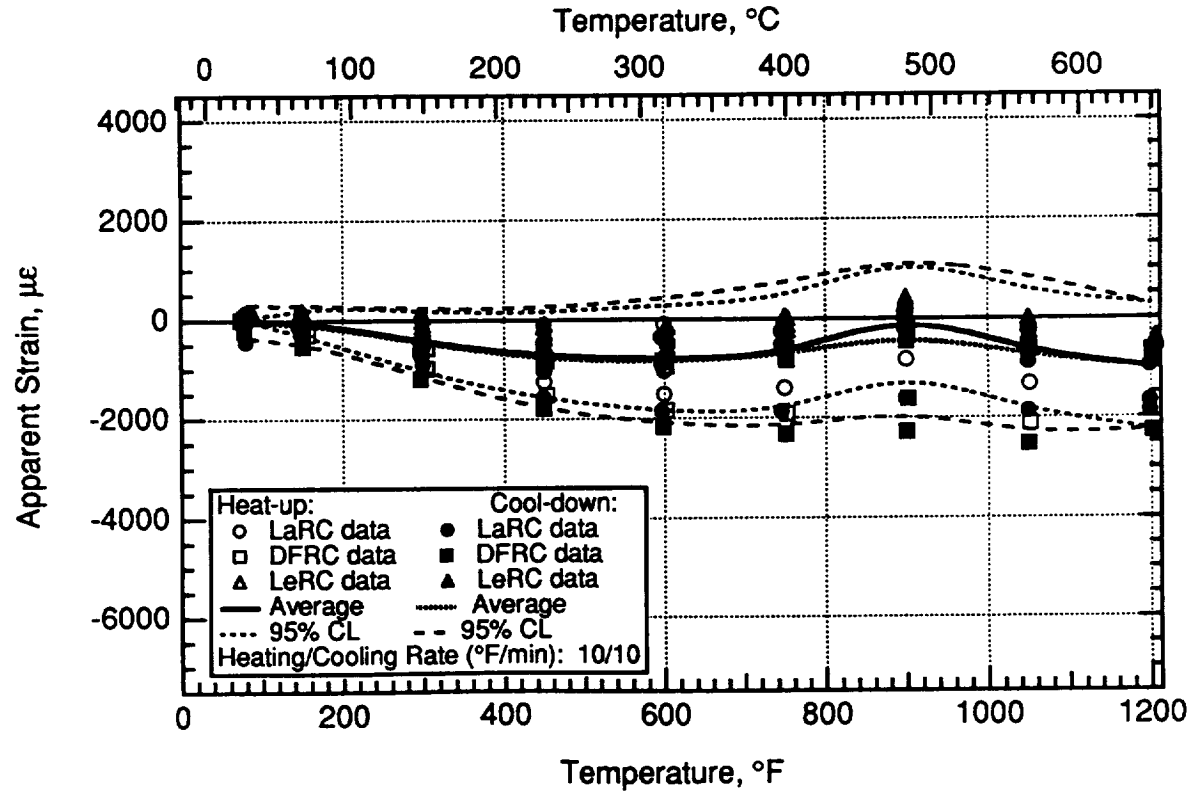

Figure 5.14.—PdCr gage cycle 2 apparent strain on IN100.

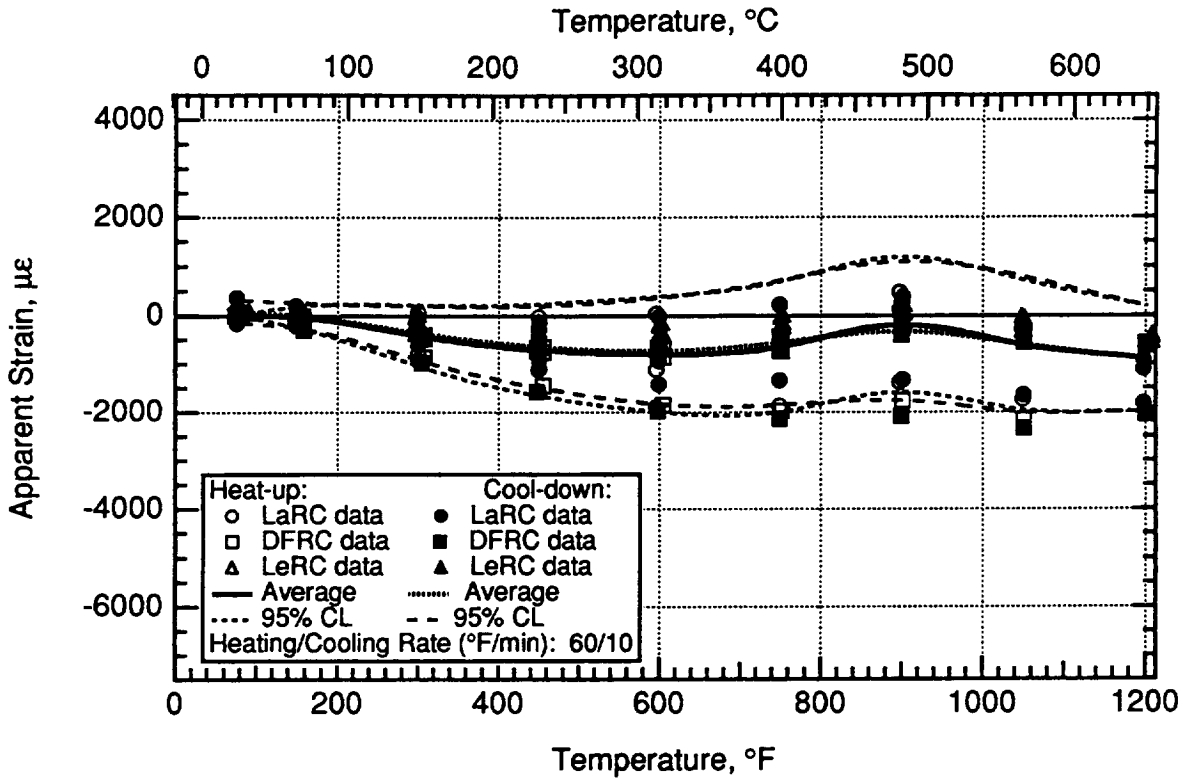

Figure 5.15.—PdCr gage cycle 3 apparent strain on IN100.

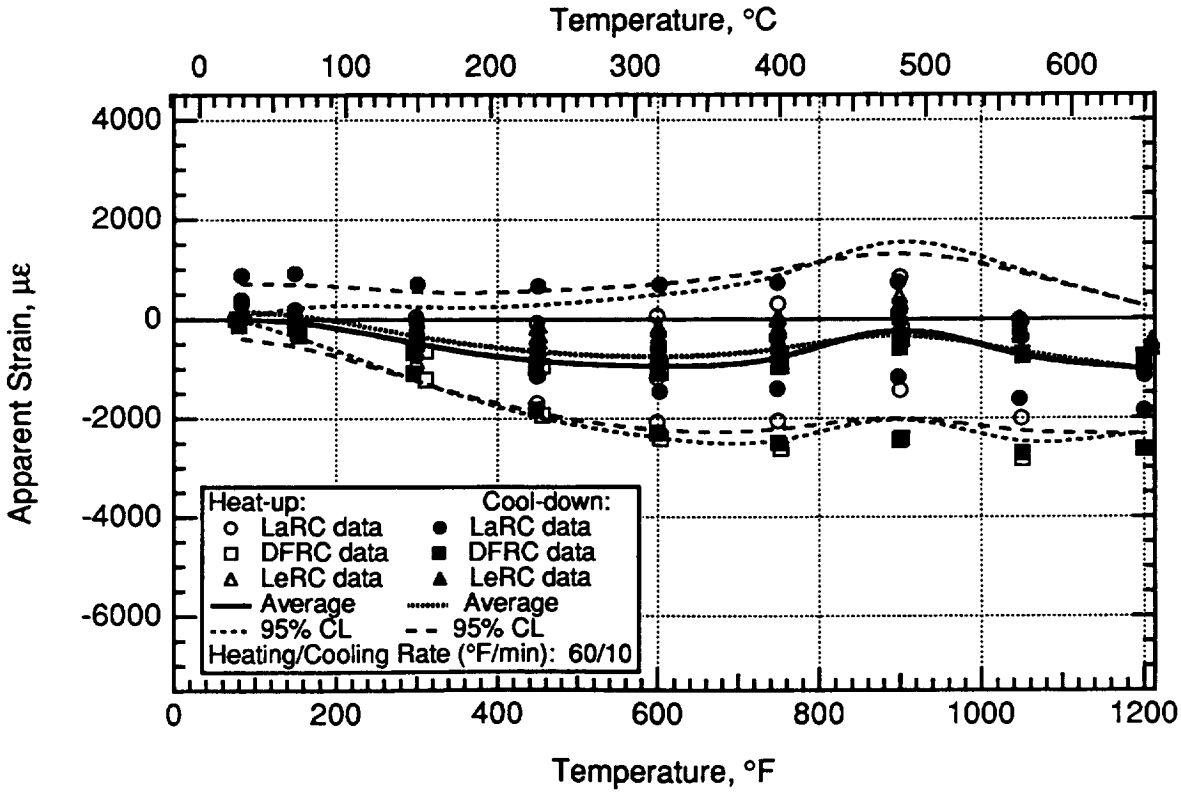

Figure 5.16.—PdCr gage cycle 4 apparent strain on IN100.

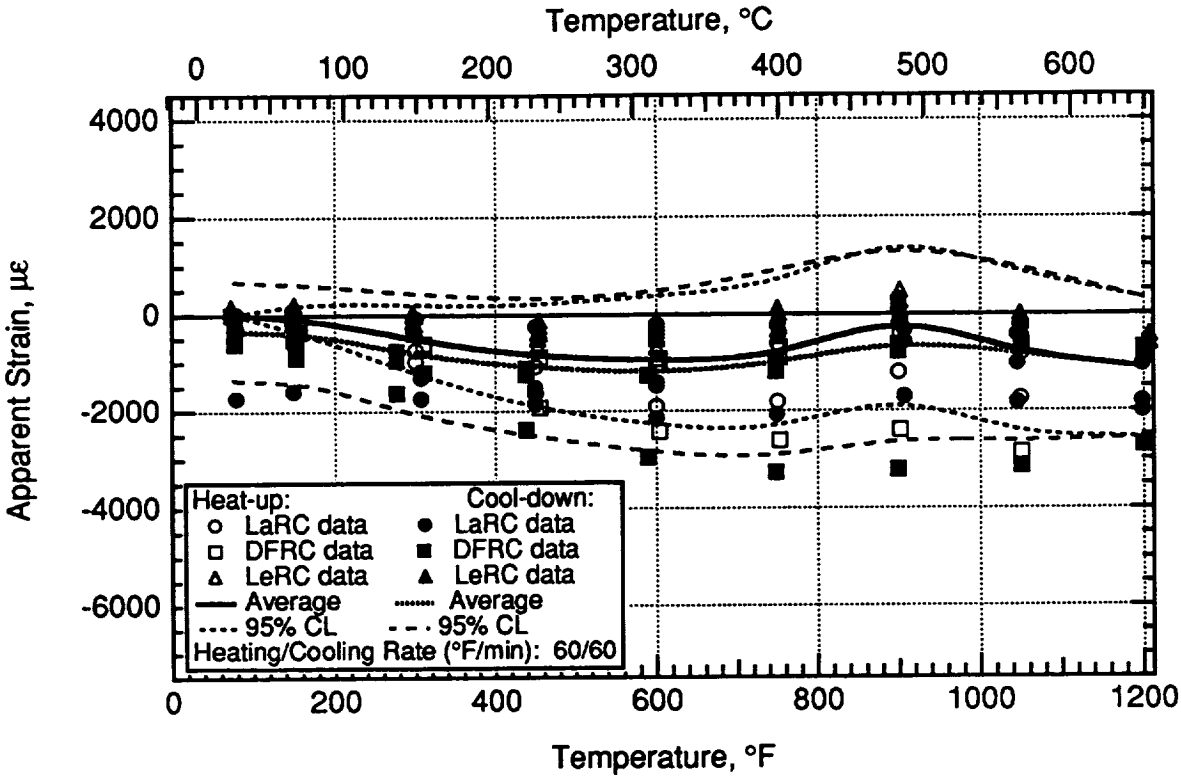

Figure 5.17.—PdCr gage cycle 5 apparent strain on IN100.

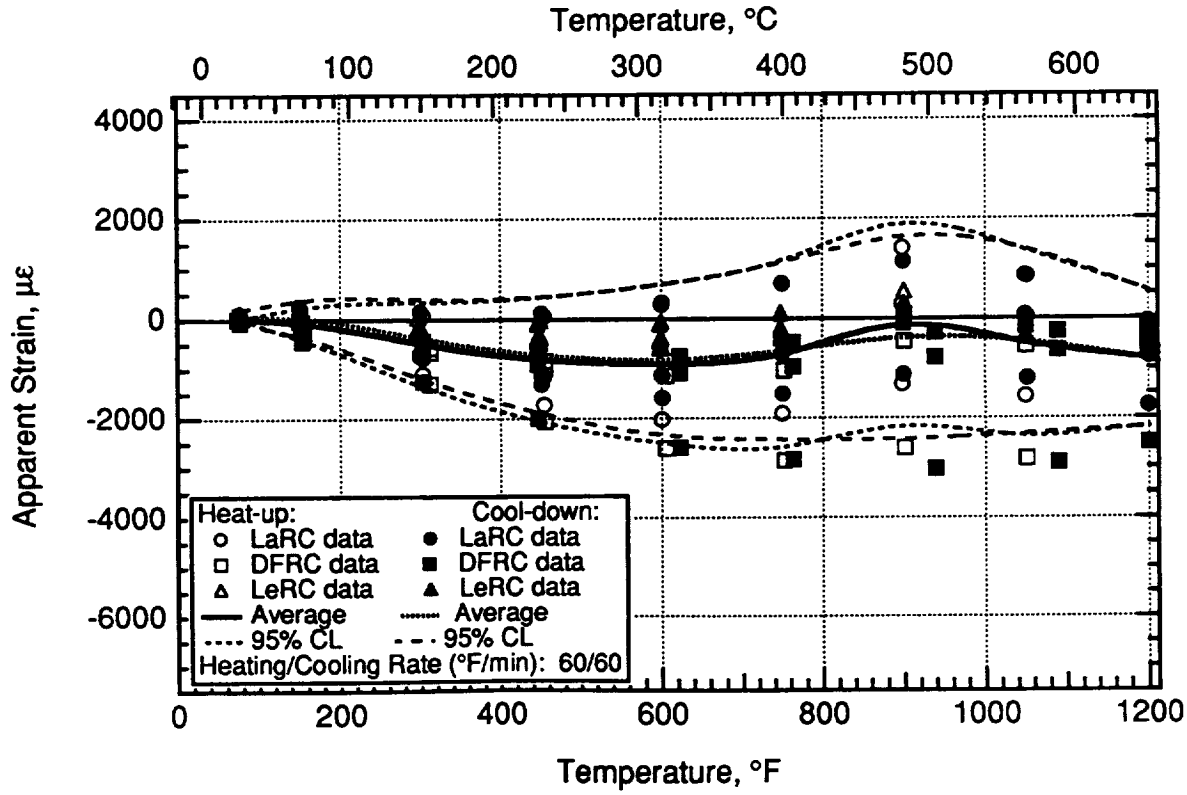

Figure 5.18.—PdCr gage cycle 6 apparent strain on IN100.

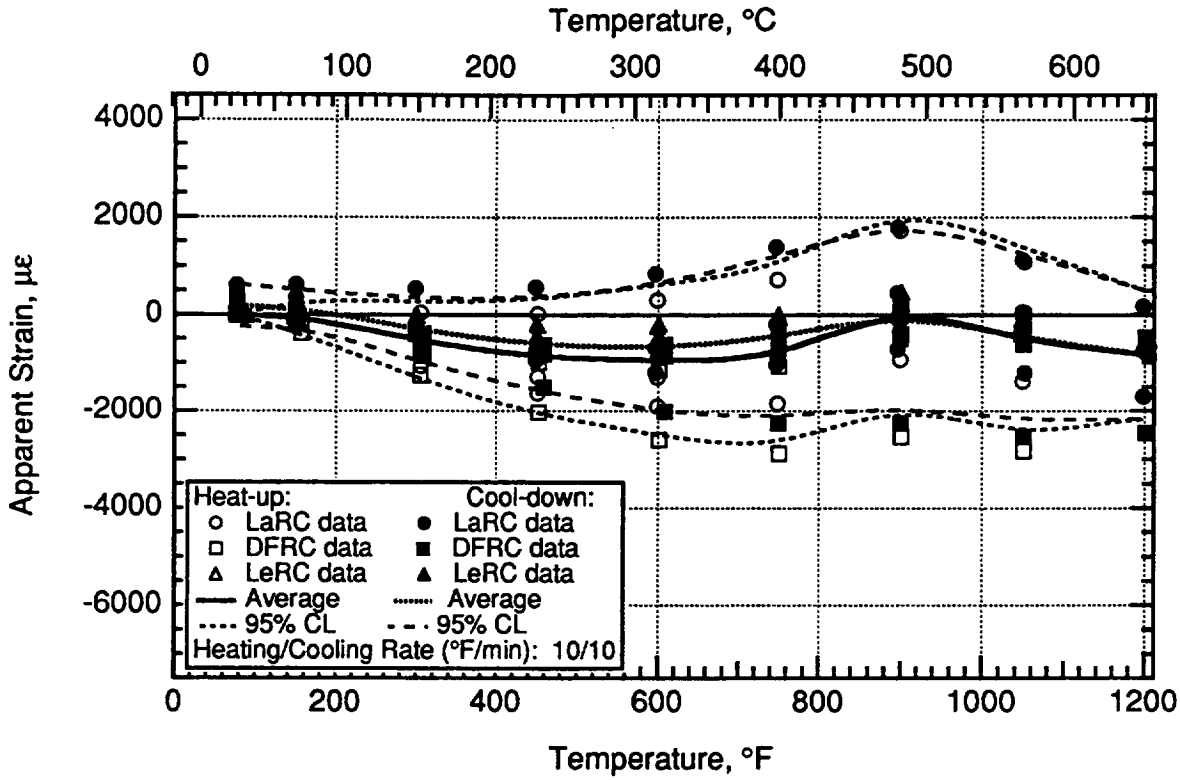

Figure 5.19.—PdCr gage cycle 7 apparent strain on IN100.

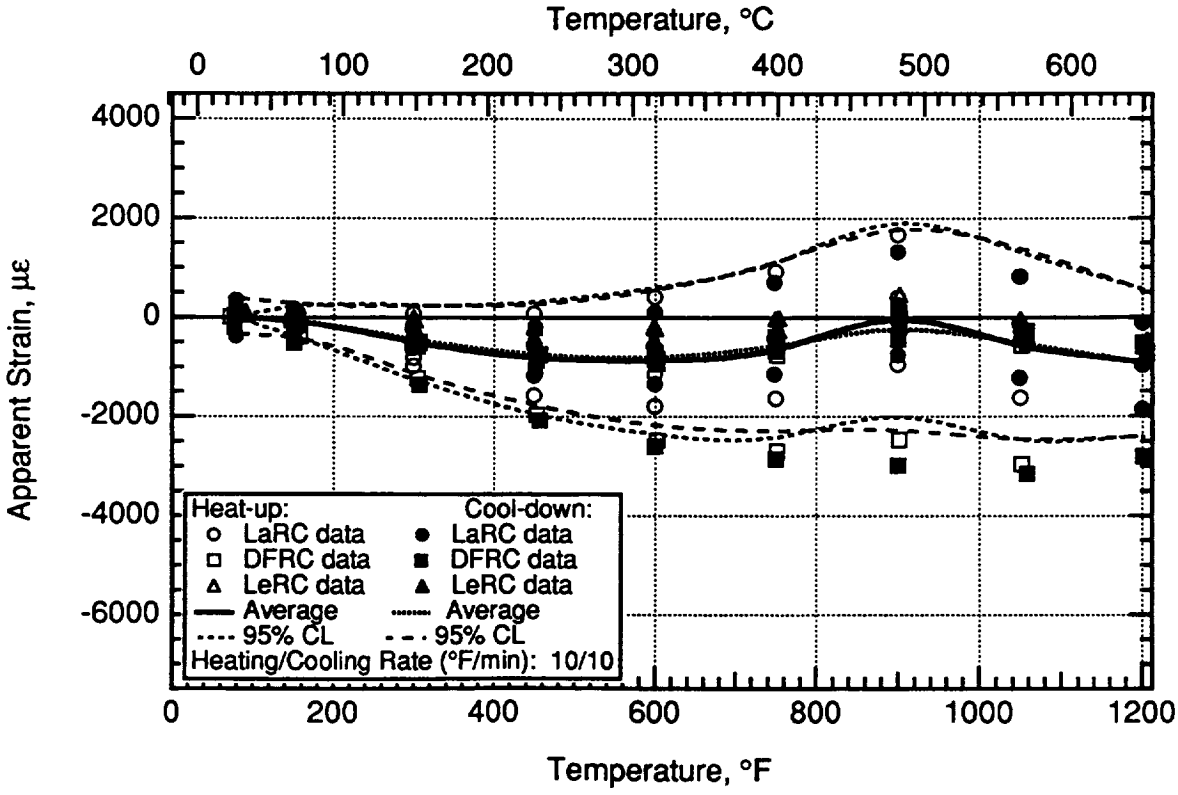

Figure 5.20.—PdCr gage cycle 8 apparent strain on IN100.

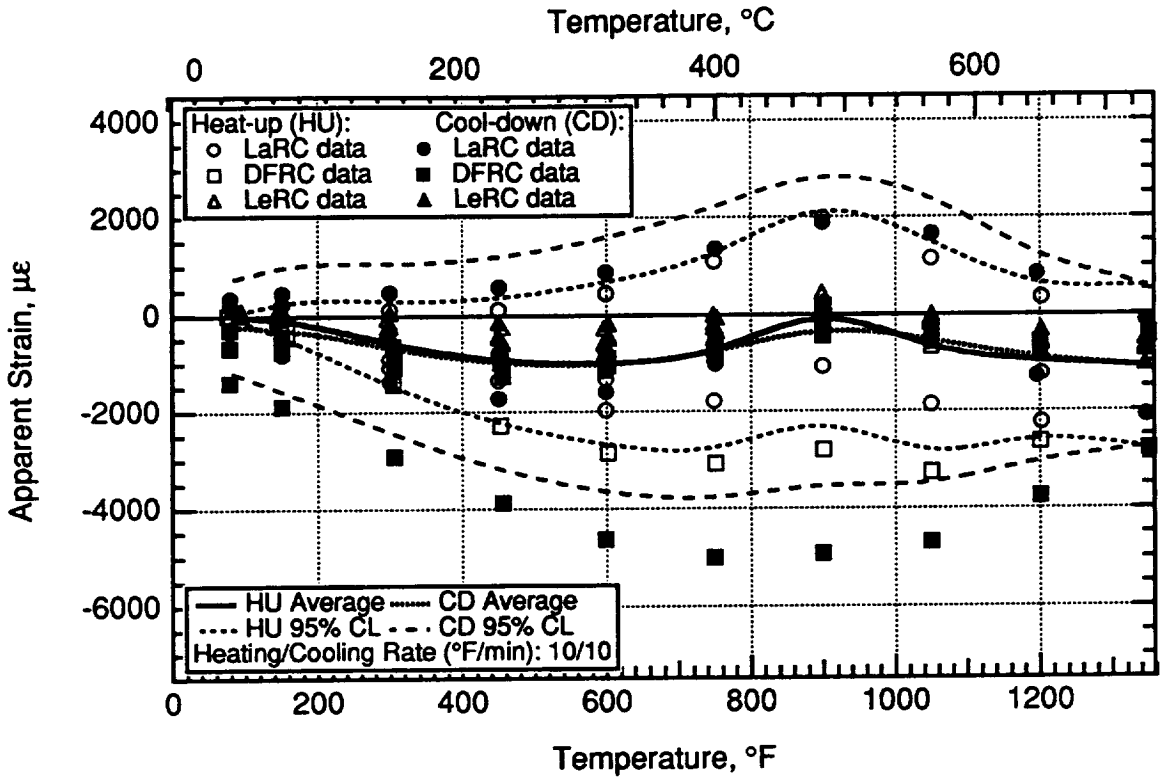

Figure 5.21.—PdCr gage cycle 9 apparent strain on IN100.

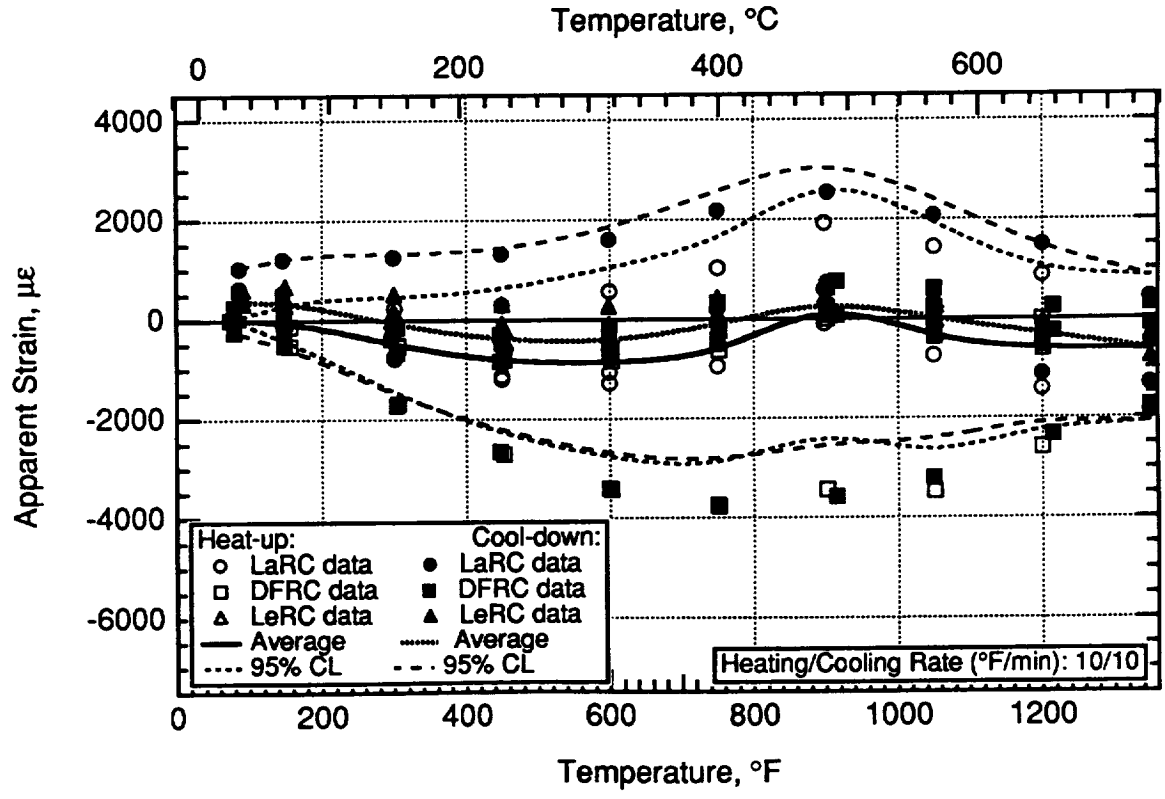

Figure 5.22.—PdCr gage cycle 10 apparent strain on IN100.

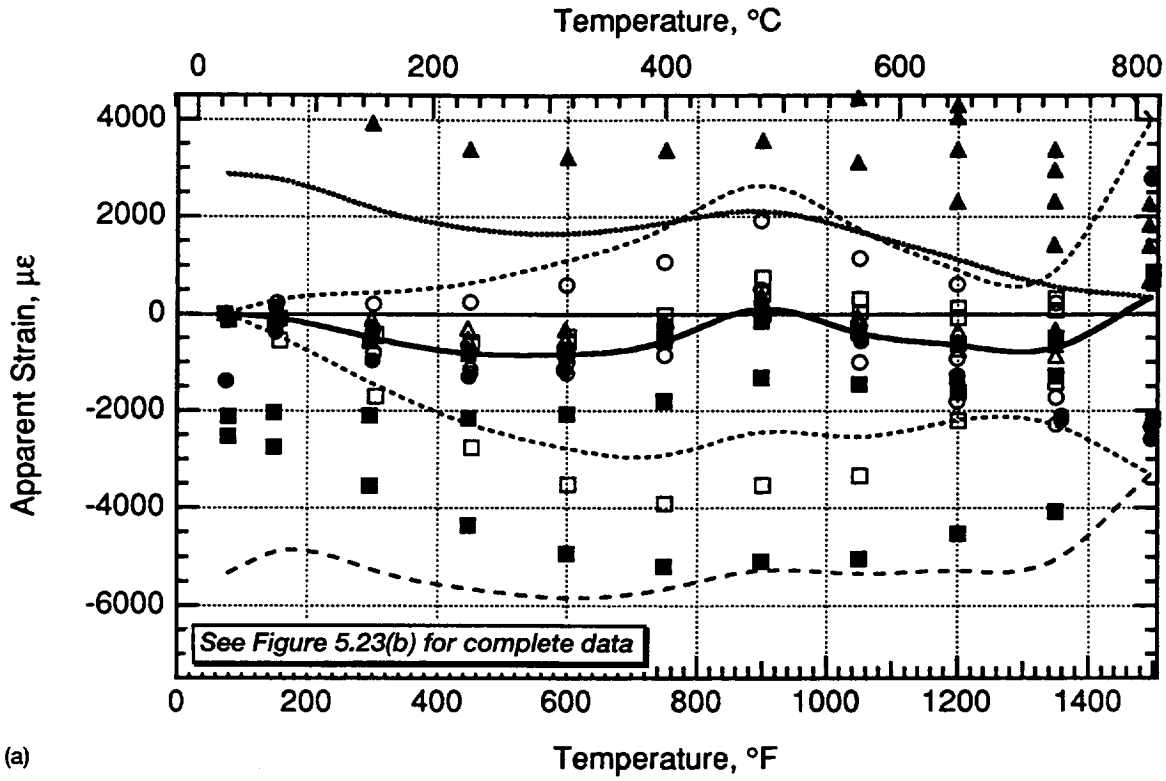

(a)

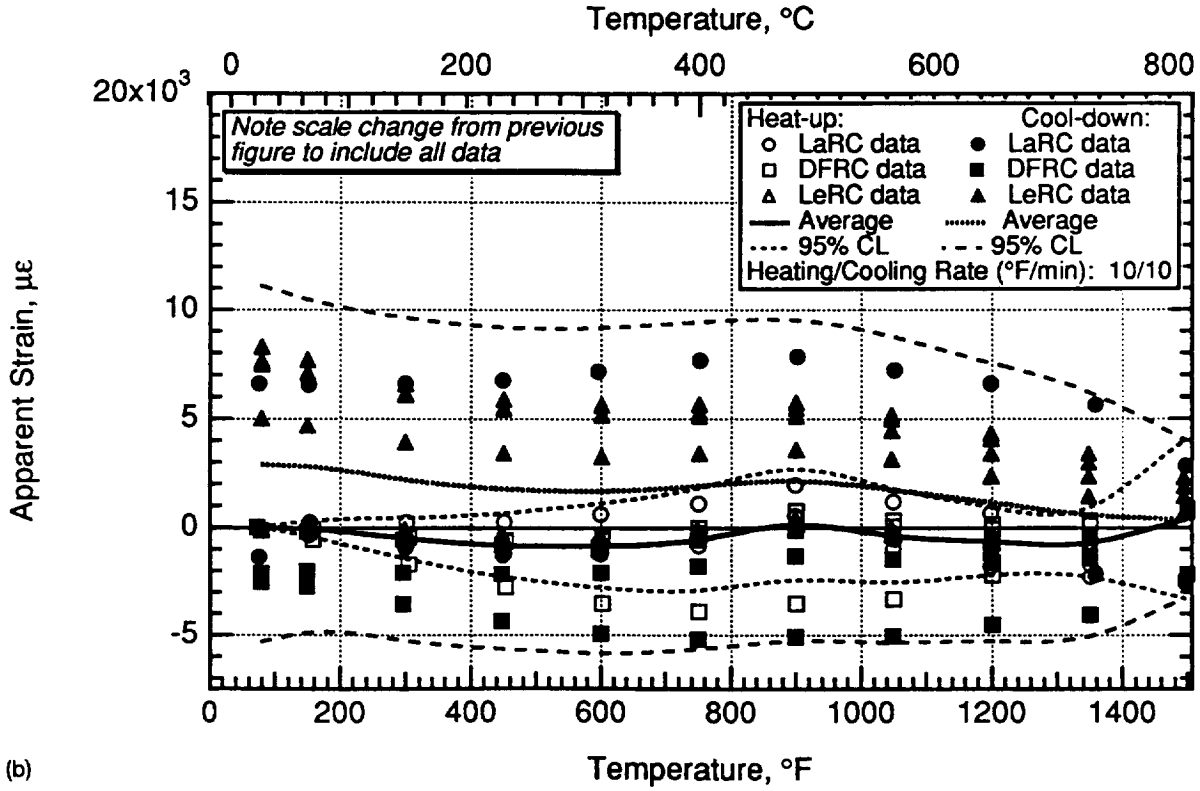

(b)

Figure 5.23.—PdCr gage cycle 11 apparent strain on IN100. (a) Partial data. (b) Complete data.

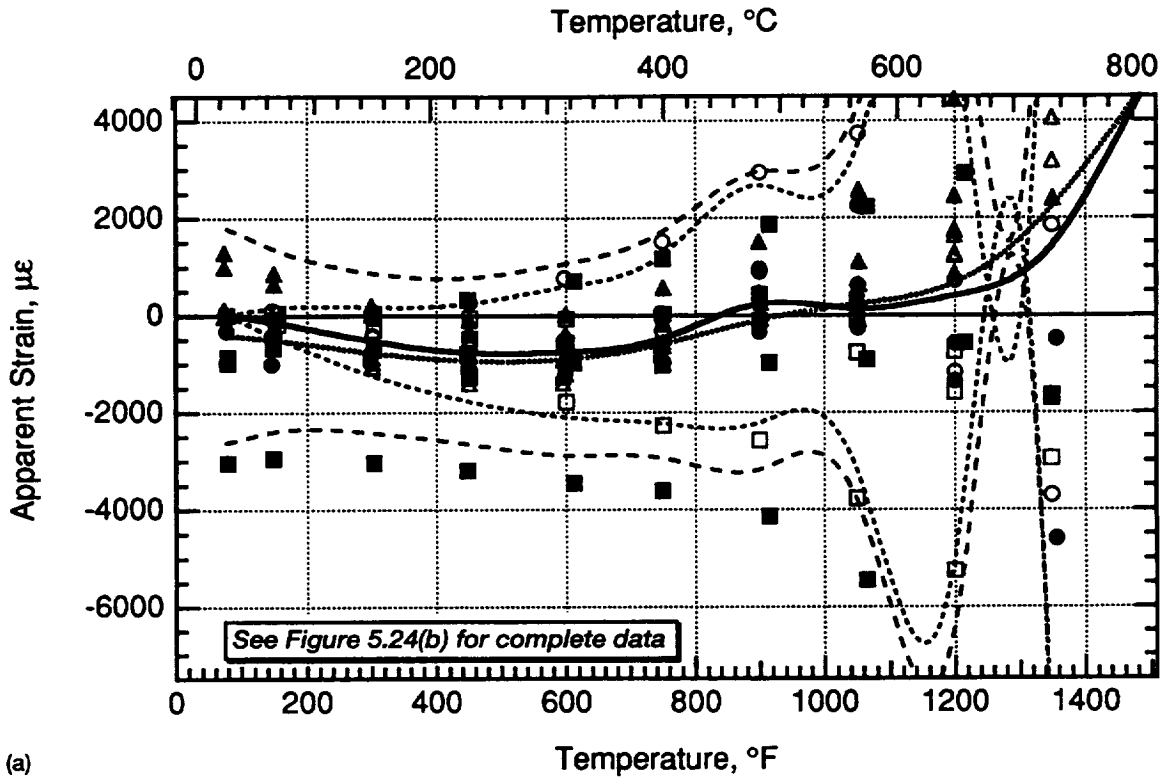

(a)

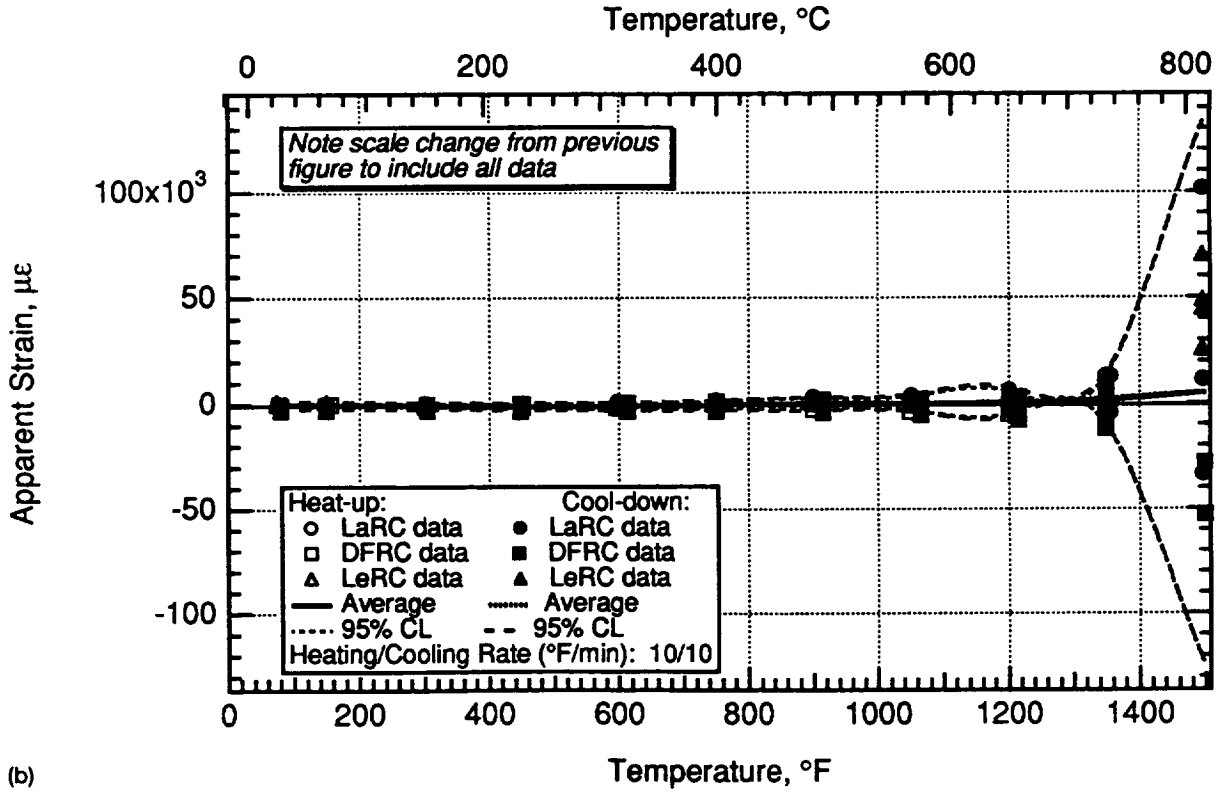

(b)

Figure 5.24.—PdCr gage cycle 12 apparent strain on IN100. (a) Partial data. (b) Complete data.

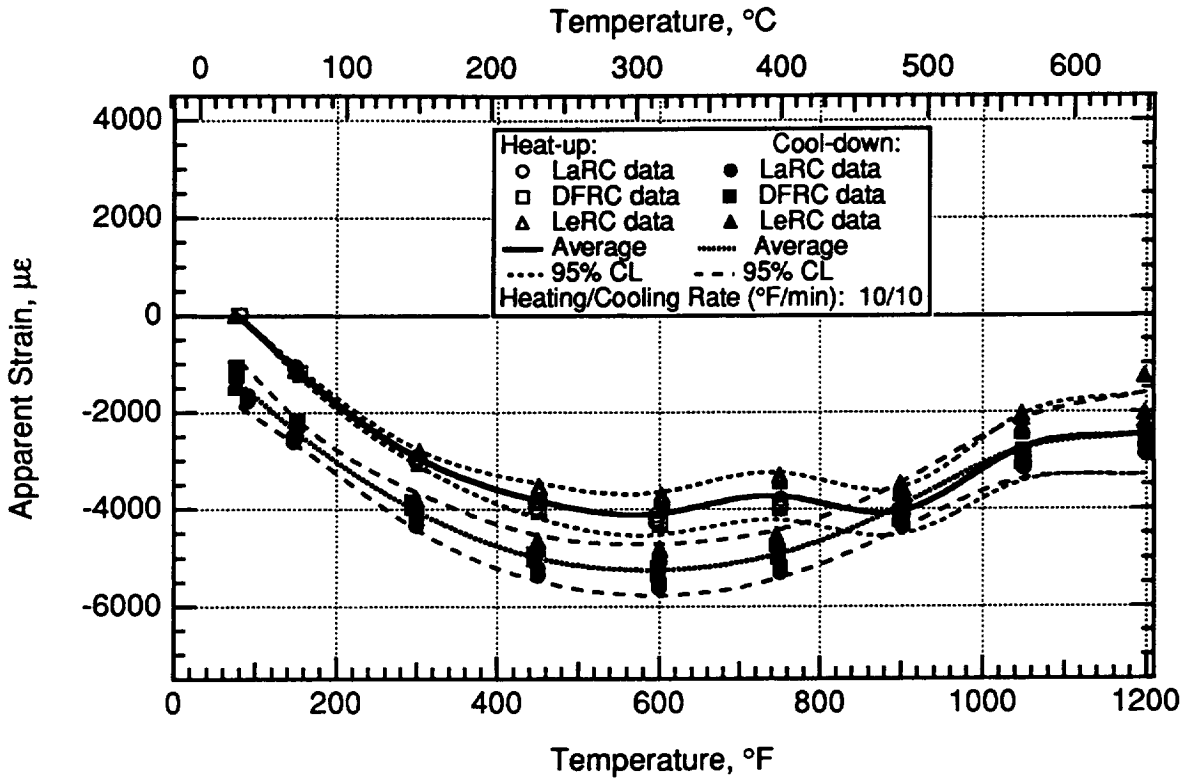

Figure 5.25.—DETCBCL gage cycle 1 apparent strain on IN100.

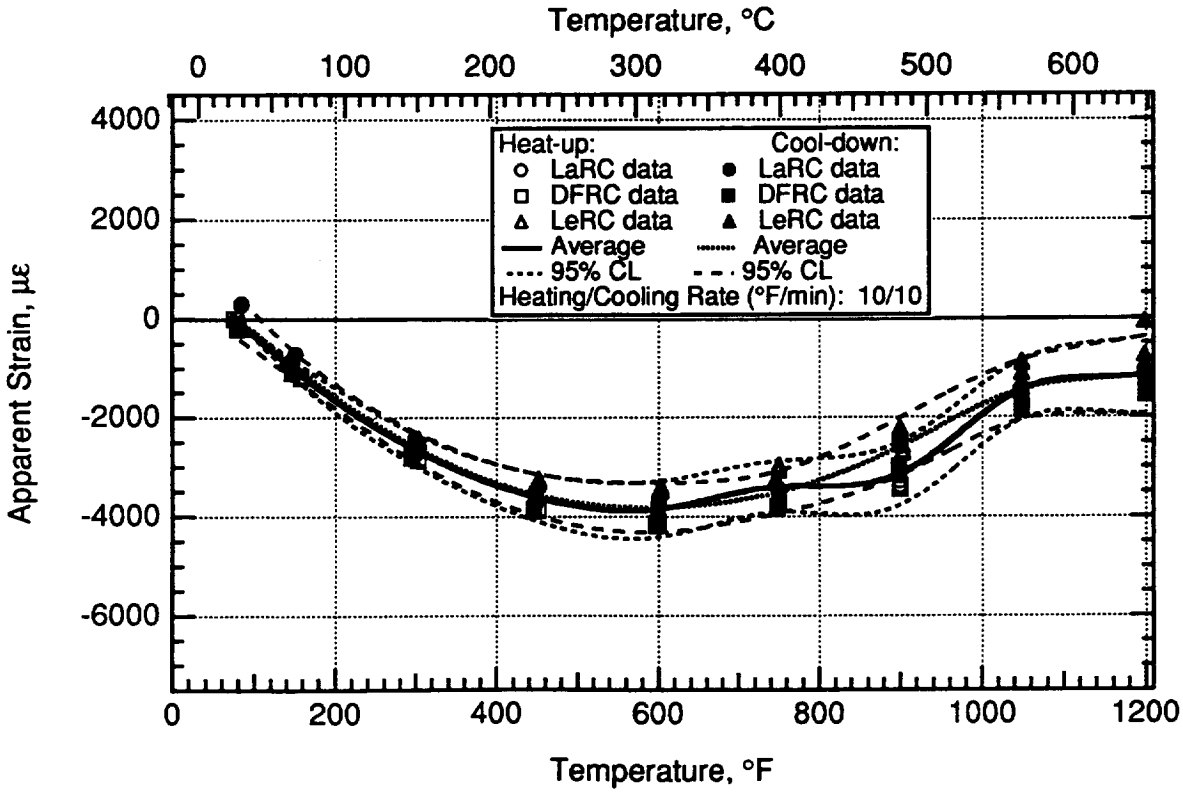

Figure 5.26.—DETCBCL gage cycle 2 apparent strain on IN100.

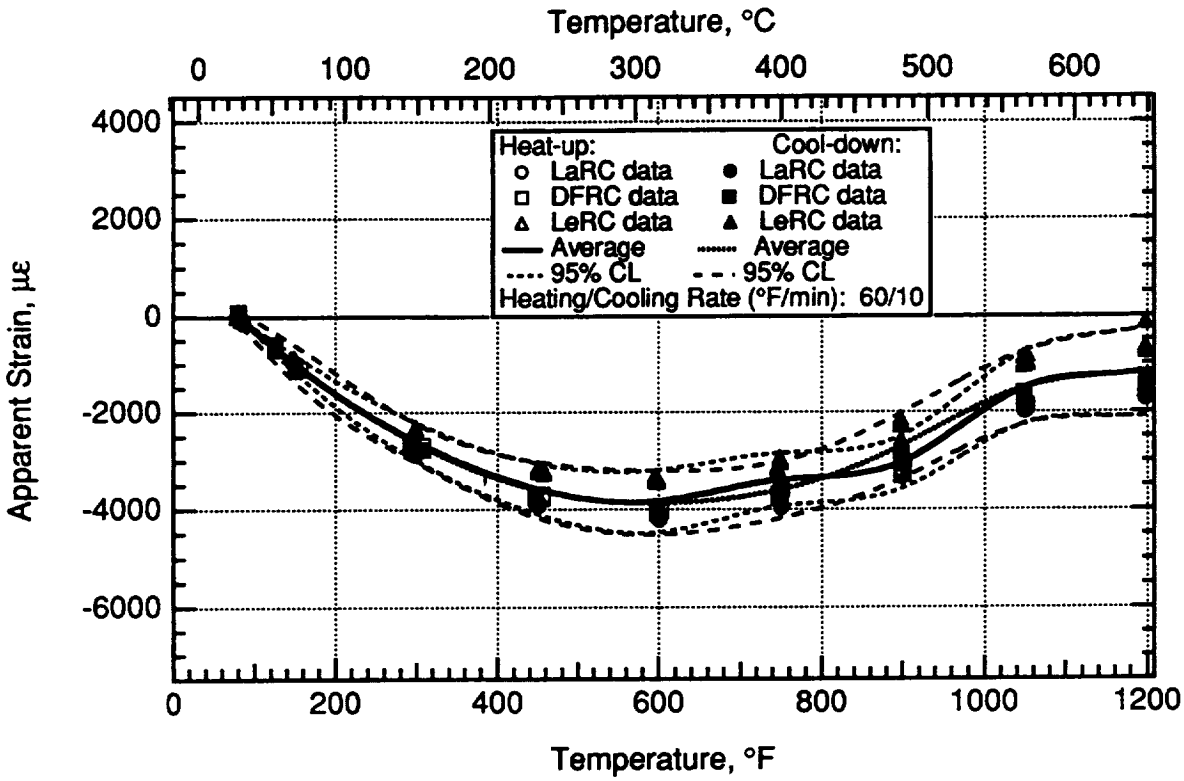

Figure 5.27.—DETCBCL gage cycle 3 apparent strain on IN100.

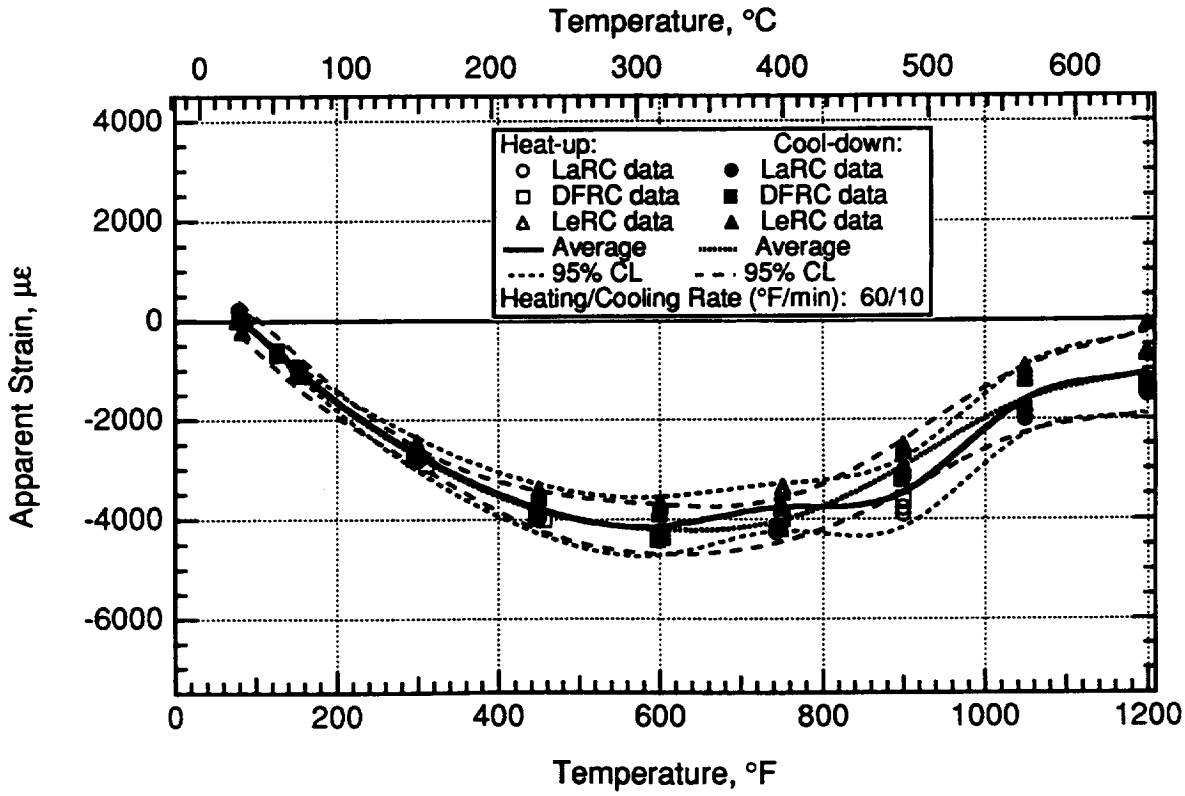

Figure 5.28.—DETCBCL gage cycle 4 apparent strain on IN100.

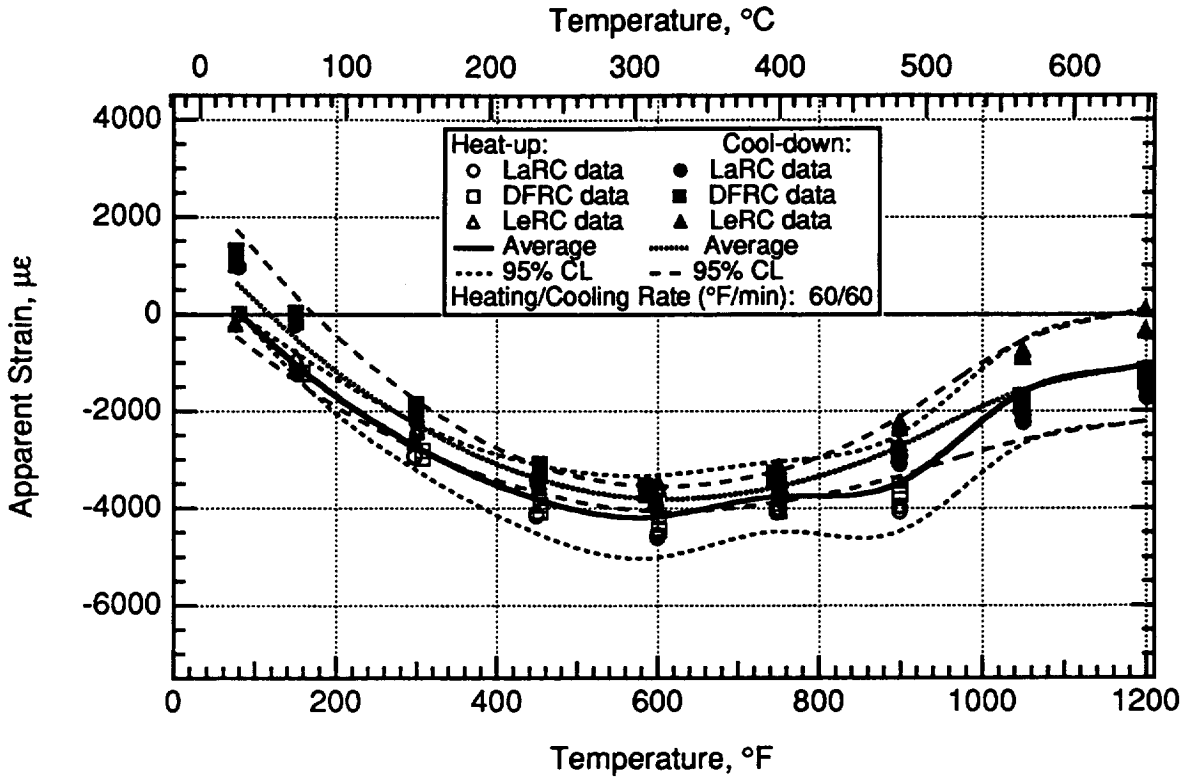

Figure 5.29.—DETCBCL gage cycle 5 apparent strain on IN100.

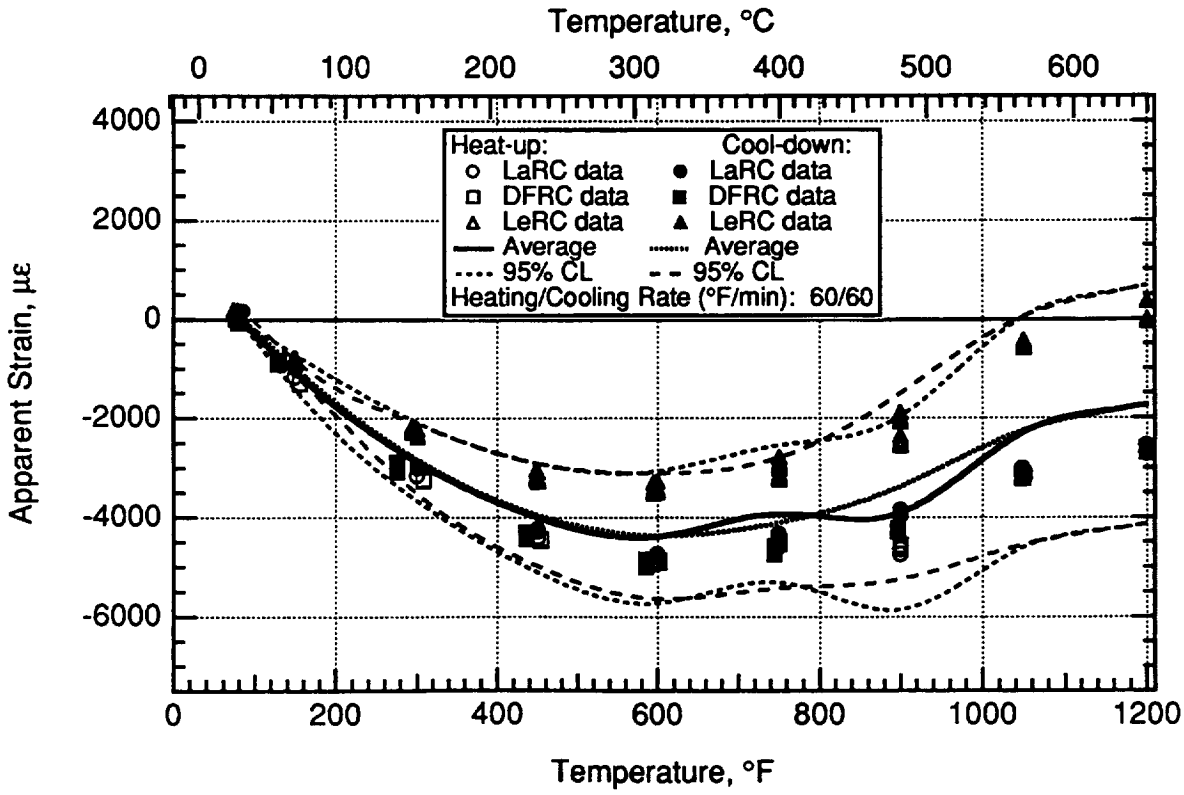

Figure 5.30.—DETCBCL gage cycle 6 apparent strain on IN100.

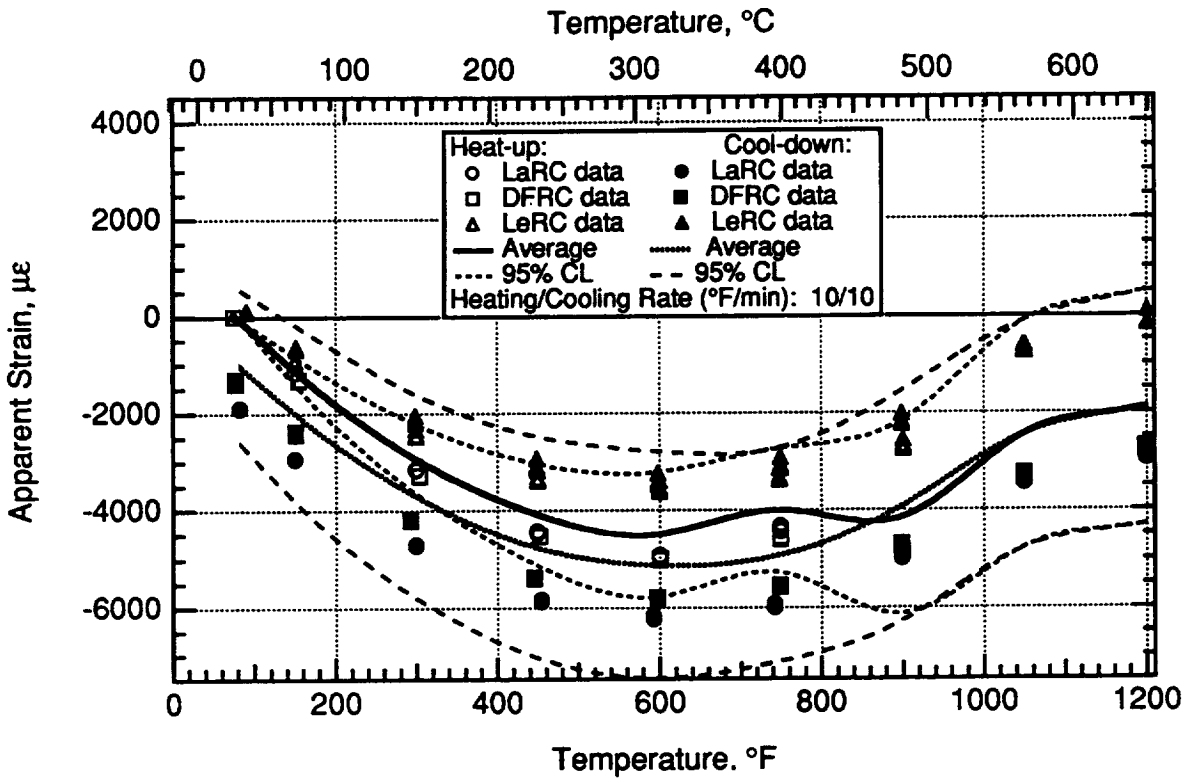

Figure 5.31.—DETCBCL gage cycle 7 apparent strain on IN100.

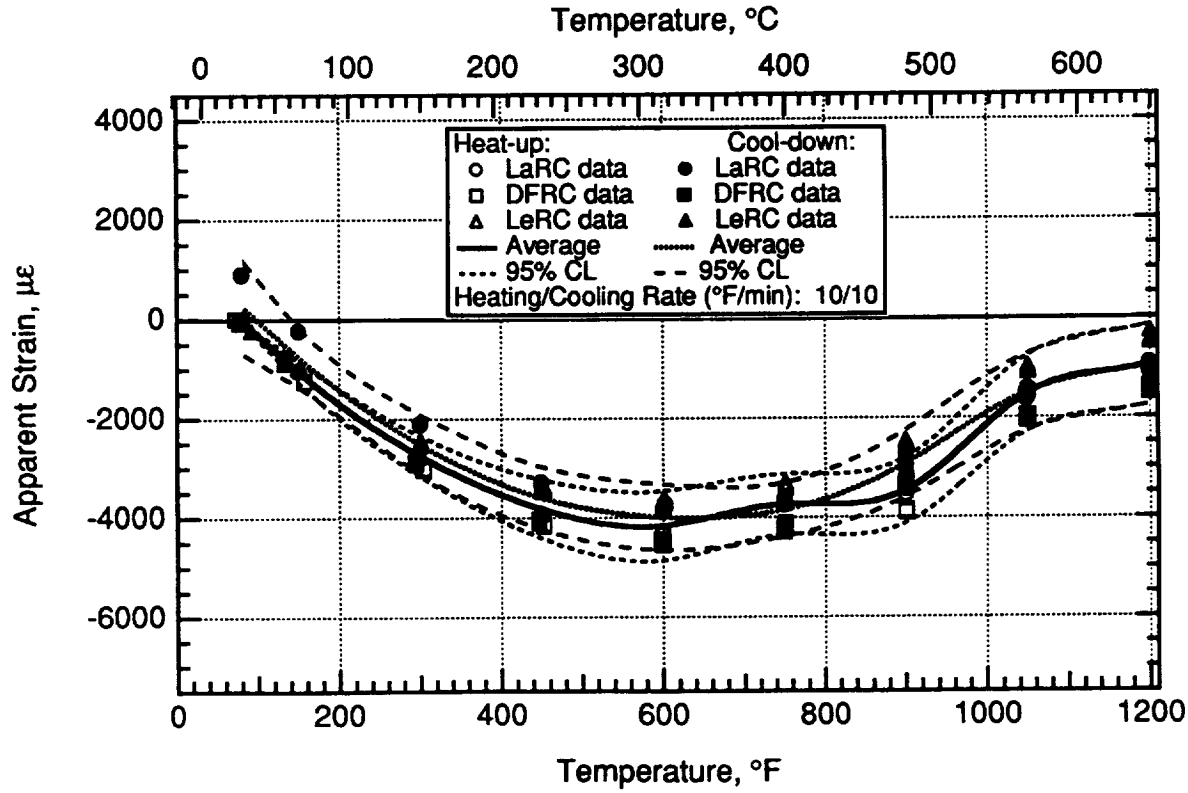

Figure 5.32.—DETCBCL gage cycle 8 apparent strain on IN100.

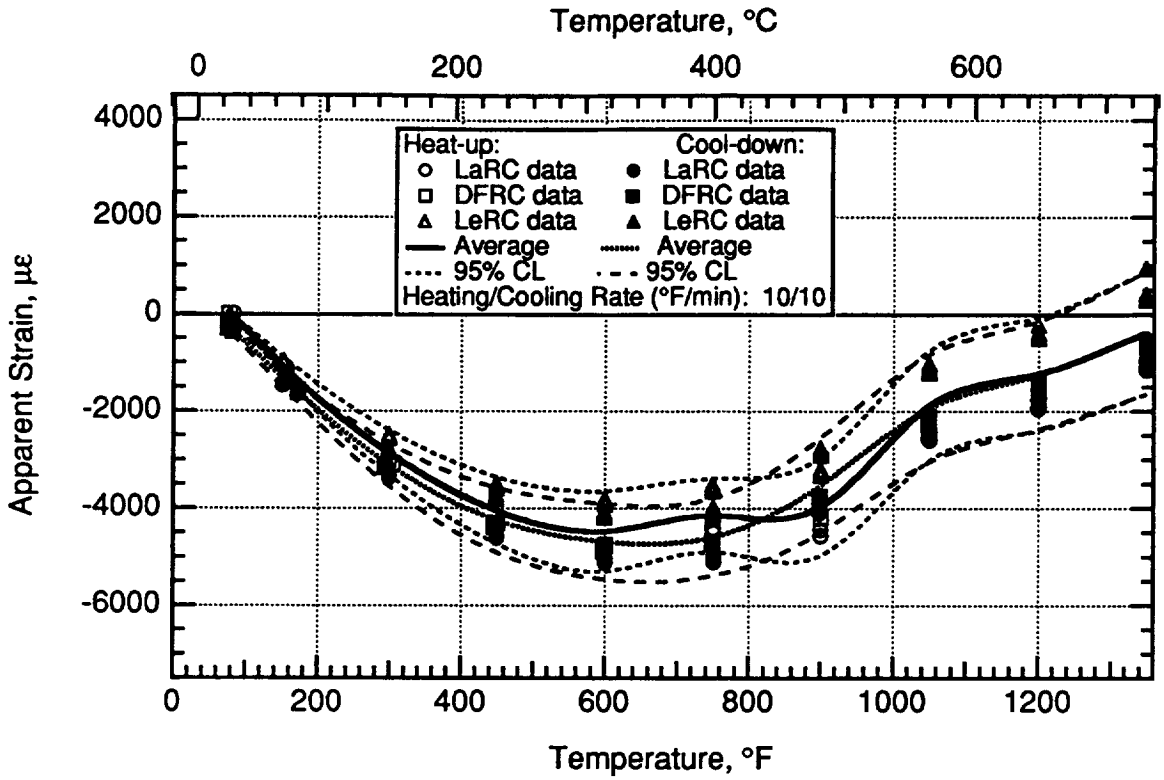

Figure 5.33.—DETCBCL gage cycle 9 apparent strain on IN100.

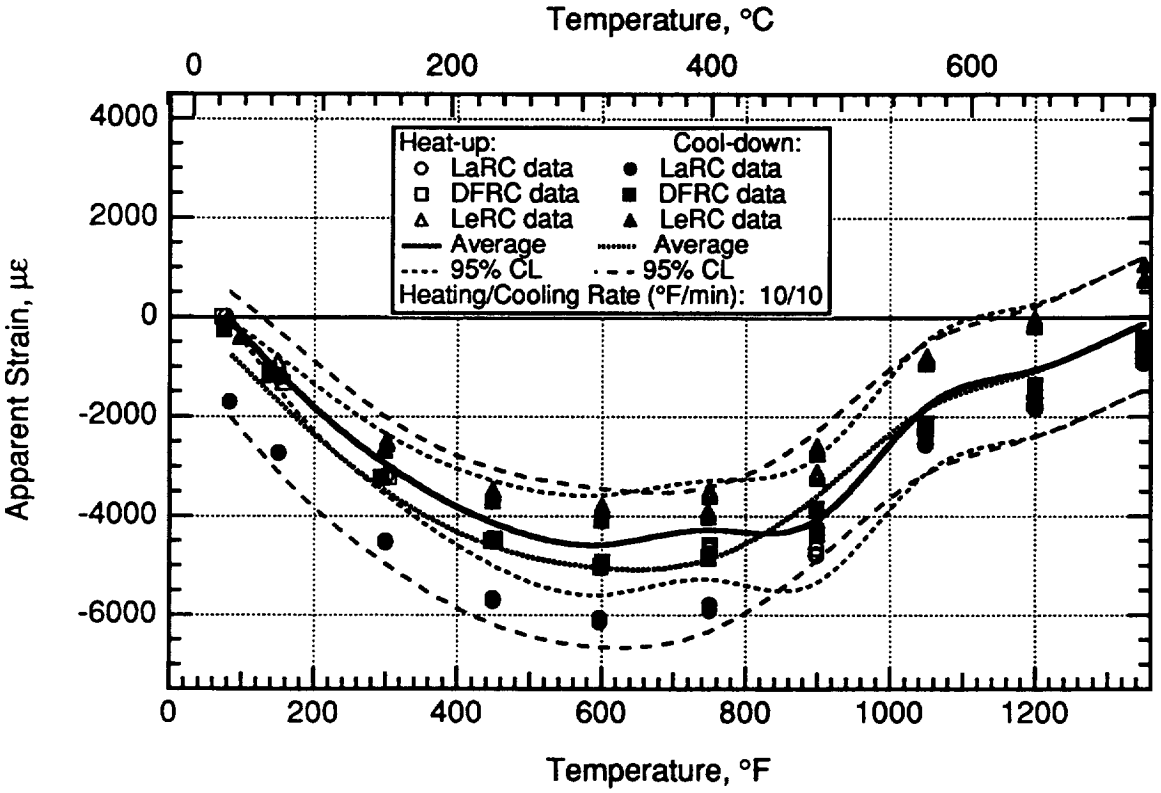

Figure 5.34.—DETCBCL gage cycle 10 apparent strain on IN100.

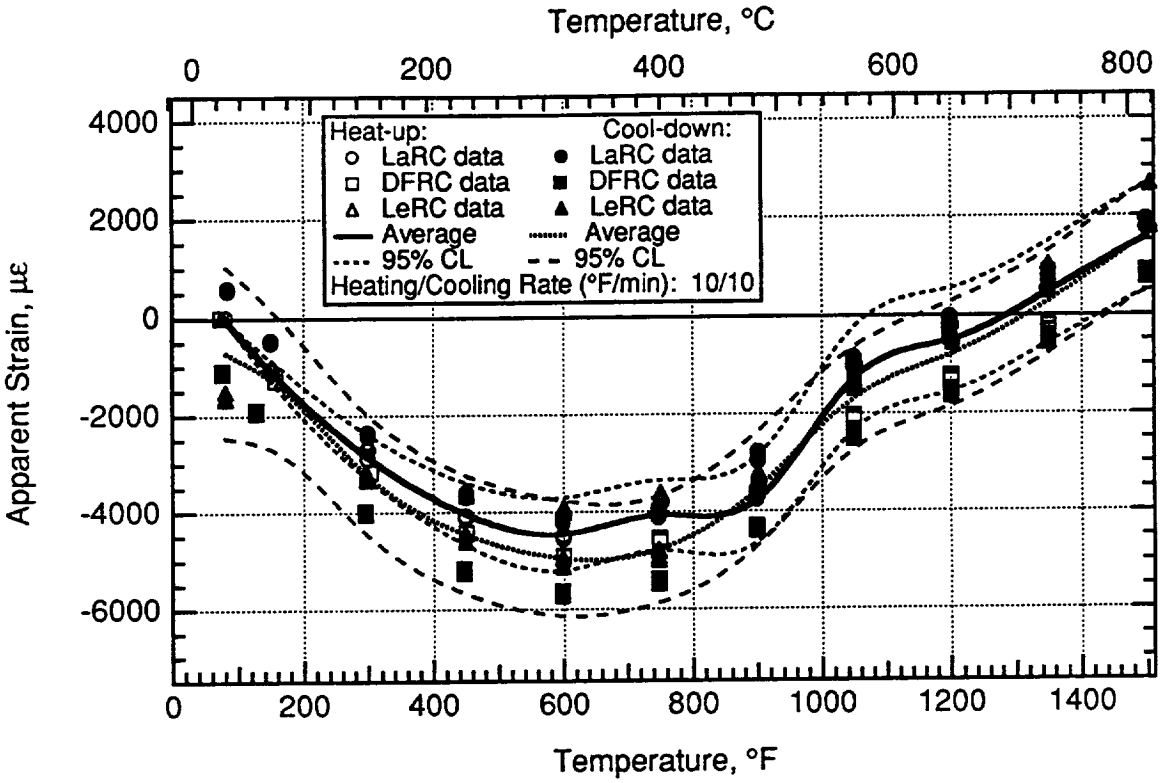

Figure 5.35.—DETCBCL gage cycle 11 apparent strain on IN100.

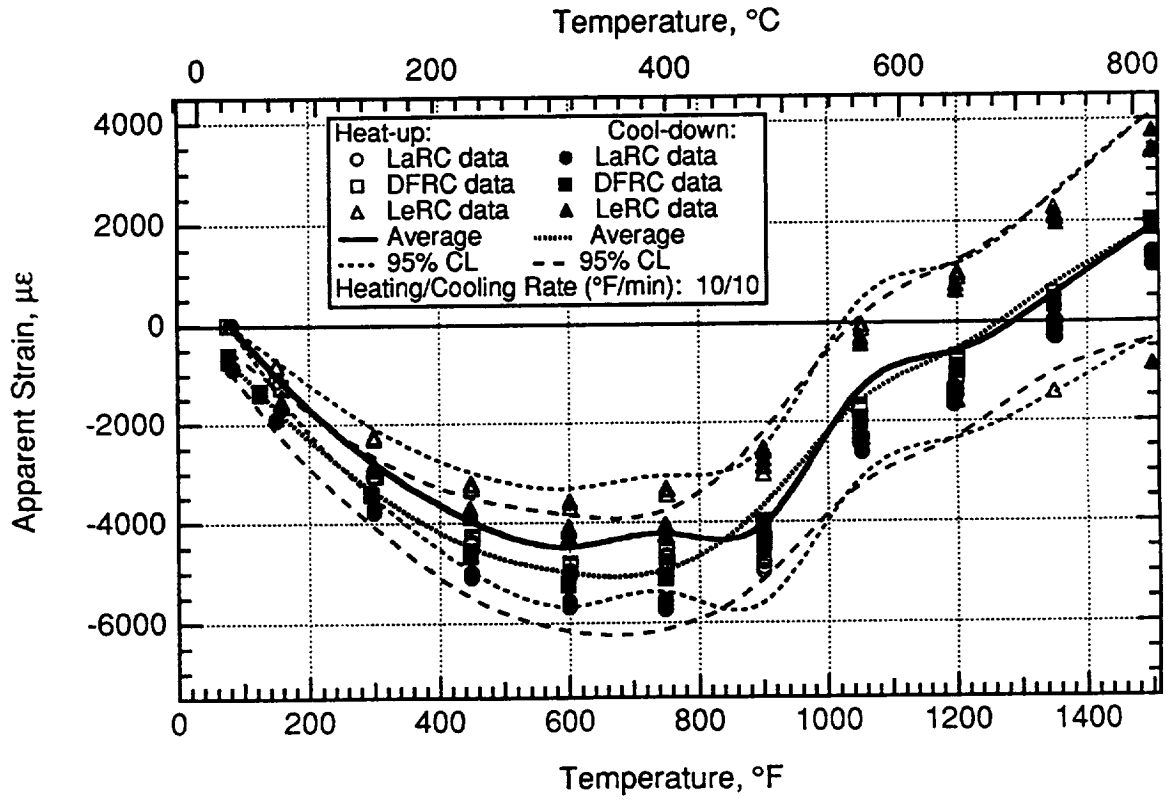

Figure 5.36.—DETCBCL gage cycle 12 apparent strain on IN100.

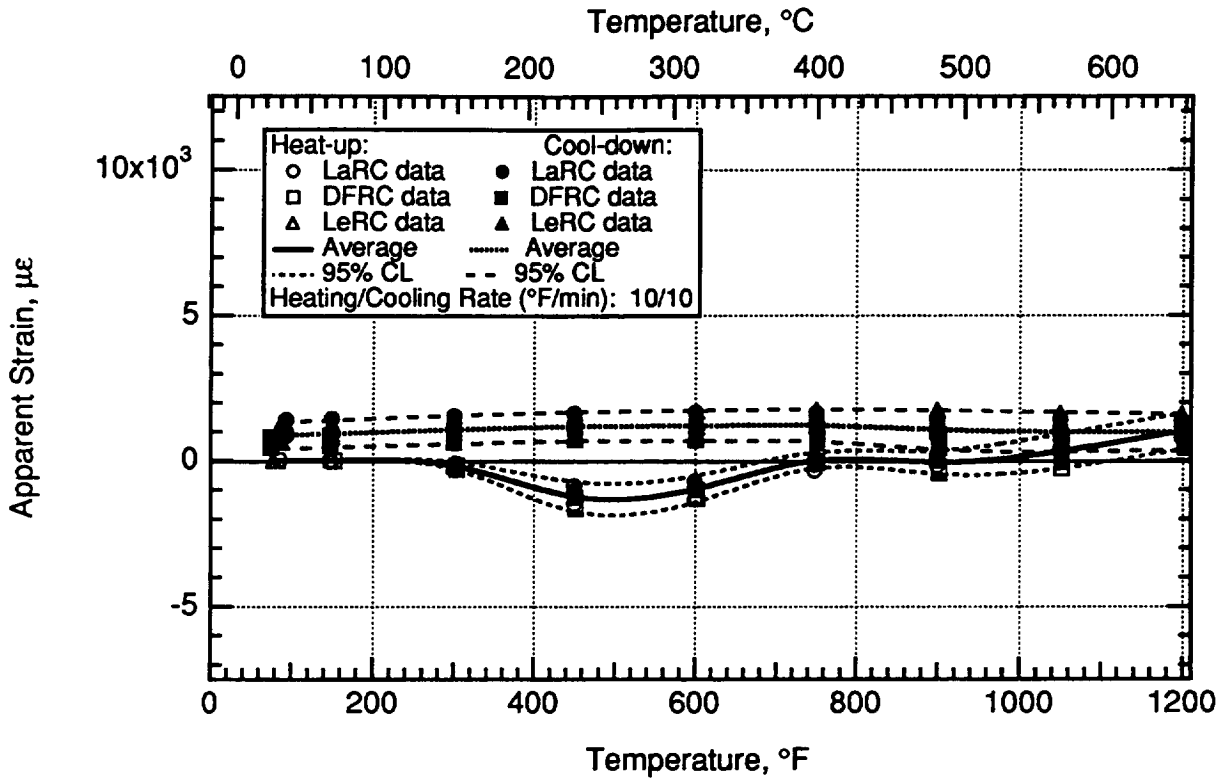

Figure 5.37.—CKA1 gage cycle 1 apparent strain on β-21S TMC.

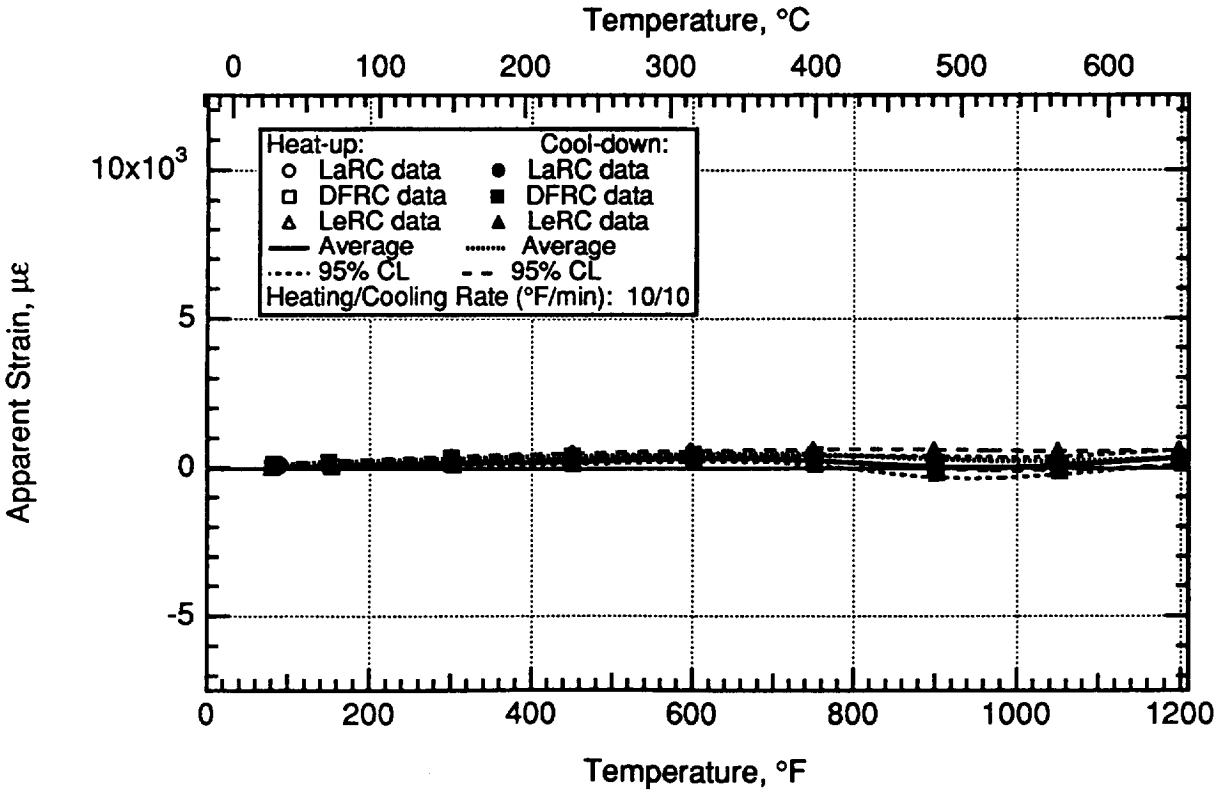

Figure 5.38.—CKA1 gage cycle 2 apparent strain on β-21S TMC.

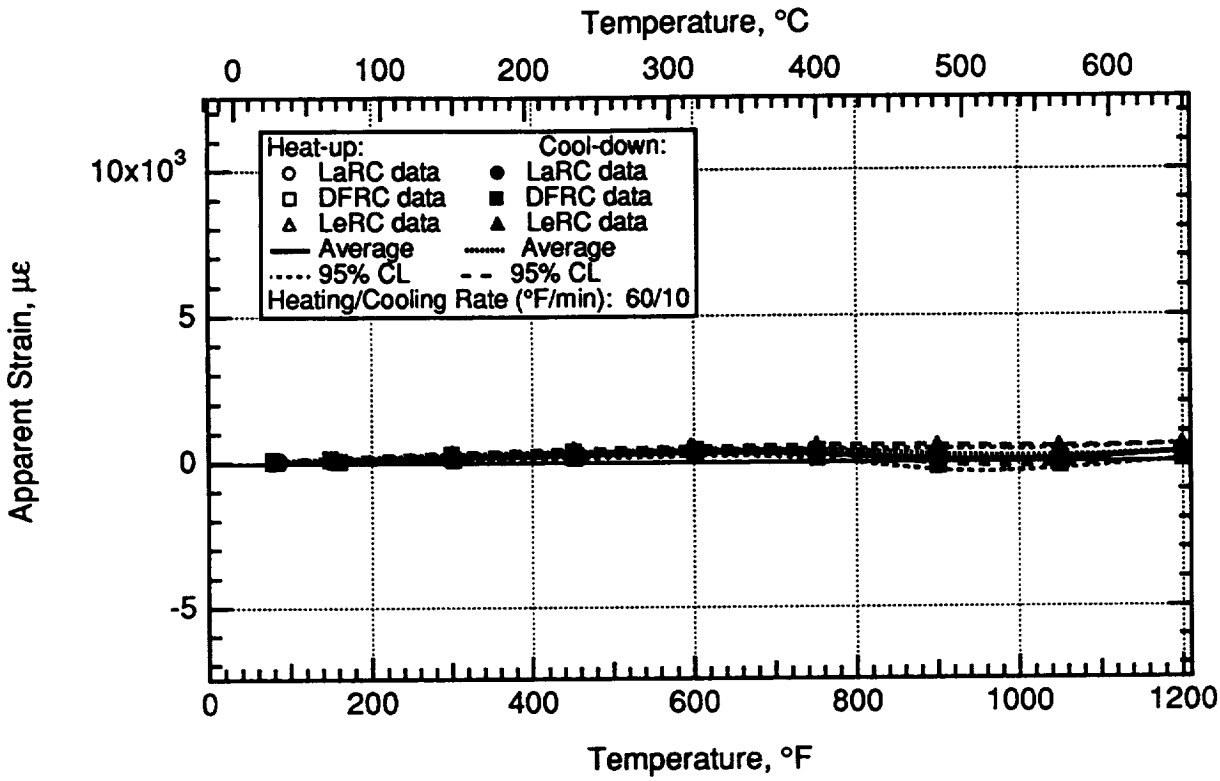

Figure 5.39.—CKA1 gage cycle 3 apparent strain on β-21S TMC.

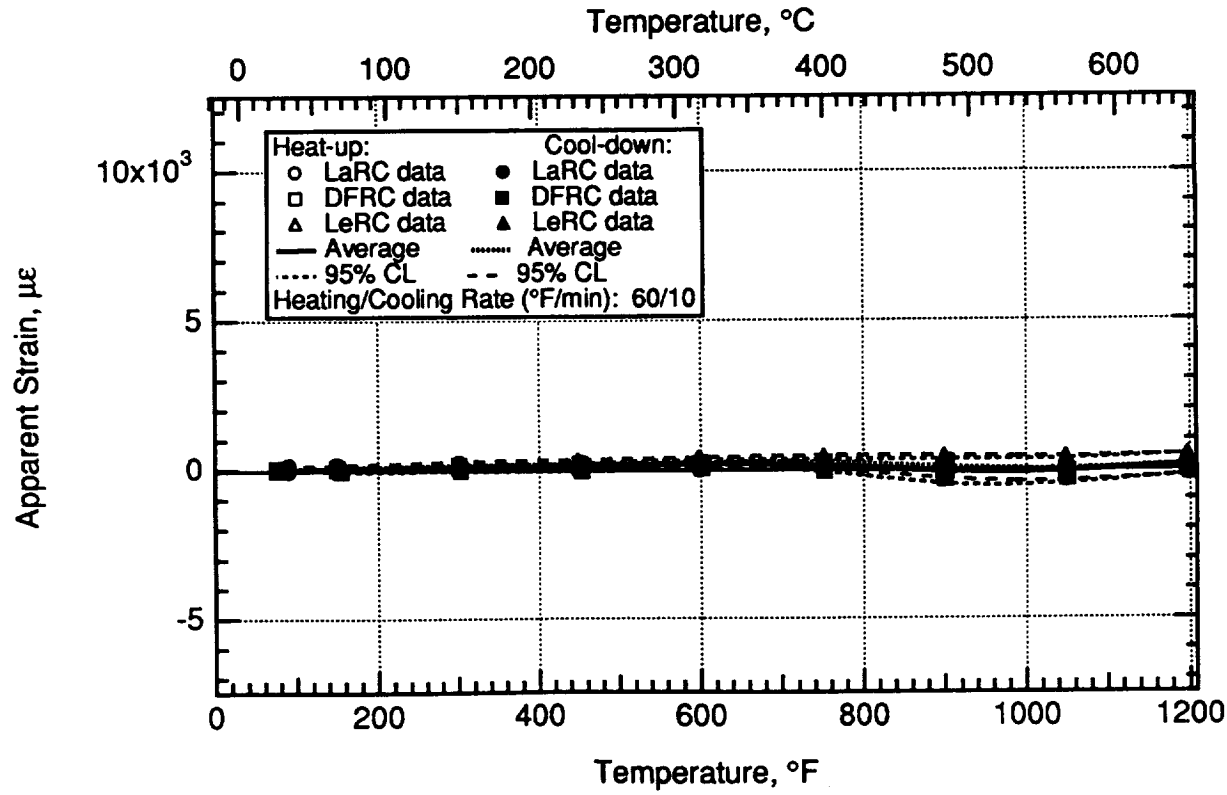

Figure 5.40.—CKA1 gage cycle 4 apparent strain on β-21S TMC.

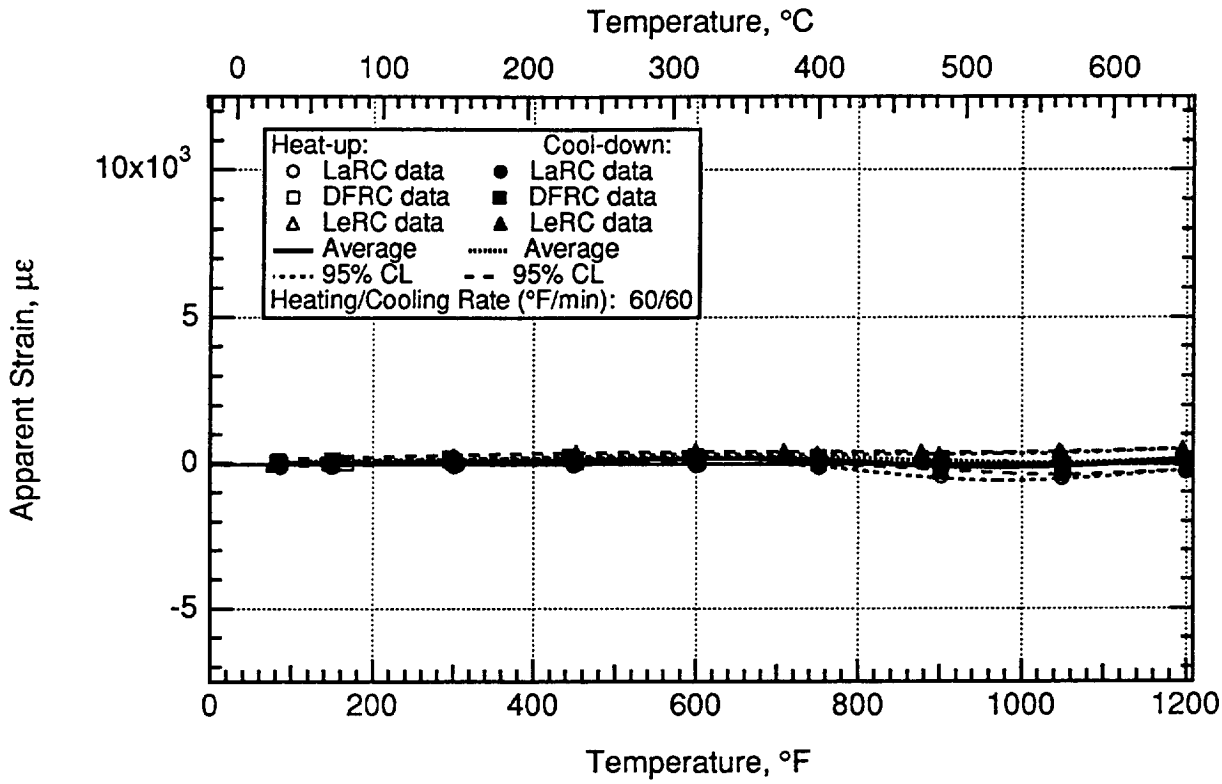

Figure 5.41.—CKA1 gage cycle 5 apparent strain on β-21S TMC.

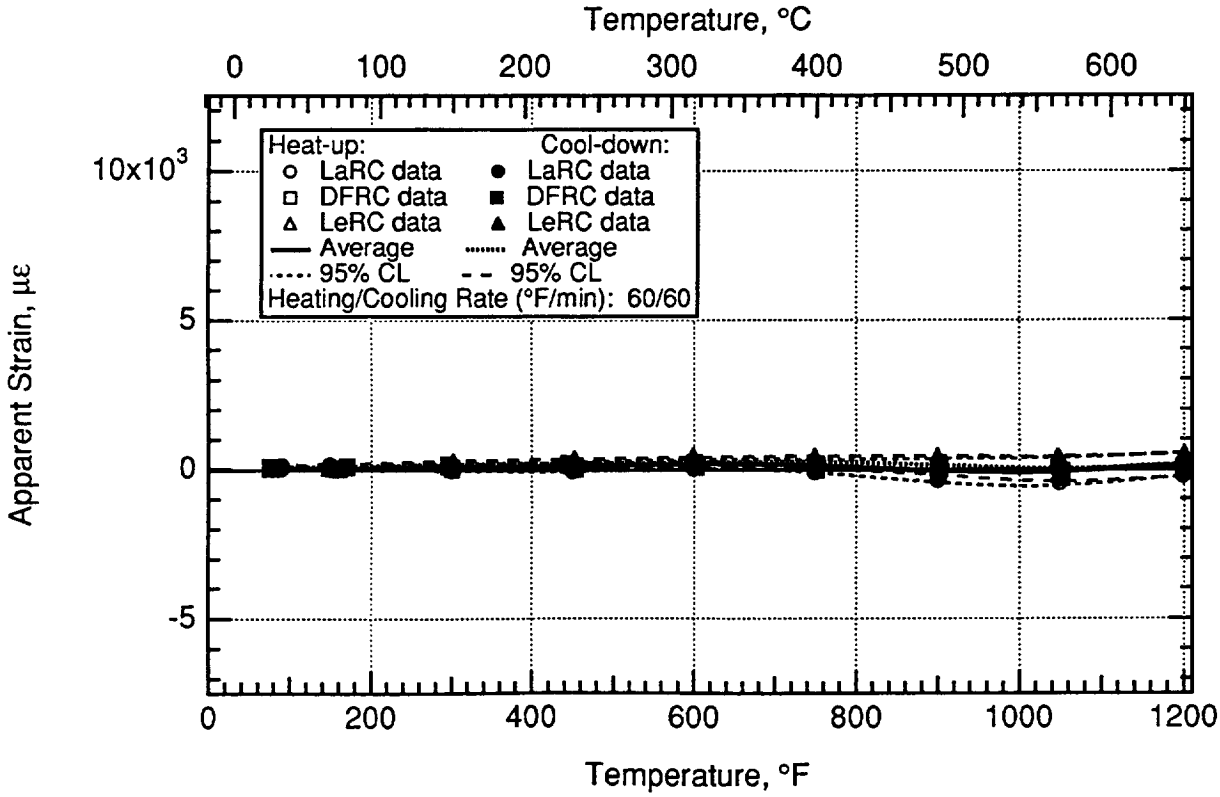

Figure 5.42.—CKA1 gage cycle 6 apparent strain on β-21S TMC.

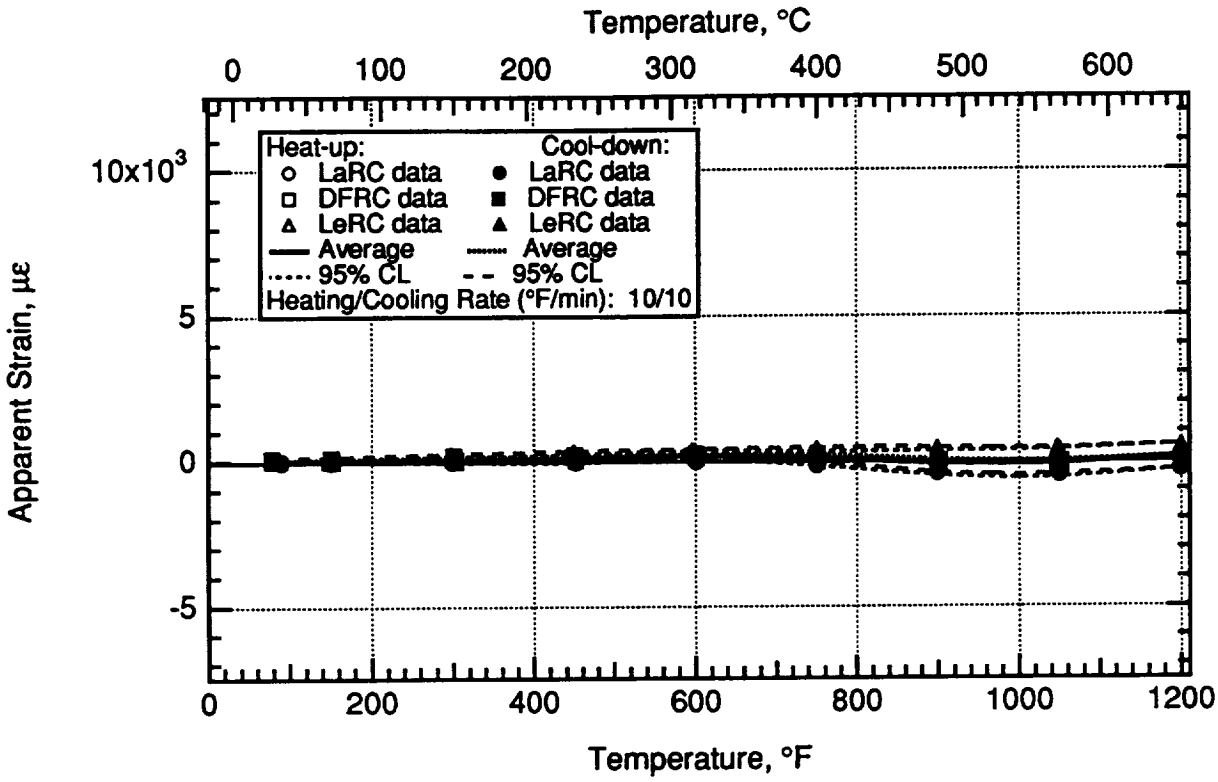

Figure 5.43.—CKA1 gage cycle 7 apparent strain on β-21S TMC.

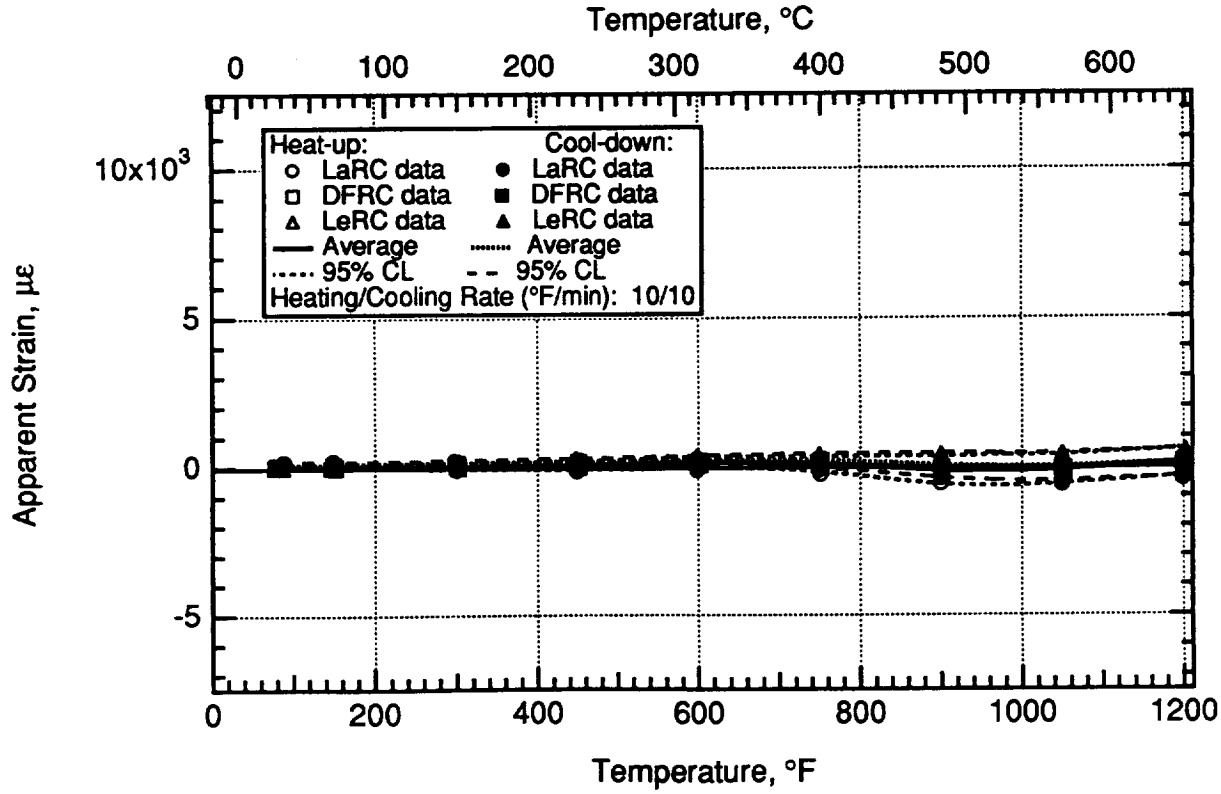

Figure 5.44.—CKA1 gage cycle 8 apparent strain on β-21S TMC.

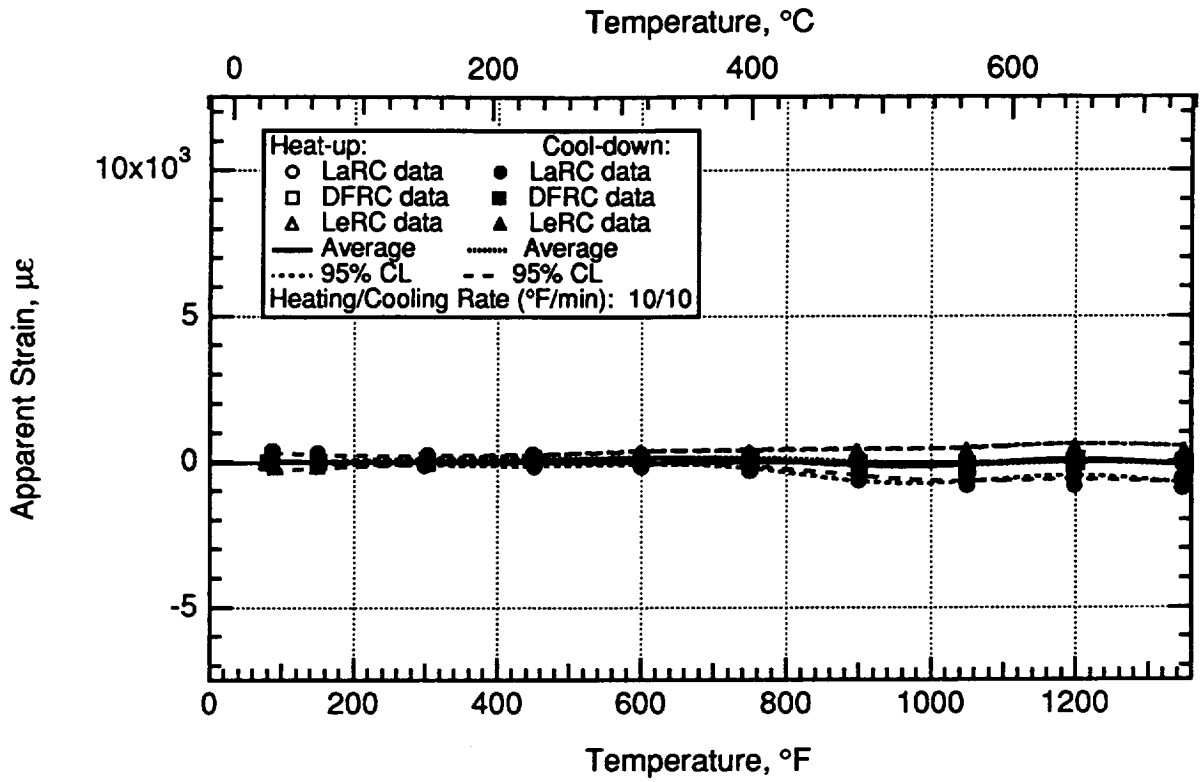

Figure 5.45.—CKA1 gage cycle 9 apparent strain on β-21S TMC.

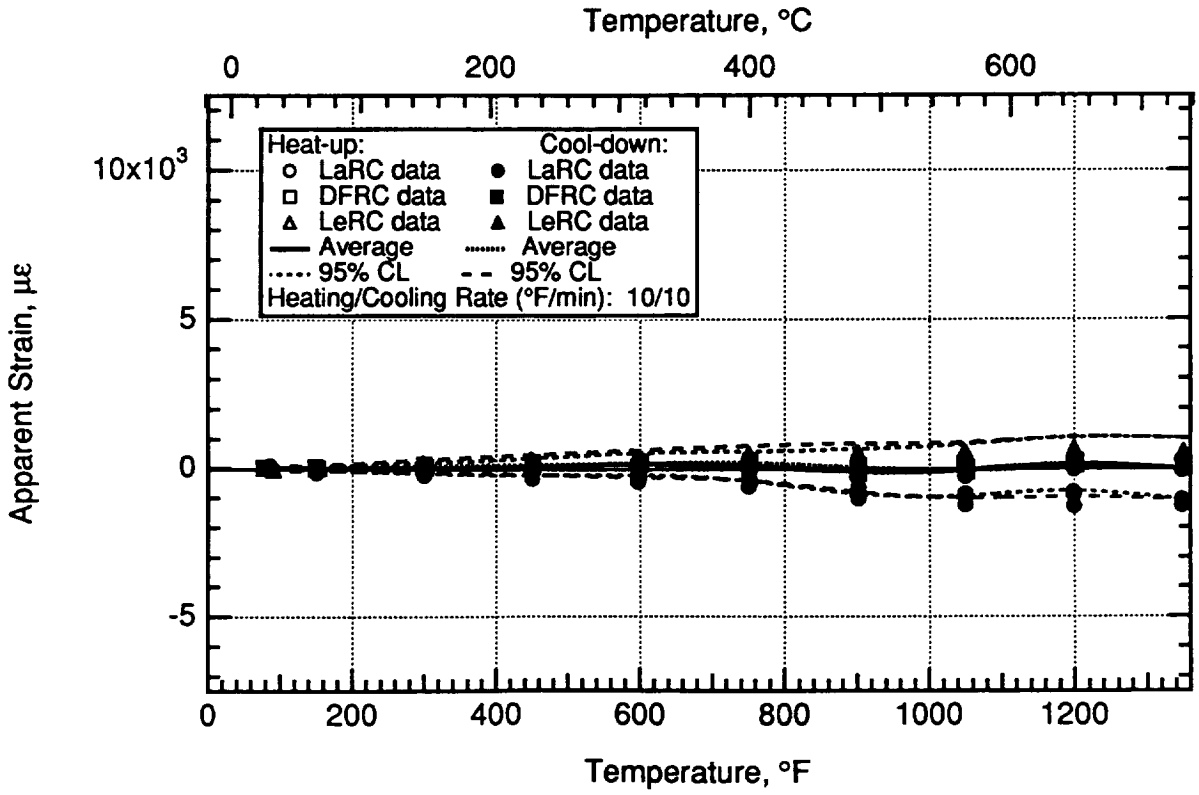

Figure 5.46.—CKA1 gage cycle 10 apparent strain on β-21S TMC.

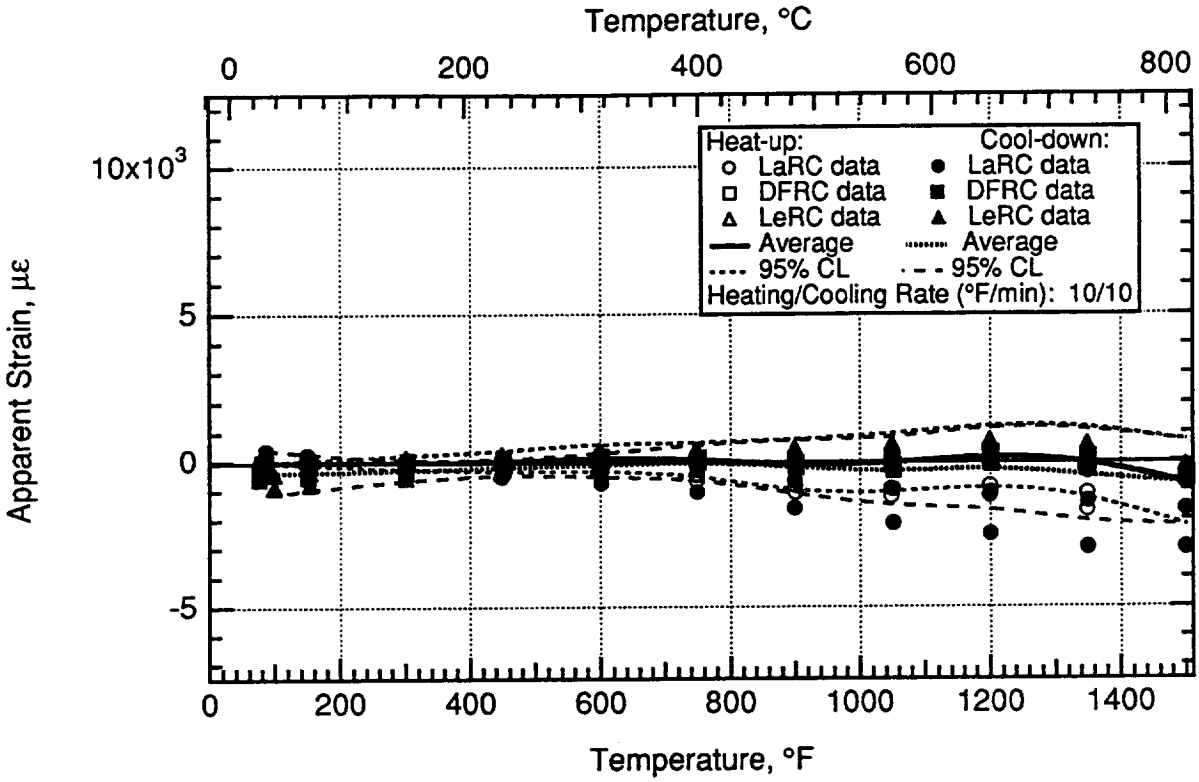

Figure 5.47.—CKA1 gage cycle 11 apparent strain on β-21S TMC.

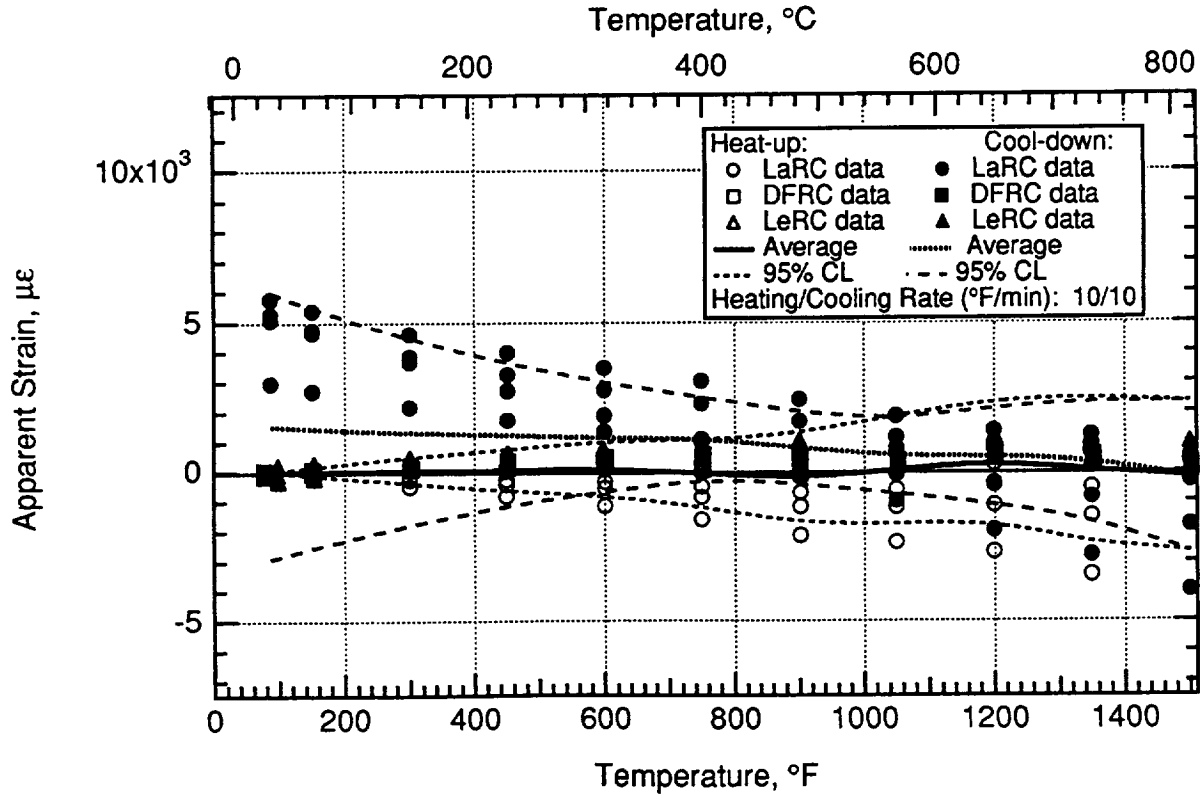

Figure 5.48.—CKA1 gage cycle 12 apparent strain on β-21S TMC.

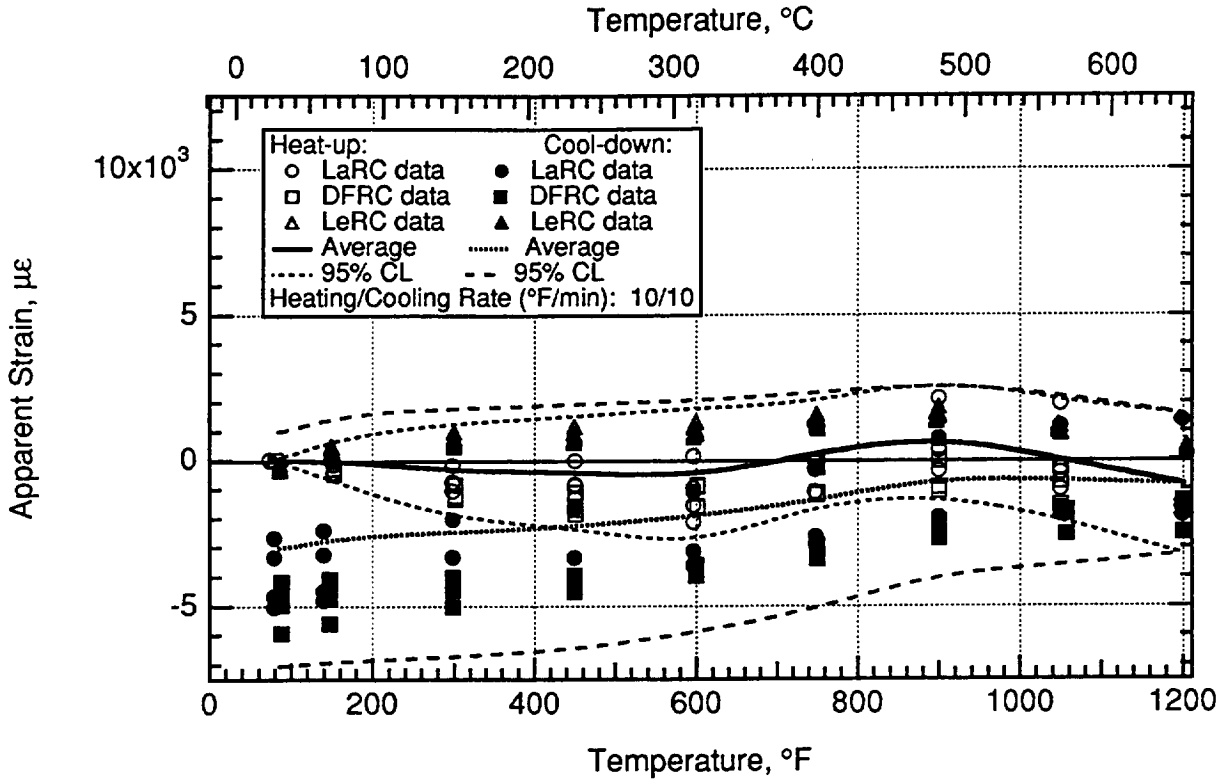

Figure 5.49.—PdCr gage cycle 1 apparent strain on β-21S TMC.

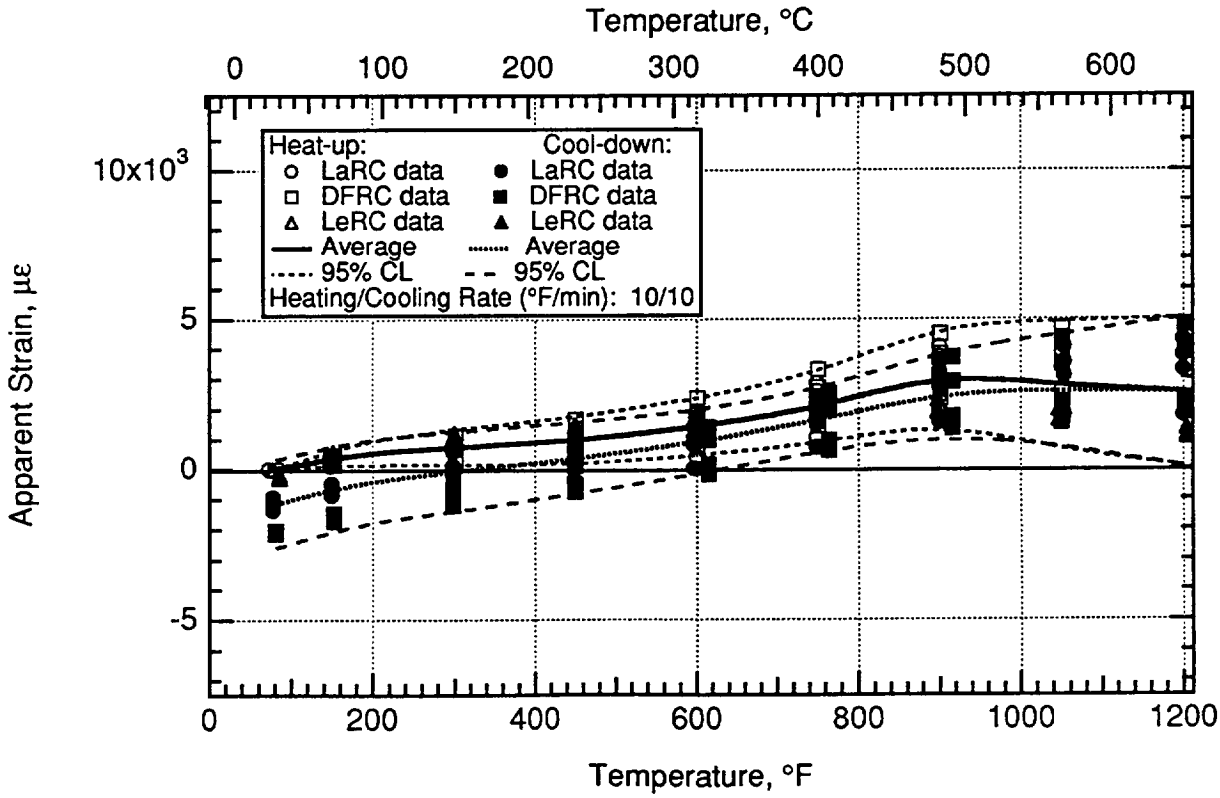

Figure 5.50.—PdCr gage cycle 2 apparent strain on β-21S TMC.

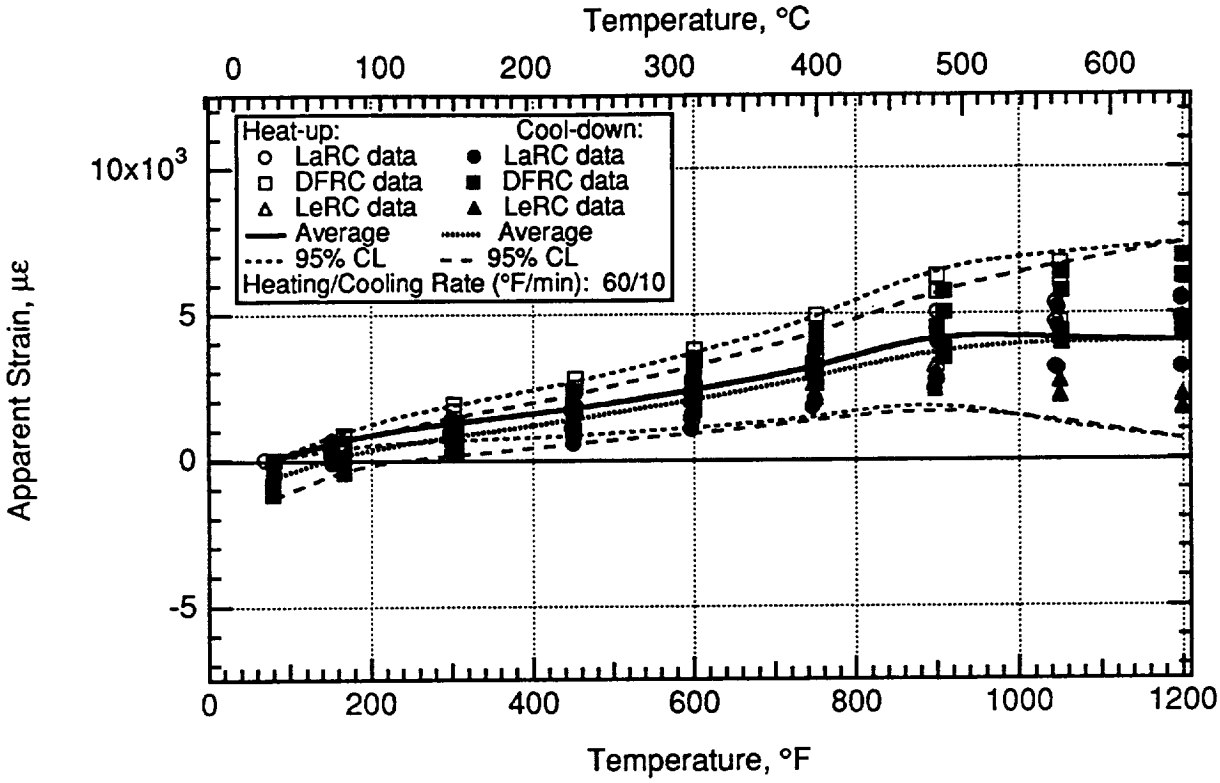

Figure 5.51.—PdCr gage cycle 3 apparent strain on β-21S TMC.

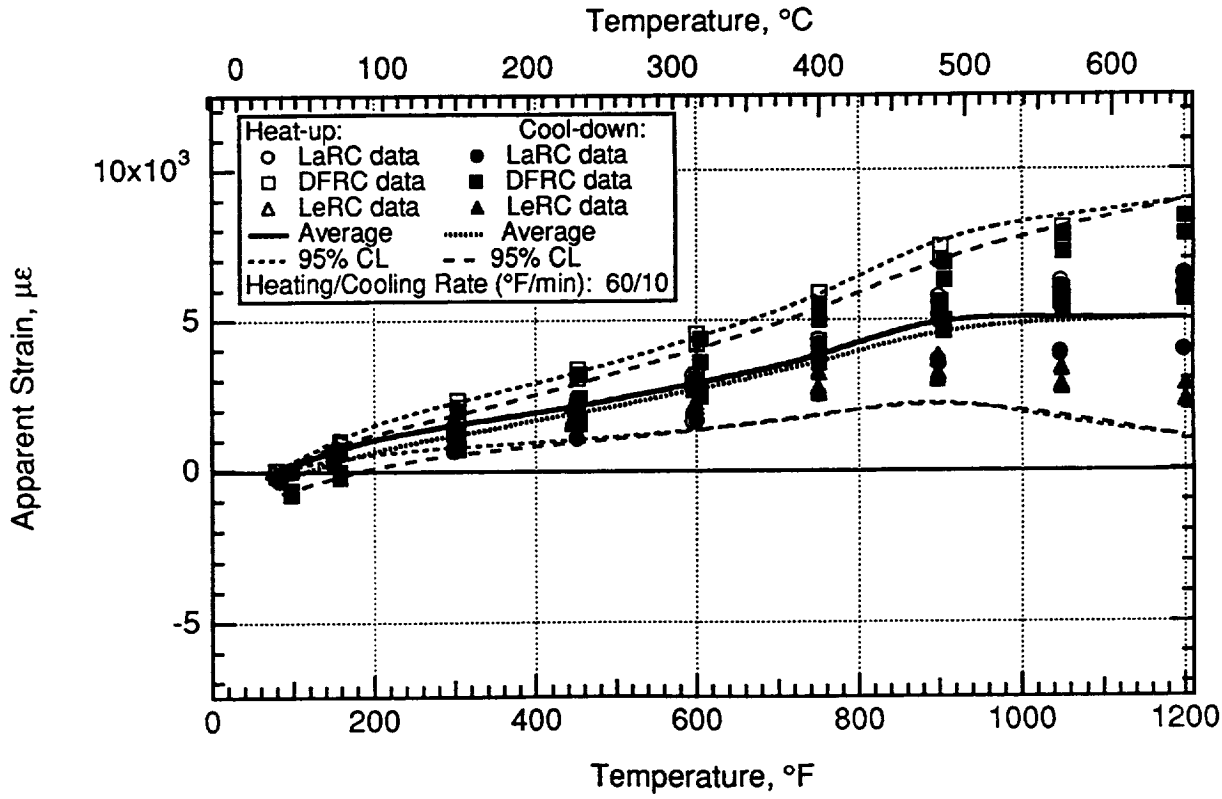

Figure 5.52.—PdCr gage cycle 4 apparent strain on β-21S TMC.

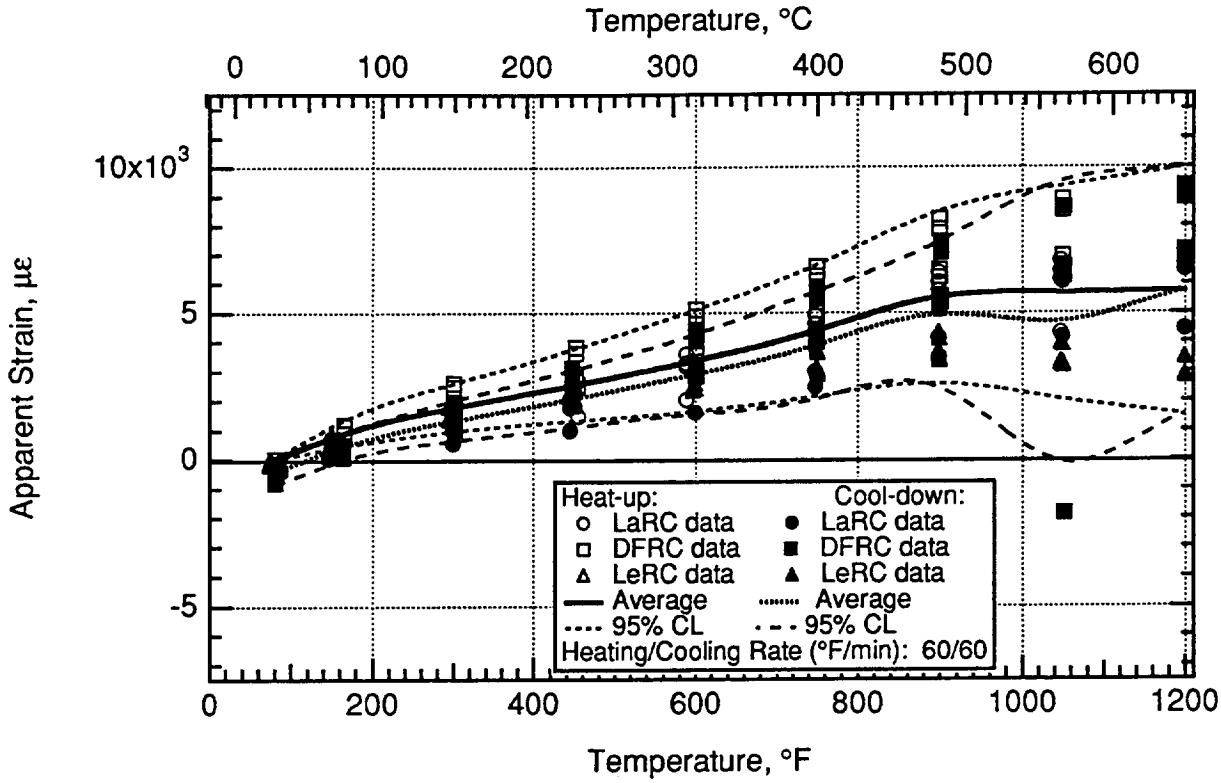

Figure 5.53.—PdCr gage cycle 5 apparent strain on β-21S TMC.

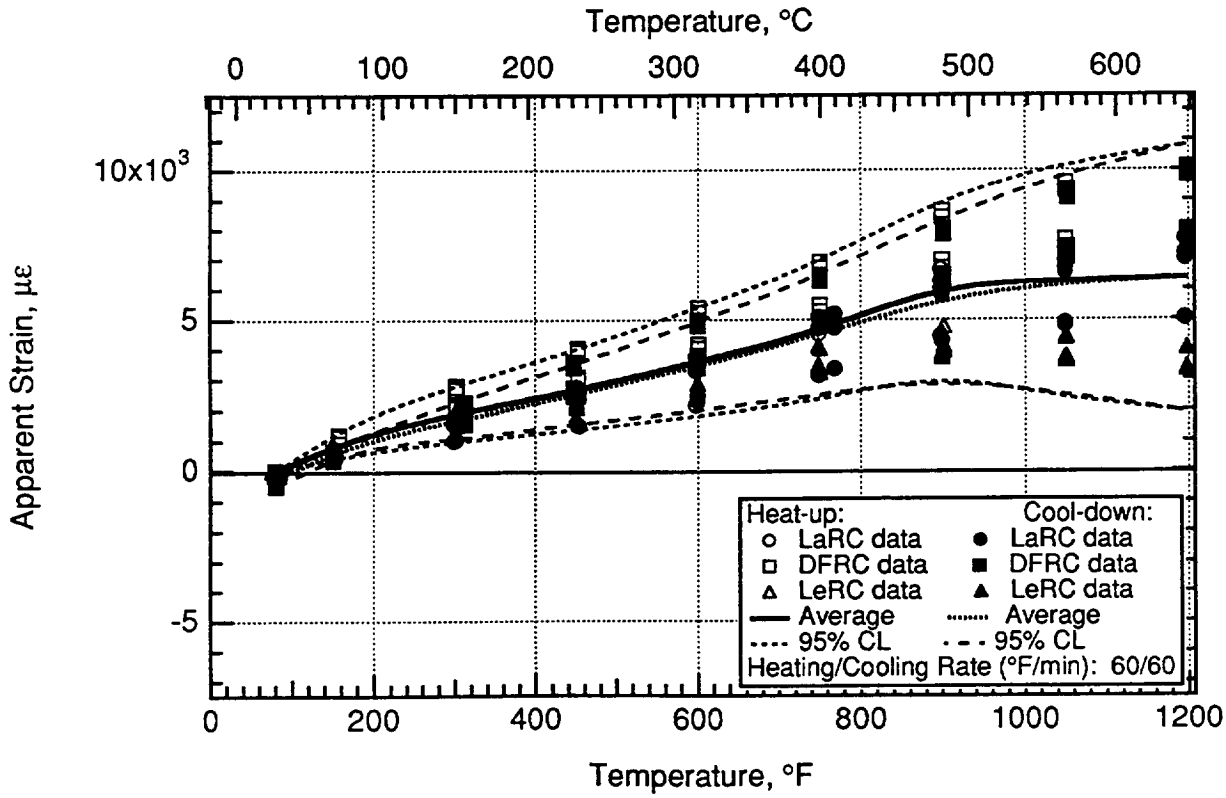

Figure 5.54.—PdCr gage cycle 6 apparent strain on β-21S TMC.

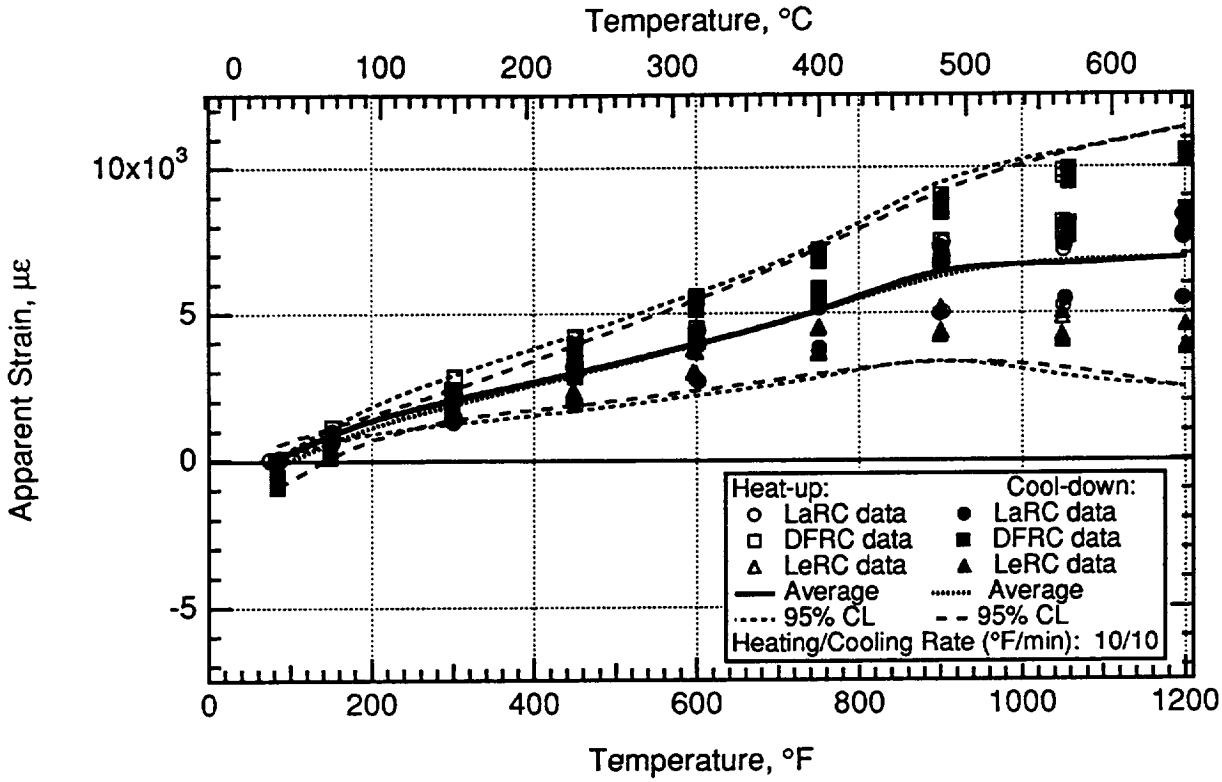

Figure 5.55.—PdCr gage cycle 7 apparent strain on β-21S TMC.

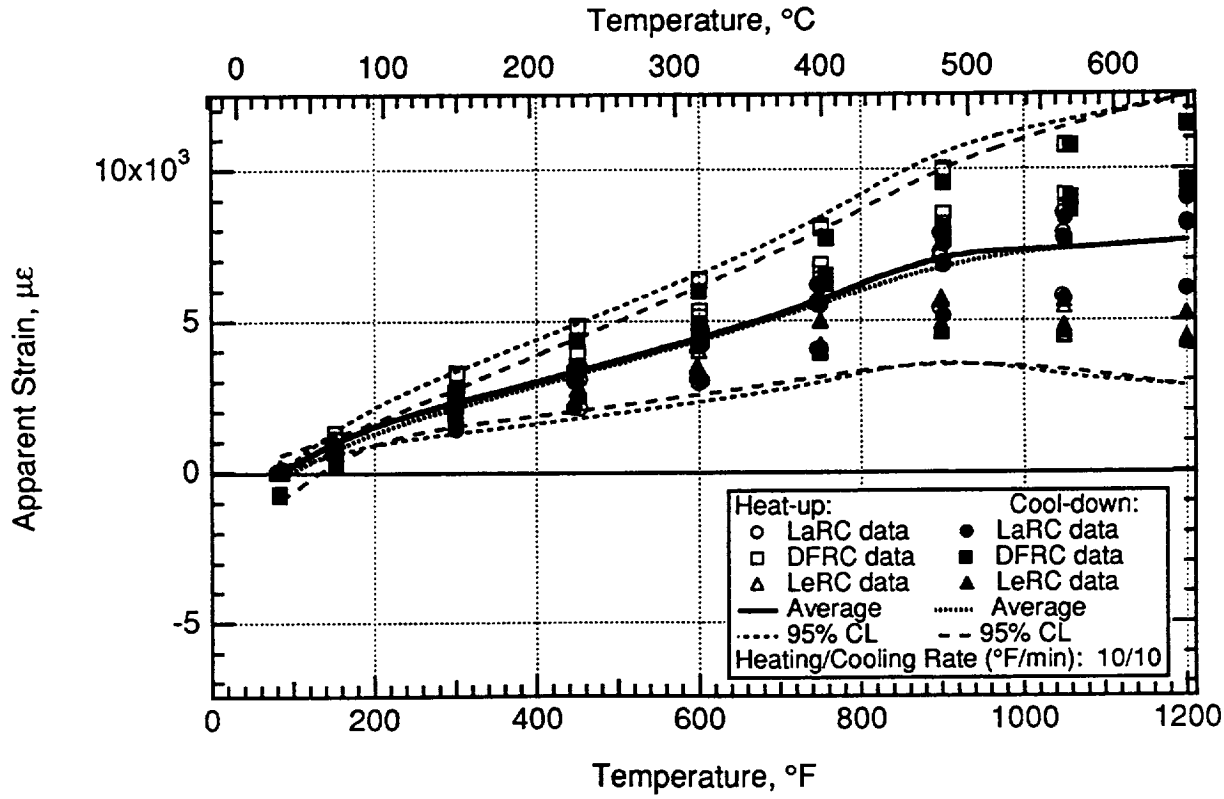

Figure 5.56.—PdCr gage cycle 8 apparent strain on β-21S TMC.

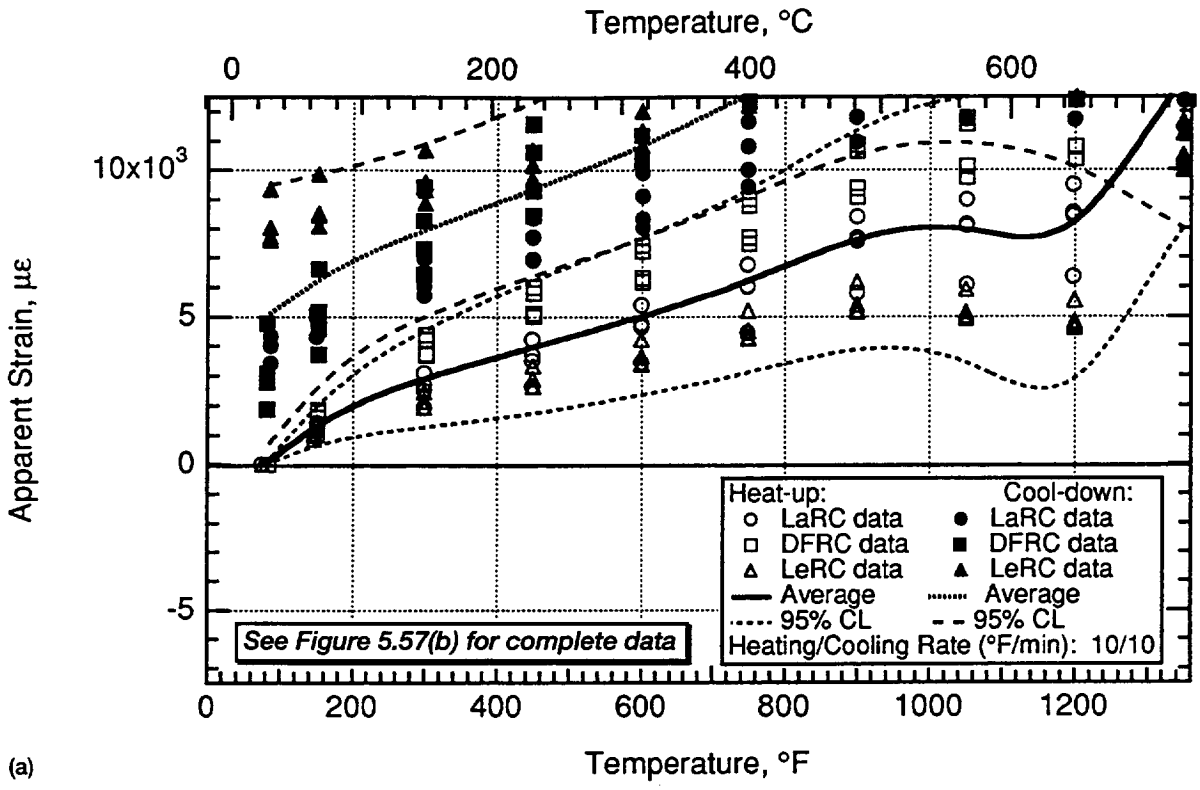

(a)

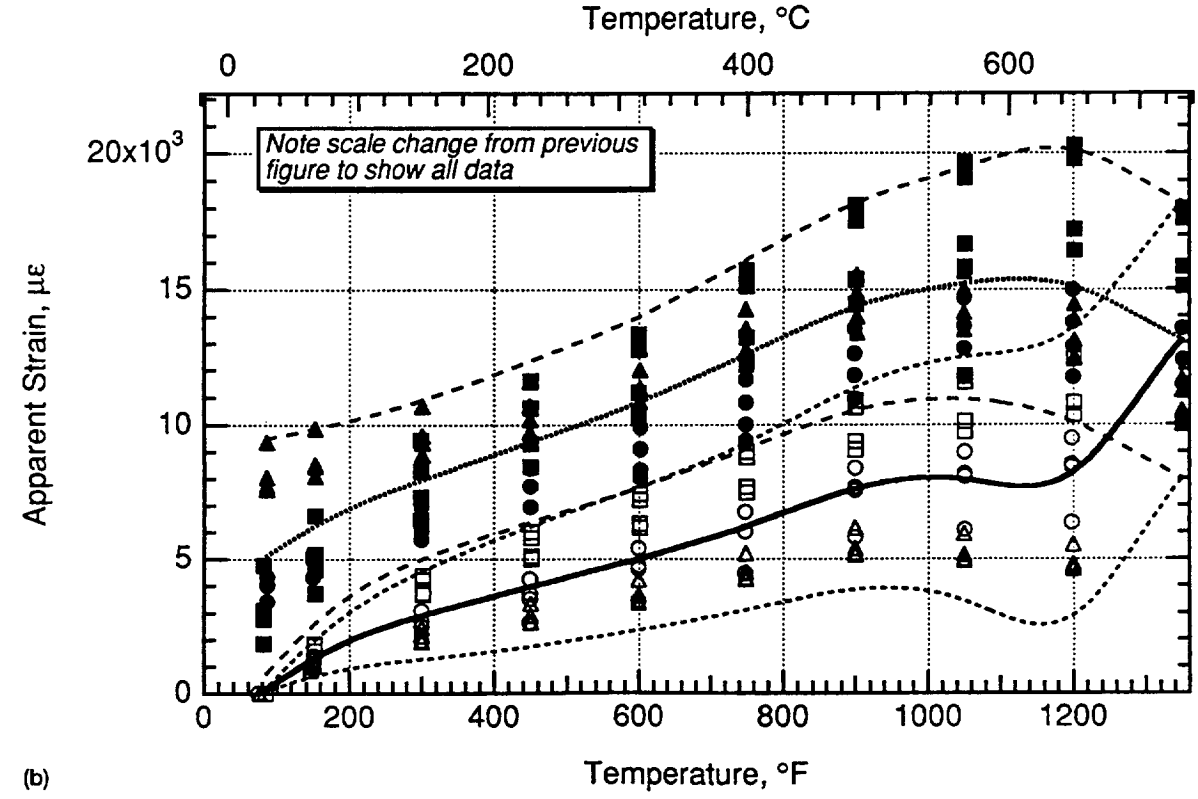

(b)

Figure 5.57.—PdCr gage cycle 9 apparent strain on β-21S TMC. (a) Partial data. (b) Complete data.

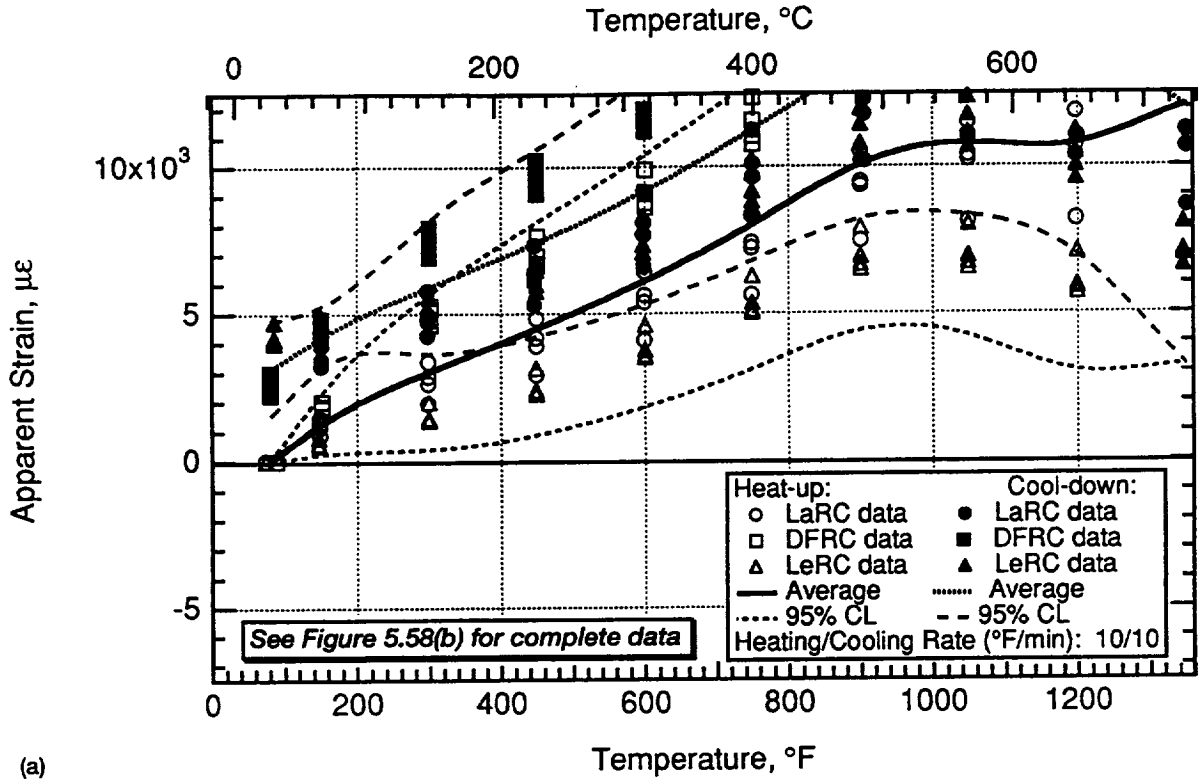

(a)

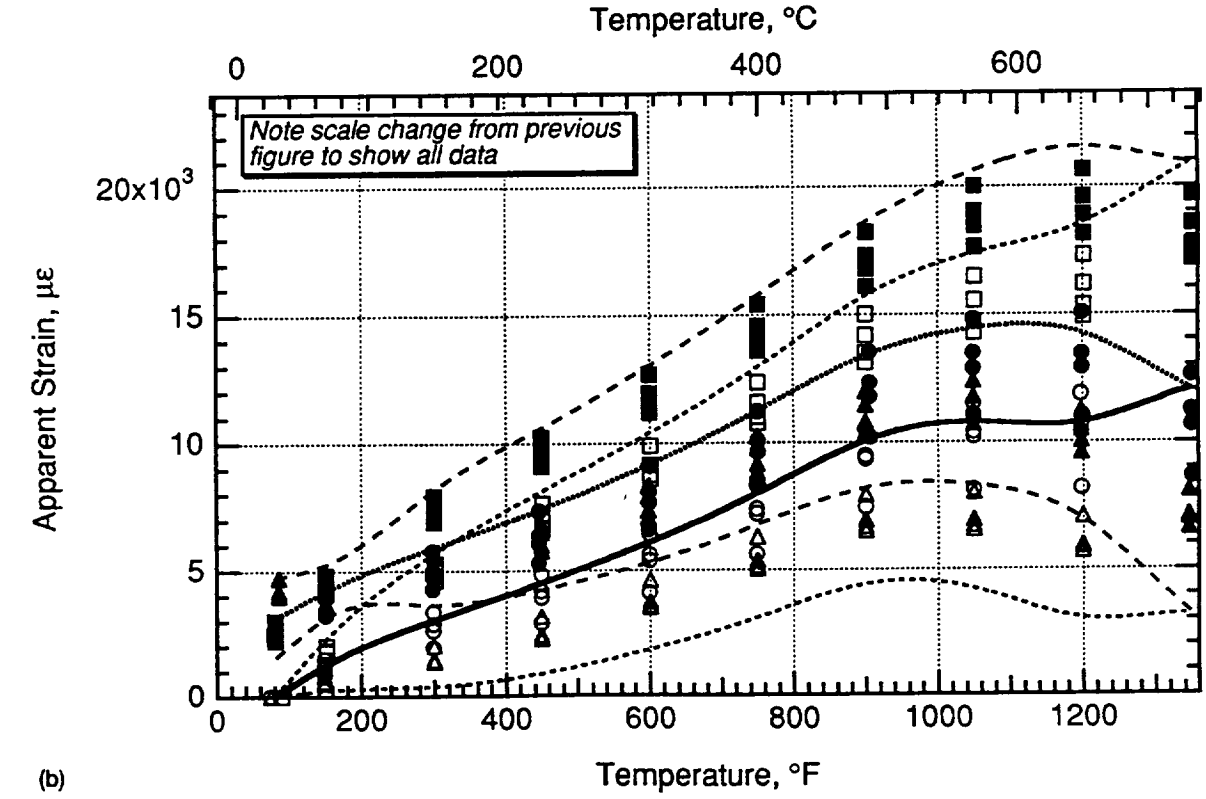

(b)

Figure 5.58.—PdCr gage cycle 10 apparent strain on β-21S TMC. (a) Partial data. (b) Complete data.

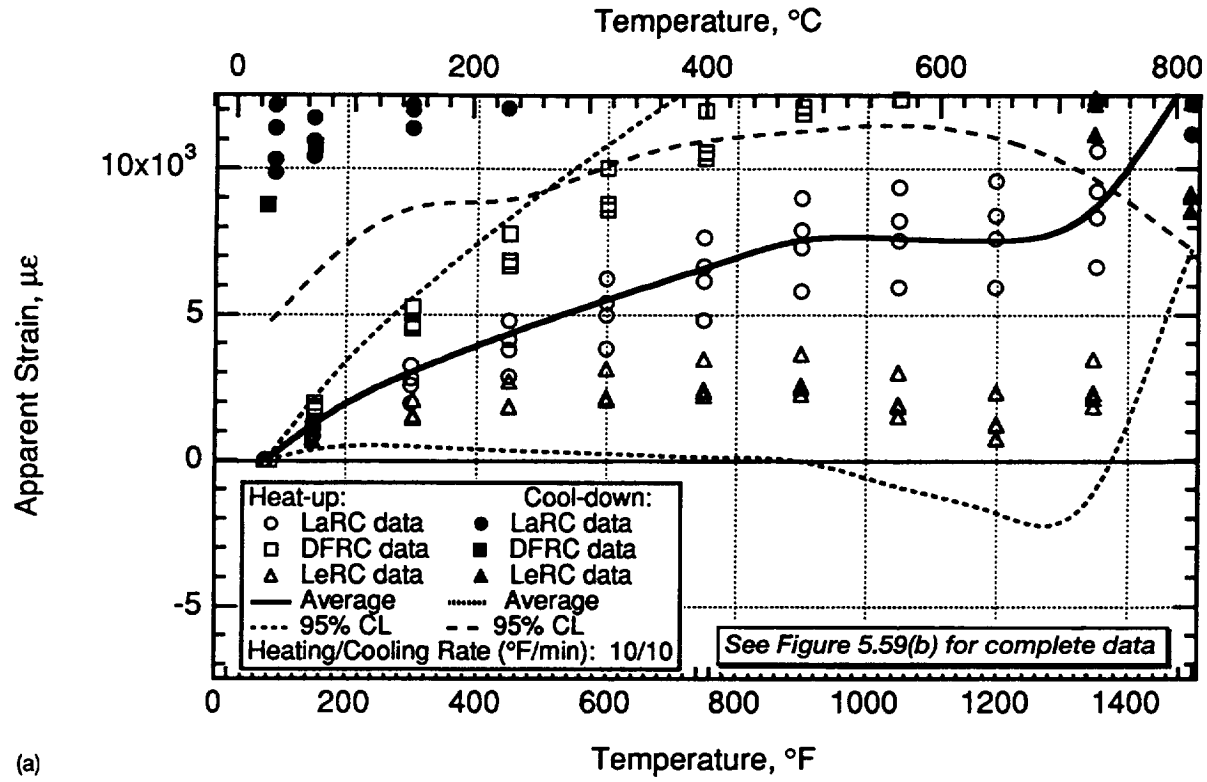

(a)

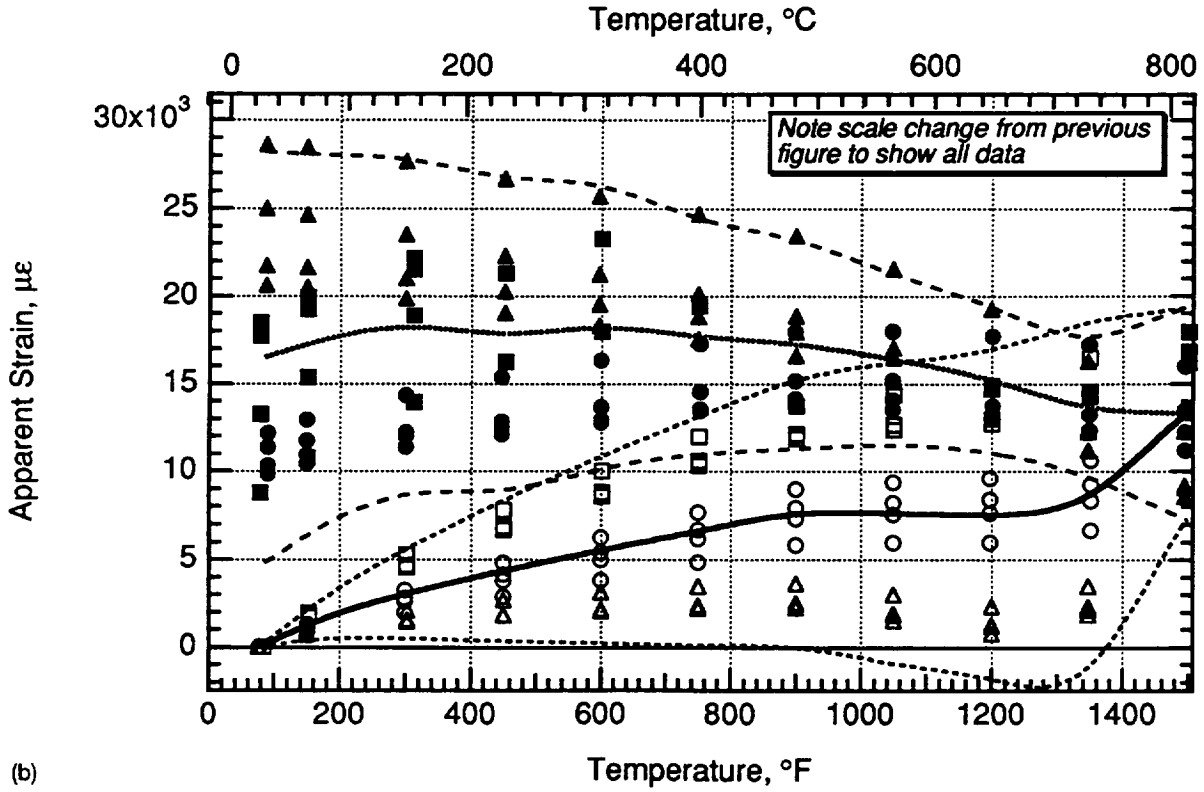

(b)

Figure 5.59.—PdCr gage cycle 11 apparent strain on β-21S TMC. (a) Partial data. (b) Complete data.

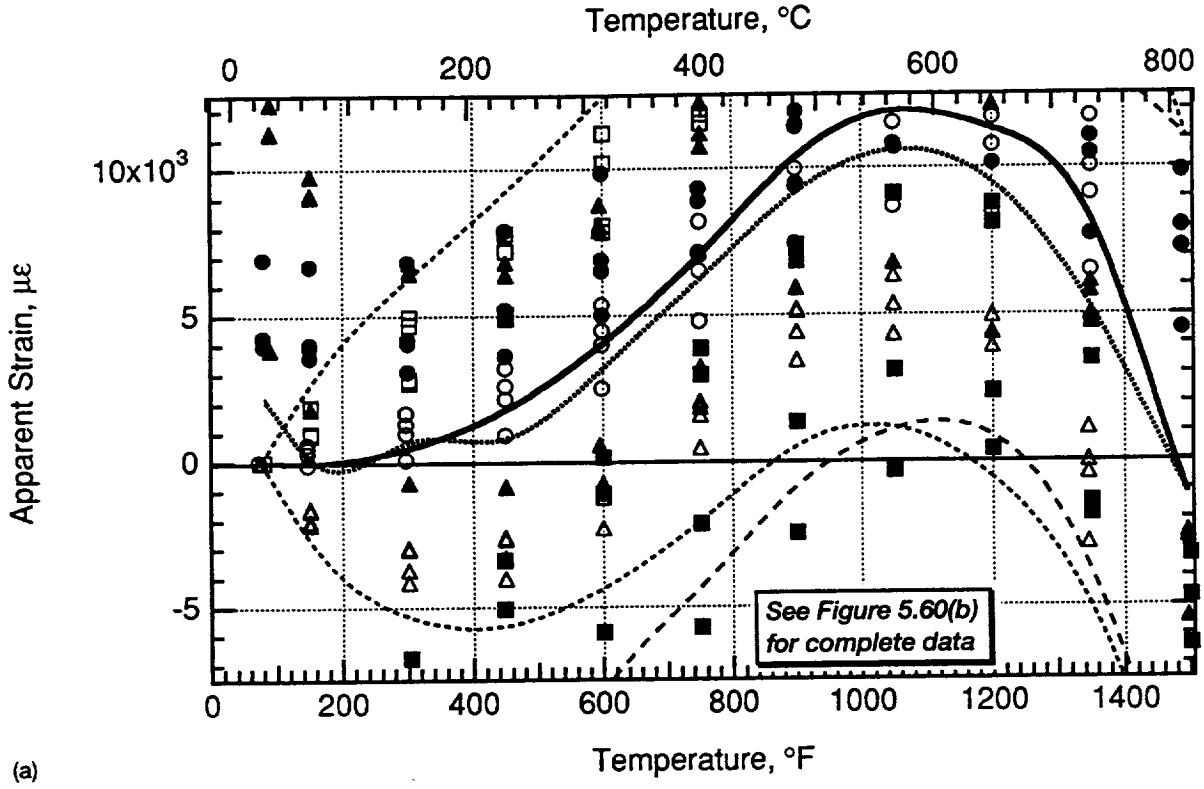

(a)

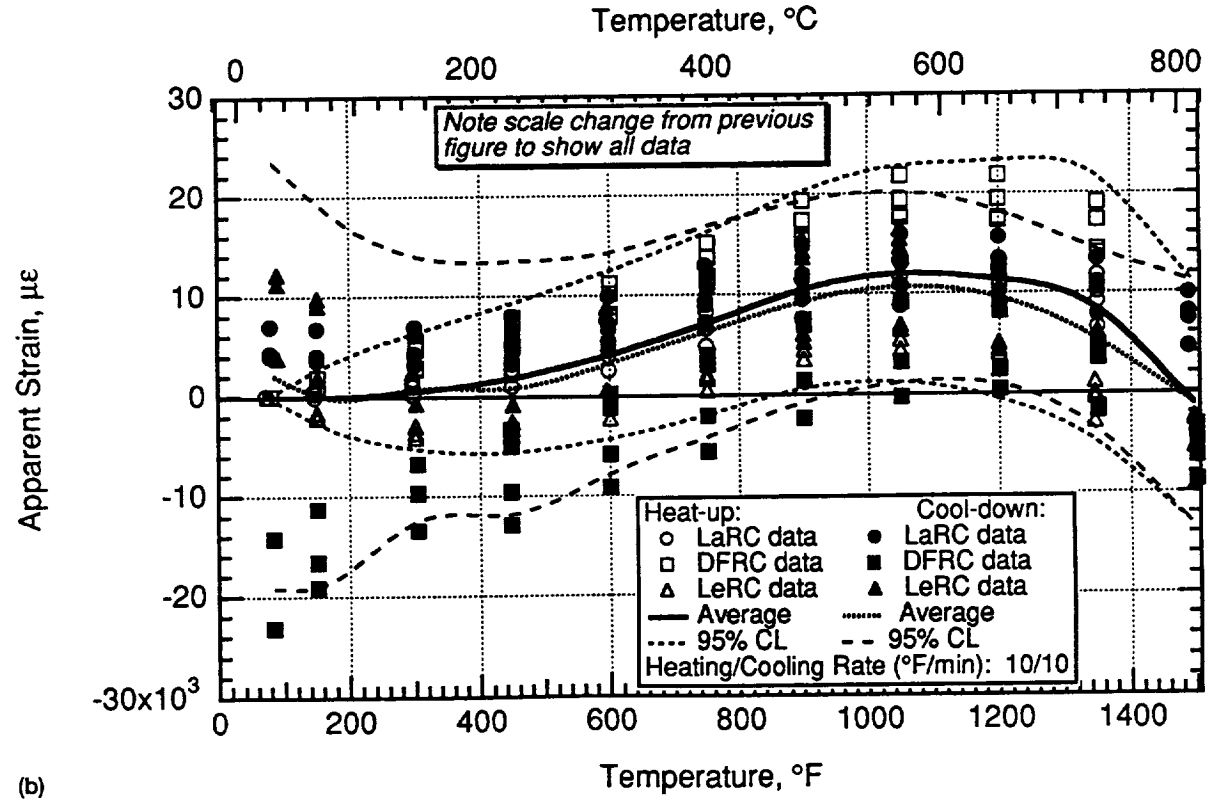

(b)

Figure 5.60.—PdCr gage cycle 12 apparent strain on β-21S TMC. (a) Partial data. (b) Complete data.

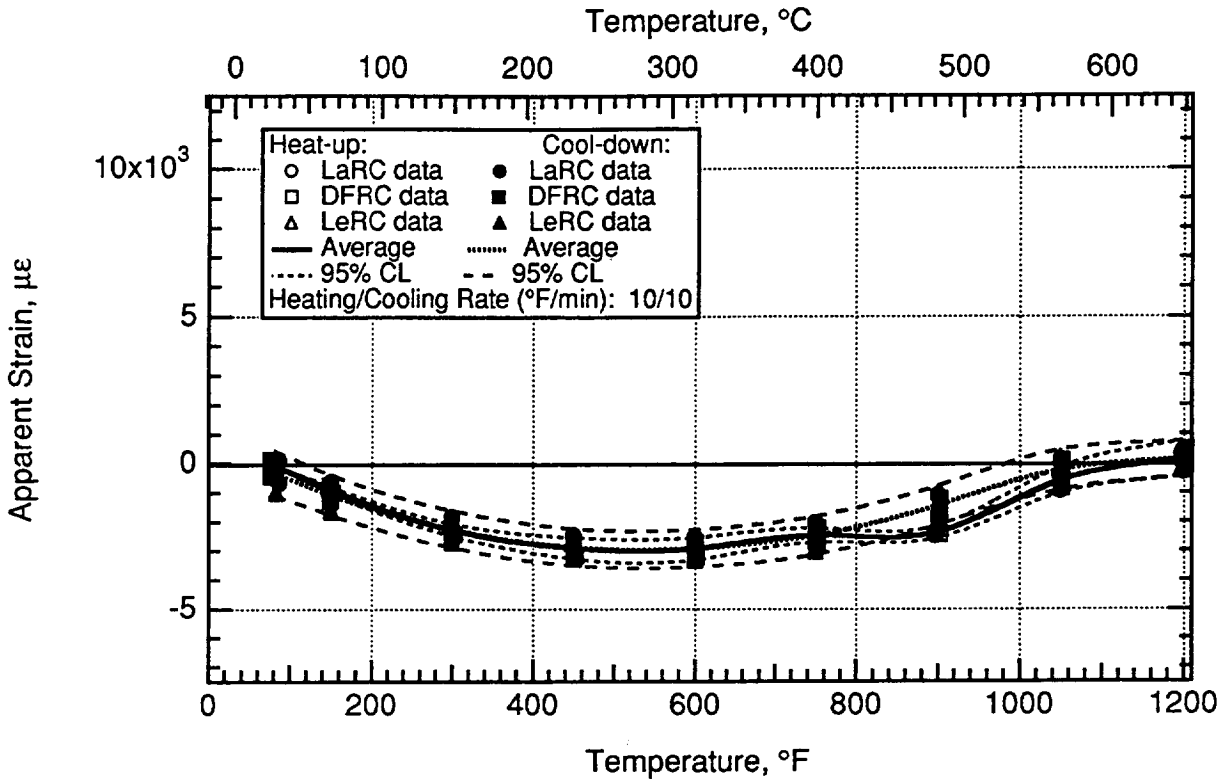

Figure 5.61.—DETCBCL gage cycle 1 apparent strain on β-21S TMC.

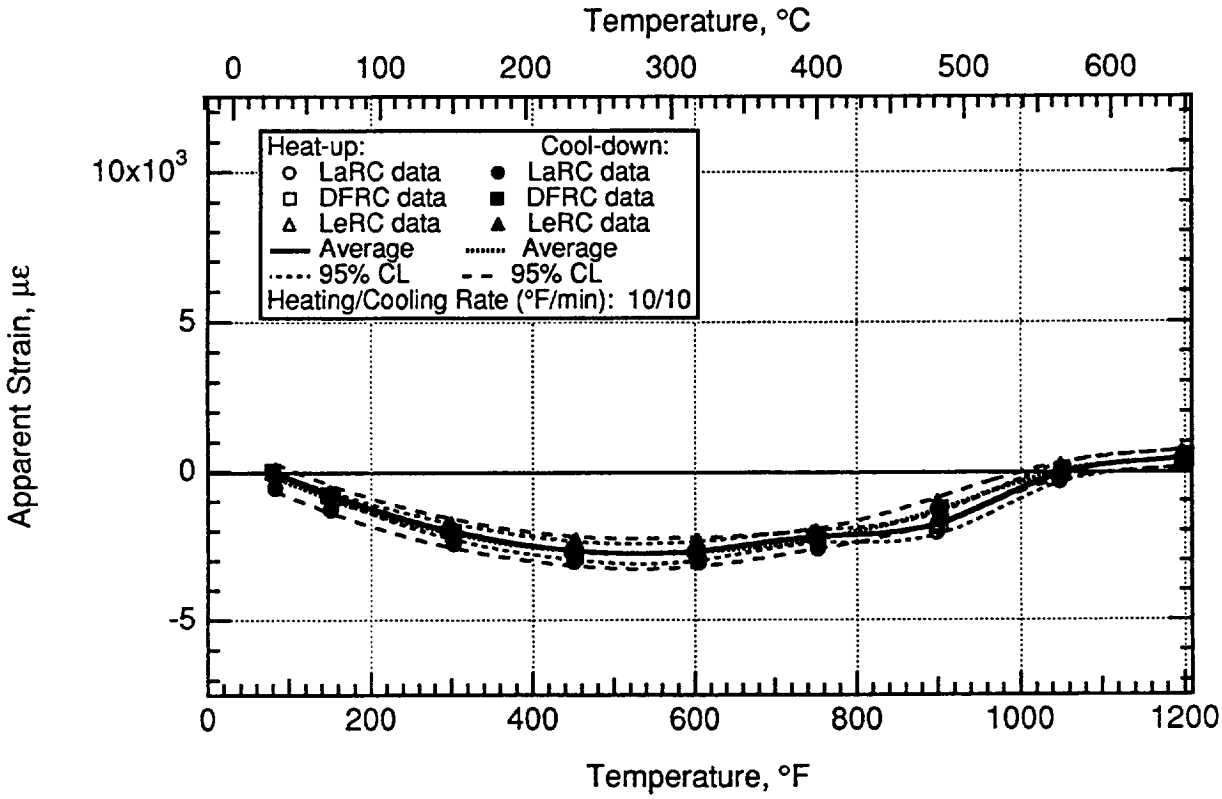

Figure 5.62.—DETCBCL gage cycle 2 apparent strain on β-21S TMC.

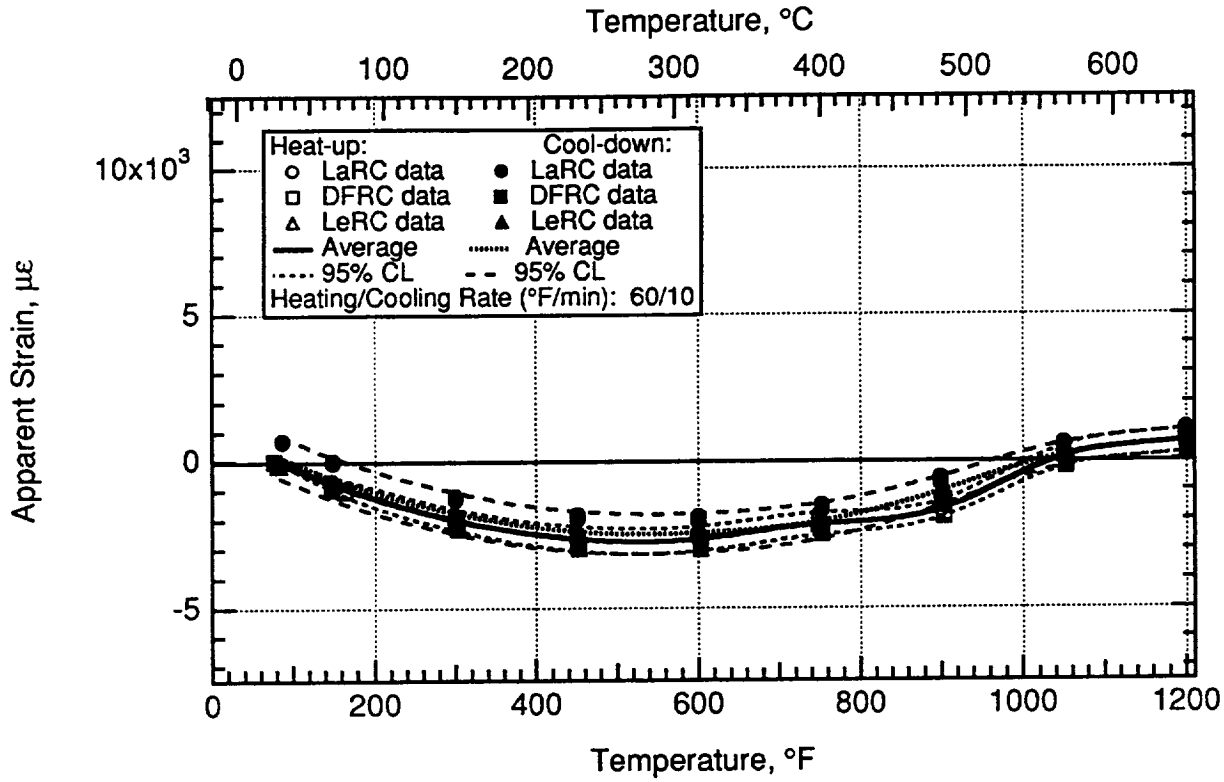

Figure 5.63.—DETCBCL gage cycle 3 apparent strain on β-21S TMC.

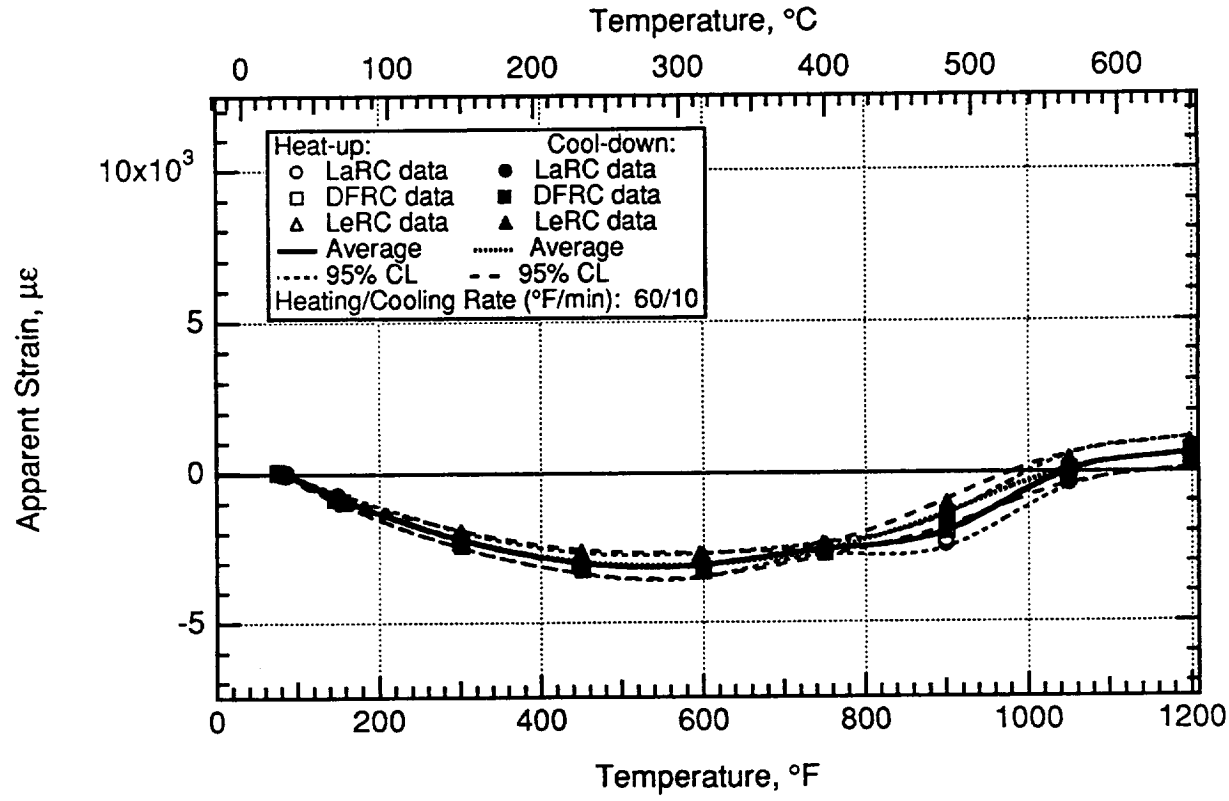

Figure 5.64.—DETCBCL gage cycle 4 apparent strain on β-21S TMC.

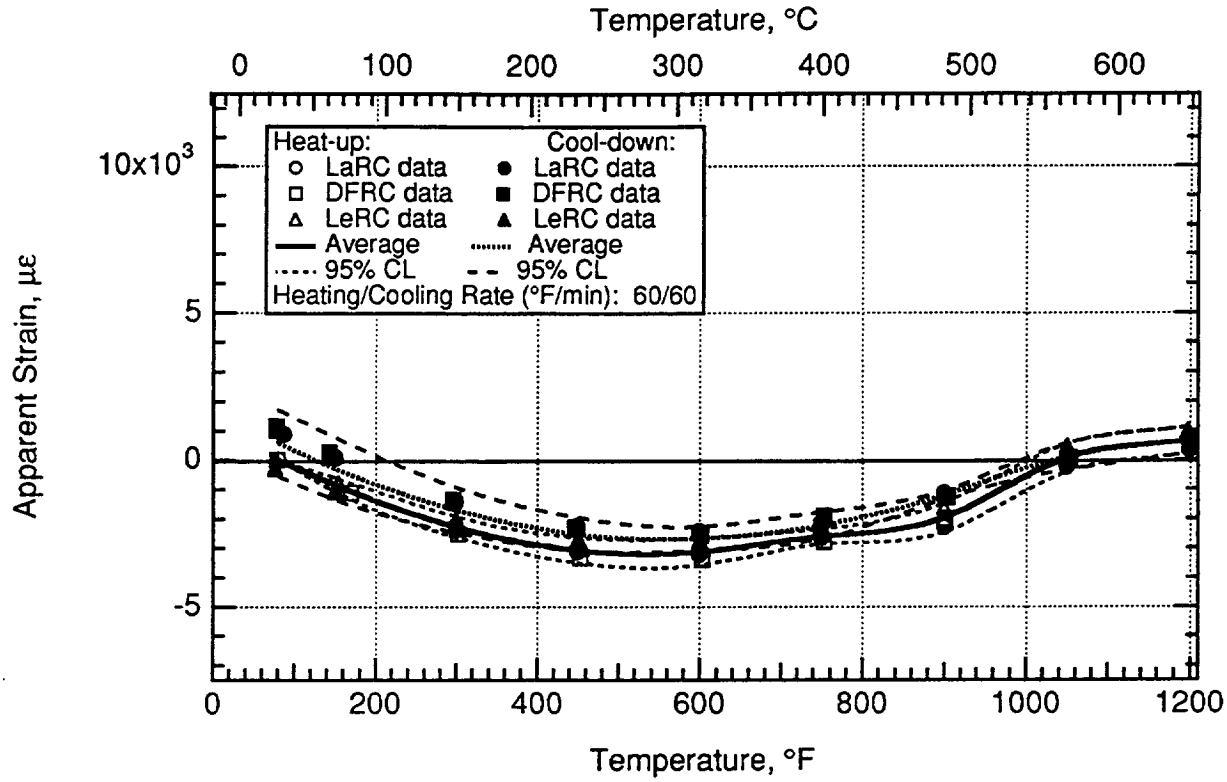

Figure 5.65.—DETCBCL gage cycle 5 apparent strain on β-21S TMC.

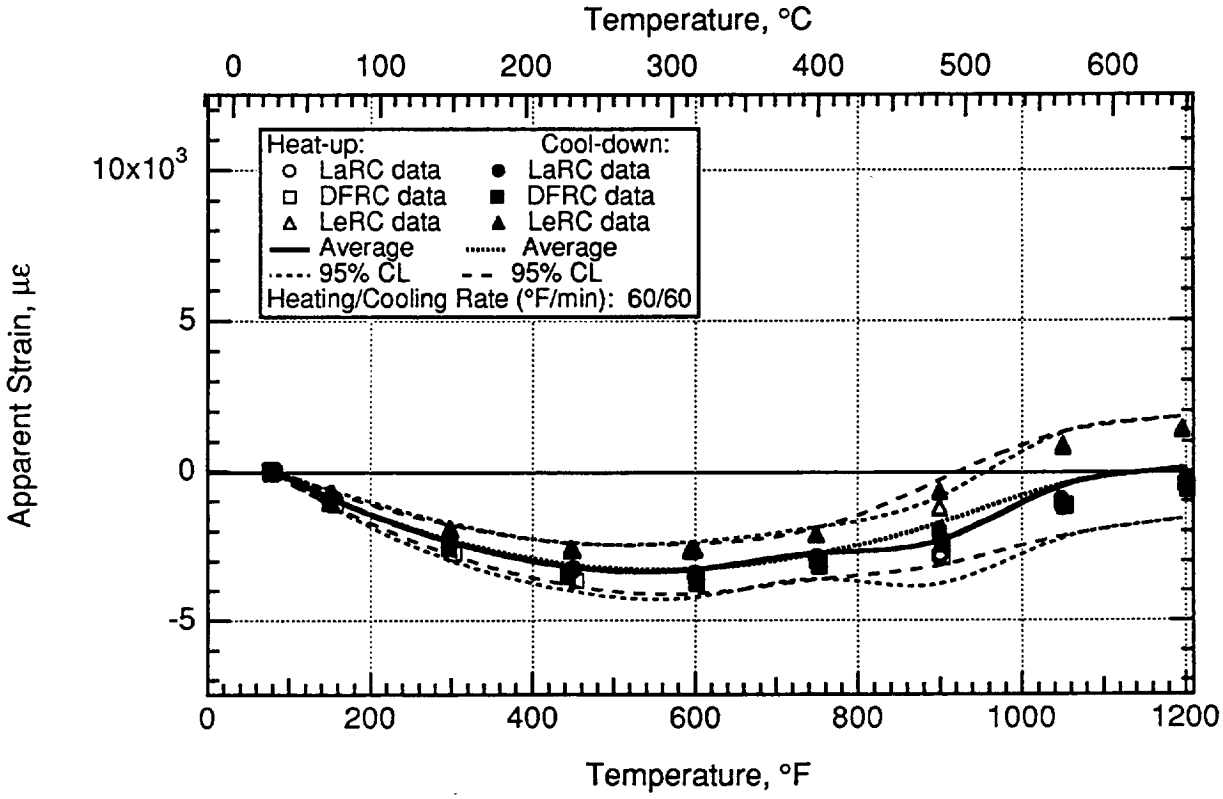

Figure 5.66.—DETCBCL gage cycle 6 apparent strain on β-21S TMC.

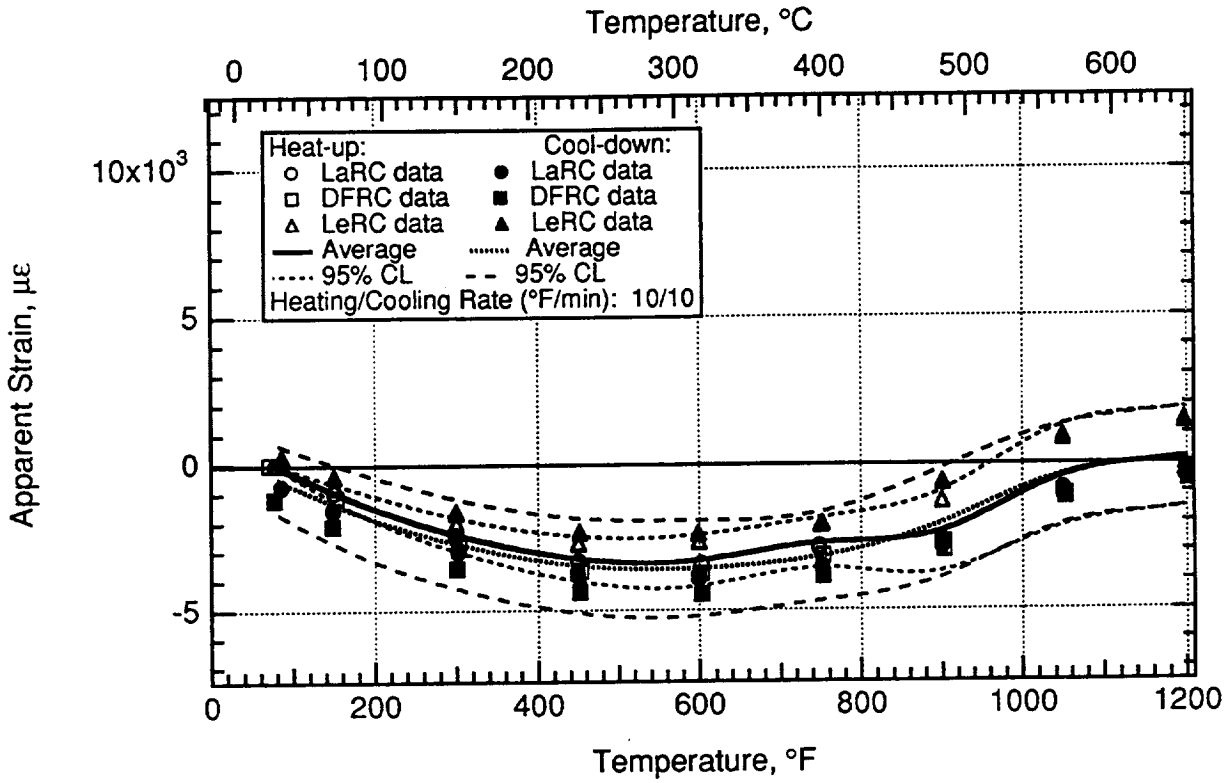

Figure 5.67.—DETCBCL gage cycle 7 apparent strain on β-21S TMC.

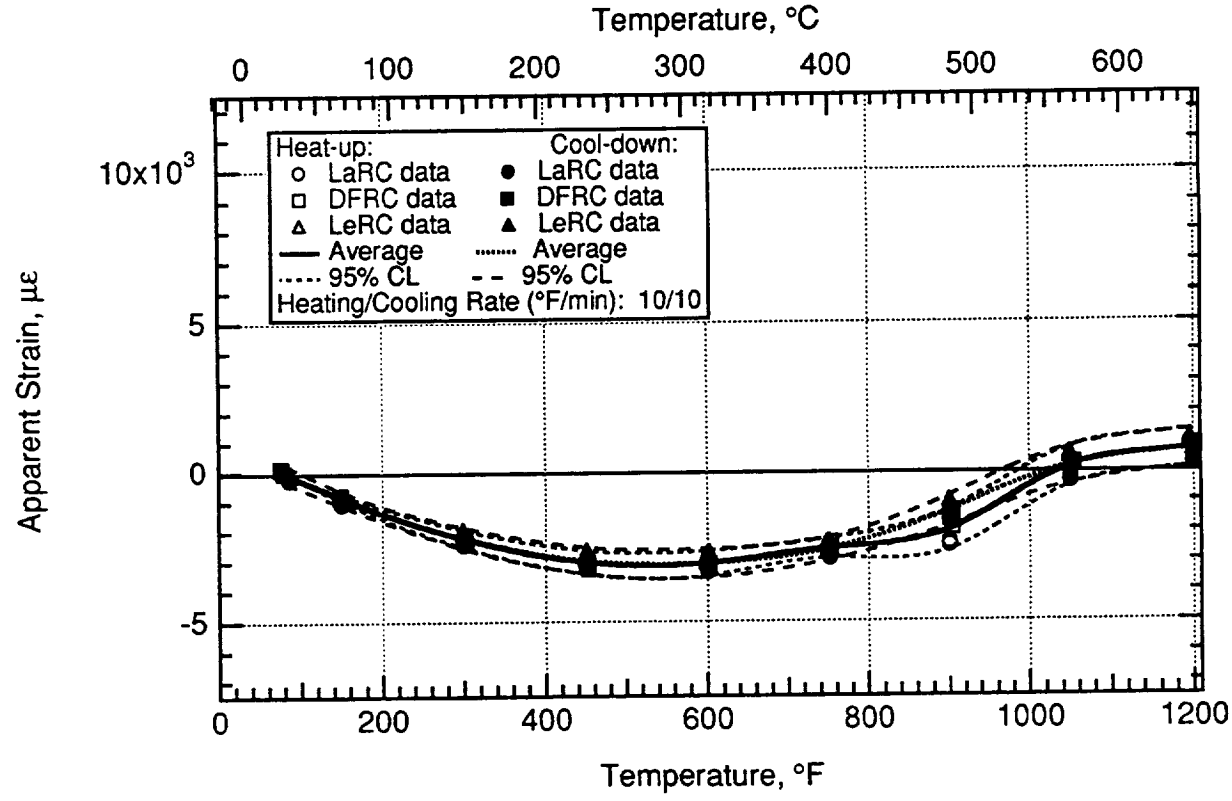

Figure 5.68.—DETCBCL gage cycle 8 apparent strain on β-21S TMC.

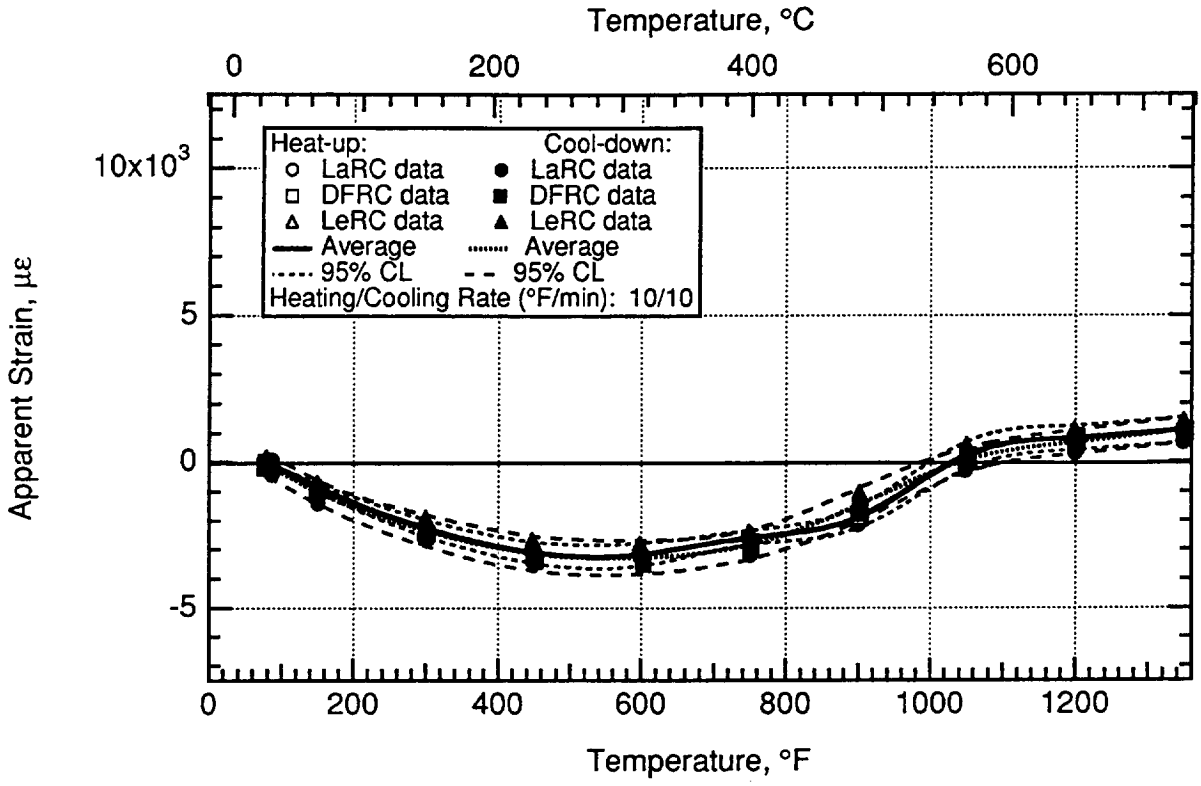

Figure 5.69.—DETCBCL gage cycle 9 apparent strain on β-21S TMC.

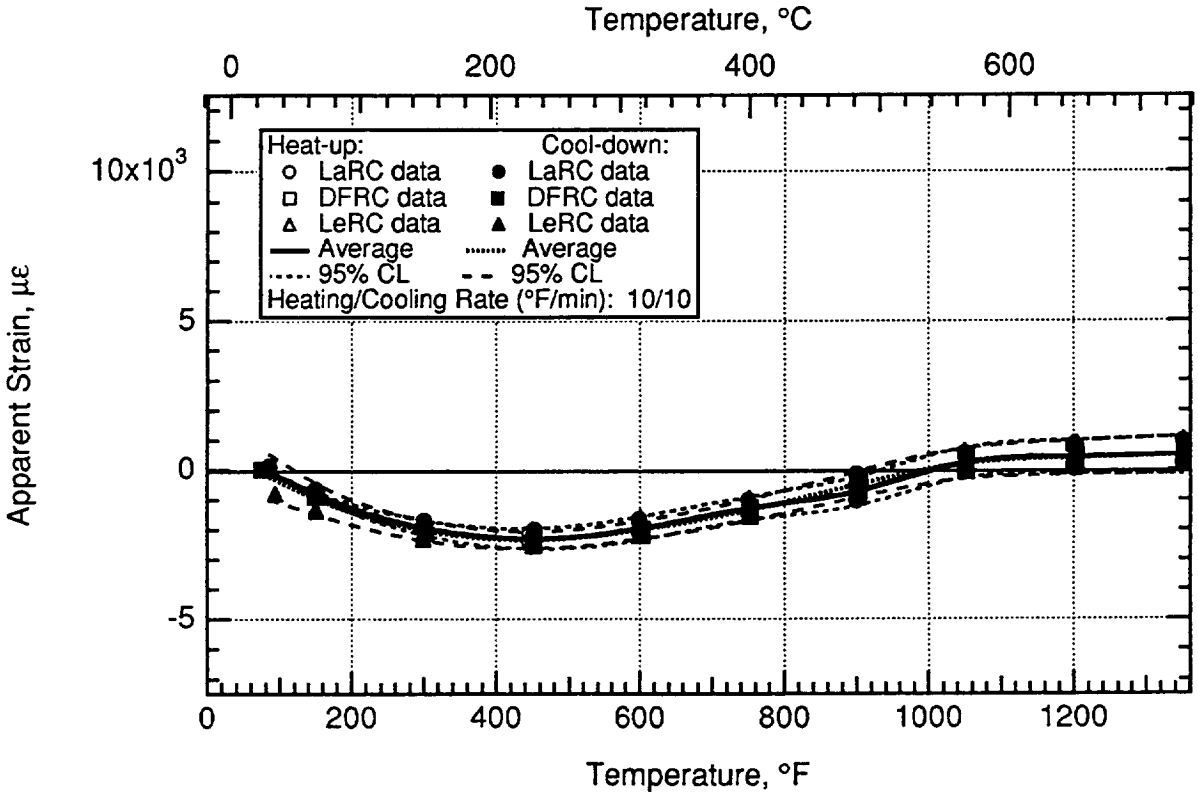

Figure 5.70.—DETCBCL gage cycle 10 apparent strain on β-21S TMC.

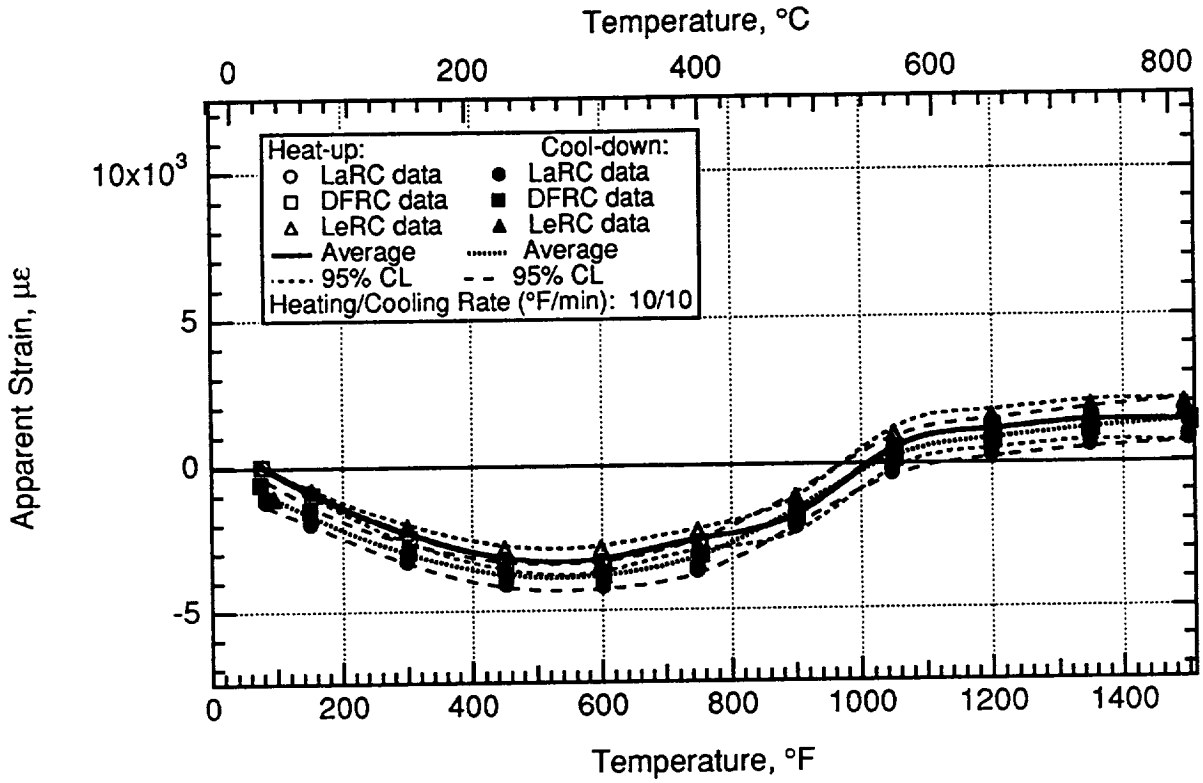

Figure 5.71.—DETCBCL gage cycle 11 apparent strain on β-21S TMC.

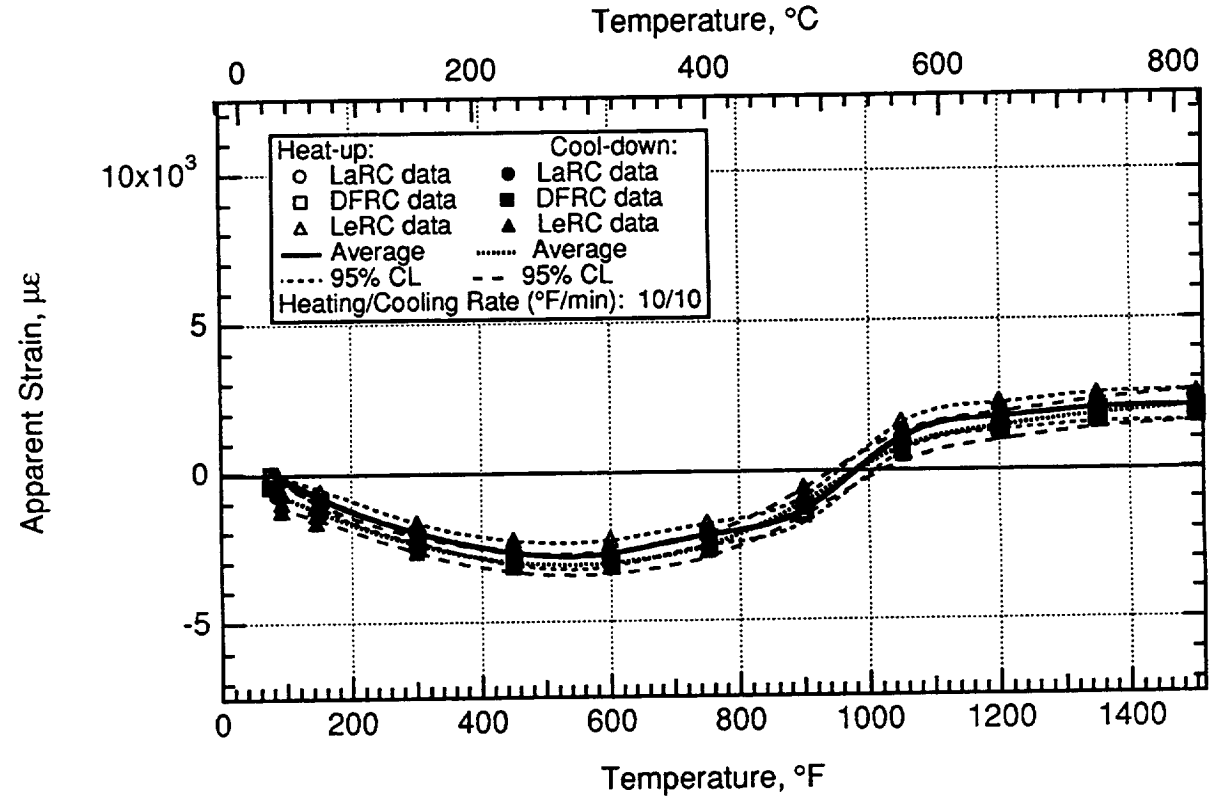

Figure 5.72.—DETCBCL gage cycle 12 apparent strain on β-21S TMC.

5.2 Drift Strain Data

The following pages contain the composite drift strain data acquired on IN100 with the CKA1 gage, the PdCr gage, and the DETCBCL gage (figs. 5.73 to 5.93). This same sequence is then repeated for the TMC material (figs. 5.94 to 5.114). Each gage/material combination was tested at 600, 750, 900, 1050, 1200, 1350, and 1500 °F (315, 400, 480, 565, 650, 730, and 815 °C). Each curve shows the results from 12 gages complete with an average drift strain and the upper and lower 95% confidence limits for that gage, material, and temperature combination. A list of the drift strain figures is given in table 5.14.

TABLE 5.14—FIGURES FOR DRIFT STRAIN

Figure	Gage type	Substrate material	Maximum temperature	
			°F	°C
5.73	CKA1	IN100	600	315
5.74	CKA1	IN100	750	400
5.75	CKA1	IN100	900	480
5.76	CKA1	IN100	1050	565
5.77	CKA1	IN100	1200	650
5.78	CKA1	IN100	1350	730
5.79	CKA1	IN100	1500	815
5.80	PdCr	IN100	600	315
5.81	PdCr	IN100	750	400
5.82	PdCr	IN100	900	480
5.83	PdCr	IN100	1050	565
5.84	PdCr	IN100	1200	650
5.85	PdCr	IN100	1350	730
5.86	PdCr	IN100	1500	815
5.87	DETCBCL	IN100	600	315
5.88	DETCBCL	IN100	750	400
5.89	DETCBCL	IN100	900	480
5.90	DETCBCL	IN100	1050	565
5.91	DETCBCL	IN100	1200	650
5.92	DETCBCL	IN100	1350	730
5.93	DETCBCL	IN100	1500	815
5.94	CKA1	TMC	600	315
5.95	CKA1	TMC	750	400
5.96	CKA1	TMC	900	480
5.97	CKA1	TMC	1050	565
5.98	CKA1	TMC	1200	650
5.99	CKA1	TMC	1350	730
5.100	CKA1	TMC	1500	815
5.101	PdCr	TMC	600	315
5.102	PdCr	TMC	750	400
5.103	PdCr	TMC	900	480
5.104	PdCr	TMC	1050	565
5.105	PdCr	TMC	1200	650
5.106	PdCr	TMC	1350	730
5.107	PdCr	TMC	1500	815
5.108	DETCBCL	TMC	600	315
5.109	DETCBCL	TMC	750	400
5.110	DETCBCL	TMC	900	480
5.111	DETCBCL	TMC	1050	565
5.112	DETCBCL	TMC	1200	650
5.113	DETCBCL	TMC	1350	730
5.114	DETCBCL	TMC	1500	815

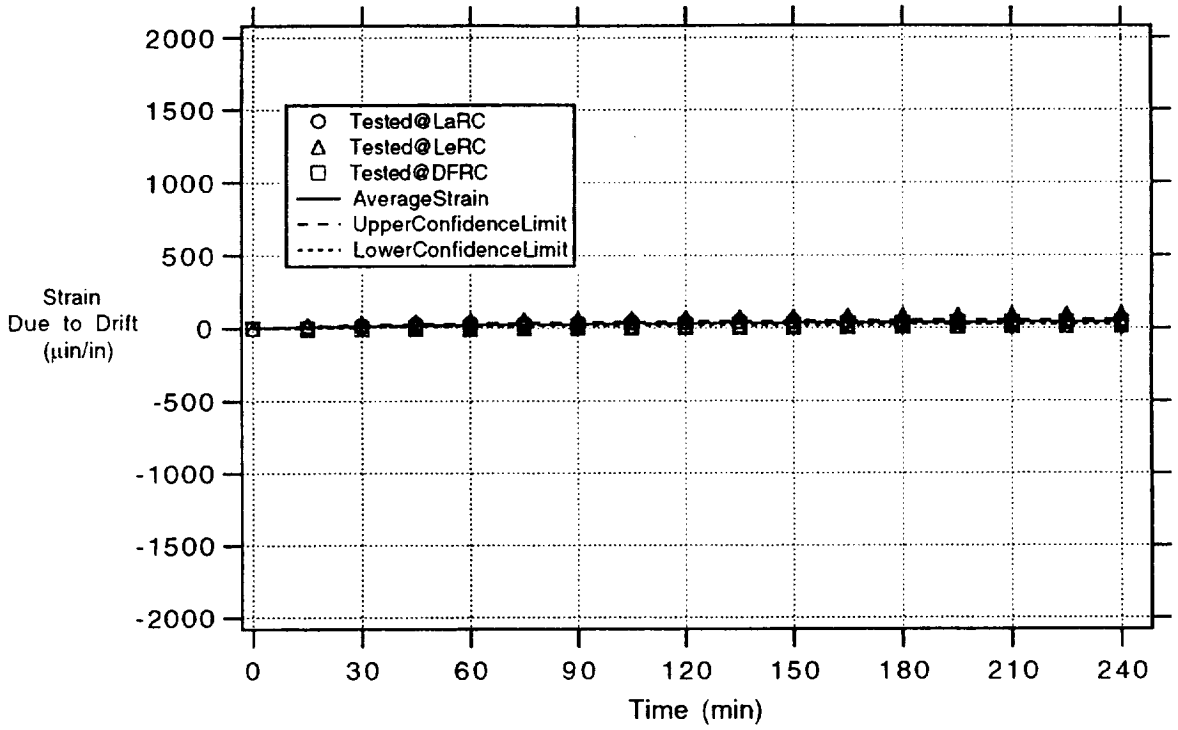

Figure 5.73.—Twelve CKA1 gages on IN100—cycle 1 (600 °F; 315 °C).

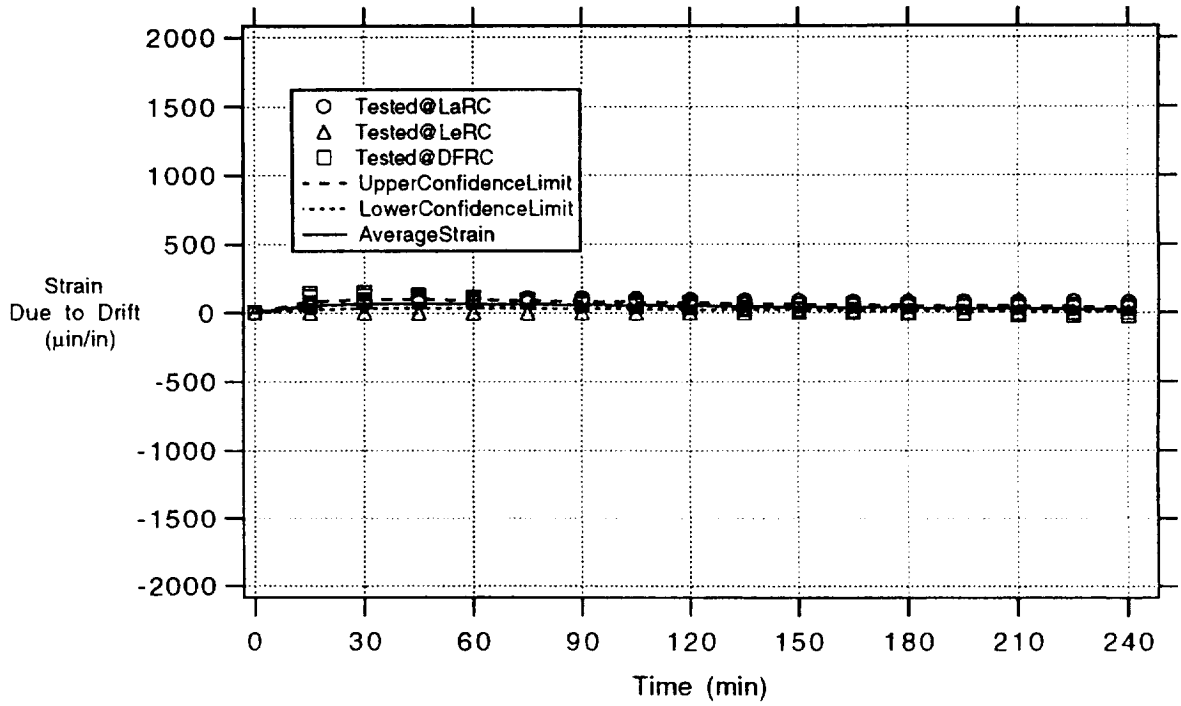

Figure 5.74.—Twelve CKA1 gages on IN100—cycle 2 (750 °F; 398 °C).

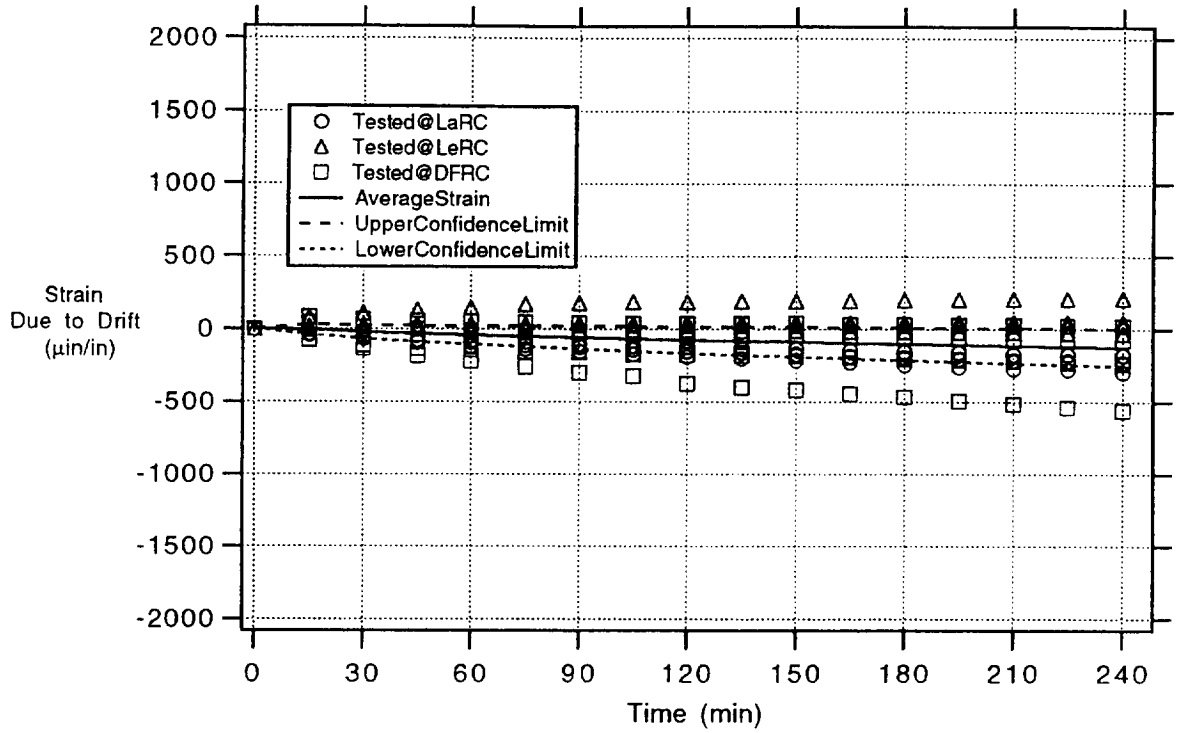

Figure 5.75.—Twelve CKA1 gages on IN100—cycle 3 (900 °F; 482 °C).

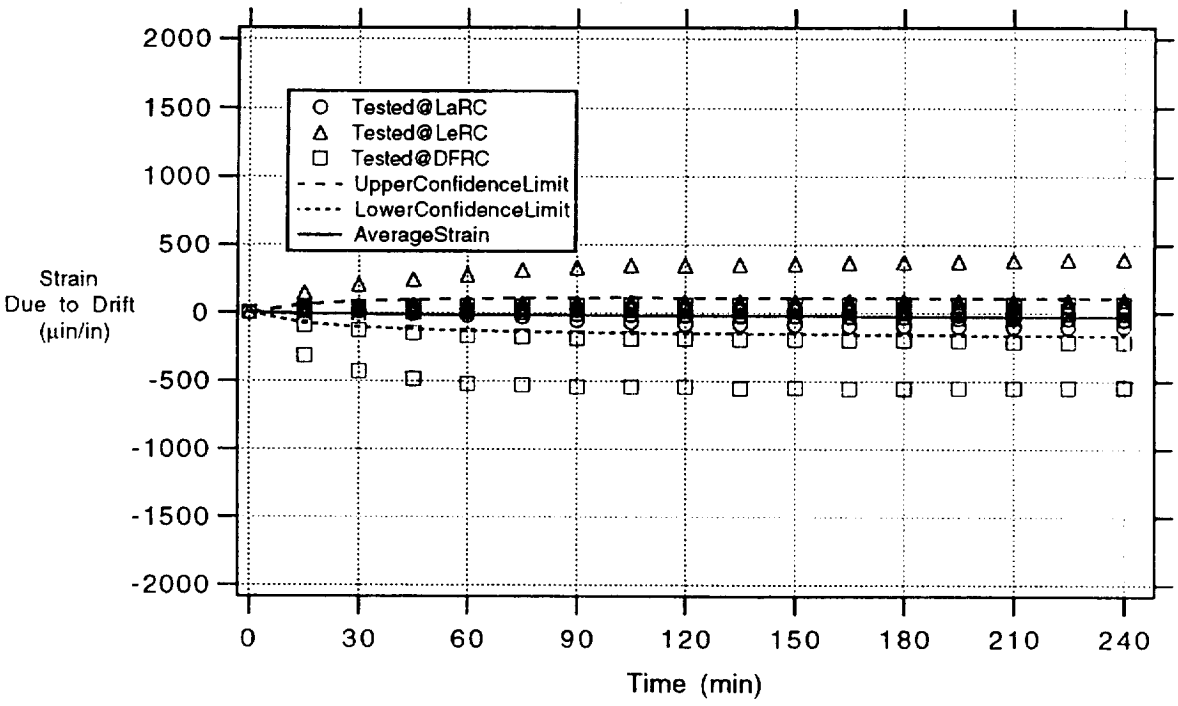

Figure 5.76.—Twelve CKA1 gages on IN100—cycle 4 (1050 °F; 565 °C).

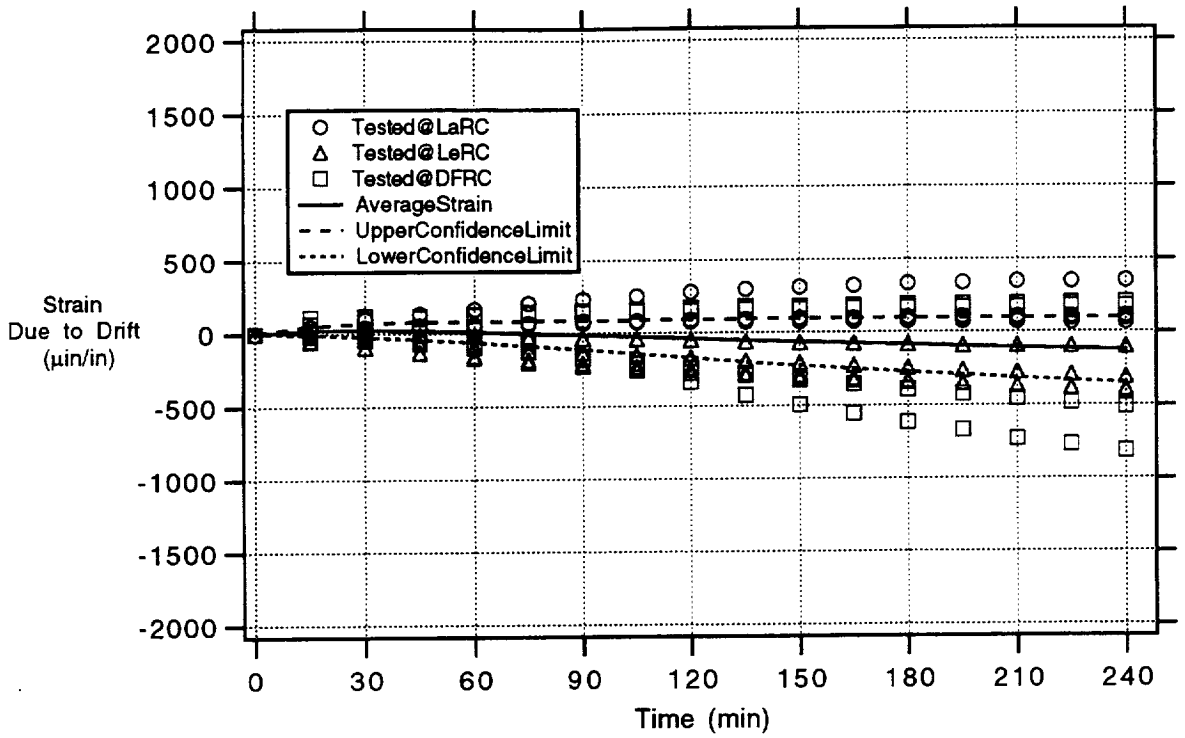

Figure 5.77.—Twelve CKA1 gages on IN100—cycle 5 (1200 °F; 648 °C).

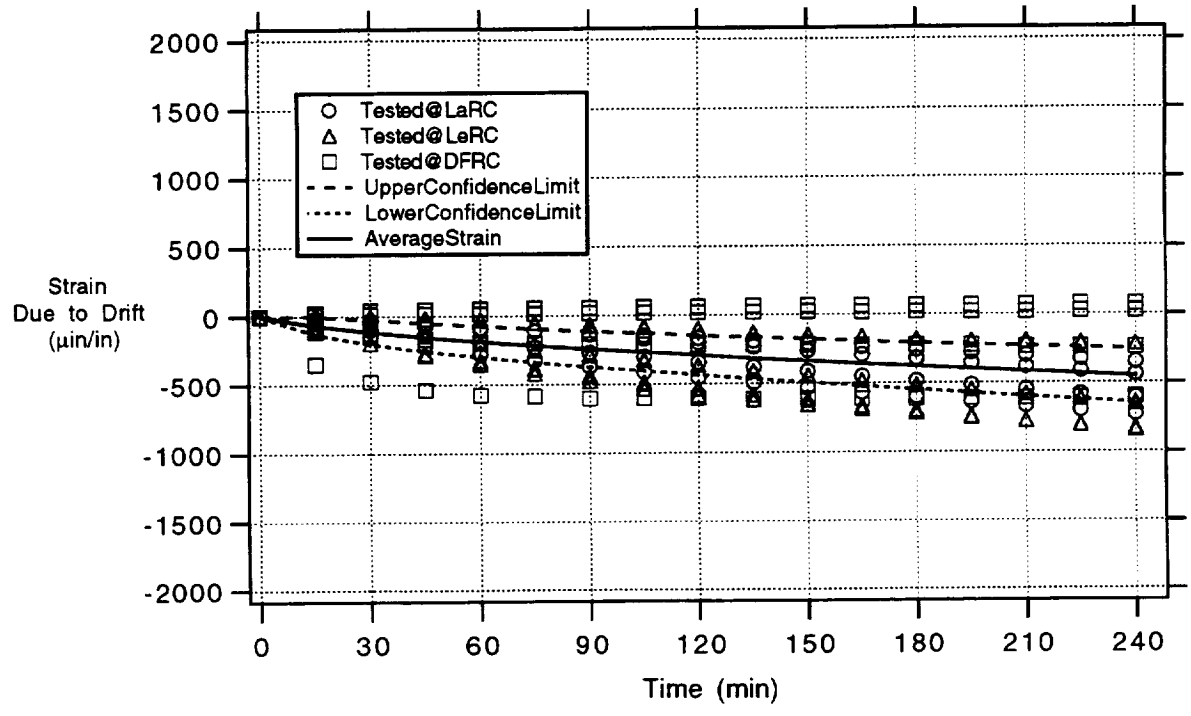

Figure 5.78.—Twelve CKA1 gages on IN100—cycle 6 (1350 °F; 732 °C).

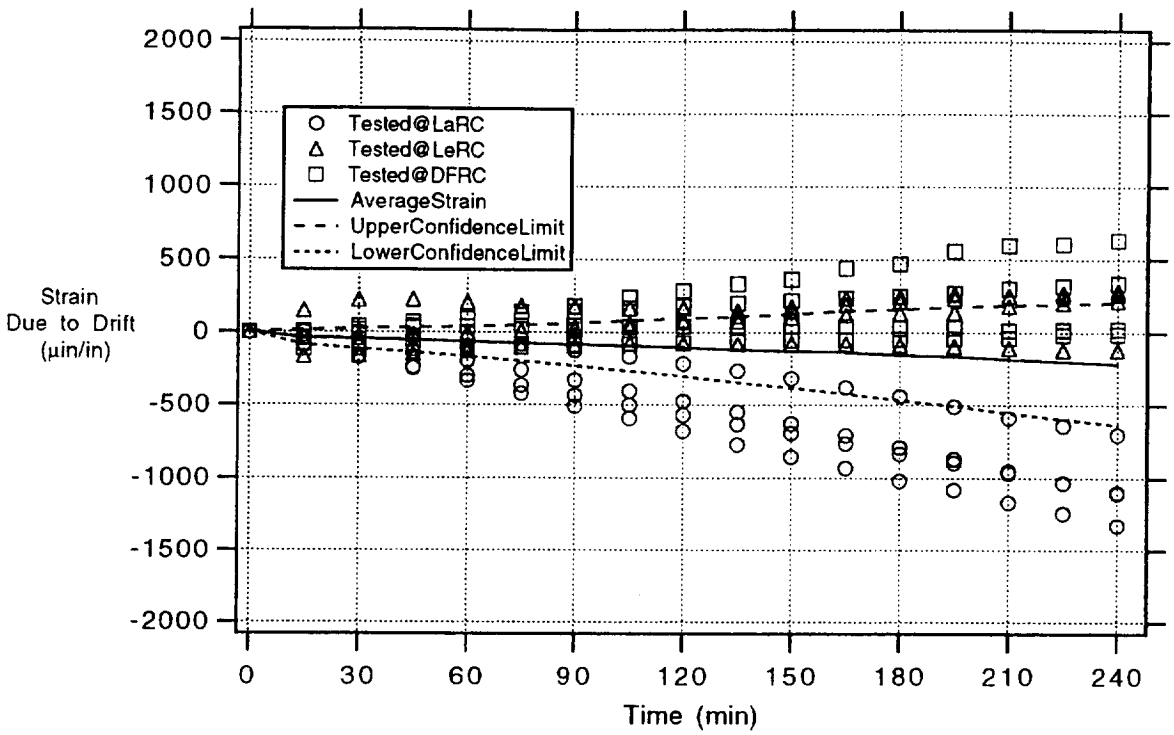

Figure 5.79.—Twelve CKA1 gages on IN100—cycle 7 (1500 °F; 816 °C).

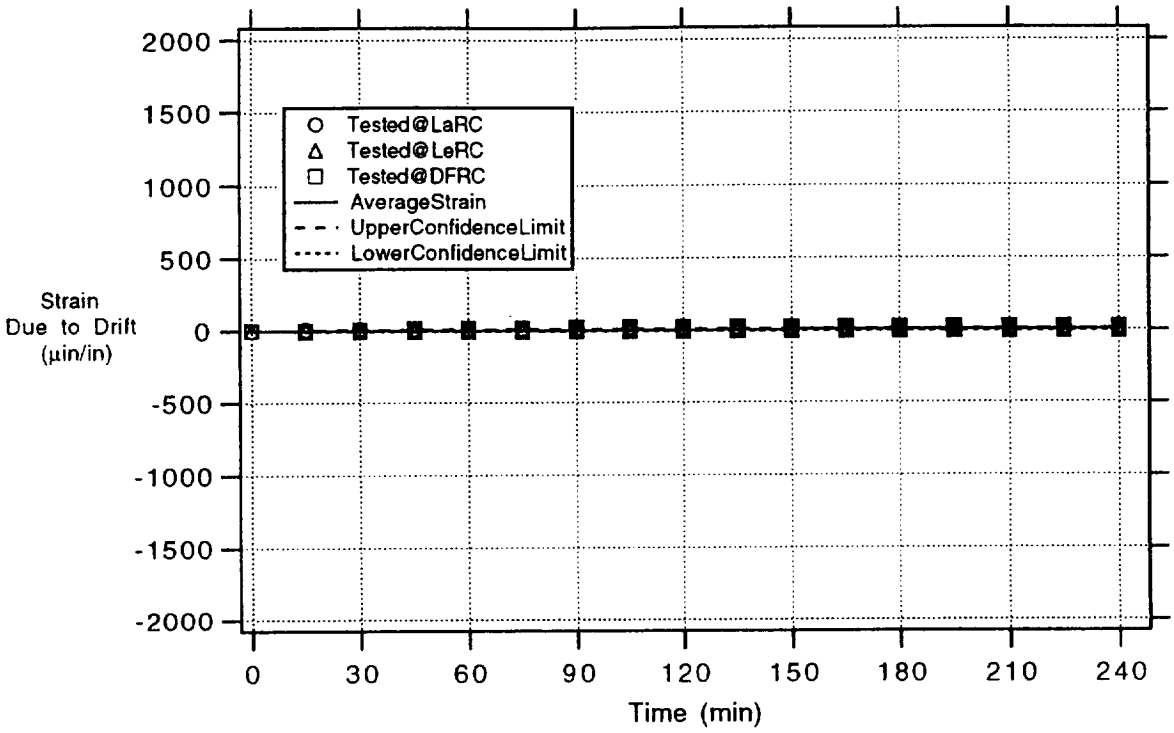

Figure 5.80.—Twelve PdCr gages on IN100—cycle 1 (600 °F; 315 °C).

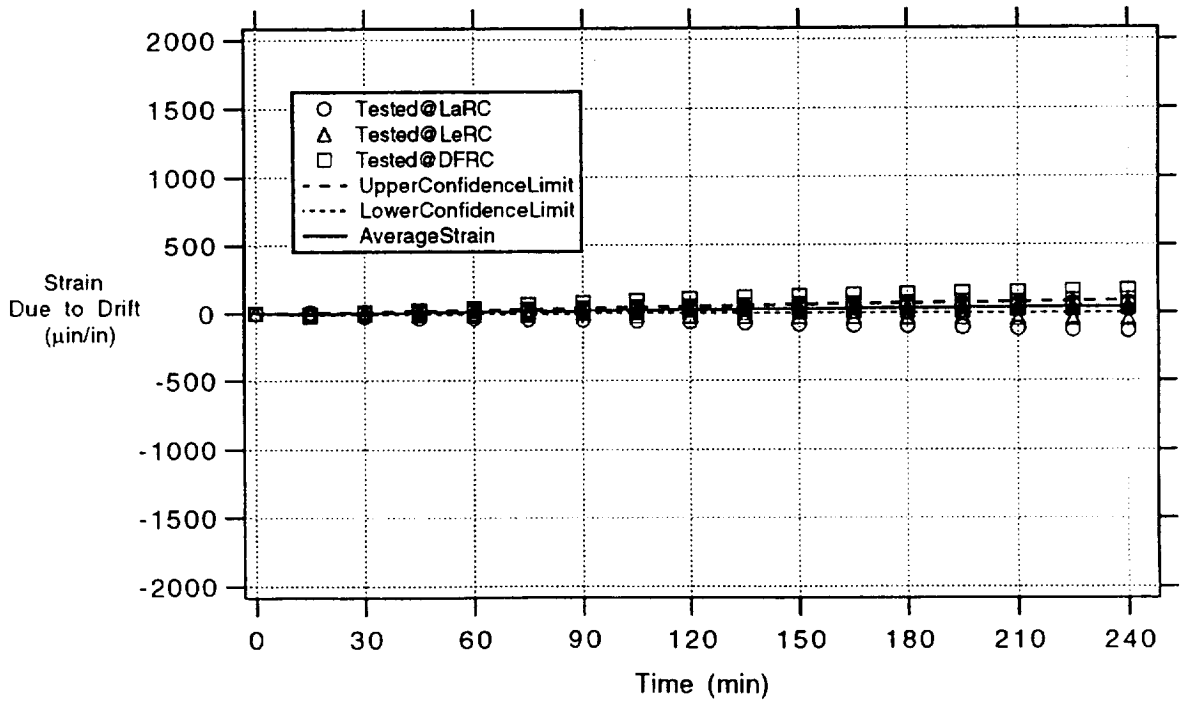

Figure 5.81.—Twelve PdCr gages on IN100—cycle 2 (750 °F; 398 °C).

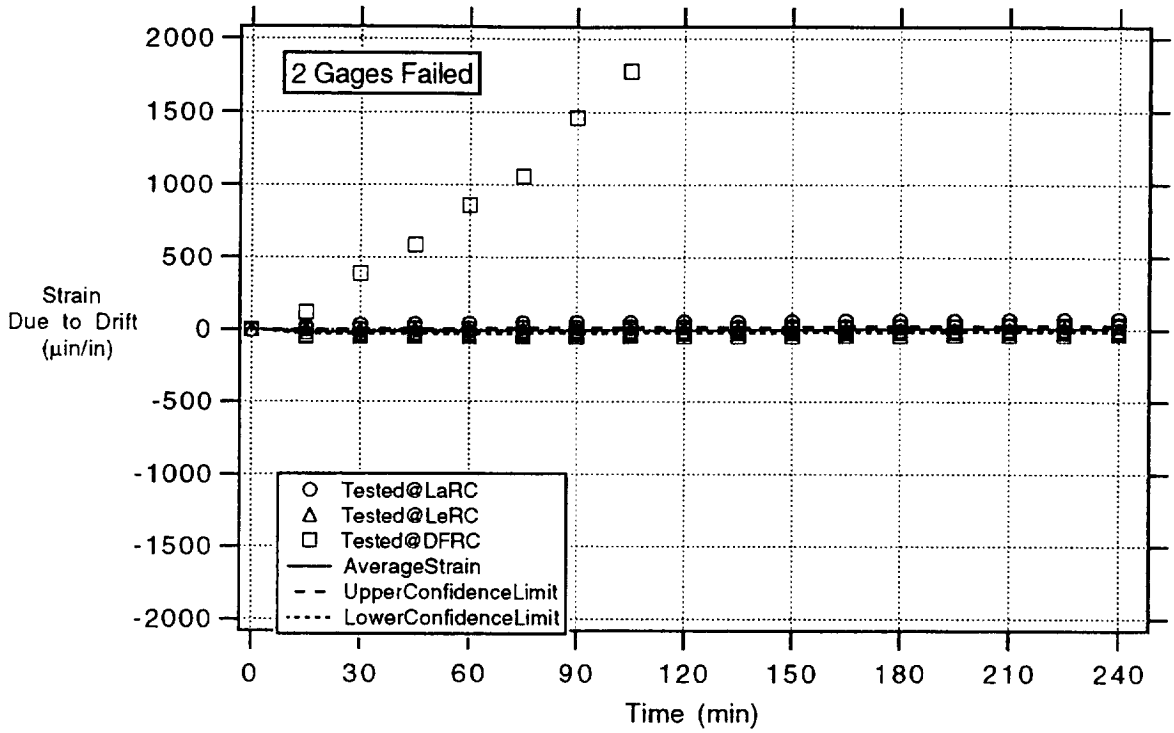

Figure 5.82.—Twelve PdCr gages on IN100—cycle 3 (900 °F; 482 °C).

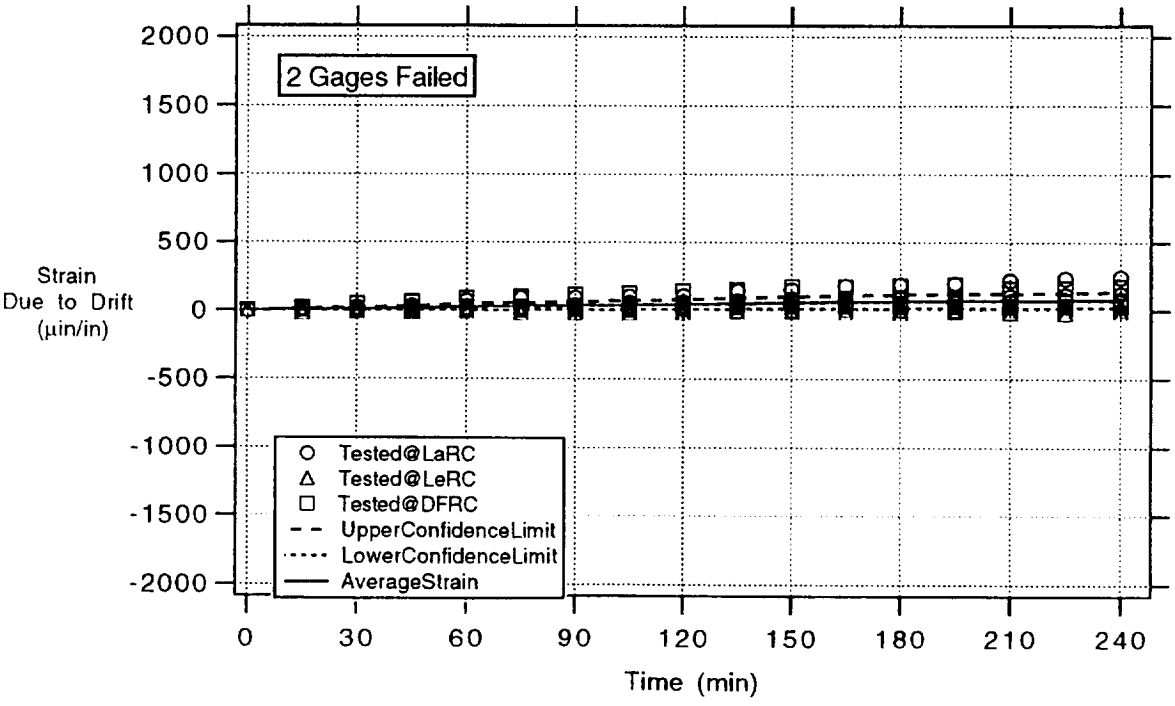

Figure 5.83.—Twelve PdCr gages on IN100—cycle 4 (1050 °F; 565 °C).

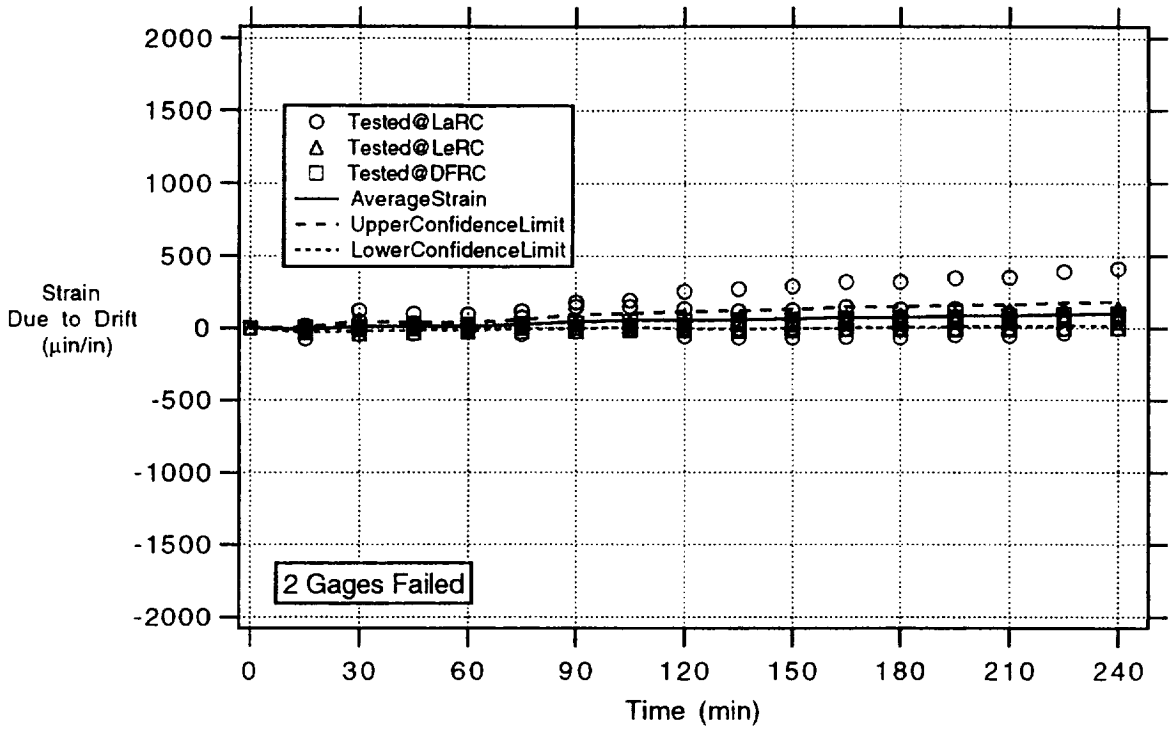

Figure 5.84.—Twelve PdCr gages on IN100—cycle 5 (1200 °F; 648 °C).

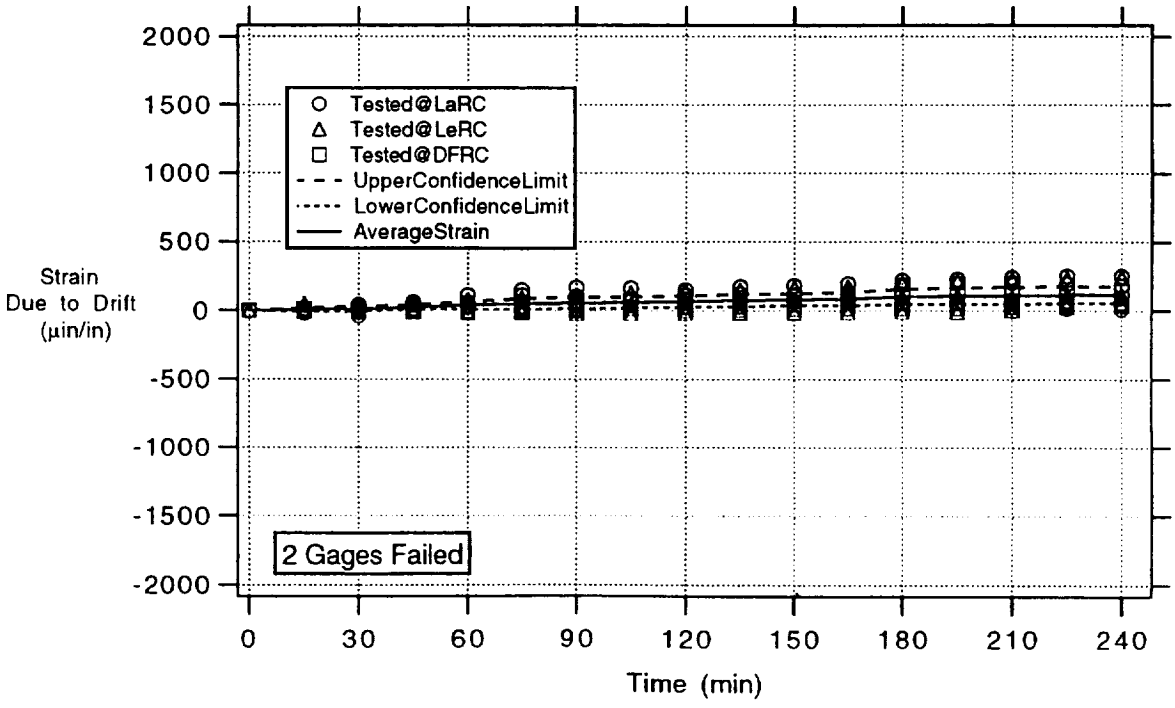

Figure 5.85.—Twelve PdCr gages on IN100—cycle 6 (1350 °F; 732 °C).

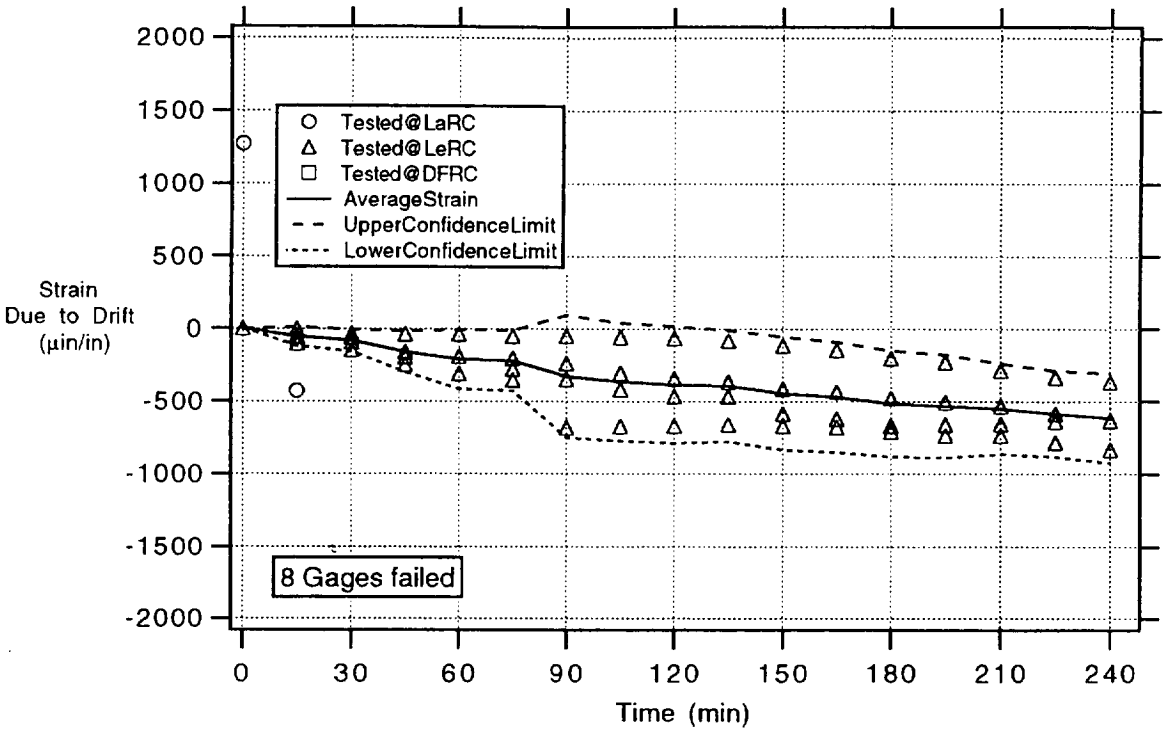

Figure 5.86.—Twelve PdCr gages on IN100—cycle 7 (1500 °F; 482 °C).

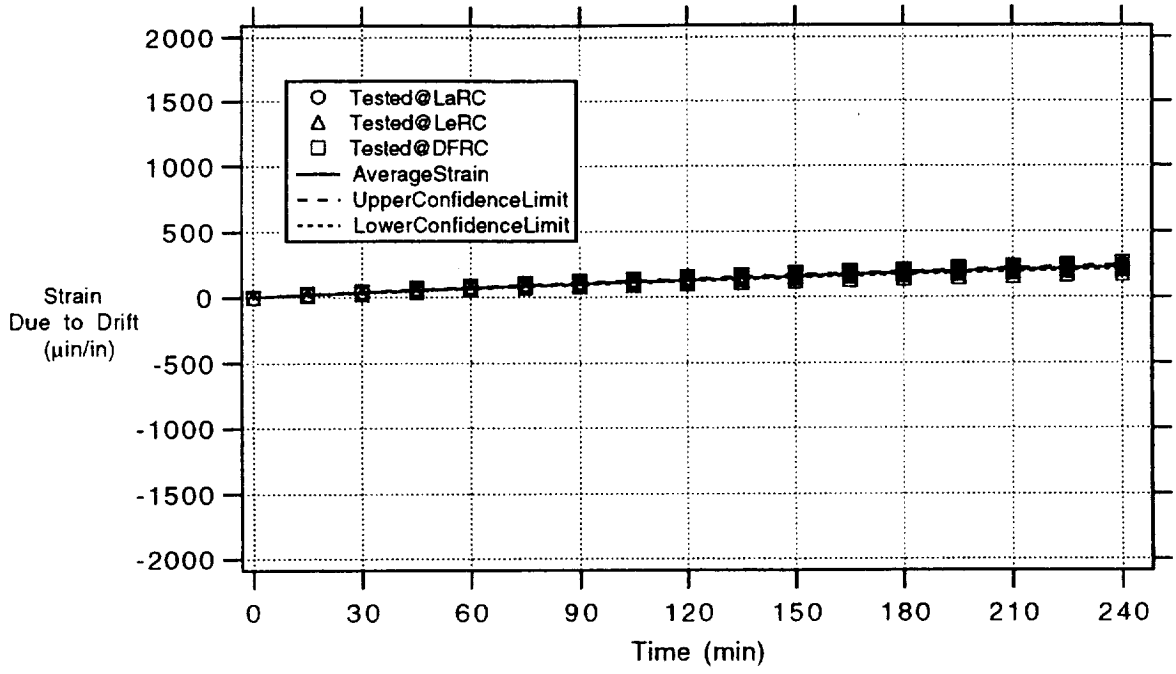

Figure 5.87.—Twelve DETCBCL gages on IN100—cycle 1 (600 °F; 315 °C).

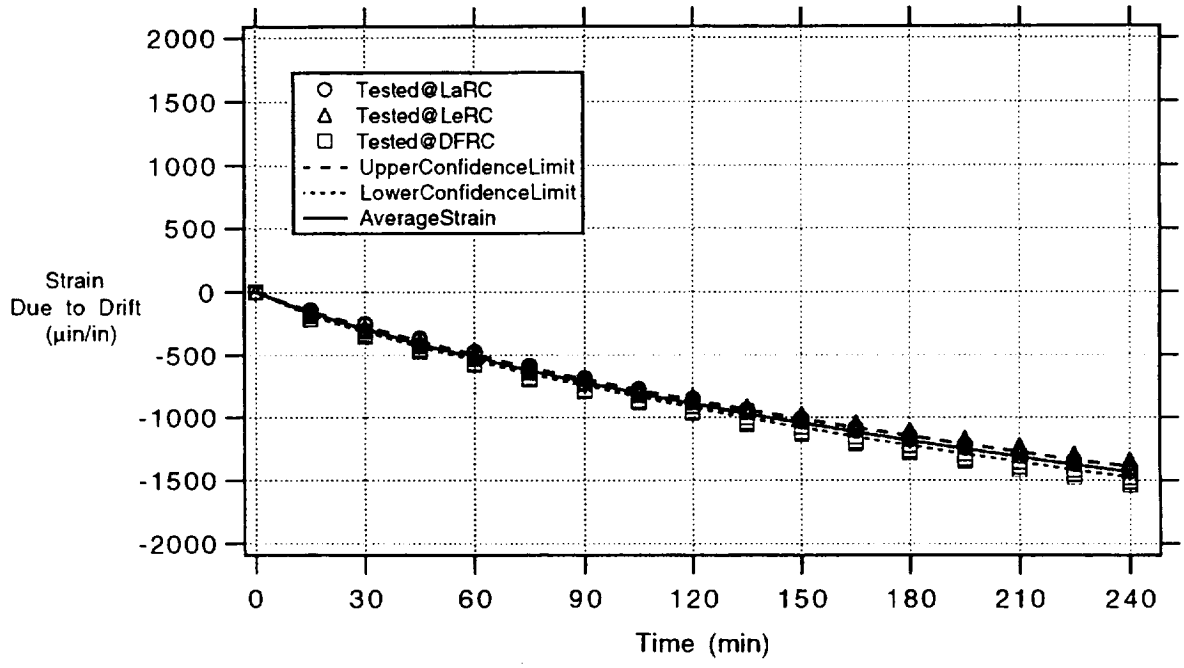

Figure 5.88.—Twelve DETCBCL gages on IN100—cycle 2 (750 °F; 398 °C).

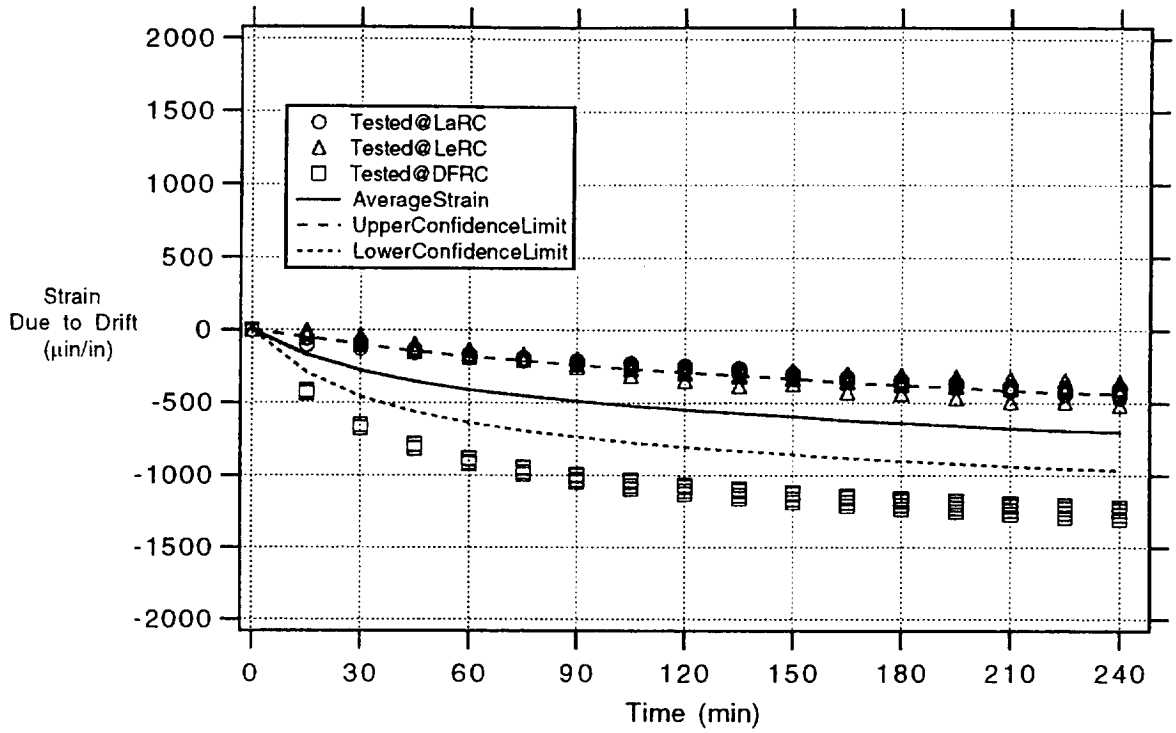

Figure 5.89.—Twelve DETCBCL gages on IN100—cycle 3 (900 °F; 482 °C).

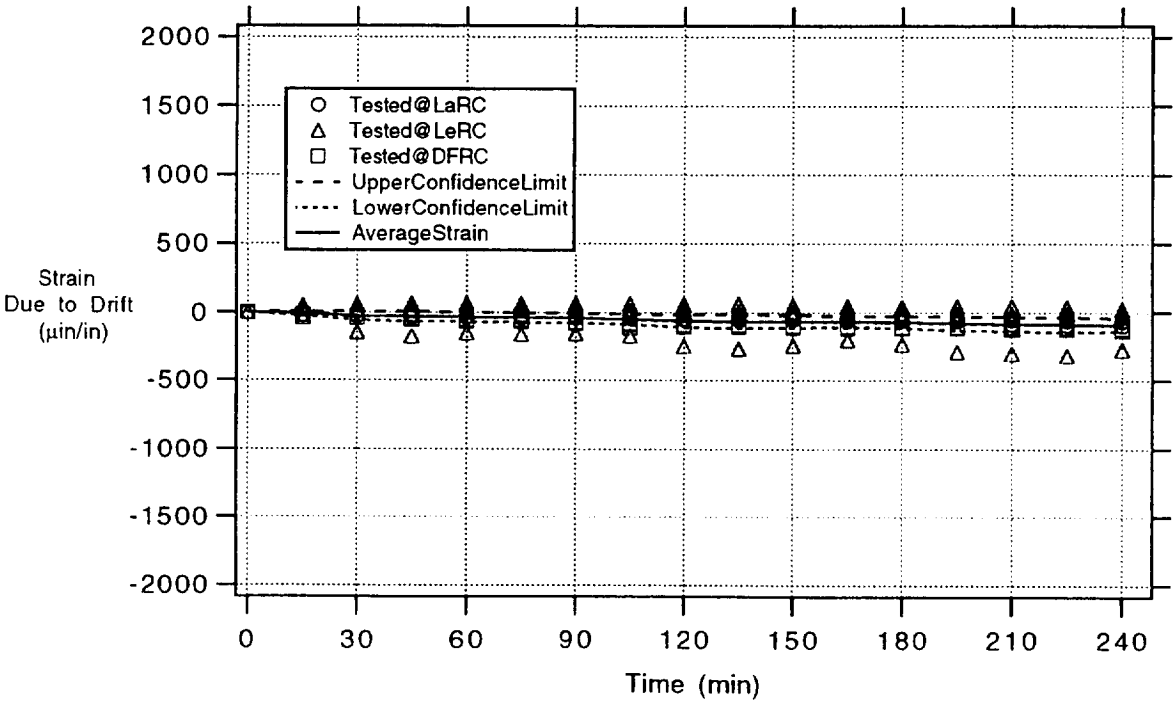

Figure 5.90.—Twelve DETCBCL gages on IN100—cycle 4 (1050 °F; 565 °C).

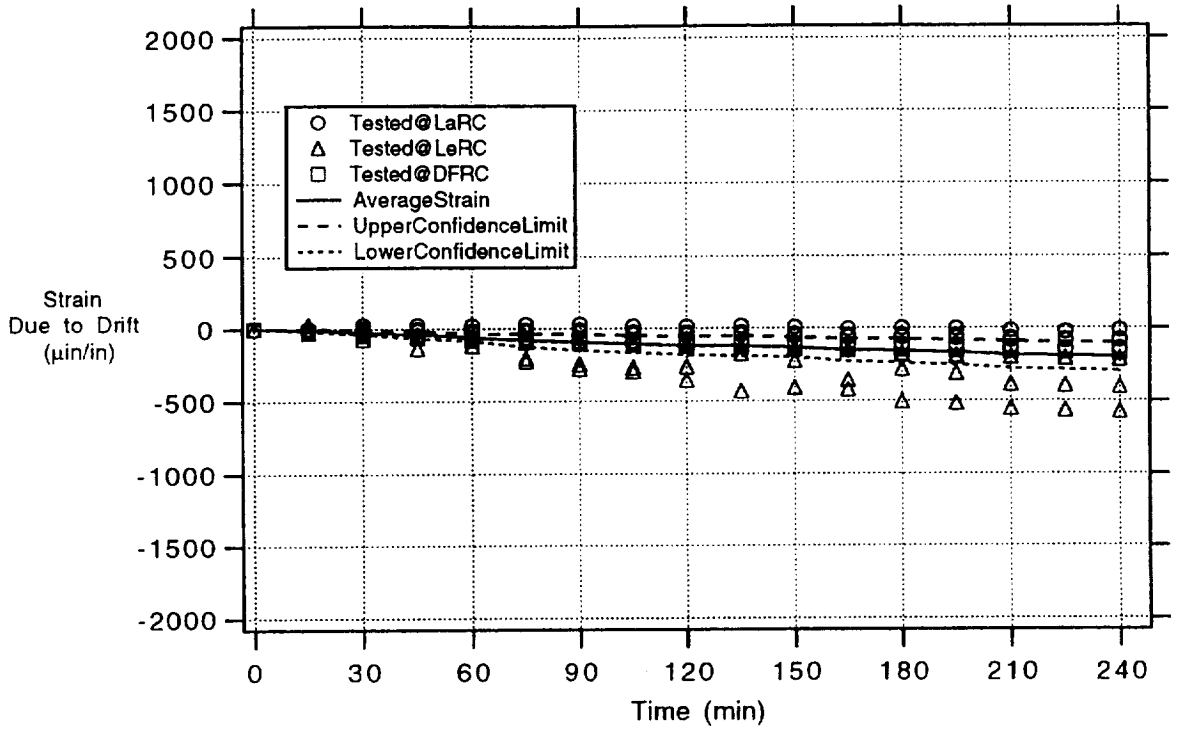

Figure 5.91.—Twelve DETCBCL gages on IN100—cycle 5 (1200 °F; 648 °C).

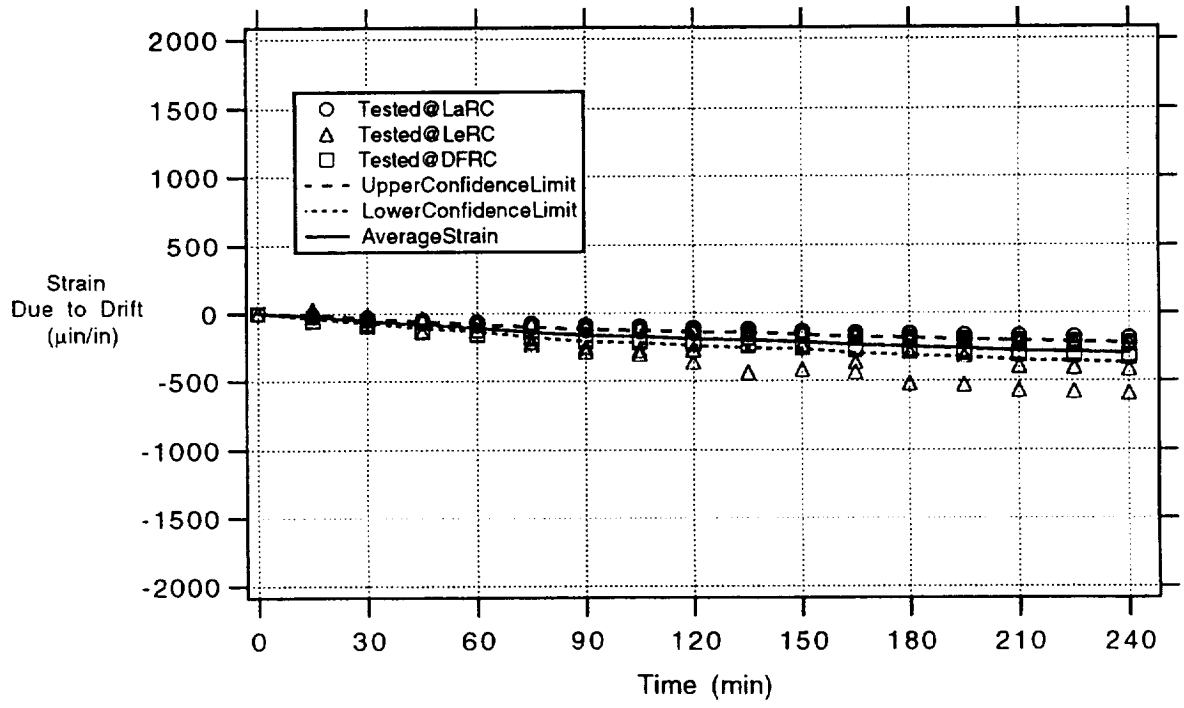

Figure 5.92.—Twelve DETCBCL gages on IN100—cycle 6 (1350 °F; 732 °C).

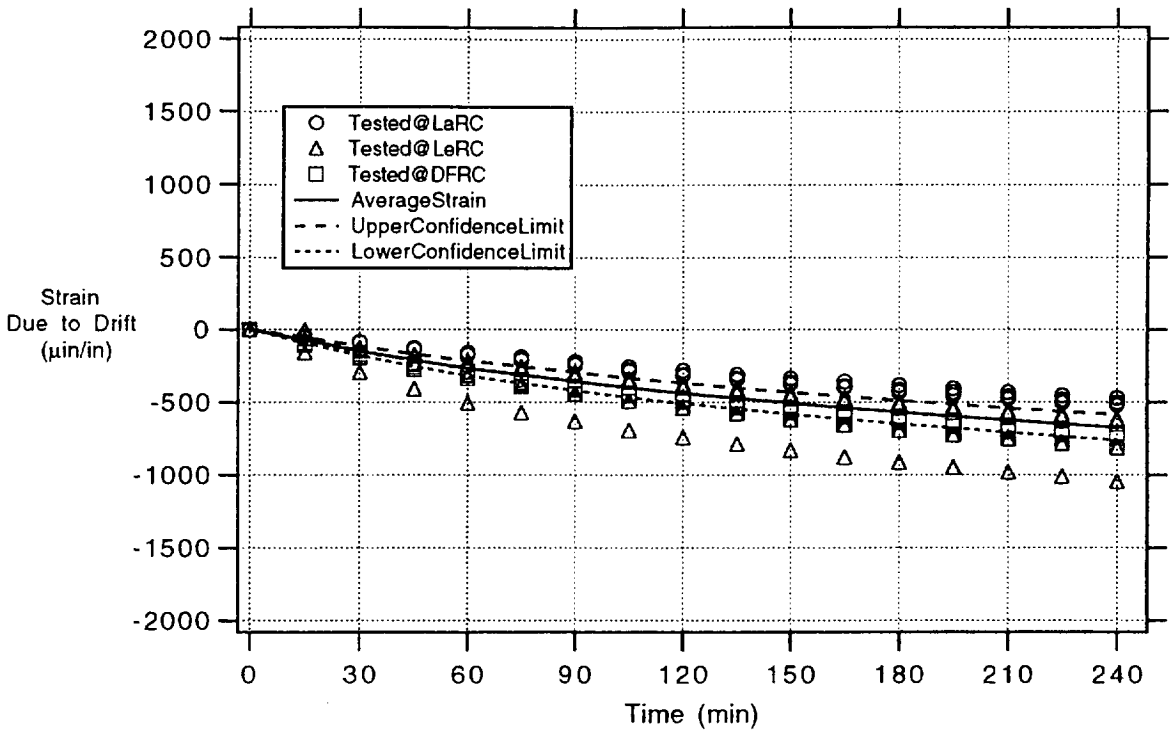

Figure 5.93.—Twelve DETCBCL gages on IN100—cycle 7 (1500 °F; 816 °C).

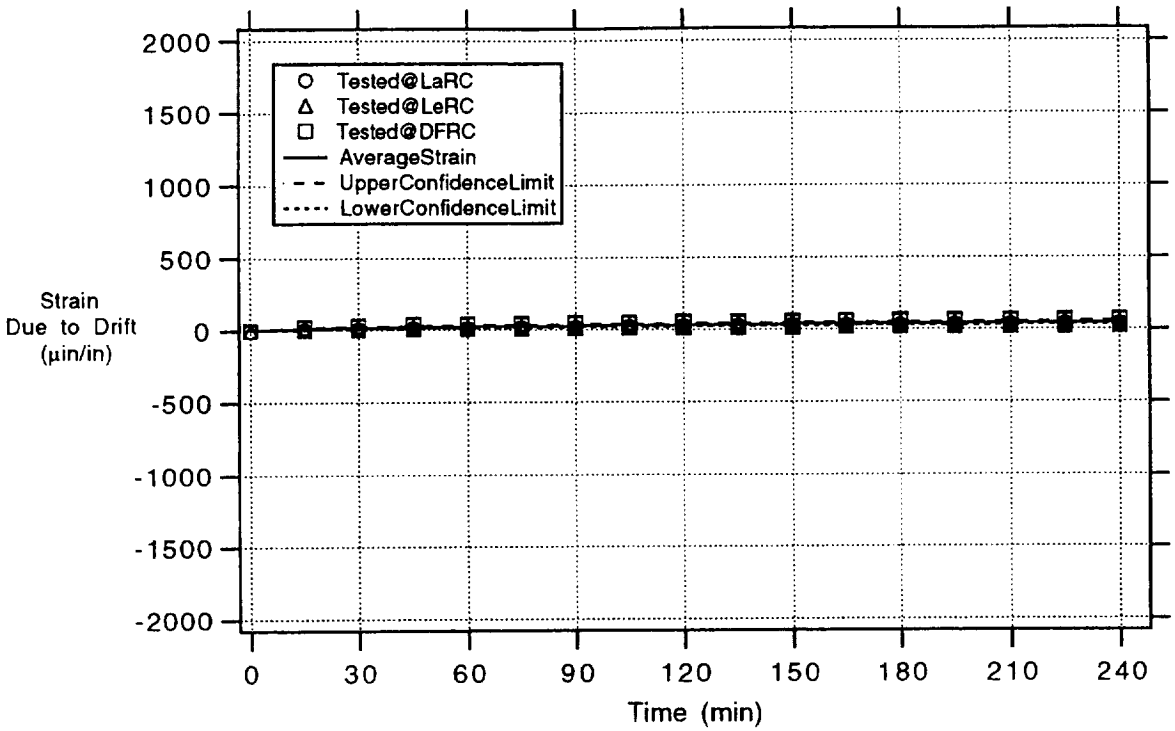

Figure 5.94.—Twelve CKA1 gages on TMC—cycle 1 (600 °F; 315 °C).

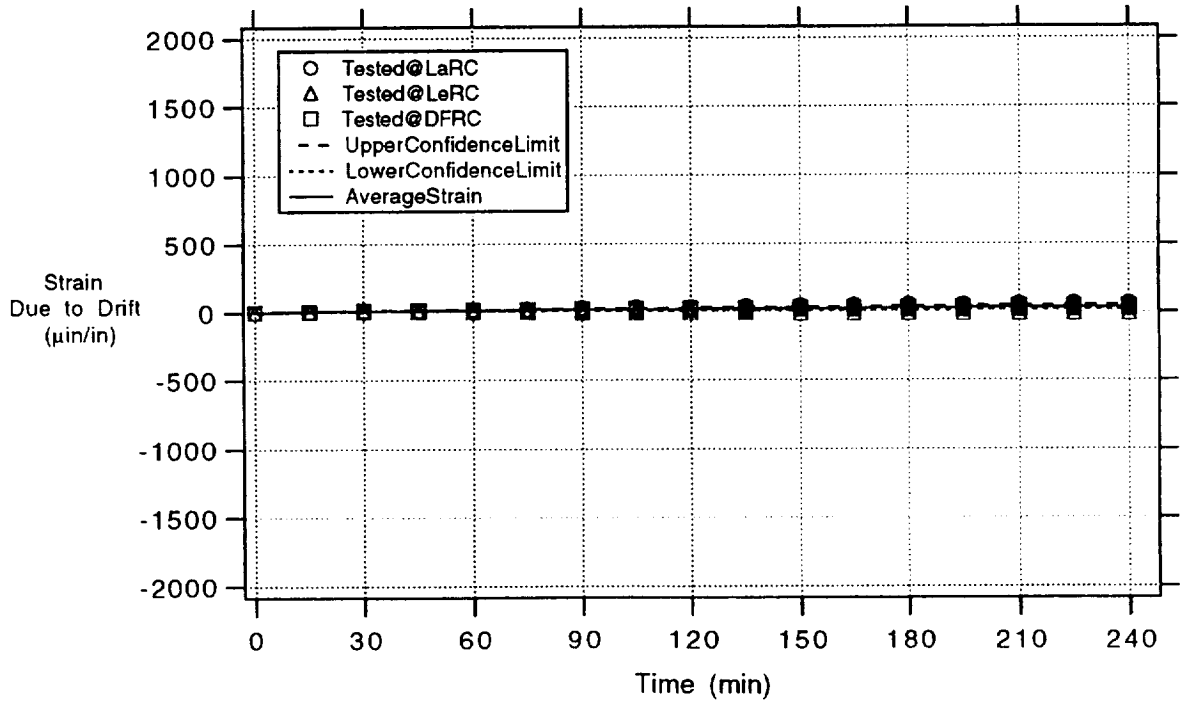

Figure 5.95.—Twelve CKA1 gages on TMC—cycle 2 (750 °F; 398 °C).

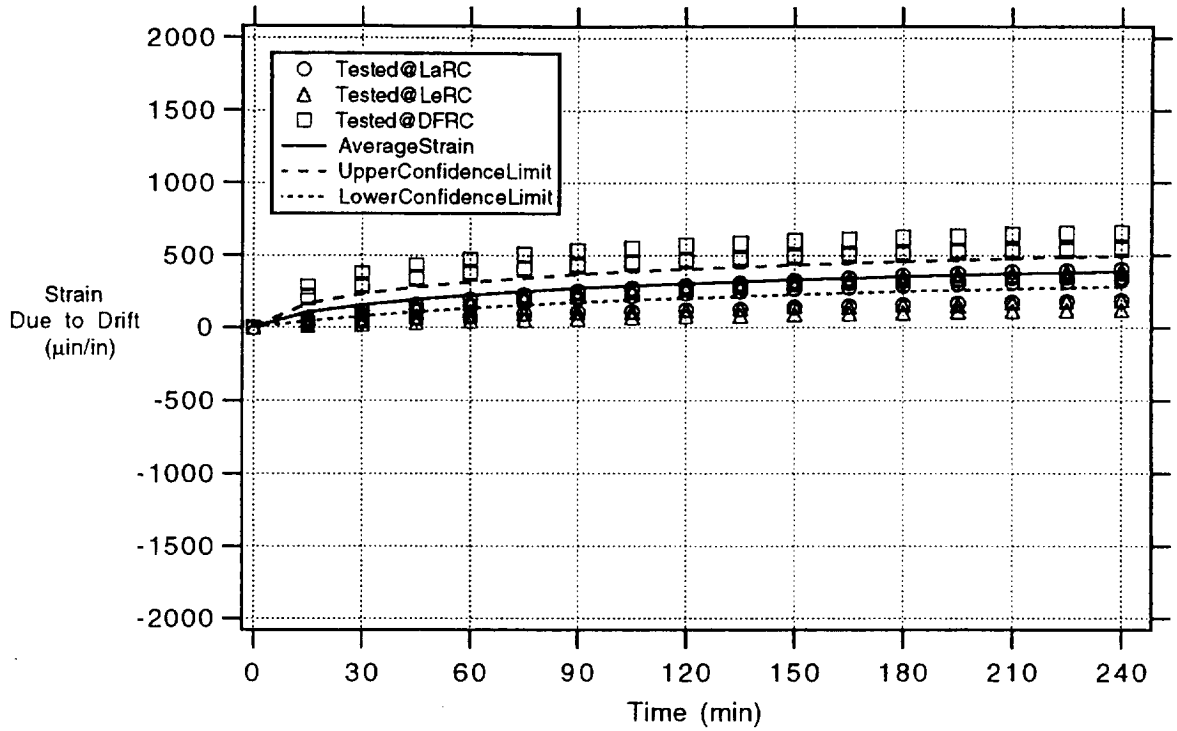

Figure 5.96.—Twelve CKA1 gages on TMC—cycle 3 (900 °F; 482 °C).

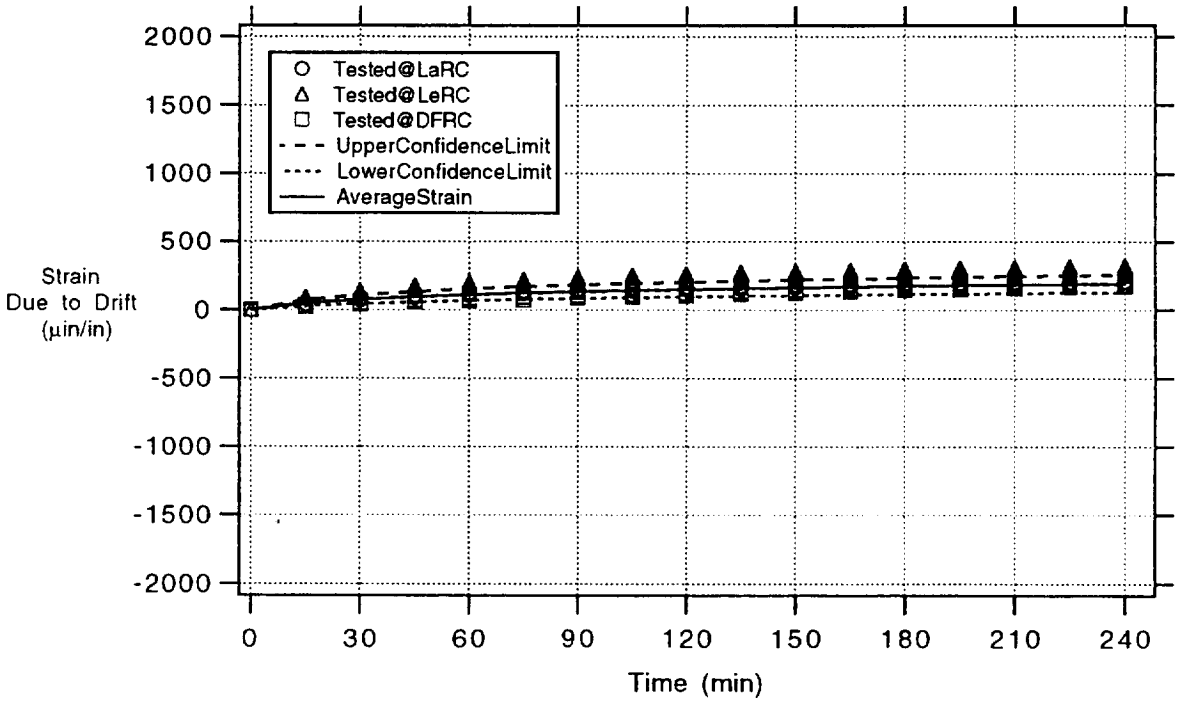

Figure 5.97.—Twelve CKA1 gages on TMC—cycle 4 (1050 °F; 565 °C).

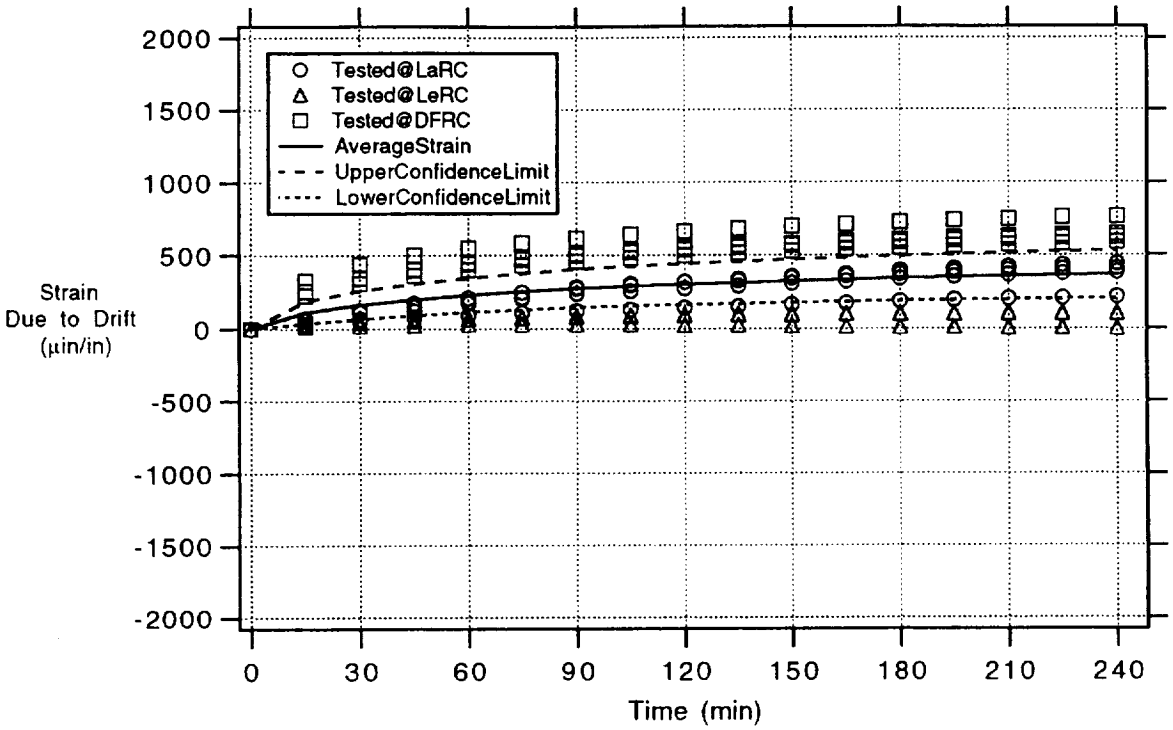

Figure 5.98.—Twelve CKA1 gages on TMC—cycle 5 (1200 °F; 648 °C).

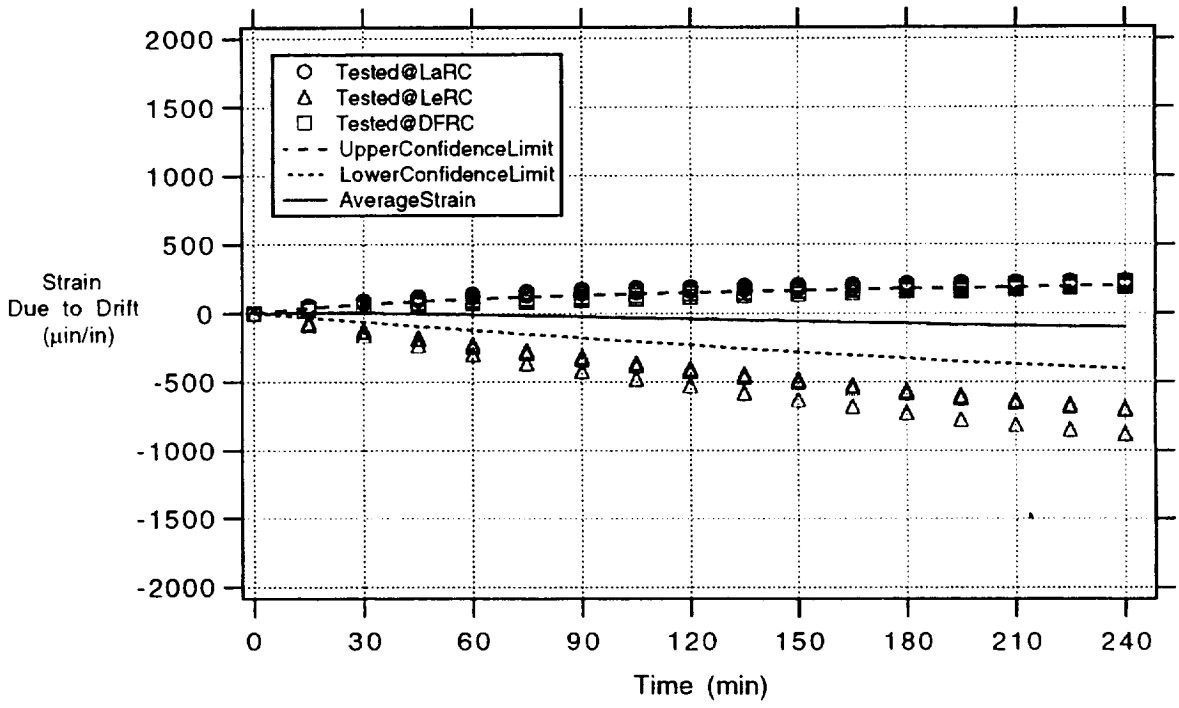

Figure 5.99.—Twelve CKA1 gages on TMC—cycle 6 (1350 °F; 732 °C).

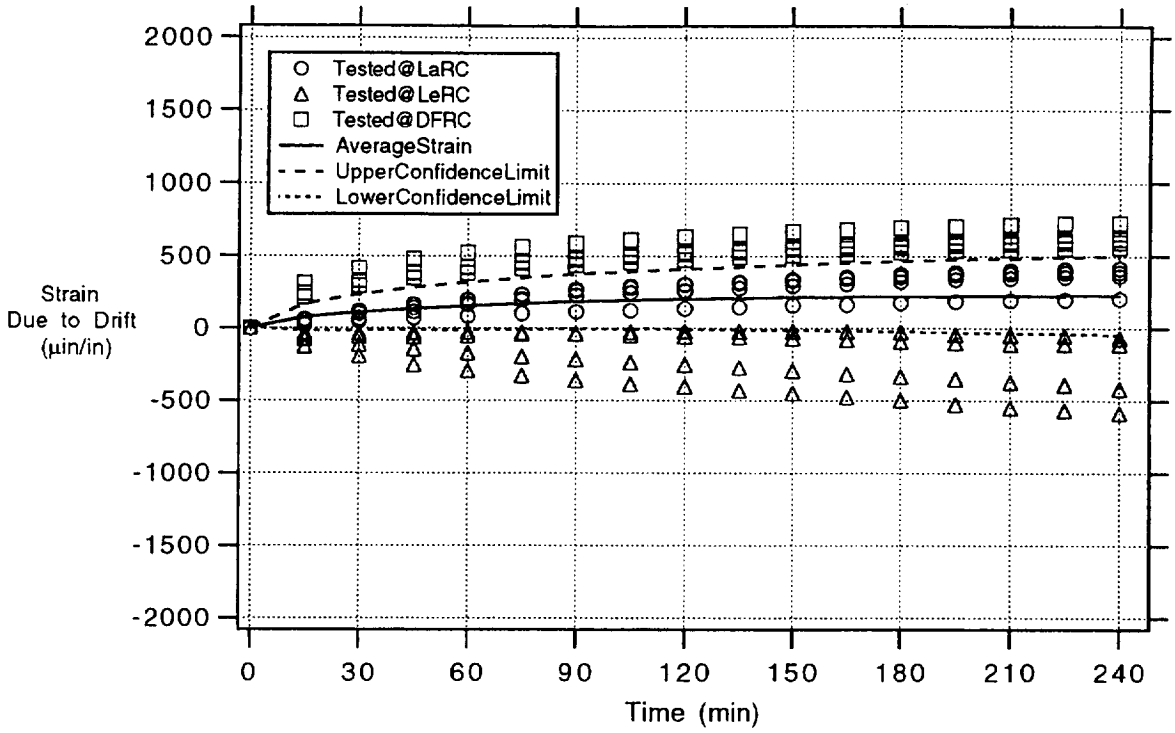

Figure 5.100.—Twelve CKA1 gages on TMC—cycle 7 (1500 °F; 816 °C).

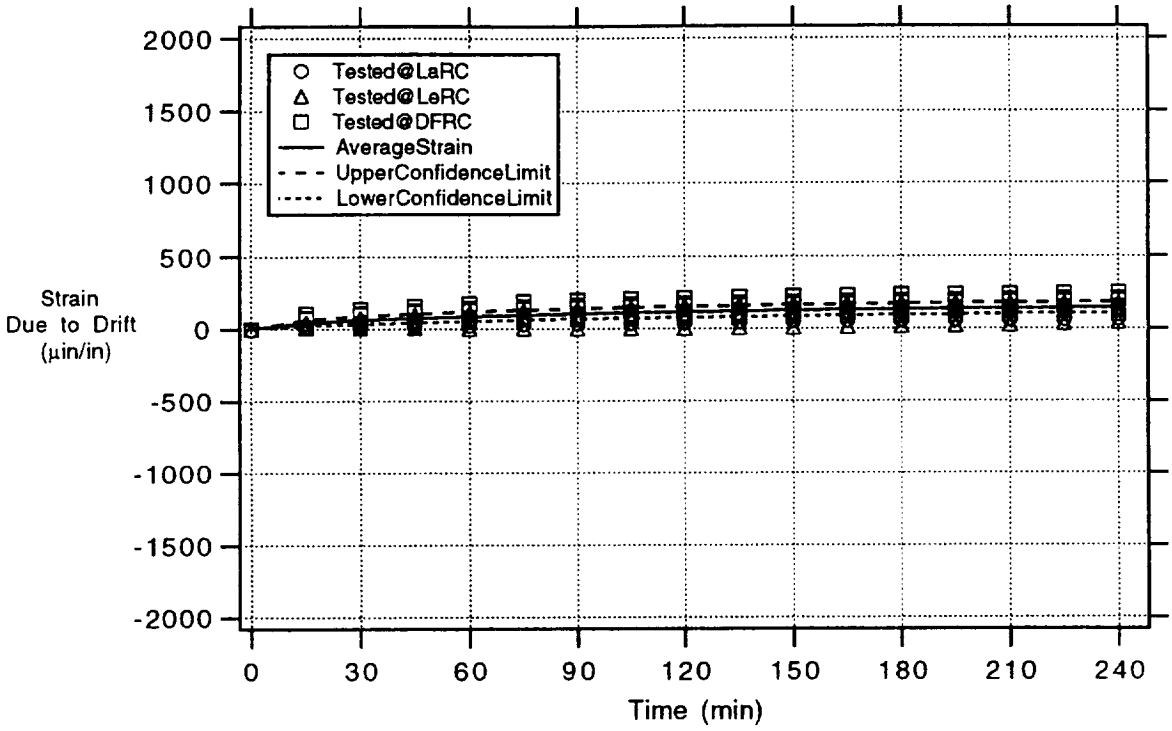

Figure 5.101.—Twelve PdCr gages on TMC—cycle 1 (600 °F; 315 °C).

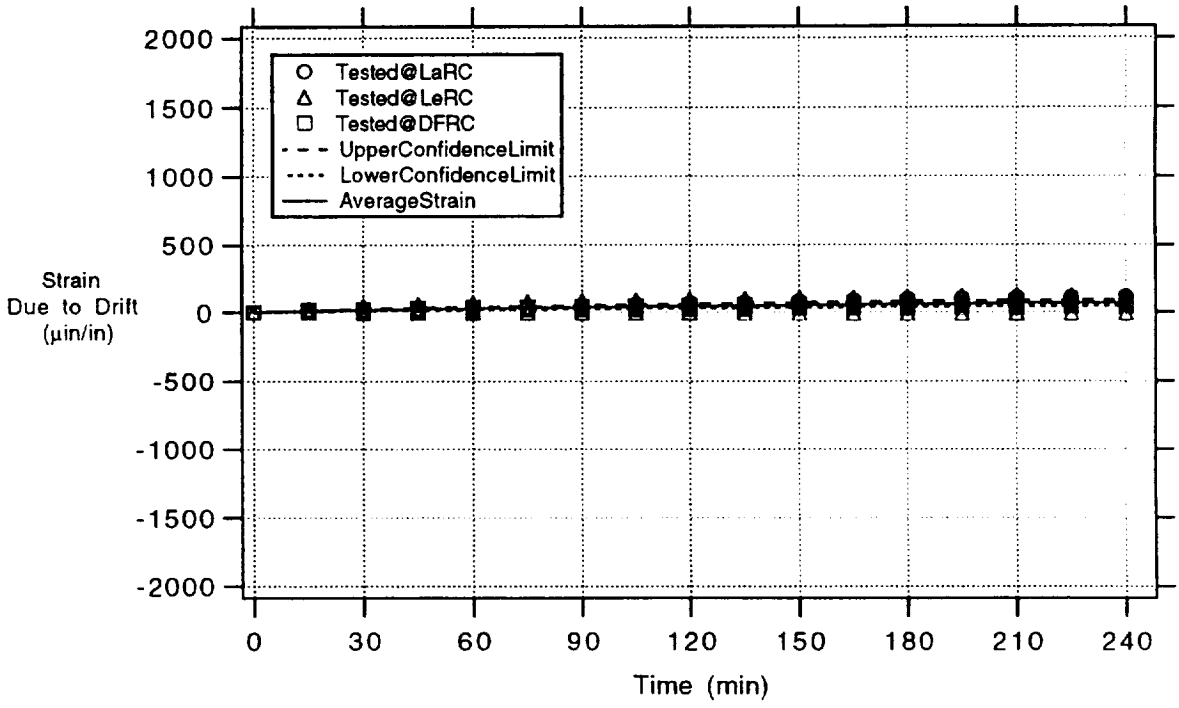

Figure 5.102.—Twelve PdCr gages on TMC—cycle 2 (750 °F; 398 °C).

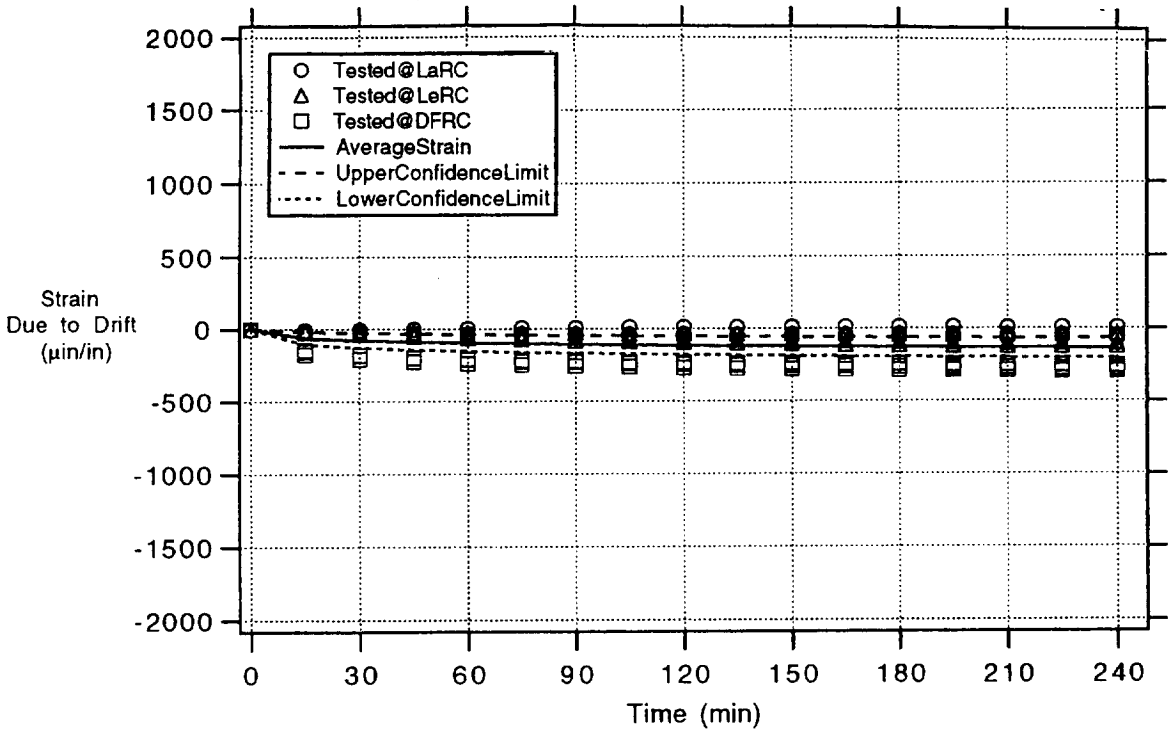

Figure 5.103.—Twelve PdCr gages on TMC—cycle 3 (900 °F; 482 °C).

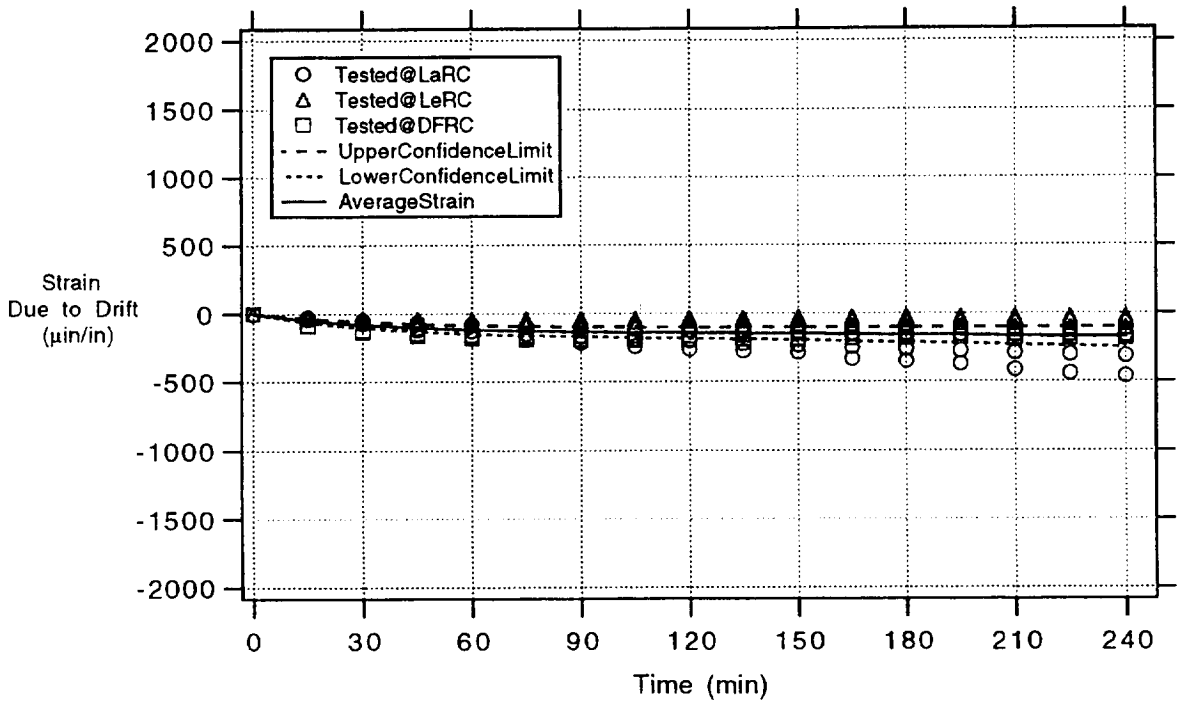

Figure 5.104.—Twelve PdCr gages on TMC—cycle 4 (1050 °F; 565 °C).

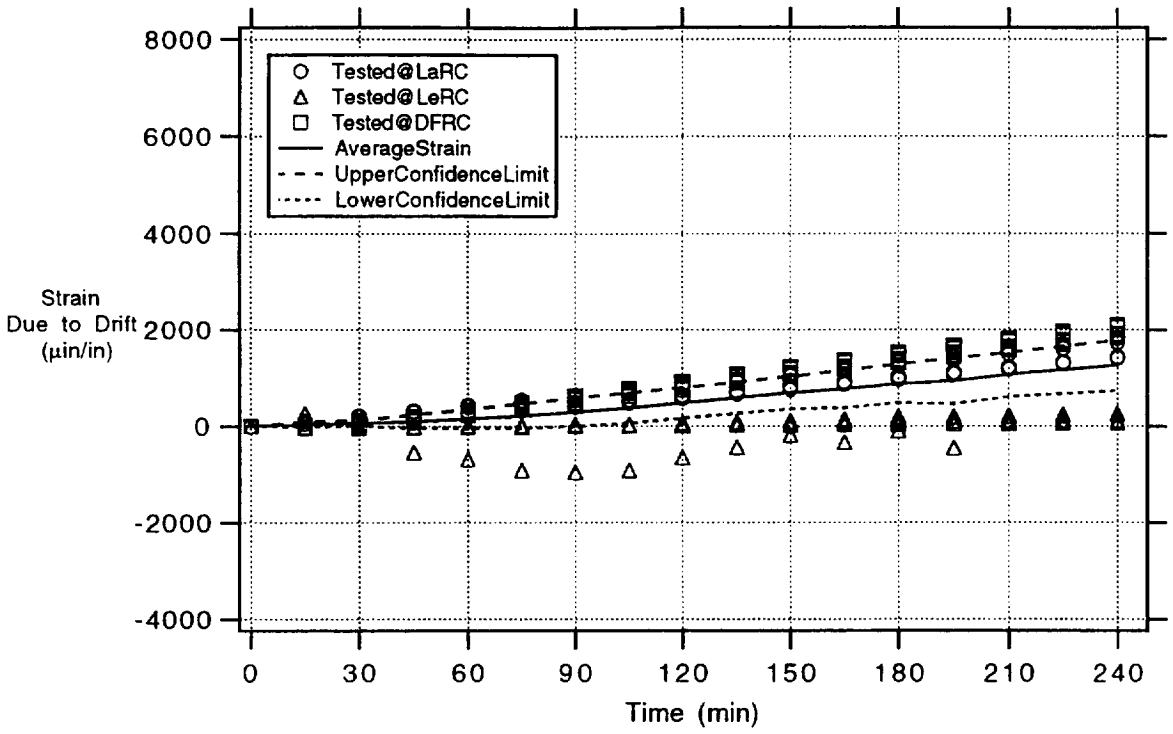

Figure 5.105.—Twelve PdCr gages on TMC—cycle 5 (1200 °F; 648 °C).

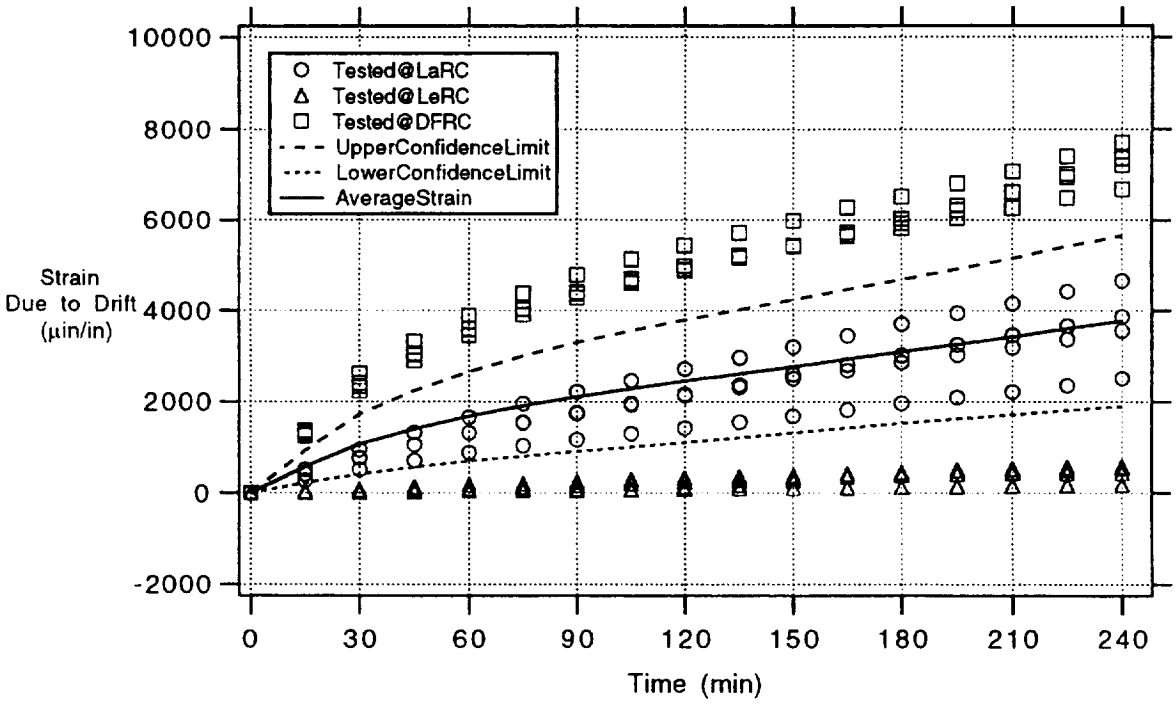

Figure 5.106.—Twelve PdCr gages on TMC—cycle 6 (1350 °F; 732 °C).

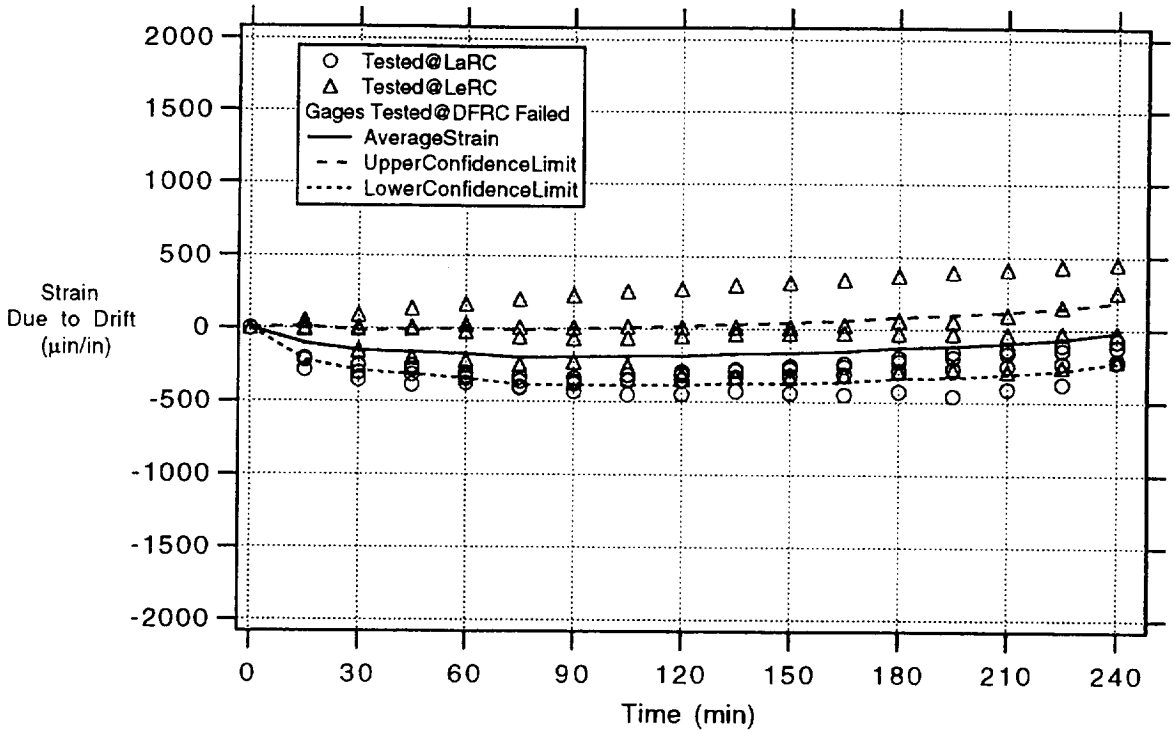

Figure 5.107.—Twelve PdCr gages on TMC—cycle 7 (1500 °F; 816 °C).

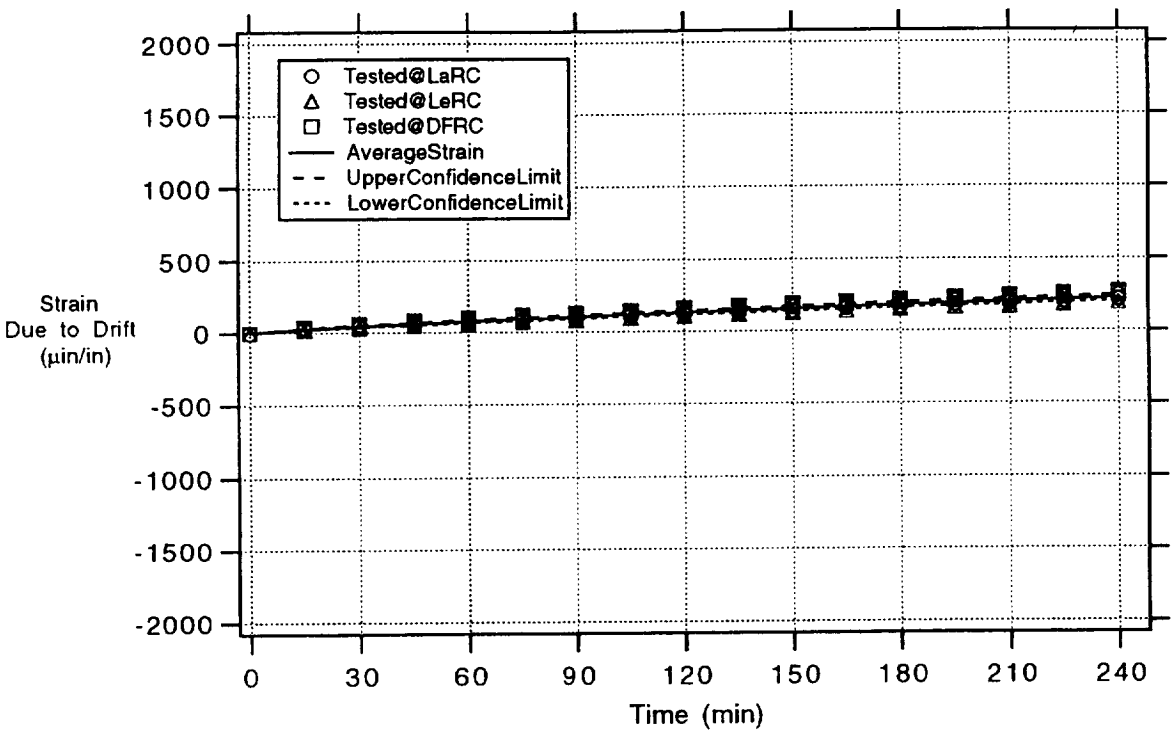

Figure 5.108.—Twelve DETCBCL gages on TMC—cycle 1 (600 °F; 315 °C).

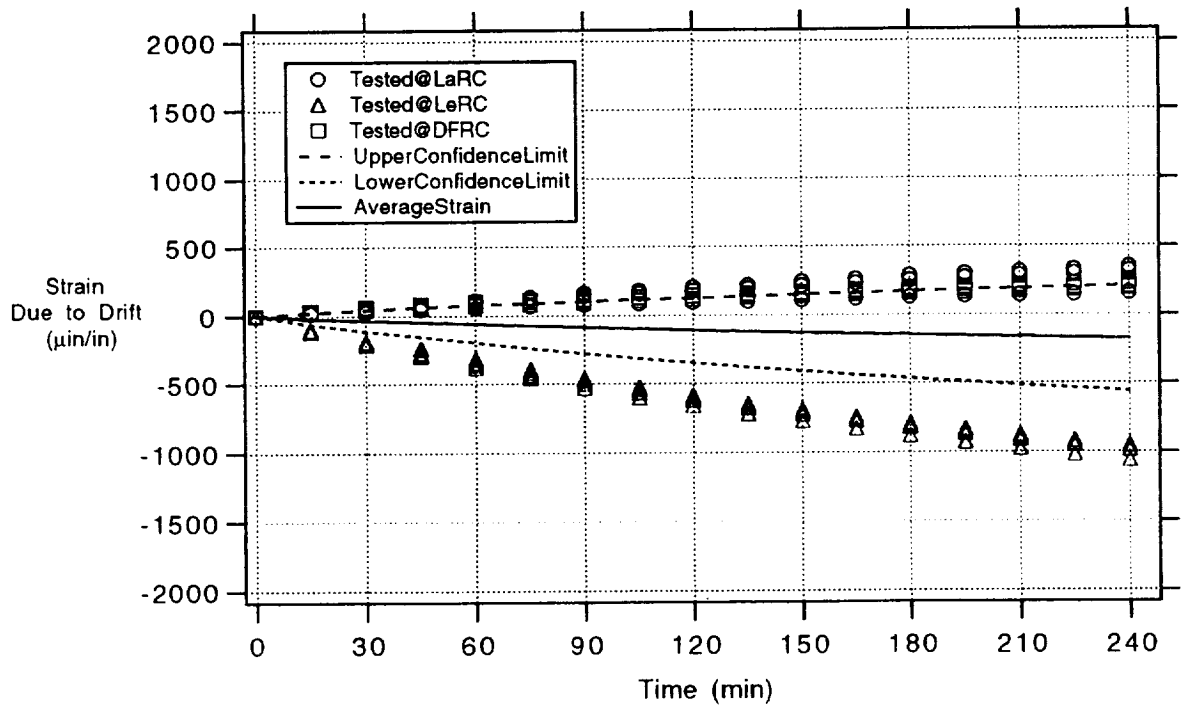

Figure 5.109.—Twelve DETCBCL gages on TMC—cycle 2 (750 °F; 398 °C).

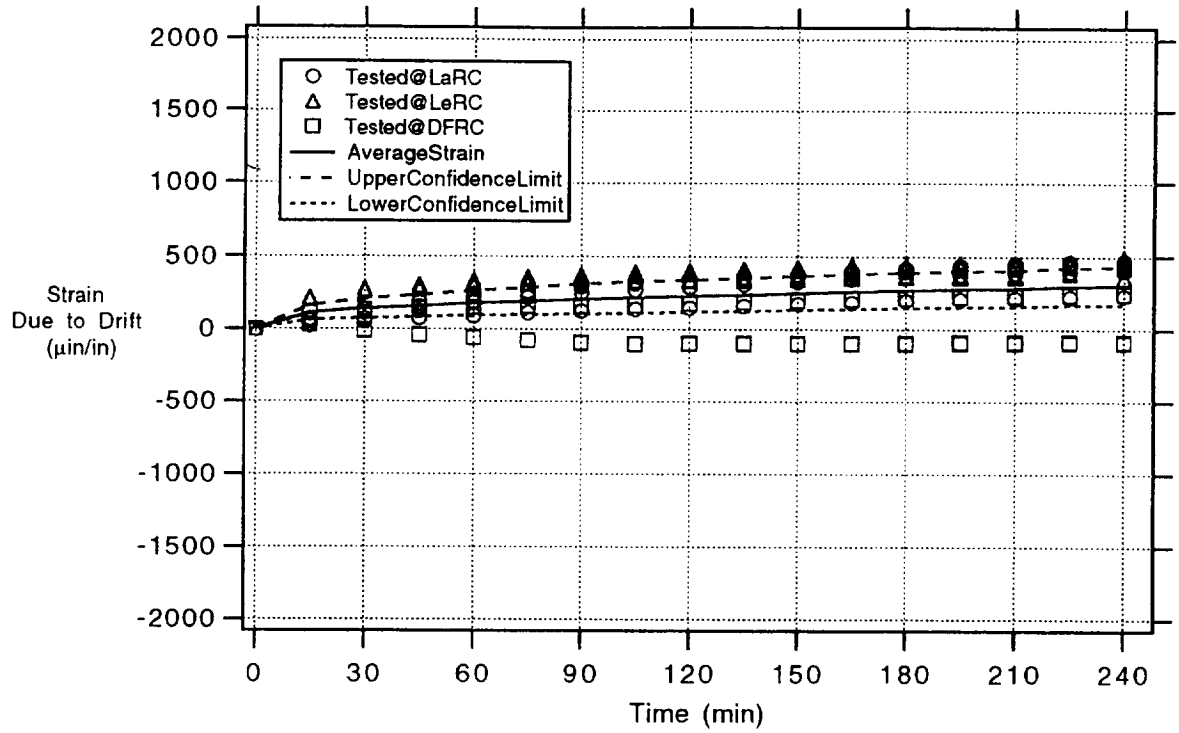

Figure 5.110.—Twelve DETCBCL gages on TMC—cycle 3 (900 °F; 482 °C).

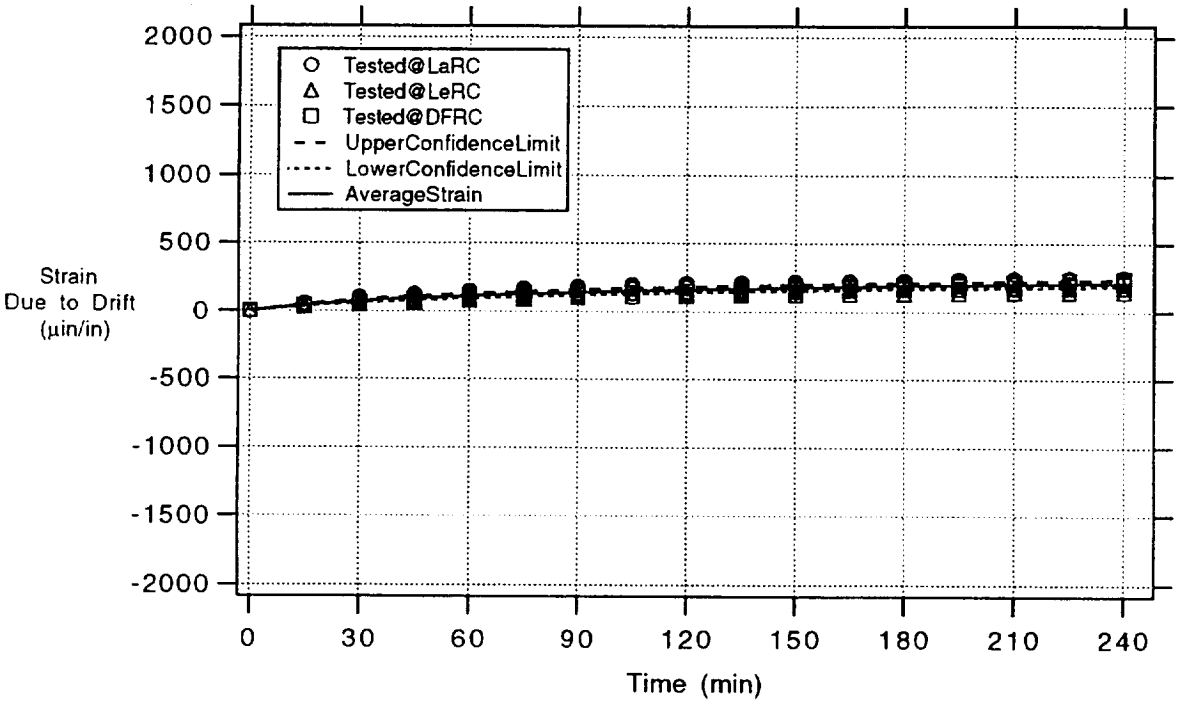

Figure 5.111.—Twelve DETCBCL gages on TMC—cycle 4 (1050 °F; 565 °C).

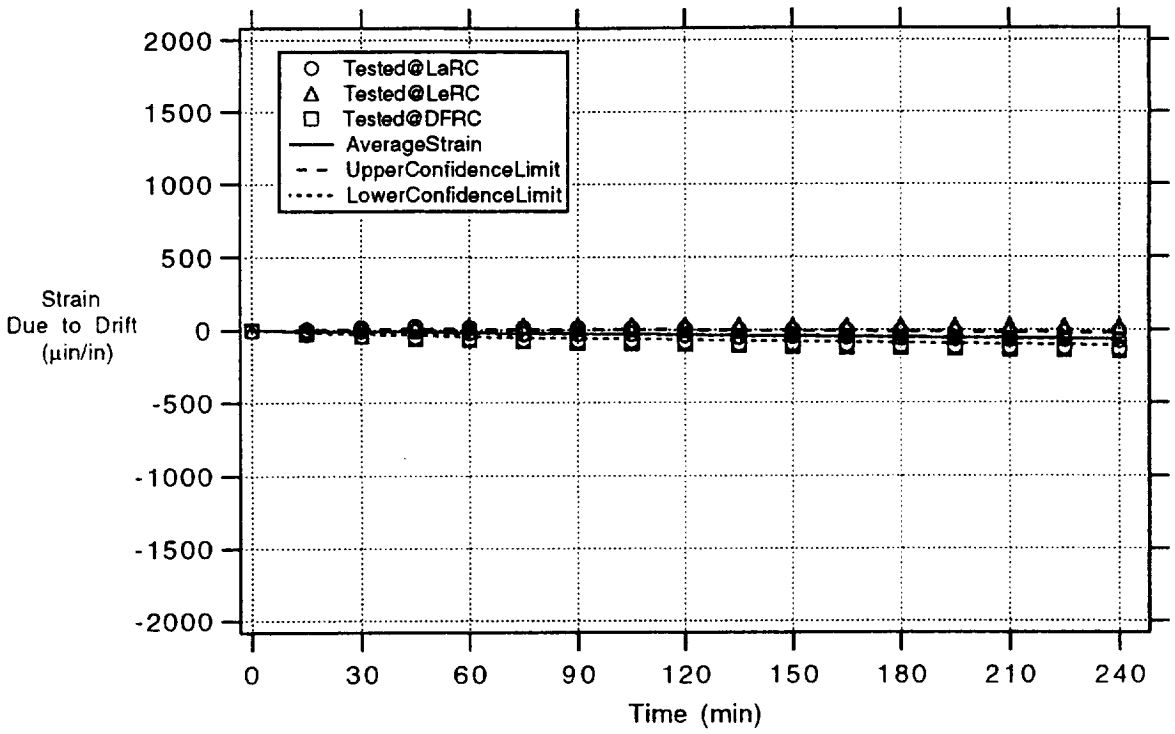

Figure 5.112.—Twelve DETCBCL gages on TMC—cycle 5 (1200 °F; 648 °C).

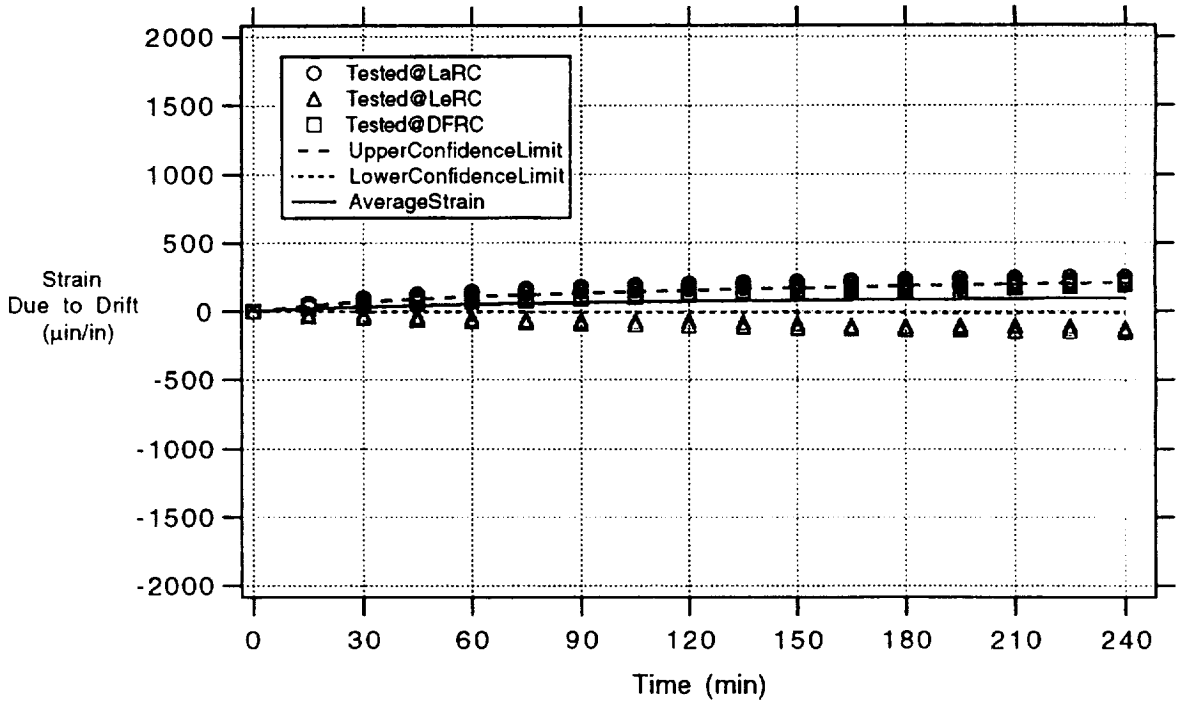

Figure 5.113.—Twelve DETCBCL gages on TMC—cycle 6 (1350 °F; 732 °C).

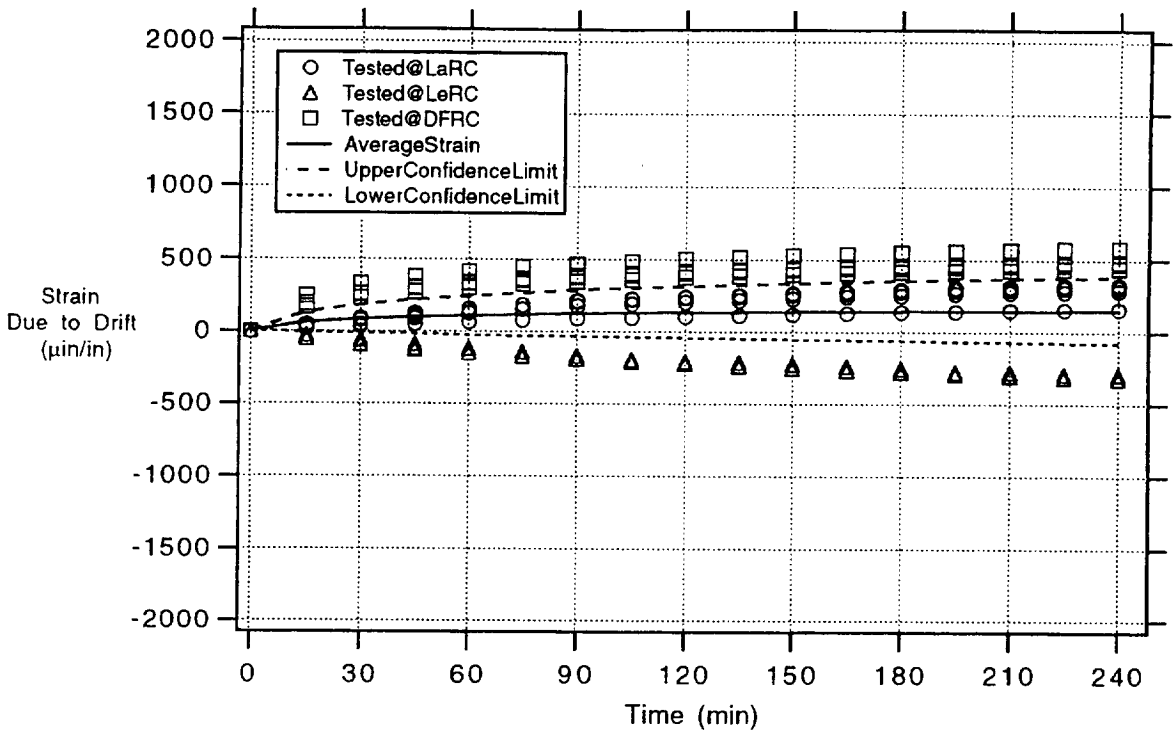

Figure 5.114.—Twelve DETCBCL gages on TMC—cycle 7 (1500 °F; 816°C).

5.3 Gage Factor Data

Figures 5.115 to 5.186 plot gage factor versus temperature for each of the three gages. There are 12 figures for each type of gage attached to either IN100 or β-21S TMC. Each figure represents a temperature heating cycle for gages under tension or compression as defined in the test plan. Unless a failure occurred, all 12 gages of a particular type are shown on the plots for tension, and all 8 gages of a particular type are shown on the plots for compression. No compression data were available from Langley, since Langley had their load bars placed under tension only. Then only surviving gages are shown. Also shown on each figure are the average values for the surviving gages and the upper and lower 95% confidence limits. A list of the gage factor figures is given in table 5.15.

Tables 5.16 to 5.27 tabulate the coefficients of the gage-factor-versus-temperature equation for each of the three gages. The equation is derived from polynomial curve fitting of the average curves shown in figures 5.115 to 5.186. There is an equation for each type of gage for each particular cycle during heating or cooling under tension or compression.

TABLE 5.15—FIGURES FOR GAGE FACTOR

Figure	Gage type	Substrate material	Cycle	Test temperature		Load mode
				°F	°C	
5.115	CKA1	IN100	1	1200	650	Tension
5.116	CKA1	IN100	1	1200	650	Compression
5.117	CKA1	IN100	4	1200	650	Tension
5.118	CKA1	IN100	4	1200	650	Compression
5.119	CKA1	IN100	5	1350	730	Tension
5.120	CKA1	IN100	5	1350	730	Compression
5.121	CKA1	IN100	6	1350	730	Tension
5.122	CKA1	IN100	6	1350	730	Compression
5.123	CKA1	IN100	7	1500	815	Tension
5.124	CKA1	IN100	7	1500	815	Compression
5.125	CKA1	IN100	8	1500	815	Tension
5.126	CKA1	IN100	8	1500	815	Compression
5.127	PdCr	IN100	1	1200	650	Tension
5.128	PdCr	IN100	1	1200	650	Compression
5.129	PdCr	IN100	4	1200	650	Tension
5.130	PdCr	IN100	4	1200	650	Compression
5.131	PdCr	IN100	5	1350	730	Tension
5.132	PdCr	IN100	5	1350	730	Compression
5.133	PdCr	IN100	6	1350	730	Tension
5.134	PdCr	IN100	6	1350	730	Compression
5.135	PdCr	IN100	7	1500	815	Tension
5.136	PdCr	IN100	7	1500	815	Compression
5.137	PdCr	IN100	8	1500	815	Tension
5.138	PdCr	IN100	8	1500	815	Compression
5.139	DETCBCL	IN100	1	1200	650	Tension
5.140	DETCBCL	IN100	1	1200	650	Compression
5.141	DETCBCL	IN100	4	1200	650	Tension
5.142	DETCBCL	IN100	4	1200	650	Compression
5.143	DETCBCL	IN100	5	1350	730	Tension
5.144	DETCBCL	IN100	5	1350	730	Compression
5.145	DETCBCL	IN100	6	1350	730	Tension
5.146	DETCBCL	IN100	6	1350	730	Compression
5.147	DETCBCL	IN100	7	1500	815	Tension
5.148	DETCBCL	IN100	7	1500	815	Compression
5.149	DETCBCL	IN100	8	1500	815	Tension
5.150	DETCBCL	IN100	8	1500	815	Compression
5.151	CKA1	TMC	1	1200	650	Tension
5.152	CKA1	TMC	1	1200	650	Compression
5.153	CKA1	TMC	4	1200	650	Tension
5.154	CKA1	TMC	4	1200	650	Compression
5.155	CKA1	TMC	5	1350	730	Tension
5.156	CKA1	TMC	5	1350	730	Compression
5.157	CKA1	TMC	6	1350	730	Tension
5.158	CKA1	TMC	6	1350	730	Compression
5.159	CKA1	TMC	7	1500	815	Tension
5.160	CKA1	TMC	7	1500	815	Compression
5.161	CKA1	TMC	8	1500	815	Tension
5.162	CKA1	TMC	8	1500	815	Compression

TABLE 5.15—Concluded.

Figure	Gage type	Substrate material	Cycle	Test temperature		Load mode
				°F	°C	
5.163	PdCr	TMC	1	1200	650	Tension
5.164	PdCr	TMC	1	1200	650	Compression
5.165	PdCr	TMC	4	1200	650	Tension
5.166	PdCr	TMC	4	1200	650	Compression
5.167	PdCr	TMC	5	1350	730	Tension
5.168	PdCr	TMC	5	1350	730	Compression
5.169	PdCr	TMC	6	1350	730	Tension
5.170	PdCr	TMC	6	1350	730	Compression
5.171	PdCr	TMC	7	1500	815	Tension
5.172	PdCr	TMC	7	1500	815	Compression
5.173	PdCr	TMC	8	1500	815	Tension
5.174	PdCr	TMC	8	1500	815	Compression
5.175	DETCBCL	TMC	1	1200	650	Tension
5.176	DETCBCL	TMC	1	1200	650	Compression
5.177	DETCBCL	TMC	4	1200	650	Tension
5.178	DETCBCL	TMC	4	1200	650	Compression
5.179	DETCBCL	TMC	5	1350	730	Tension
5.180	DETCBCL	TMC	5	1350	730	Compression
5.181	DETCBCL	TMC	6	1350	730	Tension
5.182	DETCBCL	TMC	6	1350	730	Compression
5.183	DETCBCL	TMC	7	1500	815	Tension
5.184	DETCBCL	TMC	7	1500	815	Compression
5.185	DETCBCL	TMC	8	1500	815	Tension
5.186	DETCBCL	TMC	8	1500	815	Compression

TABLE 5.16.—GAGE-FACTOR-VERSUS-TEMPERATURE EQUATION FOR CKA1 GAGE ON IN100 UNDER TENSION

$[GF(T) = a_0 + a_1 \times T + a_2 \times T^2 + a_3 \times T^3.]$

Cycle	a_0	a_1	a_2	a_3
Heating				
1	2.475	-3.095×10^{-4}	6.068×10^{-7}	-6.221×10^{-10}
4	2.526	3.049×10^{-4}	-1.074×10^{-6}	2.683×10^{-10}
5	2.368	1.125×10^{-3}	-2.527×10^{-6}	1.014×10^{-9}
6	2.367	1.099×10^{-3}	-2.652×10^{-6}	1.130×10^{-9}
7	2.380	6.185×10^{-4}	-1.979×10^{-6}	8.721×10^{-10}
8	2.276	9.073×10^{-4}	-2.303×10^{-6}	9.631×10^{-10}
Cooling				
1	2.531	-4.883×10^{-4}	6.443×10^{-7}	-5.598×10^{-10}
4	2.369	6.837×10^{-5}	-7.413×10^{-7}	2.542×10^{-10}
5	2.383	9.193×10^{-4}	-2.316×10^{-6}	9.658×10^{-10}
6	2.376	6.208×10^{-4}	-1.974×10^{-6}	8.907×10^{-10}
7	2.316	3.550×10^{-4}	-1.383×10^{-6}	6.078×10^{-10}
8	2.362	2.134×10^{-4}	-1.359×10^{-6}	6.195×10^{-10}

TABLE 5.17.—GAGE-FACTOR-VERSUS-TEMPERATURE EQUATION FOR CKA1 GAGE ON IN100 UNDER COMPRESSION

$[GF(T) = a_0 + a_1 \times T + a_2 \times T^2 + a_3 \times T^3.]$

Cycle	a_0	a_1	a_2	a_3
Heating				
1	2.610	-5.191×10^{-4}	4.251×10^{-7}	-4.936×10^{-10}
4	2.404	2.302×10^{-4}	-7.904×10^{-7}	1.157×10^{-10}
5	2.283	9.106×10^{-4}	-2.076×10^{-6}	7.987×10^{-10}
6	2.205	1.194×10^{-3}	-2.563×10^{-6}	1.048×10^{-9}
7	2.198	1.075×10^{-3}	-2.465×10^{-6}	1.031×10^{-9}
8	2.350	5.001×10^{-4}	-1.875×10^{-6}	7.975×10^{-10}
Cooling				
1	2.395	1.627×10^{-4}	-5.901×10^{-7}	9.483×10^{-12}
4	2.342	-5.594×10^{-5}	-2.450×10^{-7}	-1.032×10^{-10}
5	2.248	6.912×10^{-4}	-1.682×10^{-6}	6.437×10^{-10}
6	2.228	7.865×10^{-4}	-2.031×10^{-6}	8.705×10^{-10}
7	2.297	8.185×10^{-4}	-2.362×10^{-6}	1.040×10^{-9}
8	2.335	3.855×10^{-4}	-1.655×10^{-6}	7.064×10^{-10}

TABLE 5.18.—GAGE-FACTOR-VERSUS-TEMPERATURE EQUATION FOR PdCr GAGE ON IN100 UNDER TENSION

$[GF(T) = a_0 + a_1 \times T + a_2 \times T^2 + a_3 \times T^3.]$

Cycle	a_0	a_1	a_2	a_3
Heating				
1	1.543	1.310×10^{-3}	-2.488×10^{-6}	-1.106×10^{-9}
4	1.524	7.480×10^{-4}	-1.866×10^{-6}	8.965×10^{-10}
5	1.402	2.916×10^{-4}	-8.862×10^{-7}	4.269×10^{-10}
6	1.451	2.742×10^{-5}	-3.756×10^{-7}	1.543×10^{-10}
7	1.414	3.167×10^{-4}	-9.947×10^{-7}	4.684×10^{-10}
8	1.336	5.813×10^{-4}	-1.146×10^{-6}	4.756×10^{-10}
Cooling				
1	1.443	7.554×10^{-4}	-1.776×10^{-6}	9.707×10^{-10}
2	1.414	5.060×10^{-4}	9.267×10^{-7}	3.436×10^{-10}
5	1.338	1.002×10^{-3}	-1.895×10^{-6}	8.069×10^{-10}
6	1.428	4.780×10^{-5}	-2.945×10^{-7}	8.833×10^{-11}
7	1.351	4.324×10^{-4}	-8.737×10^{-7}	3.711×10^{-10}
8	1.331	1.442×10^{-4}	-4.120×10^{-7}	1.809×10^{-10}

TABLE 5.19.—GAGE-FACTOR-VERSUS-TEMPERATURE EQUATION FOR PdCr GAGE ON IN100 UNDER COMPRESSION

$[GF(T) = a_0 + a_1 \times T + a_2 \times T^2 + a_3 \times T^3.]$

Cycle	a_0	a_1	a_2	a_3
Heating				
1	1.622	-4.934×10^{-4}	7.710×10^{-7}	-4.742×10^{-10}
4	1.549	6.566×10^{-4}	-1.518×10^{-6}	6.115×10^{-10}
5	1.408	4.748×10^{-4}	-1.152×10^{-6}	5.026×10^{-10}
6	1.406	7.958×10^{-4}	-1.571×10^{-6}	6.328×10^{-10}
7	1.400	1.431×10^{-4}	-5.284×10^{-7}	2.348×10^{-10}
8	1.485	9.918×10^{-5}	-5.838×10^{-7}	2.727×10^{-10}
Cooling				
1	1.551	9.347×10^{-4}	-2.124×10^{-6}	1.000×10^{-9}
2	1.464	3.821×10^{-4}	-9.886×10^{-7}	4.142×10^{-10}
5	1.425	4.877×10^{-4}	-1.183×10^{-6}	5.148×10^{-10}
6	1.416	4.338×10^{-4}	-1.123×10^{-6}	4.984×10^{-10}
7	1.489	-1.023×10^{-4}	-2.067×10^{-7}	1.009×10^{-10}
8	1.477	2.011×10^{-4}	-5.932×10^{-7}	2.335×10^{-10}

TABLE 5.20—GAGE-FACTOR-VERSUS-TEMPERATURE EQUATION FOR DETCBCL GAGE ON IN100 UNDER TENSION

$[GF(T) = a_0 + a_1 \times T + a_2 \times T^2 + a_3 \times T^3.]$

Cycle	a_0	a_1	a_2	a_3
Heating				
1	2.001	3.666×10^{-4}	-1.8390×10^{-7}	-3.329×10^{-10}
4	1.8296	8.528×10^{-4}	-1.5192×10^{-6}	5.1209×10^{-10}
5	1.7900	8.550×10^{-4}	-1.8348×10^{-6}	7.7665×10^{-10}
6	1.6567	1.095×10^{-3}	-2.2133×10^{-6}	9.5722×10^{-10}
7	1.6567	1.067×10^{-3}	-2.2736×10^{-6}	1.0075×10^{-9}
8	1.5340	1.376×10^{-3}	-2.8917×10^{-6}	1.2803×10^{90}
Cooling				
1	1.7446	1.296×10^{-3}	-2.2595×10^{-6}	9.7580×10^{-10}
2	1.8232	7.853×10^{-4}	-1.9741×10^{-6}	9.7269×10^{-10}
5	1.7050	1.533×10^{-3}	-3.2409×10^{-6}	1.5165×10^{-9}
6	1.7078	9.085×10^{-4}	-2.2269×10^{-6}	1.0791×10^{-11}
7	1.6975	1.440×10^{-4}	-1.1771×10^{-6}	7.1562×10^{-10}
8	1.6873	9.724×10^{-5}	-1.1704×10^{-6}	7.0712×10^{-10}

TABLE 5.21.—GAGE-FACTOR-VERSUS-TEMPERATURE EQUATION FOR DETCBCL GAGE ON IN100 UNDER COMPRESSION

$[GF(T) = a_0 + a_1 \times T + a_2 \times T^2 + a_3 \times T^3.]$

Cycle	a_0	a_1	a_2	a_3
Heating				
1	2.0498	1.447×10^{-4}	-8.2415×10^{-7}	3.5111×10^{-10}
4	2.0800	-1.016×10^{-3}	1.0060×10^{-6}	-4.1136×10^{-10}
5	1.9860	-3.733×10^{-4}	-7.5932×10^{-8}	9.1069×10^{-11}
6	1.9003	-1.804×10^{-4}	-4.1974×10^{-7}	2.5117×10^{-10}
7	1.8923	-1.288×10^{-4}	-6.1983×10^{-7}	3.6517×10^{-10}
8	1.8191	-2.789×10^{-4}	-5.3994×10^{-7}	3.5985×10^{-10}
Cooling				
1	2.0052	-2.1579×10^{-4}	-3.0253×10^{-7}	1.9203×10^{-10}
2	2.0068	-6.4115×10^{-4}	4.4255×10^{-7}	-1.6176×10^{-10}
5	1.9055	-5.8109×10^{-5}	-7.0805×10^{-7}	4.1964×10^{-10}
6	1.8579	-1.1813×10^{-5}	-7.3070×10^{-7}	4.0604×10^{-10}
7	1.8210	-6.2049×10^{-4}	4.0729×10^{-8}	1.6660×10^{-10}
8	1.7982	-7.3916×10^{-4}	2.2393×10^{-7}	6.4192×10^{-11}

TABLE 5.22.—GAGE-FACTOR-VERSUS-TEMPERATURE EQUATION FOR CKA1 GAGE ON TMC UNDER TENSION

$[GF(T) = a_0 + a_1 \times T + a_2 \times T^2 + a_3 \times T^3.]$

Cycle	a_0	a_1	a_2	a_3
Heating				
1	2.532	3.094×10^{-4}	-3.476×10^{-7}	-1.896×10^{-10}
4	2.120	1.710×10^{-3}	-1.982×10^{-6}	4.062×10^{-10}
5	2.065	2.395×10^{-3}	-3.461×10^{-6}	1.215×10^{-9}
6	2.207	2.083×10^{-3}	-3.293×10^{-6}	1.196×10^{-9}
7	2.166	2.777×10^{-3}	-4.554×10^{-6}	1.787×10^{-9}
8	2.377	8.754×10^{-4}	-1.318×10^{-6}	2.808×10^{-10}
Cooling				
1	2.294	-7.010×10^{-4}	1.536×10^{-6}	-9.114×10^{-10}
2	2.229	1.331×10^{-4}	2.230×10^{-7}	-3.923×10^{-10}
5	2.297	4.963×10^{-4}	-9.029×10^{-7}	2.723×10^{-10}
6	2.194	1.167×10^{-3}	-1.848×10^{-6}	6.339×10^{-10}
7	2.218	1.255×10^{-3}	-2.092×10^{-6}	7.997×10^{-10}
8	2.341	2.140×10^{-4}	-5.915×10^{-7}	8.657×10^{-11}

TABLE 5.23.—GAGE-FACTOR-VERSUS-TEMPERATURE EQUATION FOR CKA1 GAGE ON TMC UNDER COMPRESSION

$[GF(T) = a_0 + a_1 \times T + a_2 \times T^2 + a_3 \times T^3.]$

Cycle	a_0	a_1	a_2	a_3
Heating				
1	2.755	-1.814×10^{-3}	2.805×10^{-6}	-1.571×10^{-9}
4	2.296	1.606×10^{-3}	-2.940×10^{-6}	1.099×10^{-9}
5	2.282	1.579×10^{-3}	2.830×10^{-6}	1.005×10^{-9}
6	2.354	7.333×10^{-4}	-1.445×10^{-6}	4.170×10^{-10}
7	2.368	7.382×10^{-4}	-1.470×10^{-6}	4.215×10^{-10}
8	2.702	-1.570×10^{-3}	1.589×10^{-6}	-6.970×10^{-10}
Cooling				
1	2.526	-1.936×10^{-3}	4.077×10^{-6}	-2.426×10^{-9}
2	2.392	-1.246×10^{-4}	4.696×10^{-7}	-6.195×10^{-10}
5	2.320	9.226×10^{-4}	-1.707×10^{-6}	5.042×10^{-10}
6	2.310	1.418×10^{-3}	-2.752×10^{-6}	1.021×10^{-11}
7	2.439	6.746×10^{-4}	-1.460×10^{-6}	4.184×10^{-10}
8	2.457	5.703×10^{-4}	-1.330×10^{-6}	3.654×10^{-10}

TABLE 5.24.—GAGE-FACTOR-VERSUS-TEMPERATURE EQUATION FOR PdCr GAGE ON TMC UNDER TENSION

$[GF(T) = a_0 + a_1 \times T + a_2 \times T^2 + a_3 \times T^3.]$

Cycle	a_0	a_1	a_2	a_3
Heating				
1	1.657	2.713×10^{-4}	-9.198×10^{-7}	4.339×10^{-10}
4	1.633	1.653×10^{-4}	-8.860×10^{-7}	4.931×10^{-10}
5	1.516	1.675×10^{-3}	-3.692×10^{-6}	1.894×10^{-9}
6	1.492	1.850×10^{-3}	-3.922×10^{-6}	1.959×10^{-9}
7	1.658	2.786×10^{-4}	-1.334×10^{-8}	9.420×10^{-11}
8	1.501	2.259×10^{-3}	-4.297×10^{-6}	1.978×10^{-9}
Cooling				
1	1.701	-4.542×10^{-4}	-4.678×10^{-7}	2.557×10^{-10}
2	1.596	3.165×10^{-4}	-1.002×10^{-6}	5.082×10^{-10}
5	1.497	2.195×10^{-4}	-4.576×10^{-6}	2.273×10^{-9}
6	1.559	1.795×10^{-4}	-3.867×10^{-6}	1.923×10^{-9}
7	1.641	9.093×10^{-4}	-1.850×10^{-6}	7.828×10^{-10}
8	1.609	2.042×10^{-4}	-4.122×10^{-6}	1.938×10^{-9}

TABLE 5.25.—GAGE-FACTOR-VERSUS-TEMPERATURE EQUATION FOR PdCr GAGE ON TMC UNDER COMPRESSION

$[GF(T) = a_0 + a_1 \times T + a_2 \times T^2 + a_3 \times T^3.]$

Cycle	a_0	a_1	a_2	a_3
Heating				
1	1.637	2.155×10^{-3}	-6.727×10^{-7}	1.814×10^{-10}
4	1.661	2.613×10^{-4}	1.026×10^{-7}	-1.463×10^{-10}
5	1.650	1.961×10^{-4}	-6.744×10^{-7}	1.971×10^{-10}
6	1.637	2.238×10^{-4}	-7.501×10^{-7}	2.530×10^{-10}
7	1.476	2.345×10^{-3}	-4.656×10^{-6}	2.127×10^{-9}
8	1.574	2.170×10^{-3}	-4.183×10^{-6}	1.827×10^{-9}
Cooling				
1	1.678	9.347×10^{-4}	6.010×10^{-7}	-3.964×10^{-10}
2	1.681	3.821×10^{-4}	9.110×10^{-7}	-5.185×10^{-10}
5	1.598	4.877×10^{-5}	-4.737×10^{-7}	1.548×10^{-10}
6	1.626	4.338×10^{-5}	-5.492×10^{-7}	1.785×10^{-10}
7	1.428	-1.023×10^{-3}	-5.672×10^{-6}	2.524×10^{-9}
8	1.596	2.011×10^{-3}	-3.313×10^{-6}	1.477×10^{-9}

TABLE 5.26—GAGE-FACTOR-VERSUS-TEMPERATURE EQUATION FOR DETCBCL GAGE ON TMC UNDER TENSION

$[GF(T) = a_0 + a_1 \times T + a_2 \times T^2 + a_3 \times T^3.]$

Cycle	a_0	a_1	a_2	a_3
Heating				
1	2.121	1.257×10^{-3}	-2.016×10^{-6}	7.771×10^{-10}
4	2.013	7.306×10^{-4}	-1.782×10^{-6}	9.053×10^{-10}
5	2.051	5.165×10^{-4}	-1.739×10^{-6}	1.004×10^{-9}
6	1.955	1.240×10^{-3}	-2.851×10^{-6}	1.481×10^{-9}
7	2.048	2.658×10^{-4}	-1.568×10^{-6}	1.113×10^{9}
8	2.048	1.352×10^{-3}	-3.308×10^{-6}	1.809×10^{-9}
Cooling				
1	2.021	6.961×10^{-4}	-1.368×10^{-6}	6.996×10^{-10}
2	1.998	7.782×10^{-4}	-1.356×10^{-6}	5.179×10^{-10}
5	1.874	1.916×10^{-3}	-3.239×10^{-6}	1.412×10^{-9}
6	1.936	1.338×10^{-3}	-2.292×10^{-6}	1.010×10^{-9}
7	2.000	1.527×10^{-3}	-2.949×10^{-6}	1.466×10^{-9}
8	1.943	2.527×10^{-3}	-4.554×10^{-6}	2.148×10^{-9}

TABLE 5.27—GAGE-FACTOR-VERSUS-TEMPERATURE EQUATION FOR DETCBCL GAGE ON TMC UNDER COMPRESSION

$[GF(T) = a_0 + a_1 \times T + a_2 \times T^2 + a_3 \times T^3.]$

Cycle	a_0	a_1	a_2	a_3
Heating				
1	2.155	2.927×10^{-4}	1.471×10^{-6}	-1.104×10^{-9}
4	2.348	-2.287×10^{-3}	3.801×10^{-6}	-1.860×10^{-9}
5	2.249	-7.114×10^{-4}	9.508×10^{-7}	-4.962×10^{-10}
6	2.367	-1.724×10^{-3}	2.278×10^{-6}	-9.653×10^{-10}
7	2.305	1.605×10^{-4}	-9.796×10^{-7}	4.825×10^{-10}
8	2.396	-9.409×10^{-4}	8.931×10^{-7}	-3.084×10^{-10}
Cooling				
1	2.126	7.513×10^{-4}	-2.031×10^{-6}	1.095×10^{-9}
2	2.025	2.980×10^{-3}	-7.221×10^{-6}	3.873×10^{-9}
5	2.056	2.367×10^{-3}	-5.332×10^{-6}	2.565×10^{-9}
6	2.106	1.953×10^{-3}	-4.641×10^{-6}	2.265×10^{-9}
7	2.406	-6.530×10^{-4}	-5.857×10^{-6}	2.172×10^{-10}
8	2.389	-1.729×10^{-4}	-1.195×10^{-6}	7.745×10^{-10}

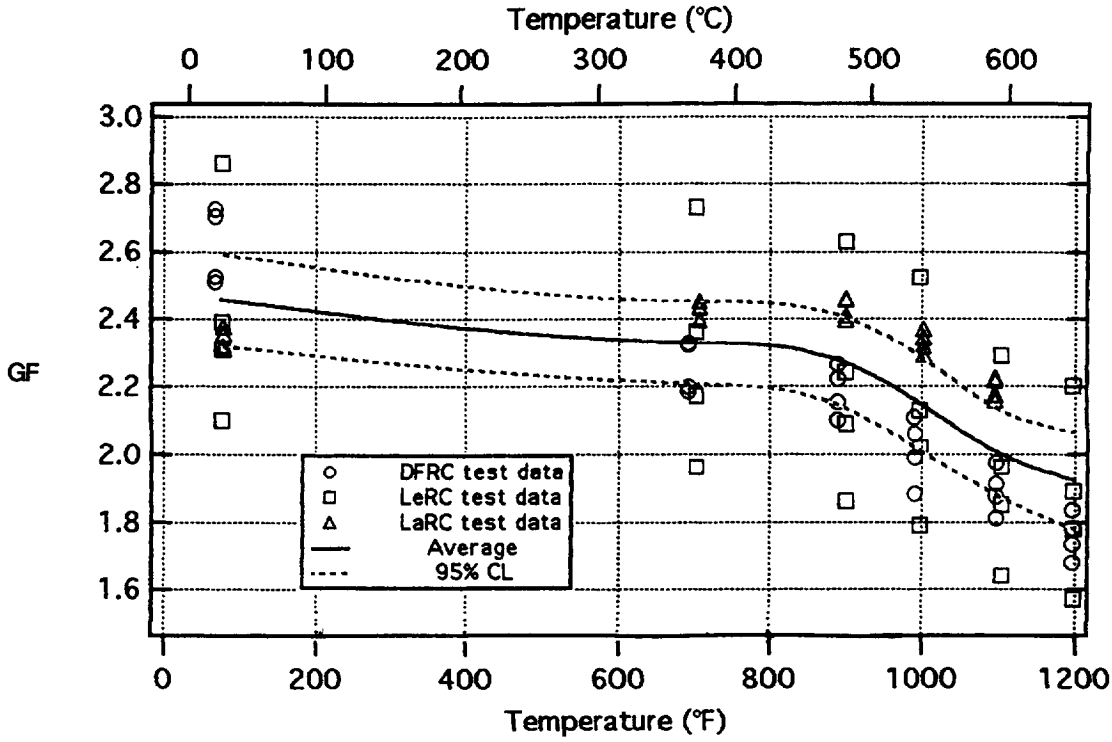

Figure 5.115.—Twelve CKA1 gages on IN100 under tension—cycle 1 heating to 1200 °F (648 °C).

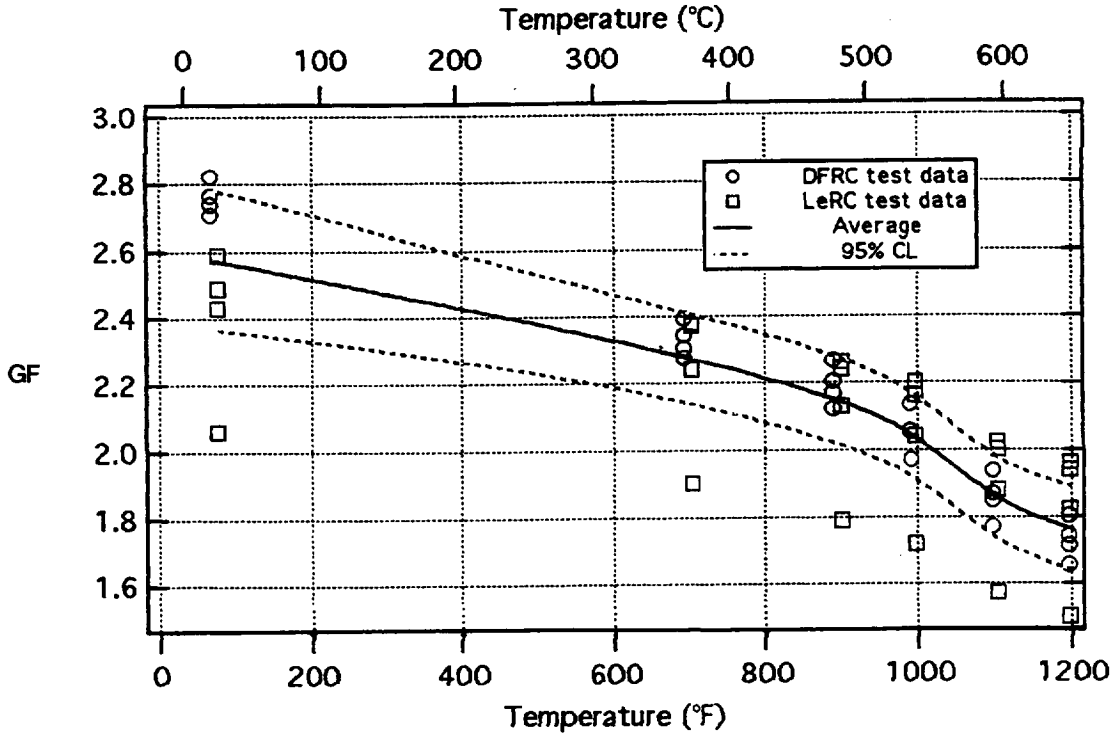

Figure 5.116.—Eight CKA1 gages on IN100 under compression—cycle 1 heating to 1200 °F (648 °C).

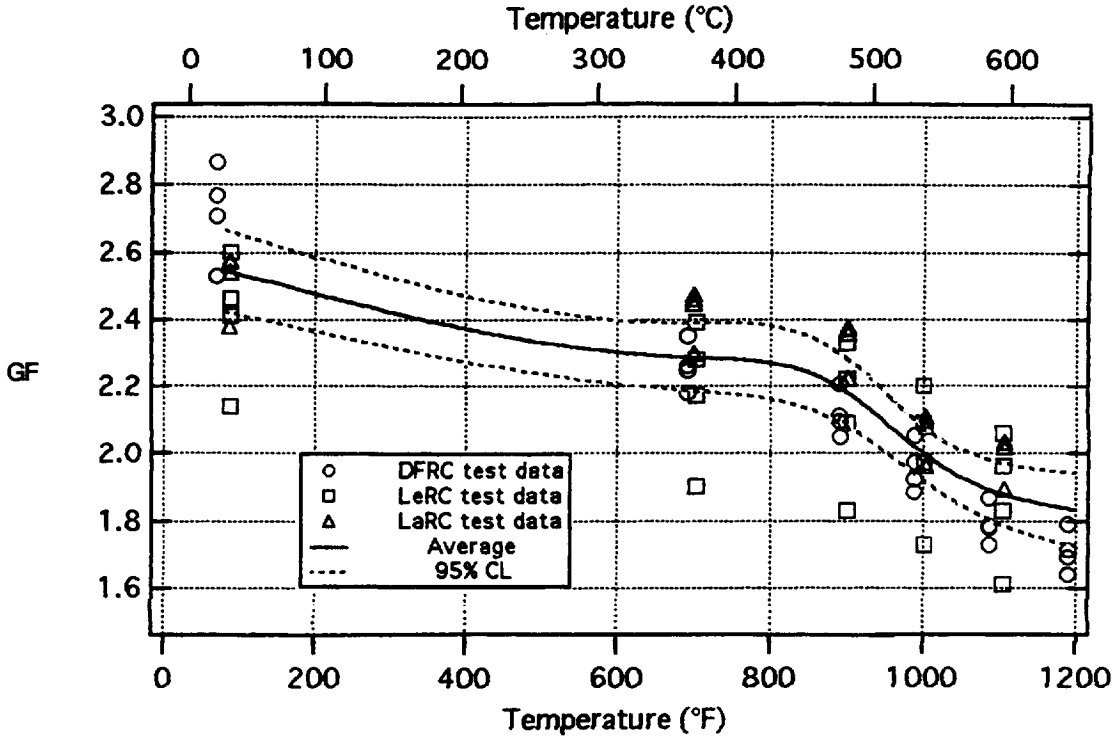

Figure 5.117.—Twelve CKA1 gages on IN100 under tension—cycle 4 heating to 1200 °F (648 °C).

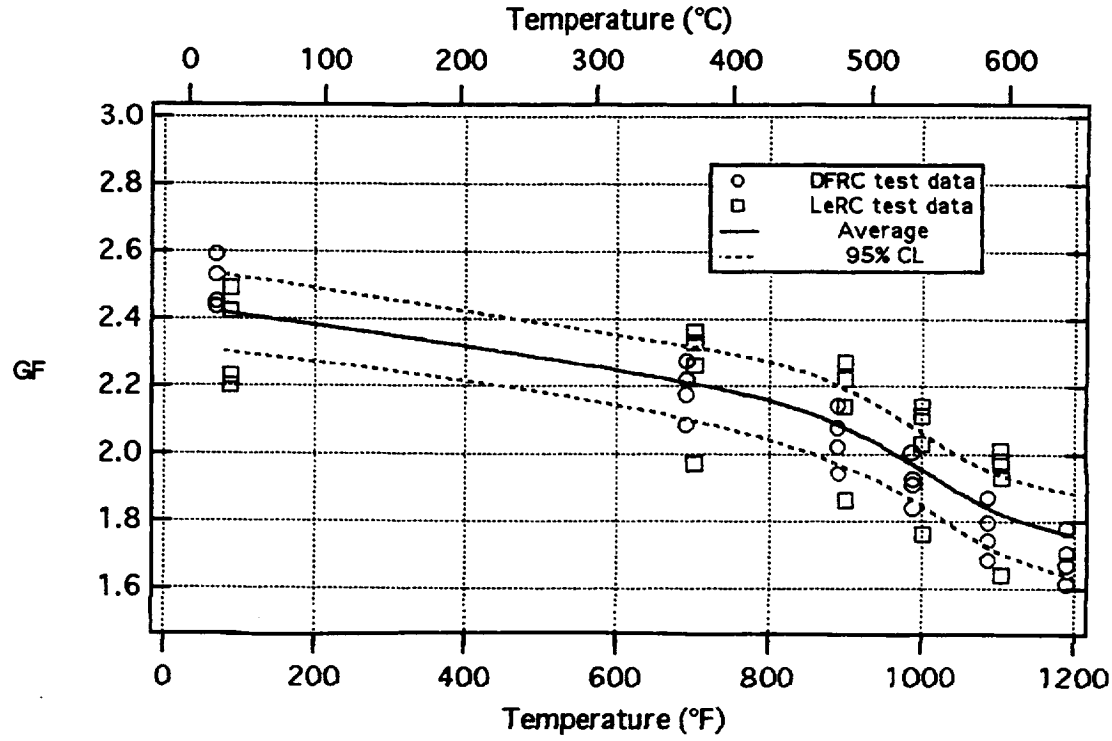

Figure 5.118.—Eight CKA1 gages on IN100 under compression—cycle 4 heating to 1200 °F (648 °C).

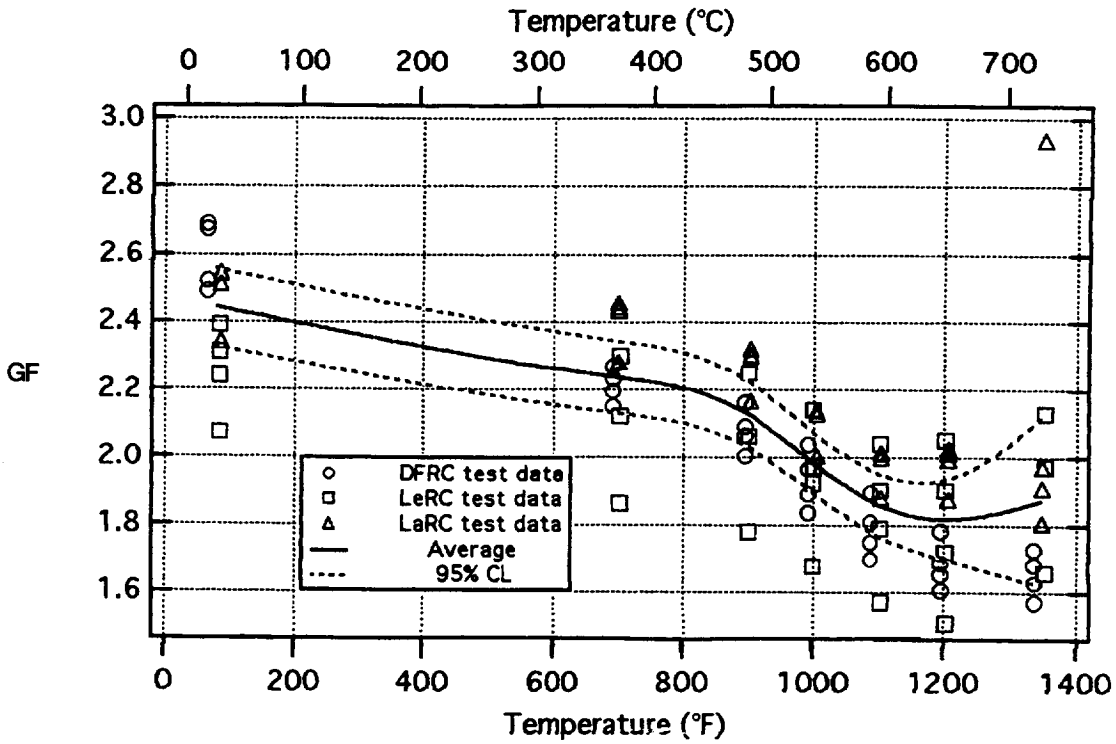

Figure 5.119.—Twelve CKA1 gages on IN100 under tension—cycle 5 heating to 1350 °F (732 °C).

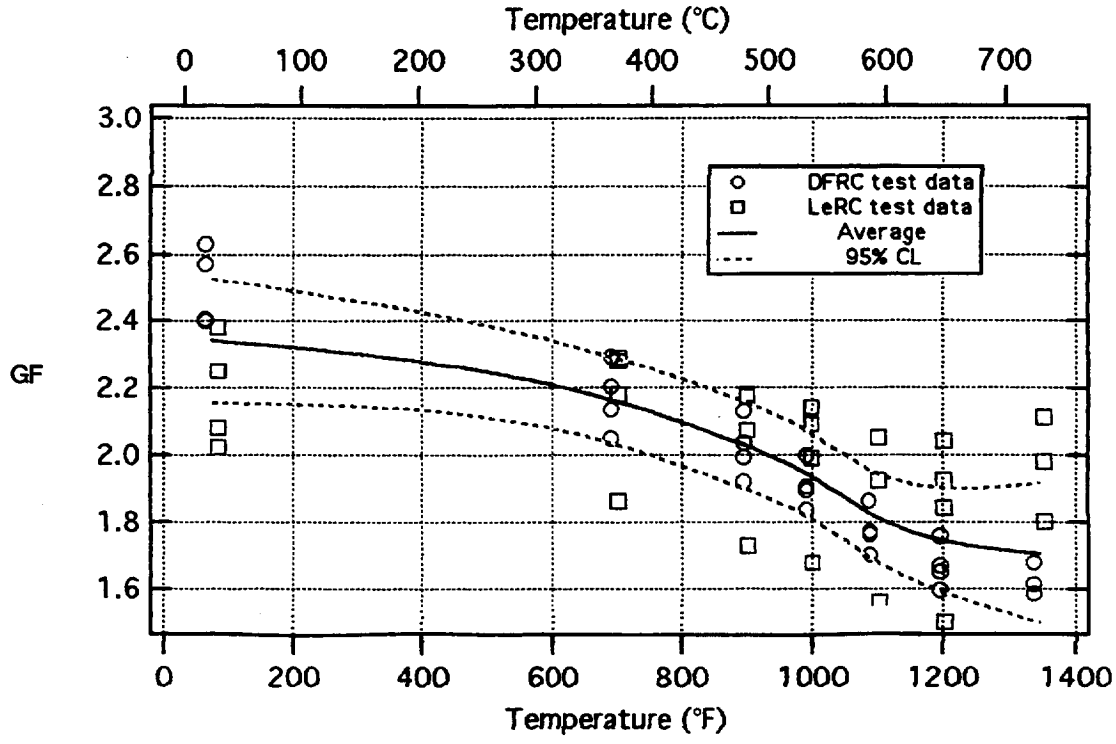

Figure 5.120.—Eight CKA1 gages on IN100 under compression—cycle 5 heating to 1350 °F (732 °C).

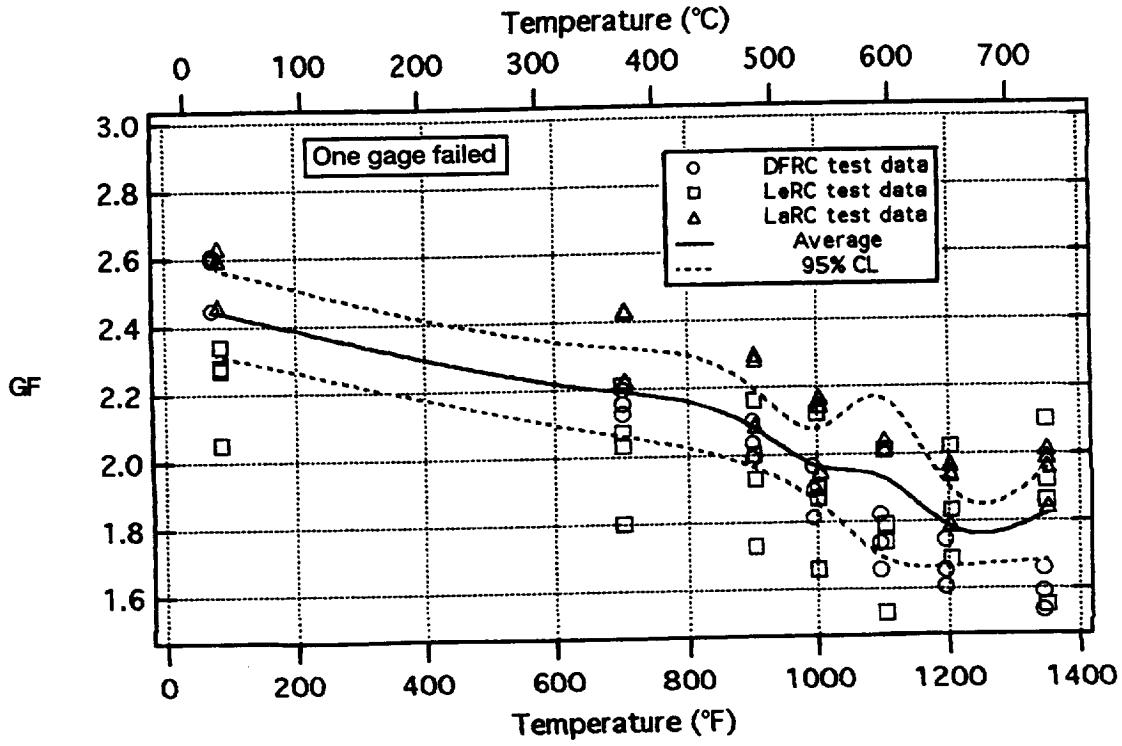

Figure 5.121.—Twelve CKA1 gages on IN100 under tension—cycle 6 heating to 1350 °F (732 °C).

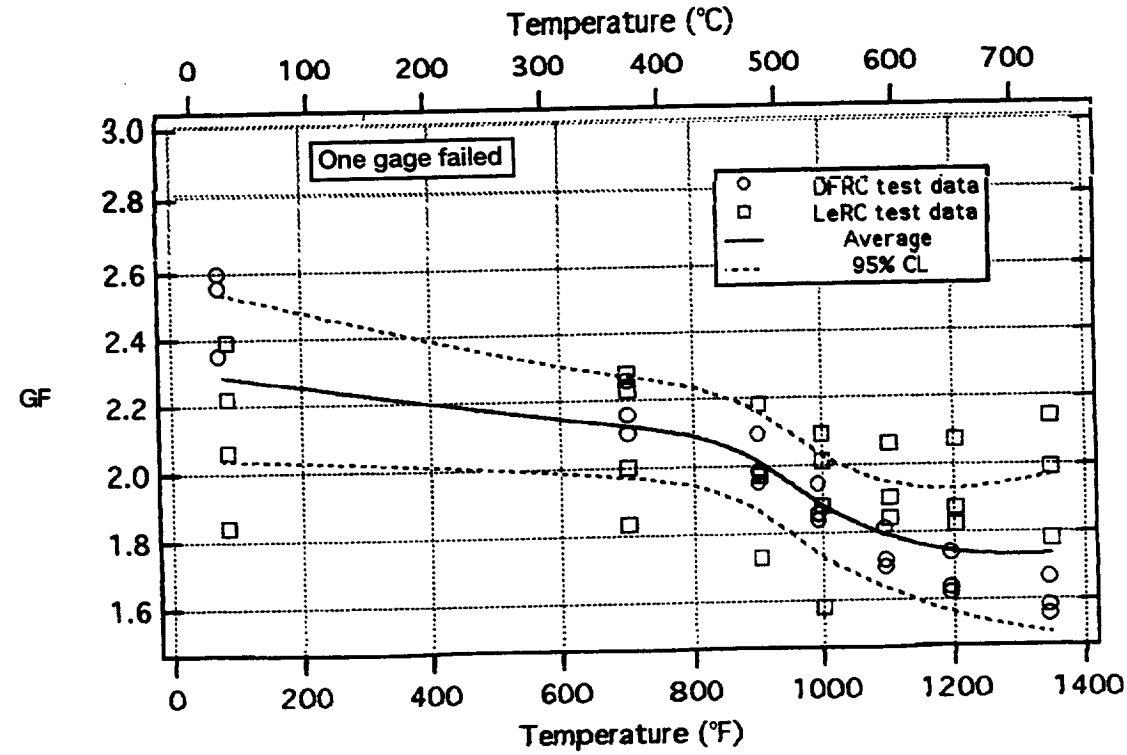

Figure 5.122.—Eight CKA1 gages on IN100 under compression—cycle 6 heating to 1350 °F (732 °C).

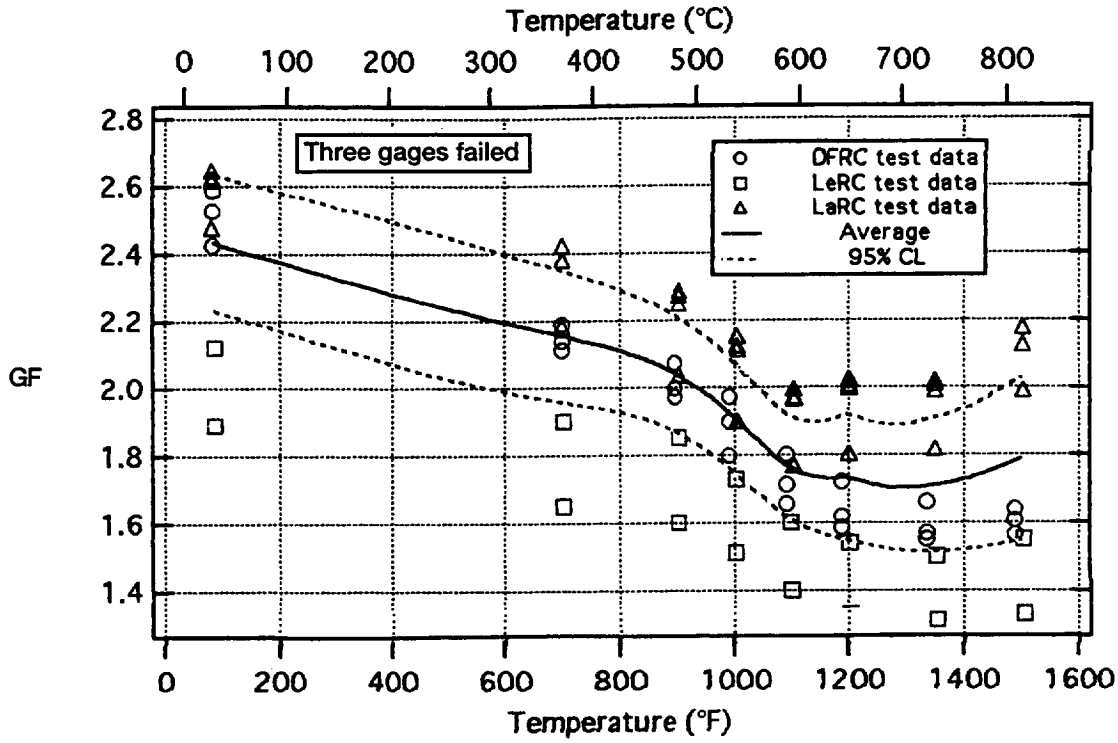

Figure 5.123.—Twelve CKA1 gages on IN100 under tension—cycle 7 heating to 1500 °F (816 °C).

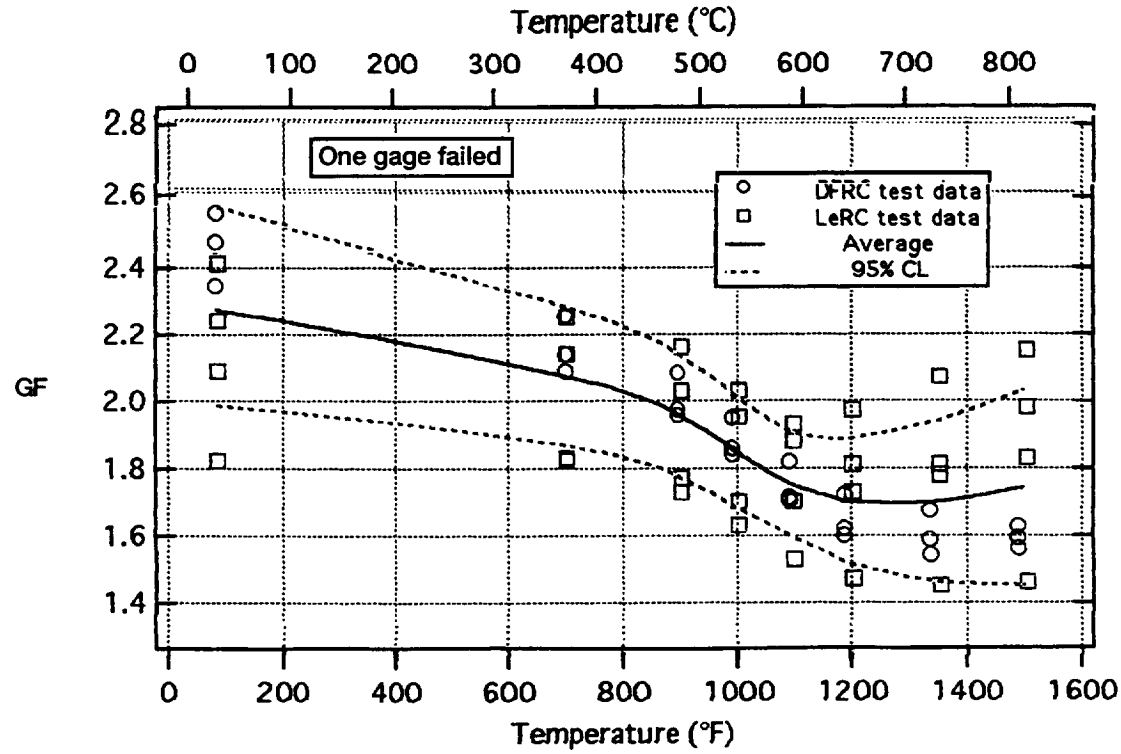

Figure 5.124.—Eight CKA1 gages on IN100 under compression—cycle 7 heating to 1500 °F (816 °C).

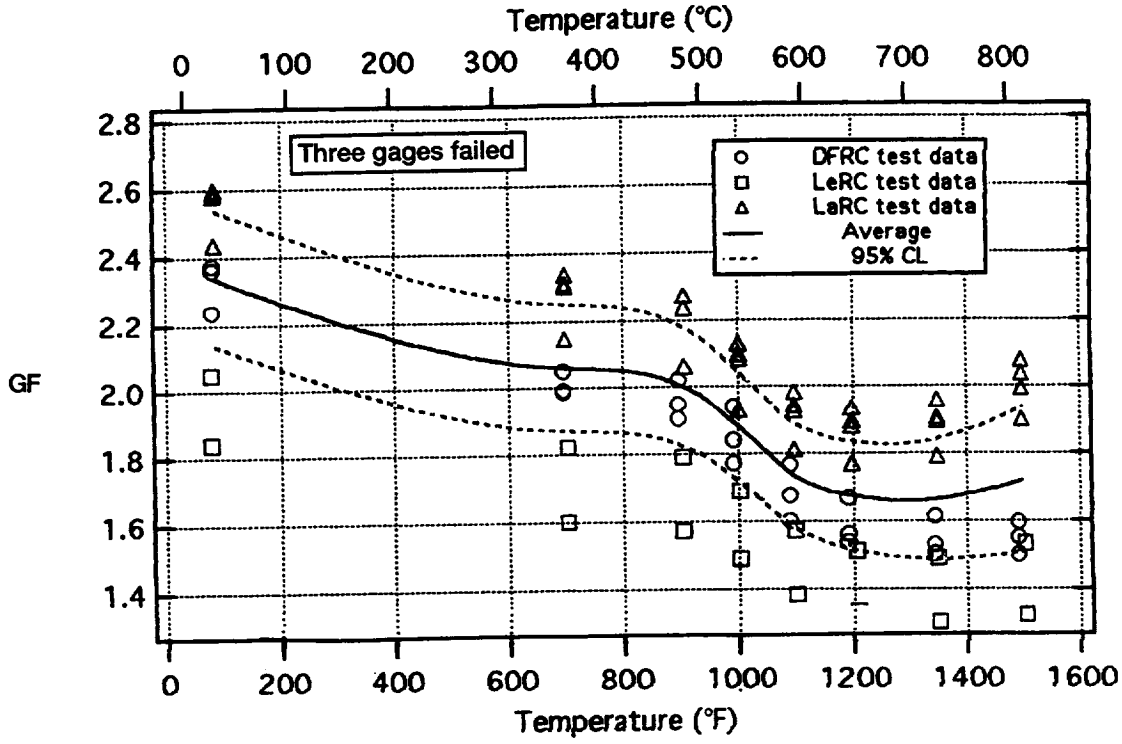

Figure 5.125.—Twelve CKA1 gages on IN100 under tension—cycle 8 heating to 1500 °F (816 °C).

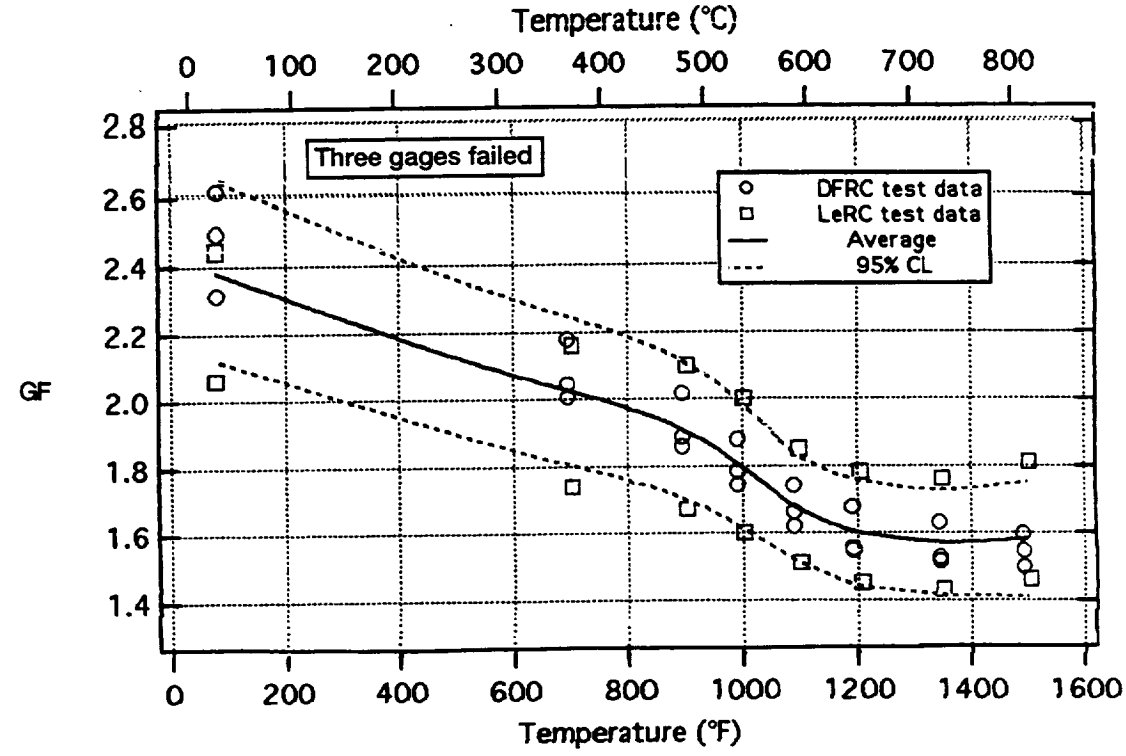

Figure 5.126.—Eight CKA1 gages on IN100 under compression—cycle 8 heating to 1500 °F (816 °C).

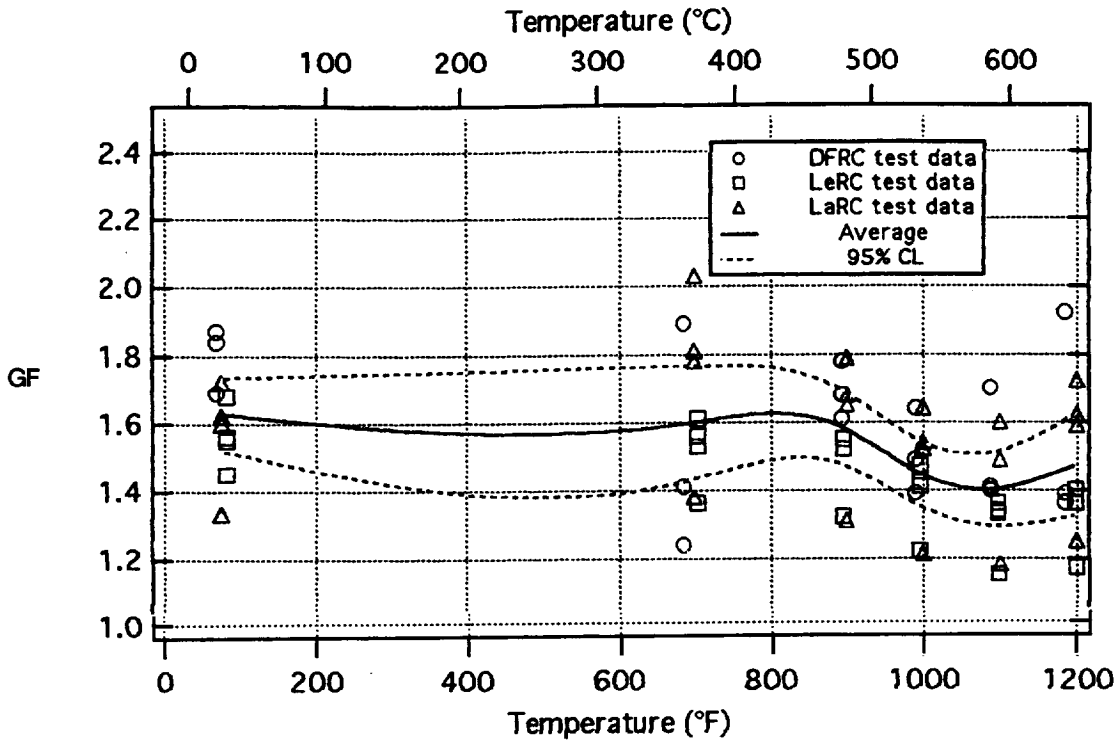

Figure 5.127.—Twelve PdCr gages on IN100 under tension—cycle 1 heating to 1200 °F (648 °C).

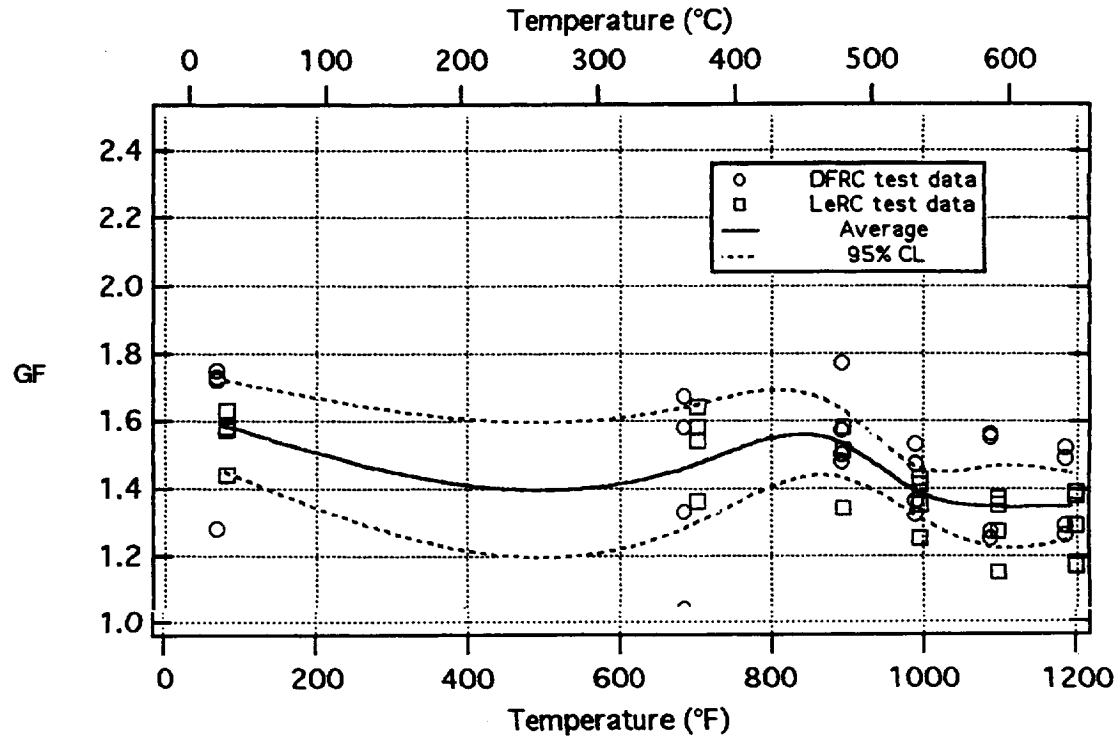

Figure 5.128.—Eight PdCr gages on IN100 under compression—cycle 1 heating to 1200 °F (648 °C).

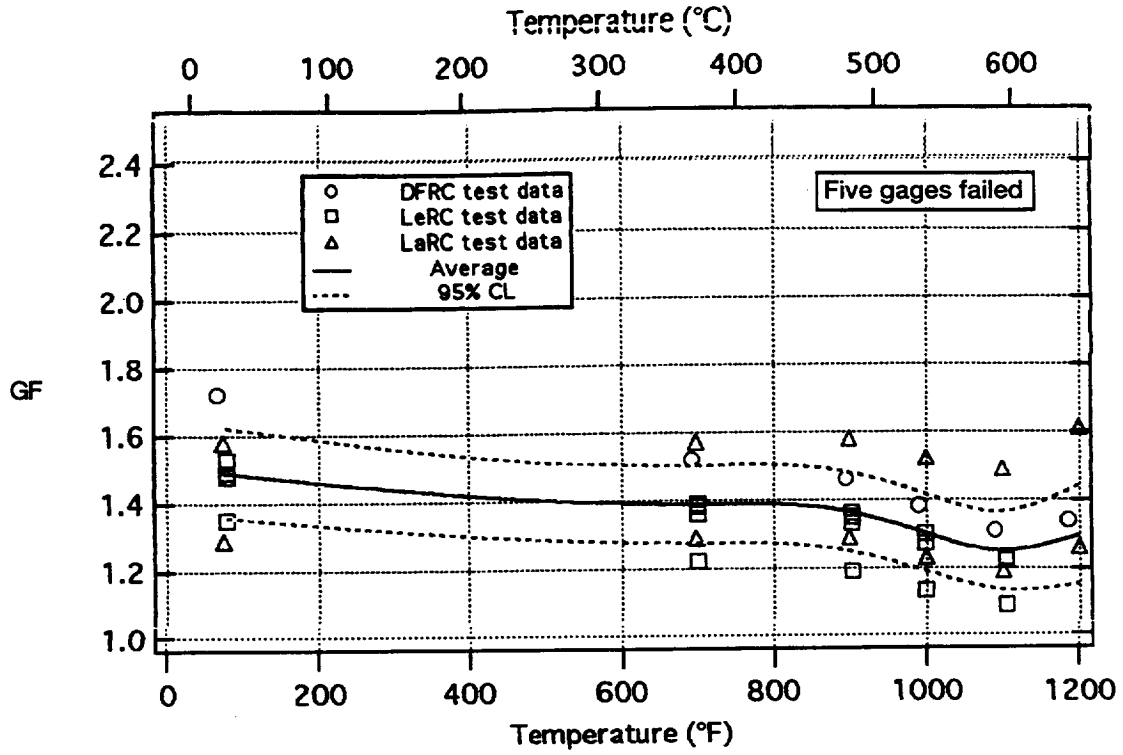

Figure 5.129.—Twelve PdCr gages on IN100 under tension—cycle 4 heating to 1200 °F (648 °C).

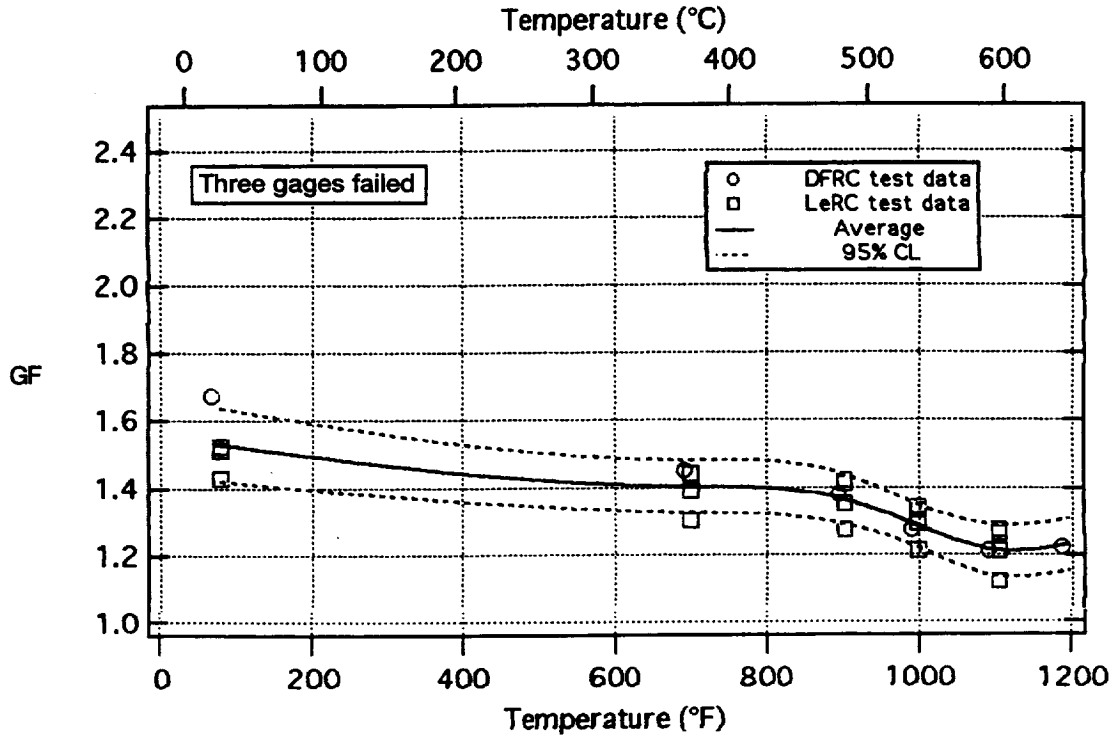

Figure 5.130.—Eight PdCr gages on IN100 under compression—cycle 4 heating to 1200 °F (648 °C).

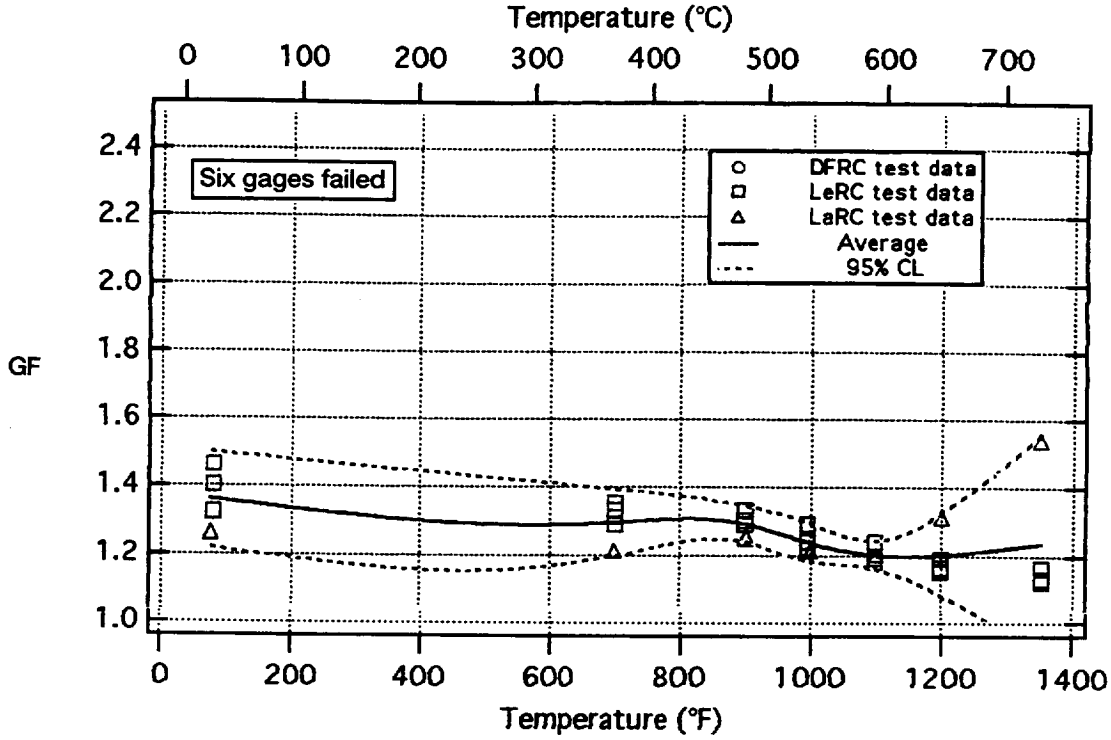

Figure 5.131.—Twelve PdCr gages on IN100 under tension—cycle 5 heating to 1350 °F (732 °C).

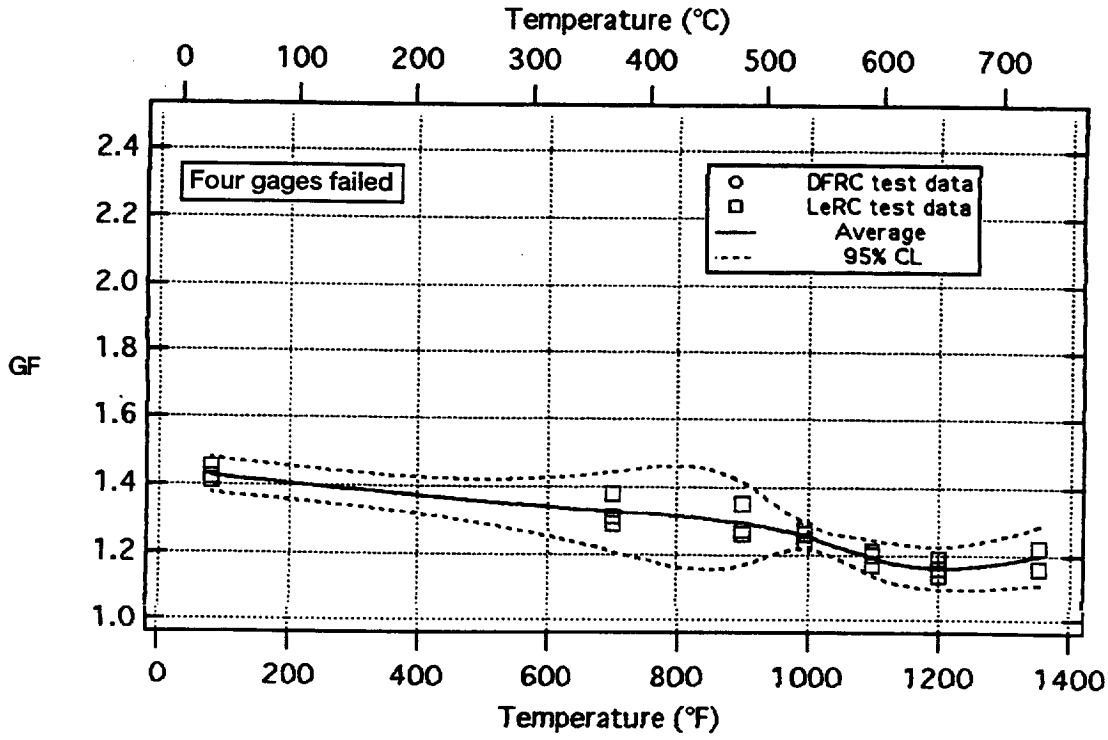

Figure 5.132.—Eight PdCr gages on IN100 under compression—cycle 5 heating to 1350 °F (732 °C).

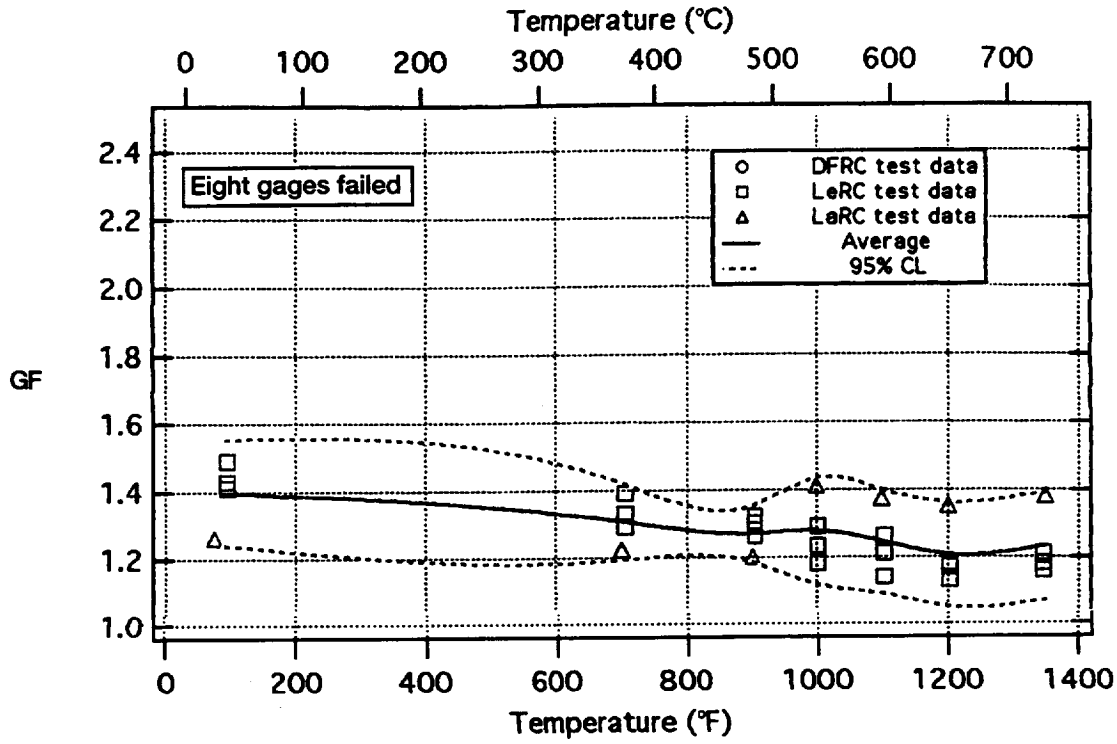

Figure 5.133.—Twelve PdCr gages on IN100 under tension—cycle 6 heating to 1350 °F (732 °C).

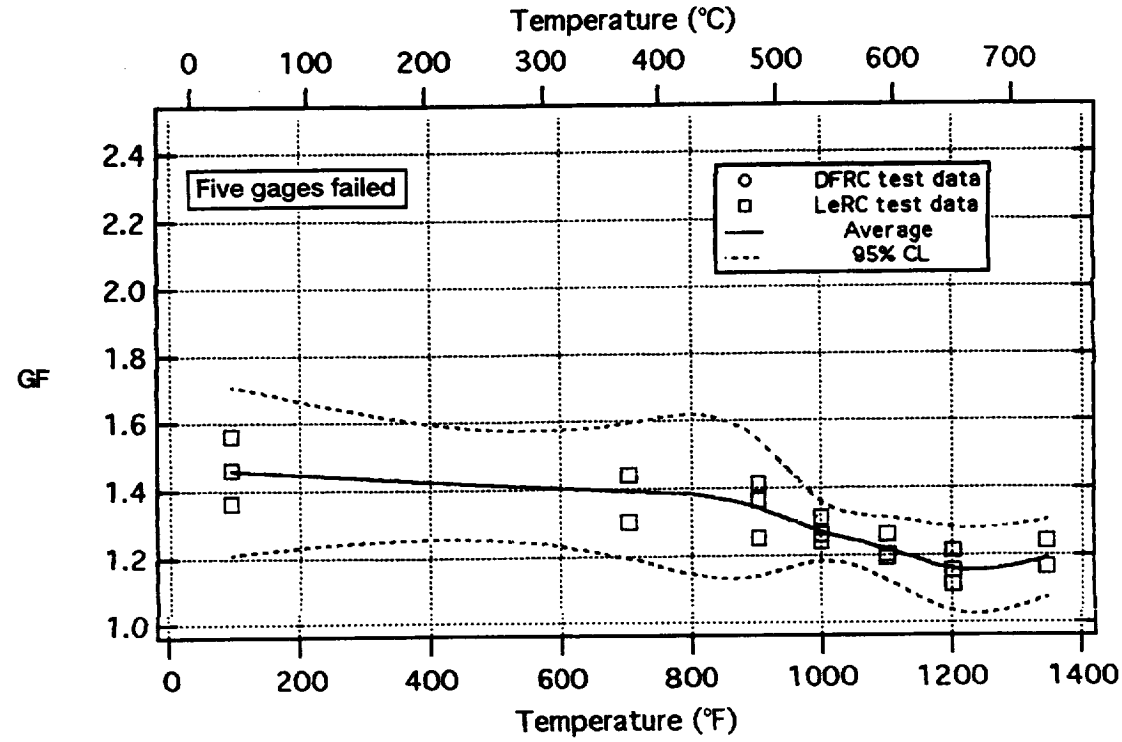

Figure 5.134.—Eight PdCr gages on IN100 under compression—cycle 6 heating to 1350 °F (732 °C).

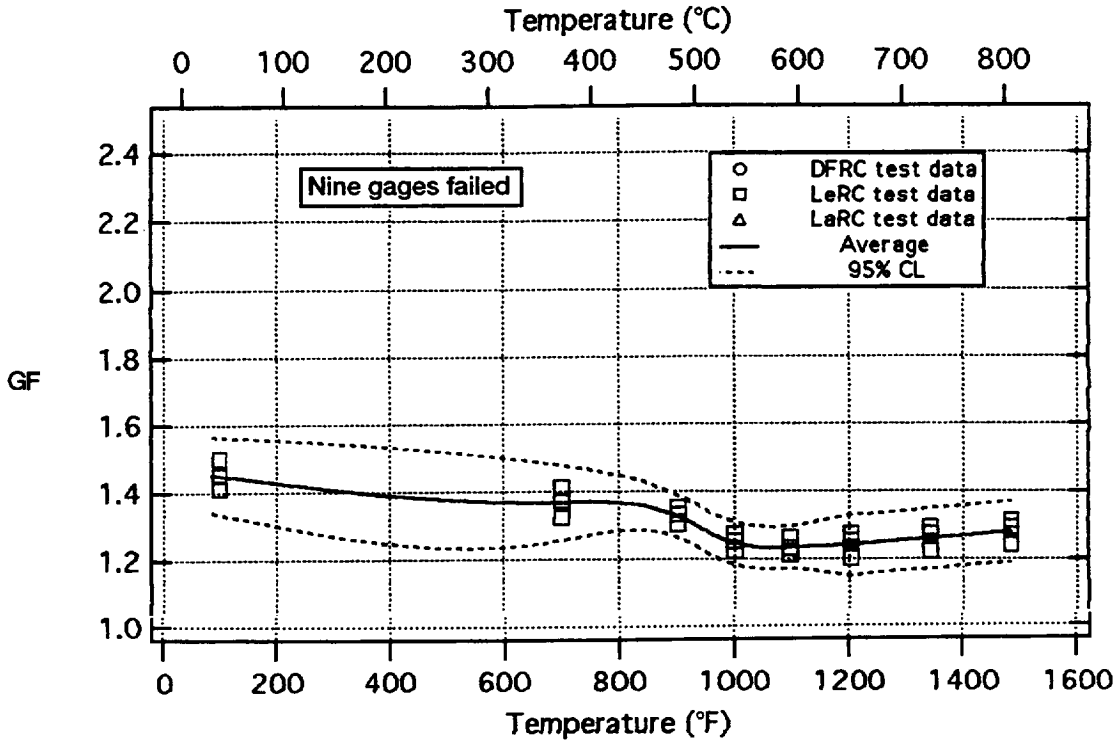

Figure 5.135.—Twelve PdCr gages on IN100 under tension—cycle 7 heating to 1500 °F (816 °C).

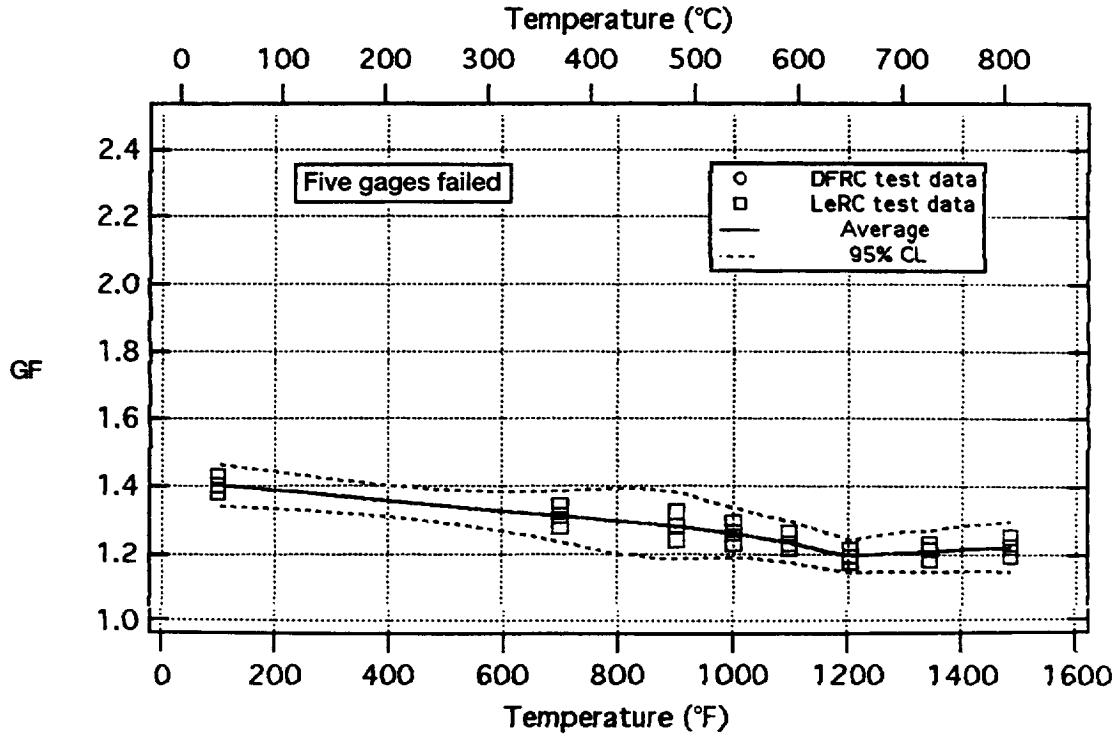

Figure 5.136.—Eight PdCr gages on IN100 under compression—cycle 7 heating to 1500 °F (816 °C).

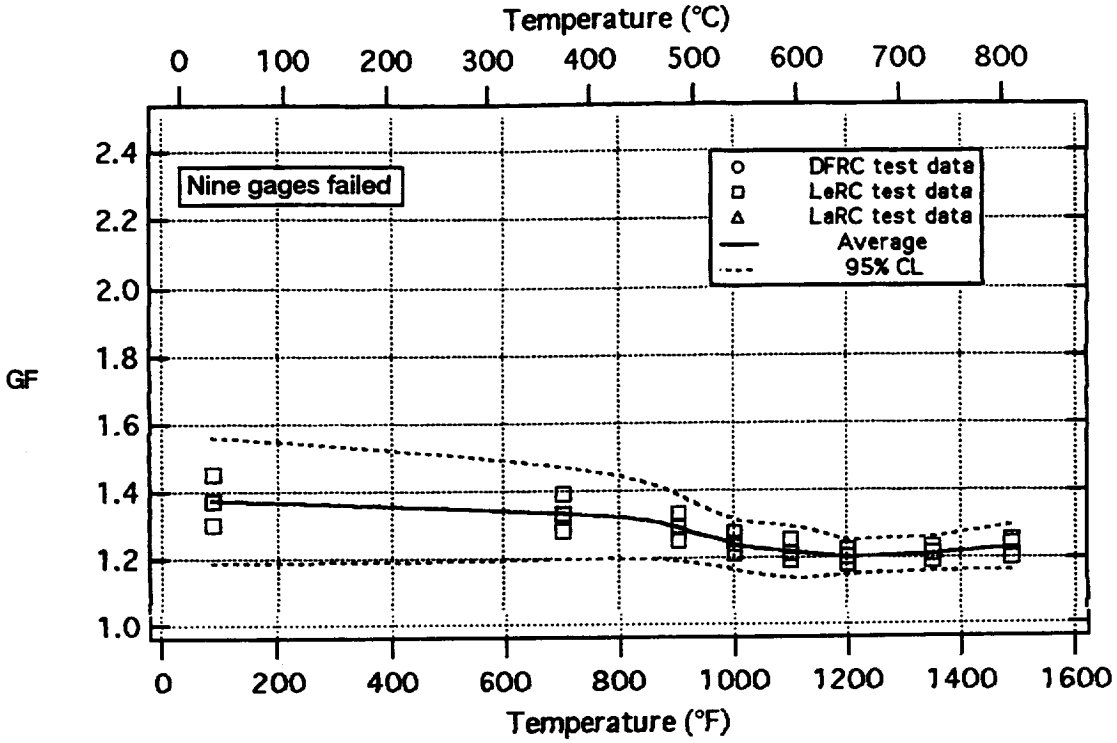

Figure 5.137.—Twelve PdCr gages on IN100 under tension—cycle 8 heating to 1500 °F (816 °C).

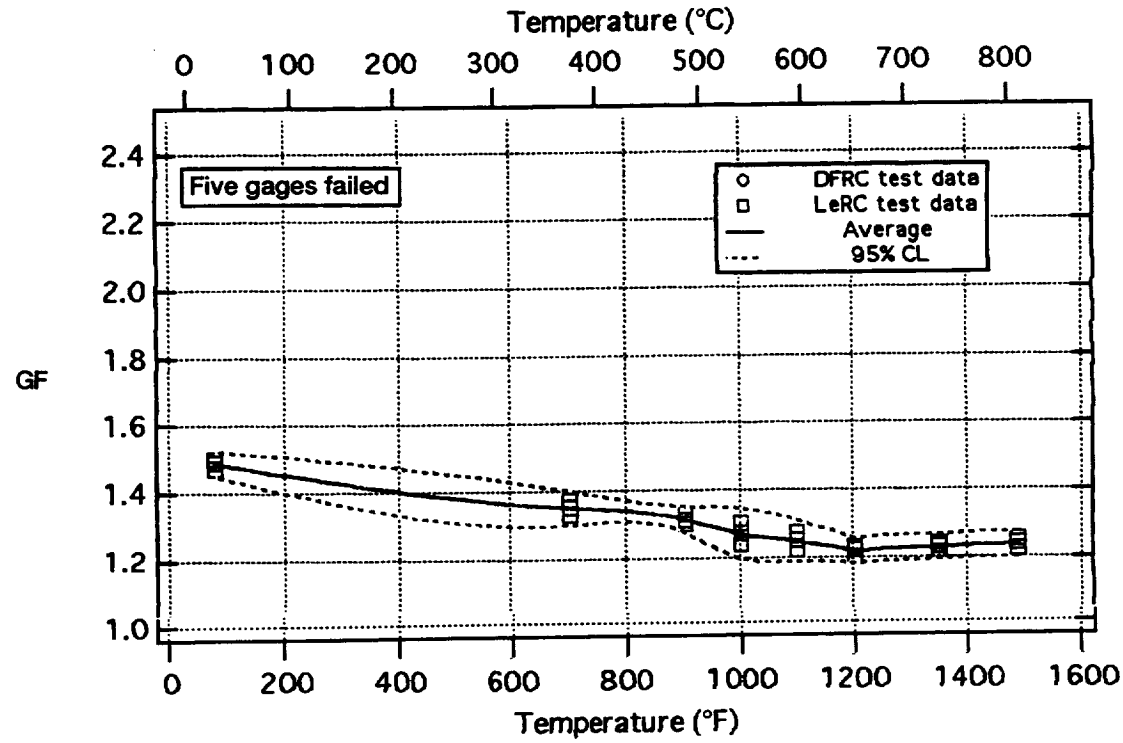

Figure 5.138.—Eight PdCr gages on IN100 under compression—cycle 8 heating to 1500 °F (816 °C).

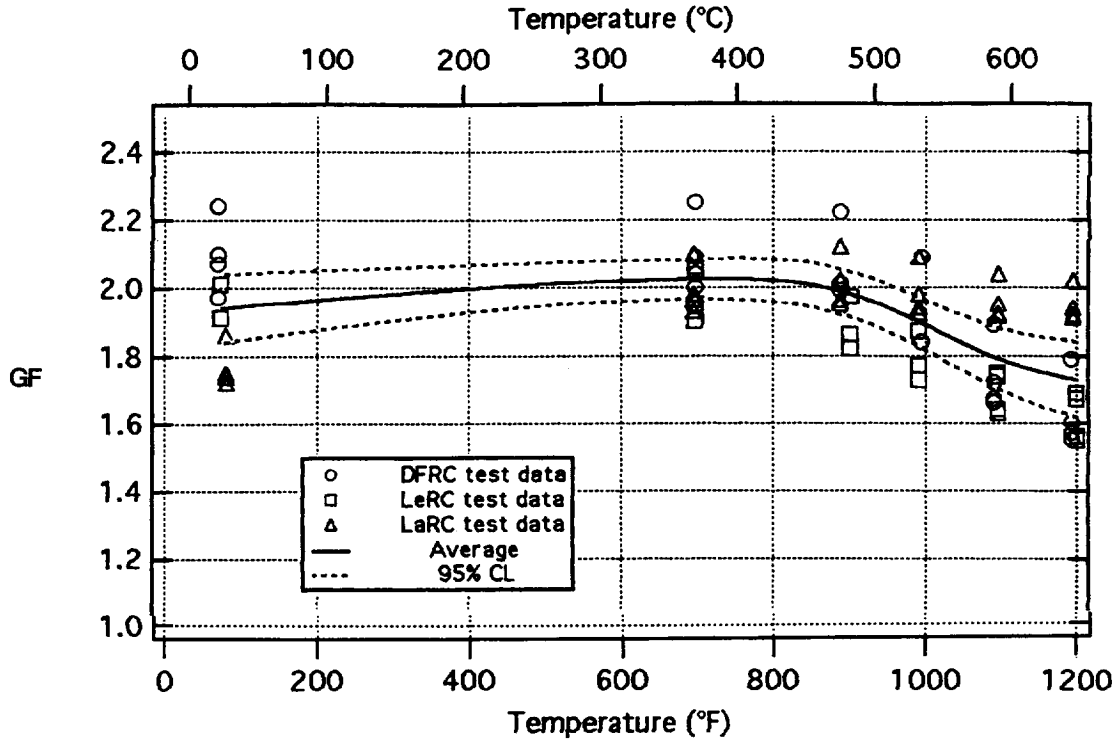

Figure 5.139.—Twelve DETCBCL gages on IN100 under tension—cycle 1 heating to 1200 °F (648 °C).

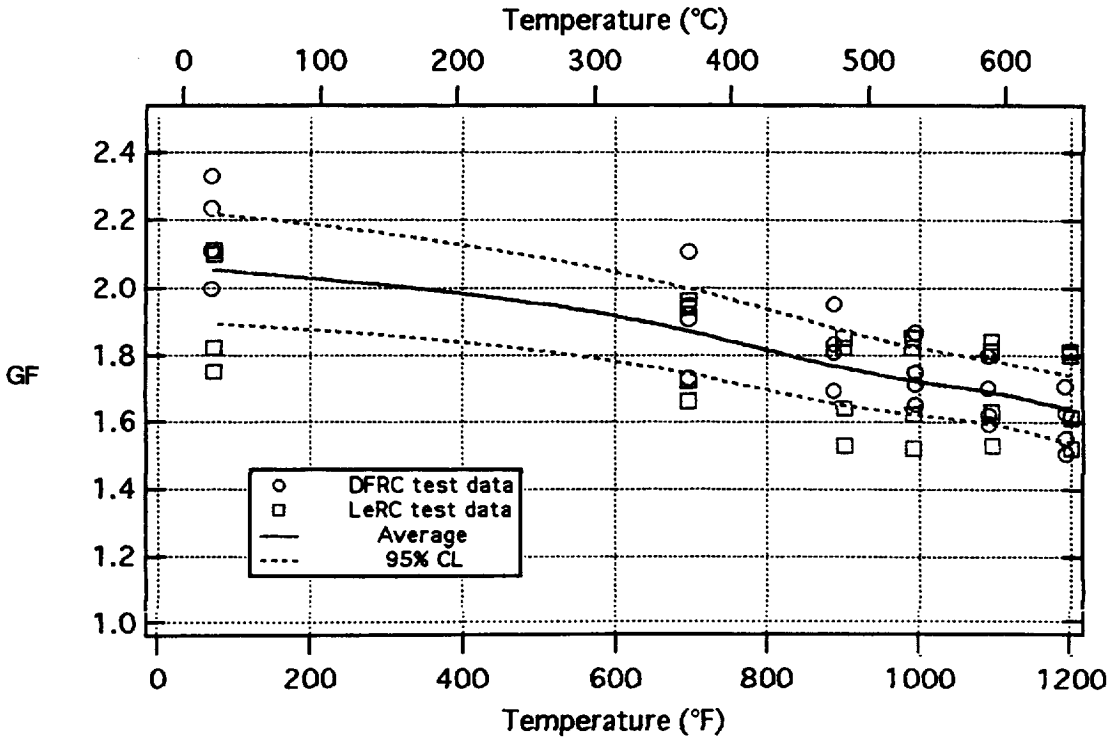

Figure 5.140.—Eight DETCBCL gages on IN100 under compression—cycle 1 heating to 1200 °F (648 °C).

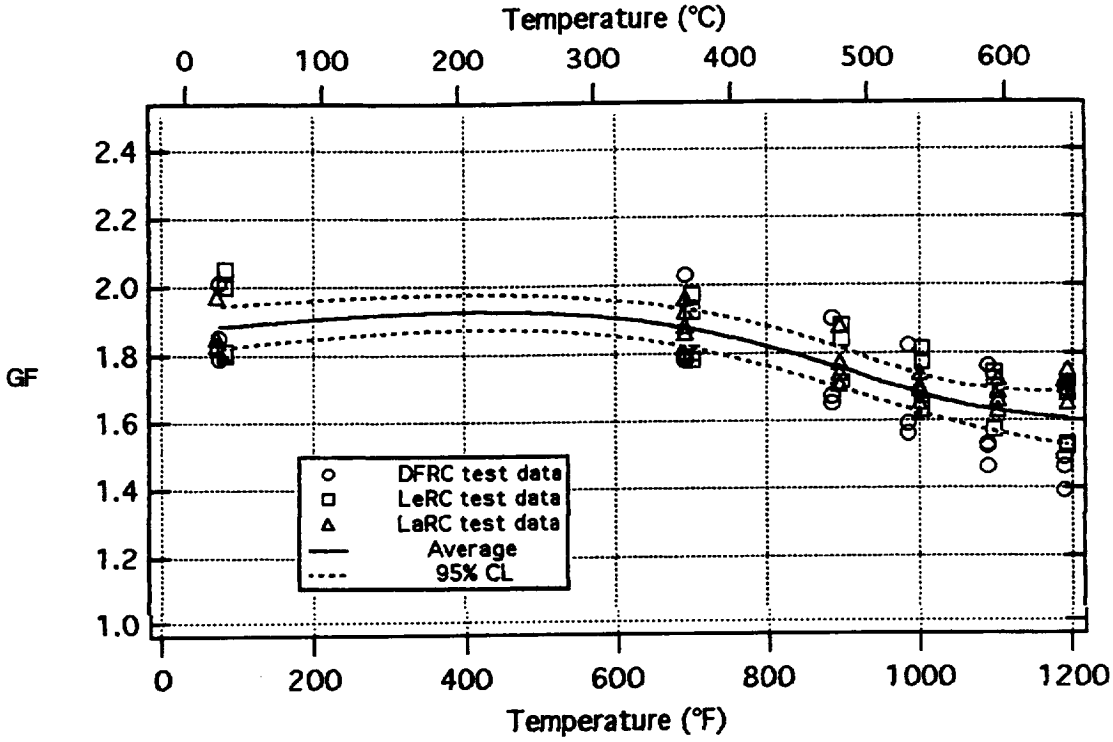

Figure 5.141.—Twelve DETCBCL gages on IN100 under tension—cycle 4 heating to 1200 °F (648 °C).

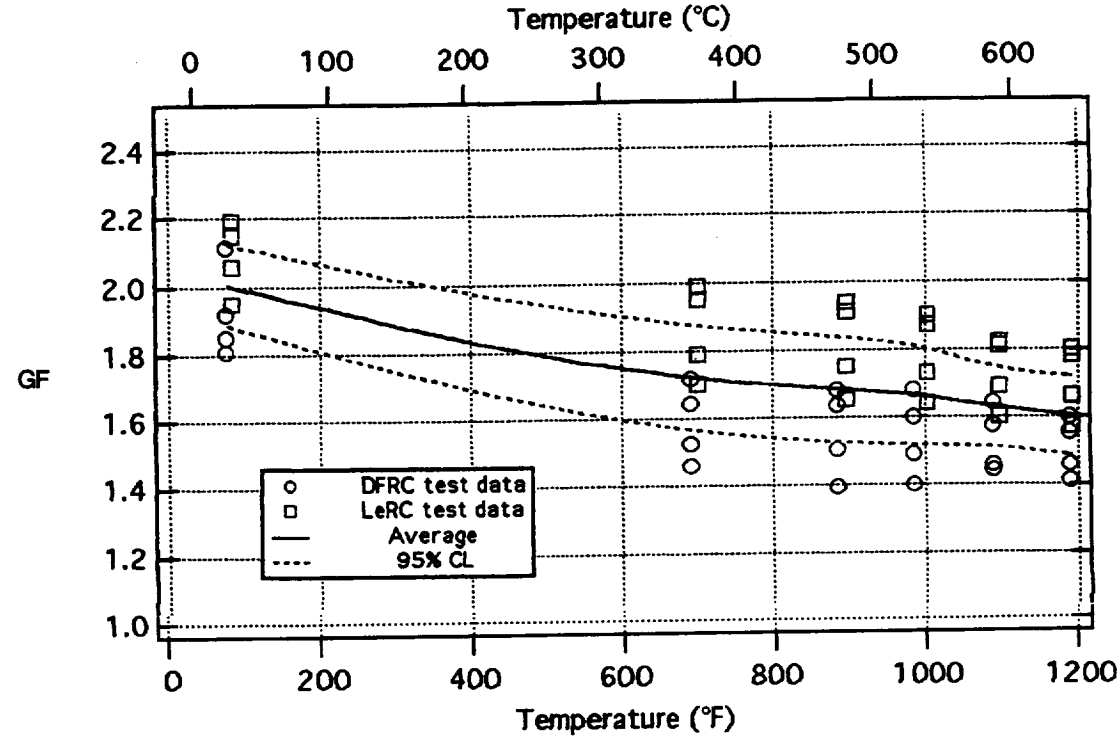

Figure 5.142.—Eight DETCBCL gages on IN100 under compression—cycle 4 heating to 1200 °F (648 °C).

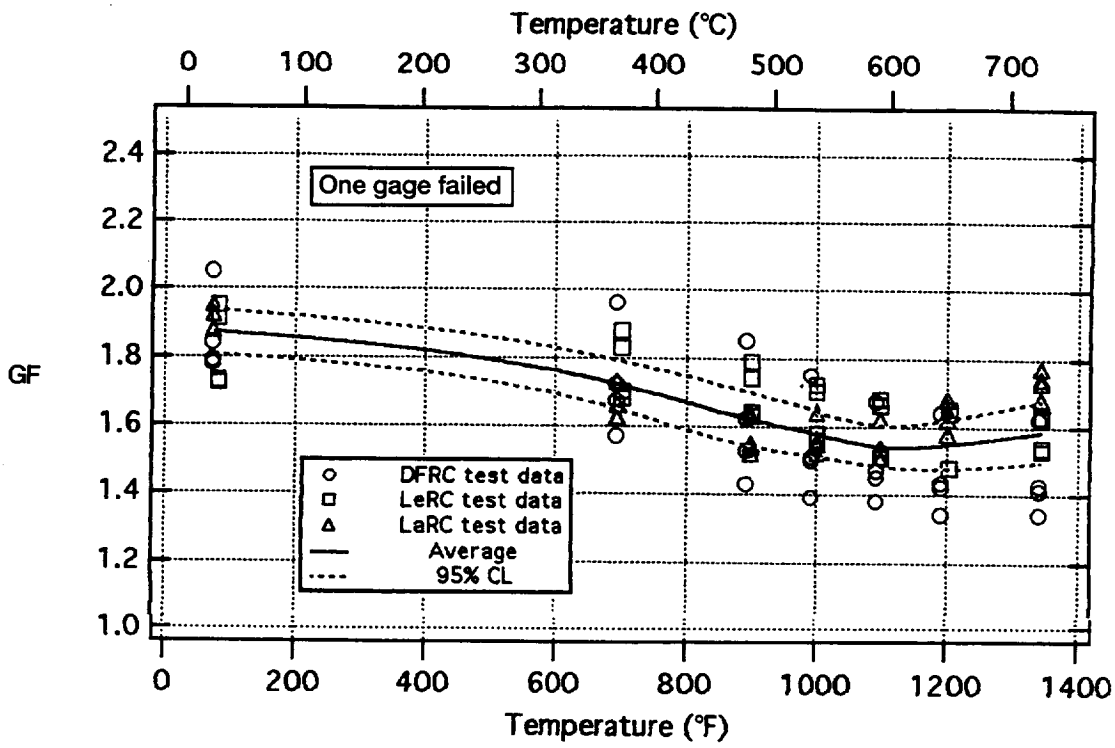

Figure 5.143.—Twelve DETCBCL gages on IN100 under tension—cycle 5 heating to 1350 °F (732 °C).

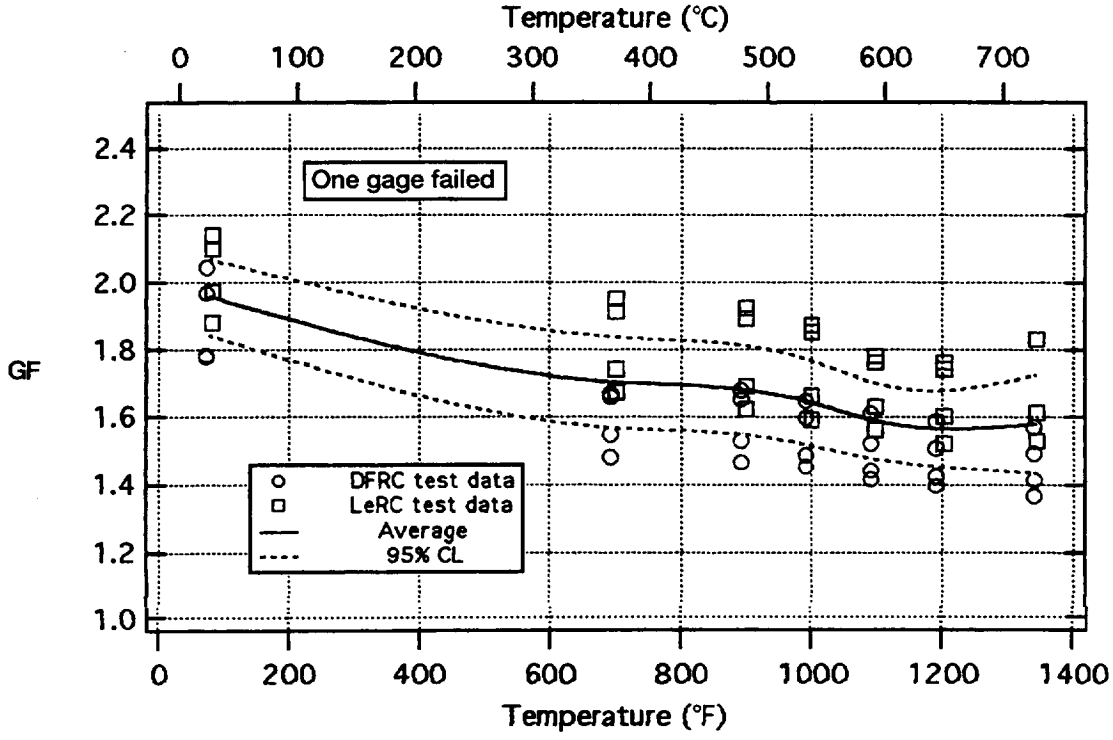

Figure 5.144.—Eight DETCBCL gages on IN100 under compression—cycle 5 heating to 1350 °F (732 °C).

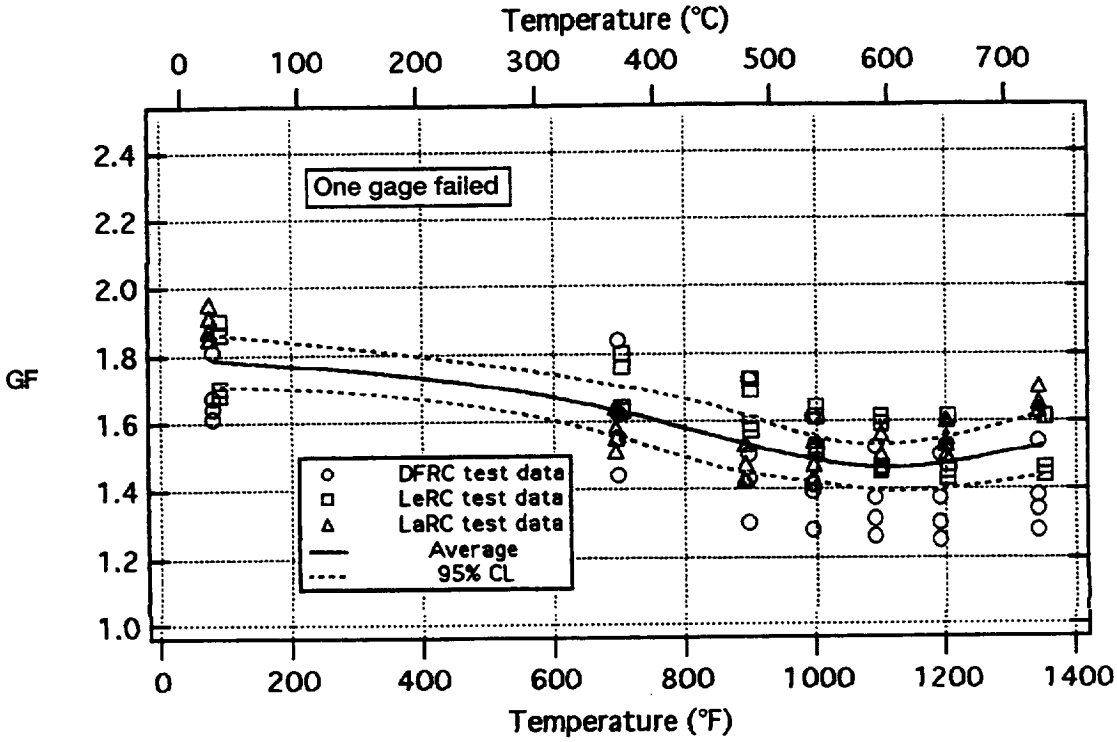

Figure 5.145.—Twelve DETCBCL gages on IN100 under tension—cycle 6 heating to 1350 °F (732 °C).

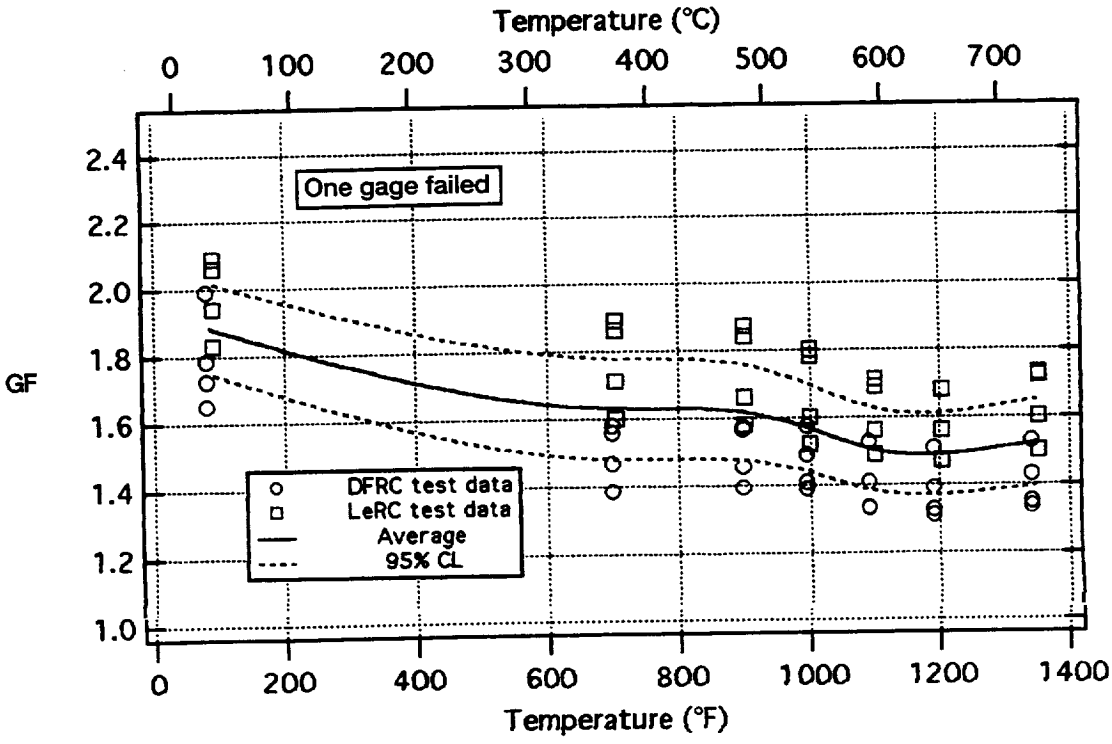

Figure 5.146.—Eight DETCBCL gages on IN100 under compression—cycle 6 heating to 1350 °F (732 °C).

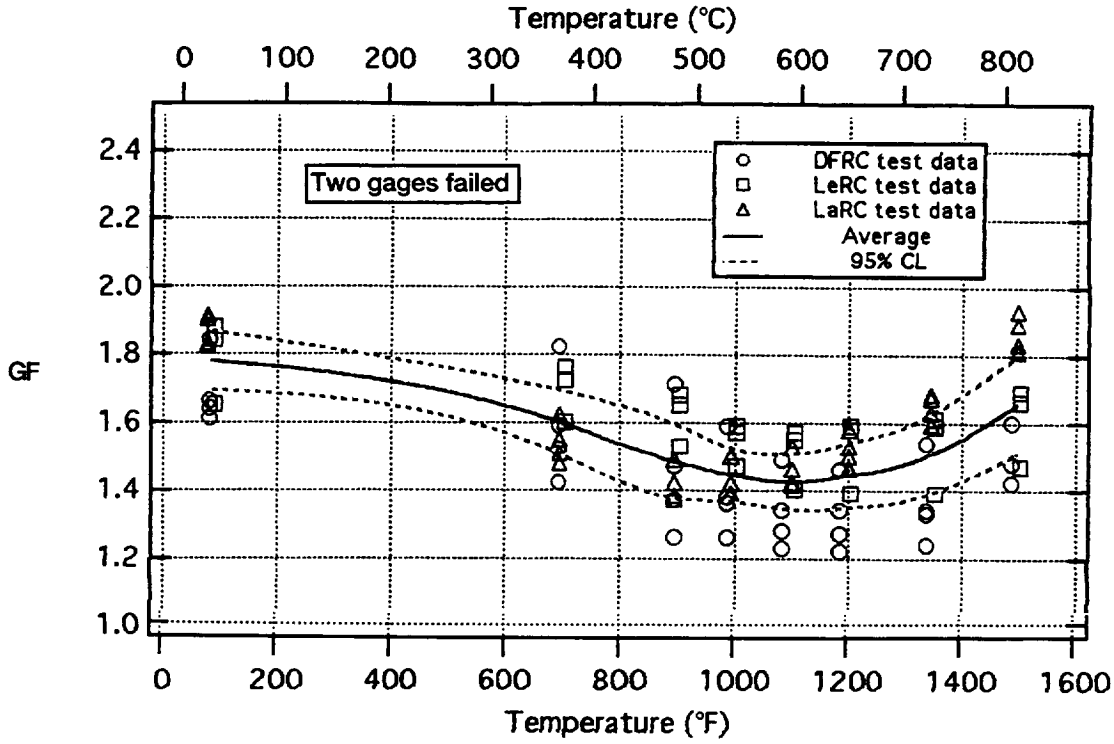

Figure 5.147.—Twelve DETCBCL gages on IN100 under tension—cycle 7 heating to 1500 °F (816 °C).

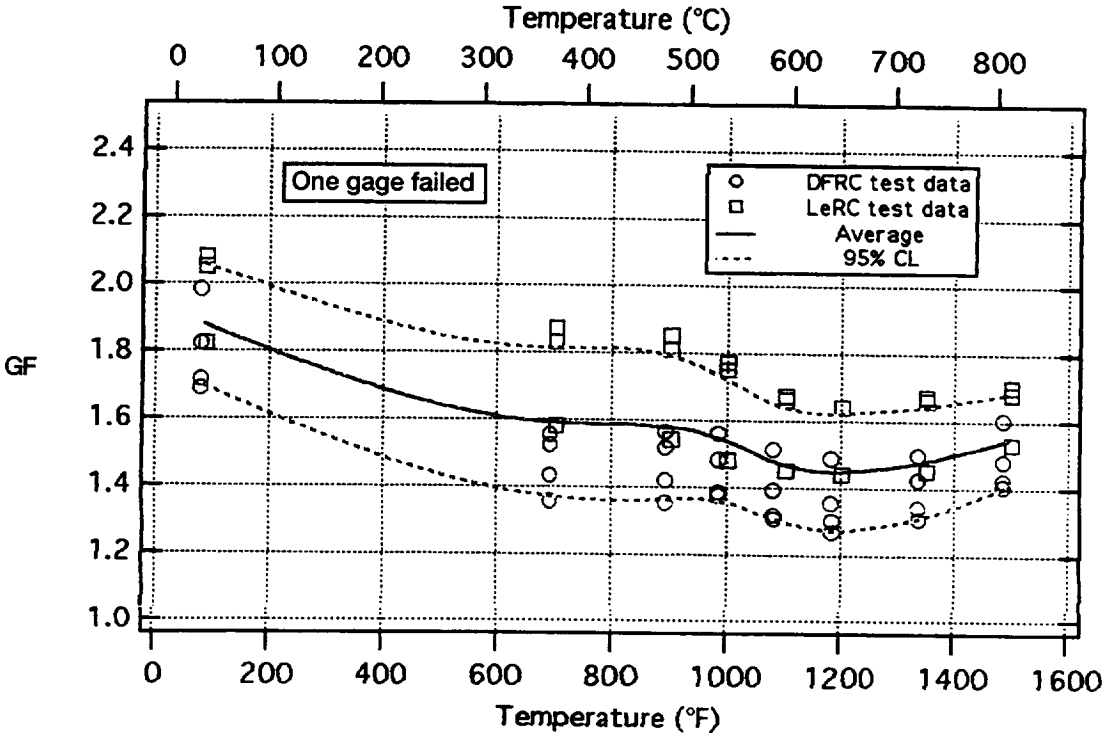

Figure 5.148.—Eight DETCBCL gages on IN100 under compression—cycle 7 heating to 1500 °F (816 °C).

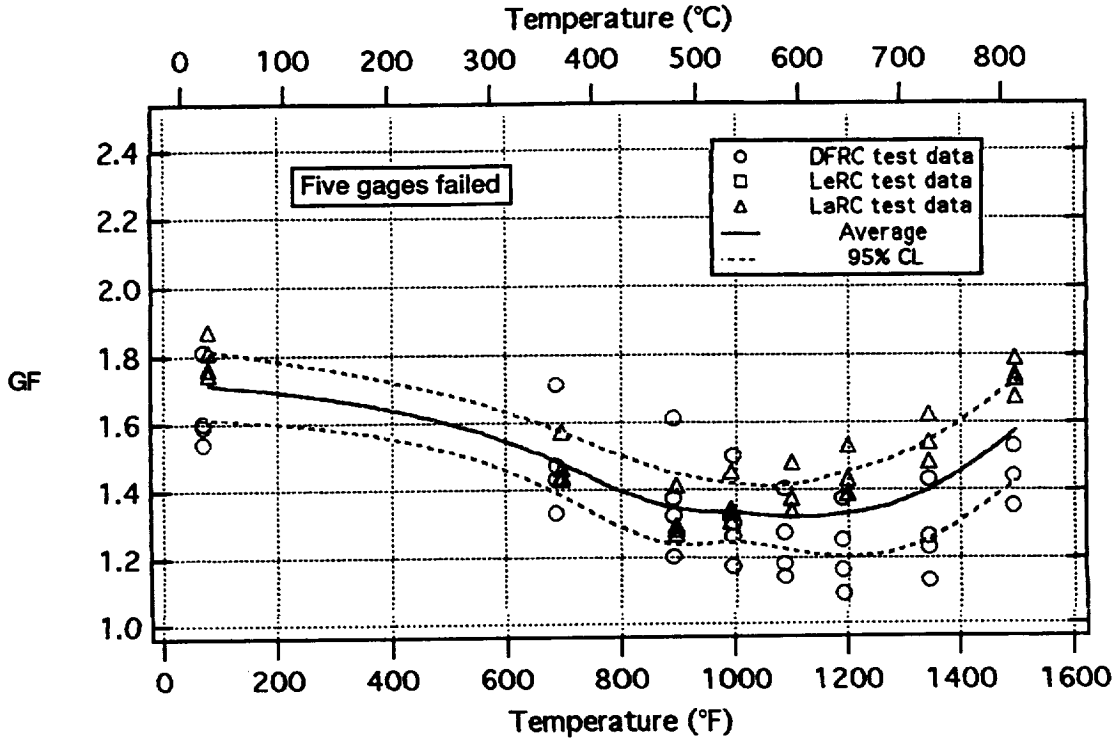

Figure 5.149.—Twelve DETCBCL gages on IN100 under tension—cycle 8 heating to 1500 °F (816 °C).

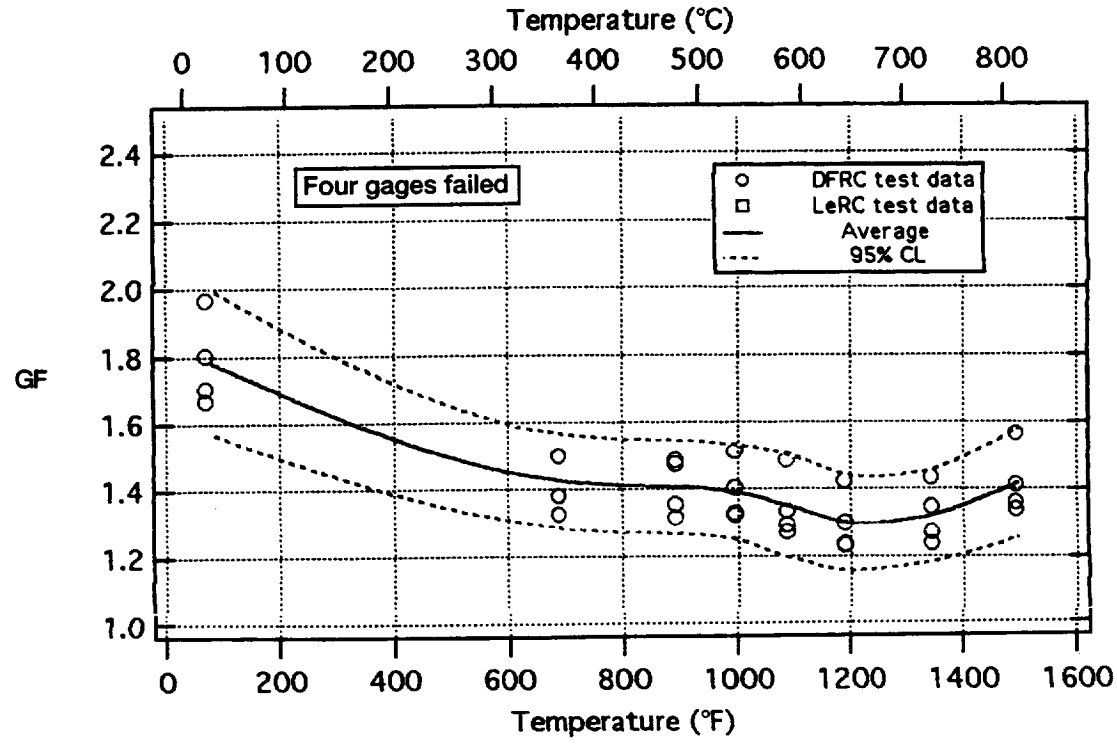

Figure 5.150.—Eight DETCBCL gages on IN100 under compression—cycle 8 heating to 1500 °F (816 °C).

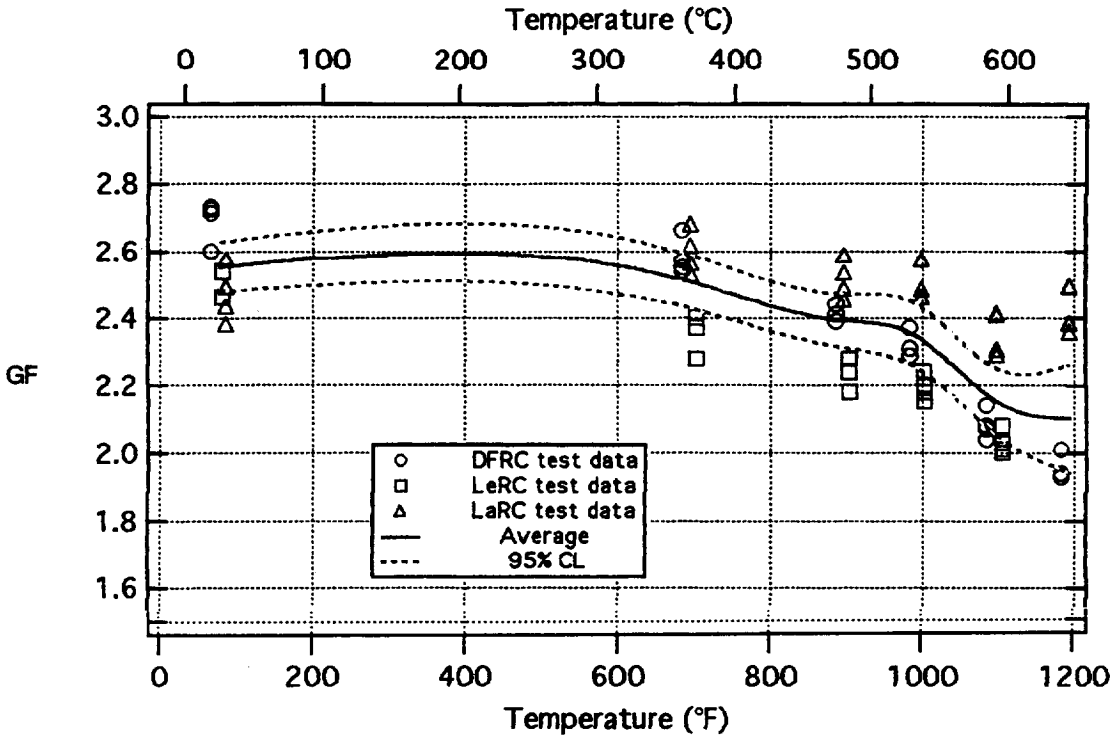

Figure 5.151.—Twelve CKA1 gages on TMC under tension—cycle 1 heating to 1200 °F (648 °C).

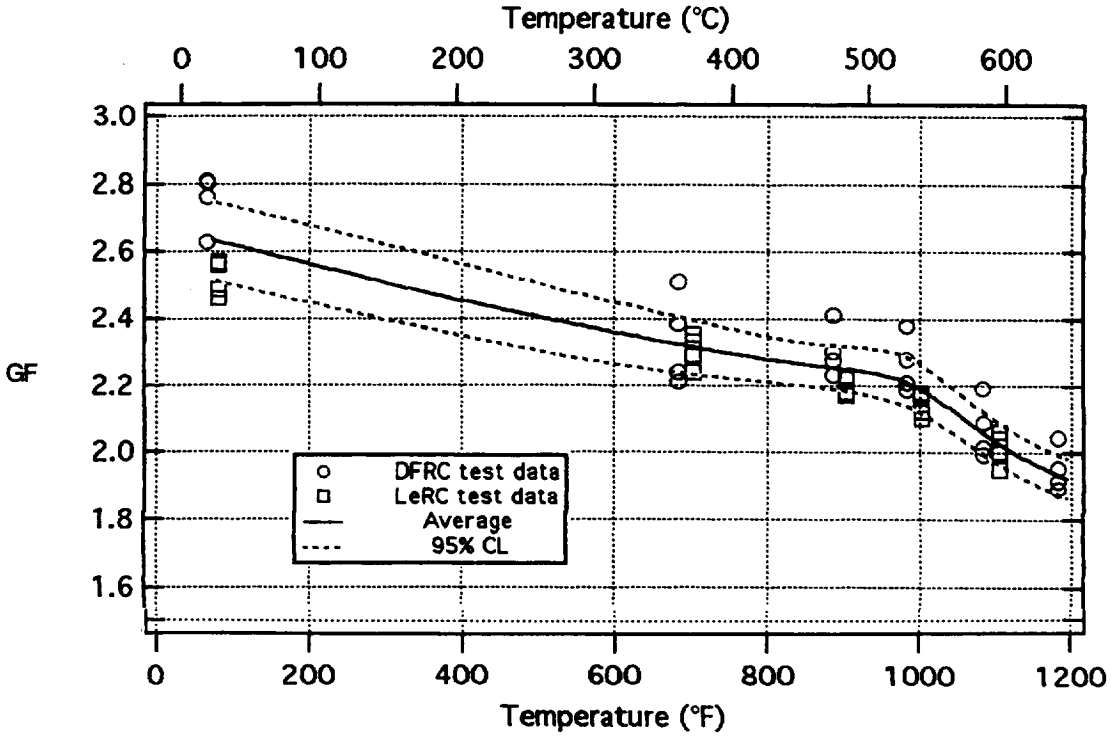

Figure 5.152.—Eight CKA1 gages on TMC under compression—cycle 1 heating to 1200 °F (648 °C).

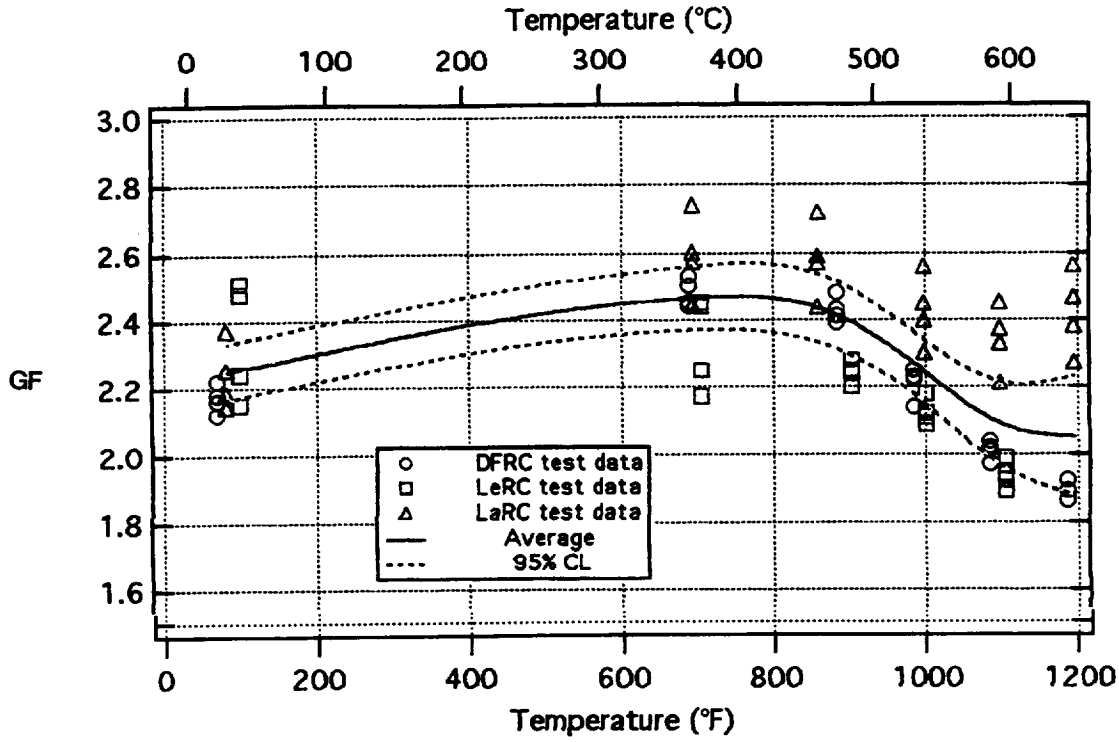

Figure 5.153.—Twelve CKA1 gages on TMC under tension—cycle 4 heating to 1200 °F (648 °C).

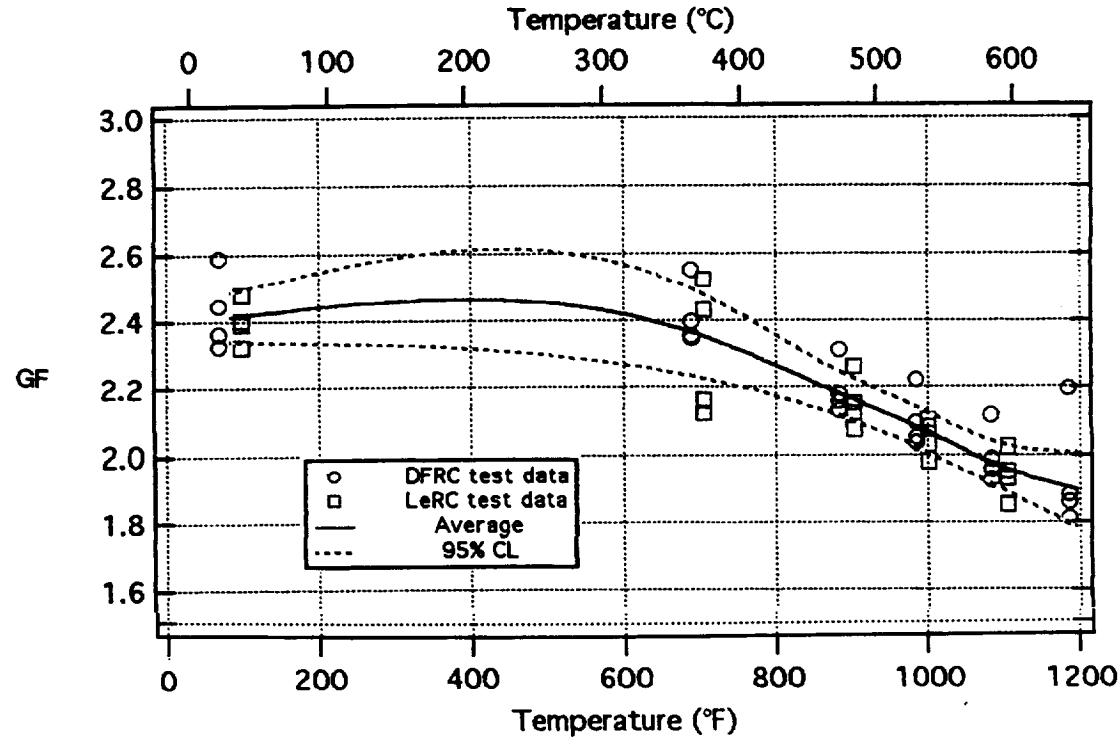

Figure 5.154.—Eight CKA1 gages on TMC under compression—cycle 4 heating to 1200 °F (648 °C).

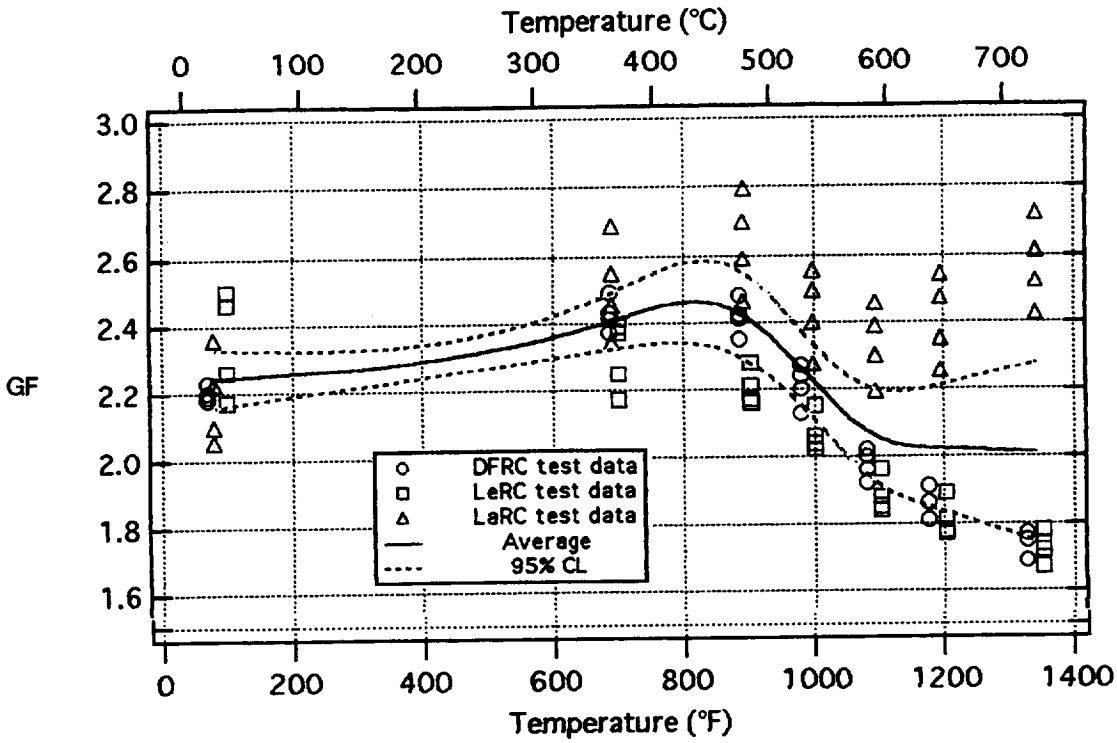

Figure 5.155.—Twelve CKA1 gages on TMC under tension—cycle 5 heating to 1350 °F (732 °C).

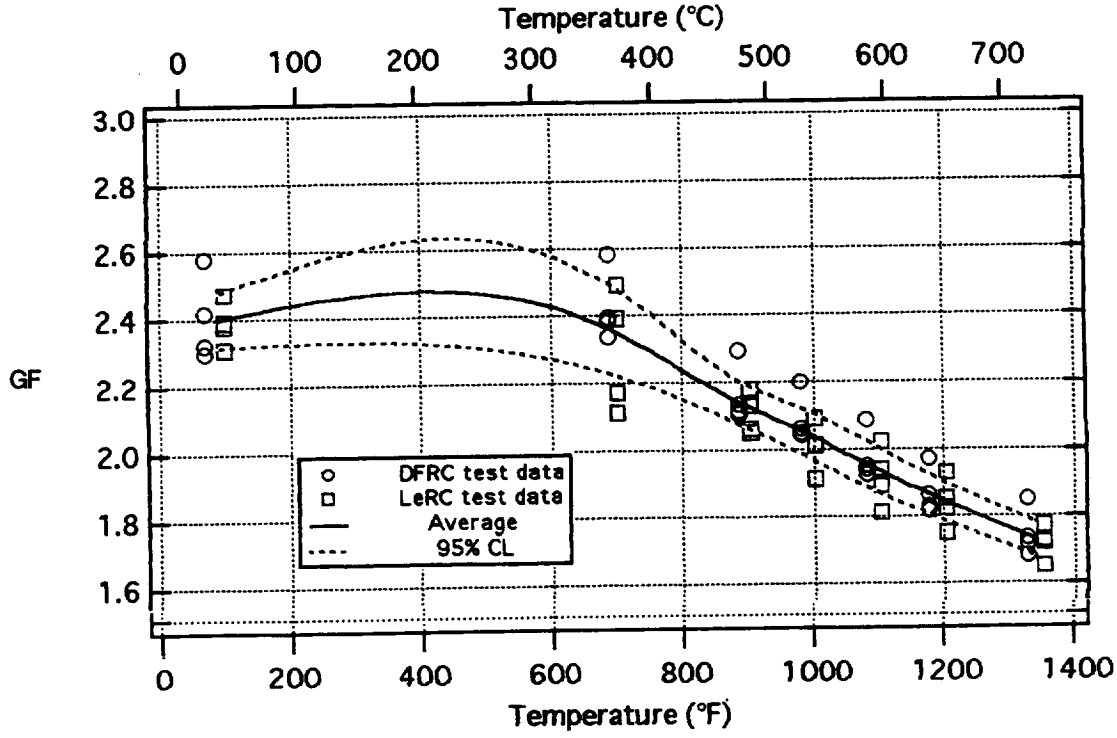

Figure 5.156.—Eight CKA1 gages on TMC under compression—cycle 5 heating to 1350 °F (732 °C).

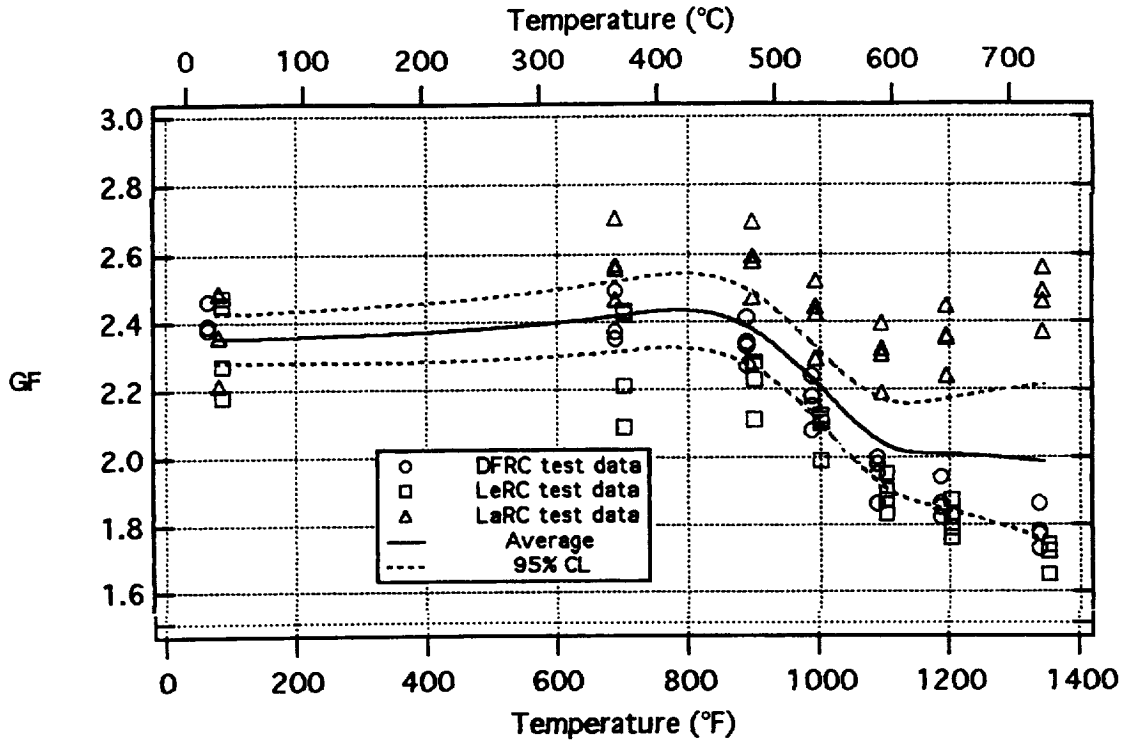

Figure 5.157.—Twelve CKA1 gages on TMC under tension—cycle 6 heating to 1350 °F (732 °C).

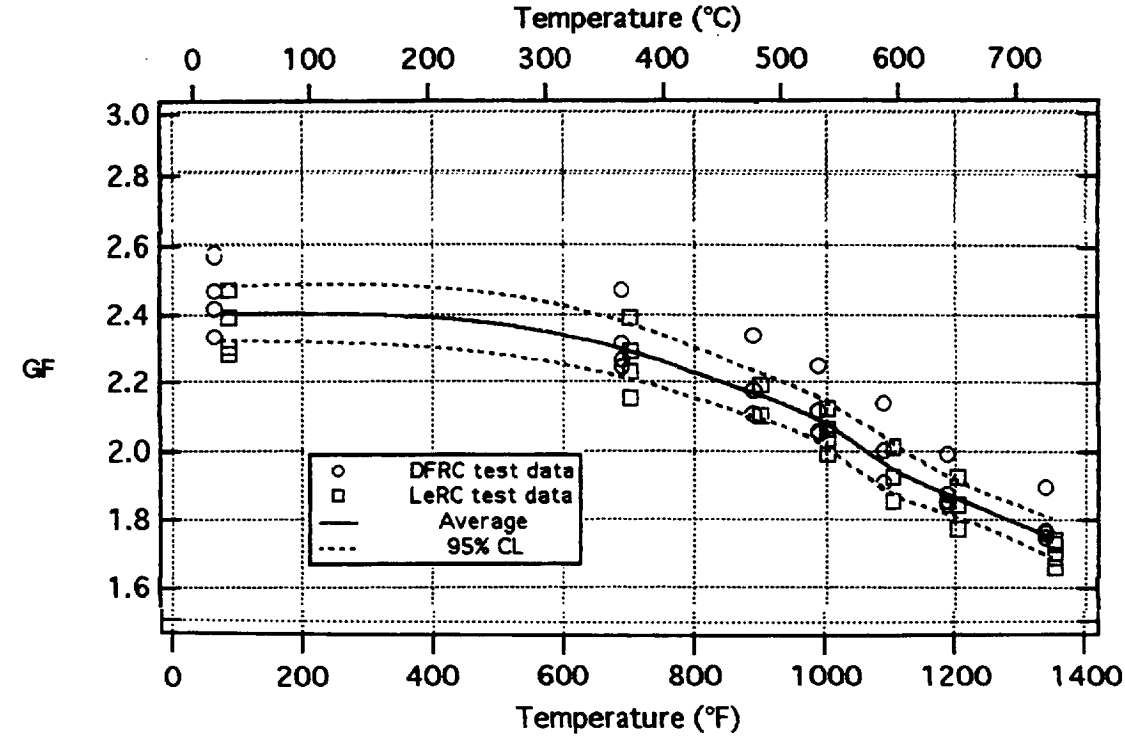

Figure 5.158.—Eight CKA1 gages on TMC under compression—cycle 6 heating to 1350 °F (732 °C).

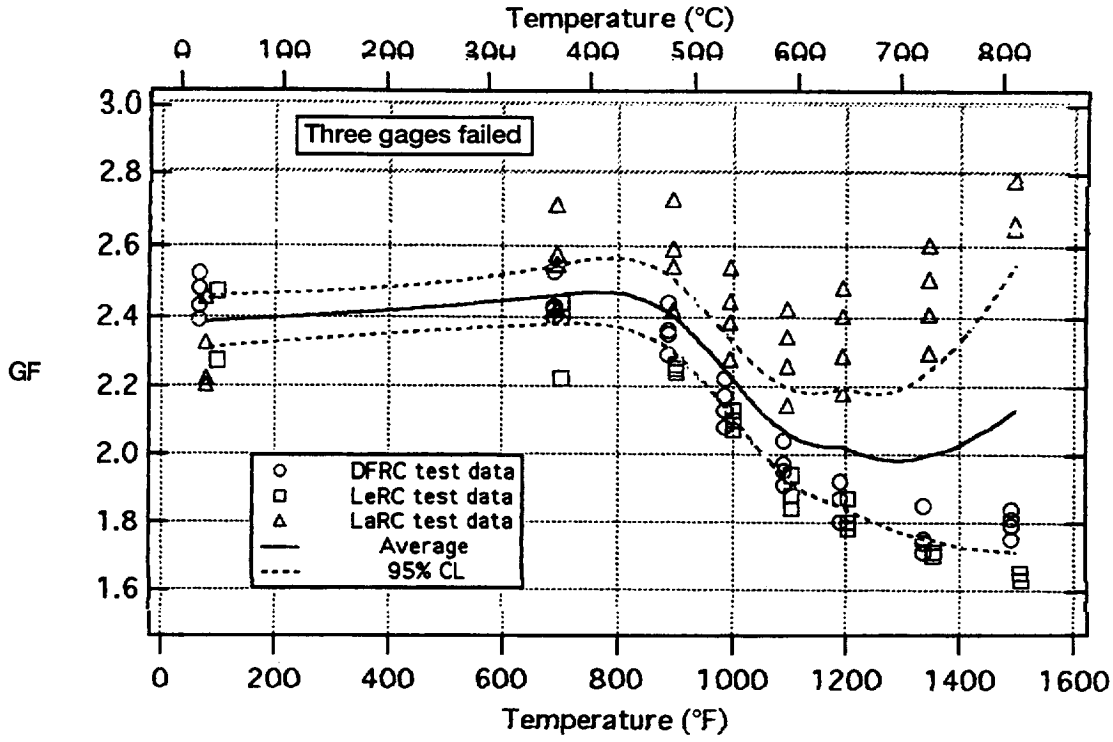

Figure 5.159.—Twelve CKA1 gages on TMC under tension—cycle 7 heating to 1500 °F (816 °C).

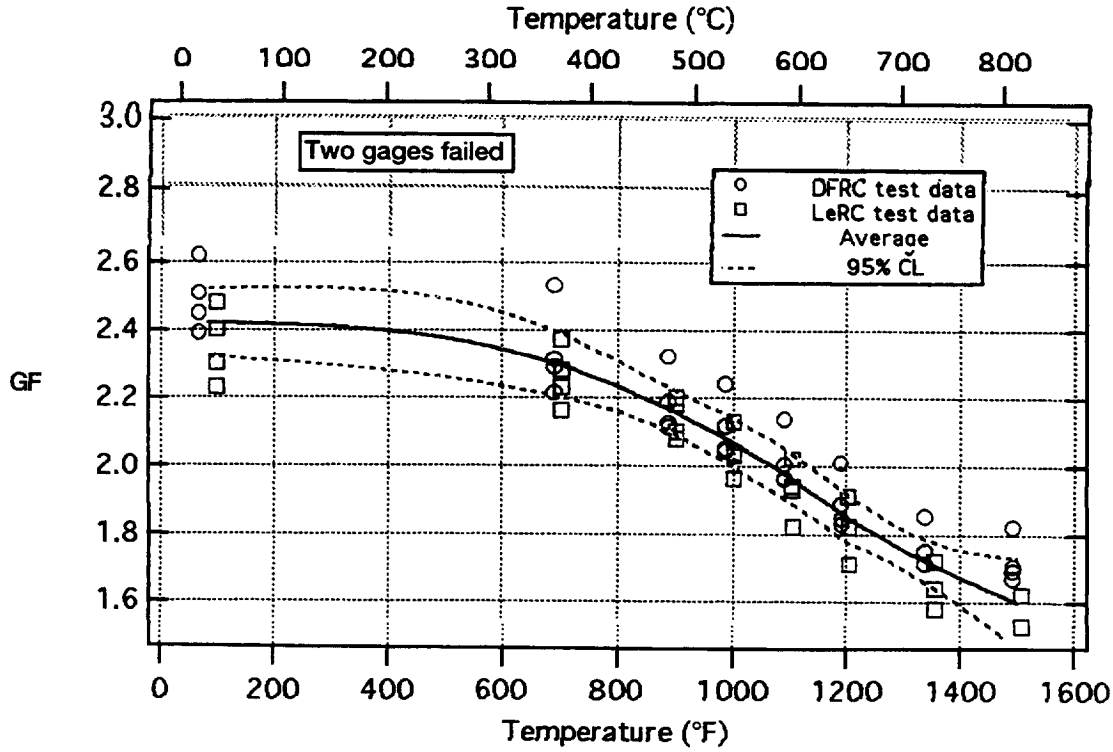

Figure 5.160.—Eight CKA1 gages on TMC under compression—cycle 7 heating to 1500 °F (816 °C).

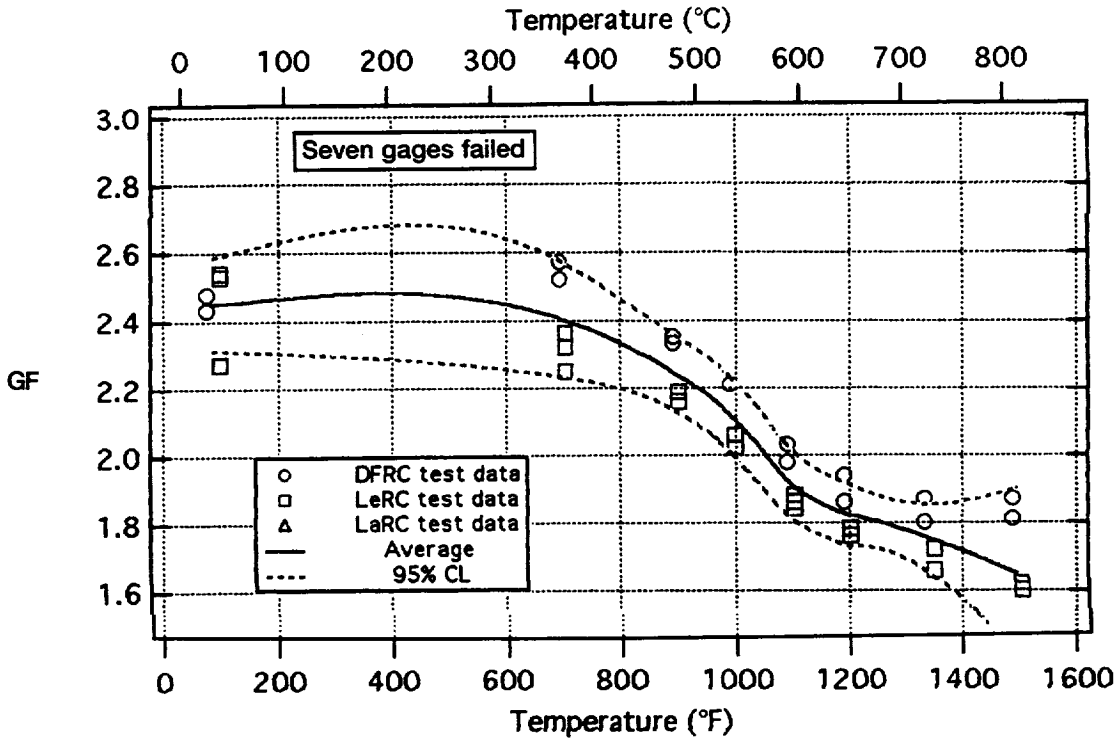

Figure 5.161.—Twelve CKA1 gages on TMC under tension—cycle 8 heating to 1500 °F (816 °C).

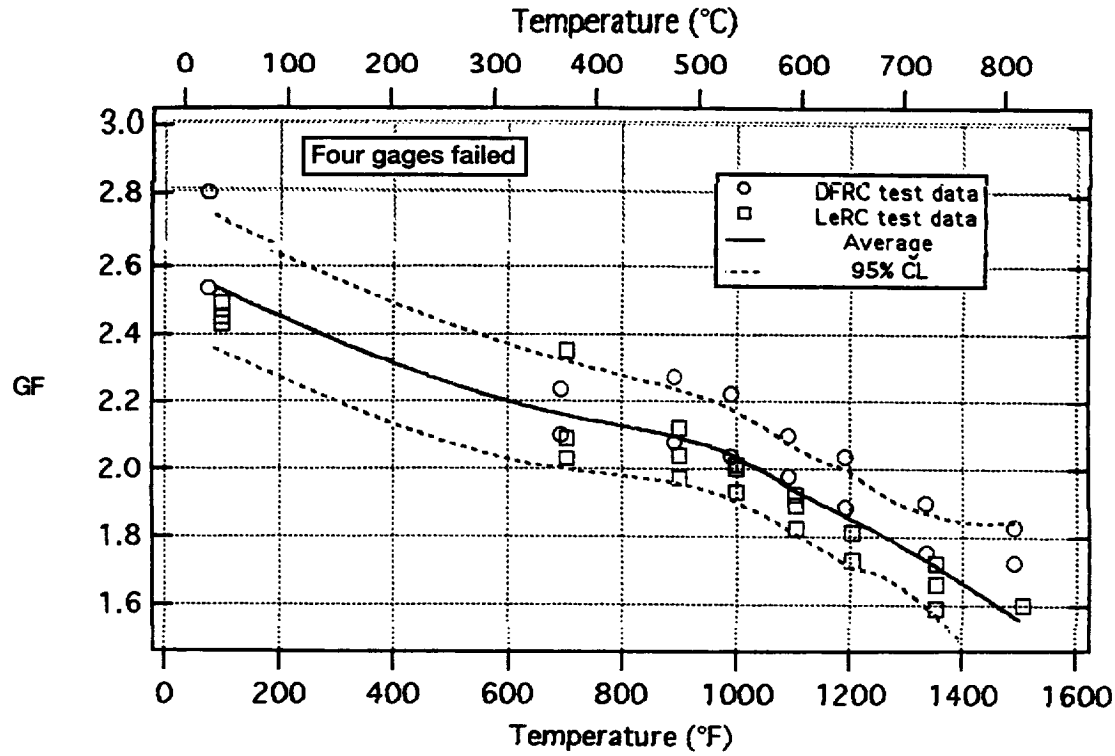

Figure 5.162.—Eight CKA1 gages on TMC under compression—cycle 8 heating to 1500 °F (816 °C).

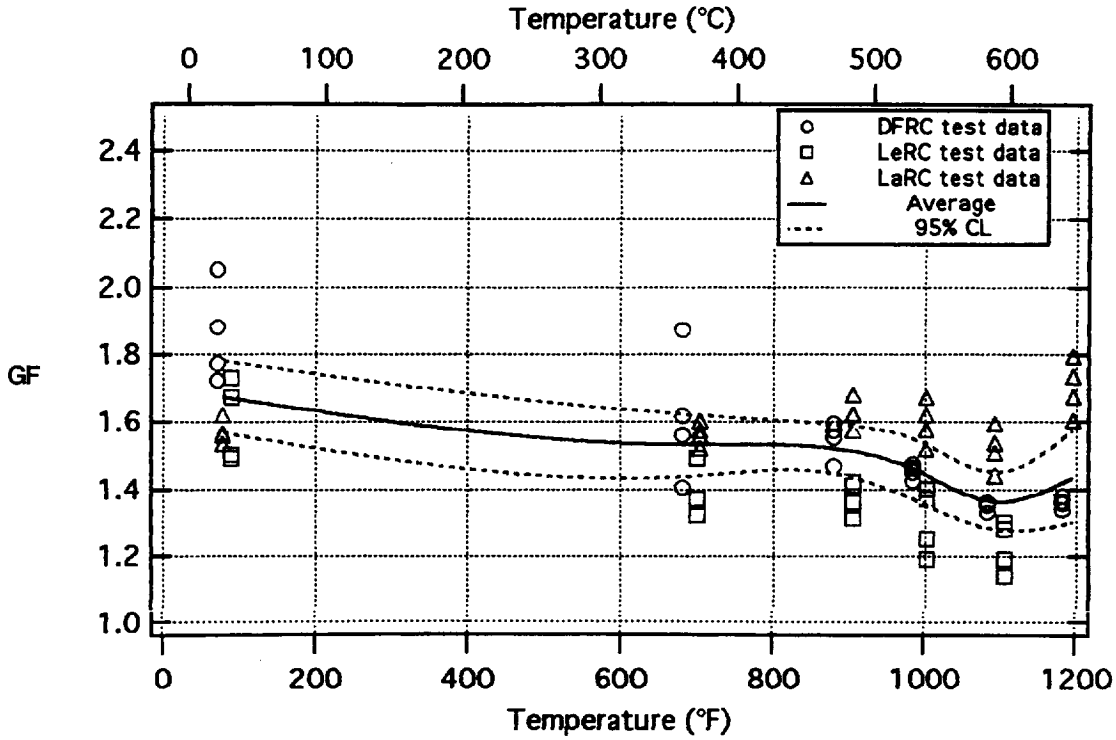

Figure 5.163.—Twelve PdCr gages on TMC under tension—cycle 1 heating to 1200 °F (648 °C).

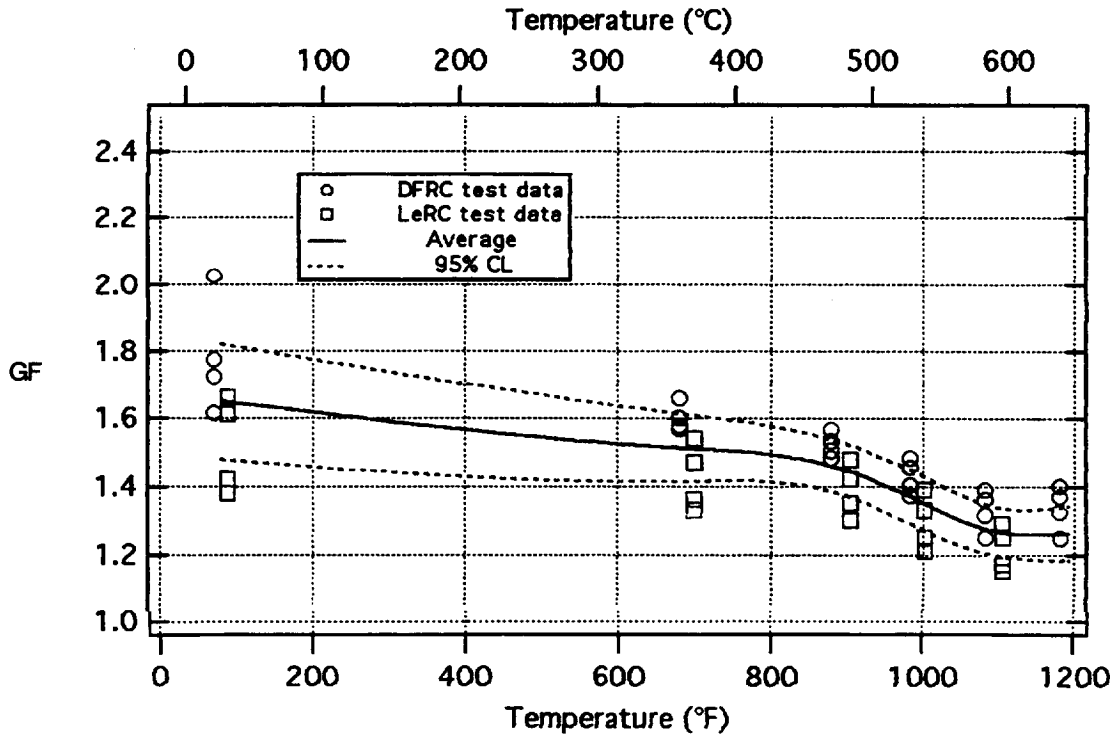

Figure 5.164.—Eight PdCr gages on TMC under compression—cycle 1 heating to 1200 °F (648 °C).

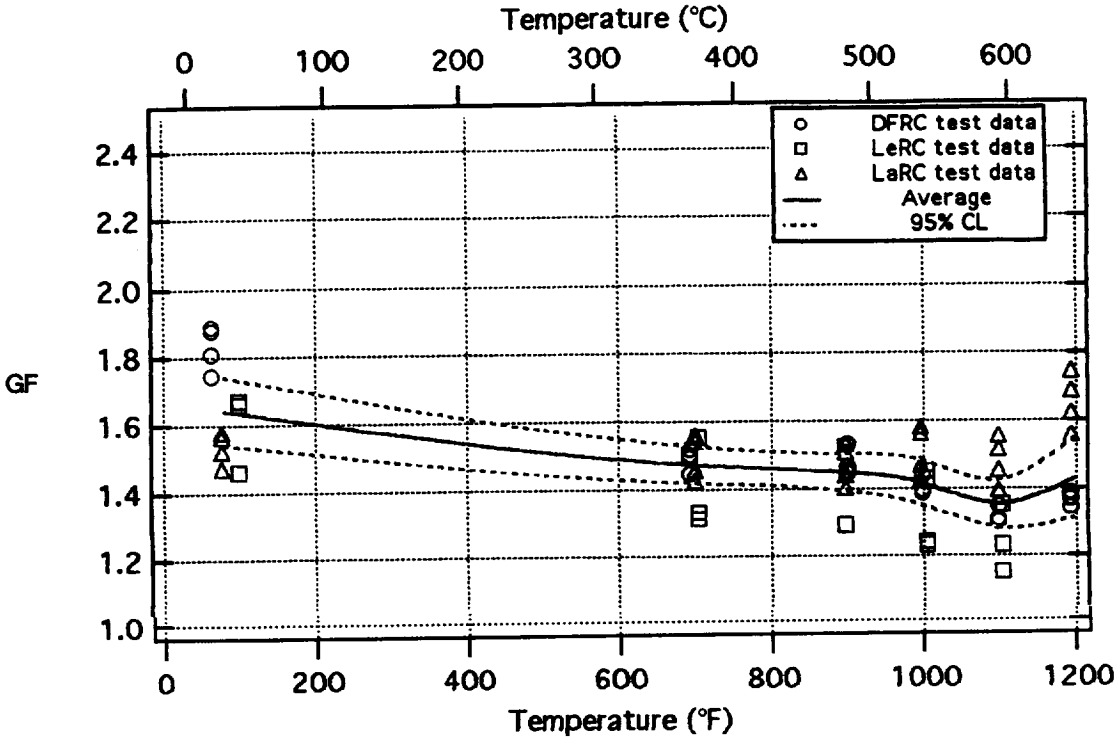

Figure 5.165.—Twelve PdCr gages on TMC under tension—cycle 4 heating to 1200 °F (648 °C).

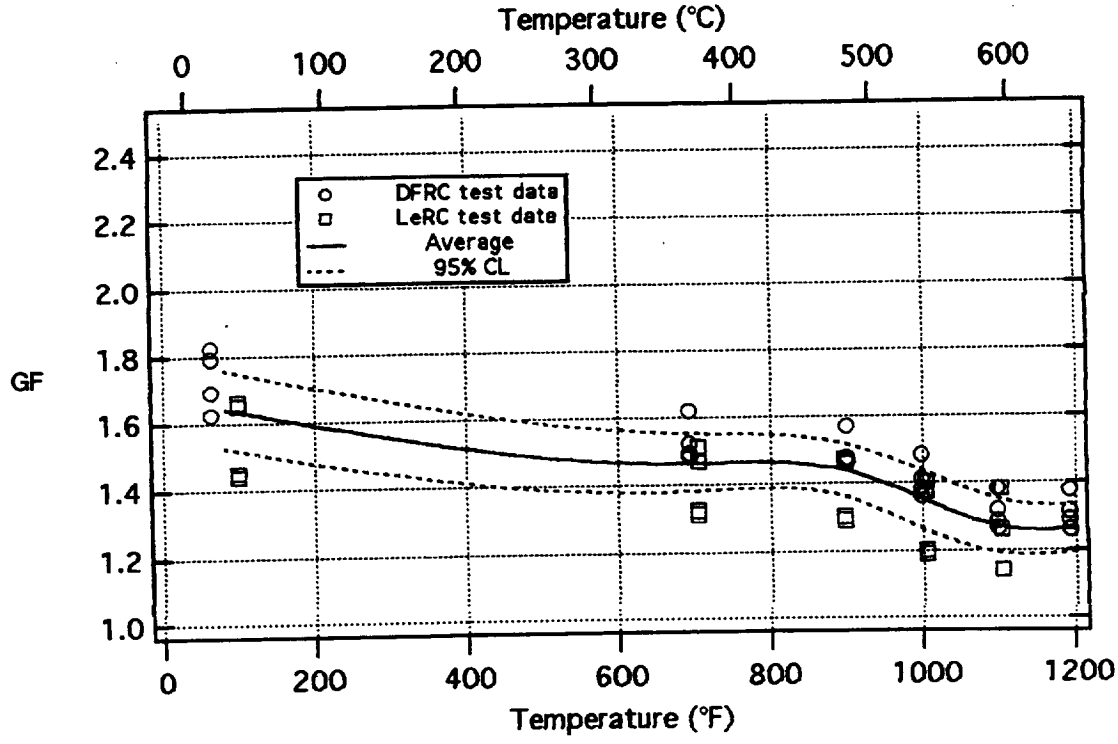

Figure 5.166.—Eight PdCr gages on TMC under compression—cycle 4 heating to 1200 °F (648 °C).

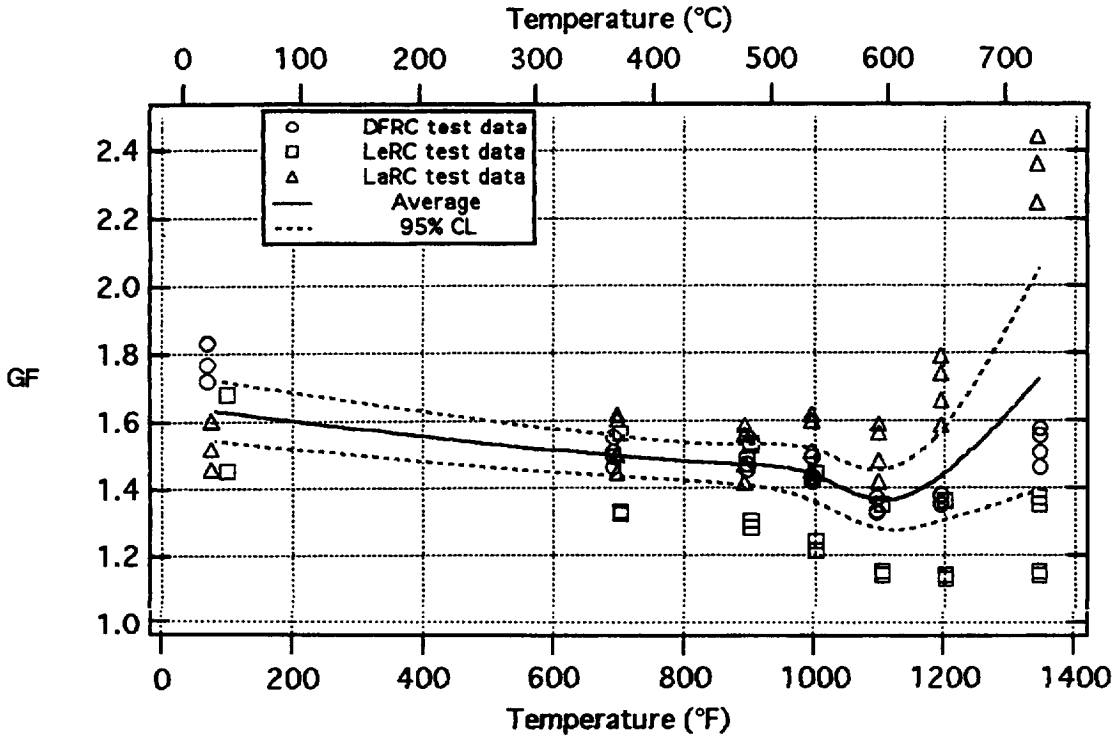

Figure 5.167.—Twelve PdCr gages on TMC under tension—cycle 5 heating to 1350 °F (732 °C).

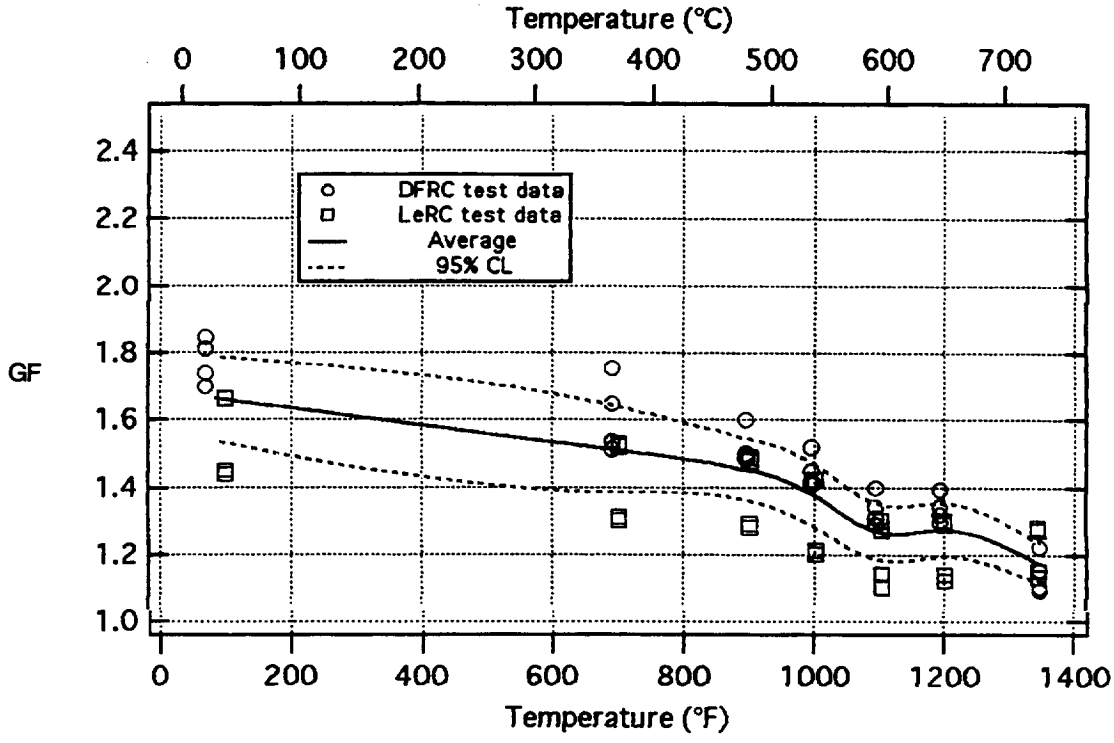

Figure 5.168.—Eight PdCr gages on TMC under compression—cycle 5 heating to 1350 °F (732 °C).

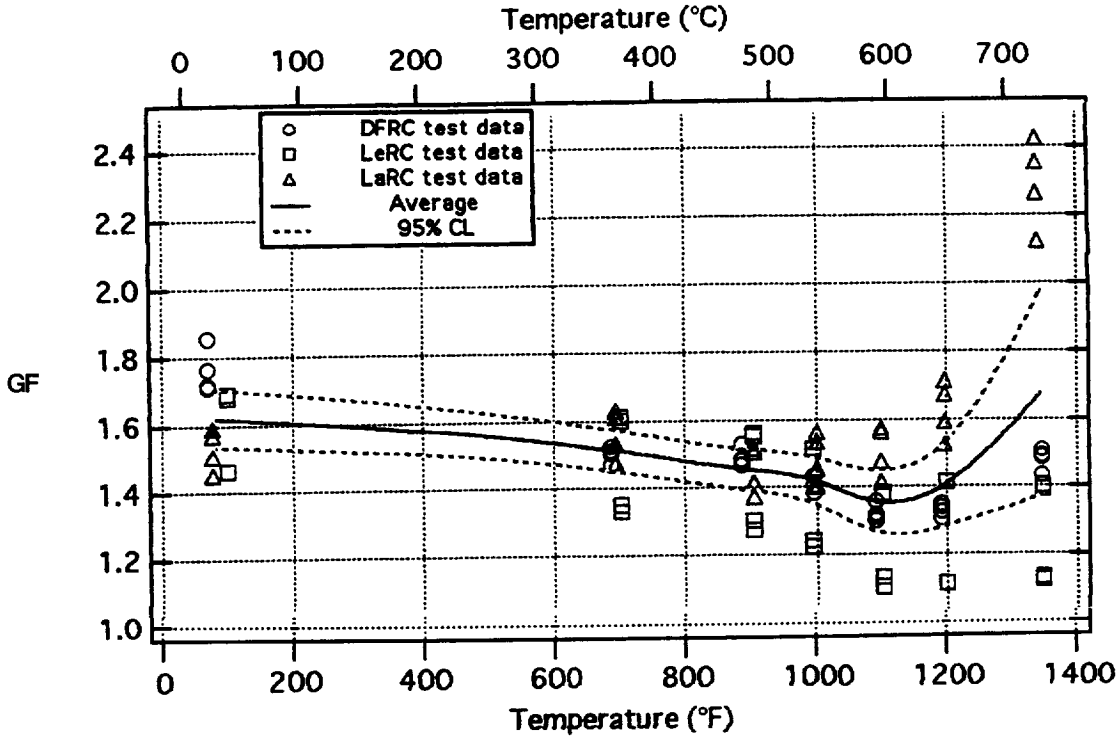

Figure 5.169.—Twelve PdCr gages on TMC under tension—cycle 6 heating to 1350 °F (732 °C).

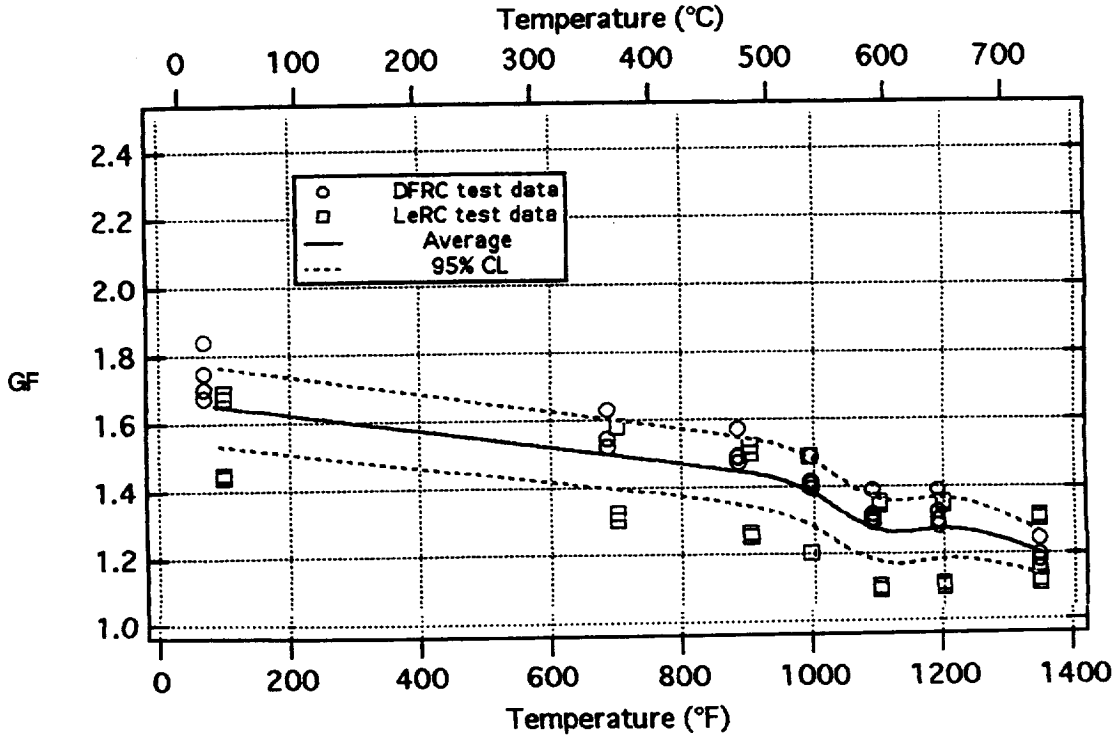

Figure 5.170.—Eight PdCr gages on TMC under compression—cycle 6 heating to 1350 °F (732 °C).

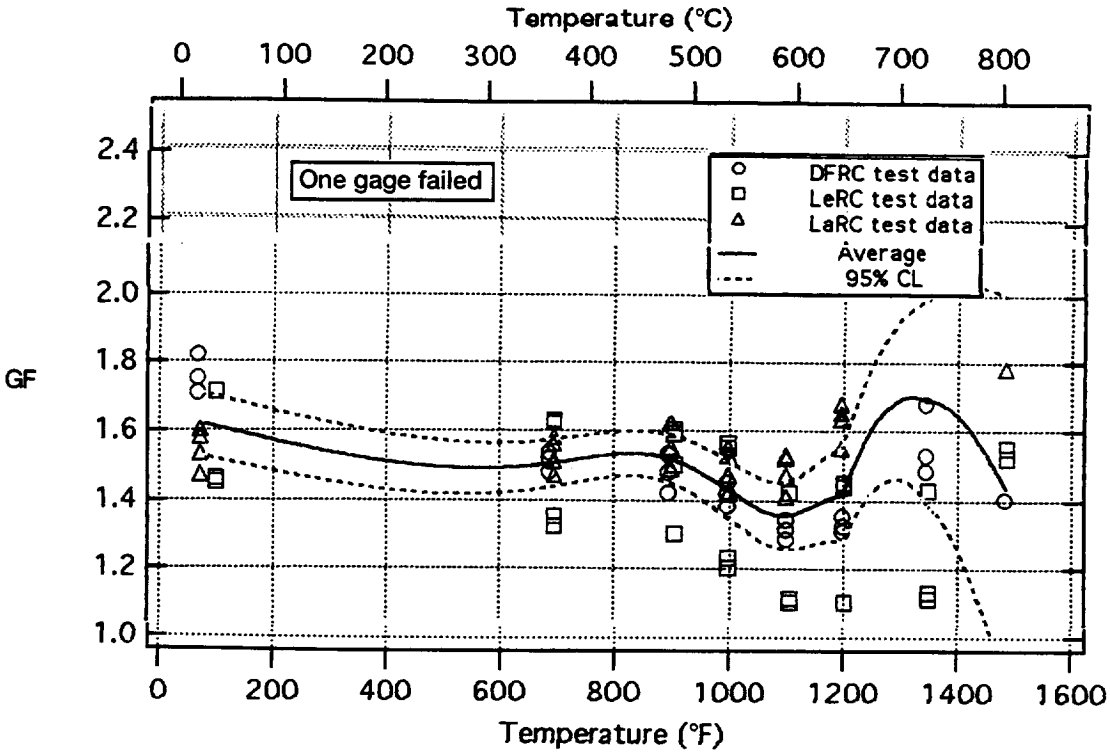

Figure 5.171.—Twelve PdCr gages on TMC under tension—cycle 7 heating to 1500 °F (816 °C).

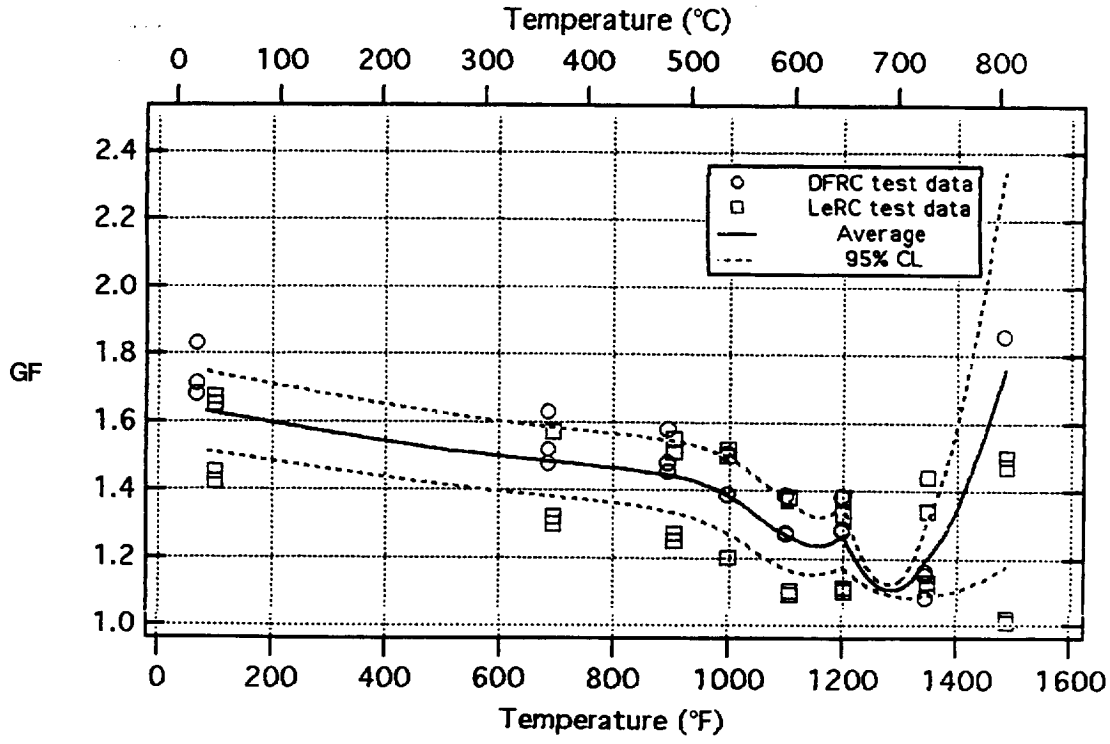

Figure 5.172.—Eight PdCr gages on TMC under compression—cycle 7 heating to 1500 °F (816 °C).

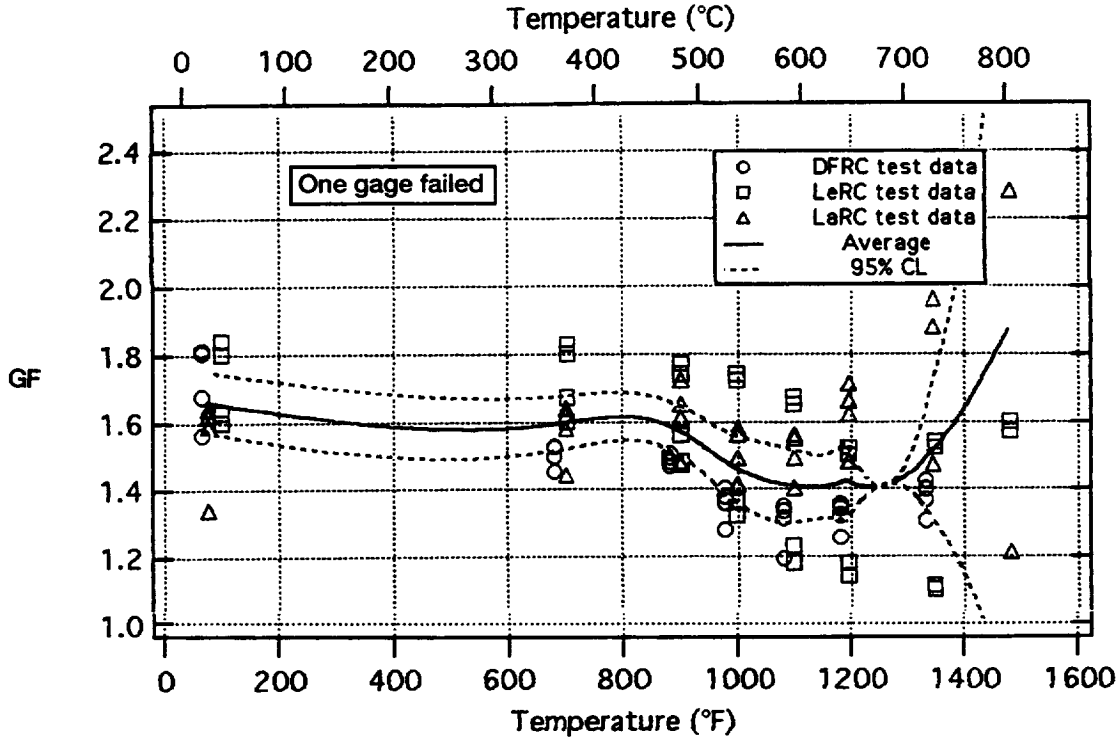

Figure 5.173.—Twelve PdCr gages on TMC under tension—cycle 8 heating to 1500 °F (816 °C).

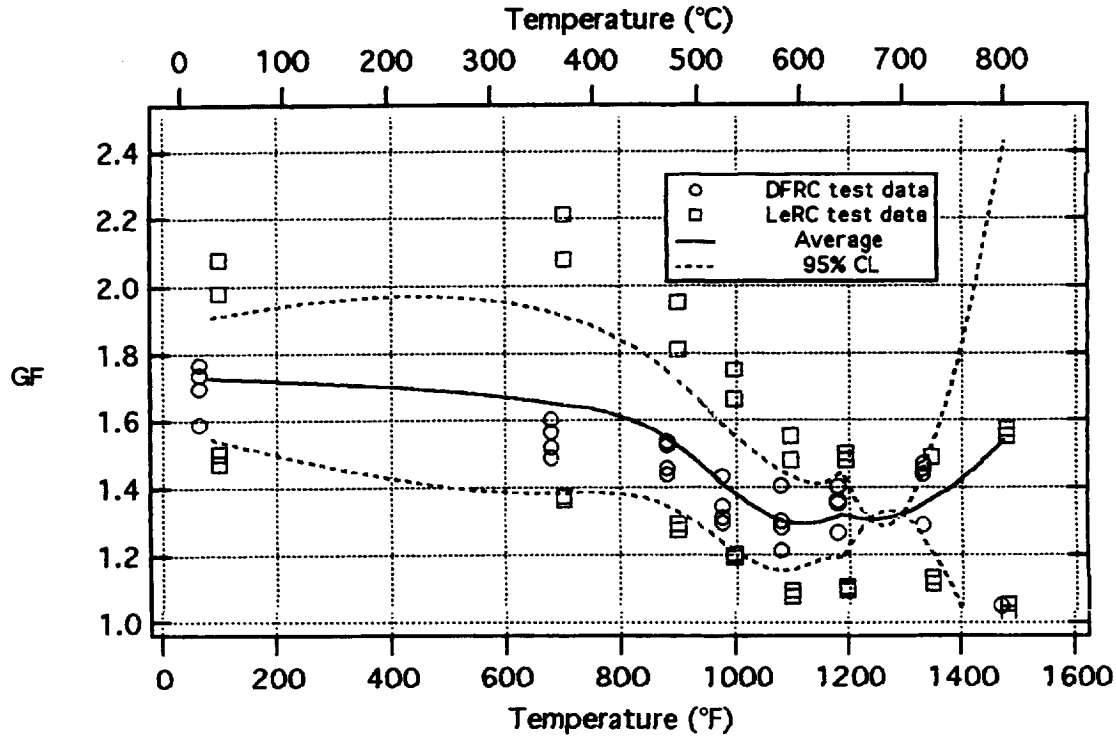

Figure 5.174.—Eight PdCr gages on TMC under compression—cycle 8 heating to 1500 °F (816 °C).

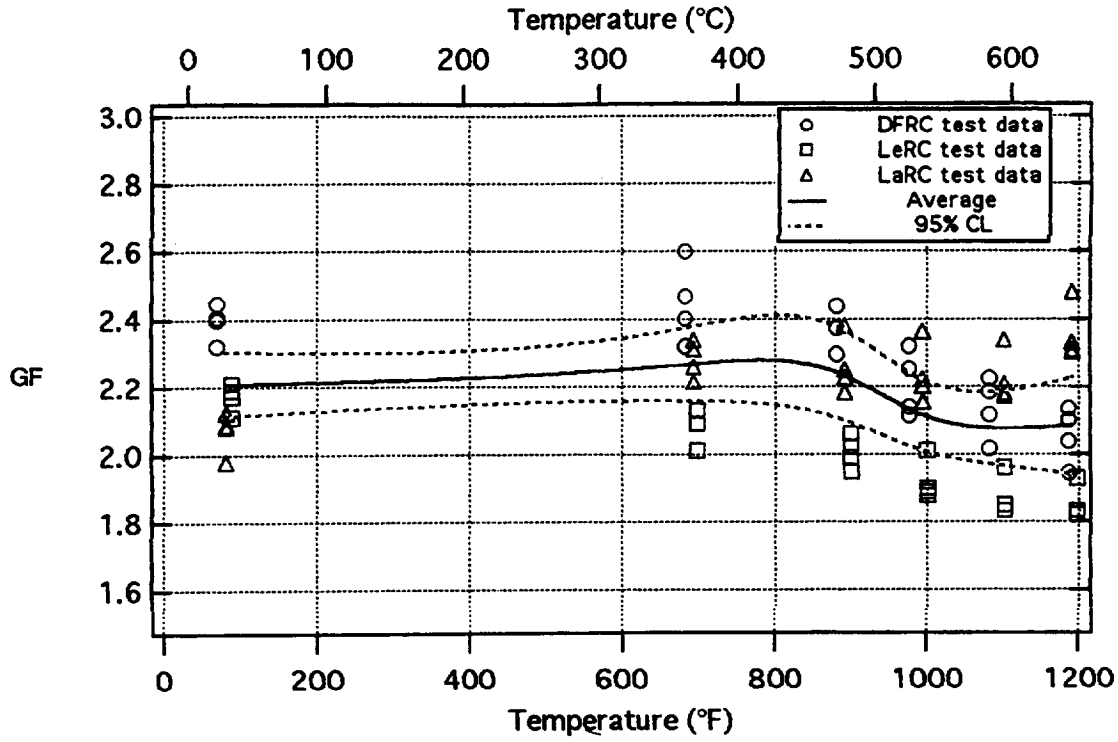

Figure 5.175.—Twelve DETCBCL gages on TMC under tension—cycle 1 heating to 1200 °F (648 °C).

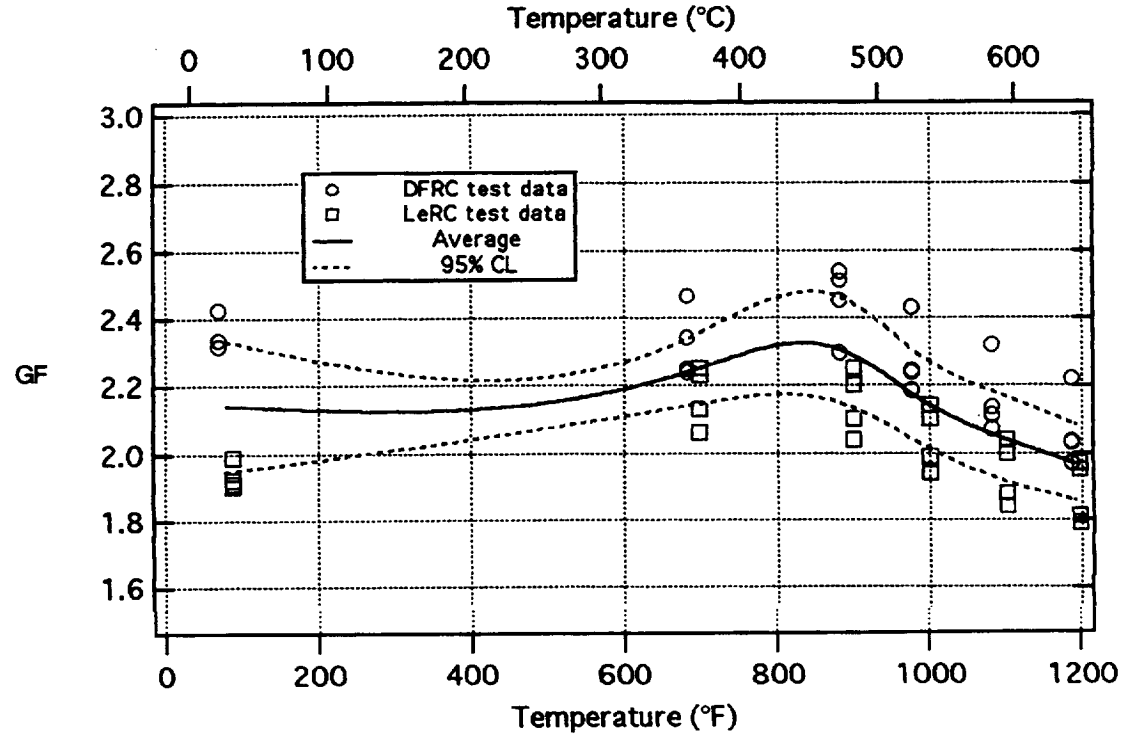

Figure 5.176.—Eight DETCBCL gages on TMC under compression—cycle 1 heating to 1200 °F (648 °C).

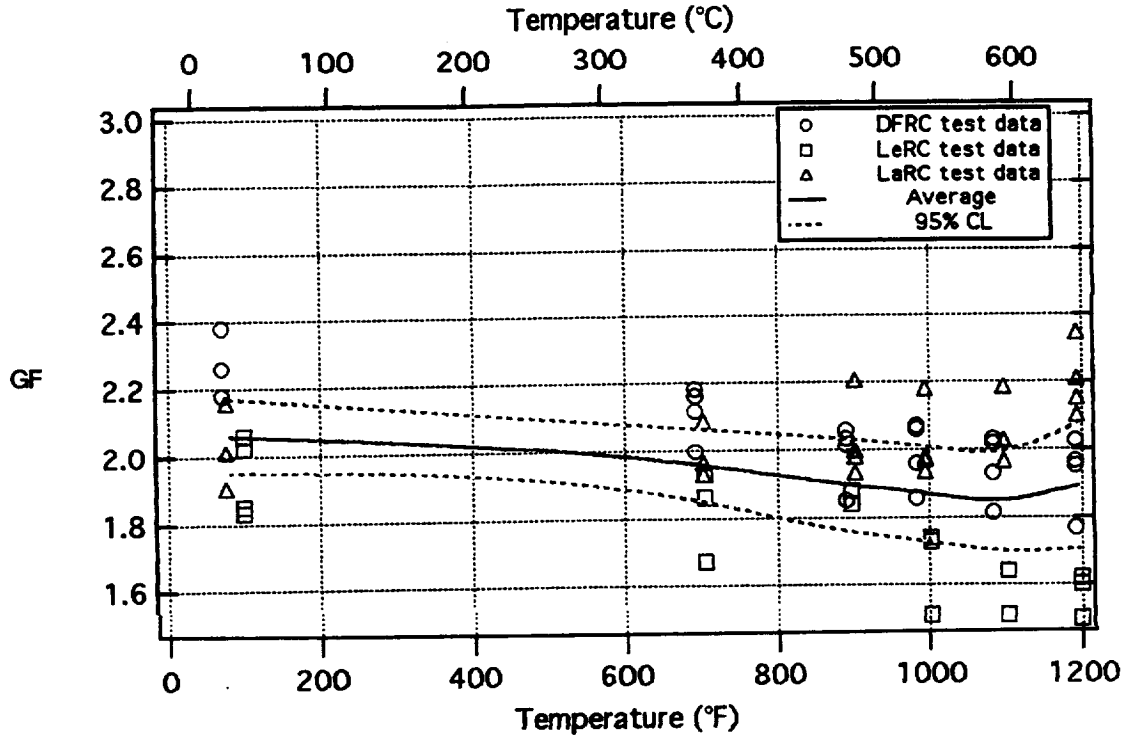

Figure 5.177.—Twelve DETCBCL gages on TMC under tension—cycle 4 heating to 1200 °F (648 °C).

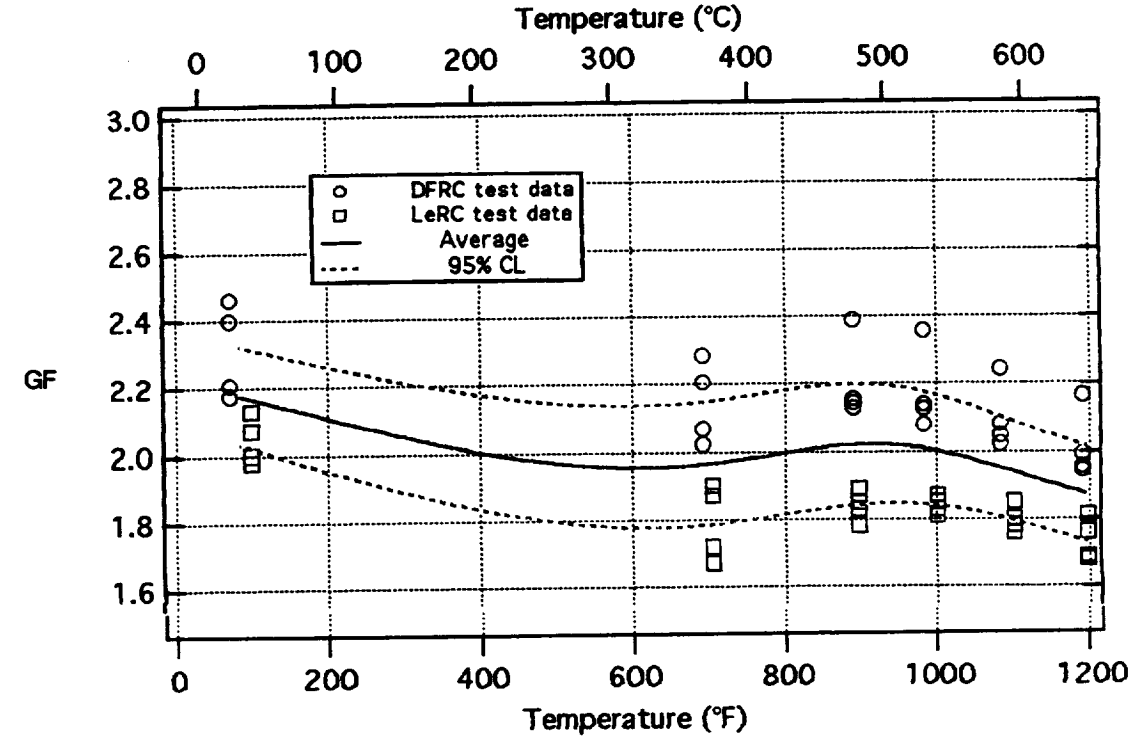

Figure 5.178.—Eight DETCBCL gages on TMC under compression—cycle 4 heating to 1200 °F (648 °C).

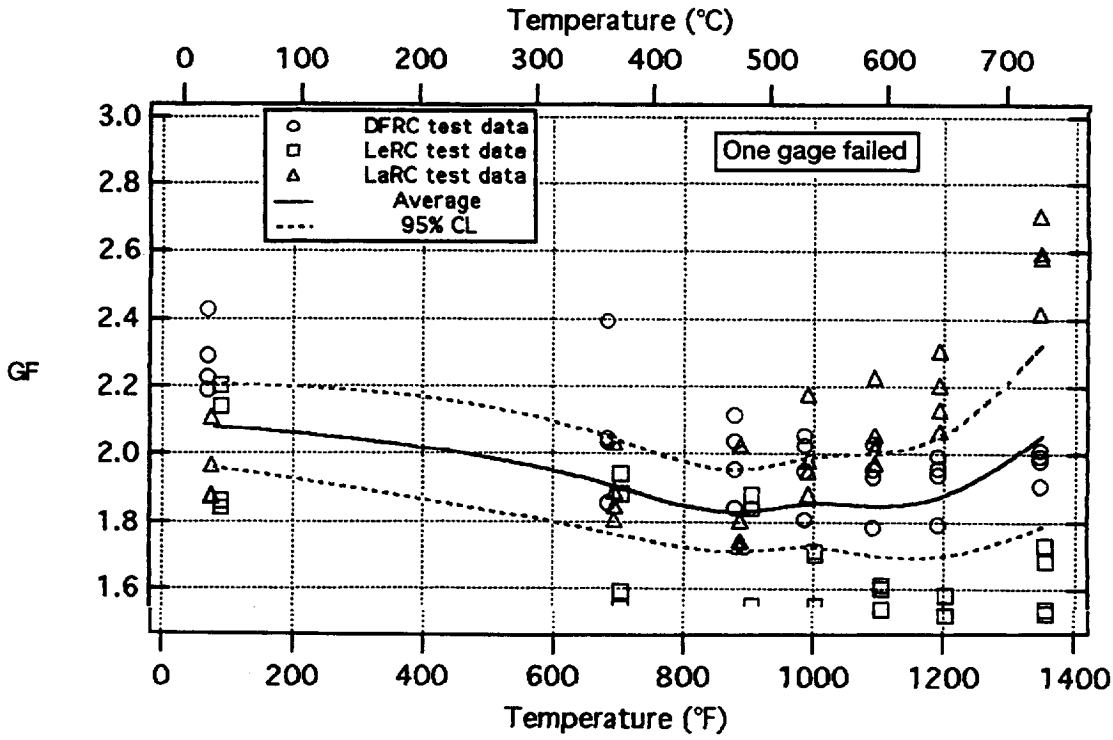

Figure 5.179.—Twelve DETCBCL gages on TMC under tension—cycle 5 heating to 1350 °F (732 °C).

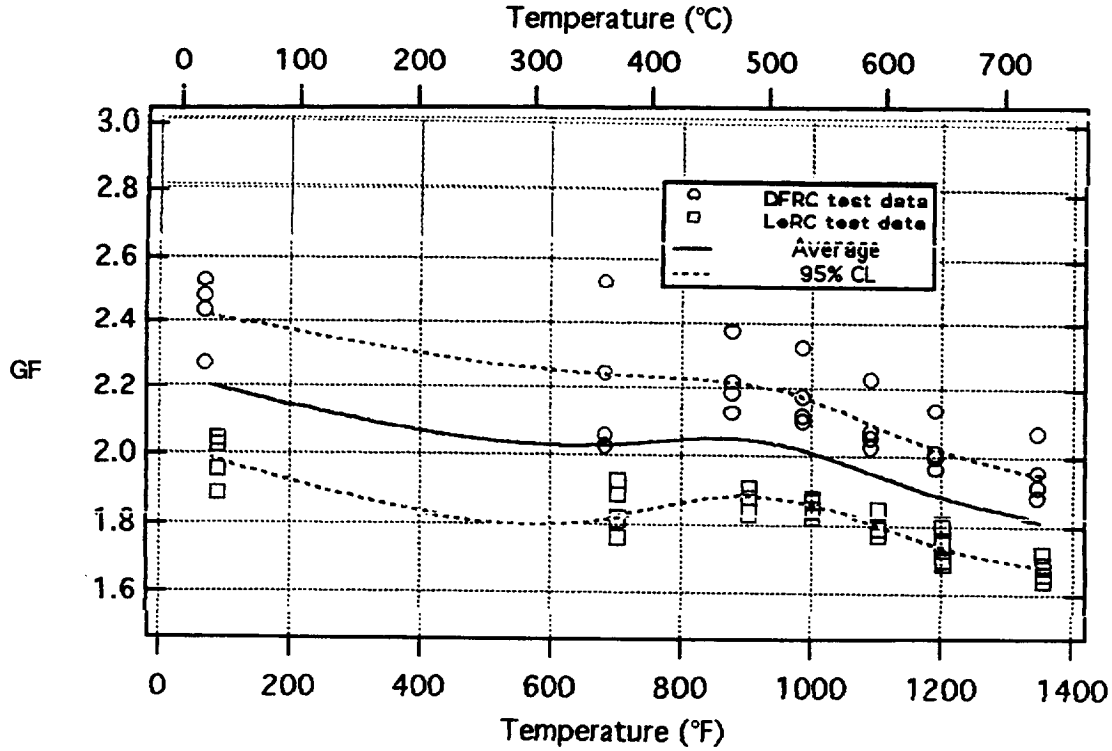

Figure 5.180.—Eight DETCBCL gages on TMC under compression—cycle 5 heating to 1350 °F (732 °C).

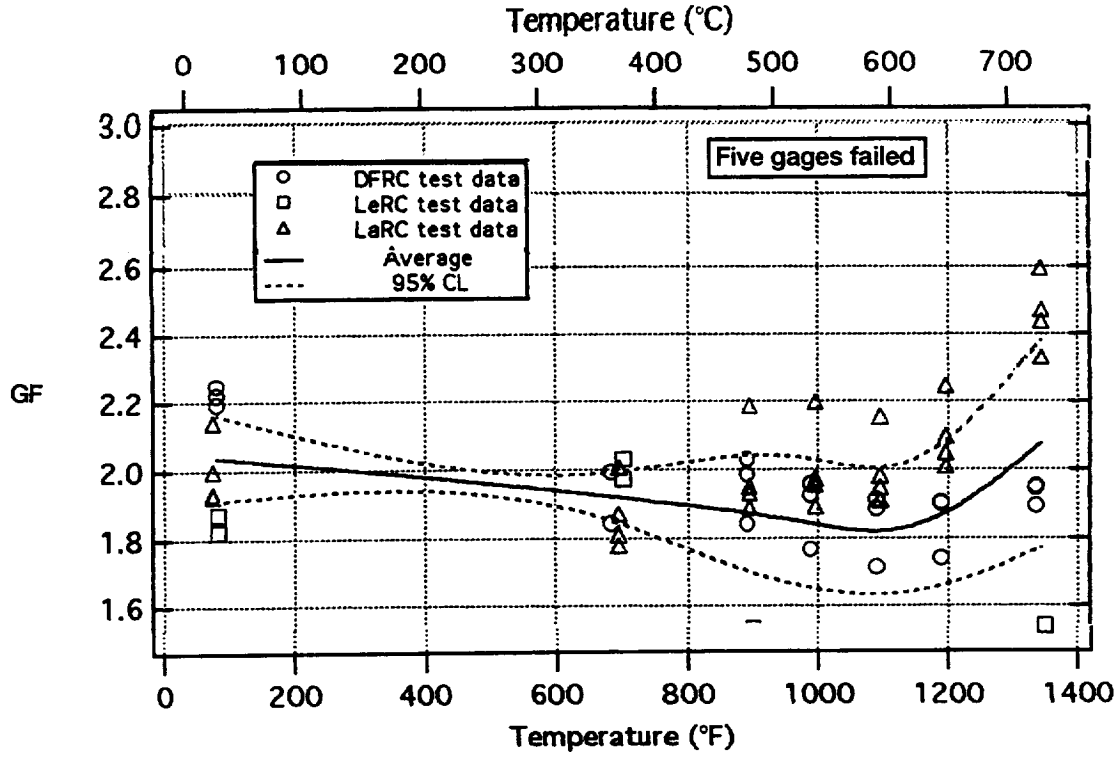

Figure 5.181.—Twelve DETCBCL gages on TMC under tension—cycle 6 heating to 1350 °F (732 °C).

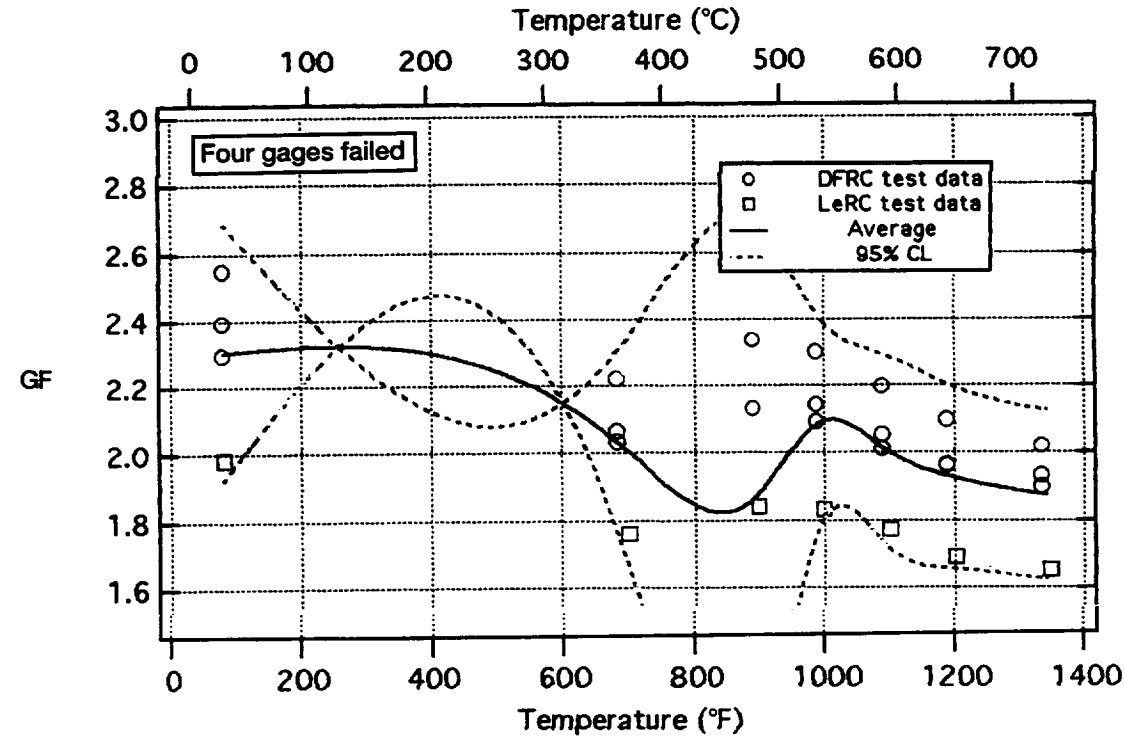

Figure 5.182.—Eight DETCBCL gages on TMC under compression—cycle 6 heating to 1350 °F (732 °C).

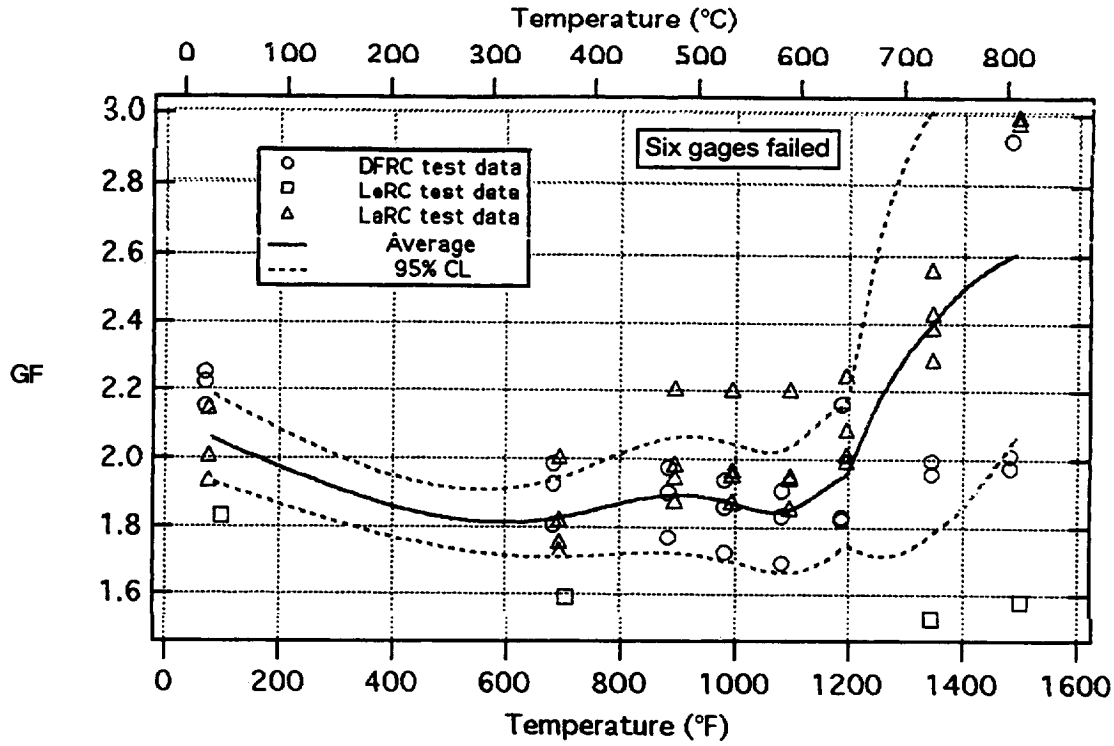

Figure 5.183.—Twelve DETCBCL gages on TMC under tension—cycle 7 heating to 1500 °F (816 °C).

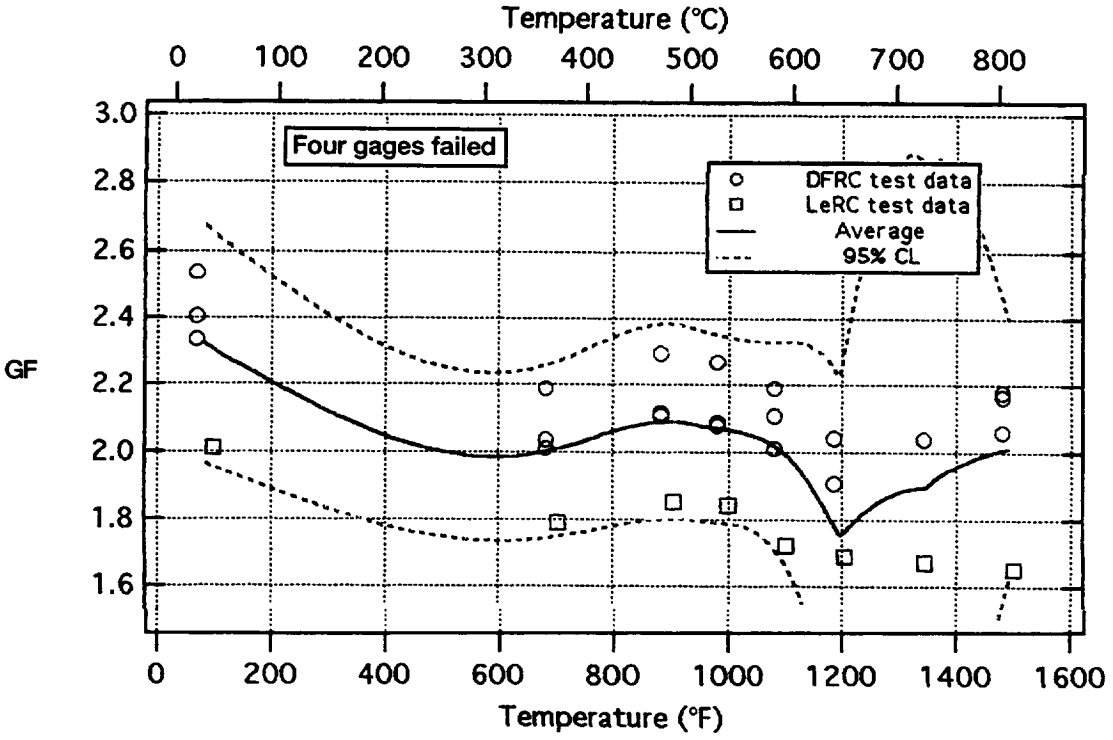

Figure 5.184.—Eight DETCBCL gages on TMC under compression—cycle 7 heating to 1500 °F (816 °C).

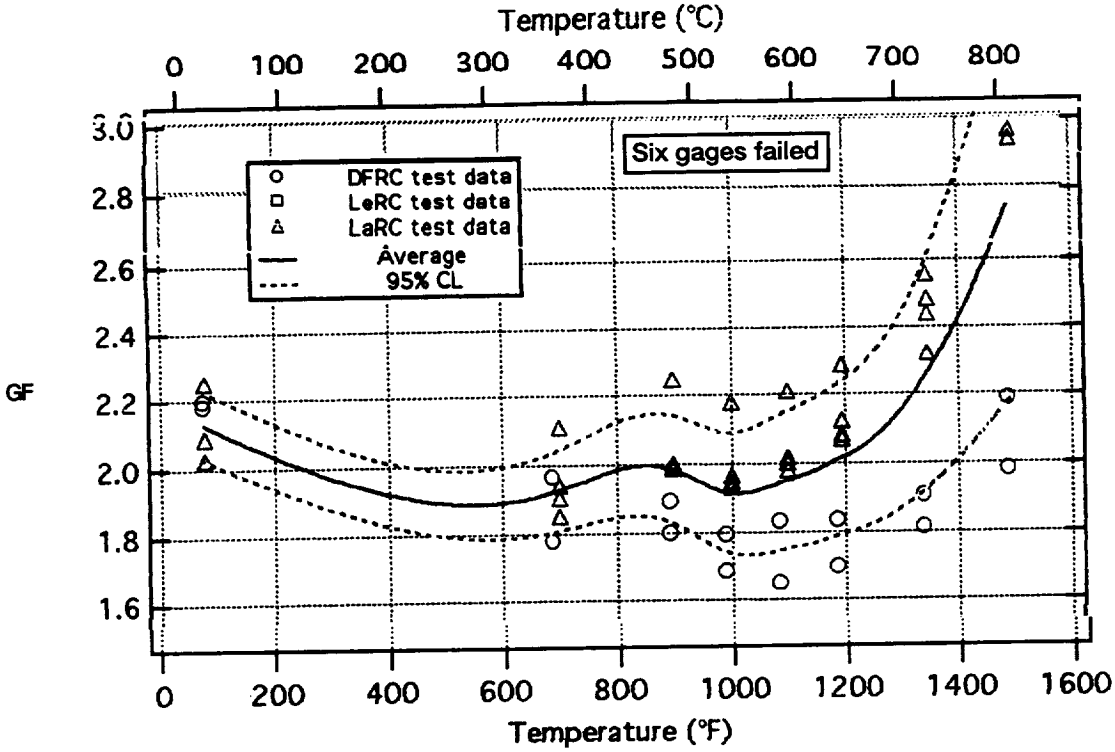

Figure 5.185.—Twelve DETCBCL gages on TMC under tension—cycle 8 heating to 1500 °F (816 °C).

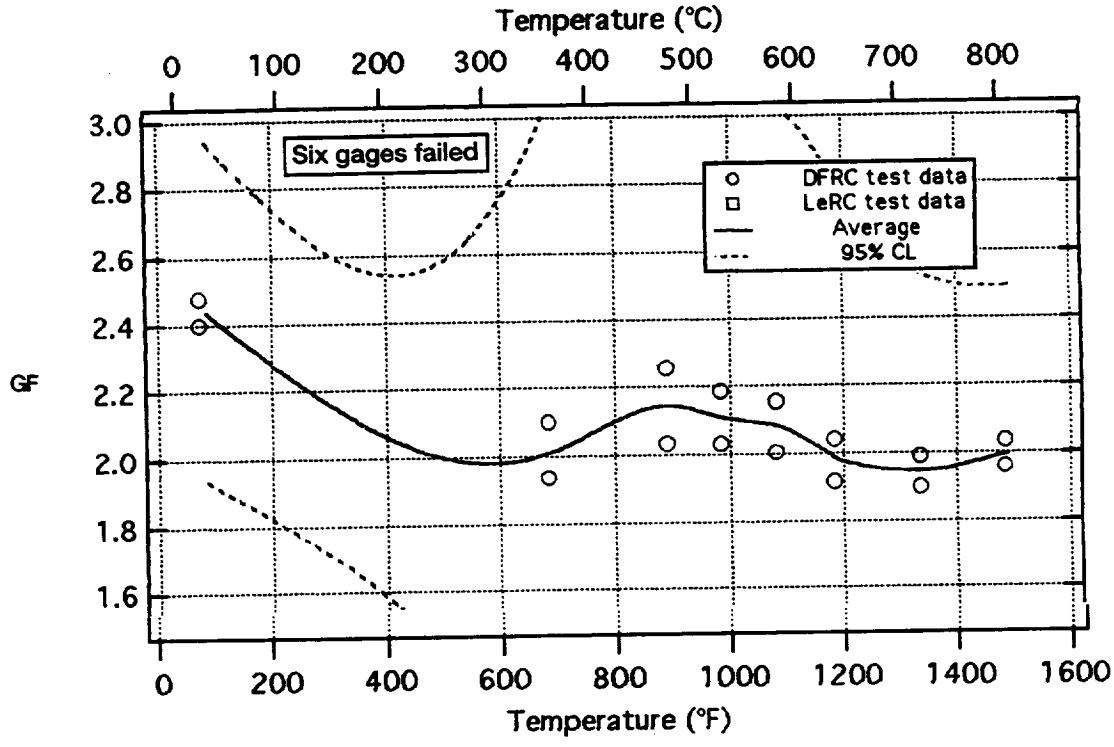

Figure 5.186.—Eight DETCBCL gages on TMC under compression—cycle 8 heating to 1500 °F (816 °C).

5.4 Figure-of-Merit Determinations

Tables 5.28 to 5.31 show the figures of merit determined for each of the parameters as described in section 2.3. Each table contains rows for the various characteristics associated with the parameter and for each cycle or temperature. Each table contains columns of figure-of-merit values for all three gage types tested on both IN100 and β-21S TMC.

TABLE 5.28.—GWP29 FIGURES OF MERIT FOR APPARENT STRAIN

Characteristic	Cycle	Gage type on IN100			Gage type on β-21S TMC		
		CKA1	PdCr	DETCBCL	CKA1	PdCr	DETCBCL
Scatter	C1HU	1.00	0.48	0.95	0.84	0.17	1.00
	C1CD	0.41	0.47	1.00	1.00	0.15	0.86
	C2HU	1.00	0.25	0.47	1.00	0.14	0.61
	C2CD	0.80	0.41	1.00	1.00	0.12	0.40
	C3HU	1.00	0.24	0.46	1.00	0.12	0.53
	C3CD	1.00	0.25	0.43	1.00	0.12	0.30
	C4HU	1.00	0.21	0.53	1.00	0.12	0.63
	C4CD	1.00	0.20	0.57	1.00	0.14	0.67
	C5HU	1.00	0.24	0.38	1.00	0.11	0.59
	C5CD	1.00	0.17	0.44	1.00	0.12	0.44
	C6HU	1.00	0.19	0.19	1.00	0.11	0.23
	C6CD	1.00	0.22	0.23	1.00	0.12	0.24
	C7HU	1.00	0.21	0.22	1.00	0.12	0.25
	C7CD	1.00	0.27	0.15	1.00	0.13	0.16
	C8HU	1.00	0.24	0.56	1.00	0.11	0.61
	C8CD	1.00	0.27	0.54	1.00	0.11	0.55
	C9HU	1.00	0.27	0.51	0.99	0.11	1.00
	C9CD	1.00	0.23	0.68	1.00	0.09	0.71
	C10HU	1.00	0.27	0.46	0.74	0.08	1.00
	C10CD	1.00	0.27	0.38	0.72	0.10	1.00
	C11HU	1.00	0.34	0.76	0.70	0.08	1.00
	C11CD	1.00	0.13	0.76	0.63	0.08	1.00
	C12HU	1.00	0.09	0.59	0.32	0.05	1.00
	C12CD	1.00	0.09	0.68	0.19	0.03	1.00
Magnitude	C1HU	1.00	0.61	0.15	0.62	1.00	0.45
	C1CD	1.00	0.26	0.07	1.00	0.15	0.11
	C2HU	1.00	0.41	0.11	1.00	0.11	0.10
	C2CD	1.00	0.32	0.08	1.00	0.09	0.11
	C3HU	1.00	0.49	0.11	1.00	0.07	0.09
	C3CD	1.00	0.40	0.10	1.00	0.07	0.11
	C4HU	1.00	0.42	0.11	1.00	0.06	0.08
	C4CD	1.00	0.33	0.09	1.00	0.05	0.07
	C5HU	1.00	0.33	0.09	1.00	0.05	0.08
	C5CD	1.00	0.35	0.07	1.00	0.03	0.06
	C6HU	1.00	0.47	0.10	1.00	0.04	0.08
	C6CD	1.00	0.47	0.09	1.00	0.03	0.07
	C7HU	1.00	0.40	0.09	1.00	0.04	0.08
	C7CD	1.00	0.41	0.10	1.00	0.03	0.06
	C8HU	1.00	0.46	0.10	1.00	0.04	0.08
	C8CD	1.00	0.41	0.09	1.00	0.03	0.06
	C9HU	1.00	0.59	0.14	1.00	0.02	0.07
	C9CD	1.00	0.60	0.12	1.00	0.03	0.06
	C10HU	1.00	0.56	0.12	1.00	0.02	0.10
	C10CD	1.00	0.51	0.10	1.00	0.02	0.09
	C11HU	1.00	0.52	0.10	1.00	0.07	0.19
	C11CD	1.00	0.32	0.12	1.00	0.14	0.13
	C12HU	1.00	0.14	0.12	1.00	0.03	0.09
	C12CD	1.00	0.17	0.14	1.00	0.15	0.33

TABLE 5.28.—Concluded.

Characteristic	Cycle	Gage type on IN100			Gage type on β-21S TMC		
		CKA1	PdCr	DETCBCL	CKA1	PdCr	DETCBCL
Slope	C1HU	1.00	0.59	0.23	0.77	1.00	0.48
	C1CD	1.00	0.21	0.06	1.00	0.23	0.10
	C2HU	1.00	0.32	0.11	1.00	0.28	0.16
	C2CD	1.00	0.22	0.06	1.00	0.18	0.12
	C3HU	1.00	0.33	0.11	1.00	0.20	0.14
	C3CD	1.00	0.34	0.09	1.00	0.15	0.12
	C4HU	1.00	0.32	0.11	1.00	0.14	0.10
	C4CD	1.00	0.30	0.08	1.00	0.11	0.09
	C5HU	1.00	0.29	0.10	1.00	0.12	0.10
	C5CD	1.00	0.24	0.06	1.00	0.07	0.07
	C6HU	1.00	0.26	0.09	1.00	0.11	0.10
	C6CD	1.00	0.29	0.07	1.00	0.08	0.08
	C7HU	1.00	0.27	0.09	1.00	0.10	0.10
	C7CD	1.00	0.30	0.09	1.00	0.08	0.08
	C8HU	1.00	0.30	0.10	1.00	0.09	0.10
	C8CD	1.00	0.28	0.08	1.00	0.07	0.08
	C9HU	1.00	0.35	0.12	1.00	0.06	0.11
	C9CD	1.00	0.32	0.08	1.00	0.05	0.08
	C10HU	1.00	0.35	0.10	1.00	0.07	0.17
	C10CD	1.00	0.30	0.08	1.00	0.04	0.12
	C11HU	1.00	0.26	0.09	1.00	0.12	0.19
	C11CD	1.00	0.29	0.09	1.00	0.15	0.14
	C12HU	1.00	0.17	0.10	1.00	0.05	0.15
	C12CD	1.00	0.18	0.10	1.00	0.07	0.22
Repeatability	C1HU,C1CD	0.64	1.00	0.13	0.18	0.15	1.00
	C1HU,C2HU	0.39	1.00	0.14	0.62	0.18	1.00
	C1CD,C2HU	0.98	1.00	0.03	0.26	0.07	1.00
	C1CD,C2CD	0.37	1.00	0.05	0.26	0.07	1.00
	C2HU,C2CD	0.62	1.00	0.82	0.75	0.22	1.00
	C2HU,C3HU	1.00	0.60	0.47	1.00	0.01	0.14
	C2CD,C3HU	0.66	1.00	0.96	0.79	0.09	1.00
	C2CD,C3CD	0.53	0.55	1.00	1.00	0.06	0.25
	C2CD,C4CD	0.73	1.00	0.38	0.92	0.10	1.00
	C3HU,C3CD	1.00	0.56	0.33	1.00	0.29	0.48
	C4HU,C6HU	1.00	0.21	0.06	1.00	0.01	0.04
	C4CD,C5CD	1.00	0.14	0.14	1.00	0.11	0.07
	C5HU,C5CD	1.00	0.13	0.08	1.00	0.16	0.19
	C6HU,C7HU	0.87	1.00	0.26	1.00	0.05	0.75
	C6CD,C7CD	1.00	0.49	0.09	1.00	0.09	0.11
	C7HU,C7CD	1.00	0.31	0.10	1.00	0.87	0.27
	C1HU,C8CD	0.68	1.00	0.21	0.62	0.07	1.00
	C9HU,C9CD	1.00	0.80	0.37	1.00	0.01	0.32
	C9CD,C10HU	1.00	0.35	0.40	1.00	0.01	0.09
	C10HU,C10CD	1.00	0.06	0.06	1.00	0.02	0.68
	C11HU,C11CD	1.00	0.08	0.48	1.00	0.02	0.57
	C11CD,C12HU	1.00	0.12	0.68	1.00	0.03	0.35
	C12HU,C12CD	1.00	0.41	0.29	0.36	0.27	1.00

TABLE 5.29.—GWP29 FIGURES OF MERIT FOR STRAIN DUE TO DRIFT

[Shaded area denotes gage type with best figure of merit. Figure of merit determined at each temperature and the figures of merit for each temperature are summed together for final figure of merit.]

Characteristic	Temperature °C (°F)	Gage type on IN100			Gage type on TMC		
		CKA1	PdCr	DETCBCL	CKA1	PdCr	DETCBCL
Rate	600 (315)	0.10	1.00	0.02	1.00	0.33	0.20
	750 (400)	0.45	1.00	0.03	1.00	0.51	0.20
	900 (480)	0.34	1.00	0.06	0.35	1.00	0.45
	1050 (565)	1.00	0.38	0.36	0.91	1.00	0.83
	1200 (650)	0.66	1.00	0.58	0.17	0.05	1.00
	1350 (730)	0.26	1.00	0.40	0.88	0.03	1.00
	1500 (815)	1.00	0.35	0.32	0.67	0.40	1.00
	Overall	**3.81**	**5.73**	**1.77**	**4.98**	**3.32**	**4.68**
Scatter	600 (315)	0.47	1.00	0.69	1.00	0.67	0.23
	750 (400)	1.00	0.95	0.80	1.00	0.58	0.04
	900 (480)	0.22	1.00	0.08	0.65	1.00	0.60
	1050 (565)	0.29	1.00	0.88	0.39	0.44	1.00
	1200 (650)	0.42	1.00	0.92	0.24	0.10	1.00
	1350 (730)	0.29	1.00	0.86	0.41	0.06	1.00
	1500 (815)	0.30	0.22	1.00	0.84	0.91	1.00
	Total	**2.98**	**6.17**	**5.24**	**4.53**	**3.77**	**4.86**

TABLE 5.30.—GWP29 FIGURES OF MERIT FOR GAGE FACTOR

(a) Tension

Characteristic	Cycle	Gage type on IN100			Gage type on β-21S TMC		
		CKA1	PdCr	DETCBCL	CKA1	PdCr	DETCBCL
Scatter	C1HU	0.58	0.52	1.00	1.00	0.89	0.85
	C1CD	0.49	1.00	0.82	1.00	0.87	0.61
	C4HU	0.57	0.48	1.00	0.74	1.00	0.61
	C4CD	0.74	0.48	1.00	0.84	1.00	0.68
	C5HU	0.61	0.58	1.00	0.87	1.00	0.61
	C5CD	0.17	0.74	1.00	0.93	1.00	0.42
	C6HU	0.56	0.50	1.00	0.79	1.00	0.71
	C6CD	0.81	1.00	0.94	1.00	0.92	0.40
	C7HU	0.48	0.91	1.00	1.00	1.00	0.73
	C7CD	0.39	0.53	1.00	0.68	1.00	0.67
	C8HU	0.57	0.91	1.00	0.89	1.00	0.60
	C8CD	0.23	1.00	0.41	1.00	0.77	0.61
Magnitude	C1HU	1.00	0.68	0.85	1.00	0.62	0.89
	C1CD	1.00	0.62	0.81	1.00	0.70	0.94
	C4HU	1.00	0.62	0.81	1.00	0.64	0.84
	C4CD	1.00	0.65	0.81	1.00	0.67	0.90
	C5HU	1.00	0.60	0.79	1.00	0.67	0.87
	C5CD	1.00	0.62	0.77	1.00	0.69	0.89
	C6HU	1.00	0.61	0.76	1.00	0.66	0.84
	C6CD	1.00	0.63	0.76	1.00	0.70	0.90
	C7HU	1.00	0.64	0.77	1.00	0.66	0.89
	C7CD	1.00	0.65	0.75	1.00	0.70	0.98
	C8HU	1.00	0.65	0.75	1.00	0.70	0.90
	C8CD	1.00	0.64	0.74	0.98	0.76	1.00
Slope	C1HU	0.72	0.93	1.00	0.53	0.74	1.00
	C1CD	0.32	1.00	0.59	0.51	0.54	1.00
	C4HU	0.40	1.00	0.79	0.40	0.72	1.00
	C4CD	0.44	1.00	0.76	0.85	0.85	1.00
	C5HU	0.35	1.00	0.63	0.72	0.77	1.00
	C5CD	0.36	1.00	0.76	1.00	0.49	0.39
	C6HU	0.32	1.00	0.60	0.91	0.81	1.00
	C6CD	0.39	1.00	0.59	1.00	0.53	0.55
	C7HU	0.34	1.00	0.47	0.95	1.00	0.55
	C7CD	0.33	1.00	0.19	1.00	0.93	0.56
	C8HU	0.28	1.00	0.31	0.97	1.00	0.74
	C8CD	0.20	1.00	0.22	1.00	0.73	0.97
Repeatability	C1HU, C1CD	1.00	0.35	0.23	0.06	1.00	0.11
	C1HU, C4HU	1.00	0.72	0.47	0.29	1.00	0.15
	C1CD, C4CD	0.13	1.00	0.19	0.94	1.00	0.58
	C4HU, C4CD	0.17	1.00	0.25	0.15	1.00	0.25
	C5HU, C5CD	1.00	0.61	0.52	0.34	1.00	0.17
	C5HU, C6HU	0.90	1.00	0.43	0.79	1.00	0.82
	C5CD , C6CD	0.69	1.00	0.54	1.00	0.86	0.44
	C6HU, C6CD	0.20	1.00	0.31	0.42	1.00	0.28
	C7HU, C8HU	0.27	1.00	0.19	1.00	0.70	0.56
	C7HU, C8HU	0.46	1.00	0.44	1.00	0.92	0.34
	C7CD, C8CD	0.66	1.00	0.64	1.00	0.37	0.25
	C8HU, C8CD	1.00	0.86	0.85	0.76	1.00	0.46

TABLE 5.30.—Concluded.
(b) Compression

Characteristic	Cycle	Gage type on IN100			Gage type on β-21S TMC		
		CKA1	PdCr	DETCBCL	CKA1	PdCr	DETCBCL
Scatter	C1HU	0.87	0.86	1.00	1.00	0.80	0.75
	C1CD	0.45	1.00	0.58	1.00	0.75	0.50
	C4HU	0.75	1.00	0.58	0.87	1.00	0.56
	C4CD	0.62	1.00	0.65	0.98	1.00	0.38
	C5HU	0.45	1.00	0.60	1.00	0.89	0.53
	C5CD	0.70	0.86	1.00	1.00	0.85	0.26
	C6HU	0.77	0.83	1.00	1.00	0.76	0.34
	C6CD	0.72	1.00	0.78	1.00	0.83	0.32
	C7HU	0.29	1.00	0.33	1.00	0.77	0.23
	C7CD	0.36	1.00	0.55	1.00	0.55	0.48
	C8HU	0.25	1.00	0.34	1.00	0.73	0.21
	C8CD	0.44	1.00	0.51	1.00	0.61	0.09
Magnitude	C1HU	1.00	0.64	0.83	1.00	0.63	0.92
	C1CD	1.00	0.68	0.83	1.00	0.65	0.92
	C4HU	1.00	0.64	0.81	1.00	0.64	0.88
	C4CD	1.00	0.64	0.82	1.00	0.66	0.88
	C5HU	1.00	0.63	0.82	1.00	0.66	0.92
	C5CD	1.00	0.64	0.81	1.00	0.66	0.89
	C6HU	1.00	0.65	0.80	1.00	0.66	0.95
	C6CD	1.00	0.64	0.78	1.00	0.67	0.93
	C7HU	1.00	0.64	0.81	1.00	0.66	0.94
	C7CD	1.00	0.67	0.77	1.00	0.68	0.95
	C8HU	1.00	0.68	0.75	1.00	0.73	0.99
	C8CD	1.00	0.70	0.75	1.00	0.68	0.94
Slope	C1HU	0.52	0.73	1.00	0.56	1.00	0.69
	C1CD	0.54	0.67	1.00	0.59	1.00	0.90
	C4HU	0.51	1.00	0.83	0.63	1.00	0.90
	C4CD	0.54	1.00	0.86	0.54	1.00	0.47
	C5HU	0.47	1.00	0.74	0.52	0.83	1.00
	C5CD	0.38	1.00	0.60	0.54	1.00	0.34
	C6HU	0.63	1.00	0.81	0.72	1.00	0.46
	C6CD	0.57	1.00	0.64	0.61	1.00	0.60
	C7HU	0.40	1.00	0.46	1.00	0.67	0.79
	C7CD	0.46	1.00	0.51	0.70	0.55	1.00
	C8HU	0.36	1.00	0.48	0.73	1.00	0.82
	C8CD	0.33	1.00	0.47	0.86	1.00	0.89
Repeatability	C1HU, C1CD	0.84	1.00	0.97	0.24	1.00	0.19
	C1HU, C4HU	1.00	0.85	0.77	0.43	1.00	0.18
	C1CD, C4CD	1.00	0.52	0.72	0.50	1.00	0.17
	C4HU, C4CD	0.26	0.75	1.00	0.14	1.00	0.11
	C5HU, C5CD	0.38	1.00	0.43	0.47	1.00	0.34
	C5HU, C6HU	0.56	1.00	0.58	0.21	1.00	0.07
	C5CD , C6CD	0.37	1.00	0.17	0.72	1.00	0.39
	C6HU, C6CD	1.00	0.88	0.48	0.44	1.00	0.27
	C7HU, C8HU	0.43	1.00	0.23	1.00	0.72	0.28
	C7HU C8HU	0.67	1.00	0.79	1.00	0.57	0.70
	C7CD, C8CD	1.00	0.57	0.83	1.00	0.52	0.25
	C8HU, C8CD	1.00	0.42	0.70	0.80	1.00	0.27

TABLE 5.31.—GWP29 GAGE SURVIVAL

(a) Summary

Parameter	Characteristic	Temperature, °F (°C)	IN100			TMC		
			CKA1	PdCr	DETCBCL	CKA1	PdCr	DETCBCL
Survival rate	Apparent strain	1200 (650)	12	10	12	12	12	12
		1350 (730)	12	10	12	12	12	12
		1500 (815)	12	10	12	12	12	12
	Drift strain	1200 (650)	12	10	12	12	12	12
		1350 (730)	12	10	12	12	12	12
		1500 (815)	12	4	12	12	8	12
	Gage factor	1200 (650)	12	7	12	12	12	12
		1350 (730)	11	4	11	12	12	7
		1500 (815)	9	3	7	5	11	6
	Overall	1200 (650)	36	27	36	36	36	36
		1350 (730)	35	24	35	36	36	31
		1500 (815)	33	17	31	29	31	30

(b) Figures of merit for gage size and survival rate

Parameter	Characteristic	Temperature, °F (°C)	IN100			TMC		
			CKA1	PdCr	DETCBCL	CKA1	PdCr	DETCBCL
Gage size	Installed area		0.42	1.00	0.60	0.42	1.00	0.60
	Calculated transverse sensitivity		0.88	1.00	0.89	0.88	1.00	0.89
	Sum		1.30	2.00	1.49	1.30	2.00	1.49
Survival rate	Apparent strain	1200 (650)	1.00	0.83	1.00	1.00	1.00	1.00
		1350 (730)	1.00	.83	1.00	1.00	1.00	1.00
		1500 (815)	1.00	.83	1.00	1.00	1.00	1.00
	Drift strain	1200 (650)	1.00	0.83	1.00	1.00	1.00	1.00
		1350 (730)	1.00	.83	1.00	1.00	1.00	1.00
		1500 (815)	1.00	.83	1.00	1.00	.67	1.00
	Gage factor	1200 (650)	1.00	0.61	1.00	1.00	1.00	1 00
		1350 (730)	.92	.33	.92	1.00	1.00	58
		1500 (815)	.75	.25	.58	.42	.92	50
	Overall	1200 (650)	1.00	0.75	1.00	1.00	1.00	1 00
		1350 (730)	.97	.67	.97	1.00	1.00	86
		1500 (815)	.92	.47	.86	.81	.86	83

5.5 Results and Discussion

Although a significant effort was made to minimize the differences in test equipment used at the three test sites (e.g., the same hardware and software were used for final data processing), each center employed a different data acquisition system and furnace configuration; therefore, some inherent differences may be evident in the final results.

5.5.1 Apparent Strain

This discussion of the characteristics of apparent strain for each type of gage (scatter, magnitude, slope, and repeatability) is based on figures 5.1 to 5.72, 5.187, and 5.188. Offsets were adjusted to zero before each heatup cycle.

5.5.1.1 CKA1 gage on IN100

Scatter:With the CKA1 gage on IN100 scatter was greater for cycle 1 than for any of the other 1200 °F (650 °C) cycles. The cooldown portion of this cycle had a wide scatterband and a large zero shift. The figures of merit from section 5.4 show that the C1HU scatter was only marginally superior and that C1CD had the poorest results for the three types of gage. C2CD improved but still had noticeable scatter; the figure of merit indicates that the DETCBCL gage was superior for this half-cycle. The scatter was stable from cycle 3 through cycle 12 even with rate changes to the temperature at cycles 9 and 11. Note the tightness of the scatterbands in cycles 3 to 8 in the temperature range 75 to 750 °F (20 to 400 °C) and the increased scatter when the temperature was between 750 and 1200 °F (400 and 650 °C). This temperature dependency in the scatterband was consistent from heatup to cooldown, suggesting that the gage design did a good job of canceling the effects of the metallurgical instabilities in the Kanthal alloy. The temperature dependency changed after the initial exposure to 1350 °F (730 °C) in cycle 9. The point at which the scatterband increased shifted from 750 °F (400 °C) in cycle 9 to 300 °F (150 °C) in cycle 10. Also, note the greater differences between the heatup and cooldown in cycles 10 and 12, indicating that second cycles at a given temperature stabilized these gages. The figures of merit from section 5.4 indicate that this gage was superior in this characteristic for first-cycle data, with the exception of the cooldown in cycle 1, C1CD.

Magnitude:Relative to other high-temperature strain gages, the CKA1 gage on IN100 had small magnitude of apparent strain throughout the temperature range tested. The figures of merit show that this gage was superior through all test cycles.

Slope:The CKA1 gage on IN100 showed very little slope in the apparent strain plots. The lack of slope change in either cycle 5 or 6 is an excellent demonstration of an insensitivity to cooling rate change, as cooling rate change is a traditional drawback of gages manufactured from FeCrAl alloys. The figures of merit show this gage to be superior for all cycles.

Repeatability:Repeatability figures of merit were determined for selected cycles as discussed in connection with table 2.9. Over this test range the CKA1 gage on IN100 showed good repeatability but was superior for only three of the seven selected cycles.

5.5.1.2 PdCr gage on IN100

Scatter: The scatterband for the PdCr gage on IN100 was nearly the same for the first four cycles except for the large zero shift in cycle 1, indicating little sensitivity to heating rate changes. Cycle 5 showed a larger zero shift and an expanded scatterband, indicating sensitivity to cooling rate change, which also is apparent in cycle 7, where another cooling rate change took place. Zero shifts from cycle 1 no longer existed in cycle 2, indicating full stabilization at this point. Scatter increased because of increased maximum exposure temperature in cycle 9. A small amount of stabilization occurred in cycle 10. The scatterbands of cycles 11 and 12 increased significantly, indicating that at 1500 °F (815 °C) there may have been a phase change in the gage material. Center-to-center differences in temperature-time histories showed up in the PdCr data. They may be explained by figures 5.187 and 5.188, which show the differences in temperature-time histories for cycle 6, a 60 F deg/sec (33 C deg/sec) heating and cooling rate test. The figures of merit for scatter show that the PdCr gage on IN100 did not perform as well as the others for all first-cycle tests.

Magnitude: The magnitude of the apparent strain was greater for the PdCr gage on IN100 than for CKA1 but was generally less than 1000 με and was relatively constant over the 12 cycles. As with all other PdCr characteristics the gage behavior broke down at 1500 °F (815 °C). The figure of merit for this characteristic places this gage second to the CKA1 for all cycles.

Slope: The slope for all cycles, except at 1500 °F (815 °C), was relatively flat and showed little change over the series of cycles. The figures of merit for slope show the PdCr gage on IN100 to be second to the CKA1 for all cycles tested.

Repeatability: Despite the cycle 1 scatter, C1HU–C1CD repeatability was significantly better than for either of the other two gage types. Repeatability was slightly affected by the rate sensitivity in cycles 5 and 7, but improved in following cycles. Repeatability was good in cycle 9 but decreased in cycle 10. It was expected that a second cycle to 1350 °F (730 °C) would stabilize the gage and improve the repeatability. Instead, we may be seeing the effects of thermal cycling. Cycles 11 and 12 show repeatability despite the widely scattered data. The figures of merit for this characteristic show the PdCr gage on IN100 to be superior in four of the designated cycles.

5.5.1.3 DETCBCL gage on IN100

Scatter:Cycle 1 scatter was low for the DETCBCL gage on IN100, despite the large magnitude of apparent strain. The other two gage types had large magnitude of apparent strain

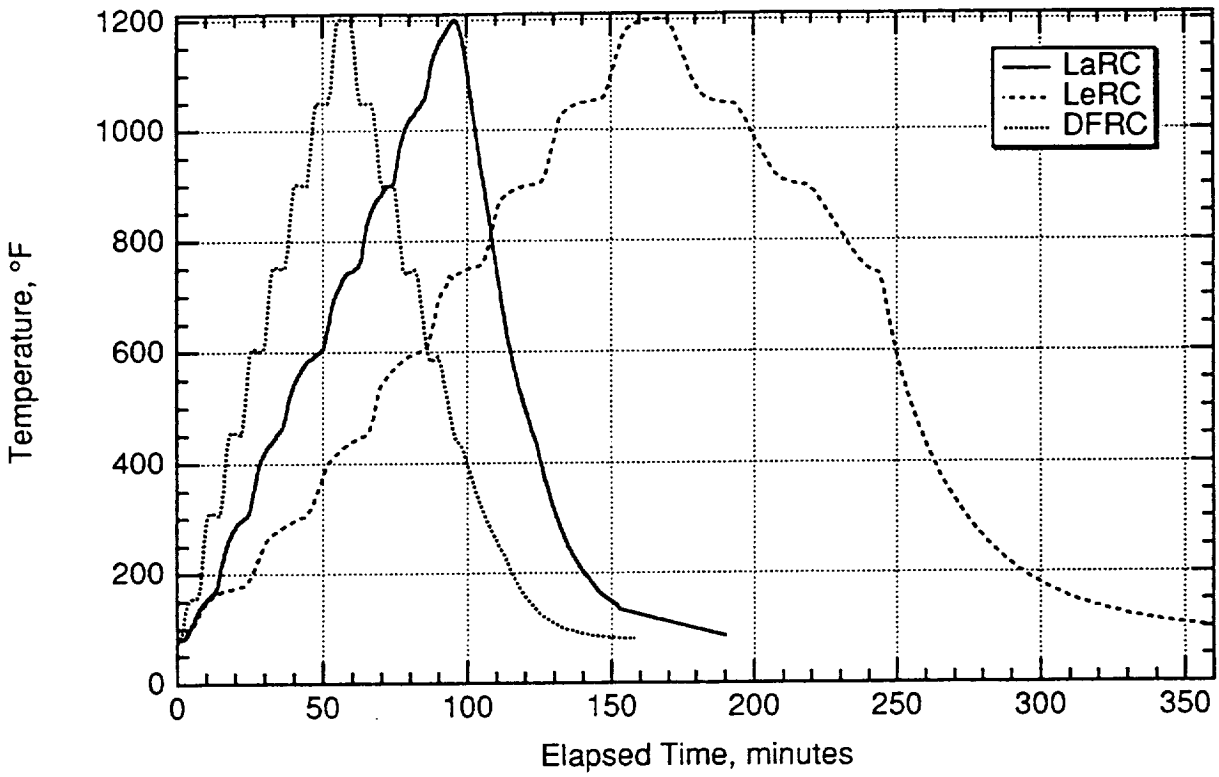

Figure 5.187.—Typical cycle 6 temperature-time profiles on IN100 (60 F deg/sec).

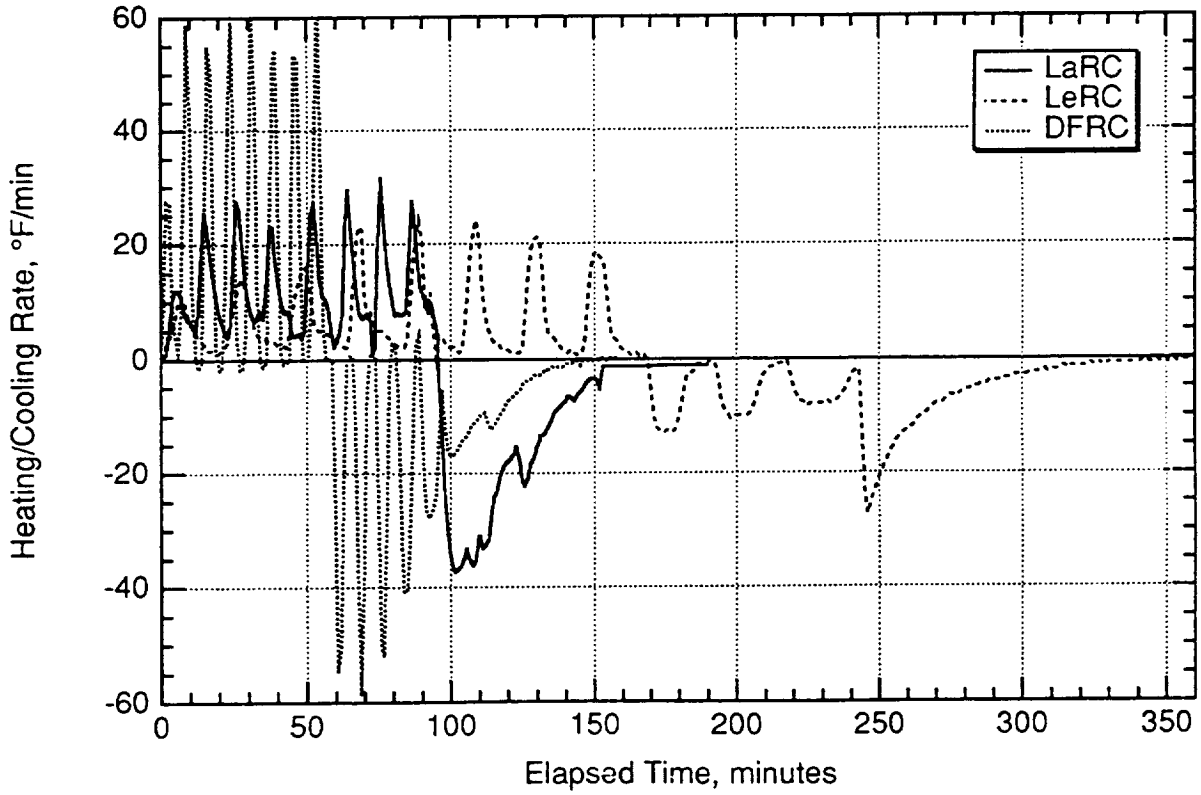

Figure 5.188.—Typical cycle 6 heating/cooling rates on IN100.

associated with large magnitude of scatter. The scatter remained fairly tight and consistent through cycle 4. Some change occurred in cycle 5, particularly in C5HU. Rate sensitivity does not explain this increase, since the heatup rate had already changed in cycle 3. It may be explained by center-to-center differences in heating and cooling profiles (figs. 5.187 and 5.188). Cycle 6 scatter was large, but center-to-center differences are evident in the data (figs. 5.187 and 5.188). BCL–3 alloy is known to be cooling rate sensitive, and there were again differences in the temperature-time profiles between the three centers. Cycle 7 scatter was large. The scatter for sets of 4 gages tested at each center was small, but when considered as a set of 12 gages it was large. Cycle 8 showed a stabilization in scatterband. Cycle 9 scatter was essentially unchanged from the cycles accomplished at lower temperatures, indicating little effect from increased exposure at temperature. Cycle 10 again appeared to be dominated by center biases. Cycle 11 showed approximately the same scatter as cycle 10, and cycle 12 showed a smaller scatter at lower temperatures and a larger scatter at 1500 °F (815 °C). The longer time at temperature shown in figure 5.187, particularly at Lewis, would cause large differences in the data. The figures of merit for scatter show that the DETCBCL gage did not perform as well on IN100 as the other two gages.

Magnitude: The magnitude for the DETCBCL on IN100 was consistent throughout all cycles but was still poor relative to the other two gages, except for cycle 12, where the magnitude was less than that for the PdCr above 1350 °F (730 °C). The figures of merit for apparent strain magnitude show that the DETCBCL was consistently poorest on all cycles. The figures of merit for cycle 12 indicate the PdCr and DETCBCL to be close to the same value, with the PdCr being only slightly superior.

Slope: The apparent strain curves all show a negative slope for the DETCBCL gage on IN100 to approximately 600 °F (315 °C), and then the slope became positive to the end test temperatures. The figures of merit for slope indicate that this type of gage did not perform as well as the other two.

Repeatability: The usual first-cycle zero shift was present below 900 °F (480 °C). Cycles 2 to 4 had good repeatability, except in the phase transformation temperature region (PTTR), 600 to 1050 °F (315 to 565 °C). Cycle 5 lost some repeatability because of cooling rate sensitivity. Cycle 6 repeatability was good outside the PTTR, despite the data scatter. Cycle 7 was similar to cycle 1. Higher temperature repeatability in cycles 9 to 12 was better than at lower temperatures. The figures of merit for this characteristic show the DETCBCL gage on IN100 to be second in two of the designated first cycles and third in the others. A factor in this poor showing was the difference in time at temperature from center to center.

5.5.1.4 CKA1 gage on β-21S TMC

Scatter: As it was for CKA1 on IN100, scatter was greater in cycle 1 for the CKA1 gage on β-21S TMC than in any of the other 1200 °F (650 °C) cycles. The scatter in the cooldown portion of this cycle, although greater than in other cycles, was less than on IN100. The figures of merit for cycle 1 show that although the DETCBCL was superior in C1HU, the CKA1 was superior in C1CD by approximately the same margin. The scatter in cycle 2 was considerably less, as reflected in the figure of merit. Although there was a slight increase in scatter as the data progressed from cycle 2 through cycle 8, the CKA1 retained its superiority in every half-cycle. Note the tightness in scatter in cycles 2 to 8 from 75 to 750 °F (20 to 400 °C) and the increased scatter from 750 to 1200 °F (400 to 650 °C). This temperature dependency in the scatterband was consistent from heatup to cooldown and followed the same trend as for CKA1 on IN100. The temperature dependency changed after the initial exposure to 1350 °F (730 °C) in cycle 9, where there was a noticeable increase in scatter in C9CD at 75 °F (20 °C). More significant changes followed in cycle 10, where there was a substantial increase in scatter, particularly at higher temperatures. Also, the temperature at which scatter increased changed from 750 °F (400 °C) in cycle 9 to 300 °F (150 °C) in cycle 10. Exposure to 1500 °F (815 °C) in cycles 11 and 12 dramatically increased the scatter in the gage. The figures of merit from section 5.4 indicate that the CKA1 gage on β-21S TMC was superior in scatter for all half-cycles through cycle 9, except for C1HU and C9CD. Thereafter, the DETCBCL gage was superior.

Magnitude: Relative to other high-temperature strain gages, the magnitude of the apparent strain of the CKA1 was small throughout the temperature range tested and was even smaller on β-21S TMC than on IN100. The figure of merit in section 5.4 shows that this gage was superior through all cycles of the test, except for C1HU, for which the PdCr gage was superior.

Slope: The CKA1 on β-21S TMC showed very little slope in the apparent strain plots. As on IN100, apparent strain for the CKA1 on β-21S TMC changed slope between 300 and 750 °F (150 and 400 °C) because installation stresses had been relieved. These changes were significant enough that the PdCr was superior in C1HU, with the CKA1 being superior in every half-cycle after that. The lack of slope change in either cycle 5 or cycle 6 was again an excellent demonstration of the insensitivity to cooling rate change.

Repeatability: Repeatability figures of merit were determined for selected cycles as discussed in connection with table 2.9. Over this test range the CKA1 on β-21S TMC showed good repeatability but was superior in only three of the seven selected cycles.

5.5.1.5 PdCr gage on β-21S TMC

The PdCr gages on the TMC at Langley and Dryden were reworked along the welds at Langley. These reworked gages showed a much larger apparent strain and poorer repeatability than those tested at Lewis with no reworking. The average results of the PdCr gages on TMC are therefore not as representative as those from gages on IN100.

Scatter: Cycle 1 scatter for the PdCr gage on β-21S TMC was large, and center-to-center differences are evident. Scatter decreased in cycle 2, with modest growth in cycles 3 to 5, again with some center-to-center differences in each cycle. Scatter remained essentially constant in cycles 5 to 7 and grew again in cycle 8. There was no clear heating or cooling rate sensitivity in the scatter, but increasing cyclic exposure did not stabilize the gage on β-21S TMC as it did on IN100. Scatter increased dramatically with increased maximum exposure temperature in cycle 9 and continued to do so in all subsequent cycles. Scatter reached extreme proportions in cycles 11 and 12, when the maximum exposure temperature increased to 1500 °F (815 °C). Center-to-center differences showed up in every cycle of the PdCr data. Differences in the temperature-time histories for the fast heatup/fast cooldown cycles explained the behavior observed on IN100. However, because center-to-center differences were present in all data for PdCr on β-21S TMC, temperature-time histories do not explain the observed data. The figures of merit for scatter show that the PdCr gage on β-21S TMC did not perform as well as the others for all first-cycle tests.

Magnitude: With the exception of C1HU the magnitude of the apparent strain was large and increased with each half-cycle. C11CD had considerably less magnitude than any of the surrounding half-cycles. The figure of merit for magnitude shows that the PdCr gage on β-21S TMC did not perform as well as the others, except for first-cycle heatup, where it was superior.

Slope: The slope characteristics of the PdCr gage on β-21S TMC were very similar to the magnitude characteristics for all cycles. In C1HU it was superior to the other gage types but thereafter had large slopes and was poorer than the other gages in the selected comparisons. The figure of merit for slope shows that this gage did not perform as well as the other two, except for first-cycle heatup, where it was superior.

Repeatability: Significant differences existed from 75 to 1200 °F (20 to 650 °C) in the C1HU–C1CD comparison, ultimately resulting in a large zero shift. Lesser but still significant offsets and zero shifts occurred in cycles 2 to 5. Repeatability improved slightly in cycles 6 to 8, and thus the PdCr did not appear to be rate sensitive as it was on IN100. Repeatability was poor in all cycles above 1200 °F (650 °C), although some improvement was made in C12CD. The figures of merit for repeatability indicate that the PdCr gage on β-21S TMC did not perform as well as the others in each of the selected comparisons.

5.5.1.6 DETCBCL gage on β-21S TMC

Scatter: Cycle 1 scatter for the DETCBCL gage on β-21S TMC was small, despite the large magnitude of apparent strain. With the other two gage types large magnitude of apparent strain was associated with large scatter. The scatter remained fairly tight and consistent through cycle 5, although there were slight increases in scatter for C3CD and C5CD. There were also more center-to-center differences in temperature-time histories for C3CD and C5CD, which are believed to be the cause of the increase in scatter. There was a large increase in cycle 6 scatter. However, center-to-center differences in the temperature-time histories, similar to what is shown in figures 5.73 and 5.74 for cycle 6 tests on IN100, are believed to be responsible for the increase. Cycle 7 scatter remained large, but center-to-center differences were also evident once again. As noted for tests on IN100, the scatter for sets of 4 gages tested at each center was small, but when considered as a set of 12 gages it was large. Cycle 8 showed a stabilization in scatterband, with much reduced center-to-center differences. C9HU scatter from 75 to 1200 °F (20 to 650 °C) was essentially unchanged from the previous cycles and was slightly lower even when the additional scatter above 1200 °F (650 °C) was added. There was a slight increase in C9CD scatter, possibly indicating a small effect from the increased exposure temperature. Cycle 10 scatter improved from that of cycle 9, indicating a stabilizing effect of cycling to temperature. A small center-to-center difference affected C10CD scatter below 300 °F (150 °C). Scatter in cycles 11 and 12 to 1350 °F (730 °C) was consistent with the scatter in previous cycles, and the small increase in overall scatter was due only to the additional scatter from 1350 to 1500 °F (730 to 815 °C). The figures of merit for scatter show that the DETCBCL gage on β-21S TMC was superior for first-cycle behavior at each temperature and was superior for first-cycle cooldowns, except in C1CD and C9CD, where it was second.

Magnitude: The magnitude of the DETCBCL gage on β-21S TMC was consistent throughout all cycles and was a distant second to the CKA1 in most cycles. After C2HU the DETCBCL had lower magnitude than the PdCr, except for C11CD where they were approximately equal. The figures of merit for magnitude show that at least one of the other gage types was always significantly better on β-21S TMC than the DETCBCL. The performances of DETCBCL and PdCr gages were very close throughout this text matrix.

Slope: The apparent strain curves all had a negative slope to approximately 600 °F (315 °C) and then the slope became positive to 1050 °F (565 °C), above which temperature it was relatively flat. As for magnitude, the slope figures of merit show that at least one of the other gage types was always significantly better on β-21S TMC than the DETCBCL.

Repeatability: The characteristic lack of repeatability of the BCL–3 alloy in the PTTR, 600 to 1050 °F (315 to 565 °C), was present in all cycles and is assumed in all further discussion. Although some first-cycle zero shift was present, it was significantly less than on IN100 and was better than that for either of the other gages. Cycles 2 to 4 had good repeatability, although center-to-center differences in temperature-time history were responsible for some slight losses in cycle 3. A combination of cooling rate sensitivity and center-to-center differences adversely affected the repeatability in cycle 5. Despite the large

scatter in the data, cycle 6 repeatability was good. Cycle 7 exhibited the heatup/cooldown differences and zero shift typified by a slow cooldown of the rate-sensitive BCL–3 alloy. Cycle 8 recovered a considerable degree of repeatability because the additional cycle had a stabilizing effect at the same conditions as the previous cycle. Only minor effects on repeatability occurred in cycles 9 and 10 because exposure temperature had increased to 1350 °F (730 °C). However, there was some loss in repeatability in cycles 11 and 12 because the maximum exposure temperature had increased to 1500 °F (815 °C). The repeatability figures of merit show the DETCBCL gage on β-21S TMC to be superior in four of the seven designated cycles and second in the other three designated cycles.

5.5.2 Drift Strain

The rate and scatter in the drift strain discussed here are shown in the data displayed in figures 5.73 to 5.114.

5.5.2.1 CKA1 gage.—This gage exhibited quite good performance with drift rate, being the best gage, on average, on TMC and second to the PdCr on IN100. The average drift strain rate was generally under 500 με throughout the range of test temperatures. In gage-to-gage scatter, however, it was second best on TMC and poorest on IN100, increasing with increasing temperature on both materials. In general, the data from the gages tested at each center seemed to cluster together, with the results obtained at Lewis and Langley tending to follow the same general trend. This result was probably attributable to the similar test ovens (rather than Dryden's radiant heater) used at those centers. It is also speculated that the less-well-protected compensating element in this gage, being only 0.001-in.-diameter wire, suffered more from oxidation effects.

5.5.2.2 PdCr gage.—This gage exhibited quite good performance on both materials and was rated the best in both drift rate and scatter on IN100 even though only the gages tested at Lewis survived at 1500 °F (815 °C). Of the gages on IN100 that were deemed failed gages, a few actually did fail (gage opened or lead-wire attachment failed) but most simply went off scale and could not be contained within the same test parameters and procedures as the others. This trend was undoubtedly exacerbated by the more complicated electrical connections required at both Langley and Dryden to interface to the data acquisition systems used at those centers. The PdCr gage on TMC, as tested at Langley and Dryden, exhibited bizarre behavior at 1200 and 1350 °F (650 and 730 °C) yet seemed to recover at 1500 °F (815 °C). This anomaly is inexplicable at this time, yet tests at both Langley and Dryden seemed to exhibit the same general behavior.

5.5.2.3 DETCBCL gage.—This gage exhibited its best performance on TMC, where it had the lowest scatter among the gages tested and was second in drift strain rate. On IN100 it was the second performer with respect to scatter but was the poorest in terms of drift strain rate. Again there was some indication of possible bias caused by the different thermal facilities used, but it was not nearly as apparent as for the other gage types.

5.5.3 Gage Factor

This section discusses the characteristics of the gage factor parameter (i.e., scatter, magnitude, slope, and repeatability) for gages tested on IN100 and β-21S TMC. This discussion is based on gage factor figures 5.115 to 5.186 and figure-of-merit table 5.30.

5.5.3.1 CKA1 gage on IN100.—The CKA1 gage had the largest gage factor magnitude among the three gage types tested for all thermal cycles under both tension and compression. This gage, however, had the largest gage-factor-versus-temperature sensitivity (highest slope) among the three gage types. Its gage factor decreased approximately 25 to 30% as the temperature increased from room temperature to 1200 °F (650 °C) and then slightly increased as the temperature increased up to 1500 °F (815 °C). The CKA1 gage had the best repeatability for the first thermal cycle to 1200 and 1350 °F (650 and 730 °C) under tension and was second to the PdCr gage for all other cycles. The gage-to-gage scatter was the largest for all thermal cycles tested. The gage factor characteristics were very similar under tension and compression. The gage factor generally decreased after thermal cycling.

5.5.3.2 PdCr gage on IN100.—The PdCr gage had the smallest gage factor magnitude among the three gage types tested for all thermal cycles under both tension and compression. It had, however, the least gage-factor-versus-temperature sensitivity (lowest slope) under tension and compression for all thermal cycles except for the first cycle to 1200 °F (650 °C) under compression; DETCBCL had the lowest slope for that cycle. The gage factor of the PdCr gages decreased approximately 15 to 20% as the temperature increased from room temperature to 1200 °F (650 °C) and then slightly increased as the temperature increased up to 1500 °F (815 °C). The PdCr gage had the best repeatability for all thermal cycles except for the first thermal cycle to 1200 and 1350 °F (650 and 730 °C) under tension; CKA1 was the best for these two cycles. The PdCr gage also had the least gage-to-gage scatter for all thermal cycles under compression and was second to the DETCBCL gage for all cycles under tension. The gage factor characteristics were very similar under tension and compression. The gage factor decreased after thermal cycling to 1200 °F (650 °C) and then increased after thermal cycling to 1350 and 1500 °F (730 and 815 °C).

5.5.3.3 DETCBCL gage on IN100.—The DETCBCL gage had the second largest gage factor magnitude among the three gage types tested for all thermal cycles under both tension and compression. It had the least gage-factor-versus-temperature sensitivity (lowest slope) for the first cycle to 1200 °F (650 °C) under compression; and it was second to the PdCr gage in the lowest slope for the rest of the thermal cycles. The gage factor

of the DETCBCL gages decreased approximately 20 to 25% as the temperature increased from room temperature to 1200 °F (650 °C) and then slightly increased (5%) as the temperature increased up to 1500 °F (815 °C). The repeatability for the DETCBCL gage was not as good as for the other gage types and its gage factor decreased approximately 15 to 20% after all the thermal cycles. It had, however, the least gage-to-gage scatter for all thermal cycles under tension and was second to the PdCr gage for all thermal cycles under compression. The gage factor characteristics were slightly different under tension and compression during cycles to 1200 °F (650 °C). The gage factor decreased after thermal cycling.

5.5.3.4 CKA1 gage on TMC.—The CKA1 gage again had the largest gage factor magnitude among the three gage types tested for all thermal cycles under both tension and compression. Its gage factor decreased approximately 20 and 30% as the temperature increased from room temperature to 1200 °F (650 °C) under tension and compression, respectively. The CKA1 gage had the best repeatability for two thermal cycles to 1500 °F (815 °C) and was second to the PdCr gage for the rest of the cycles. The CKA1 gage also had the least gage-to-gage scatter for all thermal cycles under compression and for the first cycle to 1200 °F (650 °C) under compression; it was second to the PdCr gage for the rest of the cycles. The CKA1 gage had the largest gage-factor-versus-temperature sensitivity (highest slope) among the three gage types except for the first thermal cycle to 1350 and 1500 °F (730 and 815 °C) under tension; it was the best for these two cycles. The gage factor characteristics of this gage were slightly different under tension and compression from 750 to 1050 °F (400 to 565 °C). In addition, the gage factors of the gage tested on TMC were generally larger than those of the gage tested on IN100 for all thermal cycles.

5.5.3.5 PdCr gage on TMC.—The PdCr gage again had the smallest gage factor magnitude among the three gage types tested for all thermal cycles under both tension and compression. It had, however, the least gage-factor-versus-temperature sensitivity (lowest slope) under compression for all thermal cycles except for the first cycle to 1500 °F (815 °C). The gage factor of the PdCr gage on TMC decreased approximately 15 to 20% as the temperature increased from room temperature to 1200 °F (650 °C) and then increased as the temperature increased up to 1500 °F (815 °C). The PdCr gage had the best repeatability for all thermal cycles except for the first thermal cycle to 1500 °F (815 °C); CKA1 was the best for these two cycles. The PdCr gage also had the least gage-to-gage scatter for all thermal cycles under tension and was second to the CKA1 gage for all cycles under compression. Its gage factor characteristics were very similar under tension and compression. The gage factor decreased after cycling to 1200 °F (650 °C) and then increased after thermal cycling to 1350 and 1500 °F (730 and 815 °C). Like the CKA1 gage, the gage factors of the PdCr gage tested on TMC were generally larger than those of the gage tested on IN100 for all thermal cycles.

5.5.3.6 DETCBCL gage on TMC.—The DETCBCL gage had the second largest gage factor magnitude among the three gage types tested for all thermal cycles under both tension and compression. It had however, the least gage-factor-versus-temperature sensitivity (lowest slope) for the first thermal cycle to 1200 °F (650 °C) under tension and for the first cycle to 1500 °F (815 °C) under compression. The gage factor of the DETCBCL gages decreased as the temperature increased from room temperature to 1200 °F (650 °C) and then increased as temperature increased up to 1500 °F (815 °C). The repeatability for the DETCBCL gage was not as good as for the other gage types: the gage factor varied approximately 25% between eight thermal cycles. The gage-to-gage scatter for DETCBCL on TMC was also not as good as that of the other two gage types. The gage factor characteristics of this gage were different under tension and compression from 750 to 1050 °F (400 to 565 °C). The gage factor decreased after thermal cycling to 1350 °F (730 °C) and then increased after cycling to 1500 °F (815 °C). The gage factors of this gage on TMC were generally much larger than those of the gage tested on IN100 for all thermal cycles.

5.5.4 Gage Size and Survivability

Table 5.31 shows that the PdCr required the smallest installation area of the three gages tested, the DETCBCL required a somewhat larger area, and the CKA1 required the largest area.

Table 5.31 also shows the figures of merit for survival rate. These relative numbers indicate that on IN100 the CKA1 had the superior survival, followed closely by the DETCBCL, and that on TMC the PdCr had the superior figure of merit for overall failure, followed closely by the CKA1 and the DETCBCL.

Lewis Research Center
National Aeronautics and Space Administration
Cleveland, Ohio, June 30, 1995

Appendix—Nondestructive Evaluation Tests on NASP Titanium Metal Matrix Composite

Sidney G. Allison, Min Namkung, K. Elliott Cramer, and Patrick H. Johnston
NASA Langley Research Center

Two National Aerospace Plane (NASP) titanium metal matrix composite (TMMC) panels were delivered by Rockwell to NASA Langley in June 1992 for nondestructive evaluation (NDE). Printouts of a conventional ultrasonic C-scan for each plate were also included. At NASA Langley three technologies were applied to assess the integrity of the two panels: magneto-optical imaging (MOI), thermography, and ultrasonics. The panels, which appeared to be of good quality, were returned to Rockwell in Tulsa, Oklahoma, in July 1992.

The layup of these 1/8-in.-thick, 16-ply panels was $[0,-45, 45,90, 0,-45,45,90]_s$. The lead foil strips shown in figure A.1 were removed after MOI testing. An adhesive paper was then applied to both surfaces to enhance surface emissivity for thermographic testing. The adhesive paper was removed before ultrasonic testing in a water tank.

MOI Tests

The operational principle of MOI is based on detecting the flaw-induced rotational component of electric current that produces a magnetic field normal to the test surface. Hence, two test conditions must be satisfied for the successful application of the technique. First, the electrical conductivity of the test object should be high so that strong eddy currents can be induced in the surface area of the object. Second, the size of an isolated flaw should be larger than ~5 mm so as to generate detectable normal magnetic fields (unless the flaw is created near a geometric obstacle, such a hole in the panel, which would increase the sensitivity). The two TMMC panels tested by MOI did not meet these conditions. Measurements of the electrical conductivity showed a low conductivity, much lower than that of aluminum plates (conventional test samples). Also, there were no holes in these panels. Therefore, the MOI technique did not yield any explainable results.

Thermography Tests

Thermal diffusivity imaging is a technique where a short pulse of heat is applied to one side of the test object and the time-dependent surface temperature of the other side is measured with an infrared radiometer. An image of the thermal diffusivity can be made from the time rate of change of the temperature measured. Anomalies or defects appear in these measurements as variations in the thermal diffusivity measured. Diffusivity measurements were performed on the two TMMC composite panels. The results show uniform diffusivity across both plates, giving no indication of anomalies. The average measured diffusivity of each plate was approximately 0.02 cm^2/sec. Figure A.2 is a diffusivity image of one of the plates, showing the lack of anomalies.

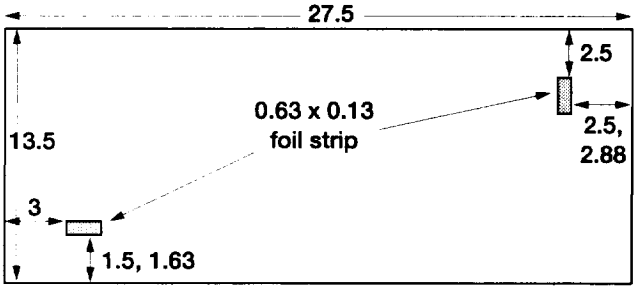

Figure A.1.—Location of lead foil strips. (Dimensions are in inches.)

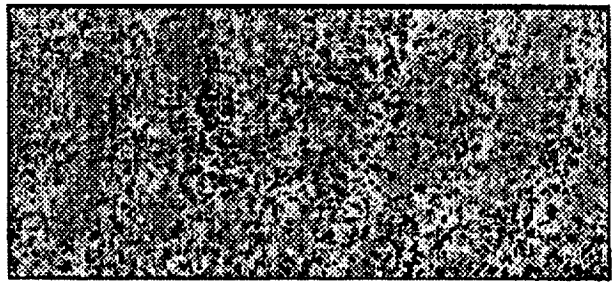

Figure A.2.—Thermal diffusivity image of TMMC test panel.

Ultrasonic Tests

Rockwell indicated that their C-scans did not show any anomalies. We repeated those types of ultrasonic C-scans on both panels in a water tank and confirmed their results (see figs. A.3 and A.4). In addition, we performed ultrasonic polar backscatter tests, which are sensitive to the conditions of fiber structures within the panels in a specific direction (see figs. A.5 and A.6). In polar backscatter measurements the ultrasonic insonification is performed at a nonnormal angle of incidence to the surface but perpendicular to a set of fibers in the plate. In principle, if the fibers are defective, increased signals will result. The surface smoothness from these samples did introduce some anomalies in polar backscatter images for the 0° direction, which was the outer layer fiber direction. These panels did not display any striking anomalies that could be attributed to flaws.

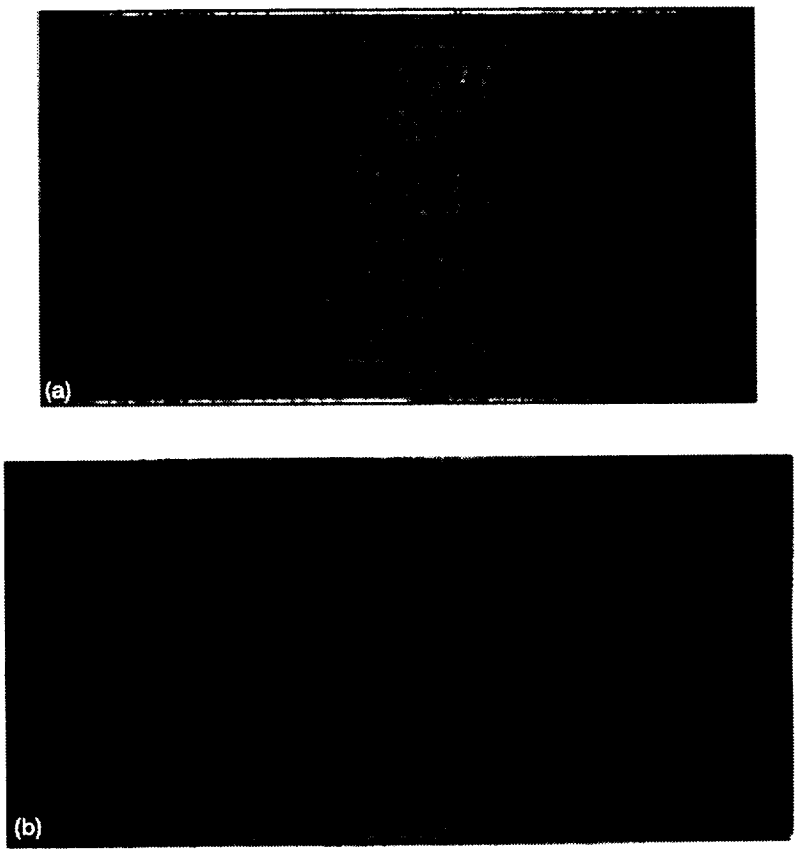

Figure A.3.—Ultrasonic C-scans of sample A. (a) Side 1. (b) Side 2.

Figure A.4.—Ultrasonic C-scan of sample B.

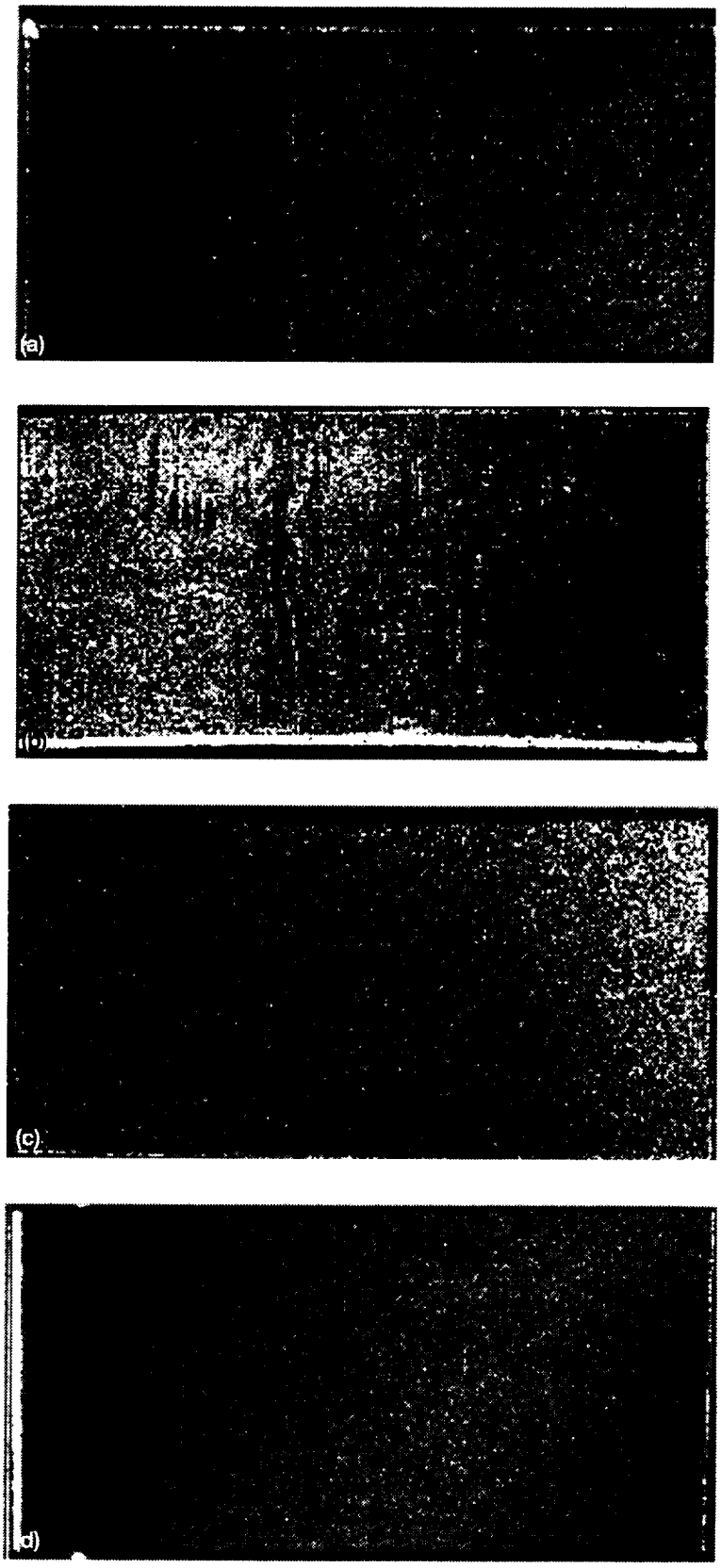

Figure A.5.—Ultrasonic polar backscatter images of sample A. (a) –45°. (b) 0°. (c) 45°. (d) 90°.

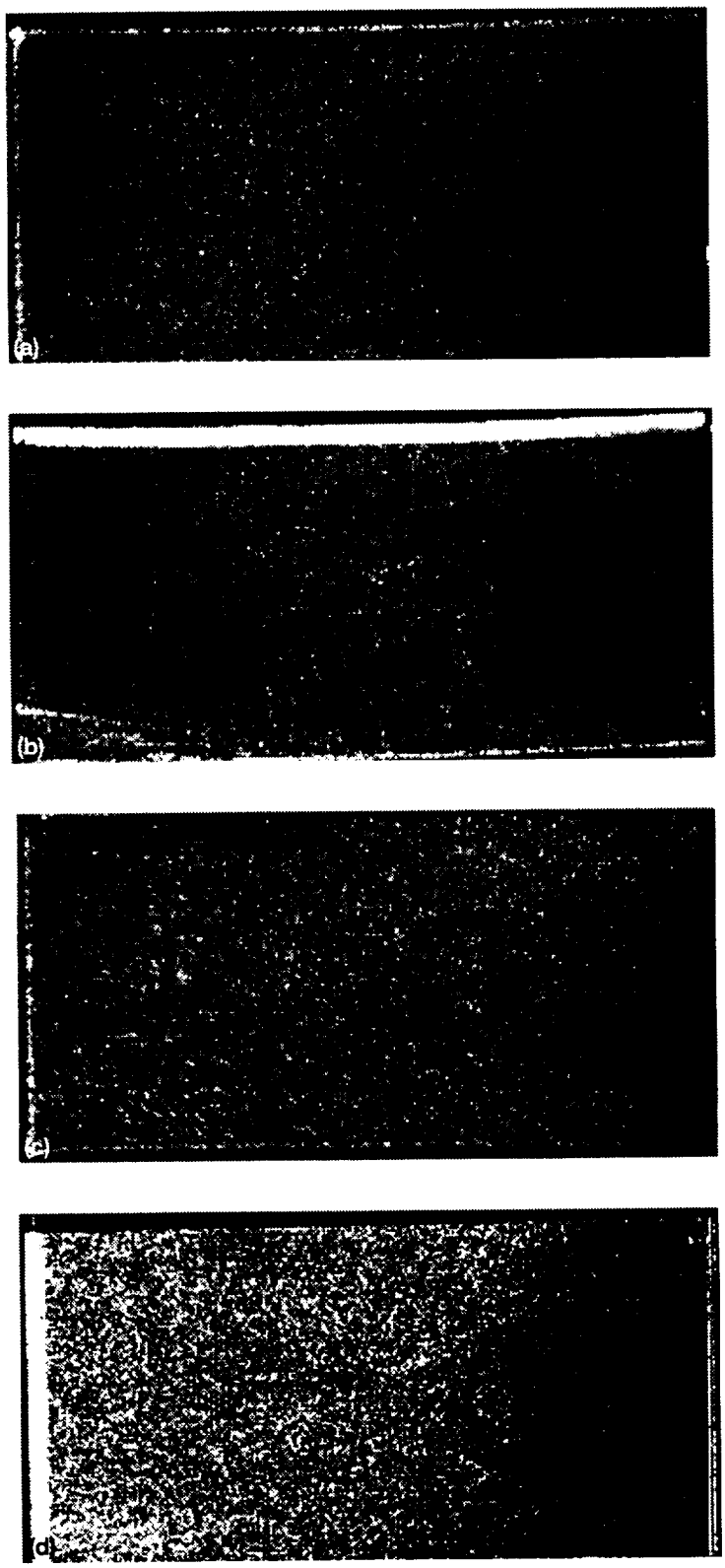

Figure A.6.—Ultrasonic polar backscatter images of sample B. (a) –45°. (b) 0°. (c) 45°. (d) 90°.

REPORT DOCUMENTATION PAGE

Form Approved
OMB No. 0704-0188

1. AGENCY USE ONLY (*Leave blank*)	2. REPORT DATE	3. REPORT TYPE AND DATES COVERED
	December 1996	Technical Paper

4. TITLE AND SUBTITLE

High-Temperature Strain Sensor and Mounting Development

5. FUNDING NUMBERS

WU-505-62-50

6. AUTHOR(S)

W. Dan Williams, Jih-Fen Lei, Lawrence F. Reardon, Keith Krake,
M.M. Lemcoe, Harlan K. Holmes, and Thomas C. Moore, Sr.

7. PERFORMING ORGANIZATION NAME(S) AND ADDRESS(ES)

National Aeronautics and Space Administration
Lewis Research Center
Cleveland, Ohio 44135-3191

8. PERFORMING ORGANIZATION REPORT NUMBER

E-9513

9. SPONSORING/MONITORING AGENCY NAME(S) AND ADDRESS(ES)

National Aeronautics and Space Administration
Washington, D.C. 20546-0001

10. SPONSORING/MONITORING AGENCY REPORT NUMBER

NASA TP-3540
NASP TM-1186

11. SUPPLEMENTARY NOTES

W. Dan Williams, NASA Lewis Research Center; Jih-Fen Lei, U.S. Army Research Laboratory, Lewis Research Center; Lawrence F. Reardon, Hugh L. Dryden Flight Research Center, Edwards, California; Keith Krake and M.M. Lemcoe, PRC, Inc., Edwards, California; Harlan K. Holmes and Thomas C. Moore, Sr., NASA Langley Research Center, Hampton, Virginia. Responsible person, W. Dan Williams, organization code 5510, (216) 433-3725.

12a. DISTRIBUTION/AVAILABILITY STATEMENT

Unclassified - Unlimited
Subject Categories 35 and 39

This publication is available from the NASA Center for Aerospace Information, (301) 621-0390.

12b. DISTRIBUTION CODE

13. ABSTRACT ***(Maximum 200 words)***

This report describes Government Work Package Task 29 (GWP29), whose purpose was to develop advanced strain gage technology in support of the National Aerospace Plane (NASP) Program. The focus was on advanced resistance strain gages with a temperature range from room temperature to 2000 °F (1095 °C) and on methods for reliably attaching these gages to the various materials anticipated for use in the NASP program. Because the NASP program required first-cycle data, the installed gages were not prestabilized or heat treated on the test coupons before first-cycle data were recorded. NASA Lewis Research Center, the lead center for GWP29, continued its development of the palladium-chromium gage; NASA Langley Research Center investigated a new concept gage using Kanthal A1; and the NASA Dryden Flight Research Center chose the well-known BCL-3 iron-chromium-aluminum gage. Each center then tested all three gages. The parameters investigated were apparent strain, drift strain, and gage factor as a function of temperature, plus gage size and survival rate over the test period. Although a significant effort was made to minimize the differences in test equipment betwen the three test sites (e.g., the same hardware and software were used for final data processing), the center employed different data acquisition systems and furnace configurations so that some inherent differences may be evident in the final results.

14. SUBJECT TERMS	15. NUMBER OF PAGES
Strain gage; NASP	240
	16. PRICE CODE: A11

17. SECURITY CLASSIFICATION OF REPORT	18. SECURITY CLASSIFICATION OF THIS PAGE	19. SECURITY CLASSIFICATION OF ABSTRACT	20. LIMITATION OF ABSTRACT
Unclassified	Unclassified	Unclassified	